UNITED STATES DEPARTMENT OF THE INTERIOR

GEOLOGICAL SURVEY

NATIONAL EARTHQUAKE HAZARDS REDUCTION PROGRAM, SUMMARIES OF TECHNICAL REPORTS VOLUME XXX

Prepared by Participants in

NATIONAL EARTHQUAKE HAZARDS REDUCTION PROGRAM

July 1990

March 3, 1849

OPEN-FILE REPORT 90-334

Menlo Park, California

1990

UNITED STATES
DEPARTMENT OF THE INTERIOR
GEOLOGICAL SURVEY

NATIONAL EARTHQUAKE HAZARDS REDUCTION PROGRAM, SUMMARIES OF TECHNICAL REPORTS VOLUME XXX

Prepared by Participants in

NATIONAL EARTHQUAKE HAZARDS REDUCTION PROGRAM

Compiled by

Muriel L. Jacobson

The research results described in the following summaries were submitted by the investigators on May 13, 1990 and cover the period from October 1, 1989 through April 1, 1990. These reports include both work performed under contracts administered by the Geological Survey and work by members of the Geological Survey. The report summaries are grouped into the five major elements of the National Earthquake Hazards Reduction Program.

Open File Report No. 90-334

The data and interpretations in these progress reports may be reevaluated by the investigators upon completion of the research. Readers who wish to cite findings described herein should confirm their accuracy with the author.

CONTENTS

Earthquake Hazards Reduction Program

Page

ELEMENT II. Earthquake Prediction Research

Collect observational data and develop the instrumentation, methodologies, and physical understanding needed to predict damaging earthquakes.

Objective (II-1): Prediction Methodology and Evaluation

Develop methods to provide a rational basis for estimates of increased earthquake potential. Evaluate the relevance of various geophysical, geochemical, and hydrological data for earthquake prediction.

1. Develop, operate and evaluate instrumentation for monitoring potential earthquake precursors.
2. Analyze and evaluate seismicity data collected prior to medium and large earthquakes.
3. Obtain and analyze data from seismically active regions of foreign countries through cooperative projects with the host countries.
4. Systematically evaluate data and develop statistics that relate observations of specific phenomena to earthquake occurrence.
5. Develop, study and test prediction methods that can be used to proceed from estimates of long-range earthquake potential to specific short-term predictions...164

Objective (II-2): Earthquake Prediction Experiments

Conduct data collection and analysis experiments in areas of California capable of great earthquakes, where large populations are at risk. The experiments will emphasize improved coordination of data collection, data reporting, review and analysis according to set schedules and standards.

1. Collect and analyze data for an earthquake prediction experiment in southern California, concentrating on the southern San Andreas fault from Parkfield, California to the Salton Sea.
2. Collect and analyze data for an earthquake prediction experiment in central California, concentrating on the San Andreas fault north of Parkfield, California...283

Page

Objective (II-3): Theoretical, Laboratory and Fault Zone Studies

Improve our understanding of the physics of earthquake processes through theoretical and laboratory studies to guide and test earthquake prediction observations and data analysis. Measure physical properties of those zones selected for earthquake experiments, including stress, temperature, elastic and anelastic characteristics, pore pressure, and material properties.

1. Conduct theoretical investigations of failure and pre-failure processes and the nature of large-scale earthquake instability.

2. Conduct experimental studies of the dynamics of faulting and the constitutive properties of fault zone materials.

3. Through the use of drilled holes and appropriate down hole instruments, determine the physical state of the fault zone in regions of earthquake prediction experiments....................................411

Objective (II-4): Induced Seismicity Studies

Determine the physical mechanism responsible for reservoir-induced seismicity and develop techniques for predicting and mitigating this phenomena.

1. Develop, test, and evaluate theories on the physics of induced seismicity.

2. Develop techniques for predicting the character and severity of induced seismicity.

3. Devise hazard assessment and mitigation strategies at sites of induced seismicity.......................

ELEMENT III Evaluation of Regional and Urban Earthquake Hazards

Delineate, evaluate, and document earthquake hazards and risk in urban regions at seismic risk. Regions of interest, in order of priority, are:

1) The Wasatch Front

2) Southern California

3) Northern California

ELEMENT IV Earthquake Data and Information Services

Seismic Monitoring of the Shumagin Seismic Gap, Alaska

USGS 14-08-0001-A0616

Geoffrey A. Abers
Lamont-Doherty Geological Observatory of Columbia University
Palisades, New York 10964
(914) 359-2900

Investigations

Seismic data from the Shumagin seismic network were collected and processed to obtain digital waveforms, origin times, hypocenters, and magnitudes for local and regional earthquakes. The data are used for earthquake source characterization, determination of seismic velocity structure, studies of regional tectonics, the analysis of possible earthquake precursors, and seismic hazard evaluation. Yearly bulletins are available starting in 1984 through 1989.

Results

Shumagin network data were used to locate 351 earthquakes from July 1 to December 31, 1989, bringing the total number of digitally recorded events in Shumagin network catalog to 5525 since 1982. The seismicity for the second half of 1989 is shown in map view on Figure 1 and in cross section on Figures 2 and 3. No events with $m_b \geq 5.0$ within the network have been recorded since July, 1988. Events shown by solid symbols are those events that meet the following selection criteria: located by 8 or more P or S arrivals, vertical error from*Hypoinverse* less than 10 km, and horizontal error less than 5 km. Other events are shown by open symbols. These criteria provide a rough indication of the location quality, and show that epicenters more than 100 km from the nearest station are rarely well determined. Additional numerical tests of hypocenter stability show that when the entire network is operating, shallow events west of 166°W, east of 156°W, or seaward of the trench can not be reliably located.

The overall pattern in Figures 1-3 resembles the long term seismicity (Figure 4). Seismicity is concentrated near the base of the main thrust zone between 35 and 50 km depth, and immediately above it within the overriding plate. The seismic below 30 km depth parallels the volcanic arc, rather than the trench, and becomes closer to the trench west of the network (Figure 1). Seismicity appears to be sparse where the main thrust zone is shallower than 35 km, between the Shumagin Islands and the trench. Deeper seismicity extends to depths of 200 km. Comparison of Figures 2 and 3 shows that much of the scatter of the seismicity in Figure 2 is a consequence of projecting events at great distance along strike onto the cross-section, although some scatter is due to poor event locations. Some locations near 100 km depth on Figure 3 are correlated with the lower plane of the double seismic zone seen on Figure 4.

Preliminary efforts have been made to assess the suitability of the Shumagin network data for determining lateral variations in seismic velocities. Locations have been redetermined in several 1D velocity models in an effort to select a set of events whose locations are relatively insensitive to velocity variations. The density of rays from selected events traced in a 1D structure (Figure 4) shows that most rays are concentrated between the south side of the Alaskan Peninsula and the Outer Shumagins, within the lower crust and uppermost mantle. Coverage appears good beneath the arc, the inner forearc, and near the top of the downgoing plate. Average residuals for each station (Figure 5) show a systematically large (.2 to .5 s) positive residuals for stations just north of the volcanic line, and somewhat large (-.14 to -.24 s) residuals at the 3 stations 15-50 km south of the volcanic line. Including these average residuals as station corrections did not significantly change the locations of the selected events. These observations give us confidence that coherent signals due to lateral velocity variations exist within the data set, and that we stand a good chance of constraining lower crust and upper mantle structure within this segment of the island arc.

Reports

Friberg, P.A., and K.H. Jacob, Processed Strong Ground Motion Data from Alaska: First Update, through June 1987., Report #2 in series "Lamont-ProcessedStrong Motion Data"; L-DGO, Palisades NY, 87 pp., 1989.

Levin, V., J.J. Taber. K.H. Jacob, G.A. Abers, M.A. Luckman, D. Johnson, M. Eubank, and J. Ramey, *Regional Seismicity Bulletin of the Eastern Aleutian Network January-December 1989*, Shumagin Seismic Network, Lamont-Doherty Geological Observatory, Palisades NY, 64 pp., 1990.

McNutt, S.R., Some seismic precursors to eruptions at Pavlof volcano, Alaska, October 1973-April 1986, *IAVCEI Proceedings in Volcanology, 1,* J.H. Latter (ed.), Volcanic Hazards, pp. 463-485, Springer-Verlag, Berlin, 1989.

Taber, J.J., S. Billington, and E.R. Engdahl, Seismicity of the Aleutian Arc, in *Neotectonics of North America*, D.B. Slemmons et al., eds., in press, 1990.

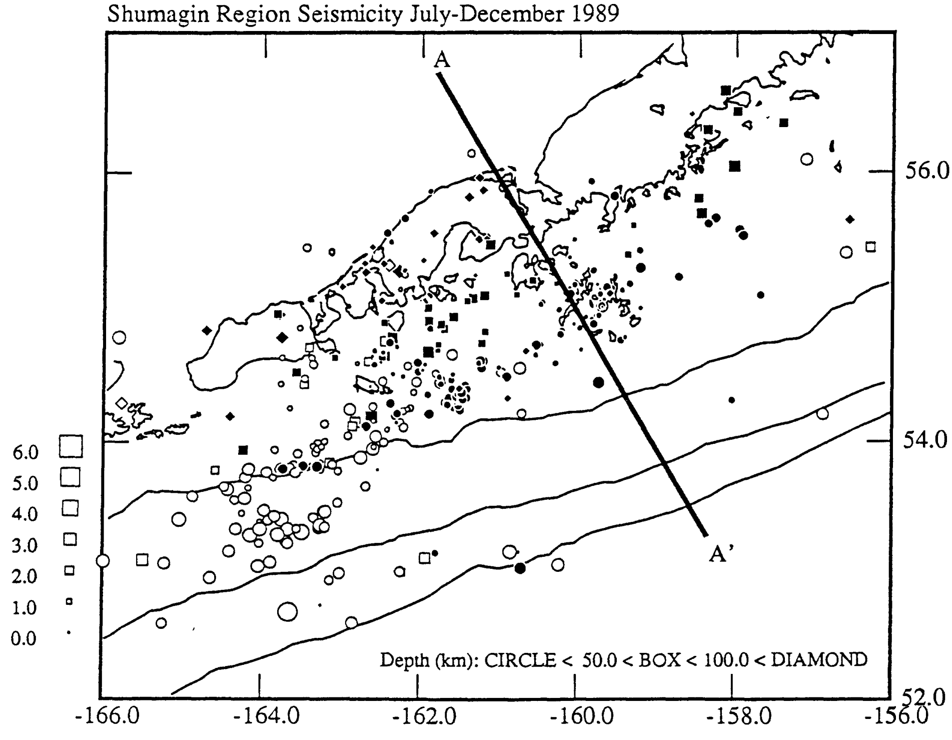

Figure 1. Map of seismicity located by the Shumagin seismic network from July to December, 1989. Symbol shapes show depths and sizes show network magnitude, as shown. Filled symbols are earthquakes that meet criteria for well-located events, discussed in text.

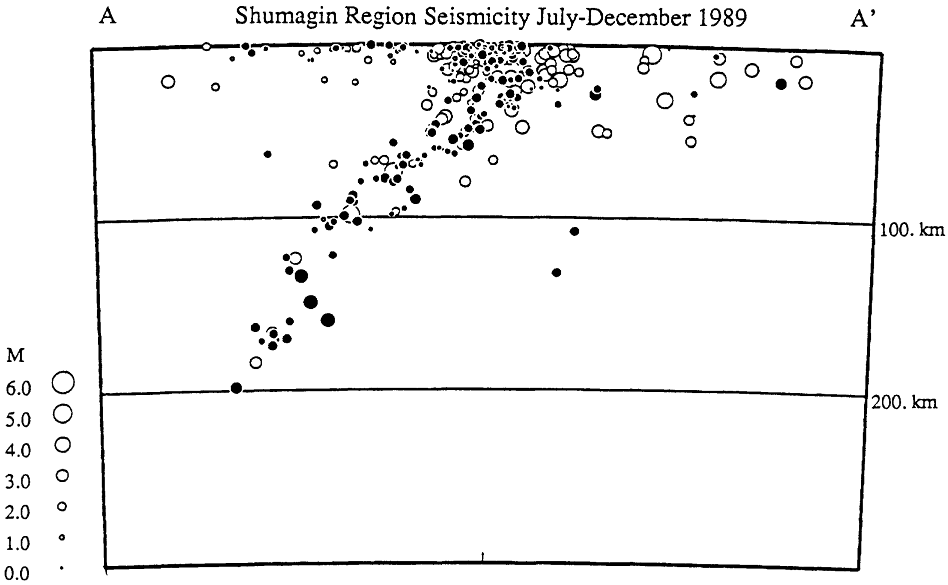

Figure 2. Cross-section of all Shumagin network seismicity, located in Figure 1 (A-A').

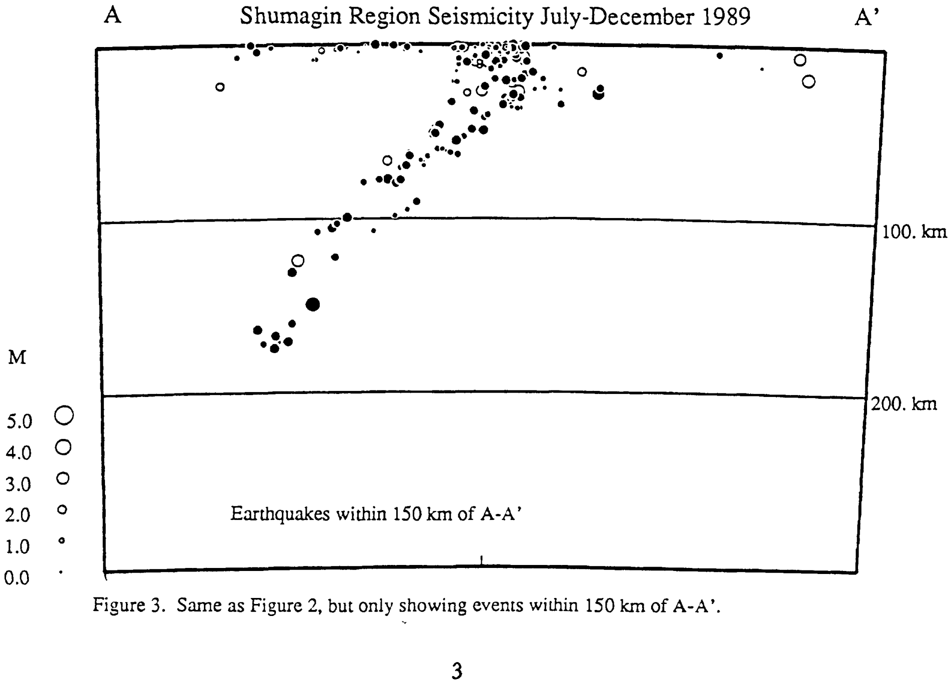

Figure 3. Same as Figure 2, but only showing events within 150 km of A-A'.

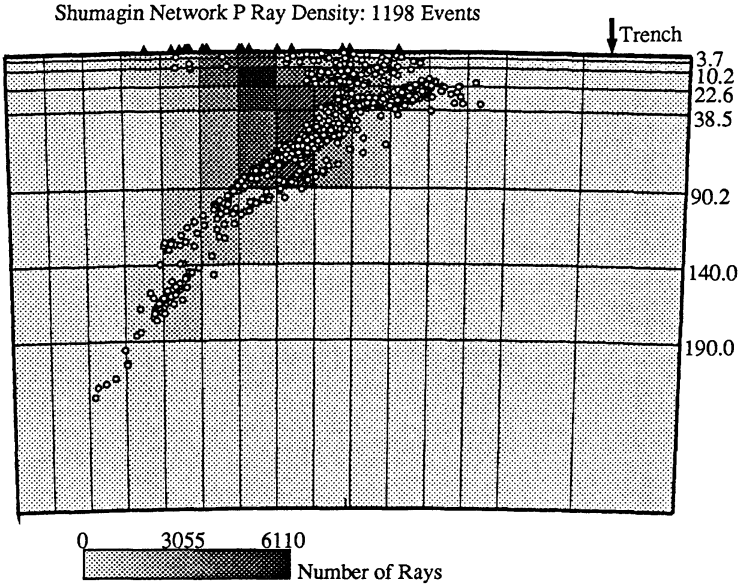

Figure 4. Number of P rays passing through a grid of 2D blocks, in cross section. Also shown are stations (triangles) and events (circles) projected onto cross section. Depths, right, in km.

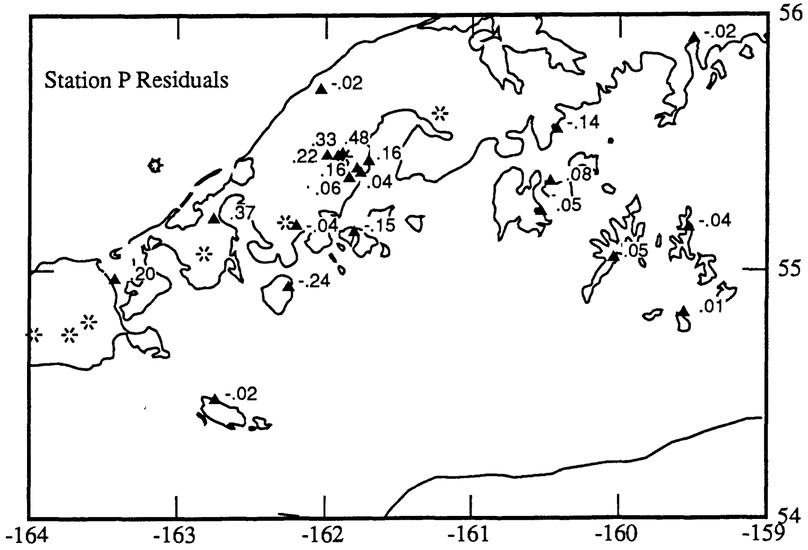

Figure 5. Average P residuals (s) at Shumagin network stations from a set of 1198 selected events 1982-1989. Triangles are stations, and stars are volcanoes.

Partial Support of Joint USGS-CALTECH Southern California Seismographic Network

#14-08-0001-A0613

Clarence R. Allen
Robert W. Clayton
Egill Hauksson

Seismological Laboratory,
California Institute of Technology
Pasadena, CA 91125 (818-356-6912)

INVESTIGATIONS

This Cooperative Agreement provides partial support for the joint USGS-Caltech Southern California Seismic Network. The purpose is to record and analyze data from local earthquakes and generate a data base of phase data and digital seismograms. The primary product derived from the data base is a joint USGS-Caltech catalog of earthquakes in the southern California region.

RESULTS

Seismicity

During the period of October 1, 1989 through March 31, 1990, the Southern California Seismographic Network recorded and processed 5002 earthquakes (Figure 1). Of these, 72 had a magnitude of 3.0 or larger, and 10 had a magnitude of 4.0 or larger. We received inquiries from the press and public on 31 of the events.

This six-month period got off to a slow start; there were no events above M4.0 in either October or November. Two significant events occurred on different areas of the San Jacinto fault in December: an M4.2 of December 2 near the town of Hemet, and an M4.5 near Lytle Creek. December also include an M4.2 northeast of Indio. This Indio site continued to be active in April 1990, producing another M4.1 and numerous smaller events. An M4.1 occurred in the Anza area, also on a branch of the San Jacinto fault, of February 18.

An M4.7 event occurred on January 15 in the northern Owens Valley area, and an M4.3 earthquake occurred south of the Mexican border, probably along the Cerro Prieto fault, on March 31.

Upland Earthquakes

The most significant event of the six-month period occurred on February 28 near the town of Upland (Figure 2). The mainshock measured M5.2 and caused moderate damage to chimneys and other weak structures throughout Upland, Claremont, and Pomona. The Upland mainshock was preceded by an M3.6 foreshock, by about 3 hours. The early part of the Upland aftershock sequence was very intense and showed promise of rivaling the 1986 Oceanside (M5.3) aftershock sequence, which is still going on. This early behavior prompted the California Office of Emergency Services to issue an advisory concerning the possibility of large aftershocks or another mainshock. After the first week, however, the Upland sequence has decayed in a relatively normal fashion for a mainshock of its size.

No surface rupture was discovered after the Upland mainshock. However, the focal mechanism was consistent with left-lateral strike-slip motion on a northeast-trending fault. The San Antonio Canyon fault has such an orientation.

Weekly Seismicity Report

In January, the Seismographic Network initiated a weekly seismicity report, patterned after a similar report issued by the U.S. Geological Survey in Menlo Park. The language of the "earthquake report" is aimed at the general public. So far, the report has been enthusiastically received. A few members of the local media have started basing regular news features on it.

Publications Using Network Data (astracts excepted).

Keilis-Borok, V. I., L. Knopoff, I., M Rotwain, and C. R. Allen, Intermediate-term prediction of occurrence times of strong earthquakes, *Nature, 335*, No. 6192, 600-694, 1989.

Jones, Lucile, Kerry E. Sieh, Egill Hauksson, and L. Katherine Hutton, The 3 December 1988 Pasadena, California, earthquake: evidence for strike-slip motion on the Raymond fault, *Bull. Seismo. Soc. Am., 80,* No. 2, 474-482, 1990.

Magistrale, Harold, Part I: Superstition Hills California earthquakes of 24 November 1989.Part II: Three-dimensional velocity structure of southern California, Ph.D. thesis, California Institute of Technology, 1990.

Magistrale, Harold, Lucile Jones, and Hiroo Kanamori, The Superstition Hills, California earthquakes of 24 November 1987, *Bull. Seismo. Soc. Am., 79*, No. 2, 239-251, 1989.

Hauksson, E. Earthquakes, faulting and stress in the Los Angeles Basin, *J. Geophys. Res.*, in press, 1990.

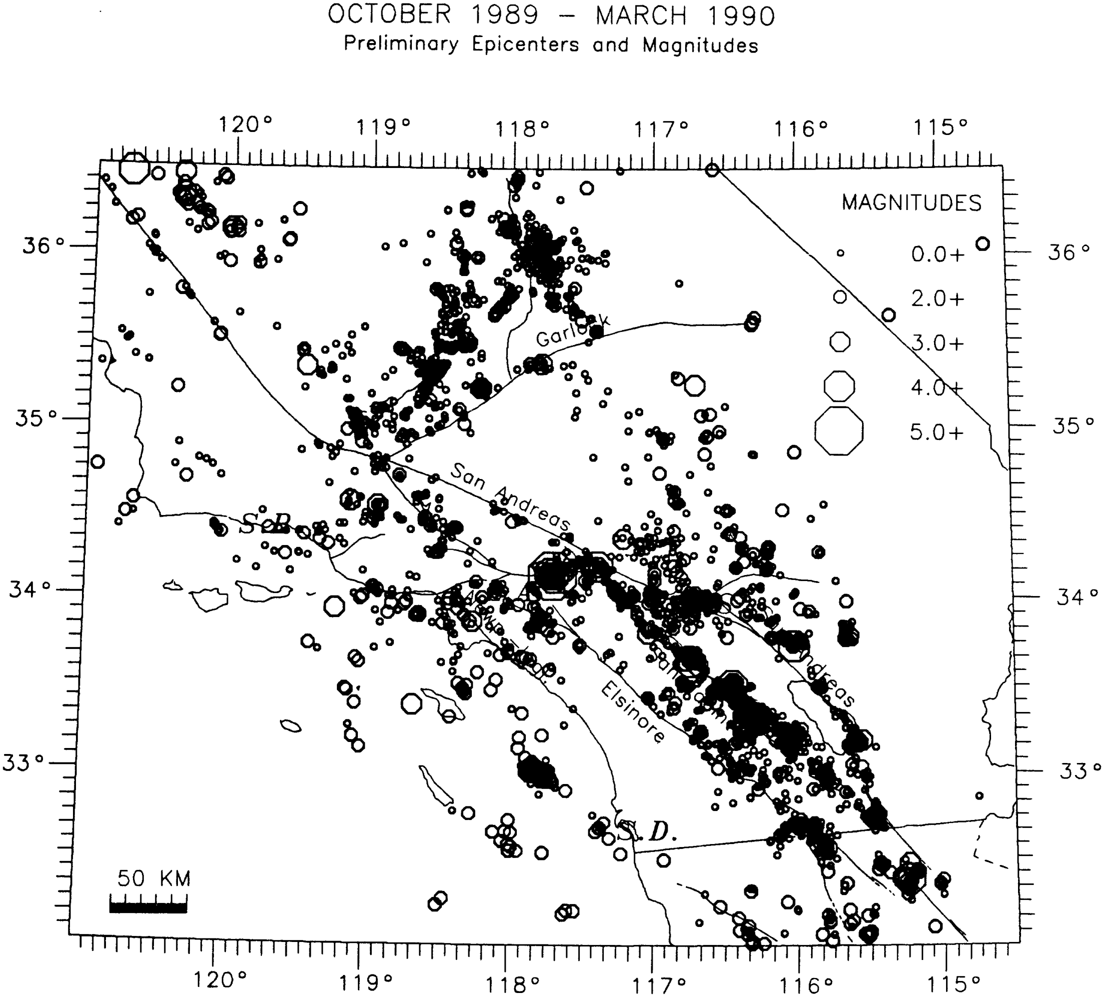

Figure 1. Map of epicenters of earthquakes in the southern California region, 1 October 1989 to 31 March 1990.

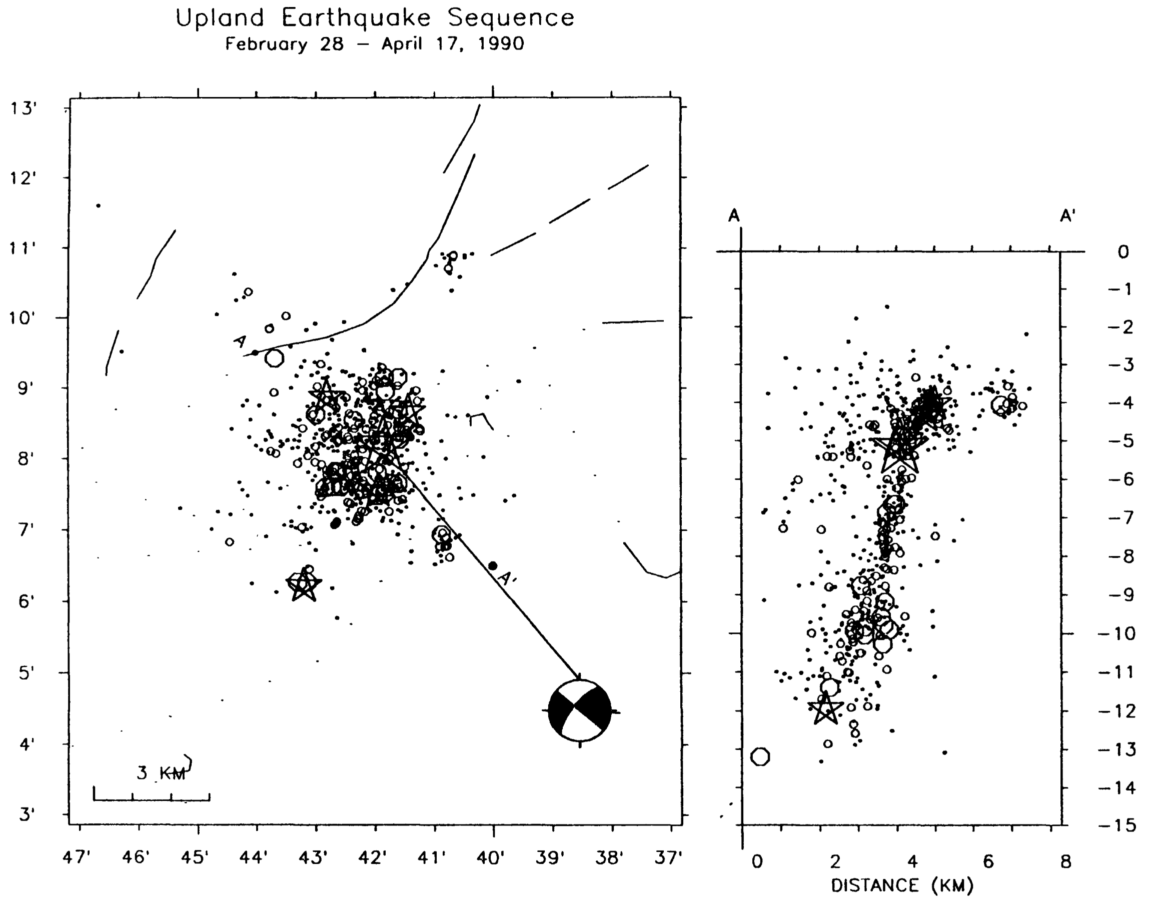

Figure 2. The 1990 Upland earthquake sequence. (Left) map showing epicenters of the mainshock (Star symbol) and aftershocks (open circles). (Right) north-northwest trending cross section (A-A') showing the depth distribution of the activity.

Regional Seismic Monitoring Along The Wasatch Front Urban Corridor And Adjacent Intermountain Seismic Belt

14-08-0001-A0621

W. J. Arabasz, R.B. Smith, J.C. Pechmann, and S. J. Nava
Department of Geology and Geophysics
University of Utah
Salt Lake City, Utah 84112
(801) 581-6274

Investigations

This cooperative agreement supports "network operations" associated with the University of Utah's 80-station regional seismic telemetry network. USGS support focuses on the seismically hazardous Wasatch Front urban corridor of north-central Utah, but also encompasses neighboring areas of the Intermountain seismic belt. Primary products for this USGS support are quarterly earthquake catalogs and a semi-annual data submission, in magnetic-tape form, to the USGS Data Archive.

During the report period, significant efforts were made in: (1) refinement of procedures for *in situ* calibration of remote telemetry stations; (2) implementation of various steps for redundancy in earthquake surveillance and response, including expansion of the channel capacity of our USGS-supplied real-time picker to 64 channels, use of a color-display terminal for rapid visual display of epicenters, and development of software for use with a battery-powered laptop computer for backup earthquake-location capability; and (3) pursuit of a major initiative to the Utah state legislature for modernizing seismic-network instrumentation in Utah as part of a state-federal partnership.

Results

Network Seismicity: October 1, 1989 - March 31, 1990

Figure 1 shows the epicenters of 246 earthquakes ($M_L \leq 3.6$) located in part of the University of Utah study area designated the "Utah region" (lat. 36.75°-42.5°N, long. 108.75°-114.25°W) during the six-month period October 1, 1989 to March 31, 1990. The seismicity sample includes four shocks of magnitude 3.0 or greater and three felt earthquakes.

The largest earthquake during the six-month report period was a shock of $M_L 3.6$ on January 24, 1990 (09:03 UTC), located 10 km north of the Great Salt Lake. This earthquake occurred in the same general area as the 1934 magnitude 6.6 Hansel Valley earthquake, one of the largest earthquakes that has occurred in Utah since settlement. During the report period, 21 additional shocks occurred in the same vicinity.

Seismic activity continued to occur in the Blue Springs Hills area of north-central Utah (clustered epicenters 45 km west of Logan), the location of an M_L 4.8 earthquake on July 3, 1989. Forty-two earthquakes were located from October 1, 1989 - March 31, 1990 in the area of the July 1989 Blue Springs Hills main shock.

Earthquakes greater than magnitude 3.0 that occurred from April 1, 1989 through September 30, 1989, are identified in Figure 1. Felt earthquakes in Utah of magnitude 3.0 or larger during the report period include an M_L3.1 event on February 5 at 10:23 UTC, felt in three small central Utah towns.

Reports and Publications

Arabasz, W. J., ed., Earthquake Instrumentation for Utah, Report and Recommendations of the Utah Policy Panel on Earthquake Instrumentation, *Utah Geological and Mineral Survey Open File Rept. 168*, 172pp., 1990.

Arabasz, W. J. and G. Atwood, Seismic Instrumentation—A Five-Element, $3M State Initiative for Utah's Earthquake Program, *Seismol. Res. Let.*, v. 61, no. 1, p.37, 1990.

Nava, S. J., Utah earthquake activity, April through June, 1989, *Survey Notes (Utah Geological and Mineral Survey)*, v. 23, no. 3, p. 14, 1989.

Nava, S. J., Utah earthquake activity, January through March, 1989, *Wasatch Front Forum (Utah Geological and Mineral Survey)*, v. 5, no. 3, p. 7, 1989.

Nava, S. J., Utah earthquake activity, April through June, 1989, *Wasatch Front Forum (Utah Geological and Mineral Survey)*, v. 5, no. 4, p. 12, 1989.

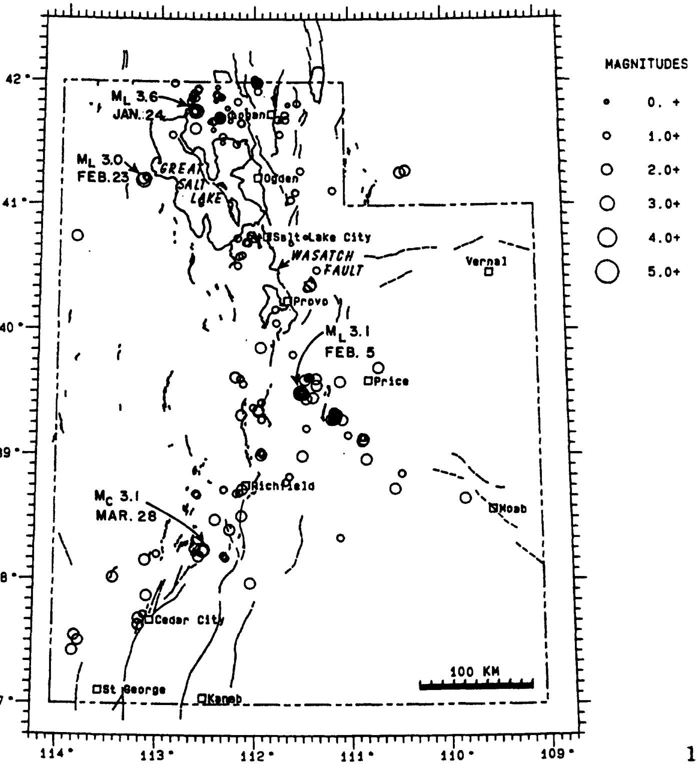

Figure 1. Earthquake Activity in the Utah Region, October 1, 1989, through March 31, 1990.

1. Regional Seismic Monitoring in Western Washington
and
2. Seismic Monitoring of Volcanic and Subduction Processes in Washington and Oregon

1. 14-08-0001-A0622
2. 14-08-0001-A0623

R.S. Crosson
S.D. Malone
A.I. Qamar
R.S. Ludwin
Geophysics Program
University of Washington
Seattle, WA 98195

(206) 543-8020

Investigations

Operation of the Washington Regional Seismograph Network (WRSN) and routine preliminary analysis of earthquakes in Washington and Northern Oregon are carried out under these contracts. Quarterly bulletins which provide operational details and descriptions of seismic activity in Washington and Northern Oregon are available from 1984 through the first quarter of 1990. Final catalogs are available from 1970, when the network began operation, though 1986. The University of Washington operates approximately 80 stations west of 120.5°W, 28 of which are supported under A0622, and 40 under A0623. This report includes a brief summary of significant seismic activity. Additional details are included in our Quarterly bulletins.

Excluding blasts, probable blasts, and earthquakes outside the U. W. network, 973 earthquakes west of 120.5°W were located between October 1, 1989 and March 31, 1990. Of these, 618 were located near Mount St. Helens, which has not erupted since October of 1986. This represents a significant increase over the previous six month period (319 events). Seven earthquakes were reported felt in western Washington during the period covered by this report. East of 120.5°W, 65 earthquakes were located, none felt.

The most notable earthquake during this reporting period was a M_L 5.1 earthquake on December 24 in the southern Washington Cascade Range near Storm King Mountain, about 30 km southwest of Mount Rainier. Although earthquakes of magnitude 5 and greater occasionally occur in the southern Washington Cascade Range, this event was somewhat unusual. In the first month after the earthquake, only 12 aftershocks were locatable, all smaller than M_C 1.5. Other events in southwestern Washington of similar magnitude (Siouxon Peak, 1961; Elk Lake, 1981, Goat Rocks, 1981) were followed by hundreds of aftershocks, including aftershocks of magnitude 3.0 and larger. This event occurred in an area where very little seismicity has been detected since the WRSN was installed, while the other magnitude 5 events were in areas with recurring seismic activity. Finally, the earthquake focal mechanism (dominantly strike-slip; with the sense of motion being either left-lateral slip on a north-south striking plane or right-lateral slip on an east-west striking plane) is markedly different from focal mechanisms for other earthquakes larger than magnitude 5 in the southern Cascade Range of Washington, which show right-lateral strike-slip on northerly-striking fault planes. Craig S. Weaver (USGS), Rick Benson (UW), John Nabelek (OSU), and William D. Stanley (USGS) are preparing a paper for JGR on this event.

In October, we recorded the greatest number of earthquakes at Mt. St. Helens since its last eruption in 1986. Since October, when 211 earthquakes were located in the vicinity of the mountain, the number of earthquakes per month has varied from 49 to 128. The largest earthquake in October was M_C 2.3, and in the entire six months only three were larger than M_C 2.5, (the largest was M_C 2.7). Thus, the rate of moment release was not significantly elevated. Depths of these earthquakes varied from the surface to 8 km and suggest stress changes within the volcanic conduit. Ash emissions occurred on December 8 1989 and January 6 1990. The last such emissions were in 1986. The December emission was accompanied by a five-hour period of elevated seismicity, and the January emission by two hours of elevated seismicity. Each emission began abruptly with the largest earthquake of the emission sequence (magnitudes ~ 2.7).

Swarms of small earthquakes at approximate depths of 4-5 km under Mount Hood were recorded on helicorder records on February 16 (30 events) and 20 (28 events). Although none were larger than magnitude 1.3, six were recorded by our digital recording system.

Publications

Barker, S.E. and S.D. Malone, 1990 (submitted), Magmatic system geometry at Mount St. Helens modeled from the stress field associated with post-eruptive earthquakes, JGR.

Ludwin, R. S., S.D. Malone, R.S. Crosson, A.I. Qamar, 1990 (in press), Washington Earthquakes 1985, in U.S. Earthquakes, National Earthquake Information Service.

Ludwin, R. S., S.D. Malone, R.S. Crosson, A.I. Qamar, 1990 (in press), Washington Earthquakes 1986, in U.S. Earthquakes, National Earthquake Information Service.

Ludwin, R. S., S.D. Malone, R.S. Crosson, A.I. Qamar, 1990 (in press), Washington Earthquakes 1987, in U.S. Earthquakes, National Earthquake Information Service.

Ludwin, R. S., C.S. Weaver, and R.S. Crosson, 1990 (in press), Seismicity of Washington and Oregon, in: Slemmons, D.B., E.R. Engdahl, D. Blackwell and D. Schwartz, editors, Decade of North American Geology associated volume CSMV-1; Neotectonics of North America.

Neri, G. and S.D. Malone, 1990 (in press), An analysis of the earthquake time series at Mt. St. Helens, Washington, in the framework of recent volcanic activity, Jour. Volcan. Geother. Res.

Thompson, K.I., 1990 (in preparation), Seismicity of Mt. Rainier - a detailed study of events to the west of the mountain and their tectonic significance, BSSA.

Univ. of Wash. Geophysics Program, 1989, Quarterly Network Report 89-C on Seismicity of Washington and Northern Oregon

Univ. of Wash. Geophysics Program, 1990, Quarterly Network Report 89-D on Seismicity of Washington and Northern Oregon

Univ. of Wash. Geophysics Program, 1990 (in preparation), Quarterly Network Report 90-A on Seismicity of Washington and Northern Oregon

Abstracts

Jonientz-Trisler, C., C. Driedger, and A. Qamar, 1989 (in press), Seismic signatures of debris flows on Mt. Rainier, WA, EOS, Fall 1989 PNAGU.

Jonientz-Trisler, C., and A. Qamar, 1989, Debris flow seismograms from Mt. Rainier and Mt. Adams, EOS, V. 70, p. 1190.

Miyamachi, H., and S.D. Malone, 1989, Relocation of earthquakes at Mount St. Helens using a three-dimensional velocity model, EOS, V. 70, p. 1195.

Semi-Annual Technical Summary (April, 1990)

Seismological Data Processing Project (#9930-03354)

John R. Evans, Greg Allen, Moses Smith
U.S. Geological Survey
Branch of Seismology
345 Middlefield Road, MS-977
Menlo Park, California 94025
415-329-4753

This Project provides UNIX computer support to the Branch of Seismology. "Investigations, results and reports" *per se* are not part of our duties. We supply network management, system management, installation, backups, maintenance, and trouble shooting to Branch UNIX computers, including other Projects' workstations. We also supply and maintain a number of peripherals for Branch use (9-track tape, optical disk, ExaByte tape, Ethernet backbone, laser printers, etc.).

During the first six months of FY90 we provided the following services for the Branch:

- Purchased and installed a Sparcstation I for monitoring the Real Time Picker. Maintained RTP data system buffer service to Branch UNIX and VAX computers.
- Upgraded Branch Administrative Office PC's and largely completed their PC network. Installed file server, printer, networked data base, and travel manager for this net. This was the lead project in Admin-PC networks for the Division in Menlo Park; it is the model by which others will be built.
- Installed workstations for two Projects; installed three system disks and one other disk on other Projects' workstations.
- Purchased and installed a large disk for "andreas", roughly doubling available disk space on this server. /we is much larger and scratch space will be available for general use soon.
- Installed erasable optical disk for Alaska Project. Purchased and installed erasable optical disk for "andreas", providing 270 MB formatted on each side of each removable disk. The "andreas" disk is available to all users and will serve mainly as high-speed random-access archive space for any user purchasing a blank disk ($200). It is the appropriate repository for digital seismograms and other voluminous data.
- Purchased and installed an ExaByte tape drive for "andreas" for doing disk backups of "andreas" and Branch workstations.
- Purchased and managed a software-maintenance contract for the Sun workstations, and a "parts and labor" hardware-maintenance contract for the Sun workstations. About $2500 of the allocated $10,000 has been spent so far on just two repairs—the Suns are finally getting old. Arranged and managed various repairs for "isunix".
- Paid for Branch portion of the ISD contract for doing backups of the Office VAX.
- Purchased and installed miscellaneous parts and components for maintaining and extending Ethernet, and miscellaneous supplies for laser printers and other peripherals.
- Extended Ethernet trunk in Building 7 to service north hallway, and added more cable in Building 8.
- Installed X Windows and Mathematica on "andreas"; obtained "ptroff" software to run on "andreas".
- Work on InterNet mailers and name servers is continuing. Solved uncounted hardware and software problems throughout the Branch network.

We have continuing problems with short staffing. The Project has fewer full-time people than a few years ago, yet we are now supporting Ethernet, many more computers, more software, and a much larger disk farm than before. The strain of reduced purchasing power, hiring restrictions, and uncompetitive salaries are affecting us at least as seriously as other Projects, particularly since we are competing directly with Si Valley. We hope users will recognize that resources are finite, seriously strained, and breakable and appreciate that our level of service is high in spite of these obstacles.

Northern and Central California Seismic Network Processing

9930-01160

Fredrick W. Lester
Branch of Seismology
U.S. Geological Survey
345 Middlefield, MS 977
Menlo Park, CA 94025
(415) 329-4747

Investigations

1. In 1966 a seismographic network was established by the USGS to monitor earthquakes in central California. In the following years the network was expanded to monitor earthquakes in most of northern and central California, particularly along the San Andreas Fault, from the Oregon border to Santa Maria. In its present configuration there are over 500 single and multiple component stations in the network. The primary responsibility of this project is to monitor, process, analyze, and publish data recorded from this network.

2. This project continues to maintain the primary seismic data base for the years 1969 to the present on both computers and magnetic tapes for those interested in doing research using the network data. As soon as older data are complete and final the preliminary data base is updated with the final phases and locations.

3. Lately video has become increasingly useful in documenting research activities being conducted by the USGS, especially activities related to the Parkfield Prediction Experiment. In addition, computer animation of geophysical data sets have allowed researchers to study the data in time series and in 3-dimensions. The two technologies work well in communicating the research being done here to a wide audience that includes other geoscientists as well as untrained but interested laymen who are able to understand the material when it is presented in a visually appealing way.

4. As time permits some research projects are underway on some of the more interesting or unusual events or sequences of earthquakes that have occurred within the network.

Results

1. Figure 1 illustrates 13252 earthquakes located in northern and central California and vicinity during the time period October 1989 through March 1990. This level of seismicity is higher than normal for a six month period. The increase is due primarily to the most important earthquake sequence in California in many years, the Loma Prieta earthquake and it's aftershocks. That earthquake occurred on October 17, 1989 in the Santa Cruz Mountains, approximately 16 kilometers northeast of Santa Cruz. Currently we have located more than 6000 aftershocks and they are continuing at a rate of about 5 per day of all magnitudes. The largest aftershocks recorded include a magnitude 5.2 aftershock 37 minutes after the mainshock and a magnitude 5.0 aftershock on October 19. The aftershocks are occurring in a 55 kilometer long zone from south of Los Gatos at the north end to east of Watsonville at the south end (Figure 1)

   Some of the overall increase in rate of seismicity is also due to an increase in two areas of

Long Valley caldera. Two prominent clusters of activity continue to persist. Those are under Mammoth Mountain, near the southeast corner of the caldera, and near Casa Diablo Hot Springs in the south-central portion of the caldera. These areas are of concern because of their possible relationship to subsurface magma movement in or near the caldera.

Seismic data recorded by the network are being processed using the CUSP (Caltech USGS Seismic Processing) system. CUSP was designed by Carl Johnson in the early 1980's and has since undergone some revisions for the Menlo Park operation. On September 1, 1989 we began using revised CUSP software in a generic format. This new format will make CUSP more universally acceptable to groups that are using or plan to use it in the future because the commands are relatively non-specific to any particular group operation.

In the future we plan to begin publishing, probably on a monthly basis, a preliminary catalog of earthquakes for northern and central California. The format is not yet established but it will probably be some type of listing of events accompanied by a text explaining the processing and what is in the catalog, and a map showing the epicenters. The catalog will be approximately complete at the magnitude 1.5 in the central core of the network and something approaching M2.0 in the more remote portions of the net.

2. The current catalog is relatively complete and correct through December 1989. The data from January 1990 are complete but some work remains to make corrections on some problem events and identify the quarries that have been located. Data from February and March 1990 are still incomplete and some errors still remain to be identified and corrected.

3. Steve Walter has co-produced an Open File Video Report (OFR 89-669) that consists of Computer animations of aftershocks of the Loma Prieta Earthquake. The animations are recorded on videotape and accompanied by both narration and musical sound track. The video runs 22 minutes in length. It has been favorably received at AGU poster sessions and has been recorded by the BBC, NOVA, and National Geographic produceers, among others, for possible inclusion in special programs on the Loma Prieta earthquake.

4. Steve Walter has been investigating the seismicity in the Medicine Lake region following a magnitude 4.0 earthquake occurred in that area on September 30, 1988 followed by many aftershocks. The seismicity has subsided to a very low level at the present time but there has been renewed interest in this region because of this activity and it's possible relationship to associated volcanic activity. Steve is currently co-authoring a paper in progress that will describe the historical seismicity and crustal deformation in the Medicine Lake region.

Reports

Klein, F.W., and Walter, S.R., 1989, Aftershocks of the Loma Prieta earthquake: Computer animations, U.S.G.S. Open-File Report 89-669 (video).

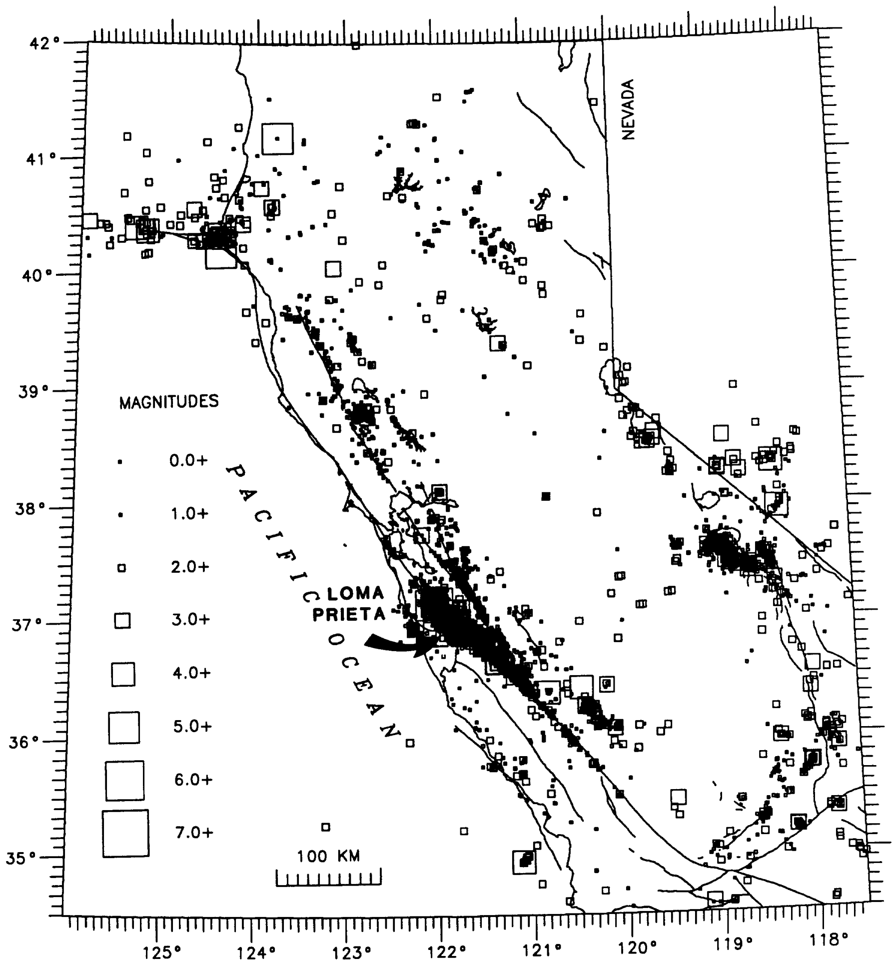

FIGURE 1. Seismicity for northern and central California and vicinity during October 1989 - March 1990

Central California Network Operations

9930-01891

Wes Hall
Branch of Seismology
U.S Geological Survey
345 Middlefield Road-Mail Stop 977
Menlo Park, California 94025
(415)329-4730

Investigations

Maintenance and recording of 345 seismograph stations (446 components) located in Northern and Central California. Also recording 68 components from other agencies. The area covered is from the Oregon border south to Santa Maria.

Results

1. Bench Maintenance Repair	
A. seismic VCO units	102
B. summing amplifier	15
C. seismic test units	2
D. VO2H/JO2L VCO Units	40
E. FBA VCO Units	2
F. DC-DC converters	16
2. Production/Fabrication	
A. J512A VCO units	9
B. J512B VCO units	24
C. dc-dc converter/regulators	10
D. lightning protectors	24
E. V02H / V02L VCO units	6
3. Modifications	
summing amplifiers	26
4. Discriminator Tuning	
J120	27

5. Increased clamping circuit tlme constants of all J120 discriminators. (419ea)

6. Equipment Shipped
   - A. 7ea, J120 discriminators to Cal Tech
   - B. 1ea, J512B (dual) VCO to Cal Tech
   - C. 2ea, J512A VCO's to Cal Tech

7. New seismic stations: CMKI, CMKJ, CMKK, (Monumont Peak FBA's)
   JLPI, JLPJ, JLPK, JLPF, JLPZ (Loma Prieta)
   JNAF, JNAZ (New Almaden Mine)
   JUMF, JUMZ (Mt. Umunhum)
   HER (Elkorn Road)
   JEL (Ellicot)
   HFMI, HFMJ, HFMK (Fremont Peak FBA's)

8. Stations deleted: 4-W circuit from California Divison of Mines & Geology;
   PPR (Paso Robles)

9. Install alarm experiment with stations JNA, JUM in telemetry center. Signal transmitted to Cypress Structure in Oakland CA.

10. Connected additional 64 channel input to Willie Lee's portable IBM based monitor.

11. Moved location of Bell & Howell tape decks and removed most non-plenum cables from ceiling area.

12. Completed computer plotsof Northern & Central California telemetry system showing radio, telephone line and microwave paths.

Central Aleutians Islands Seismic Network

Agreement No. 14-08-0001-A0259

Carl Kisslinger, Sharon Kubichek, and Robin Wright
Cooperative Institute for Research in Environmental Sciences
Campus Box 216, University of Colorado
Boulder, Colorado 80309

(303) 492-6089

Brief Description of Instrumentation and Data Reduction Methods

The Adak seismic network consists of 13 high-gain, high-frequency, two-component seismic stations and one six-component station (ADK) located at the Adak Naval Base. Station ADK has been in operation since the mid-1960s; nine of the additional stations were installed in 1974, three in 1975, and one each in 1976 and 1977.

Data from the stations are FM-telemetered to receiving sites near the Naval Base, and are then transferred by cable to the Observatory on the Base. Data were originally recorded by Develocorder on 16 mm film; since 1980 the film recordings are back-up and the primary form of data recording has been on analog magnetic tape. The tapes are mailed to CIRES once a week.

At CIRES, the analog tapes are played back into a computer at four-times the speed at which they were recorded. This computer then digitizes the data, automatically detects events, demultiplexes each event, and writes them to disk. These events are edited to eliminate spurious triggers, and a tape containing only seismic events is created. All subsequent processing is done from this tape. Times of arrival and wave amplitudes are read from an interactive graphics display terminal. The earthquakes are located using a program originally developed for this project by E. R. Engdahl, which has been modified several times since.

Data Annotations

A minor maintenance trip was conducted during the end of January through early February 1990, in Boulder, CO. The Boulder site had not been visited since 1988 so many adjustments and recalibrations were necessary. One of the major improvements was the replacement of the data cable between the tape playback system and the digitizing unit resulting in a significant reduction of noise levels in the digitized data. A remote control unit was also installed offering improved tape handling and control. The 1989 minor maintenance trip to Adak was not conducted since that money was needed to purchase batteries for the remote stations due to funding changes. At present, the only major unit not working on Adak is the satellite link with the GOES time clock. The next major maintenance trip (summer 1990) will address this problem and routine maintenance issues. Three stations are down as a result of a lightning strike at the end of the 1988 summer maintenance trip.

Current Observations

Since August 1989, we have been digitizing and locating all of our data on a SUN workstation with a Cutler Digital Design analog to digital converter (a-to-d). In January 1990, this workstation was upgraded to a SUN 3/60 level CPU with 8 megabytes of internal memory (RAM). This has helped with our system hang problems, however, we still have a system hang an average of twice per day when digitizing. Discussion with SUN hardware personnel revealed that this level of workstation can adequately support no more than three peripherals on the SCSI bus. With our disk drives, cartridge tape unit, and the a-to-d, we have 4 peripherals on the SCSI bus. SUN personnel expressed some surprise that we were functioning at all with this load. This situation cannot be improved without purchase of a second workstation for which we do not have funding. As a result of this problem, we are about 3 months behind in digitizing data and 6 months behind in locating data. We are continuing to erase analog data tapes with good film backup before they are digitized in order to maintain the data tape supply to Adak.

The location work has proceeded well despite delays; 84 earthquakes were located during January 1 - 8 and February 1 - 8, 1987; and 158 earthquakes were located during July and August 1989. An additional 73 select earthquakes were located during the period of March 21 through July 29, 1987 for a special study of a large intermediate depth swarm. The grand total of events located for all time periods is 315, about half the rate prior to 1989 due to complications with the digitizing process.

Epicenters of *all* the located events for 1987 and 1990 are shown in Figures 1a and 1b and vertical cross-sections are given in Figures 2a and 2b.

Sixteen of the events located with data from the Adak network for 1987 were large enough to be located teleseismically (U.S.G.S. PDEs). A number of other teleseismically located aftershocks within the network region are difficult for us to locate due to their arrivals being masked by the codas of other aftershocks. Also, 3 of the events located with data from the Adak network in 1989 were large enough to be located teleseismically (U.S.G.S. PDEs). Due to the large number of aftershocks of the May 7, 1986 main event, a decision was made not to locate earthquakes with duration magnitudes (M_d) of less than 2.3 for 1986 and 1987. However, *all* events are being located for 1988 and 1989.

More detailed information about the network status and a catalog of the hypocenters determined for the time period reported are included in our Semi-Annual Data Report to the U.S.G.S. Recent research using these data is reported in the Technical Summary for U.S.G.S. Grant No. G1368.

Recent Seismic Activity

On March 12, 1990 at 14:41:23 UTC, a M_b 6.3 earthquake occurred at 51.632N and 174.851W. It was followed by almost 100 aftershocks over the next four days. Due to the proximity of this event to the epicenter of the May 7, 1986 major event (M_s 7.7), we have jumped ahead and begun locating the aftershocks.

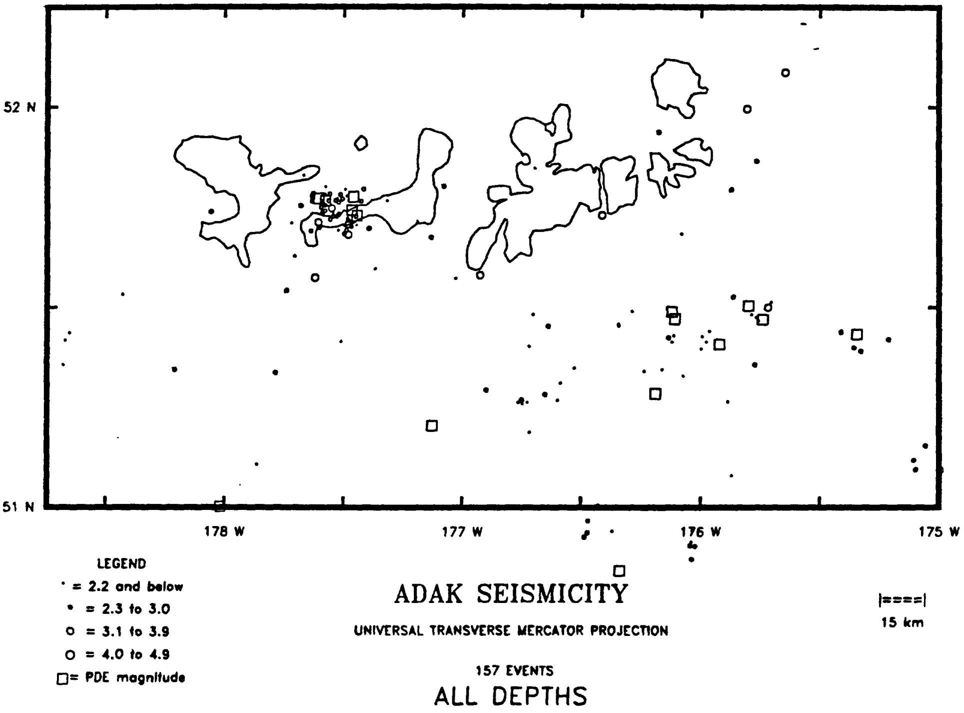

Figure 1a: Map of seismicity located during January and February 1 - 8, 1987 and a sampling of select events between March 21 and July 29, 1987. All epicenters were determined from Adak network data. Events marked with squares are those for which a teleseismic body-wave magnitude has been determined by the U.S.G.S.; all other events are shown by symbols which indicate the duration magnitude determined from Adak network data. The islands mapped (from Tanaga on the west to Great Sitkin on the east) indicate the geographic extent of the Adak seismic network. The cluster of events in the Kanaga Pass region (51.7° N, 177.5° W) is the result of a special study of an intermediate depth mainshock-aftershock sequence beginning on March 21, 1987.

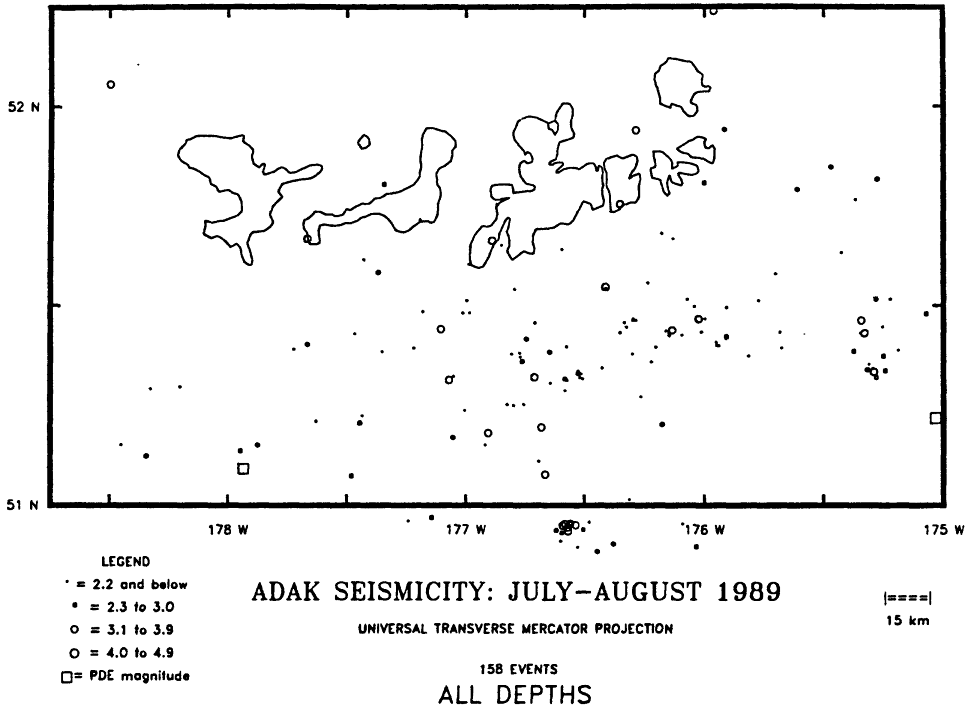

Figure 1b: Map of seismicity which occurred July and August, 1989. Symbols as in Figure 1a.

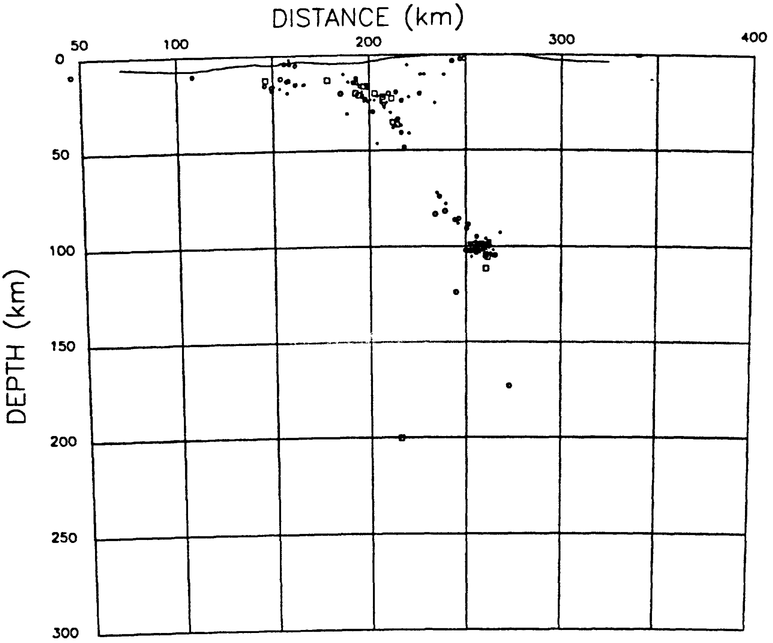

ADAK SEISMICITY

Figure 2a: Vertical cross section of seismicity located during January and February 1 - 8, 1987 and a sampling of select events between March 21 and July 29, 1987. Events are projected according to their depth (corresponding roughly to vertical on the plot) and distance from the pole of the Aleutian volcanic line. The zero-point for the distance scale marked on the horizontal axis of the plot is arbitrary. Events marked with squares are those for which a teleseismic body-wave magnitude has been determined by the U.S.G.S.; all other events are shown by symbols which indicate the duration magnitude determined from Adak network data. The irregular curve near the top of the section is bathymetry. The cluster of events in the Kanaga Pass region (distance: 250 km; depth: 100 km) is the result of a special study of an intermediate depth mainshock-aftershock sequence beginning on March 21, 1987.

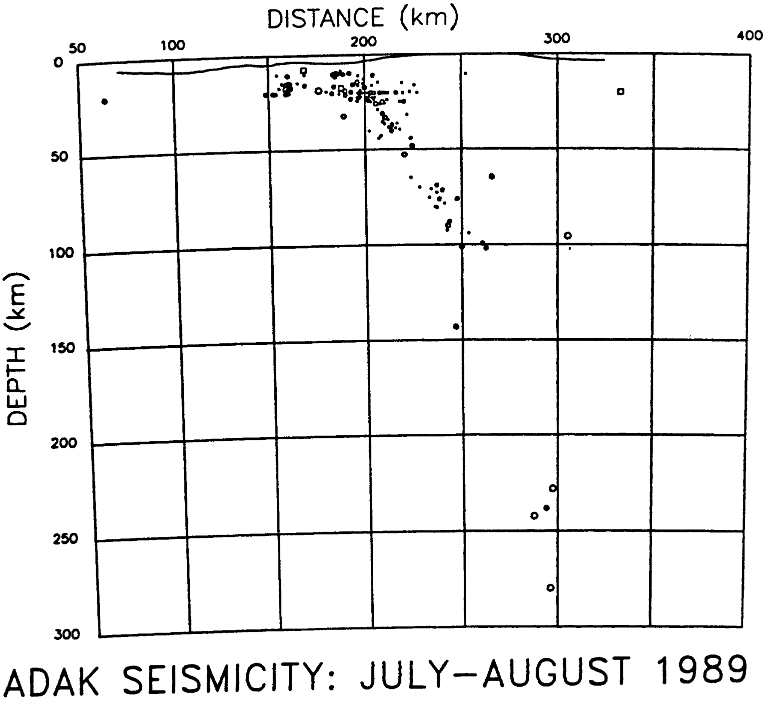

Figure 2b: Vertical cross section of seismicity which occurred July and August, 1989. Projection and symbols as in Figure 2a.

Alaska Seismic Studies

9930-01162

John C. Lahr, Christopher D. Stephnes,
Robert A. Page, Kent A. Fogleman
Branch of Seismology
U. S. Geological Survey
345 Middelfield Road
Menlo Park, California 94025
(415) 329-4744

Investigations

1) Continued collection and analysis of data from the high-gain short-period seismograph network extending across southern Alaska from the volcanic arc west of Cook Inlet to Yakutat Bay, and inland across the Chugach Mountains. This region spans the Yakataga seismic gap, and special effort is made to monitor for changes in seismicity that might alter our assessment of the imminence of a gap-filling rupture.

2) Cooperated with the USGS Branch of Alaskan Geology, the Geophysical Institute of the University of Alaska (UAGI), and the Alaska Division of Geological and Geophysical Surveys in operating the Alaska Volcano Observatory (AVO). Under this program, our project monitors the seismicity of the active volcanoes flanking Cook Inlet and operates six- and an eight-station arrays of seismographs near Mt. Spurr and Mt. Redoubt, respectively.

3) Cooperated with the Branch of Engineering Seismology and Geology and UAGI in operating 16 strong-motion accelerographs in southern Alaska, including 11 between Icy Bay and Cordova in the area of the Yakataga seismic gap.

Results

1) Preliminary hypocenters determined using data from the regional network for the period July - December 1989 are shown in Figures 1 and 2. Other than an apparent decrease in the level of activity in an around the Yakataga seismic gap (probably a systematic effect due to an elevated magnitude threshold for completeness in this area), general features in the spatial distribution of hypocenters south of the Denali fault remain relatively unchanged compared to the previous six-month period. Notable shallow earthquakes that occurred within this time period include: 1) a magnitude 4.1 M_a (4.4 m_b) shock on July 16, located near latitude 61.5° N, longitude 149° W. This event is within the aftershock zone of the 1984 Sutton earthquake (Lahr and others, 1986), and is the largest shock to occur within this area since 1984. The focal mechanism of this earthquake is similar to that of the Sutton mainshock. 2) a crustal shock of magnitude 5.4 m_b on December 21 located about 50 km SSE of McGrath, between

the mapped traces of the Iditarod-Nixon Fork and Farewell faults (near latitude 62.4° N, longitude 155.6°W). This latter event is significant because crustal shocks of about magnitude 5 and larger have been rare in southern Alaska since the regional network was established in the early 1970's. However, because of the remote location of this event with respect to the regional network, the focal depth and focal mechanism determined from polarities of initial P-waves are poorly constrained. Only one aftershock, an event of magnitude 3.0 M_L, was located from the 24-hour period following the mainshock. The mainshock did not occur near any known or suspected Late Cenozoic faults (Plafker and Jacob, 1986).

2) In December 1989, after 23 years of quiescence, Redoubt volcano began erupting (Alaska Volcano Observatory Staff, 1990). A series of phreatomagmatic and ash-rich explosions that began on December 14 marked the initial vent-clearing phase of the eruption sequence. During the ensuing months, repeated episodes occurred in which dome growth from magma extrusion was culminated by major dome-destroying eruptions. Significant hazards from the eruptions that have occurred thus far include the production of airborn ash and ash deposits, pyroclastic and debris flows, and flooding.

Since prior to the first eruption on December 14, seismic data from the local seismograph array, and in particular the three new stations installed in March 1990 within 3 km of the summit, have proven critical for monitoring the evolution of the eruptive sequence and forecasting most of the major eruptions. One of the key observations that has been indicative of impending eruptions is an increase in the rate of occurrence and size of long-period seismic events (Koyanagi and others, 1987; Chouet, 1988, 1990) which are characterized by dominant frequencies of about 2-2.5 Hz and are thought to be caused by oscillations within pressurized, fluid- or vapor-filled cracks. The two largest eruptions, on December 14 and January 2, were preceded by intense swarms of LP's that began 1-3 days prior to the eruptions. The largest of these events could be easily observed at seismographs located up to 80 km from the summit of the volcano and contributed to marked increases in amplitudes on records from a system that monitors the average absolute amplitude of the seismic signals (RSAM; Murray and Endo, 1989). LP swarms that preceded later eruptions were generally comprised of much smaller events that could be observed clearly only at stations within about 3 km of the summit. Forecasting eruptions from these later episodes of premonitory LP activity was aided by the use of spectragrams (Figure 3) constructed from signals generated by the on-line seismic monitoring system (Rogers, 1989).

3. Upgrades under development for the PC-based seismic monitoring system include a new, more efficient data aquisition program with 128-channel capability (XDETECT, written by Dean Tottingham and modified by John Rogers), and the design and construction of a

printed-circuit board to multiplex 128-channel data (based on a design by Ellis, 1989). Also, a computer program was written to analyze automatic calibration signals detected from the remote field instruments and provide parameters that include the station identification, battery voltage, and amplifier and geophone response.

References

Chouet, Bernard, 1988, Resonance of a fluid-driven crack: Radiation properties and implications for the source of long-period events and harmonic tremor, J. Geophys. Res., v. 93., p. 4375-4400.

Chouet, Bernard, 1990, Seismic Model for the Source of Long-Period Events and Harmonic Tremor, Springer-Verlag, New York, (in press).

Ellis, J. O., 1989, Expanding the input multiplexer for the Data Translation, Inc. Model DT2821 analog-to-digital converter, U. S. Geological Survey Open-File Report 89-191 6 p.

Koyanagi, R. B, Bernard Chouet, and Kei Aki, 1987, Volcanic tremor in Hawaii. Part 1: Compliation of seismic data from the Hawaiian Volcano Observatory 1969-1985, U. S. Geological Survey Professional Paper 1350, p. 1221-1258.

Lahr, J. C., R. A. Page, C. D. Stephens and K. A. Fogleman, 1986, Sutton, Alaska, earthquake of 1984: Evidence for activity on the Talkeetna segment of the Castle Mountain fault system, Bull. Seismol. Soc. Amer., v. 76, p. 967-983.

Murray, T. L., and E. T. Endo, 1989, A real-time seismic amplitude measurement system (RSAM), U. S. Geological Survey Open-File Report 89-684, 26p.

Plafker, George, and K. H. Jacob, 1986, Seismic sources in Alaska, in Proceedings of Conference XXXI, A Workshop on Evaluation of regional and Urban Earthquake Hazards and Risk in Alaska, U. S. Geological Survey Open-File Report 86-79, p.76-82.

Rogers, J. A., 1989, Frequency-domain detection of signals using a DSP coprocessor board, IASPEI Software Library, v. 1, pp. 151-172, Seismological Society of America, El Cerrito, CA.

Reports

Alaska Volcano Observatory Staff, 1990, The 1989-1990 eruption of Redoubt volcano, EOS, Trans. Amer. Geophys. Union, v. 71, p. 265-275.

Alpha, T. R., J. C. Lahr, and R. A. Page, 1989, Oblique map of the north half of the Loma Prieta, California, earthquake rupture zone and environs, U. S. Geological Survey Open-File Report 89-633, map with discussion.

Alpha, T. R., J. C. Lahr, and L. F. Wagner, 1989, How to construct a paper model showing the motion that occurred on the San Andreas fault during the Loma Prieta, California, earthquake of October 17, 1989, U. S. Geological Survey Open-File Report 89-640, 9 p.

Page, R. A., George Plafker, J. N. Davies, and Hans Pulpan, 1989, Block rotation and seismicity in east-central Alaska, EOS, Trans. Amer. Geophys. Union, v. 70, p.1337.

Rogers, J. A., 1989, Frequency-domain detection of signals using a DSP coprocessor board, IASPEI Software Library, v. 1, pp. 151-172, Seismological Society of America, El Cerrito, CA.

Rogers, J. A., 1989, Data format conversion program for the PC and SUN computer, U. S. Geological Survey Open-File Report 89-662, 6 pp.

Stephens, C. D., R. A. Page, and J. C. Lahr,1990, Reflected and mode-converted sesimic waves within the shallow Aleutian subduction zone, southern Kenai Peninsula, Alaska, J. of Geophys. Res. (in press).

CENTRAL AND SOUTHERN ALASKA

July – December 1989; Depths shallower than 30 km

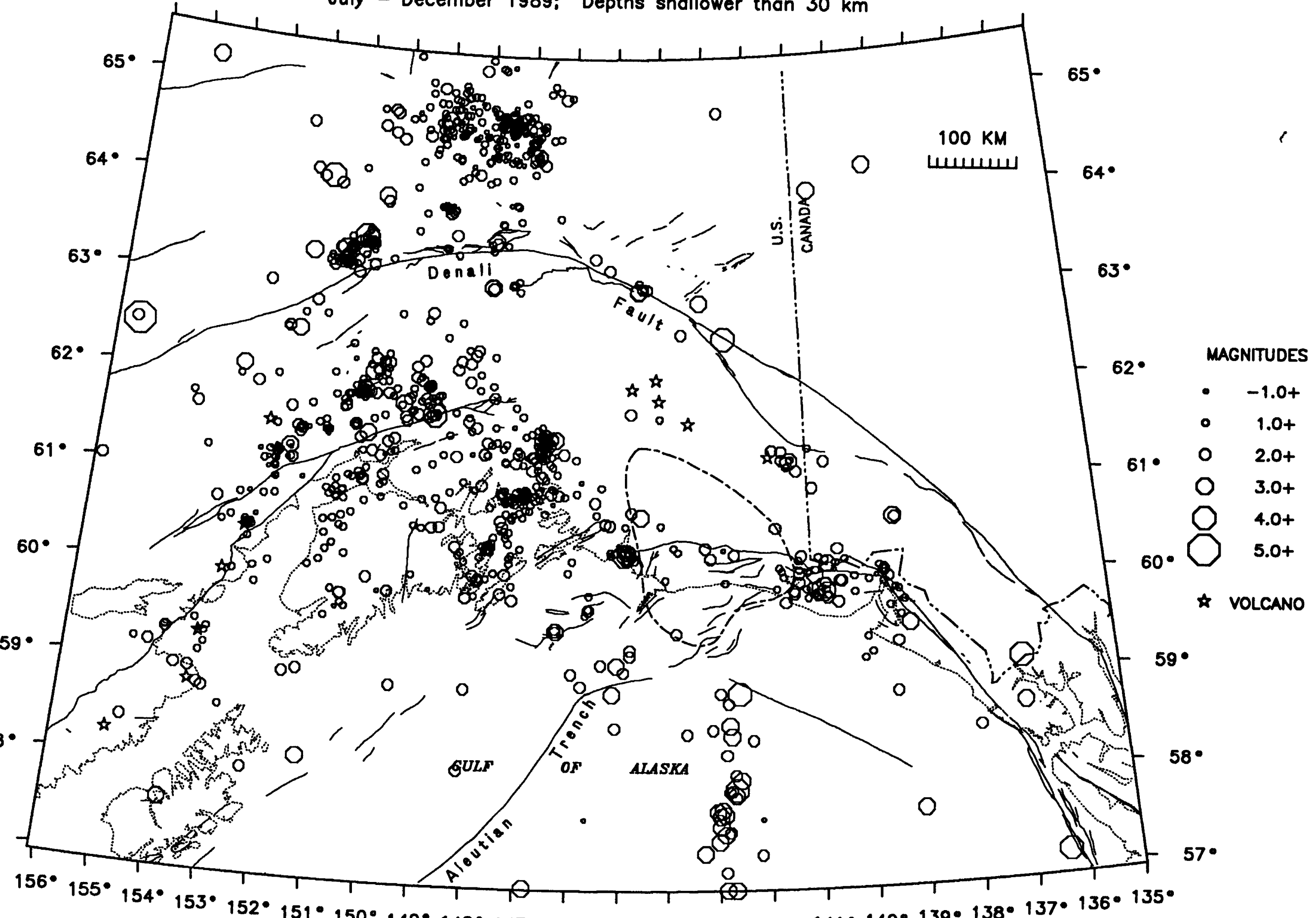

CENTRAL AND SOUTHERN ALASKA

July – December 1989; Depths equal to and below 30 km

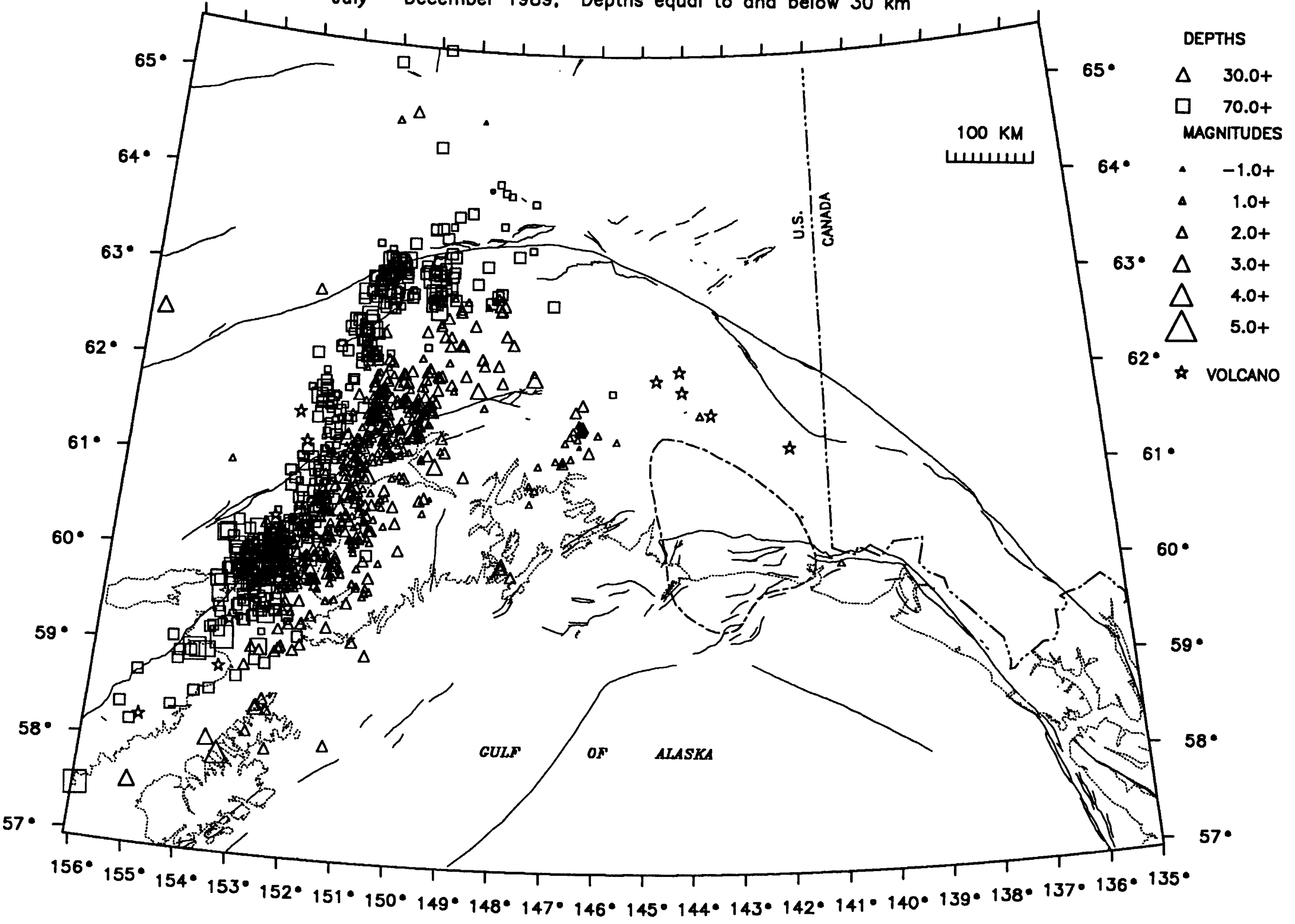

1—MIN FFT DATA

BAND:	0	1	2	3	4	5	6	7	8	9
BASE AMPLITUDE:	9	8	7	7	6	5	5	5	4	3

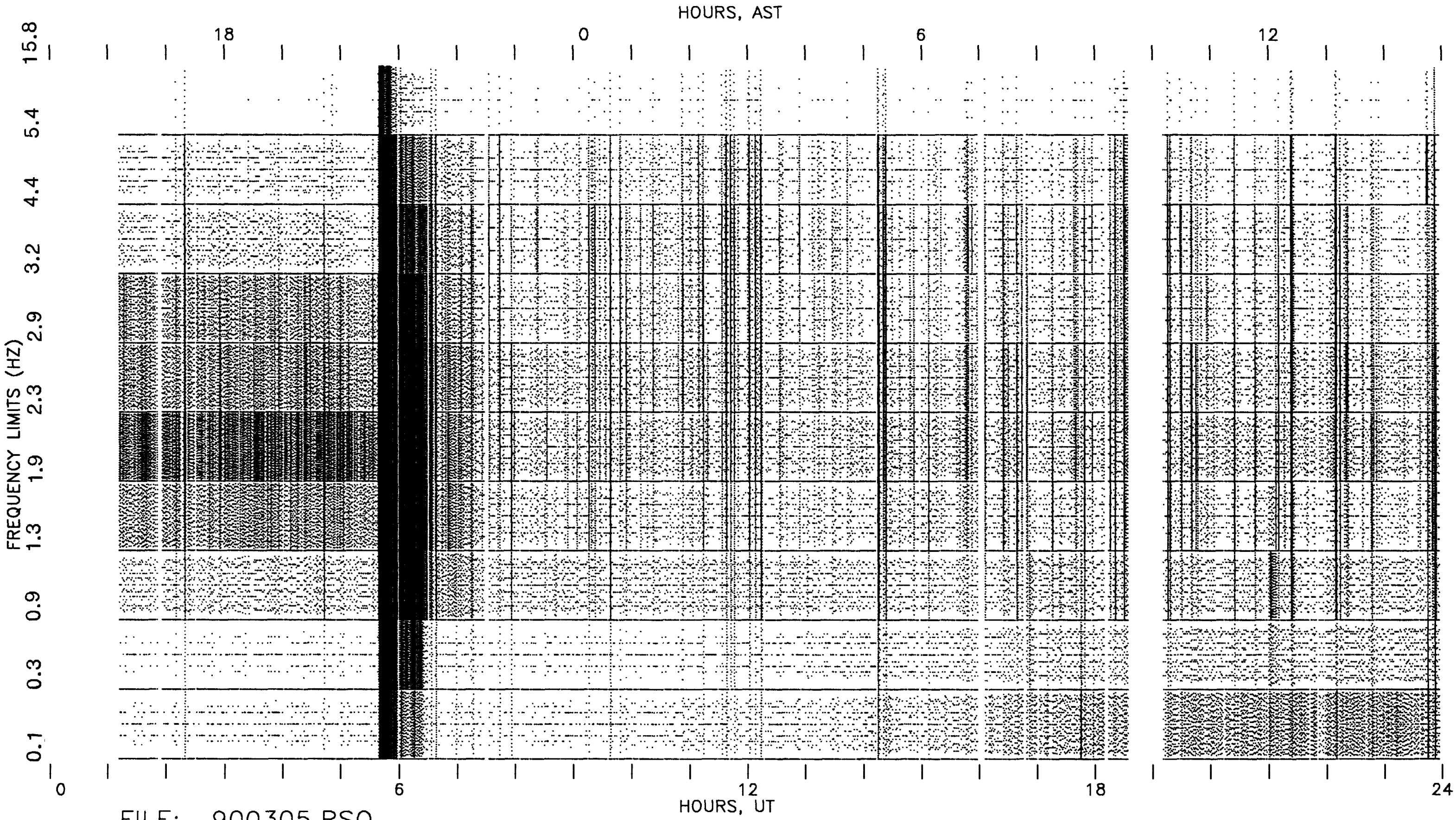

FILE: 900305.RSO

Figure captions

Figure 1. Epicenters of 1062 shallow earthquakes that occurred between July and December 1989 (processing for this time period is not yet completed). Magnitudes are determined from coda duration or maximum amplitude; the magnitude threshold for completeness varies across the network. Contour with alternating long and short dashes outlines inferred extent of Yakataga seismic gap. Neogene and younger faults (Plafker and Jacob, 1986) are shown as solid lines.

Figure 2. Epicenters of 1054 intermediate and deep shocks that occurred between July and December 1989. See Figure 1 for details about magnitudes and identificaton of map features.

Figure 3. Spectragram from the seismograph station RSO for March 5, 1990. RSO is located about 2.4 km south of the summit of Mt. Redoubt, and recording began this day only 4½ hours before an eruption at 05:39 UT. In each of ten spectral bands the average amplitude during successive minute intervals is plotted as a grey scale that darkens with increasing amplitude (a base amplitude, indicated at the top, is subtracted from each value before plotting). Note the strong signal peaked in the frequency range 2.0-2.5 Hz, the dominant frequencies observed for typical LP events, prior to the eruption.

Western Great Basin - Eastern Sierra Nevada Seismic Network

Cooperative Agreement 14-08-0001-A00
1 October 1989 - 31 March 1990

M.K. Savage and W.A. Peppin
Seismological Laboratory
University of Nevada
Reno, NV 89557
(702) 784-4315

Investigation

This contract supported continued operation of a seismic network in the western Great Basin of Nevada and eastern California, with the purpose of recording and locating earthquakes occurring in the western Great Basin, and acquiring a data base of phase times and analog and digital seismograms form these earthquakes. Research using the data base was performed under USGS contract 14-08-0001-G1524 and is reported elsewhere in this volume.

Results

During the time period 1 October 1989 to 31 March 1990 2,332 earthquakes were registered by the University of Nevada within the University of Nevada seismic network, which monitors the eastern Sierra Nevada - Western Great Basin area with special emphasis on the regions west of Reno, Nevada, within the Excelsior Mountains, and near Long Valley caldera (Figure 1). Of these, 34 were magnitude 3 and greater and two exceeded 4 in magnitude, the 15 January 1990 Fishlake Valley earthquake (Mc 4.53) and the 24 March 1990 Luning earthquake (Mc 4.51). Figure 2 shows a map of these events. Most of the earthquakes (1,659) are located near Long Valley caldera, showing a significant increase in overall seismicity near the caldera during the last six months, owing largely to the continuing swarm under Mammoth Mountain and the increased seismicity under the south moat of the caldera, site of the 1983 earthquake swarm. Although seismicity has been intense in the caldera, this statistic is misleading because of the very dense station coverage near this area.

Seismicity in the vicinity of the caldera is shown in Figure 3, and is dominated by four groups of events, numbered 1 through 4 in this figure. 1 is the ongoing swarm of earthquakes under Mammoth Mountain which started in May of 1989 and continues to this writing, and the earthquake swarm near the caldera south boundary. Activity under Mammoth Mountain has been gradually subsiding following the initiation of the south-moat activity (December 1989), but continues at this writing. Because of the reactivation of uplift (Dec 1989) and the close proximity of the two swarms to the town of Mammoth Lakes, this activity commands special attention and warrants careful monitoring. 2 is the seismicity in the mountain block south of the caldera, which appears to be the most consistent and steady source of earthquakes in this region. 3 are continuing aftershocks of the the November 1984 Round Valley earthquake, and 4 are continuing aftershocks of the 1986 Chalfant Valley sequence.

Catalogs covering the seismicity are shortly to be published for the time period up to 31 December 1989. The previous network computer system, consisting of a PDP11/70 and a PDP11/34 was replaced by the Microvax/CUSP system on 7 November 1989. The completion of a bulletin through 1989 will put, in a single place, all of the information taken from the PDP11/70 system. Every effort has been made to maintain consistent procedures in making the transfer to the CUSP system, so that the completeness of the catalog, the computation of magnitudes, and the location procedures will be comparable. However, researchers should note that some inconsistency is bound to creep in, and so use of UNR catalog data through 1989 must be made with caution. Before 7 November 1989 all of the catalog locations were obtained from the PDP11/70 system; after 1 January 1990 all come from the CUSP system; for the two months November and December 1989 the catalog contains a mix of events. Because of considerable computer down time in December 1989, quite a bit of data was lost. We are now working on merging data with the USGS CUSP system in Menlo Park to recover this lost data, and plan to include this in our bulletin as well.

With the onset of the CUSP system, the network data stream now includes calibrated digital waveforms from nine wideband (0.05 to 20 Hz) three-component digital stations located around this region (Figure 1). Therefore, the MEM/GRM file pairs after 7 November 1989 also contain this information together with the uncalibrated vertical waveforms used for earthquake timing. Also operating on the Microvax system is an Exabyte data logger, which continuously records the incoming digital data on tape, and is being kept as an ongoing data library, providing access to data for distant teleseisms and large events. Calibration pulses for the digital stations (not complete at this writing) are found on the UNR Microvax system in ROOT$DUA0:[CALPULSES]. The UNR computer can be reached either by 1200-baud remote modem (numbers 702-784-1592 or 702-784-4270): please call Bill Peppin at 702-784-4975 for information how to log onto the computer (KERMIT is available). The microvax cluster can also be accessed through the TELNET addresses 134.197.33.248 and 134.197.33.249 and supports TCP/IP communications through the FTP file transfer package from Wollongong and Associates.

Figure 1

UNR Seismic Stations (Digitals Named)

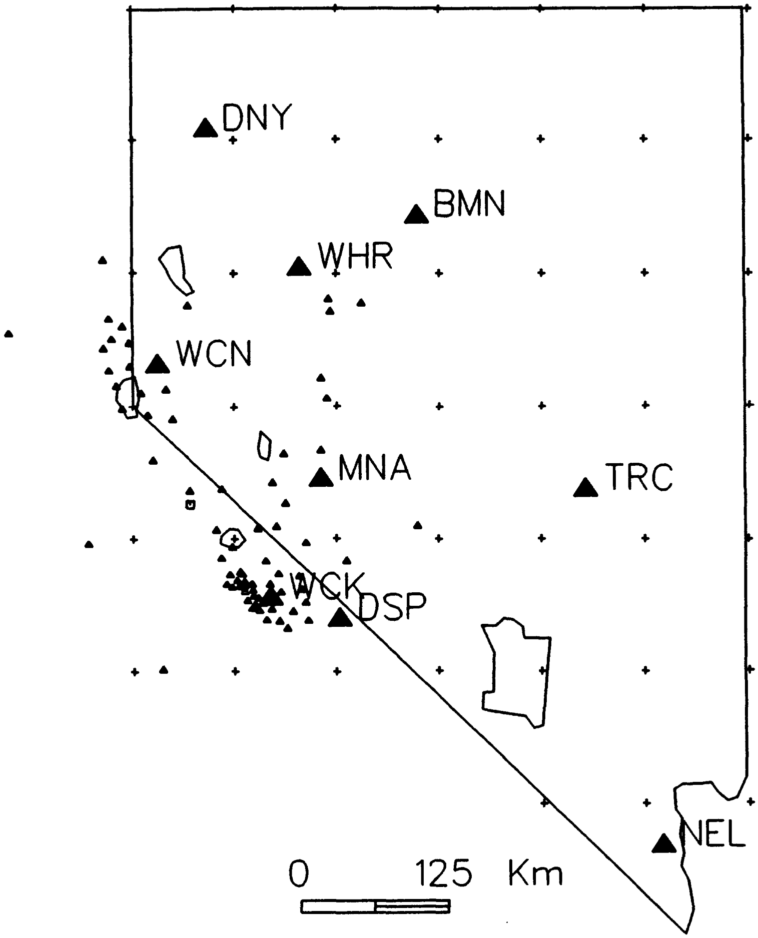

Figure 2

Nevada – Western Great Basin Seismicity
1 October 1989 through 31 March 1990

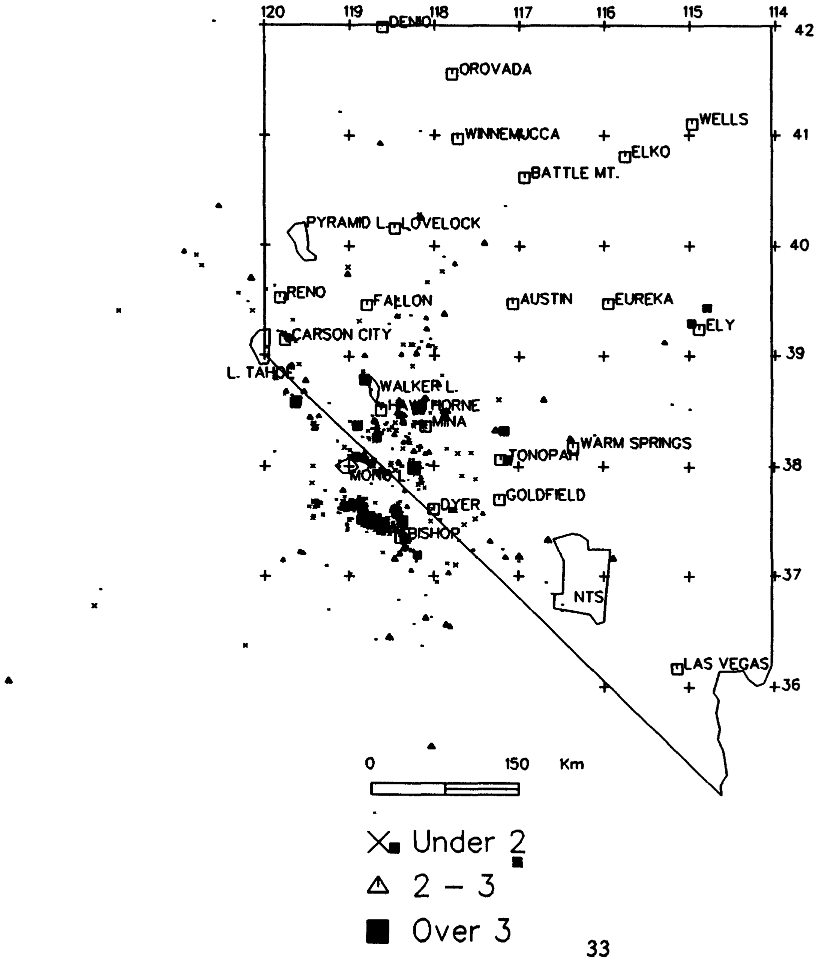

Figure 3

Mammoth – White Mountains Seismicity
1 October 1989 through 31 March 1990

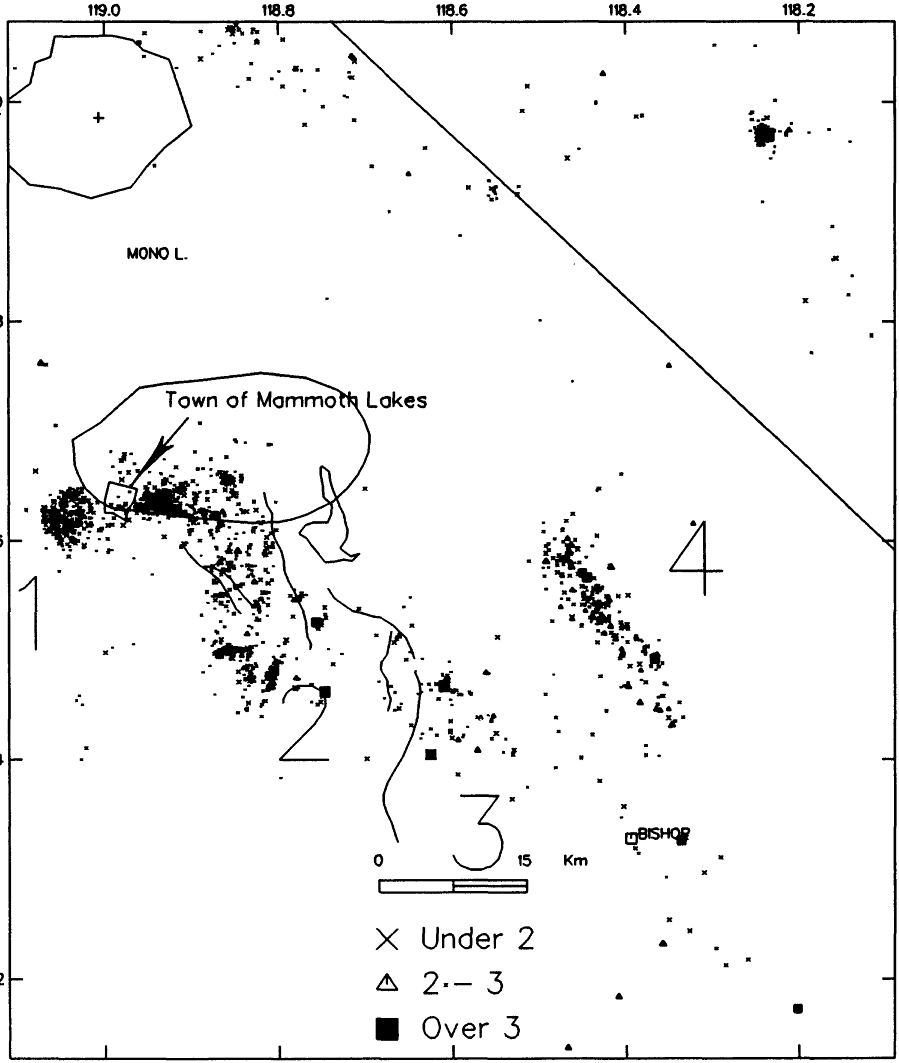

Regional Microearthquake Network in the Central Mississippi Valley

14-08-0001-A0619

William V. Stauder and Robert B. Herrmann
Department of Earth and Atmospheric Sciences
Saint Louis University
3507 Laclede
St. Louis, MO 63103
(314) 658-3131

Investigations

The purpose of the network is to monitor seismic activity in the Central Mississippi Valley Seismic zone, in which the large 1811-1812 New Madrid earthquakes occurred. The following section gives a summary of network observations during the last six months of the year 1989, as reported in Network Quarterly Bulletins No. 61 and 62.

Results

In the last six months of 1989, 51 earthquakes were located by the 42 station regional telemetered microearthquake network operated by Saint Louis University for the U.S. Geological Survey and the Nuclear Regulatory Commission. Figure 1 shows 51 earthquakes located within a 4° x 5° region centered on 36.5°N and 89.5°W. The magnitudes are indicated by the size of the open symbols. Figure 2 shows the locations and magnitudes of 43 earthquakes located within a 1.5° x 1.5° region centered at 36.25°N and 89.75°W.

In the last six months of 1989, 49 teleseisms were recorded by the PDP 11/34 microcomputer. Epicentral coordinates were determined by assuming a plane wave front propagating across the network and using travel-time curves to determine back azimuth and slowness, and by assuming a focal depth of 15 kilometers using spherical geometry. Arrival time information for teleseismic P and PKP phases has been published in the quarterly earthquake bulletin.

The significant earthquakes occurring in the last six months of 1989 include the following:

1. September 14 (1731UCT). New Madrid, Missouri. $m_{bLg} = 3.5$ (SLM). 3.2 (TEIC). Felt(IV) at Conran and Lilbourn; (III) at Gideon, Grayridge, and Portageville; (II) at Kewanee.

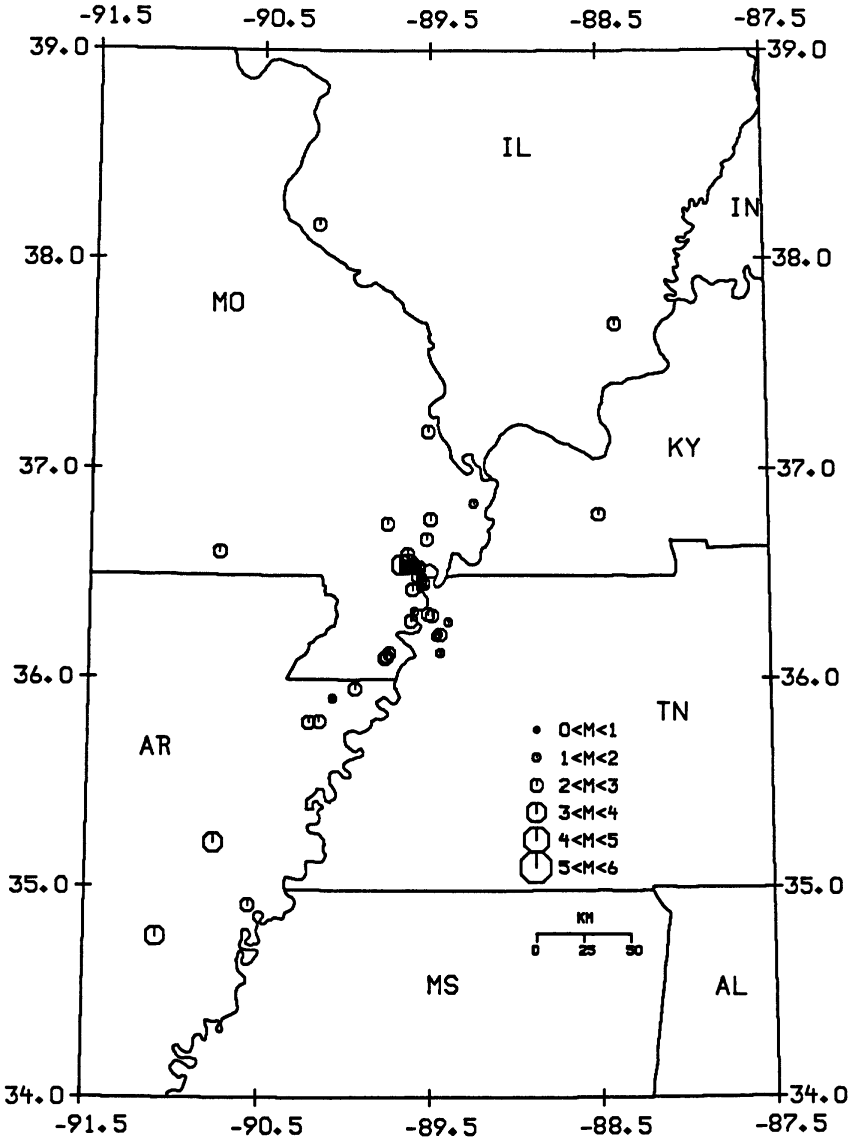

FIGURE 1

CUMULATIVE EVENTS 01 JUL 1989 TO 31 DEC 1989

LEGEND . ▲ STATION ⊙ EPICENTER

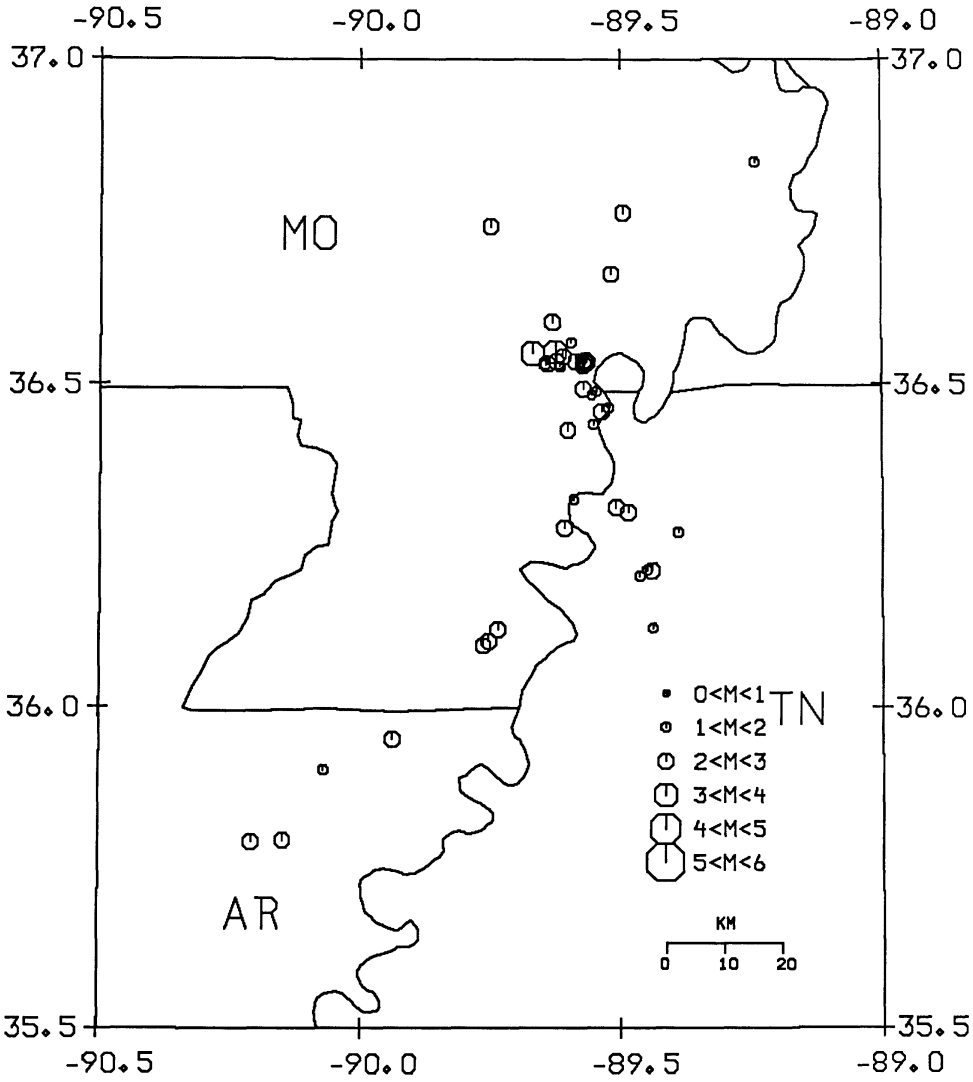

FIGURE 2
CUMULATIVE EVENTS 01 JUL 1989 TO 31 DEC 1989
LEGEND . △ STATION ⊙ EPICENTER

Consolidated Digital Recording and Analysis

9930-03412

Sam Stewart
Branch of Seismology
U. S. Geological Survey
345 Middlefield Road Mail Stop 977
Menlo Park, California 94025

Investigations.

The "Consolidated Recording and Analysis " project has as its primary goal the design, development and support of computer-based systems for processing earthquake data recorded by large, telemetered seismic networks. This includes (1) realtime systems capable of monitoring up to 1000 stations and detecting and saving waveforms even from earthquakes registering just slightly above background noise level, (2) near-realtime and offline graphics systems to analyze, catalog and archive the detected waveforms, (3) support and documentation for the users of the system.

Hardware for these systems is based upon Digital Equipment Corporation (DEC) VAX series of micro-computers. Currently, this includes the VAX 750, microVAX II, and VAXstations 2000 and 3200.

Software is based upon the DEC/VMS operating system, the CUSP database system, and the GKS graphics system. VMS is a major operating system, well documented and developed, and has a rich variety of system services that facilitate our own system development. CUSP is a state-driven data base system specifically designed and developed by Carl Johnson of the USGS.

GKS is an international-standard graphics analysis package that provides interactive input facilities as well as graphical output to a workstation. We use the DEC implementation of GKS.

The main goal for the last year has been to complete development of the "Generic" version of CUSP. This is a more modular, more generalized, more integrated version of CUSP than the one we have used since 1984. The Generic CUSP consists of a realtime earthquake event detection and processing module, the earthquake (offline) processing module (QED, Quake Editor) a new interactive graphics module known as "TMIT", a new interactive station display program known as "STNMAP", and extensive online documentation in the form of "help" files. Generic CUSP retains the use of the Tektronix 4014 graphics terminals with the high-speed graphics interface, and adds the ability to use the DEC VS2000 and VS3xxx series of workstations.

Results.

1. The various modules of Generic CUSP are essentially complete.

   Pre-release versions are being used at some sites, or are being tested by us. The Halliburton and Varian sites at Parkfield have been using the realtime system for many years. University of Nevada (Reno) is using the realtime system. USGS (Menlo Park) is using QED and the HELP files modules. We are also comparing performance of the realtime system to that of the 11/44-based realtime system in use since 1984, and are testing the TMIT module. A few comments follow.

2. The Generic CUSP realtime module is a complete re-write of versions that run on the DEC PDP series, and of older versions of CUSP that run on DEC VAX/VMS systems. It was recently modified to run under VMS 5.2, in a VAXCluster environment. It is being used to digitize analog tapes, and to read and process directly-transmitted digital data, as well as perform its original function of digitizing and monitoring the (analog) signals from large earthquake networks.

3. The QED analysis module has been modified to work with the TMIT module in a multi_windows workstation environment. The main features of QED have been retained from older versions of CUSP.

4. Two new modules, TMIT and STNMAP, have been written. TMIT is the interactive earthquake trace analysis and timing module. STNMAP is the interactive station display and selection module. Both can run alone, or simultaneously along with QED. Both work on the DEC VS2000 and VS3xxx series of workstations. They use the DEC version of the GKS interactive graphics software. They do not use DECWINDOWS or XWINDOWS.

5. The main analysis modules (QED, TMIT and STNMAP) are each individual programs, capable of running by themselves. However, they communicate with each other by using shared data space in memory, and synchronize with each other by using 'event flags' and 'status words'. One advantage is that Generic CUSP is not a huge, bulky "one shot" executable image, but is a collection of more manageable, individual modules. Another advantage is that new applications can be added, without rebuilding the entire system. Only those modules that you want to use need be activated.

Reports:

Dollar, R.S., 1989. Realtime CUSP: Automated earthquake detection system for large networks. USGS Open-File Report 89-320

Earthquake Hazard Research in the Greater Los Angeles Basin and Its Offshore Area

#14-08-0001-A0620

Ta-liang Teng,Egill Hauksson,Thomas L. Henyey

Center of Earth Sciences
University of Southern California
Los Angeles, CA 90089-0740
(213) 743-6124

INVESTIGATIONS

Monitor earthquake activity in the Los Angeles Basin and the adjacent offshore area. Upgrade of instrumentation by installing Optimum Telemetry System (OTS) for onscale recording of waveforms from local earthquakes, and installation of more downhole seismometers for improved coverage and sensitivity.

RESULTS

The 1 January - 31 December, 1989 Los Angeles Basin Seismicity

The 1989 seismicity (Figure 1A) is characterized by a strong cluster of events in the Santa Monica bay with a mainshock being a $M_L = 5.0$ event on January 19 some, 25 km south of Malibu. This cluster is followed by a $M_L = 4.0$ event 10 km offshore southwest of Point Dume on February 2, a $M_L = 4.5$ event (with many aftershocks along the Newport-Inglewood fault trend) at Newport on April 7, and a group of Whittier Narrows aftershocks with the two largest ones being $M_L = 4.1$ and 4.4 on June 12. The overall seismicity in the Greater Los Angeles Basin and its offshore area has been very active during 1989 as compared with earlier years. It is apparent that the Newport-Inglewood fault zone, the Malibu Coast-Santa Monica-Raymond Hill fault zone, as well as the Whittier fault zone, are all very active during 1989. While the characteristics of the hypothetical Elysian Park buried thrust are not yet clearly understood, tectonic stress operative in this area clearly produces right-lateral strike-slip events on NW-trending structures, thrust events on EW-trending structures, and left-lateral strike slip events on NE-trending structures.

The group of NE-trending events near 34° 10' N and 117° 50' W are the aftershocks of the Upland sequence that first occurred on 26 June 1988, with the mainshock magnitude $M_L = 4.6$. This group of events actually lead to the second and larger earthquake sequence on February 28, 1990, with mainshock magnitude $M_L = 5.5$ (see cluster on the top right of Figure 1B). Both the 1988 and the 1990 sequences occurred on the same fault as the two set of aftershocks overlap the same NE-trending fault zone and practically the same fault-plane solution is obtained for the two mainshocks. In Figure 1B, seismic activity of the Greater Los Angeles Basin and its Offshore area is given for the 6-month period from October 1989 to March 1990. Besides the Upland sequence mentioned above, the basic pattern of the 1989 seismicity continues in the monitoring area. We note that the recent 1987 Whittier Narrows events and the 1988 Pasadena events may have some surface manifestations. For several years buckling at the joining part of the concrete freeway slabs has been observed near the northern terminus of the Pasadena Freeway between Fair Oak Street and Orange Grove Boulevard overpasses. The significance and nature of this buckling needs further study.

A plot of cumulative number of earthquakes in the monitoring area during 1989 is given in Figure 2A. Clearly, the largest jump of this curve occurs in January 1989 and that is the Santa Monica bay sequence reported above.

The focal mechanisms of five M > 4.0 events that occurred during 1989 in the Greater Los Angeles Basin and its offshore area are shown in Figure 2B. Four of the five are thrust events that include the January 19 Santa Monica bay event, February 2 Point Dume event, and two aftershocks of the Whittier Narrows earthquake. The Newport event of April 7 gives a standard right-lateral strike slip faulting typical of the focal mechanism along the Newport-Inglewood fault. These focal mechanisms suggest the importance of compressional tectonic stress in the Los Angeles Basin that cause NS shortening together with associated strike slip motions.

A new downhole seismic station (LOM) was installed in December 20, 1989, at Lomita. It improves the network coverage of the Torrance area. Excellent signals began to arrive at our central recording system on December 27.

REFERENCES

Hauksson, E. and L. M. Jones, The 1987 Whittier Narrows earthquake sequence in Los Angeles, southern California: Seismological and tectonic analysis, J. Geophys. Res., 94, 9569-9590, 1989.

Hauksson, E. and G. V. Saldivar, Seismicity (1973-1986) and active compressional tectonics in the Santa Monica Bay, southern California, J. Geophys. Res., 94, 9591-9606, 1989.

Hauksson, E. and R. S. Stein, The 1987 Whittier Narrows earthquake: a metropolitan shock, J. Geophys. Res., 94, 9545-9547, 1989.

Jones, L. M., K. E. Sieh, E. Hauksson and L. K. Hutton, The December 3, 1988 Pasadena, California Earthquake: Evidence for Strike-slip Motion on the Raymond fault, Bull. Seism. Soc. Amer., to appear in February 1990.

Hauksson, E., Earthquakes, active faulting, and stress in the Los Angeles Basin, submitted to J. Geophys. Res., August 1989.

Hauksson, E., T. L. Teng, T. L. Henyey, M. Robertson, J. K. McRaney and L. Hsu, Earthquake hazard research in the Los Angeles Basin and its offshore area, Annual Technical Report, submitted to the U.S. Geological Survey, December 1988, 90 pp.

Hauksson, E., Comparison of broad-band waveforms of local earthquakes recorded art crystalline and sedimentary rock sites in the Los Angeles Basin, submitted to fall AGU meeting, 1989.

Robertson, M. C. and E. Hauksson, Three-dimensional fine velocity structure of the Los Angeles Basin, submitted to fall AGU meeting, 1989.

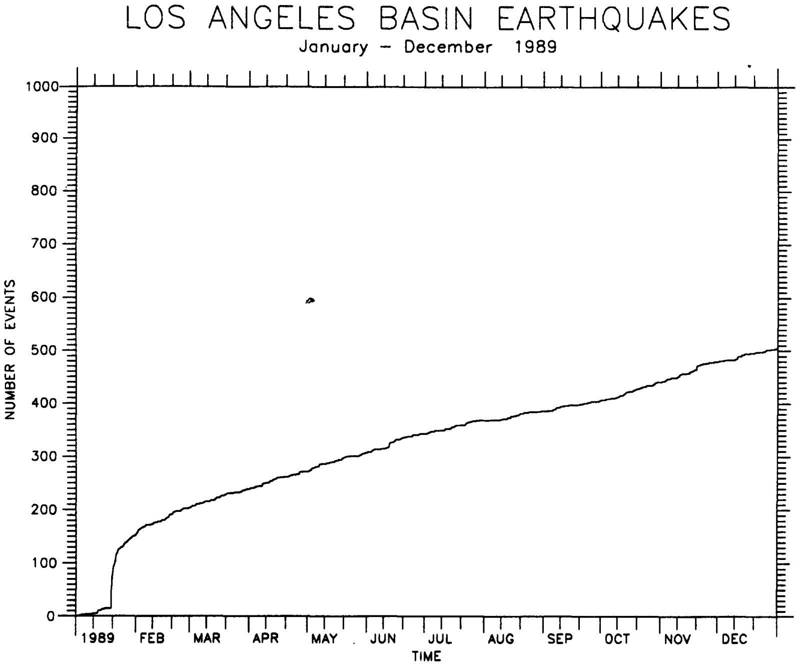

Figure 2A. Cumulative number of earthquakes in the Los Angeles basin recorded by the USC Los Angeles basin network in 1989.

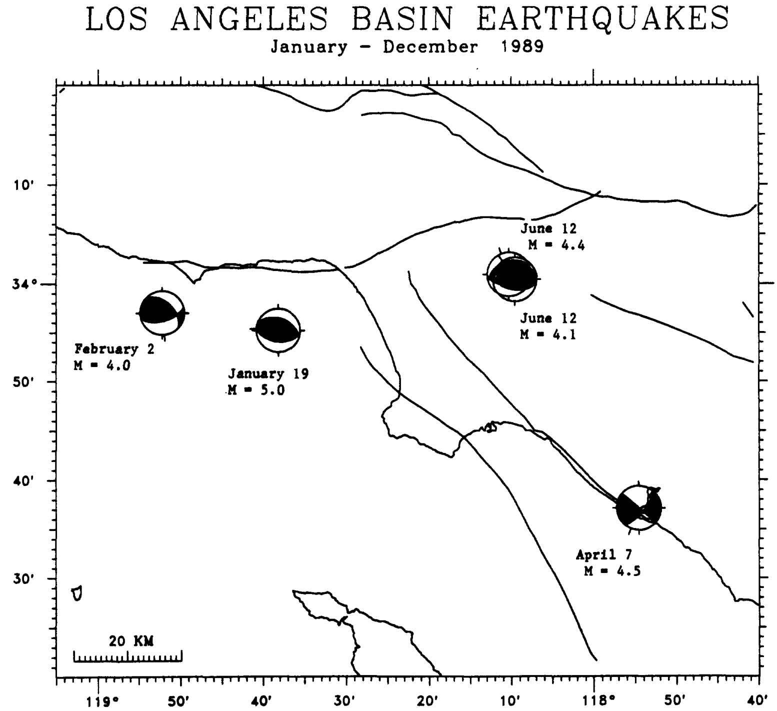

Figure 2B. Focal mechanisms of M ≥ 4.0 earthquakes recorded in the Los Angeles basin in 1989.

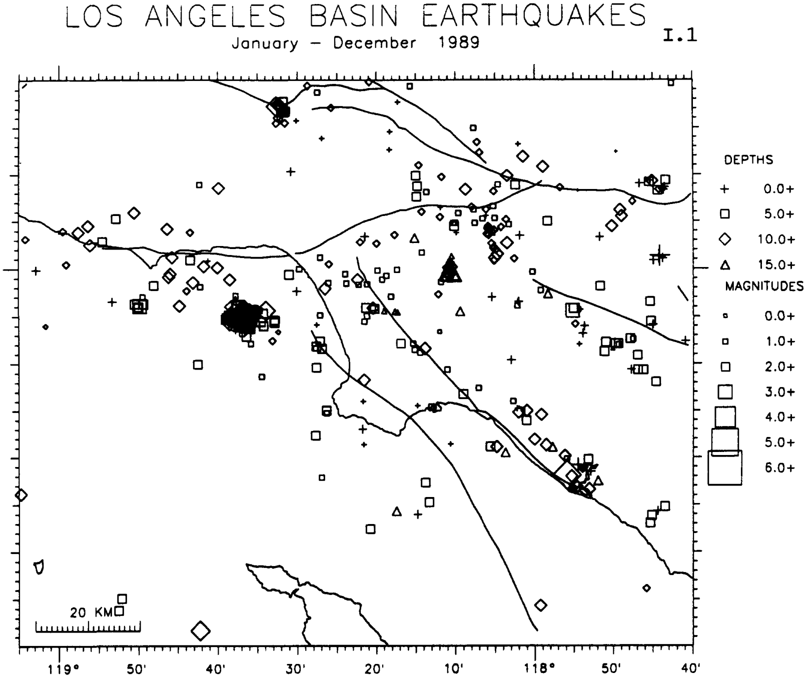

Figure 1A. Seismicity recorded during 1989 by the USC Los Angeles basin network.

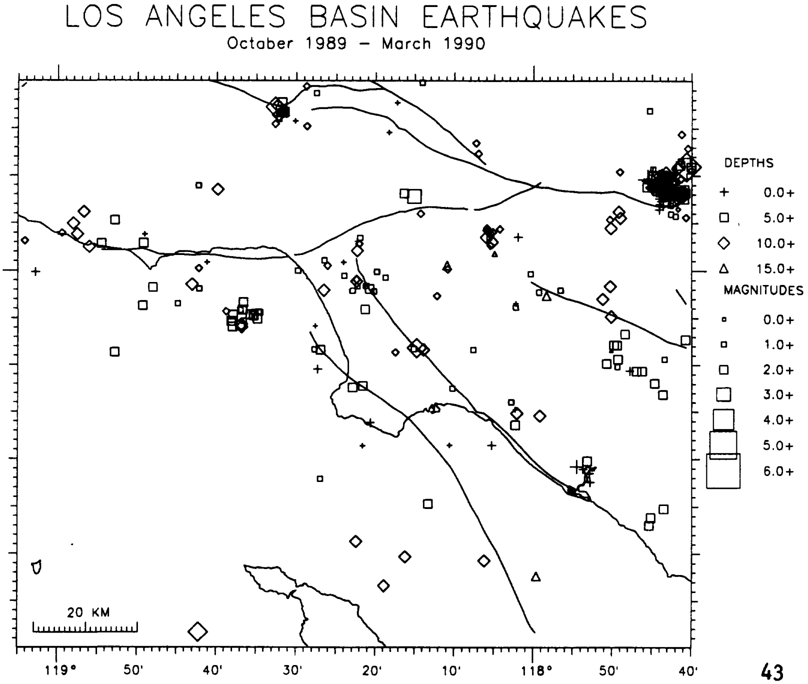

Figure 1B. Seismicity recorded between 01 October, 1989 and 31 March, 1990 by the USC Los Angeles basin network.

Field Experiment Operations

9930-01172

John VanSchaack
Branch of Seismology
U.S. Geological Survey
345 Middlefield Road, MS-977
Menlo Park, California 94025
(415) 329-4780

Investigations

This project performs a broad range of management, maintenance, field operation, and record keeping tasks in support of seismology and tectonophysics networks and field experiments. Seismic field systems that it maintains in a state of readiness and deploys and operates in the field (in cooperation with user projects) include:

A. 5-day recorder portable seismic systems.
B. "Cassette" seismic refraction systems.
C. Portable digital event recorders.

This project is responsible for obtaining the required permits from private landowners and public agencies for installation and operation of network sensors and for the conduct of a variety of field experiments including seismic refraction profiling, aftershock recording, teleseism P-delay studies, volcano monitoring, etc.

This project also has the responsibility for managing all radio telemetry frequency authorizations for the Office of Earthquakes, Volcanoes, and Engineering and its contractors.

Personnel of this project are responsible for maintaining the seismic networks data tape library. Tasks includes processing daily telemetry tapes to dub the appropriate seismic events and making playbacks of requested network events and events recorded on the 5-day recorders.

Results

Seismic Network Operations:

The major effort during this period was in support of Loma Prieta earthquake monitoring. The microwave network, which telemeters about 60% of the data, operated without failure. An early alert monitoring system was developed and installed about 4 days after the Loma Prieta mainshock. This small net consisted of 3 separate dual gain vertical sensor systems. The stations were installed near Loma Prieta Mountain in a triangular pattern with each side about 2 miles. The signals were independently transmitted to Menlo Park. The signals were fed into a trigger which actuated if 2 of the 3 units sensed a signal equivalent to a magnitude 3.8 earthquake. The trigger actuated a radio code which was received by radios at the Cypress Structure CalTrans headquarters. The warnings of earthquakes were received there about 15-18 seconds before the arrival of the S waves. The system had 1 false trigger in 2 months and did not fail to trigger on any earthquake larger then M3.8.

Geothermal Seismotectonic Studies

9930-02097

Craig S. Weaver
Branch of Seismology
U. S. Geological Survey
at Geophysics Program AK-50
University of Washington
Seattle, Washington 98195
(206) 442-0627

Investigations

1. Continued analysis of the seismicity and volcanism patterns of the Pacific Northwest in an effort to develop an improved tectonic model that will be useful in updating earthquake hazards in the region. (Weaver, Yelin)

2. Continued acquisition of seismicity data along the Washington coast, directly above the interface between the North American plate and the subducting Juan de Fuca plate. (Weaver, Yelin, Norris, UW contract)

3. Continued seismic monitoring of the Mount St. Helens area, including Spirit Lake (where the stability of the debris dam formed on May 18, 1980 is an issue), Elk Lake, and the southern Washington-Oregon Cascade Range (north of Newberry Volcano). The data from this monitoring is being used in the development of seismotectonic models for southwestern Washington and the interaction of the Basin and Range with the Oregon Cascades. (Weaver, Grant, Norris, Yelin, UW contract)

4. Study of Washington and northern Oregon seismicity, 1960-1989. Earthquakes with magnitudes greater than 4.5 are being re-read from original records and will be re-located using master event techniques. Focal mechanism studies are being attempted for all events above magnitude 5.0, with particular emphasis on the 1962 Portland, Oregon event. (Yelin, Weaver)

5. Study of earthquake catalogs for the greater Parkfield, California region for the period 1932-1969. Catalogs from the University of California (UCB) and CalTech (CIT) are being compared, duplicate entries noted, and the phase data used by each reporting institution are being collected. The study is emphasizing events greater than 3.5, and most events will be relocated using station corrections determined from a set of master events located by the modern networks. (Meagher, Weaver)

6. Study of estuaries along the northern Oregon coast in an effort to document probable subsidence features associated with paleosubduction earthquakes (Grant).

Results

1. Portland, Oregon lies in the southern half of an approximately rectangular basin measuring 30 by 50 km. Since 1969, there have been no earthquakes of magnitude 4.0 or greater on the margins of the Portland basin, but this level of seismicity may not be characteristic of the region. Using microseismicity data collected by the University of Washington regional short-period seismograph network for the period mid-1982 through 1989, we have determined P-wave focal mechanisms for four individual earthquakes and three groups of earthquakes. We

have also relocated the the $M_w = 5.1$ Portland earthquake of 6 November 1962 and analyzed regional surface-wave recordings of this event, using the seismic moment-tensor inversion technique. The results of these seismic analyses, along with geologic and other geophysical data, are integrated into a seismo-tectonic model of the Portland basin. The P-wave mechanisms are compatible with dextral strike-slip motion along approximately NW trending fault zones bounding the eastern and western margins of the basin. We propose the existence of a dextral strike-slip fault zone, which we call the Frontal Fault Zone, along the eastern margin of the Portland basin The western margin has been previously recognized as a zone of dextral strike-slip faulting, the so-called Portland Hills Fault Zone. The epicenter of the 1962 earthquake is located between the two fault zones, and lies approximately 15 km NE of downtown Portland. Our preferred mechanism is normal faulting on NE or NNE trending fault planes. These results support the hypothesis posed by previous investigators that the Portland basin is a pull-apart basin and further support the existence of contemporary crustal extension between the Frontal and Portland Hills Fault Zones.

2. On December 24, 1989, a magnitude 5.1 earthquake occurred in the southern Washington Cascade Range near Storm King Mountain, about 30 km southwest of Mount Rainier. Although earthquakes of magnitude 5 and greater occassionally occur in the southern Washington Cascade Range, this event was unusual for three reasons. First, in the first month after the earthquake, only 12 aftershocks were locatable, and all of these events were less than magnitude 1.5. In contrast, other events in southwestern Washington of similar magnitude (Siouxon Peak, 1961; Elk Lake, 1981, Goat Rocks, 1981) have been followed by many tens to hundreds of aftershocks and the largest magnitude aftershock in all previous sequences has been at least 3.0. Second, this event occurred in an area where very little seismicity has been detected since the regional Washington seismic network was installed in 1972. The other magnitude 5 events have occurred in areas with recurring seismic activity. Third, the earthquake focal mechanism is decidely different than others calculated for events in the southern Washington Cascades. The focal mechanism is dominantly strike-slip; however, the sense of motion, left-lateral slip on a north-south striking plane or right-lateral slip on an east-west striking plane, is in contrast to the right-lateral strike-slip on northerly-striking fault planes observed elsewhere for focal mechanisms calculated for earthquakes in the southern Cascade Range of Washington.

The epicentral locations of the Storm King Mountain event is within a region of very high conductivity, referred to as the Southern Washington Cascade Conductor (SWCC). Previous interpretations of the relation between seismicity and the SWCC have emphasized the horizontal limits of the conductor, and suggested that earthquake activity was concentrated along the boundary of the SWCC. For example, the St. Helens seismic zone occurs at the western boundary between the SWCC to the east and Eocene marine volcanic rocks known as Siletzia to the west. The hypocentral depth of the Storm King Mountain event places the earthquake below the interpreted lower boundary of the SWCC, perhaps near the eastern edge of Siletzia. We conclude that the Storm King Mountain earthquake is further evidence of the importance of the major crustal blocks in determining the pattern of crustal seismicity in the southern Washington Cascade Range.

Reports

Grant, W. C. and Weaver, C. S., 199?, Seismicity of the Spirit Lake area: Estimates of possible earthquake magnitudes for engineering design, in *The formation and significance of major lakes impounded during the 1980 eruption of Mount St. Helens, Washington, U. S. Geological Survey Professional Paper,* edited by R. L Shuster and W. Meyer, (still in press). Funded by Earthquake, Geothermal, and Volcano Hazards.

Mooney, W. and C. S. Weaver, 1989, Regional crustal structure and tectonics of the Pacific Coastal States: California, Oregon, and Washington, in, *GSA Memoir 172, Geophysical*

Framework of the Continental United States, L. Pakiser and W. Mooney, eds., 129-161. This project's contribution funded by Volcano, Geothermal and Earthquake Programs.

Zollweg, J. E., 1990, High frequency earthquakes following the 1985 eruption of Nevada del Ruiz, Columbia, *J. Volcan. and Geotherm. Res.*, 19 pages, 8 figures, (in press). Funded by Volcano Hazards.

Ludwin, R., C. S. Weaver, and R. S. Crosson, 1990, Seismicity of Washington and Oregon, *GSA Decade of North American Geology Associated Volume, Neotectonics,* 35 pages, 10 figures, (in press). Funded by Geothermal, Volcano Hazards and Earthquake Programs.

Zollweg, J. E. and P. Johnson, 1989, The Darrington seismic zone in northwestern Washington, *Bull. Seism. Res. Amer.*, 1833-1845. Funded by Earthquake Program.

Shedlock, K. M. and C. S. Weaver, 1989, Rationale and outline of a program for earthquake hazards assessment in the Pacific Northwest, in *U.S. Geol. Surv. Open-File Report 89-465,* 2-10. Funded by Geothermal and Earthquake Programs.

Weaver, C. S. and K. M. Shedlock, 1989, Potential subduction, probable intraplate, and known crustal earthquake source areas in the Cascadia subduction zone, in *U.S. Geol. Surv. Open-File Report 89-465,* 11-26. Funded by Geothermal and Earthquake Programs.

Fournier, R. O. and C. S. Weaver, Heat flow from the Washington Cascades and adjacent regions estimated using variations in depth of the seismogenic crust, submitted to *J. Geophys. Res.*, 21 pages, 8 figures. Funded by Geothermal Program.

Finn, C., Weaver, C. S., and W. D. Stanley, 1989, Relation of earthquakes and aeromagnetic anomalies to crustal structure of western Washington, (abs), *EOS, Trans. Amer. Geophys. Union, 71,* 1329.

Grant, W. C., Atwater, B. F., Carver, G. A., Darienzo, M. E., Nelson, A. R., Peterson, C. D., Vick, G. S., 1989, Radiocarbon dating of late Holocene coastal subsidence above the Cascadia subduction zone--compilation for Washington, Oregon and northern California, (abs), *EOS, Trans. Amer. Geophys. Union, 71,* 1331.

Shedlock, K. M., Weaver, C. S., Opppenheimer, D., King, G. C. P., 1989, Seismic deformation in the Pacific Northwest, *EOS, Trans. Amer. Geophys. Union, 71,* 1330.

Yelin, T. S. and H. J. Patton, 1989, Seismotectonics of the Portland, Oregon region, (abs), *EOS, Trans. Amer. Geophys. Union, 71,* 1330.

Norris, R. D., 1990, Seismograms from the 16 August 1989 rockfall from Russell Cliff, Mount Rainier, (abs), *EOS, Trans. Amer. Geophys. Union, xx,* in press (presented at Pacific Northwest AGU section meeting).

Yelin, T. S. and H. J. Patton, Seismotectonics of the Portland, Oregon region, manuscript for *Bull. Seis. Soc. Am.*, (38 pages, 11 figures, in branch review). Funded by Earthquake and Geothermal Programs.

Weaver, C. S., Norris, R. D., and C. Jonientz-Trisler, 1990, Seismological monitoring in the Cascade Range, 1962-1989: Earthquakes, eruptions, avalanches, and other curiosities (abs), in *Proceedings of the Geological Association of Canada Annual Meeting,* (in press).

Rupture Histories of the 1934 and 1966 Parkfield, California, Earthquakes: A Test of the Characteristic Earthquake Hypothesis

14-08-0001-G1784

Gregory C. Beroza and Thomas H. Jordan

Rm. 54-518, Massachusetts Institute of Technology, Dept. of EAPS, Cambridge, MA, 02139
(617) 253-3382

Near-Source Modeling of the 1966 Parkfield Earthquake

We have carried out an analysis of the near-source records for the 1966 Parkfield earthquake to try to determine the extent of coseismic rupture. Because of the distribution of stations with respect to the rupture zone it is difficult to infer the complete rupture history. In particular we found it practically impossible to distinguish effects due to changes in the rupture time from effects due to changes in the slip amplitude.

Instead of trying to solve for both rupture time and slip amplitude, we assume a range of rupture velocities parameterized by the fraction of the shear wave velocity β, and solve for the slip amplitude. A consequence of this is that our results do not provide a definitive rupture history for the entire fault and could be biased if rupture velocity varied a great deal during the earthquake. On the other hand, they do allow us to place constraints on the extent of coseismic rupture and estimate the range of possible rupture velocities.

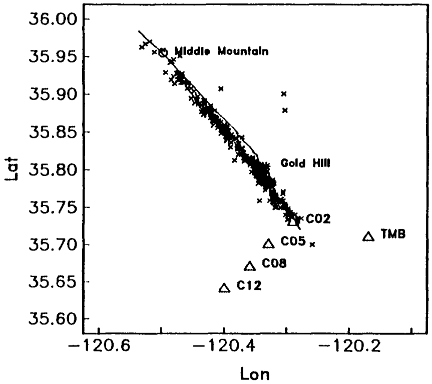

Figure 1. The location of strong-motion stations that recorded the 1966 Parkfield earthquake are shown as triangles. Well located aftershocks [*Eaton et al.*, 1970] are shown together with the surface trace of the San Andreas Fault. The right-step near Gold Hill is apparent in the aftershock distribution.

In our analysis we used the horizontal components of the Cholame-Shandon array: C05, C08, C12, and Temblor (Figure 1). C02 was excluded from the analysis due to the possibility that the data were affected by propagation effects and because the high-frequency, near-source approximation would be invalid if shallow coseismic rupture extended beyond Gold Hill.

Rupture velocities in excess of 0.80β fit the data very poorly and were characterized by slip distributions that had very little slip over most of the rupture surface. Rupture velocities of 0.65β or less resulted in unreasonable models with a large amount of slip on a very short fault, which is inconsistent with the geodetic data and teleseismic estimates of the seismic moment [*Tsai and Aki*, 1969].

Our best-fitting slip model, which assumes a rupture velocity of 0.70β, is shown in figure 2. this model has a region of high slip occurring about 10 km to the southeast of the hypocenter at a depth of about 10 km. There is a small region of high slip near the hypocenter and a larger region of high slip from 25-30 km to the southeast. This model suggests that rupture propagated well past the right-step at Gold Hill and very near to station C02. The fact that this region appears disconnected from the rest of the slip in our model does not necessarily make it infeasible. The barrier model provides a mechanism for disconnected regions of slip during earthquakes [*Das and Aki*, 1978]. Moreover, our data are band-limited and we are unable to recover the low-wavenumber components of the source.

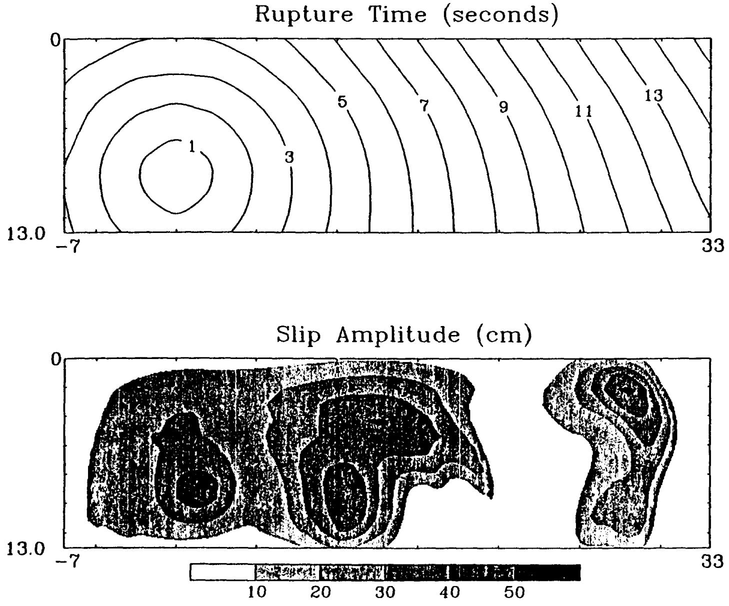

Figure 2. The best-fitting constant rupture velocity model for the Parkfield earthquake has a rupture velocity of 0.70β. This model has slip occurring as far as 30 km from the hypocenter–near the Cholame-Shandon array; however, it is inconsistent with the geodetic model of slip during the 1966 sequence [*Segall and Harris*, 1987].

However, a more troublesome aspect of this rupture model is that there is very little slip on a large part of the fault over which the geodetic data [*Segall and Harris*, 1987] indicate that the slip was highest–about 15-25 km to the southeast of the hypocenter. Unless a great deal of post-seismic slip occurred over that entire area, this model is inconsistent with the geodetic data.

A model that we prefer, which assumes a slightly higher rupture velocity of 0.75β and fits the strong-motion data nearly as well, is shown in Figure 3. In this model slip extends to about 24 km to the southeast of the hypocenter, near the offset in the fault at Gold Hill. There is a small region of high slip 33 km along-strike, but this is not significant. The majority of slip occurs from 10-23 km along-strike and at depths ranging from 2-12 km. The region of high slip is located at the same distance along the fault as in the geodetic model of *Segall and Harris* [1987]. This model is also supported by independent estimates of the rupture velocity [e.g. *Trifunac and Udwadia*, 1974; *Lindh and Boore*, 1981].

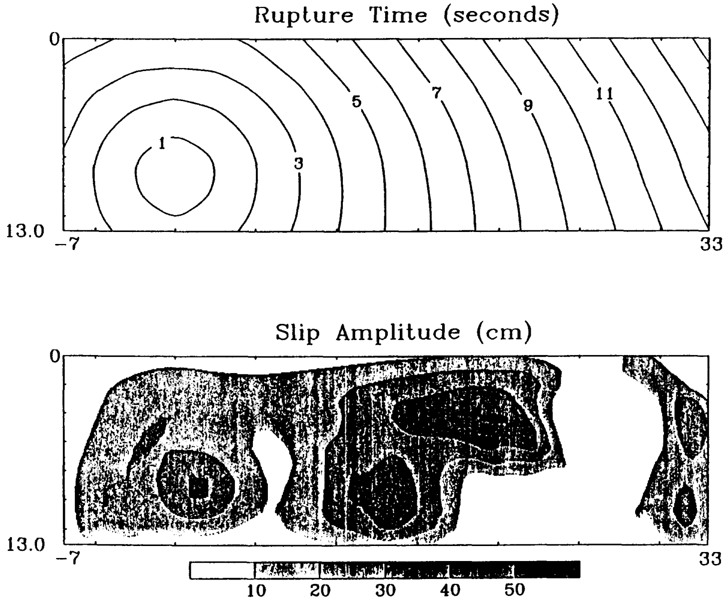

Figure 3. The constant rupture velocity model for the Parkfield earthquake assuming a rupture velocity of 0.75β. Although this model fits the data slightly less well than the model shown in Figure 2, it is consistent with geodetic models of slip in the 1966 sequence. For this reason we favor it over the model in Figure 2. The sensitivity of our rupture models for this earthquake to the rupture velocity is a consequence of the poor source-station distribution. The regional-distance data have a much better azimuthal distribution with respect to the source and will not be nearly as sensitive to the assumed rupture velocity.

To summarize, the results from the near-source data indicate that the rupture velocity was fairly low in this earthquake, $0.65\beta < v < 0.80\beta$. We also obtain lower values for the shear fracture energy ~ 5×10^5 J/m^2 for the Parkfield earthquake relative to that found for the Morgan Hill and Imperial Valley earthquakes ~ 2×10^6 J/m^2 [*Beroza and Spudich*, 1988; *Beroza*, 1989].

The extent of coseismic slip is not well determined by the near-source data alone. However, taken together with models derived from the geodetic data our results suggest a model in which coseismic rupture terminates near the offset in the San Andreas fault at Gold Hill with post-seismic slip occurring farther to the southeast. These conclusions could change; however, if there are strong variations in the rupture velocity during the earthquake. A definitive determination of the extent of rupture in the 1966 earthquake and in the 1934 earthquake requires the analysis of the regional-network Wood-Anderson data.

Analysis of the 1934 and 1966 Parkfield Earthquakes Using Wood-Anderson Data

We have already collected Wood-Anderson seismograms from the Archives of the University of California at Berkeley and the California Institute of Technology for earthquakes dating from 1931 to 1975 in the Parkfield region. The seismograms have all been reproduced and enlarged for digitization with funding and support from the U.S. Geological Survey. We are currently working on the digitization of the dataset.

The digitized Wood-Anderson data will be used to infer the rupture history of the 1934 and 1966 events and to test the characteristic earthquake hypothesis. The Wood-Anderson data should substantially increase our resolution of the rupture history of the 1966 earthquake. This is especially true given the poor distribution of strong motion stations relative to the 1966 earthquake with the associated pitfalls demonstrated above. How well we will be able to recover the rupture history of the 1934 earthquake will depend on the accuracy of the regional-distance Green's functions calculated using the proposed techniques. Analysis of geodetic measurements at the southern end of the rupture zone bracketing the 1934 earthquake indicate that there were substantial differences in the 1934 and 1966 sequences [*Segall et al.*, 1990].

The techniques we develop have the potential to open up a new window on older earthquakes, which in turn will allow a better understanding of earthquake rupture. They may also provide a starting point for the analysis of broad-band, high-dynamic-range, digital data from future earthquakes.

References

Anderson, J., A., and H. O. Wood, Description and theory of the torsion seismometer, *Bull. Seismol. Soc. Am.*, *15*, 1-72, 1925.

Beroza, G. C., Near-source imaging of seismic rupture, Ph.D. Thesis, 198 pp., Mass. Inst. of Technol., Cambridge, 1989.

Beroza, G. C., and P. Spudich, Linearized inversion for fault rupture behavior: application to the 1984, Morgan Hill, California, earthquake, *J. Geophys. Res.*, *93*, 6275-6296, 1988.

Das, S. and K. Aki, Fault plane with barriers: a versatile earthquake model, *J. Geophys. Res*, *82*, 5658-5670, 1977.

Eaton, J. P., M. E. O'Neill, and J. N. Murdock, Aftershocks of the 1966 Parkfield - Cholame, California earthquake: a detailed study, *Bull. Seismol. Soc. Am.*, *60*, 1151-1197, 1970.

Lindh, A. G., and D. M. Boore, Control of rupture by fault geometry during the 1966 Parkfield earthquake, *Bull. Seismol. Soc. Am.*, *71*, 95-116, 1981.

Segall, P., Y. Du, and W. Thatcher, Were the 1934 & 1966 Parkfield earthquakes similar?, *Seismological Research Letters*, *61*, 22, 1990.

Segall, P., and R. Harris, Earthquake deformation cycle on the San Andreas fault near Parkfield, California, *J. Geophys. Res.*, *92*, 10,511-10,525, 1987.

Trifunac, M. D., and F. E. Udwadia, Parkfield, California, earthquake of June 27, 1966: a three-dimensional moving dislocation, *Bull. Seismol. Soc. Am.*, *64*, 511-533, 1974.

Seismic Source Analysis Using Empirical Green's Functions

9910-02676

J. Boatwright, and L. Wennerberg
Branch of Engineering Seismology and Geology
345 Middlefield Road, MS 977
Menlo Park, California 94025
(415) 329-5609, 329-5607, 329-5659

Investigations

1. Inversion for the distribution of stress release in an earthquake rupture process.

2. Recording and analysis of aftershocks of the 1989 Loma Prieta earthquake.

3. Analysis of accelerograms written by the mainshock and aftershocks of the 1983 Coalinga earthquake.

Results

1. Boatwright, DiBona, Cocco (1989) have designed, programmed, and applied an iterative inversion scheme which uses positivity constraints to deconvolve recordings of small earthquakes from recordings of larger earthquakes, and which minimizes the number of sub-events necessary by using an F-test to check the statistical significance of each added subevent. The inversion determines the space-time distribution of the stress release comprising the earthquake. It has been applied to a set of 9 unfiltered accelerograms of body-waves radiated by a $M_L = 5.3$ Coalinga aftershock; the error reduction from the inversion was 75%. Different methods of constraining the solution were tested: the most physical solution was obtained by constraining the rupture velocity of the process to be less than the S-wave velocity.

2. GEOS digital event recorders were deployed at 21 sites in San Francisco and 14 sites extending from Woodside to Fremont across the Southern San Francisco Bay. These instruments recorded some 85 aftershocks of the Loma Prieta earthquake over a period of two months following the earthquake. The set of recordings represents one of the most extensive data sets ever obtained in an urban or suburban environment, and can be expected to yield significant information for the evaluation of seismic hazard in these areas. In particular, these recordings can be used to complement the strong motion recordings of the mainshock in the Bay Area. Boatwright, Seekins, and Mueller (1990) have completed an analysis of the recordings obtained in the Marina District which yielded estimates of the ground amplification throughout the Marina, as well as upper bounds for the main shock ground motion in the Marina.

3. Wennerberg (1990a) has derived a variant of Boatwright's (1988) filtering strategy in which the recordings of small earthquakes are amplified a long periods using a zero-phase-shift filter to simulate the recordings of large simple earthquakes or of large subevents within a complex rupture

process. Wennerberg (1990b) applies this technique to synthesize the accelerograph recording of the $M_L = 6.7$ Coalinga mainshock, using the recording of a $M_L = 5.3$ aftershock. A sum of filtered accelerograms corresponding to eleven subevents gives a credible match to the main shock accelerogram. Corresponding stress parameters for the sub-events vary over a factor of five, and the sum of the subevent moments is consistent with independent estimates of the seismic moment of the main shock.

References

Boatwright, J., 1988, The seismic radiation from composite models of faulting, *Bulletin of the Seismological Society of America*, v. 78, p. 489-508.

Wennerberg, L., 1990a, Stochastic summation of empirical Green's functions, Bulletin of the Seismological Society of America, in press.

Publications

Boatwright, J., M. DiBona, and M. Cocco, 1989, The dynamic decomposition of the earthquake rupture process, EOS, p. 243.

Boatwright, J., L.C. Seekins, and C.S. Mueller, 1990, Ground motion amplification in the Marina District, U.S. Geological Survey Open-File Report 90-253., p. F1-F18.

Wennerberg, L., 1990b, Observing source complexity in locally recorded accelerograms from Coalinga, California, Earthquake Notes, in press.

Analysis of the 1957 Andreanof Islands Earthquake
14-08-0001-G1766

Thomas M. Boyd
Colorado School of Mines
Department of Geophysics
Golden, CO 80401
(303) 273-3522

Project Summary and Goals

Recent studies have indicated that the spatial distribution of moment release can be quite heterogeneous along any particular rupture zone. The most common explanation for this heterogeneity has been the rupture of strong patches, or asperities, along the fault plane [e.g., Ruff and Kanamori, 1983]. These strong patches could possibly arise from spatial variations in the frictional characteristics of the fault surface or from geometrical barriers inherent to the fault's shape. Alternatively, the spatial distribution of moment release could have little to do with the physical characteristics of the fault's surface and may be related to the dynamics of slip and how regions of a fault interact with neighboring regions [e.g., Rundle and Kanamori, 1987; Horowitz and Ruina, 1989].

Distinctions between these two models can not be made by the analysis of single events [e.g., Thatcher, 1990]. Conclusive observations can only be drawn from a study of the moment-release distribution generated by several great earthquakes, all of which rupture the same fault segment. If this distribution is controlled by the physical characteristics of the fault's surface, then one might expect the moment distributions to be similar for each of the earthquakes. One might also expect to be able to identify the sites of large moment release during the next great earthquake from the spatial distribution of the smaller interseismic events. If, however, the distribution of moment release is controlled by fault interactions, then one might expect the moment distributions to differ, particularly if the events have different, but overlapping rupture bounds.

In this context, an excellent region of study is the central Aleutian Arc. In 1986, a magnitude 8.0 (M_w) earthquake occurred along the Aleutian Arc near the Andreanof Islands. The slip distribution, aftershock, and preshock sequence of this earthquake have been described in a number of recent studies. Prior to 1986, the central Aleutian Arc was ruptured by another great earthquake in 1957 ($M_w > 8.5$). The 1957 Andreanof Islands earthquake remains poorly understood. Its seismic moment, slip distribution, and even rupture area have not been well constrained. The short time span between the 1957 and 1986 earthquakes provides us with a unique opportunity to study a complete seismic cycle bounded by two instrumentally recorded great earthquakes. In fact, it represents the only complete seismic cycle along the Alaska-Aleutian Arc which has been instrumentally observed. Currently published and ongoing research efforts have focused mainly on the final two-thirds of the rupture cycle. To help supplement our picture of the seismic process' involved during the entire rupture cycle, verify the recently proposed set of seismic hazard estimates, and shed light on the possible mechanical consequences of the seismically observed moment distribution, a more fundamental understanding of the rupture characteristics of the 1957 event, including more robust estimates of its rupture bounds, seismic moment, and slip distribution are needed.

In this study, we initially concentrate on describing the aftershock sequence of the 1957 event and tying these observations together with studies of recent seismicity and the spatial distribution of moment release during great earthquakes. The spatial distribution of moment release during the 1957 event will then be determined from an analysis of surface and bodywave observations.

Compilation of Travel-Time Observations

Since it appears to take several years for the rate of aftershock activity to return to the backround level and because we would ultimately like to compare the spatio-temperal distribution of the 1957 aftershock sequence with that of the 1986 event and the interseismic events (i.e., those occurring after 1963) already relocated by Engdahl et al. [1989] we will relocate events that occurred between 1957 and 1963. Unfortunately, the travel-time observations listed in both the *ISS* and the *BCIS* for this time period are not available in computer readable form. This problem is also complicated by the fact that several apparently large events ($m_b > 5.0$) are not included in the *ISS* but are included in the *BCIS*. We have, therefore, compiled a list of all the known events along the Aleutian Arc and are beginning to tabulate, and enter the appropriate travel-time observations. To facilitate data entry we are experimenting with, and hope to employ Optical Character Recognition software.

Aftershock Relocations and Depths

Previous relocation efforts have either ignored the laterally varying velocity structure near the arc or accounted for it using the method of Joint Epicenter Determination (JED). Although JED locations are expected to be more consistent than single event locations, this procedure assumes that the source corrections applied to the location of each event are constant in a direction perpendicular to the arc. Many studies have shown, however, that the magnitude and direction of the earthquake mislocation vector can vary substantially with event position and recording station distribution. The relative mislocation of teleseismically recorded events can, however, be explained with the inclusion of a near-source velocity perturbation in the form of a high-velocity slab.

Using the slab geometry described by Boyd and Creager [1990] and Creager and Boyd [1990], we have calculated *P-wave* travel-time perturbations to 476 stations as a function of epicentral position. As a first pass, we are only considering shallow thrust earthquakes. As such, residuals are calculated assuming a source depth of 33 km. Differences in an event's actual source depth should not greatly affect the residual pattern since variations in source depth trade-off with origin time, but do not greatly affect epicentral estimates. The spatial variation in the theoretical travel-time residuals for two stations is shown in Figure 1. Notice that the residuals vary not only with changes in an event's arc-normal position, but also with changes in an event's along strike position. This is mainly a result of changes in the local strike and dip of the slab.

These calculated residuals will be used directly as epicentrally varying station corrections to generate relocated epicenters without additional ray tracing. We have performed preliminary locations on events listed in the *ISS* during the years 1961 through 1963. The relative relocations vectors for this set of events are shown in Figure 2. The relocations vectors are spatially consistent and amount to as much as 30 km. Preliminary relocations of the aftershock sequence will be presented at the Fall, 1990 AGU meeting.

Waveform Inversion for Mainshock Source Parameters

Ruff et al. [1985] constrained the spatial distribution of moment release for the 1957 event by inverting surface wave observations from Pietermaritzburg. Their results indicate that most of the seismic moment was released in the western 600 km of the rupture zone. We will repeat Ruff's inversion, but include additional observations. For example, we have found seismograms in the World Data Center A that might provide additional constraints. The most encouraging of these are records recorded on Wiechert seismometers at Abuyama, Japan. The vertical component contains unclipped R_1. Although the seismometer period is only 5 seconds, surface waves with periods of up to 40 seconds are clearly visible on the raw record. If after digitizing and low-pass filtering this record, significant energy can be seen at periods of greater than 50 seconds these observations will provide important constraints on distribution of moment release since Japanese stations are located along strike of the arc. We will also try to include the N/S component of the 30-90 seismometer recorded at Pasadena. This record shows clear R_3 and R_2 phases. We plan on presenting the preliminary results of this portion of study at the Fall, 1990 AGU meeting.

References

Boyd, T. M., and Creager, K. C., The Geometry of Aleutian Subduction: Three-Dimensional Seismic Imaging (submitted), *J. Geophys. Res.*, 1990

Creager, K. C., and T. M. Boyd, The Geometry of Aleutian Subduction: Three Dimensional Kinematic Flow Model (submitted), *J. Geophys. Res.*, 1990.

Engdahl, E. R., S. Billington, and C. Kisslinger, Teleseismically recorded seismicity before and after the May 7, 1986, Andreanof Islands, Alaska, earthquake, *J. Geophys. Res.*, *94*, 15,481-15,498, 1989.

Horowitz, F. G., and A. Ruina, Slip patterns in a spatially homogeneous fault model, *J. Geophys. Res.*, *94*, 10,279-10,298, 1989.

Houston, H., and E. R. Engdahl, A comparison of the spatio-temoral distribution of moment release for the 1986 Andreanof Islands earthquake with relocated seismicity, *Geophys. Res. Lett.*, *16*, 1,421-1,424, 1989.

Ruff, L., and H. Kanamori, The rupture process and asperity distribution of three great earthquake from long-period diffracted P-waves, *Phys. Earth and Planet. Inter.*, *31*, 202-230, 1983.

Ruff, L., H. Kanamori, and L. R. Sykes, The 1957 great Aleutian earthquake (abstract), *EOS*, *66*, 298, 1985.

Rundle, J. B., and H. Kanamori, Application of an inhomogeneous stress (patch) model to complex subduction zone earthquakes: A discrete interaction matrix approach, *J. Geophys. Res.*, *92*, 2606-2616, 1987.

Thachter, W., Oreder and diversity in the modes of Circum-Pacific earthquake recurrence, *J. Geophys. Res.*, *95*, 2609-2624, 1990.

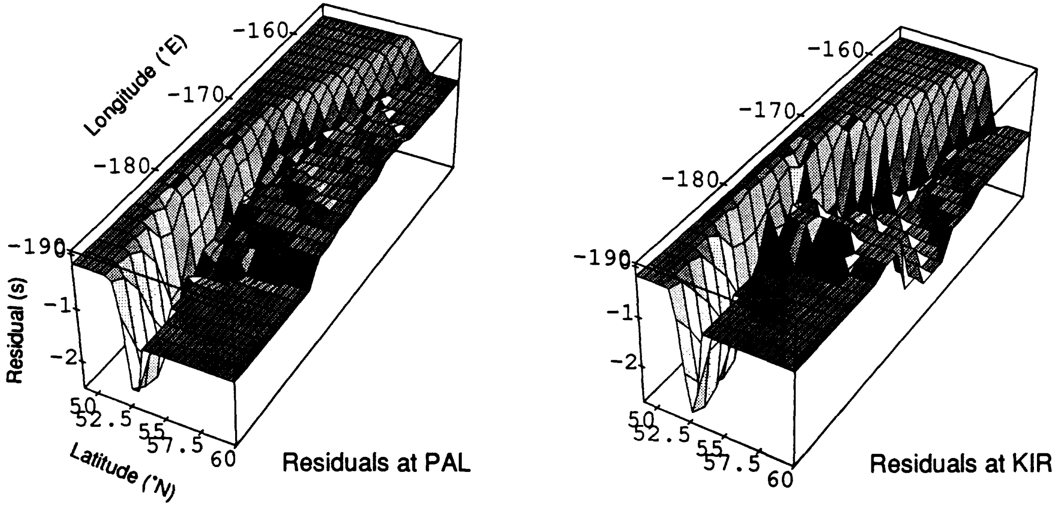

Figure 1: *P-wave* travel-time residuals calculated from the slab model of Creager and Boyd [1990] and Boyd and Creager [1990]. Residuals are calculated by assuming event positions that vary from the trench to 40 km north of the volcanic arc. Source depth is fixed to 33 km. The constant residual patterns observed to the north in each plot are artifacts of the limited spatial extent of event position.

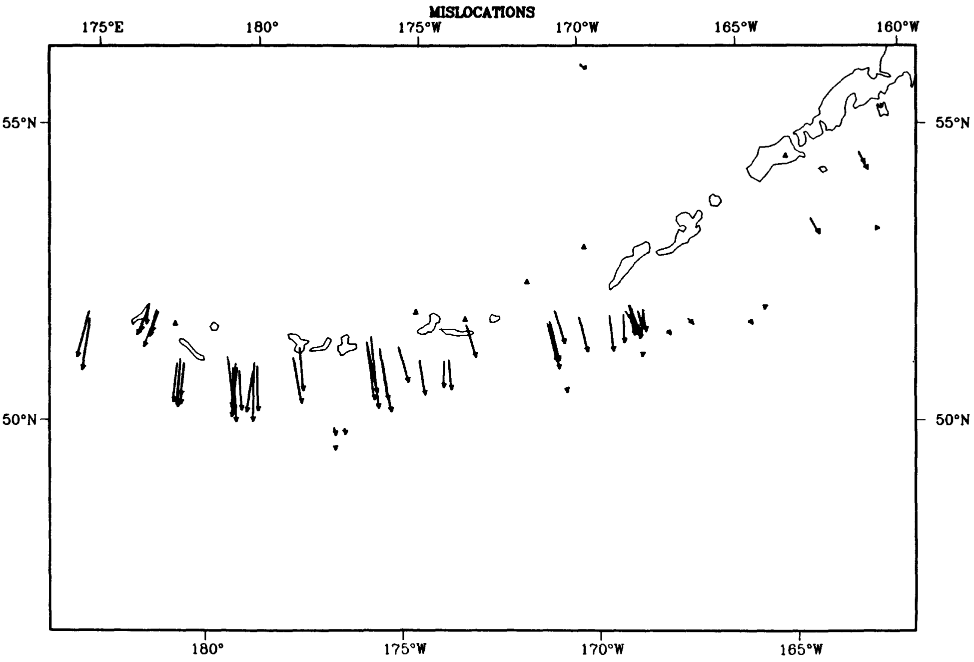

Figure 2: Relocation vectors computed for all of the events listed in the *ISC* between 1961 and 1963. Tail of each arrow is located at the spherically symetric earth model location. Each arrow points in the direction of the slab corrected location.

Earthquake Hazard Investigations in the Pacific Northwest

14-08-0001-G1803

R.S. Crosson and K.C. Creager
Geophysics Program
University of Washington
Seattle, WA 98195
(206) 543-8020

Investigations

The objective of this research is to investigate earthquake hazards in western Washington, including the possibility of a large subduction-style earthquake between the North American and Juan de Fuca plates. Improvement in our understanding of earthquake hazards is based on better understanding of the regional structure and tectonics. Current investigations by our research group focus on the configuration of the subducting Juan de Fuca plate, differences in characteristics of seismicity between the overlying North American and the subducting Juan de Fuca plates, kinematic modeling of deformation of the Juan de Fuca slab, and modeling of lateral velocity variations in the shallow crust. Accomplishments this quarter include final publication of the 3-D crustal velocity model for Puget Sound resulting from tomographic inversion of earthquake travel times, submission of an article describing a technique for incorporating gravity data as a constraint in the tomographic inversion of earthquake travel times for crustal structure, and publication of a paper on an automatic method for more accurate determination of teleseismic relative phase arrival times. We are continuing development of non-linear inversion techniques for use in the inversion of teleseismic travel times for deep structure of the Cascadia Subduction Zone. Research during this contract period concentrated on the following topics:

1. Investigation of anomalous phase arrivals from sub-crustal earthquakes.

2. Modeling of 3-D kinematic flow of the subducted slab.

Results

1. Anomalous Phase Arrivals

We are completing an investigation of the lower crust and uppermost mantle of western Washington using anomalous high amplitude phase arrivals at stations on the Olympic Peninsula from subcrustal earthquakes. These phases are observed at distances of 100-200 km for subcrustal earthquakes at south-east azimuths, and have apparent velocities of 5.8-6.2 km/s. We interpret these arrivals as resulting from energy trapped within the low-velocity subducting oceanic crust. We used 2-D raytracing to model these phase amplitudes and arrival times.

From observed P_n arrivals we find that, along a NW-SE azimuth, the subducting plate has an apparent dip of 8-11°. The observed 5.8-6.2 km/s velocity of the low velocity oceanic crust is somewhat lower than that observed in a similar study of Southwestern Japan, where subducting crust velocities of 6.8-7.0 km/s at around 40 km depth were obtained. The lower velocity observed in the subducting crust below western Washington may be related to a layer of metasediments being subducted within the basaltic crust as described by Cochrane et. al (1988, PAGEOPH, V.128, pp. 767-800), with the observed apparent velocities of the anomalous phases being an average of the two low velocity layers.

2. Slab Kinematics

Well-located subcrustal microseismicity recorded by the Washington Regional Seismograph Network (WRSN) since 1970 is concentrated in the Puget Sound Basin. The catalog of subcrustal earthquakes greater than magnitude 6 in Washington during the last century indicates an even more pronounced concentration of seismic moment release of events beneath the Puget Sound Basin; from Olympia, Washington to Victoria, British Columbia. Intra-slab moment release in this area is four orders of magnitude higher than to the north and south.

Wadati-Benioff zone seismicity dips 20° under central Vancouver Island, 10° across the Olympic Peninsula-Puget Sound area, and about 20° under Oregon, defining an arching slab geometry with the axis of the arch running east-west under Puget Sound. The arch coincides with the Olympic Mountains, a horseshoe-shaped, post-Eocene accretionary prism. This unusually wide and deep accretionary wedge extends 200 km from the deformation front, but is confined to less than 100 km along arc. To the north and south the prism is much smaller. All these observations seem to be related to the ~ 35° concave oceanward bend of the trench adjacent to the Olympic Peninsula. The subduction process forces an initially spherical shell of oceanic lithosphere to pass through the trench, whose curvature is backwards relative to most island arcs, and into the mantle. Even though the descending slab retains much of the strength it had as a tectonic plate, in-plane deformation is required to obtain the observed slab geometry. To explore the three-dimensional consequences of the concave oceanward trench, we have developed a numerical scheme to determine the kinematic flow field of a thin sheet of stiff fluid that enters the mantle along the trench at the known relative plate velocities, is constrained to remain on a given slab geometry, and minimizes various global norms of the in-plane strain rate tensor. Minimizing the integrated effective strain rate to the power [1+ 1/n] is equivalent to determining the flow field that minimizes the global dissipation power associated with internal deformation of the slab for a power rheology with power n. We constructed two basic models of the geometry based on constraints from subcrustal seismicity, receiver function analysis and marine seismic reflection data. We utilized a criteria of "least change of curvature" to interpolate at places where no direct geometric constraint is available. The 'constant dip' model has a uniform 20° dip along any cross section normal to the trench, while the 'arch' model has 20° dip under Vancouver Island and Oregon, but has a shallower 11° dip under the Olympic Peninsula and Puget Sound, adjacent to the bend in the trench. For all slab geometries and rheologies analyzed the calculated flow field is dominated by high values of along-strike compression concentrated landward of the bend in the trench. The region of high calculated strain rates is coincident with the region of high observed seismic activity. The largest in-plane strain rates are $10^{-16}s^{-1}$. The following effects have been examined in detail: (1). *Sphericity*. The compressional in-plane strain rates adjacent to the bend in the trench are a factor of two larger if the incoming lithosphere is a spherical shell than if it is planar. (2). *Arch*. The 'arch' model reduces the total dissipation power by a factor of 3 compared with the 'constant dip' model.

Fixing the dip to the north and south at 20°, we performed several calculations varying the dip along the arch axis and found that the minimum total integrated dissipation power occurs at a dip of 10-12°. Thus, the observed arch geometry matches the optimum slab configuration in the sense that it requires the least amount of in-plane deformation. (3.) *Non-linear rheology*. The experiments discussed above assume a linear Newtonian rheology, which is not likely to be appropriate for the cold core of a slab. We have extended the calculations to a power-law rheology with a power of n= 3.5 and n= 100000. The power law rheology has little effect on the pattern of strain rates, except to concentrate regions of peak strain rate, and to produce large areas of very small strain rates.

Articles

Boyd, T.M., and K.C. Creager, 1989 (revised), The geometry of Aleutian subduction: Three-dimensional seismic imaging, JGR.

Creager, K.C. and T.M. Boyd, 1989 (revised), The geometry of Aleutian subduction: Three-dimensional kinematic flow modeling, JGR.

Lees, J.M. and R.S. Crosson, 1989 (in press), Bayesian ART versus conjugate gradient methods in tomographic seismic imaging: An application at Mount St. Helens,

Washington, AMS-SIAM: Conference on spatial statistics and imaging - June, 1988.

Lees, J.M. and R.S. Crosson, 1989 (in press), Tomographic imaging of local earthquake delay times for 3-D velocity variation in western Washington, JGR

Lees, J.M. and J.C. VanDecar, (submitted to PAGeophys.), Seismic tomography constrained by Bouguer gravity anomalies, with application to western Washington, U.S.A..

VanDecar, J.C. and R. S. Crosson, 1990, Determination of teleseismic relative phase arrival times using multi-channel cross correlation and least squares, BSSA, V. 80, pp. 150-169.

Reports

Final Technical Report: 1989, 1990 (in preparation), Earthquake Hazard Research in the Pacific Northwest, USGS Grant # 14-08-0001-G1390.

Abstracts

Boyd, T.M., and K.C. Creager, 1989, Temperature dependence of seismicity within subducted slabs, EOS, V. 70, p. 1315.

Chiao, L.Y. and K.C. Creager, 1989, Kinematic deformation of the subducted Cascadia slab, EOS, V. 70, p. 1333.

Creager, K.C., L.Y. Chiao, and T.M. Boyd, 1989, In-plane slab deformation and seismic moment distributions, EOS, V. 70, p. 1315.

Crosson, R.S., 1989, Application of spectral constraints in tomography and linear inversion: extension to non-uniformly sampled models (abstract), EOS, V. 70, p. 1223.

Mundal, I., M. Ukawa, and R.S. Crosson, 1989 (submitted), Evidence of subducting Juan de Fuca plate in apparent velocities observed from subcrustal earthquakes, EOS, 1989 PNAGU.

Ukawa, M. and R.S. Crosson, 1989, Investigation of deep crustal and uppermost mantle structure in the Pacific Northwest through subcrustal earthquakes (abstract), EOS, V. 70, p. 1329.

VanDecar, J.C., R.S. Crosson, and K.C. Creager, 1990, Teleseismic Arrivals recorded over the Cascadia Subduction Zone: amplitude variation and Calibration of the Washington Regional Seismic Network, Seismol. Res. Lett., V. 61, p. 32.

Seismotectonics in the Northeastern United States

14-08-001-G1796

John E. Ebel
James W. Skehan, S.J.
David C. Roy
Weston Observatory
Dept. of Geology and Geophysics
Boston College
Weston, MA 02193
(617) 899-0950

Objective: The primary objective of this research is to improve the calculated locations of earthquake hypocenters in New England (particularly to better constrain the event focal depths) by relocating earthquakes using new network station travel-time residuals. These residuals are to be found from a time-term tomographic analysis of the P wave arrivals on the New England Seismic Network (NESN) stations from the 1984 Maine Seismic Refraction Profile (MSRP) and from the 1988 New York-New England Seismic Refraction Experiment (NY-NEX). The relocated earthquake hypocenters will be used to reexamine the present seismotectonics of the northeastern United States in an effort to identify seismically active structures in the region.

Data Preparation and Analysis: The time during the first 3 months of the contract has been spilt between reading the P wave arrival times from the NY-NEX blasts from the NESN stations and writing the computer code to perform the tomographic time-term analysis on the full data set. As part of reading the arrival times from the NESN stations, we are also accumulating measurements of S wave arrival times whenever possible. We hope to use those data to make some estimates of Poisson's ratios under the individual stations. The data analysis and computer programming are going on schedules and we hope to have this part of the analysis completed by June.

Preliminary Results: While we have no results from the data analysis yet to report, we do note from the NY-NEX waveforms from which we have read arrival times that many, but not all, of these refraction explosions gave easily recognized P-wave first arrivals at many stations. This gives us confidence in the accuracy of the source-receiver travel times which we have calculated. We have also seen a preliminary crustal model for the New England and Adirondack part of the NY-NEX profile as calculated by the U.S.G.S. from their instrumentation (W. Mooney and J. Luetgert, personal communication, 1989, 1990). We regard this work as vital to our own effort since we need to use the best available average crustal models as the starting input into our time-term tomographic analysis.

Investigation of the Late Quaternary Slip Rate of the Northern San Andreas Fault at the Vedanta Wind Gap, Marin County, California

NEHRP Contract 14-08-0001-G1777

N. Timothy Hall[1]
Tina M. Niemi[2]

Earth Sciences Associates
701 Welch Road
Palo Alto, California 94304

The 1906 trace of the San Andreas fault (SAF) at the Vedanta research site lies along the southwest base of a ridge of late Pleistocene terrace deposits here called the "medial ridge." The site of this paleoseismologic study is an abandoned water gap which was cut across the medial ridge in an orientation nearly orthogonal to the trend of the SAF. The following summarizes the past nine months of the project.

1. The results of the 1988 field season were written as a final technical report last summer. We have developed a preliminary reconstruction of the evolution of the wind gap that is based primarily on strata exposed in our 1988 trenches east of the SAF. If we assume late Holocene slip events on the SAF produced geomorphic changes similar to those documented after the 1906 earthquake, (slight subsidence of the western block and development of a shallow tectonic trough along the fault trace), then we can infer that these changes served to prevent Gravel Creek from flowing through the gap, at least temporarily. Based on this model, be are able to identify at least three pre-1906 episodes of faulting: between 2,000 and 1,900 B.P. (Figure 1, sketches 1 and 2), between 1,850 and 1,500-1,100 years B.P. (sketches 3 and 4), and between 1,100 years B.P. and 1906 (sketches 5 and 6). Channelized stream deposits located at the northern end of the wind gap at a depth of two meters are truncated on the west by the SAF. Wood and charcoal samples from this channel have been radiocarbon dated at 1,850±50 years B.P. The correlative channel presumably lies northwest of the wind gap and is now buried under marsh sediments. Our FY 1990 proposal focuses on investigating the northwest side of the SAF.

2. Trenching began at the Vedanta Wind Gap site on April 23, 1990. In order to dewater the marsh around the targeted area on the northwest side of the SAF, we deepened and extended a drainage ditch from the lower end of the marsh. During excavation of the ditch, we encountered well-preserved trees buried at various depths in the marsh. At least one tree lies across the SAF and appears to be offset by faulting. Orientation of the trees across the SAF and possible seismic events captured in their tree rings provide a unique opportunity to investigate both slip rate and recurrence intervals at this site.

---

[1] Now at: Geomatrix, One Market Plaza, Spear Street Tower, Suite 717, San Francisco, CA 94105

[2] Also at: Geology Department, Stanford University, Stanford, CA 94305

(PAGE 64 FOLLOWS)

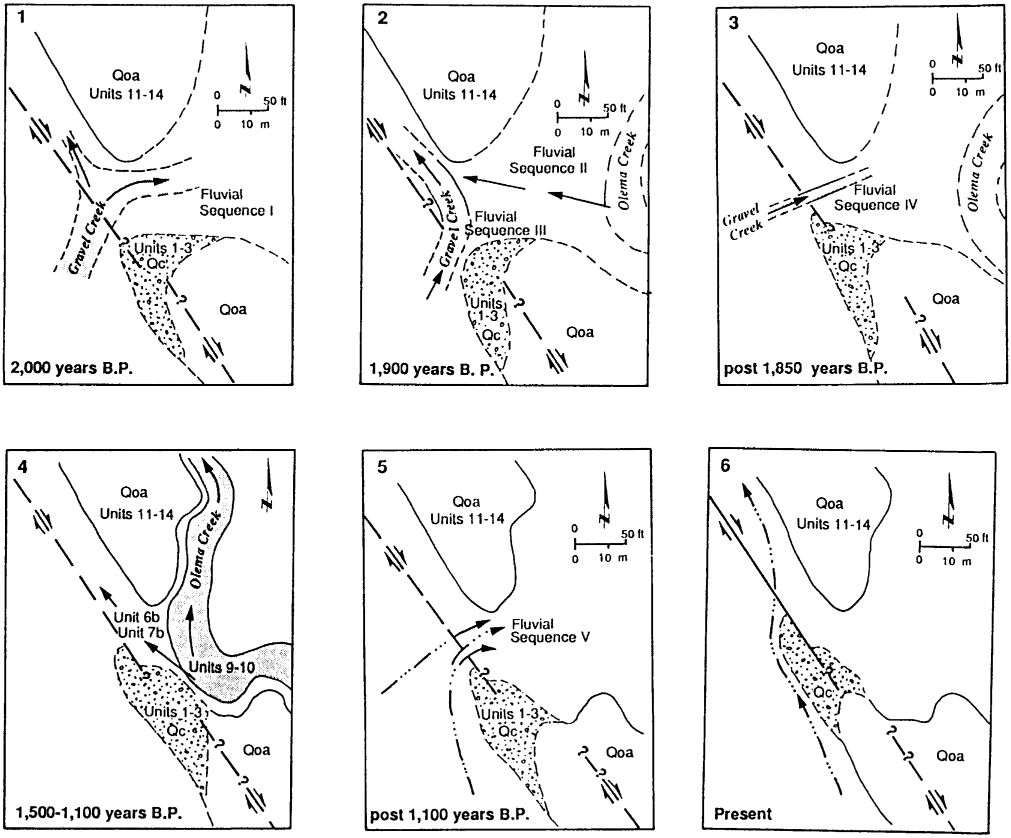

Figure 1: *Late Holocene evolution of the Vedanta wind gap. Qoa = older Quaternary terrace deposits; Qc = colluvial units.*

1. Gravel Creek deposits a sheet of gravel through the gap from west to east and fills a tectonic depression between the fault and the medial ridge.
2. Gravel Creek drains to the northwest parallel to the fault, but does not cross through the water gap, possibly as a response to temporary damming of the gap by colluvium and/or by local subsidence on the western block caused by slip on the SAF. A flood event on Olema Creek deposits crevasse splay sediments on the Pacific plate.
3. Gravel Creek erodes a channel across the north end of the gap depositing the gravels and wood of our target buried piercing point channel. Stream flow is from west to east across the San Andreas fault.
4. An Olema Creek meander cuts the deposits within the gap and deposits a point bar sequence. The deposits fine upward into floodplain silts. Gravel Creek is diverted to the northwest possibly by slip on the SAF.
5. Gravel Creek resumes flow from west to east across the gap and deposits a sheet of gravel.
6. Subsidence on the western block accompanying at least one pre-1906 slip event on the SAF causes abandonment of the water gap. At present, a tributary of Gravel Creek flows in a man-made ditch along the fault.

3. Publications to date include:

1990, Niemi, T.M., and Hall, N.T., The San Andreas Fault at the Vedanta Retreat, *in* B.J. Bilodeau and S. Davis, eds., *Geologic Guidebook to the Point Reyes Area, Northern California*, NCGS Field Trip #1: American Association of Petroleum Geologists Annual Meeting, SF, CA, June 3-6, 1990.

1989, Hall, N.T., and Niemi, T.M., Stop 1: Overview of the San Andreas Fault Valley and Stop 2: San Andreas Fault at the Vedanta Retreat, *in* C. Wahrhaftig, ed., *Geology of San Francisco and Vicinity*: Field Trip Guidebook T105, 28th International Geological Congress, p. 57.

1989, Niemi, T.M., and Hall, N.T., Subsurface Characteristics and Style of Faulting along the 1906 Trace of the San Andreas Fault at the Vedanta Wind Gap Site, Marin County, California (abst.): Cordilleran Section Meeting, Spokane, Washington, April 7-9, 1989, *Geological Society of America Abstracts with Programs,* v. 21, no. 5, p. 123.

4/30/90

Spatial and Temporal Patterns of Seismicity in the Garm Region, USSR: Applications to Earthquake Prediction and Collisional Tectonics

14-08-0001-G1382

Michael W. Hamburger, Gary L. Pavlis
Department of Geology, Indiana University
Bloomington, Indiana 47405
(812) 855-2934

Investigations

This program focuses on the highly active seismic zone between the Pamir and Tien Shan mountain belts in Soviet Central Asia. The Garm region is located directly atop the collisional boundary between the Indian and Eurasian plates, and is associated with a dense concentration of both shallow and intermediate-depth earthquakes. Since the early 1950's, Garm has been the home of the Complex Seismological Expedition (CSE), whose primary mission is the prediction of earthquakes in the USSR (Nersesov *et al.*, 1979). Beginning in 1975, the USGS, in cooperation with the CSE, has operated a telemetered seismic network nested within a stable CSE network that has operated in the area for over thirty years. The fundamental aims of the present research project are: (1) to elucidate the structures and processes involved in active deformation of the broad collisional plate boundary, and (2) to examine the temporal variations in seismicity near Garm, in the form of changing spatial, depth, and stress distribution of microearthquakes that precede larger events. The data base for this study includes the combined resources of the global, regional, and local seismic networks.

Results

The research reported here is based on two main data sources: (1) the *Soviet regional catalog* ("Earthquakes in the USSR," Acad. Sci. USSR), which covers an area of approximately 15° x 25° and includes over 30,000 events since 1962 (compiled in collaboration with D.W. Simpson, Lamont-Doherty Geol. Obs.), and (2) the *CSE network catalog,* which covers an area of about 2° square surrounding Garm, and includes over 90,000 events since the early 1950's. Our research during this period included collaborative studies with three visiting Soviet seismologists, A. Lukk, S. Yunga, and G. Popandopulo, who were working at Indiana University for the period January - March 1990. The work included research on velocity inversion using teleseismic travel time residuals, analysis of earthquake focal mechanisms, and earthquake relocation problems. We have also continued our work on analysis of aftershock properties of intermediate-depth earthquakes.

Teleseismic Travel Time Inversion. In collaboration with Alek Lukk (Institute of Physics of the Earth, Moscow), we have compiled traveltime data from 218 teleseismic earthquakes recorded at the Garm network stations, in order to obtain information on mid- to lower crustal velocities. These data have been augmented by arrival time data from fourteen regional seismic stations operating in the Pamir, in the Tadjik Depression, and in Afghanistan. We have begun work with a teleseismic inversion routine based on the work of Aki et al. (1977), and incorporated into Fortran code by Evans (1986). To date, we have succeeded in calculating travel time residuals from the raw arrival time data, removing unreliable readings, and examining azimuthal characteristics of the traveltime residuals. Based on our preliminary results, we are reexamining the original seismograms for teleseismic arrival times; we anticipate obtaining a three-dimensional velocity model for the crust and upper mantle of the Garm region by the fall of this year.

Earthquake Focal Mechanisms. As a result of our collaboration with Sergei Yunga and Alek Lukk (Institute of Physics of the Earth, Moscow), we have gained access to a remarkable data base of earthquake focal mechanisms from the Garm network. The Soviet seismologists have accumulated over 15,000 earthquake focal mechanisms in this area (Lukk and Yunga, 1988). As part of the bilateral exchange, we have gained access to both the focal mechanism solutions and the first motion data on which the solutions are based. Our work to date has included comparison of Soviet and American techniques in focal mechanism determination (to examine the influence of local velocity structure, earthquake relocation, and computational algorithms on mechanism determination) and seismotectonic analysis of average mechanism characteristics.

Single-event mechanism solutions for the larger events in the data base (magnitudes greater than 3.0) are summarized in Figure 1. We observe a remarkable uniformity to the mechanisms, which are dominated by thrust- and strike-slip fault plane solutions. The mechanisms' P-axes generally trend north-northwest to northwest, with a gradual fanning out of the stress axes about the syntaxis of the Pamir. We have also redetermined focal mechanisms for 3380 events for the period 1980-1987, using the American program FPFIT (Reasenberg and Oppenheimer, 1985). Significant differences were observed for approximately 30% of the events examined, and the discrepancies increased for events located outside the network. What was somewhat surprising was that despite significant discrepancies for individual events, the average stress tensor determined for the overall region, as well as those for individual sub-areas, proved to be highly stable. Average orientations of P- and T-axes, for instance, seldom differed by more than 2 degrees. This result suggests that while individual earthquake focal mechanism determinations may be subject to significant random errors, there are few systematic errors that influence the determination of the overall stress field. The results thus provides support for Lukk and Yunga's (1988) summary of stress orientations within the Garm region, which documented subhorizontal compression as the dominant component of the stress system acting throughout the region.

Earthquake Relocations. As part of our collaborative work with Gyorgi Popandopulo (Institute of Physics of the Earth, Moscow), we have been studying a new algorithm that permits resolution of three-dimensional P and S velocity structure and earthquake location in the presence of significant lateral inhomogeneity in the earth's crust (Popandopulo *et al.*, 1990). The VELGA algorithm has been applied to seismotectonic and earthquake prediction problems in the Garm region. We have compared the results with those obtained using U.S. 1-D velocity inversion and earthquake location programs (VELEST and HYPOELLIPSE). The VELGA algorithm offers several distinct advantages over other earthquake location and velocity inversion schemes: (1) the program takes advantage of all available arrival time data, rather than being restricted to a small group of well constrained hypocenters. In the case of the Garm study, we used over 80,000 earthquake locations and over 1,200,000 arrival time data to constrain the velocity structure; (2) The program requires no *a priori* knowledge of the velocity structure of the region; (3) because the program uses iterative, rather than simultaneous, inversion for velocity structure and earthquake location, it is not extraordinarily demanding of computer speed or memory; (4) the use of a laterally varying velocity structure appears to circumvent the pitfalls common to one-dimensional, single-event location algorithms, in which earthquake hypocenters tend to cluster around layer boundaries; (5) the use of the entire 30-year data base permits resolution of temporal variations in P- and S-wave velocity that may be associated with precursory deformation prior to major earthquakes; (6) because the program works with effective, rather than absolute, velocities, it does not require sophisticated 3-D ray-tracing subroutines to calculate travel times; and (7) the program works with S-P times, rather than with absolute P or S arrival times, making the earthquake locations less affected by timing errors at individual stations.

As an independent test of the VELGA algorithm, we have relocated hypocenters recorded by the Garm network, using the single-event location algorithm HYPOELLIPSE (Lahr, 1986). In general, well recorded earthquakes within the seismic network show little difference between the two location schemes (Figure 2). In general, the discrepancies increase at the fringes of the network, increasing to 5 km or more. Over 80% of the events compared showed epicentral discrepancies less than 2 km. A small number of events show larger deviations, which may be attributable to very poorly constrained events. In general, the VELGA events are systematically offset to the south relative to the HYPOELLIPSE events. This is likely to result from lateral velocity heterogeneities within the study area, possibly accounted for by the 3-D velocity model used by VELGA.

Aftershock Properties of Intermediate-Depth Earthquakes. In our previous NEHRP Technical Report we presented evidence that confirms Lukk's (1968) observation that earthquakes in the Pamir-Hindu Kush region are followed by clear mainshock-aftershock sequences. This observation is remarkable as the events involved have focal depths of approximately 200 km, contradicting the widely held view that deep earthquakes do not have aftershock sequences (e.g., Page, 1968). Building on the overview of Central Asia aftershock properties of Thomas (1989), Pavlis et al. (1989) examined seismicity associated with all intermediate-depth earthquakes with magnitude larger than 5.5 for the period 1962-1984. They examined these sequences by two different methods: (1) a qualitative method based on examination of epicentral maps to discriminate space-time clustering of earthquakes after a large earthquake, and (2) a quantitative method based on a robust estimator of a Poisson rate. They found that of the 36 earthquakes examined 16 showed no evidence of aftershock behaviour, 15 showed subtle suggestions of aftershock behaviour, and only 3 were followed by unambiguous aftershock sequences. The three clear aftershock sequences, however, show a remarkable property seen in Figure 3: they all occurred in essentially the same place at an interval of approximately 9 years. Furthermore, the aftershock seismicity that follows these large events is primarily associated with an persistent nest of earthquakes that occurs near a major change in strike of the Pamir-Hindu Kush seismic zone, at approximately 36.5°N and 70.4°E. We suggest that the aftershock behaviour of these large, intermediate-depth earthquakes is probably caused by the transient load applied to this nest by the disruption of the local stress field following the mainshock. This transient load could trigger increased activity in the nest which would decay with time as the load was relaxed.

References

Aki, K., A. Christofferson, and E. Husebeye, 1977, Determination of the three-dimensional seismic structure of the lithosphere, *J. Geophys. Res., 82,* 277-296.

Evans, J. R., 1986, Teleseismic traveltime residual analysis system: A user's manual, unpublished computer documentation, Draft Dec. 31, 1986.

Lukk, A. A., 1968, Aftershock sequence of the Dzhurm deep-focus earthquake of 14 March 1965, *Izvestiya, Physics of the Solid Earth, 5,* 83-85.

Lukk, A. A., and S. L. Yunga, 1988, Stress-strain state of the earth's crust in the Garm region (II): Results of reconstructions [in Russian], *Izvestiya, Fiziki Zemli, 24:7,* 10-22

Nersesov. I.L., Yu, P. Skovorodkin, and T.V. Guseva, 1979, Results of complex studies in the Garm geodynamic polygon, *Izvestiya, Physics of the Solid Earth, 15:4,* 47-55.

Page, R., 1968, Focal depths of aftershocks, *J. Geophys. Res., 73,* 12-16.

Pavlis, G.L., M.W. Hamburger and M.W. Thomas, 1989, Aftershock sequences associated with intermediate-depth earthquakes in the Pamir-Hindu Kush region [abstract], *EOS Trans. Am. Geophys. Un.,* in press.

Popandopulo, G.A., M.W. Hamburger and G.L. Pavlis, 1990, An iterative approach to inversion for 3-D velocity structure and earthquake location *[abstract],* IRIS Annual Meeting, Hilton Head, S.C., 5-7 March 1990.

Reasenberg, P.A. and D. Oppenheimer, 1985, FPFIT, FPPLOT, and FPPAGE: Fortran computer programs for calculating and displaying earthquake fault-plane solutions, *U.S. Geol. Surv. Open-file Rept. 85-739,* 108 pp.

Thomas, M.W., 1989, Temporal distribution of seismic activity within the Soviet regional earthquake catalog, Central Asia, M.S. thesis, Indiana University, 149 pp.

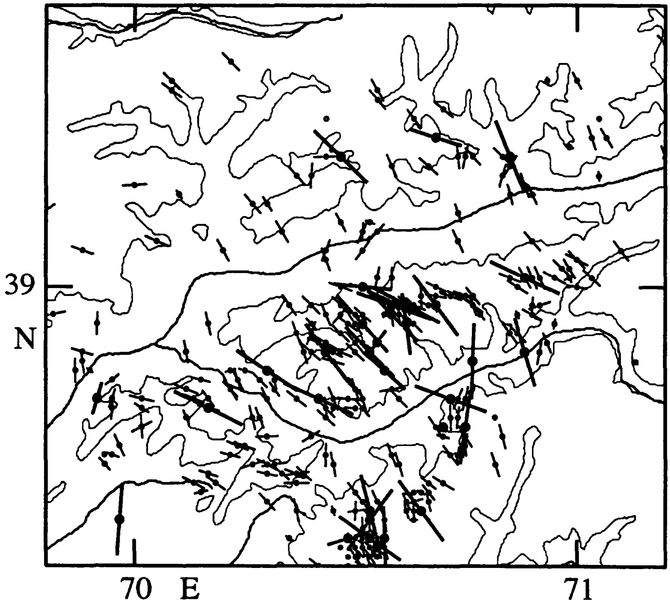

Figure 1. Earthquake focal mechanism solutions for moderate-sized events ($M_L \geq 3.0$) in the Garm region, 1971-1988. Shown are the horizontal projections of the axes of maximum compression of earthquake mechanisms determined by Lukk and Yunga (1988). Small symbols indicate earthquakes with $3.0 \leq M_L \leq 4.0$; large symbols indicate earthquakes with $M_L \geq 4.0$. Light lines indicate the 9000 foot topographic contour, and heavy lines indicate rivers.

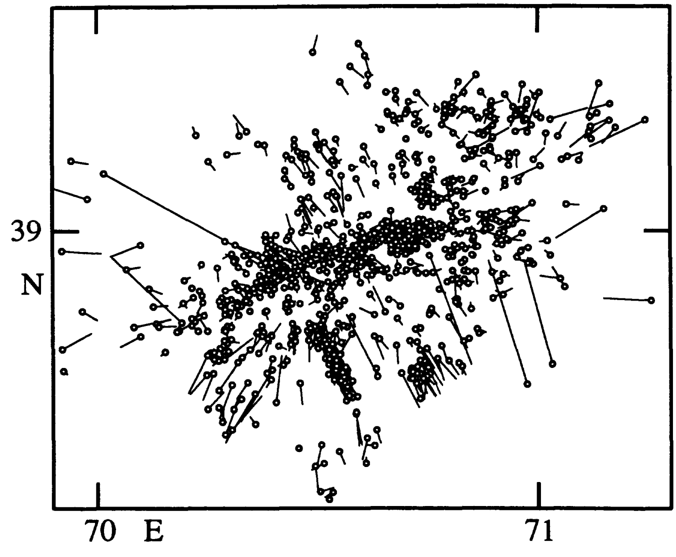

Figure 2. Comparison of earthquake locations determined by VELGA (ends of line segments) and HYPOELLIPSE (open circles) for a single year (1980). The map area is approximately the same as in Figure 1.

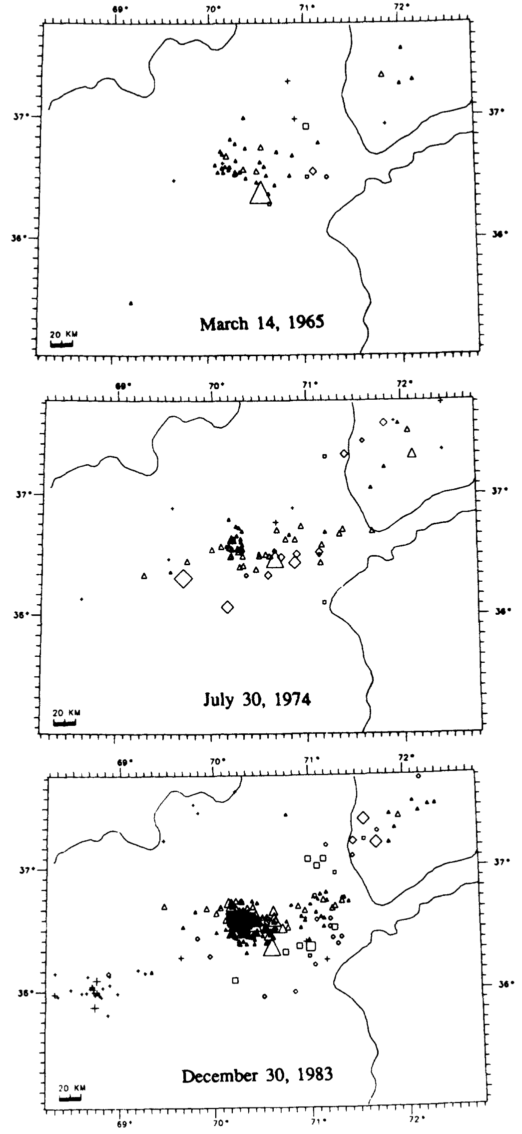

March 14, 1965

July 30, 1974

December 30, 1983

Figure 3. Intermediate-depth aftershock sequences in the Pamir-Hindu Kush region. Shown are map views of aftershocks of the three clear sequences we have identified in this region. Dates listed are those on which the mainshock occurred. Time period shown in each map is from the beginning of the sequence until the seismicity rate drops below the mean background rate at a 95% confidence level. Symbols are keyed by depth: crosses, $h < 50$ km; squares, $50 \leq h < 100$; diamonds, $100 \leq h < 150$; triangles ≥ 150. Symbol size increases with magnitude. Light line indicates the Afghan border.

Analysis of Earthquake Data from the Greater Los Angeles Basin and Adjacent Offshore Area, Southern California

#14-08-0001-G1761

Egill Hauksson

Seismological Laboratory,
California Institute of Technology,
Pasadena, CA 91125
818-356 6954

INVESTIGATIONS

Seismotectonic analysis of earthquake data recorded by the CIT/USGS and USC networks during the last 15 years in the greater Los Angeles basin. Improve models of the velocity structure to obtain more accurate earthquake locations including depth and to determine focal mechanisms. Studies of the earthquake potential and the detailed patterns of faulting along major faults in the metropolitan area and adjacent regions.

A comprehensive study entitled: *Earthquakes, faulting and stress in the Los Angeles basin* , has been accepted for publication in Journal of Geophysical Research.

RESULTS

State of Stress in the Los Angeles Basin

The seismicity, active faulting and folding in the Los Angeles basin are caused by a regional tectonic stress field. Close correspondence between the orientations of the P- and T-axes from focal mechanisms and borehole breakouts determined by Mount [1989] is observed. For instance, at the northern end of the Newport-Inglewood fault both the thrust focal mechanisms and the borehole breakout data show northeast to east-northeast trending P-axes. This suggests that the trends of the principal stress axes do not change significantly with depth and that borehole breakouts in the Los Angeles basin although taken from shallow depth are representative of the tectonic stress field.

The P-axes show some spatial variations in orientation with mostly northerly trending azimuths along the north and eastern sides of the basin but more northeasterly azimuths in the southwest. A similar variation can be seen in the azimuths of fold axes. The fold axes were grouped into three sets of sliding windows along latitudes 33° 42', 33° 52', and 34° 2'. These overlapping windows, with a constant radius of 23 km, are spaced 23 and 22 km apart in longitudinal and latitudinal direction, respectively. Azimuths of fold axes within these windows plotted in rose diagrams show how fold axes in the north and the eastern parts of the basin have azimuths that differ about 30-40° from azimuths of fold axes in the southwestern part of the basin.

The P- and T-axes or fold axes alone, however, do not adequately represent the local stress field, because the trend of the P-axes can differ from the maximum principal stress by 45° [McKenzie, 1969]. To determine the average deviatoric stress field in the Los Angeles basin the data set of focal mechanisms was inverted for the orientations of the principal stresses and their relative magnitude. Furthermore, to determine spatial variations in the deviatoric stress field across the basin the data set was divided up into 15 spatial groups and each group was inverted separately.

The Whole Data Set

The stereonet plots in Figure 1 show the data and the directions of the maximum principal stresses with 95% confidence limits obtained from the inversion. As discussed earlier these stresses were calculated by selecting one of the two nodal planes from each focal mechanism as the actual fault plane. The 95% confidence limits were calculated assuming that 30% of the planes were picked incorrectly. The average stress state in the Los Angeles basin has a maximum horizontal principal stress with an azimuth of 13°±3° and a vertical intermediate stress axis. The value of ϕ=0.22 shows that the relative magnitudes of the three principal stresses are all different, with S_2-S_3 smaller than S_1-S_3 indicating a small but significant thrust faulting component. This stress state reflects the coexistence of strike-slip and thrust faulting regime in the basin. This is also consistent with the prominent late Quaternary strike-slip faults and the strike-slip faulting observed for more than half of the focal mechanisms. This stress state is also consistent with previous results obtained for the Newport-Inglewood fault [Hauksson, 1987], Santa Monica Bay [Saldivar and Hauksson, 1989], and San Fernando aftershocks [Gephart and Forsyth, 1984]. This stress state also fits within the average stress trajectories of central and southern California determined from borehole breakouts by Mount [1989].

Spatial Stress Variations

To determine the spatial distribution of stress within the Los Angeles basin the slip vectors from the 244 focal mechanisms were grouped into three sets of sliding windows, like the fold axes, along latitudes 33° 42', 33° 52', and 34° 2'. These overlapping windows, with a constant radius of 23 km, are spaced 23 and 22 km apart in longitudinal and latitudinal direction, respectively. The overlapping windows provide increased stability of the stress inversion, and some smoothing of the stress field. The stereonet projections of the selected planes and slip vectors for each window are shown in Figure 2. Each projection is plotted at the origin of the circle of 23 km radius that was used to select data for the inversion. The orientations of the maximum principal stress axes and the associated 95% confidence limits determined assuming 30% of the planes were picked incorrectly are shown for the 15 data sets in Figure 3. The large misfit angles from the stress inversions for events in the southwestern part of the basin are caused mostly by the normal faulting mechanisms. This suggests that the normal faulting mechanisms are caused by localized spatial variations in the stress field and further supports the interpretation that the normal faulting reflects local geometric readjustments.

The state of stress varies significantly across the Los Angeles basin. The most important spatial variation in the state of stress is the variation from N1°W to N31°E in the trend of the maximum principal stress. The east side of the basin has a nearly north trending maximum principal stress. From east to west, along the northern edge of the basin the principal stress rotates to the east from 0° to 13°. This is also consistent with the orientation of the fold axes along the northern flank.

The 32° variation in azimuth of the maximum principal stress, from a north trending axis to a northeast trending axis, occurs between the northeast basin and the southern segment of the Newport-Inglewood fault and the San Pedro Bay. This deviation is statistically significant because the 95% confidence limits do not overlap, and shows that a different stress state exists in the southwest part of the Los Angeles basin. Fold axes in San Pedro Bay have a more northwesterly trend than observed elsewhere in the Los Angeles basin. The agreement between average trends of fold axes (shown as petals in Figure 3) and the trend of the minimum horizontal principal stress suggests that the current stress field has existed over the lifetime of the folds or for the last 2-4 Ma [e.g., Davis et al., 1989].

The second most important spatial variation in the stress field is the variation in ϕ or the relative magnitude of S_2 and S_3, which shows where strike-slip faulting and thrust faulting dominate in the basin (Figure 3). In the central part of the basin and along its eastern edge, ϕ=0.25-0.49 (i.e., S_2 is significantly larger than S_3), and the plunge of S_2 is close to 90° so that the stress state is equivalent to strike-slip faulting. Along the Elysian Park and the Torrance-Wilmington fold and thrust belt, ϕ=0.08-0.25 (i.e. S_2 is approximately equal in magnitude to S_3), so the stress state is equivalent to thrust faulting. These spatial variations in the magnitudes and orientations of the principal stresses suggest that the flanks of the basin locally influence the state of stress.

PUBLICATIONS and REPORTS

Jones, Lucile, Kerry E. Sieh, Egill Hauksson, and L. Katherine Hutton, The 3 December 1988 Pasadena, California, earthquake: evidence for strike-slip motion on the Raymond fault, *Bull. Seismo. Soc. Am., 80,* No. 2, 474-482, 1990.

Hauksson, E., Earthquakes, active faulting,and stress in the Los Angeles Basin, J. Geophys. Res., in press, 1990.

Hauksson, E., Comparison of broad-band waveforms of local earthquakes recorded at crystalline and sedimentary rock sites in the Los Angeles basin, presented at fall AGU meeting, 1989.

Robertson, M. C., and E. Hauksson, Three-dimensional fine velocity structure of the Los Angeles basin, presented fall AGU meeting, 1989.

Hauksson, E. The 1993 Long Beach earthquake and its aftershocks, (Abstract), Seis. Res. Letters, 61, 42, 1990.

LOS ANGELES BASIN : STRESS STATE
30% OF FAULT PLANES ASSUMED PICKED INCORRECTLY

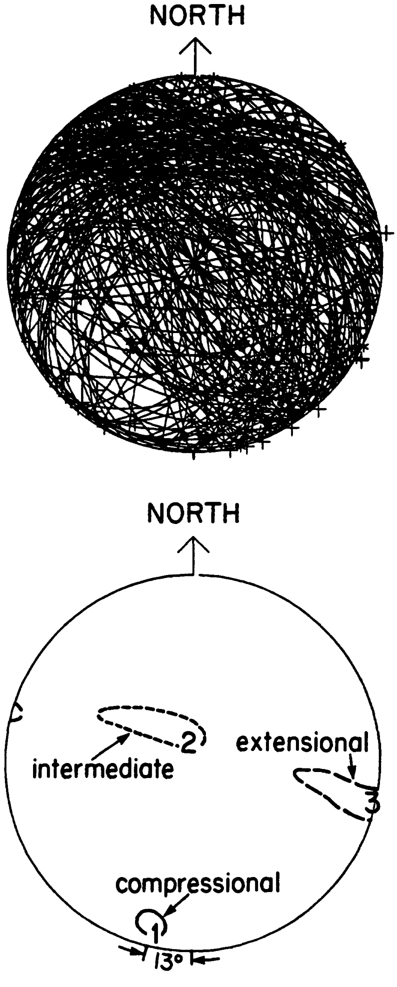

Figure 1. Data from the 244 focal mechanisms and results from the stress inversion. (a) lower hemisphere projection of all selected nodal planes (one from each focal mechanisms). Location of the slip vector is shown on each nodal plane as a plus symbol (with a normal component) or a star (with a thrust component). (b) The orientations of the principal stress axes with 95% confidence areas, determined assuming that 30% of the planes were picked incorrectly, indicated with solid, heavy dashed or light dashed lines. 1, 2, and 3 are the maximum, intermediate and minimum principal stress axes.

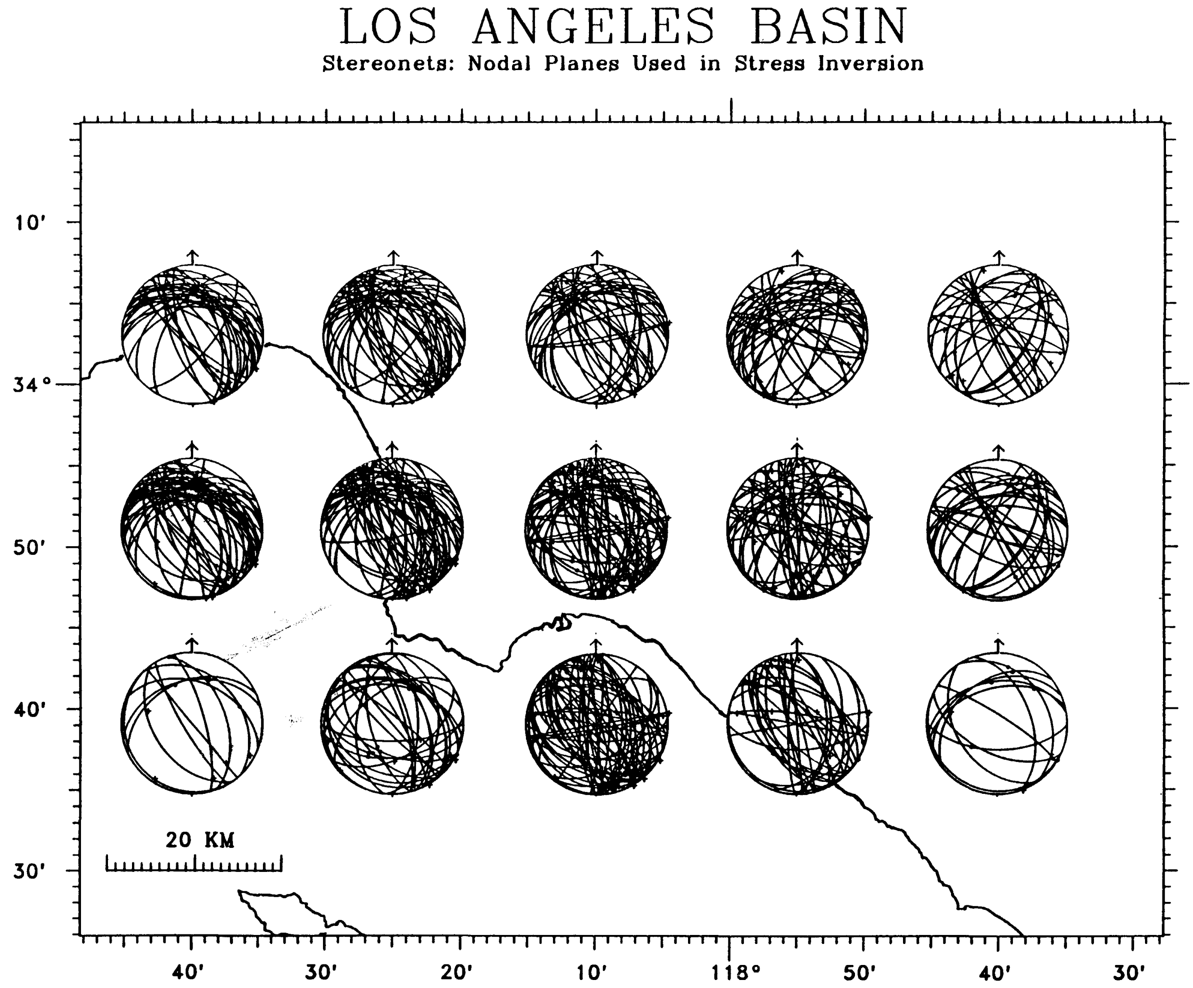

Figure 2. Map showing the 15 data sets inverted for the stress field. See also caption of Figure 1a.

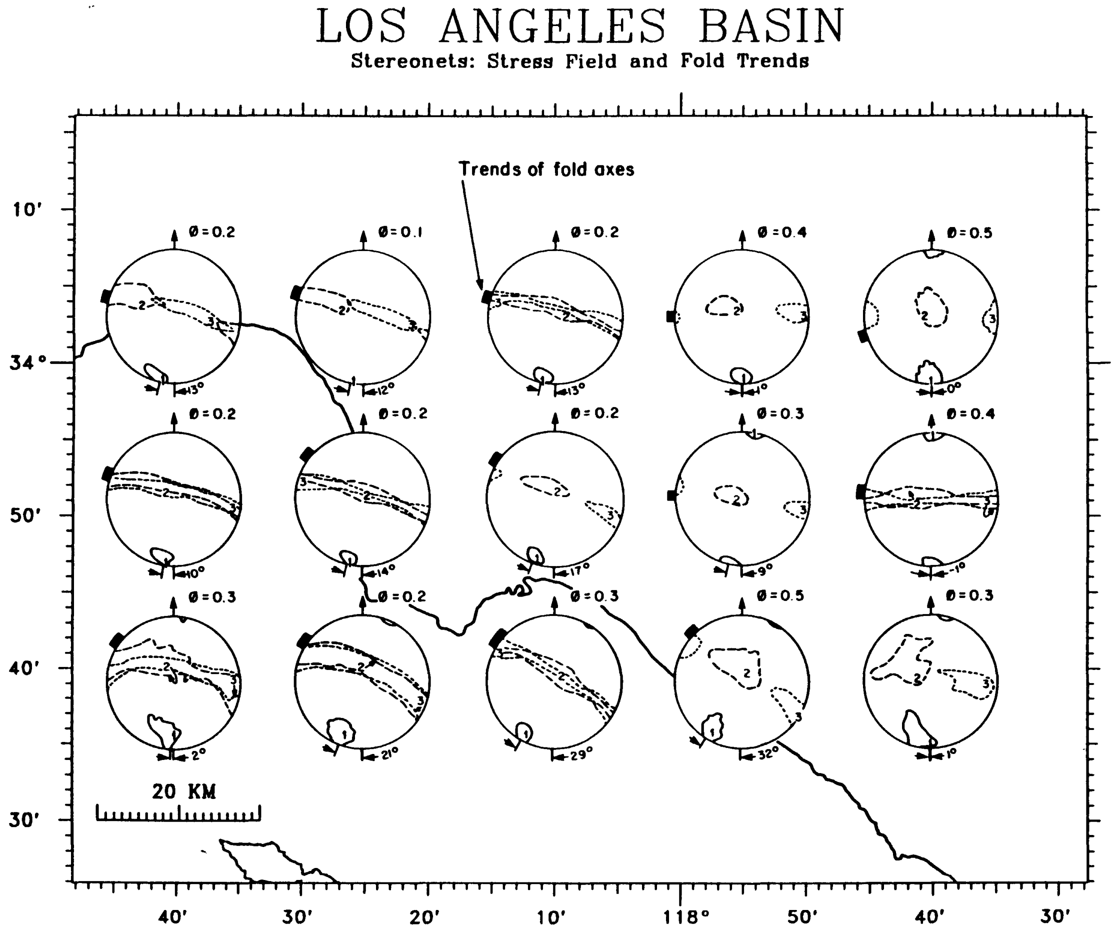

Figure 3. Map showing the stress field in stereonet projection at the 15 sites. The largest petals from each of the rose diagrams of fold orientation are also shown as petals on the outside of each stereonet circle. See also caption of Figure 1b.

Source Characteristics of California Earthquakes and Attenuation Effects

14-08-001-G1872

Donald V. Helmberger
Seismological Laboratory
California Institute of Technology
Pasadena, CA 91125
(818)356-6998

Investigations: Our long term objective is to determine the characteristics of earthquakes occurring in Southern California. The basic strategy has been to study the larger modern events since they are well-recorded and then to compare the records from these events (Masters) to interpret historic events or recent ones to obtain quick preliminary results. The primary data sets for these studies are the PAS (low gain recording), long term running teleseismic stations such as DeBilt, starting in 1917, some local strong motion recordings (SMA's), and some of the older Caltech array (wa.sp). Essentially we think better locations can be obtained using a combination of waveform data and travel time constraints.

Two approaches will be applied to these four basic data sets in source determination, namely empirical (using observed records as Green's functions) and completely theoretical (local models fitting particular events and hoping that Green's function computed for neighboring distances are accurate). We think that there are some regions now that are well enough modeled to make these approaches powerful enough to simply invert the smaller events, 5 to 3.5, directly given one three component station and fitting portions of records.

Three manuscripts are presently in press, see references, titled:
a) Broad-band modeling of local earthquakes.
b) Rupture process of the 1987 Superstition Hills earthquake from the inversion of strong motion data.
c) A re-examination of historic earthquakes in the San Jacinto fault zone, California.

Results: The first of these concerns the modeling the Upland events on the Pasadena broad-band, high dynamic range instrument. The Upland area has had two earthquake sequences with mainshock magnitudes of M=4.6 and M=5.5, the first in June 1988 and the second started on 28 February 1990. The second sequence is very rich in aftershocks with continuing activity, see figures 1 and 2.

At long periods the largest event of the l988 sequence, namely the June 26 event (M_L=4.6) located at 6 km depth, and the 1990 mainshock are very similar in waveform and can be modeled with the 1988 focal mechanism (ϕ=220, δ=40, λ=8), see figure 3. First motion studies from the Caltech-USGS array provide a slightly different focal mechanism for the 1990 event relative to the 1988 event, namely the dip is steeper (ϕ=220, δ=70, λ=0). We obtain better fits to the waveform data using the 1988 mechanism and it seems that these two sequences are very similar in source orientation.

The second paper concerns a pair of significant earthquakes on conjugate faults in western Imperial Valley. The first event was located on the Elmore Ranch fault, M_S=6.2, and the larger event on the Superstition Hills fault, M_S=6.6. the latter event is seen as a doublet teleseismically with the amplitudes in the ratio of 1:2 and delayed by about 8 seconds. This 8 second delay is also seen in about a dozen strong motion records. These strong motion records are used in a constrained least-squares inversion scheme to determine the distribution of slip on a two-dimensional fault. Upon closer examination, the first of the doublets was found to be itself complex requiring two episodes of slip. Thus, the rupture model was allowed to have three separate subevents, treated as separate ruptures, with independent locations and start times. The best fits were obtained when all three events initiated at the northwestern end of the fault near the intersection of the cross-fault. Their respective delays are 2.1 and 8.6 seconds relative to the first subevent, and their moments are 0.4, 0.8 and 4.0 x 10^{25} dyne-cm which is about half of that seen teleseismically. This slip distribution suggests multi-rupturing of a single asperity with stress drops of 60, 200 and 15 bars, respectively. The first two subevents were confined to a small area around the epicenter while the third propagated 18 km southwestward, compatible with the teleseismic and afterslip observations.

The third paper relocates and provides estimates of historic earthquakes in the western Imperial valley. The historic events considered occurred in 1937, 1942 and 1954. the recent events consist of the 1968 Borrego Mountain, 1969 Coyote Mountain, and 1987 Elmore Ranch earthquakes. We use regional and teleseismic data from continuously operating stations, with Pasadena, De Bilt, Ottawa and St. Louis recording most of the events. The waveforms imply that all the events. The waveforms imply that all the events are almost pure strike-slip events on vertical or near-vertical faults. The earthquakes are relocated by comparing S-P and surface wave -S travel times of historic events with the presumably well-located recent events. The moment estimates are obtained by direct comparison of the maximum amplitudes. The moment estimates imply that the 1968 and not the 1942 earthquake is the largest to have occurred in the region this century. Previous magnitude estimates suggested the 1942 event was the largest. The relocations change in location for the 1954 event and a larger adjustment in the I942 epicenter. It also appears that the 1969 earthquake may have been mislocated.

<u>References</u>:

Bent, A. L. and D. V. Helmberger (1990). A re-examination of historic earthquakes in the San Jacinto fault zone, California, submitted to BSSA.

Wald, D. J., D. V. Helmberger and S. H. Hartzell (1990). Rupture process of the 1987 Superstition Hills Earthquake from the inversion of strong motion data, BSSA (in press).

Dreger, D. S. and D. V. Helmberger (19990). Broad-band modeling of local earthquakes, BSSA (in press).

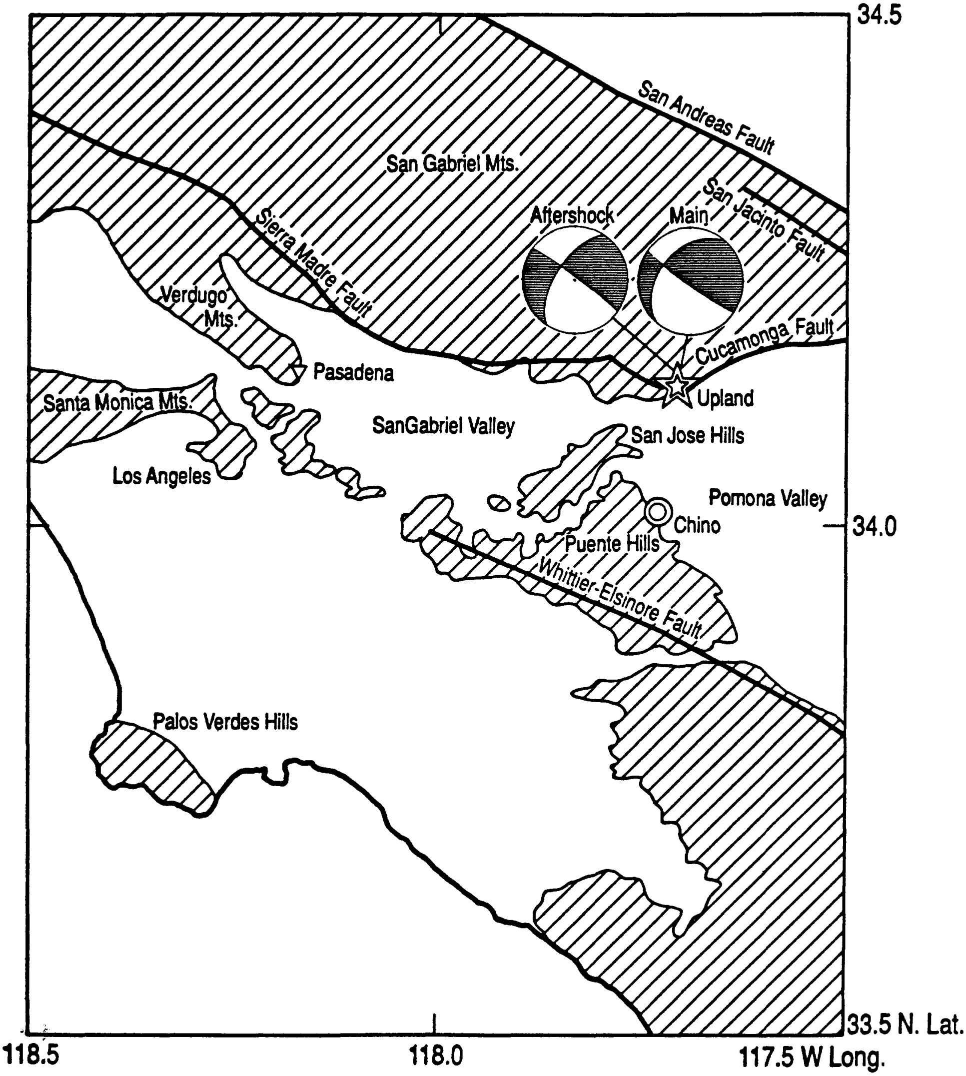

Figure 1. Locations Map: the inverted triangle is the Pasadena station, the circles mark the Chino events, and the stars denote the Upland events. Focal mechanisms for the two 1988 Upland events determined from USGS/Caltech seismic array first motion polarities are also given. Hatched regions represent areas of shallow or surficial basement rocks after Yerkes et al. (1965).

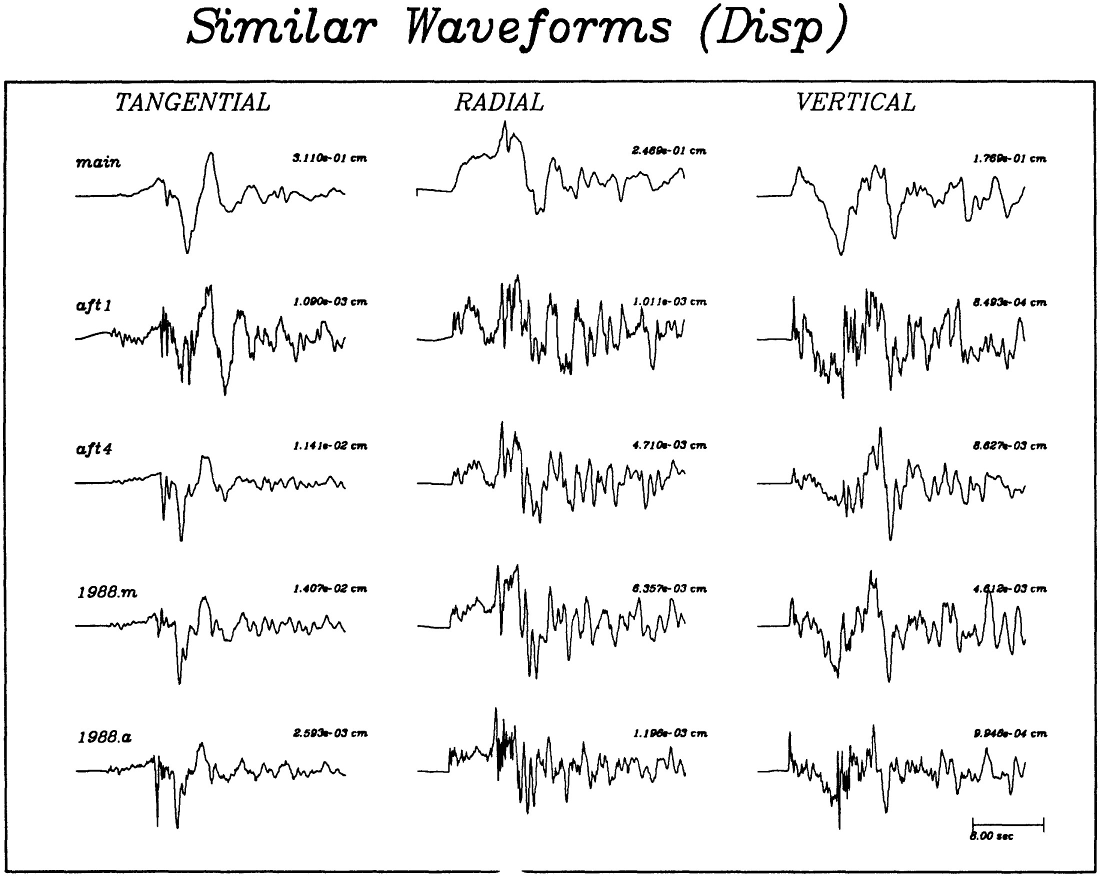

Figure 2. Comparisons of broad-band observations of a few Upland events occurring in 1988 (lower two) and 1990 (upper three). The 1988 mainshock had a magnitude of 4.6 and the aftershock a magnitude of 3.7. Note the relative event strengths of their peak displacements in cm. Synthetic seismograms computed for the best fitting model, see Dreger and Helmberger (1990), were used to estimate a long-period moment of $(6\pm 2)\times 10^{22}$ dyne-cm (M_L=4.6) and 1×10^{22} dyne-cm (M_L=3.7) with identical triangular source time durations of 0.3 seconds. Assuming the same fault dimension of 0.4 km from standard scaling laws, stress drop estimates of 410 and 70 bars are obtained for the two events, respectively. Generally, we found that it is possible to reproduce local waveforms at frequencies up to 1 Hz without a complete knowledge of fine structural detail. Resulting Green's functions can be useful in studying historic events, and in simulations of large events from a given source region. For example, we were able to determine the orientation and moment of the 1990 mainevent, mechanism similar to the 1988 mainevent and moment (M_o=1.7×10^{24} dyne-cm), within minutes.

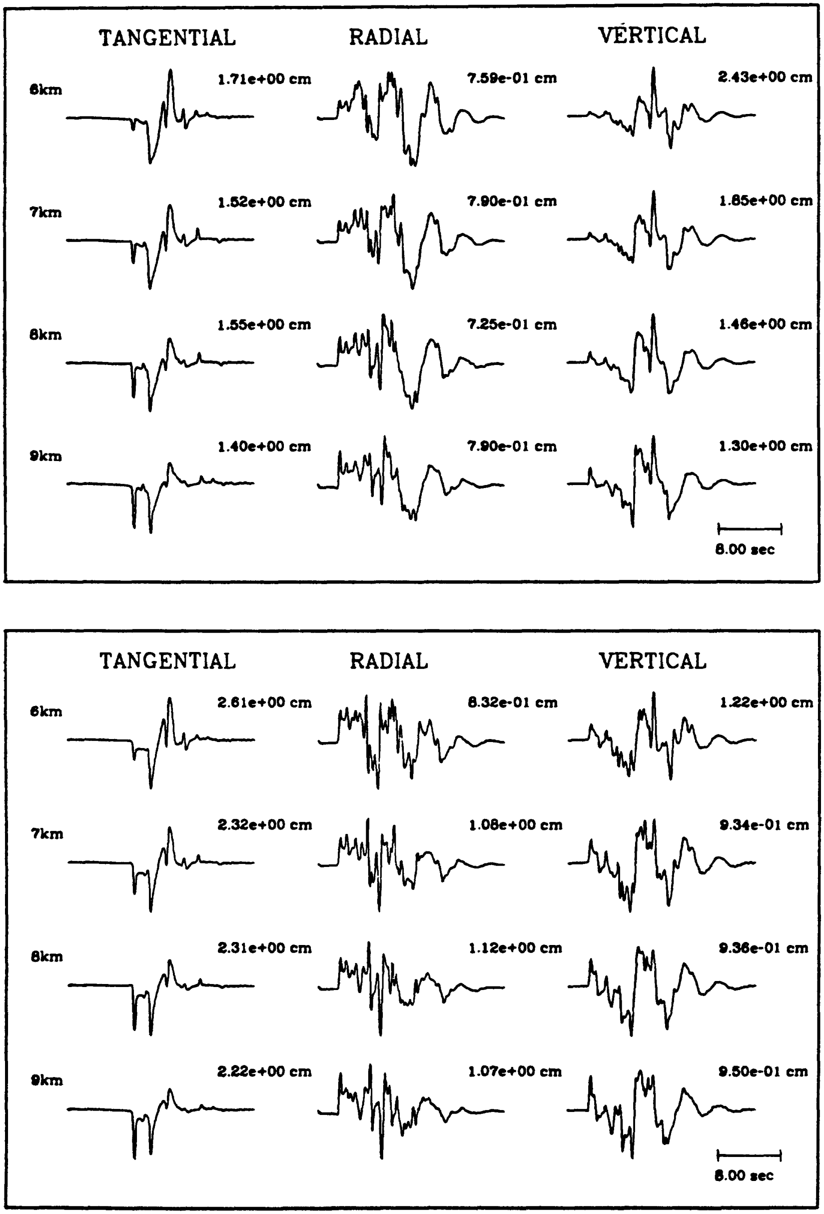

Figure 3. The upper panel displays profiles of synthetic seismograms for source depths from 6 km to 9 km constructed with the 1988 mainshock focal mechanism given in figure 1. The lower panel displays results assuming the aftershock mechanism. A moment of 10^{25} dyne-cm was used in these synthetics, see Dreger and Helmberger (1990).

Geologic Mapping of the Island of Hawaii - Kaoiki Fault Zone

Program Task No. I.2

Marie D. Jackson
Branch of Igneous and Geothermal Processes
U. S. Geological Survey
2255 N. Gemini Drive
Flagstaff, Arizona, 86001
(602) 527-7186

Investigations

Field and mechanical study of ground cracks associated with the 1974 M_L=5.5 and 1983 M_L=6.6 Kaoiki, Hawaii, earthquakes.

Results

1. *Importance of the Kaoiki Fault Zone.* The Kaoiki seismic zone, a young tectonic feature of Mauna Loa volcano, Hawaii (Fig. 1), is the site of recurrent moderate- and large-magnitude earthquakes that cause serious damage. The Kaoiki is the subject of a forecast for a $M_L \geq 6$ earthquake before the turn of the century (Wyss, 1986). Investigation of the relation between volcano-seismic processes and faulting within the Kaoiki zone will increase our ability to evaluate earthquake hazards and test Wyss's prediction methodology within this area.

   The November 30, 1974 M_L=5.5 and November 16, 1983 M_L=6.6 Kaoiki earthquakes generated zones of left-stepping, en echelon ground cracks that extend for several kilometers on the lower SE flank of Mauna Loa. Most large magnitude earthquakes occur along preexisting faults; in contrast, these major Kaoiki earthquakes propagated new ruptures, at least in their surface expression. The Kaoiki seismic zone is unique because its ground ruptures record the initial stages in the development of a strike-slip fault zone: future ground ruptures should be expected to merge into a mature fault zone Geologic mapping by this project and by Endo (1985) shows that at least four ground-rupture zones are concentrated within an area of 30 km^2.

   The 1983 M=6.6 earthquake caused significant damage to the Island of Hawaii and preceded an eruption on the NE-rift zone of Mauna Loa volcano in March 1984. Similiarly, the November 1974 Kaoiki earthquake preceded the July 1975 Mauna Loa summit eruption. Many aftershocks of the 1983 event are strike-slip but an equal number are low-angle thrust events. Based on aftershock data and body-wave modelling, Thurber et al. (1989) suggested that the 1983 main shock initiated as a strike-slip event of moderate magnitude, which preceded the main moment release on a low-angle thrust fault. Here, I use geologic field data collected along the zone of ground breakage and mechanical analysis to evaluate the importance of strike-slip faulting in the 1983 earthquake.

2. *General Objectives.* This project provides important information on the history and mechanisms of faulting within the Kaoiki zone. This data will form the basis for seismic hazard evaluations for the Island of Hawaii. This

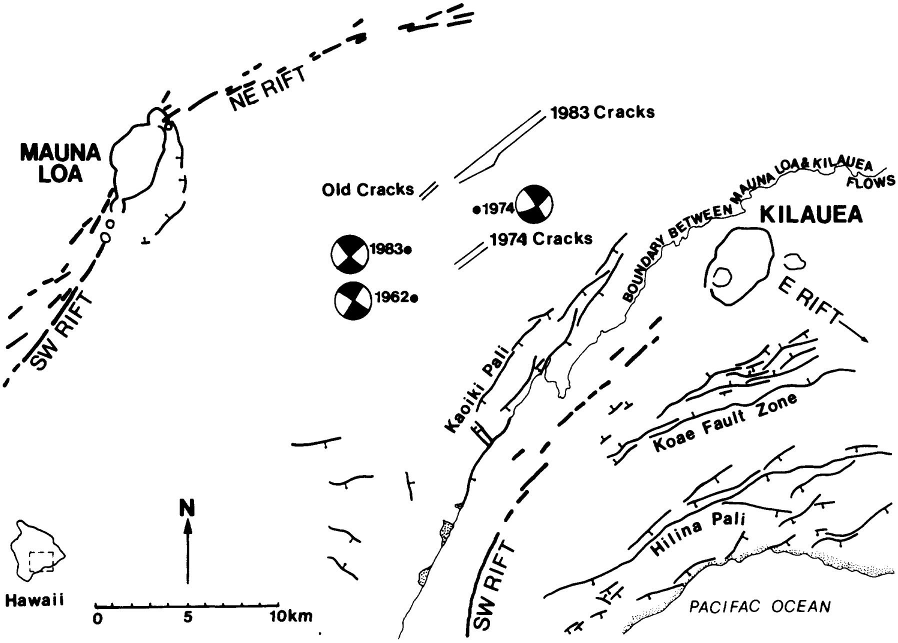

Figure 1. Generalized map showing locations of ground ruptures, focal mechanisms and locations of important strike-slip Kaoiki earthquakes, and major fault and rift systems within the southeast flank of Mauna Loa volcano and the southwest portion of Kilauea volcano, Hawaii.

study investigates: 1) the faulting and earthquake mechanisms involved in the 1974 and 1983 Kaoiki events; and 2) the deformation of the Mauna Loa and Kilauea volcanic edifices resulting from the mutual inflation of their summit magma chambers and the seaward migration of Mauna Loa's SE flank. Field work undertaken by this study includes: 1) the preparation of a 1:10,000 geologic map of the rupture zones generated by the 1983 and 1974 earthquakes and another, much older, undated earthquake; and 2) detailed outcrop-scale mapping (<1:1000) of three critical exposures of the 1983 ground cracks and one excellent exposure of the oldest crack zone. Endo (1985) mapped the 1974 ground cracks at 1:1360, and these data are included in this study. Analytical work includes mechanical analysis of the nature and depth of faulting underlying the 1974 and 1983 cracks and will include analysis of sparse geodetic data spanning the epicentral region.

3. *Summary of Data Collected.* In the past six months, Jackson completed compilation of the 1:10,000 scale map of the 1983 rupture (Fig. 2), and four detailed (<1:1000) maps of the cracks (e.g., Fig. 3). These maps are part of a manuscript, to be submitted to Journal of Geophysical Research, that describes the structure of the 1974 and 1983 Kaoiki ground ruptures, and their relation to the long-term geologic history and recent seismicity of Mauna Loa's SE flank. The manuscript will be submitted to Branch review this spring; all figures are drafted. Jackson also made several very detailed maps of short segments of the 1983 cracks. These show: 1) how pre-existing joints in the pahoehoe host rock control the propagation paths of some cracks; and 2) how the cracks probably initiated as opening-mode fractures that subsequently accomodated small amounts of right-lateral shear.

4. *Analysis of Field Data.* Ground ruptures from the 1983 M_L=6.6 earthquake, the 1974 M_L=5.5 earthquake and an older, undated earthquake trend N48°-55°E, a direction nearly parallel to nodal planes of the 1983 and 1974 main shocks' focal mechanisms (Fig. 1). Individual ruptures consist of arrays of left-stepping, en echelon cracks, with predominantly opening displacements, which strike roughly EW, about 30°-50° clockwise from the overall trend of the zones. The orientation and geometry of the cracks are consistent with right-lateral shear and they strike parallel to a transect joining the summit magma chambers of Mauna Loa and Kilauea volcanoes.

   Geologic mapping of the 1974 rupture (Endo, 1985) shows that:

   - The 1974 cracks extend for 2.2 km, about 3.5 km downslope and SW of the 1983 rupture zone (Fig. 1). Left-stepping, echelon ground cracks from the 1974 M_L=5.5 event may have reactivated two crack sets associated with the 1962 M_L= 6.2 event.

   - The rupture is composed of seven 100--150-m-long, left-stepping, en echelon arrays of cracks. These arrays, in turn, form two 600--700-km-long, left-stepping arrays with a 100-m step between them. Both scales of arrays are joined by prominent pop-up blocks and zones of rubble breccia.

   - In contrast to the 1983 cracks, the 1974 cracks have greater components of right-lateral slip, and linkages between cracks at all scales are more well-developed. These features indicate coalescence at depth. They may

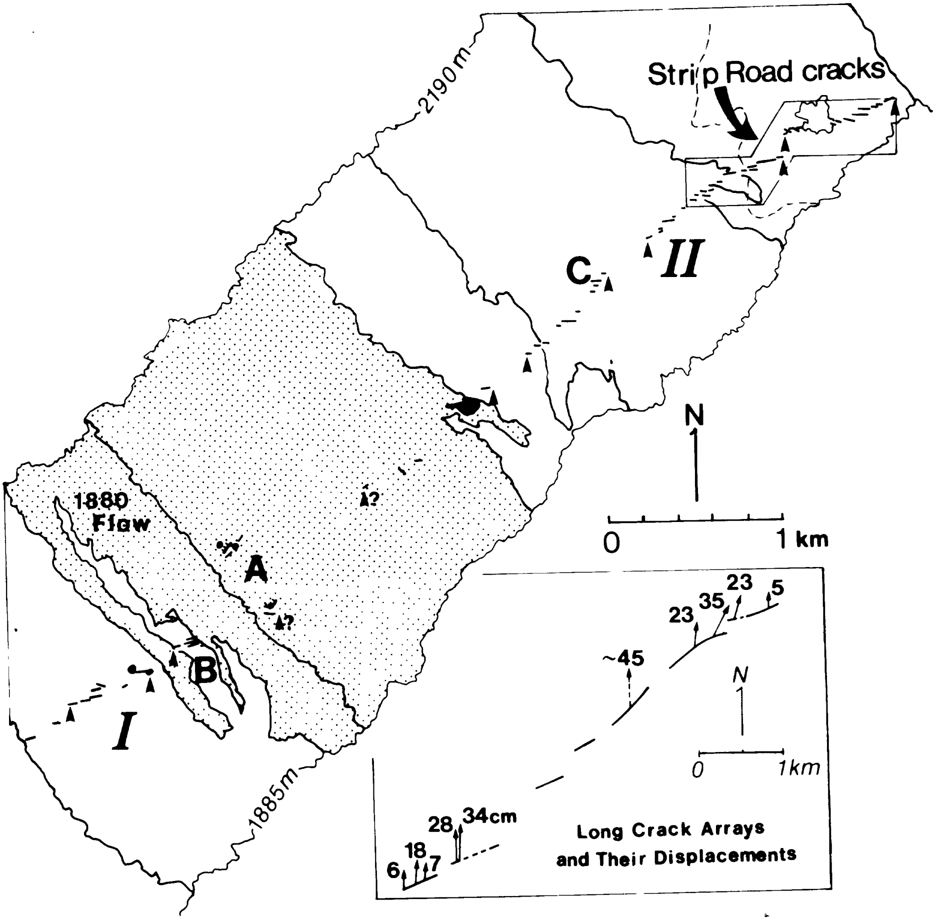

Figure 2. Geologic map of the 1983 Kaoiki ground rupture (1:10,000 scale). Large aa fields (stippled pattern) make detection of some of the cracks impossible. Arrows show the tips and terminations of 300--900-m-long arrays. I and II show the two longest arrays, 1.3 and 3.8 km in length. Inset shows the distribution of these arrays and cumulative displacements across the zone.

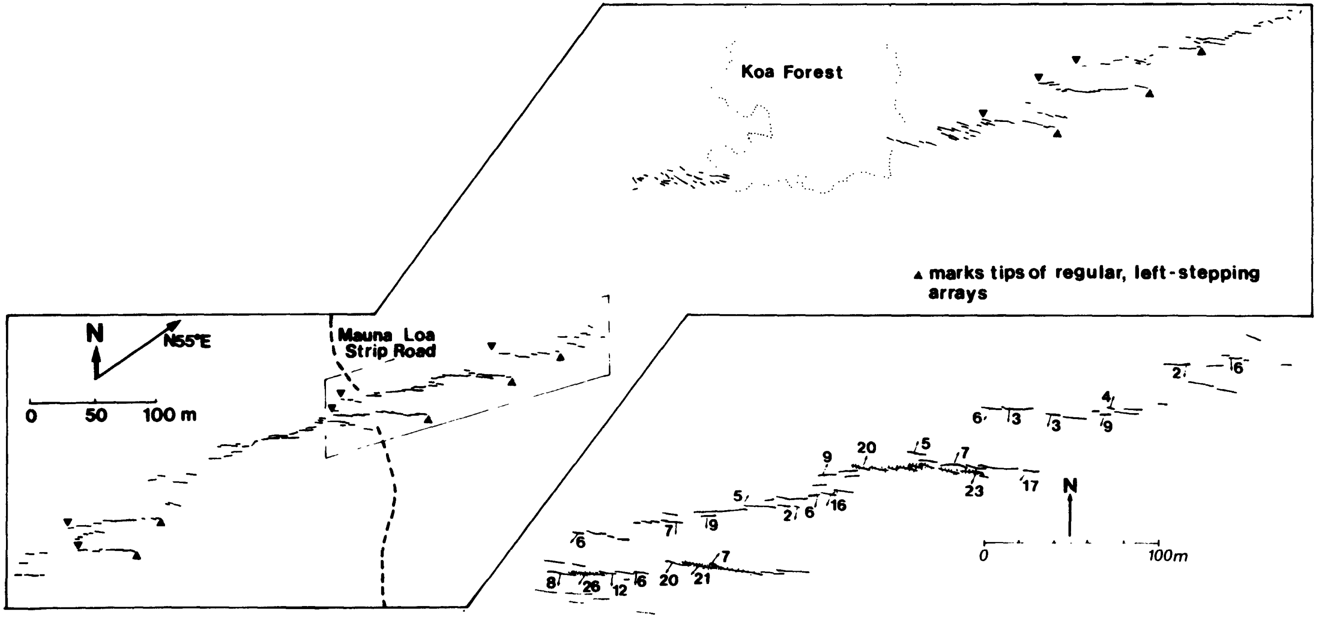

Figure 3. Geologic map of 1983 ground cracks in the Mauna Loa Strip Road area. Left-stepping arrays of cracks form two 1-km-long arrays with a 100-m-long step between them. Inset shows individual crack segments and their displacements.

result from reactivation of yet another zone of cracks, perhaps associated with a 1962 M_L=6.2 event, or they may be a result of the 1974 event's shallower hypocenter, 4--5 km deep (compared with 9--10 km depth in 1983), that allowed the tip of the underlying parent crack to propagate closer to the earth's surface and form a more continuous zone of strike-slip ground breakage.

Geologic mapping of the 1983 rupture shows that:

•Exposures of the 1983 cracks begin about 4.3 km NE of the mainshock epicenter and continue for over 7 km to the NE (Fig. 1). The rupture apparently grew upwards and to the NE, propagating from a focal depth of 11 km to the earth's surface along a distance of about 4 km. The surface area of the fault is about 130 km^2.

•Displacements vary along the rupture zone. Maximum displacements of about 0.5 m occur within the central portions of the 300--900 m-long-arrays, and displacements are zero at the tips of these structures (Fig. 2). Individual crack segments have small, predominantly opening displacements of <5 cm. Crack segments with larger opening displacements also have a component of right-lateral shear parallel to their walls, and commonly these segments are linked to their neighbors by small patches of rubble breccia.

•The ground cracks form three scales of en echelon arrays. Detailed maps show that the left-stepping crack segments form en echelon arrays that range in length from 25--120 m (Fig. 3). These arrays form still longer arrays, 300--900-m-long, that step more-or-less continuously through the entire rupture zone (Fig. 2). Near the tips of these longer arrays, the fairly regular, left-stepping pattern of 25--120-m-long-arrays breaks down into zones of disordered short cracks (Fig. 3). Longer arrays strike progressively more northeastwardly so that the two longest mapped arrays, which are 1.3- and 3.8-m long, deviate only 5°-10° from the N56°E trend of the rupture (Fig. 4).

With depth, crack segments coalesce to form progressively longer, left-stepping arrays of twisted surfaces that become sub-parallel to the overall trend of the rupture zone. The geometry of the 1983 rupture appears to confirm the self-similarity of earthquake produced fractures in hierarchial arrays that range in length from a few meters to several kilometers.

•The ground cracks are a "fracture-process zone" above a parent fault that, during propagation, stressed the rocks above its tip (Pollard et al., 1982). An approximate calculation that uses an estimated fault size and the observed seismic moment, and treats the 1983 Kaoiki earthquake as a Mode-III crack, demonstrates that motion along a parent fault that extends to a height of somewhat less than a kilometer below the earth's surface generates sufficient tensile stress above its tip to induce failure (Jackson et al., 1988). The analysis suggests that if the 300--900-m-long en echelon arrays have heights equal to their lengths, then they may connect directly with the parent fault at depth.

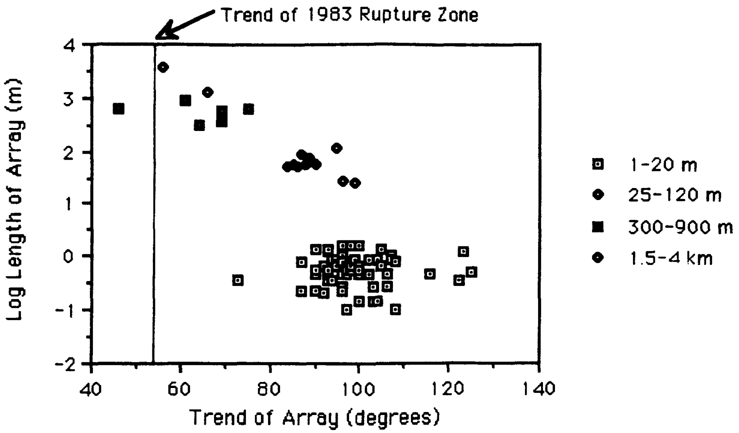

Figure 4. Orientations and lengths of hierarchial arrays forming the 1983 rupture. Progressively longer, left-stepping, en echelon arrays of cracks become sub-parallel to the overall trend of the 1983 rupture zone.

•Estimation of the seismic moment release from field data using $M_0=ADG$, where the fault area $A=130$ km^2; the average displacement $D=0.5$ m, based on surface displacements, and the seismically determined shear modulus $G=50$ GPa, gives M_0 = 3.6 x 10^{18} Nm. NEIS data for the 1983 event give M_0= 1.2 x 10^{19} Nm, and the close agreement between these values indicates that the main moment release was indeed accomodated by strike-slip faulting along a NE-striking plane. These data are not in agreement with Thurber's (1989) hypothesis that low-angle thrusting dominated the moment release of the 1983 event.

References cited

Endo, E. T., 1985, Seismotectonic framework for the southeast flank of Mauna Loa volcano, Hawaii: Ph.D. Thesis, Univ. of Wash., Seattle.

Jackson, M. D., E. T. Endo, P. T. Delaney, 1988, Ground rupture from the 1983 Kaoiki earthquake, Mauna Loa volcano, Hawaii (abs.): Seismol. Res. Letters, v. 59, p.35.

Pollard, D. D., P. Segall, P. T. Delaney, 1982, Formation and interpretation of dilatant echelon cracks: Geol. Soc. Am. Bull., v. 93, p. 1291-1303.

Thurber, C. H., Y. Li, and C. Johnson, 1989, Seismic detection of a low-velocity layer beneath the southeast flank of Mauna Loa, Hawaii: Geophys. Res. Letters, v. 16, p., 649-652.

Wyss, M., 1986, Regular intervals between Hawaiian earthquakes: Implications for predicting the next event: Science, v. 234, p. 726-728.

Reports

Jackson, M. D., and E. T. Endo, 1989, Genesis of a strike-slip fault zone: the 1974 and 1983 Kaoiki ground ruptures, Mauna Loa Volcano, Hawaii (abs): Trans. Am. Geophys. Union, v. 70, p. 1409. To BWTR 8/89.

Earthquake and Seismicity Research Using SCARLET and CEDAR

Grant No. 14-08-0001-G1774

Hiroo Kanamori, Clarence R. Allen, Robert W. Clayton
Seismological Laboratory, California Institute of Technology
Pasadena, California 91125 (818) 356-6914

Investigations

1. Seismotectonics of the Southern Sierra Nevada, California: Early Stages of an Intracontinental Transform?, Helen Qian, Craig H. Jones, and Hiroo Kanamori.
2. Teleseismic Source Parameters and Rupture Characteristics of the 24 November 1987, Superstition Hills Earthquake, Lorraine J. Hwang, Harold Magistrale, and Hiroo Kanamori, (partial support).
3. A Slow Seismic Event Recorded in Pasadena, Hiroo Kanamori.

Results

1. Seismotectonics of the Southern Sierra Nevada, California: Early Stages of an Intracontinental Transform?

The Lake Isabella region of the southern Sierra Nevada lies between the epicenters of the 1946 Walker Pass earthquake (M_L 6.3) and of the 1952 Kern County earthquake (M_S 7.7). Earthquakes in this area occurring during the summer of 1988 were located from P and S arrival times at stations of the Southern California Seismic Network and a temporary array of 17 digital seismometers using the velocity structure of Jones and Dollar (1986).Two prominent features radiate from the epicenter of the 1946 Walker Pass earthquake: a linear band of earthquakes trending SW to the eastern edge of surface displacement from the 1952 Kern County earthquake, and a north-south band extending north about 10 km from the epicenter of the 1946 Walker Pass earthquake. Numerous other more diffusely distributed earthquakes are found north of the NE-SW trending lineament, but there are far fewer earthquakes south of the lineament. Focal mechanisms determined from P first-motions indicate that the earthquakes in this trend have ruptured on a NE trending, near-vertical left-lateral fault; such a fault is unknown from the surface geology. Focal mechanisms from the events north of this trend indicate slip on roughly north-south striking normal faults; this is similar to mechanisms found by Jones and Dollar (1986) for events of the Durrwood Meadows swarm north of this area. This geometry of deformation is strongly reminiscent of the NE trending Garlock fault, which separates the WNW-ESE oriented extension of the California Basin and Range to the north from the Mojave Desert to the south. If, as suggested by Jones and Dollar (1986), the Durrwood Meadows swarm represents the early stages of Basin and Range deformation in the Sierra, then the NE-SW trending seismic lineament might represent the early stages in the creation of an "intracontinental transform" analogous to the Garlock Fault. The existence of an active structure connecting Basin and Range deformation in the "eastern California seismic belt" with the left-lateral reverse White Wolf fault system suggests that the seismic risk and neotectonics of this region should be reexamined.

2. Teleseismic Source Parameters and Rupture Characterics of the 24 November 1987, Superstition Hills Earthquake.

Long-period body waves from the 24 November 1987, Superstition Hills earthquake are studied to determine the focal mechanism and spatial extent of the seismic source. The earthquake is a complex event consisting of two spatially distinct subevents with different focal mechanisms. Two consistent models of rupture are developed. For both models the second subevent begins 8 sec after the initiation of the first subevent and the preferred centroid depth lies between 4 to 8 km. Model 1 consists of two point sources separated by 15-20 km along strike of the Superstition Hills fault. Model 2 consists of one point source and one line source with a rupture velocity of 2.5 km/sec with moment release distributed along strike of the focal plane at a distance of 10 to 22 km from the epicenter. These moment release patterns show that a significant amount of long-period energy is radiated from the southern segment of the fault. Total moment release for both models is approximately 8×10^{25} dyne-cm. Both models also suggest a change of dip from near vertical near the epicenter to steeply southwesterly dipping along the southern segment of the fault. The difference in rupture characteristics and fault dips seen teleseismically is also reflected in aftershock and afterslip data, and crustal structure underlying the two fault segments. The northern segment had more aftershocks and a smaller proportion of afterslip than the southern segment. The boundary between the two segments lies at a step in the basement that separates a deeper metasedimentary basement to the south from a shallower crystalline basement to the north.

3. A Slow Seismic Event Recorded in Pasadena, Hiroo Kanamori.

A prominent long-period wave with a duration of 2000 sec or longer was recorded with a very-broadband system in Pasadena on June 18, 1988. This wave was not observed elsewhere, and is considered of local origin. The acceleration amplitude is 2.5×10^{-5} cm/sec^2 in the northwest direction, with the vertical component less than 10% of the horizontal. The horizontal acceleration can be interpreted as due to a tilt of the ground of 2.5×10^{-8} radians to the northwest. A slowly propagating pressure wave with an amplitude of about 15 mbars could be the cause of the tilt; however, there were no reports suggesting such pressure changes. A more likely cause is a slow tectonic event near Pasadena. The required magnitude of such a slow event is $M_W = 0$, 2, and 4, for a distance of 0.1, 1, and 10 km respectively. This event could be part of a tectonic episode associated with the larger earthquakes which occurred in southern California around this time, especially the December 3, 1988, Pasadena earthquake ($M_L = 4.9$) which occurred six months later within 4 km of the Pasadena station.

Publications

Hwang, Lorraine J., Harold Magistrale, and Hiroo Kanamori, Teleseismic source parameters and rupture characteristics of the 24 November 1987, Superstition Hills earthquake, *Seismo. Soc. Am., Bull., 80,* No. 1, 43-56, 1990.

Kanamori, Hiroo, A slow seismic event recorded in Pasadena, *Geophys. Res. Lett., 16,* No. 12, 1411-1414, 1989.

Kanamori, Hiroo and Harold Magistrale, State of stress in seismic gaps along the San Jacinto fault, in *Observatory Seismology,* A Centennial Symposium for the Berkeley Seismographic Stations, edited by Joe J. Litehiser, University of California Press, Berkeley, Los Angeles, London, 179-186, 1990.

Kanamori, Hiroo, Jim Mori, and Thomas Heaton, The 3 December 1988 Pasadena earthquake ($M_L = 4.9$) recorded with the very broadband system in Pasadena, *Seismo. Soc. Am, Bull., 80,* No. 2, 483-487, 1990.

Magistrale, Harold, Part I: Superstition Hills California earthquakes of 24 November 1987. Part II: Three-dimensional velocity structure of southern California, Ph.D. thesis, California Institute of Technology, 1990.

Seismicity Patterns and the Stress State in Subduction-Type Seismogenic Zones

Grant Number 14-08-0001-G1368/G1810

Carl Kisslinger
Cooperative Institute for Research in Environmental Sciences
Campus Box 216, University of Colorado
Boulder, Colorado 80309-0216
(303)-492-6089

Research during October, 1989 through May, 1990 was focused on the following topics: (1) analysis of earthquake doublets for evidence of changes in material properties associated with preparation for and occurrence of a strong earthquake; (2)modeling stresses in a subduction zone; (3)analysis of aftershock sequences in southern California.

Doublet Analysis

The study of earthquake doublets is in the final stages of analysis. Doublets from three source regions (marked 1,2 and 3 in Figure 1) have been analyzed in order to obtain a good azimuthal coverage of the source-station geometry. A 'set' refers to two or more events of different origin times that behave as doublets. For 'sets' with more than two events, any combination of two events form a doublet pair. Each doublet pair yields very similar seismograms at all recording stations, so that, on the average, ten pairs of seismograms are analyzed for each doublet pair. From region 1, two sets of doublets have been analyzed. The first set consists of three events from January, 1981, December, 1985 and July, 1986 while the second set consists of two events from May, 1985 and July, 1986. From region 2, two differents sets of doublets have been studied. One set consists of two events from July, 1984 and July, 1986 and the other set consists of four events from September, 1981, July, 1983, August, 1985 and December, 1986. For region 3, only one doublet with two events from June, 1983 and January, 1986 has been studied. Several of these doublet pairs span the May 7 1986 Andreanof Islands earthquake (M_w=8.0), the primary target of the study.

Every event has been corrected for instrumental time-drift using a method previously developed. Seismograms from all the stations have been analyzed using a modified Cross Spectral Analysis Method (CSAM). This produced delay times (in the order of millisecs) as a function of running time along the seismograms recorded at each station for every doublet pair. In all, over 100 pairs of seismograms from different stations have been analyzed.

All the events were relocated as accurately as possible to take out the delays due to location error. For each set of doublets, a 'master event' was chosen relative to which all the other events were located. The master event had the best routine location, with minimum errors involved. It was recorded by maximum number of stations and had good, relatively noise-free seismograms. It turned out that the events from 1986 satisfied most of these requirements and were therefore chosen as the master events for all the doublet sets. These events were all recorded by a minimum of six stations and had overall location errors of 0.2 km or less. Most of the seismograms had distinct P and S-wave arrivals and background noise was relatively small.

The master events were first located using the network routine location method after rereading all P and S- arrivals. When the best solution was obtained, synthetic travel times of P and S waves at all the stations from the master event location were obtained. The synthetic S-P times were noted for each station.

The individual events for each set of doublets were located relative to the 'master event' of that set by first calculating the observed S-P delays from the doublet analysis; then adding these delays to the synthetic S-P times of the master event; and finally using these new S-P times to relocate the individual events. This is a relative means of relocation and the absolute locations are only as good as the locations of the 'master event'. However, the quality of the data in the network and the present available means of location do not permit individual location of these events to such great accuracy. Usually, the routine locations have standard errors of 0.4 km or more. The relative locations obtained from the doublet delays often differ only by 0.2 km or less. For the interpretation desired, it is the relative location that is important and not the absolute locations.

Figure 2 shows the relative locations for two doublet sets from regions 1 (doublet 6) and 2 (doublet 8) along with the best routine location of the master event (marked as 1986). The maximum difference in location (≈ 280 meters) is between the 1985 event and the other events in doublet no. 8 from region 1. All the other locations are around 100 meters. A careful scrutiny did not reveal any systematic bias of the original locations.

From the relative locations, synthetic S-P times to each station was noted for all events. The difference between these S-P times and the master event S-P times for the same station, gives the S-P delays due to location difference of each event. Subtracting these from the observed S-P delays between the master event and individual event, gave the S-P delays that could be due to velocity changes along the path of travel. Figure 3 shows the S-P delays before and after relocation for doublets sets 6 and 8. A systematic bias was observed in the delays for station AD8. It always shows a unusually higher magnitude of delay than all the other stations. The seismograms at this station are also markedly different from all other stations and appear to have considerable amplification of all wave energy arriving at this station. A nearby station , ADK, does not exhibit any such behavior and it is therefore proposed that this station probably overlies some local rock type that enhances the apparent delays in the doublet analysis.

The S-P delays from doublet set 6 shows positive delays to the east and negative delays to the west. For doublet 8, the delays appear to have an oscillatory nature with a period of 80^0 and peak-to-peak amplitude of about 36 msecs. An oscillatory behavior was shown by Nur (1971) to be a result of stress-induced velocity anisotropy in rocks with cracks. However, the period of this variation was suggested by Nur(1971) to be 180^0 (i.e. $\approx \mathrm{Sin}(2\alpha)$) where α is azimuth around the source location. At present, there is no theoretical basis for the type of (S-P) azimuthal variation observed for this doublet. Similar analysis with S-P delays have been done with all the other doublet pairs. report.

After the above analysis, the delays in the S-coda for each individual pair can be used to interpret for possible S-velocity change. The fractional velocity change is given in terms of the slope of the delays as:

$$\frac{d\delta}{dt} = -\frac{\Delta V_s}{V_s}.$$

Such a fit has been done to the S-coda delays of doublet no. 6 and is shown in figure 4. The fractional S-velocity changes observed are mostly negative and range in values from .0002 to -.009. As before, if AD8 is neglected, there is a definite trend as a function of azimuth. In any case, it can be confidently stated from this result that there appears to be a marked decrease in the S-velocity for the path of travel between region 2 and all the stations between July, 1984 and July, 1986. This suggest that the 1986 Andreanof Islands earthquake was accompanied by a decrease in S-velocity. Similar analyses are nearly completed for all other doublets considered.

Stresses in a Subduction Zone

A study to model stresses in a subducting slab has been initiated. The forces assumed in the model are: the negative buoyancy due to the relatively low temperature and higher density of the slab material; viscous drag on the slab by the surrounding mantle material; and stresses due to the bending of the slab. The distribution and characteristics of the subduction zone earthquakes provide constraints on the parameters needed to construct the stress model. The geometric constraints are the length of the seismically active part of the slab, the angle of subduction, and the radius of curvature of the bent part of the slab. In many subduction zones, there is a change in focal mechanism with depth along the Wadati-Benioff zone, indicating a change in the deviatoric stress from extensional to compressional at some depth. In the neighborhood of the transition depth, seismicity is reduced. The spatial distribution of seismicity and stress drop data from microearthquakes, provided by local network seismograms, further constrains the stress distribution.

The negative buoyancy force, which drives the slab, can be estimated from the slab's age at subduction, the thermal diffusivity, the temperature difference between the mantle and the surface, and the coefficient of thermal expansion. The viscous friction force can be estimated by assuming the slab is not accelerating, and, therefore, the friction force balances the buoyancy force. The ratio of the maximum bending stress to the maximum buoyancy stress can be estimated by setting the bending moment equal to the component of negative buoyancy normal to the slab. The ratio is a function of the slab length, D, thickness, h, the subduction angle ϕ, and Poisson's ratio, ν.

$$\frac{\sigma_{bend}}{\sigma_{buoy}} = \frac{3D}{h(1-\nu^2)^2} cot(\phi)$$

This implies that either the bending stresses are much greater than the other stresses in the problem, or some other force, acting perpendicular to the slab, enters into the moment balance. The model assumes the latter, another force acting at the lower end of the slab. This force is probably due to the increasing viscosity with depth, perhaps complicated by a component of mantle velocity normal to the plate velocity.

Preliminary results from this model indicate:

1) The magnitudes of the modeled stresses are roughly 10 times typical earthquake stress drops of 100 bars.

2) Some force normal to the slab, other then the three primary ones, is necessary for the bending stresses to be of the same order as the tensional stresses in the slab.

3) Forces must be transmitted from below the end of the seismically active part of the slab in order to satisfy focal mechanisms. This implies an increase in

viscosity, as well as some integrity of the slab below the deepest seismicity.

Southern California Aftershock Sequences

As part of the investigation of aftershock sequences as indicators of fault properties, 39 sequences in southern California, 1933-88 were modeled by the modified Omori relation. Maximum likelihood estimates of the parameters K, p, c, with standard errors, were found by applying the Ogata algorithm. The corresponding b-values were also determined. Many of the active faults in the region were sampled. Most of the sequences were well represented by the Omori relation. The program for the analysis has been improved, in cooperation with P. Reasenberg, U.S.G.S., Menlo Park.

The p-values, which describe the decay rates of the sequences, differed among the sequences by more than the estimated errors. The mean value of p is 1.126 ± 0.266, with values ranging from 0.688 to 1.816. Correlations of the p-values with b-values, mainshock magnitudes, and the differences between the mainshock magnitude and that of the strongest aftershock were tested. No significant correlations were found. No significant differences in decay rates were found for strike-slip and thrust mainshocks, when the hypocenters are in the same general region. A geographical distribution has been found, with high p-values, 1.5 to 1.8, to the southeast, especially in the Imperial Valley, low values, 0.7 to 0.9, for a majority of the events offshore and some along the coast, and "normal" values, close to 1 in the Mojave block, on the San Jacinto fault, and in and around the Los Angeles Basin.

The most important finding is that p-value differences greater than the error bars on the values do exist. The interpretation of these values is in terms of models of aftershock generation. If we ascribe the variations to differences in fault zone properties, rather than some as yet undefined differences in fault loading, we conclude that the fault surfaces in the Imperial Valley are more homogeneous than those in the offshore region, or to the northwest along the San Andreas and San Jacinto fault systems.

This work was done in cooperation with L.M. Jones, U.S.G.S., Pasadena.

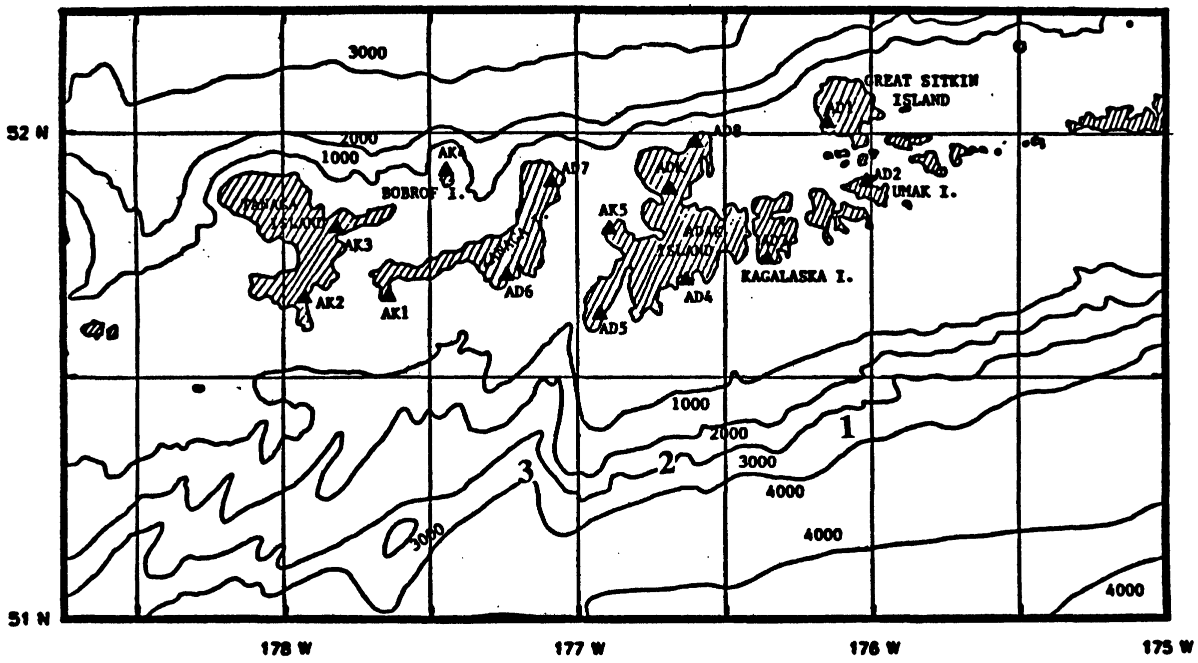

Figure 1. Map showing the Central Aleutian Seismic Network (CASN) seismic stations (solid triangles) and the general area covered by the network. The three source regions of interest are marked as 1, 2 and 3 (referred to as regions 1, 2 and 3 in text).

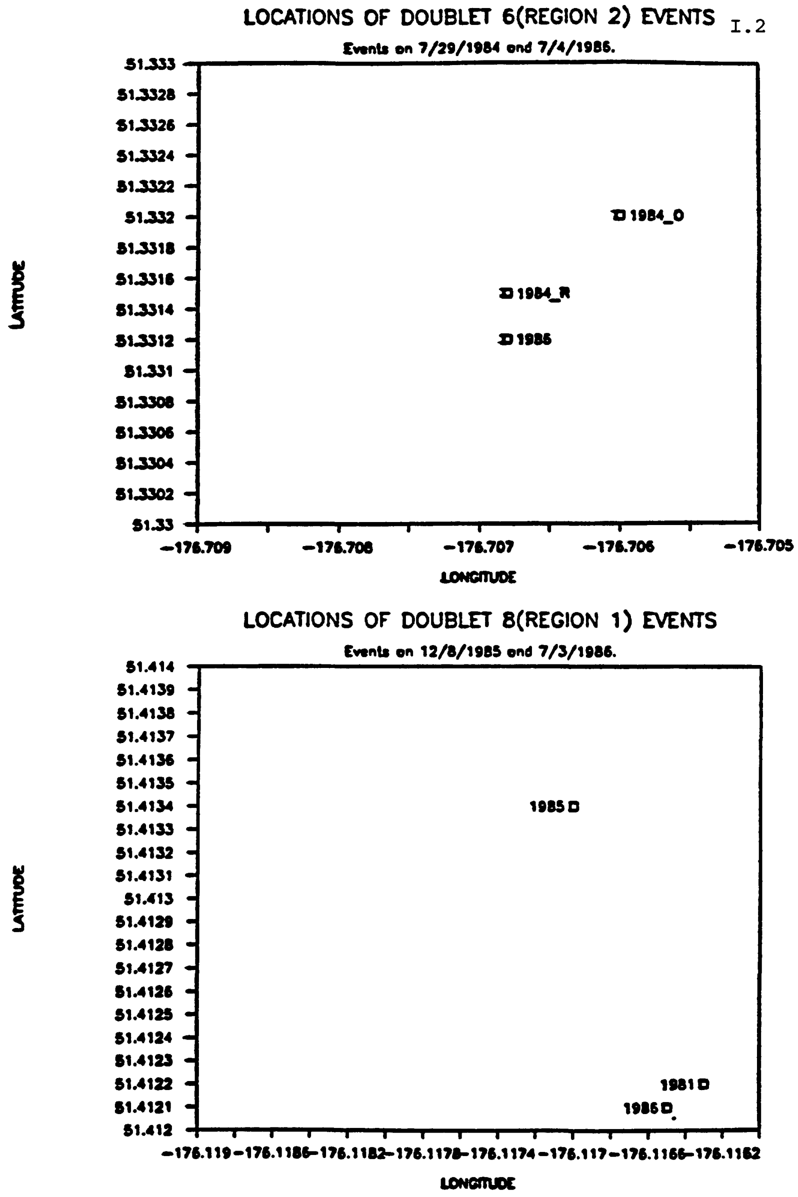

Figure 2. Locations of doublet sets 6 (top) and 8 (bottom). For doublet 6, O - original location and R - relocated positions. For doublet 8, only the relocated positions are shown as the original locations are outside the range of the figure.

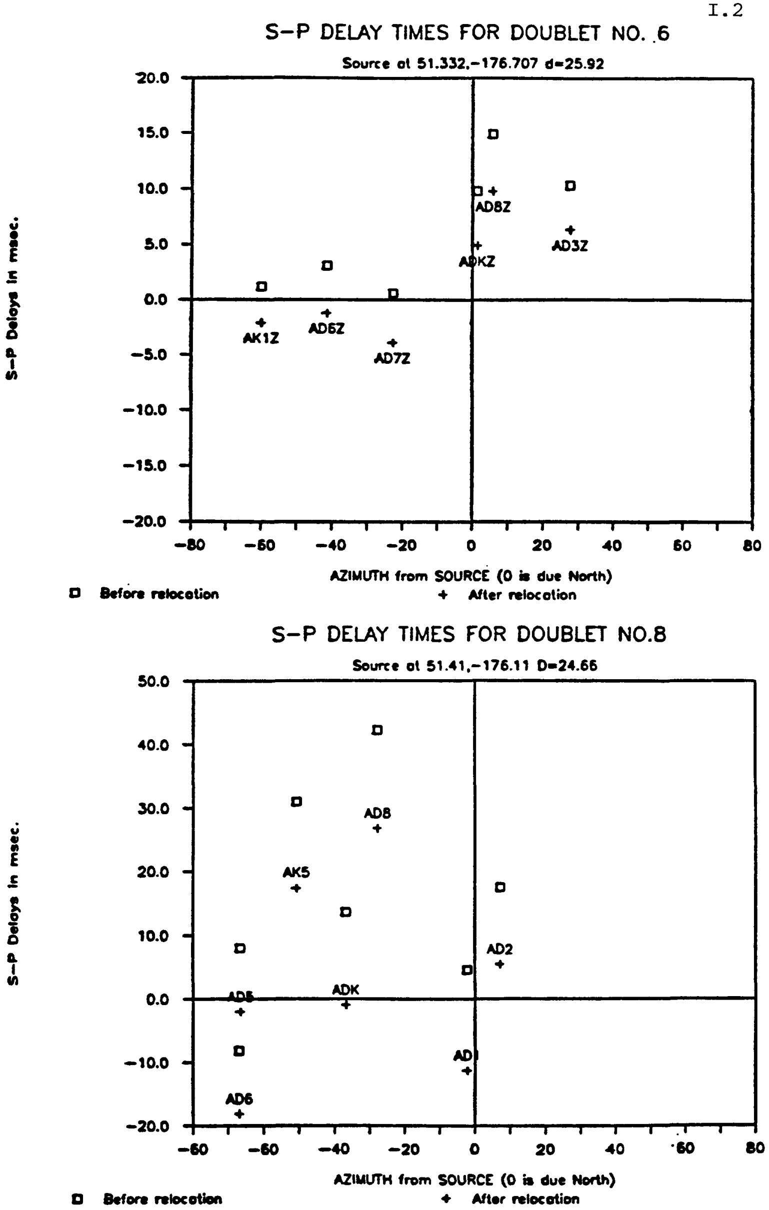

Figure 3. S-P delay times measured as a function of azimuth measured at each station for doublets 6 (top) and 8 (bottom) from regions 1 and 2 respectively (see figure 1). Note station AD8 has anomalous high value.

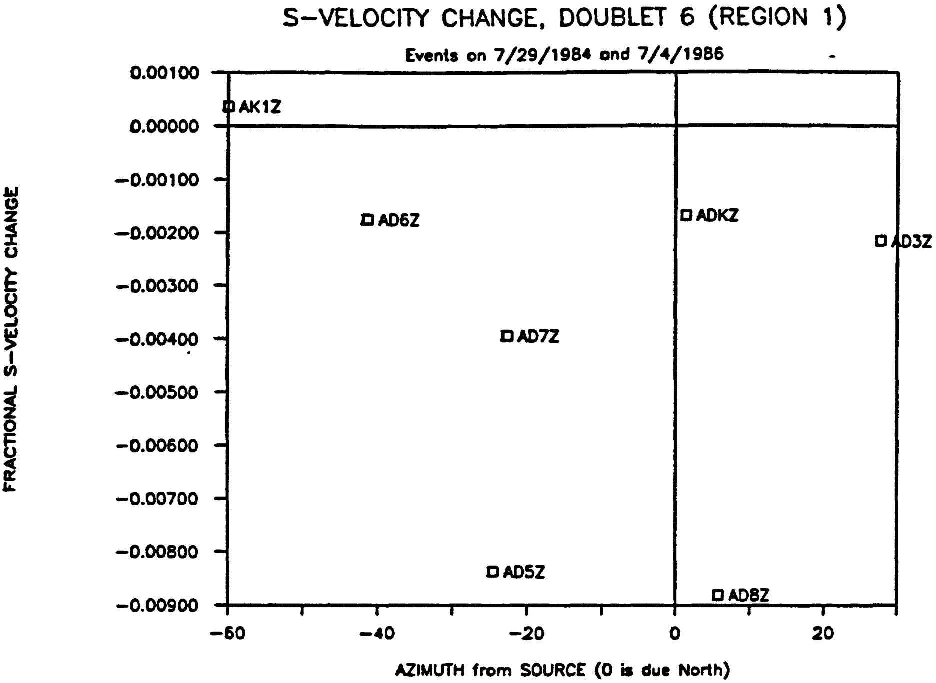

Figure 4. Fractional S-velocity change measured from doublet 6 in region 1 shown as a function of azimuth from source area. Overall S-velocity decrease is observed. Note station AD5 and AD8 has high negative values.

Slip History of San Andreas and Hayward faults

9910-04192

J. J. Lienkaemper
Branch of Engineering Seismology and Geology
U.S. Geological Survey
345 Middlefield Road, MS 977
Menlo Park, California 94025
(415) 329-5642

Investigations

Determine slip rates and earthquake recurrence intervals on the San Andreas and Hayward faults. Compare rates of geologically determined surface slip to rates of historic creep and geodetically determined deep slip. Analyze the effects of structural complexity and fault segmentation upon inferring recurrence times from slip rate.

Results

1. Earlier Hayward Fault Work and Progress Report. The manuscript, *Borchardt et al.* [in prep.], on joint USGS/CDMG trenching in Fremont 1986-1987 is completed and going into internal review. Along a ≥62-km length of the creeping trace of the Hayward fault offset curbs, fences, and buildings indicate that the creep rate over several decades has averaged about 3.5-6.5 mm/yr, but a 4-km long segment in southern Fremont has been creeping at 8-10 mm/yr [*Lienkaemper and Borchardt, in prep.*] Our earlier conclusions about creep rate in Oakland [*Lienkaemper and Borchardt,* 1988, *EOS 69,* 1306] have been significantly modified by new measurements in El Cerrito, Berkeley, and Oakland, that show a gradual decent of creep rate southeastward into central Oakland. Creep in central Oakland is at least 3.5-4 mm/yr, but may not be any greater than that. Thus, we tentatively conclude that Oakland probably does contain a fault segment showing low creep rate, contrary to our earlier opinion. We are now monitoring creep rates in Oakland to test this conclusion.

The Holocene slip rate of 5.5 mm/yr we measured in central Fremont may be too low because of local structural complications, thus the 8 to 10 mm/yr creep rate measured by us in southern Fremont may better represent the full amount of long-term slip rate on the fault. To test this possibility, in April-June 1989 we trenched at the Masonic Home site in Union City where the Holocene-active fault zone appears to be narrower.

2. Holocene and Late Pleistocene Slip Rates at Masonic Home, Union City. Six buried fan units offset by the fault were identified, yielding values of total slip (inferred from projected locations of fan apexes): C) 20? ± 7 m, E) 46 ± 5 m, G) 66 ± 5 m, I) 88 ± 5 m, K) 131 ± 6 m, and M) 167 ± 6 m. We have submitted 24 radiocarbon samples (all charcoal) for dating. Thus far 7 dates are available. These yield fairly well-constrained slip rates for 2 apexes: 8.0 ± 0.6 mm/yr (8260 ± 90 yr old, tree-ring correction made) for apex G, and ≤9.2 mm/yr (14,200 ± 260 radiocarbon yr BP, correction not currently possible) for apex K. Dates on apex E bracket slip rate between ≥7.4 and ≤9.9 mm/yr. Samples at what appear to be the same stratigraphic horizon give distinctly different ages that limit the age of onset of apex E to between ≥4670 ± 185 to ≤6190 ± 150 yr old (tree-ring corrected.) The discrepancy could result either from a mistake in our stratigraphic interpretation or from charcoal that was already many centuries old when deposited (e.g., old tree or reworked charcoal.) Further logging and dating of other samples should clarify

the disparity. More parallel trenching in 1990 will verify and improve both stratigraphic control and accuracy of inferred offsets.

Although the Holocene and late Pleistocene slip rates at the Masonic site seem to be only about 8 mm/yr in our preliminary analysis, it should be kept in mind that geologically derived slip rate is frequently only a minimum estimate of the entire slip rate. Despite the fact that we chose the Masonic site for the relative narrowness of the fault zone here, we do know from a trench dug in 1970 about 100 m to the southeast, that Holocene, secondary thrust faulting can extend well into the alluviated flat, even farther out than our 1989 trench. Our main intent with the Masonic site trenching effort was to test the hypothesis that the 9 mm/yr creep rates observed in southern Fremont may represent the long-term slip rate for the entire Hayward fault. Ideally this theory should be tested by trenching several sites along the fault, but the Masonic Home evidence clearly supports ~9 mm/yr as the underlying or driving slip rate of the Hayward fault. Of greater concern may be that we are still underestimating the long-term slip rate of the Hayward fault, because the fast creeping segment in southern Fremont had visible surface rupture in 1868, and thus this segment could be expected to have a long-term rate even larger than the current 9 mm/yr creep rate.

Reports

Borchardt, G., J. J. Lienkaemper, and K. Budding, ----, Holocene slip rate of the Hayward fault at Fremont, California: manuscript in preparation for J. Geophys. Res.

Bonilla, M. G., and J. J. Lienkaemper, 1990, The visibility of fault strands in exploratory trenches and timing of rupture events: *Geology 18,* 153-156.

Lienkaemper, J. J., ----, Amount of slip along the San Andreas fault near Cholame, California, associated with the great 1857 earthquake: evidence from offset stream channels: manuscript in preparation.

Lienkaemper, J. J., and G. Borchardt, ----, Historic creep rate and potential for seismic slip along the Hayward fault, northern California: manuscript in preparation for J. Geophys. Res.

Lienkaemper, J. J., G. Borchardt, J. F. Wilmesher, and D. Meier, 1989, Holocene slip rate along the Hayward fault, northern California (abs.): *EOS, Abstr. Am. Geophys. Union 70,* 1349.

Lienkaemper, J. J., and W. H. Prescott, 1989, Surface slip along the San Andreas fault near Parkfield, California: *J. Geophys. Res.. 94,* 17,647-17,670.

Earthquake Research in the Eastern Sierra Nevada Western Great Basin Region

Contract 14-08-0001-C1524, October 1989

W.A. Peppin
Seismological Laboratory
University of Nevada
Reno, NV 89557
(702) 784-4315

Investigations

This contract supports continued research focused on the eastern Sierra Nevada and western Great Basin region. We have investigated: (1) seismicity near the south moat of the caldera using an array of portable event recorders and waveform inversion of these for the seismic moment tensor, (2) seismicity in the White Mountains seismic gap, and (3) pulse-width studies for estimates of stress drops. Some of these results are described below.

Results

(1) Waveform Inversion

Following preliminary work by Steve Horton in August of 1989, a more concerted effort was made during February and March to record digital waveforms close to the sources of the swarm earthquakes in the south moat of Long Valley caldera. These earthquakes were accompanied by a sudden increase in the uplift near the caldera, possibly leading to a resumption of seismicity involving large events such as occurred in May of 1980. Activity has been quite intense in this region, and we deployed an array of six three-component EDA digital event recorders. After considerable effort in both hardware and software, Steve was able to operate these instruments in seismic event-triggering mode, and has collected a considerable library of useable data. Seismic transducers used included three Kinemetrics intermediate-period instruments and three-component velocity transducers. The data has been successfully uploaded to floppy discs, where a body of processing programs is available. Testing has been done on use of Brian Stump's program FREFIT for frequency-domain fitting of seismograms. Green's functions are now being computed for a halfspace using a program written by Bill Peppin, and we are attempting to get programs PROSE and SEIS running to produce proper input for Brian's program with a layered halfspace. Andres Mendez is working to put up a simpler version of the multilayer codes from Paul Spudich. Some runs on the data are occurring at the time of this writing, but we have no result to show yet. The driving motivation is to investigate whether or not any of the swarm events in the south moat have a non double-couple component. The portable array, supported by the network data being taken by the CUSP system, provides quite dense coverage right over the active swarm region.

(2) Seismicity Within the White Mountains Seismic Gap

Figure 1 shows seismicity drawn from the complete UNR catalog extending through January 1990 of the region encompassing the north end of the White Mountains, within an area recognized as a possible seismic gap, lying as it does between the 1932 Cedar Mountains and 1872 Owens Valley rupture zones. Seismicity seems to cluster around the end of the northern Fish Lake Valley - Death Valley fault system (Figure 1). Near the northern termination of this fault system is an earthquake cluster (star in Figure 1) which began with an M 4.6 event on 14 January 1990. This was a particularly vigorous sequence as a few hundred aftershocks were recorded within the first few days. Preliminary locations of the first of these earthquakes define a tight cluster about 2 km in maximum dimension, as resolved by onset times at the two close stations BON and MIL, at a shallow depth of 3 to 5 km. The mainshock had a strike-slip focal mechanism (Figure 1), which is the norm rather than the exception for this area. The north-northwest nodal plane parallels the trend of the Fish Lake Valley fault zone. We are examining these earthquakes (Johnson, dePolo, and Peppin, 1990), which are still continuing; it appears that the cluster may be growing in size as the intensity dies out.

It is known that three paleoseismic events have occurred in the last 1800 years on this north section of the Fish Lake Valley fault (Sawyer, 1989, M.S. Thesis). We are preparing a manuscript (dePolo, Peppin, and Johnson) which catalogs the active faults in the White Mountain seismic gap and which attempts to identify those regions most likely to produce a large earthquake. In this region of complex faulting and numerous identifiable trends, we believe that several stand out as likely candidates for such an event, if it happens.

(3). Pulse-Width Studies

Smith and Priestley (1990) have presented estimates of stress drops as obtained by the pulse-width method of Frankel and Kanamori (1983). Their results are significant for use in arrays such as ours where most of the signals are uncalibrated vertical waveforms. Their results show low stress drop in the region believed to have ruptured in the main event of the 1984 Round Valley sequence and higher stresses around the edges of this zone. During this contract period we are working on application of the pulse-width method to the 1986 Chalfant sequence, and on events recently recorded by the CUSP system. Software now available on CUSP should permit routine application of this method during standard event timing, which should facilitate application of the method to the ongoing intense earthquake sequences near Long Valley caldera.

Written Submittals, This Contract Period

Horton, S.P., Anderson, J.G. and A.J. Mendez, 1989. Performance of EDA PRS-4 Portable Seismic Recorder, EOS, Trans. Am. Geophys. Un., 70, 1224.

Johnson, P.A., dePolo, C.M. and W.A. Peppin, 1990. The M 4.6 Fish Lake Valley, Nevada earthquake of 15 January 1990 and the White Mountains Seismic Gap, Seis. Res. Lett., 61.

Peppin, W.A., 1990. Real-time analog and digital data acquisition through CUSP, Seis. Res. Lett., 61 no 1.

Peppin, W.A., Delaplain, T.W. and J.S. Lewis, 1989. Pre-S observations at station SLK, NW of Long Valley caldera, California and their relation to possible magma bodies, Bull. Seism. Soc. Am., 79, 1894-1904.

Savage, M.K., Shih, X.R., Meyer, R.P. and R.C. Aster, 1989. Shear-wave anisotropy of active tectonic regions via automated S-wave polarization analysis, Tectonophysics, 165, 279-292.

Savage, M.K., Silver, P.G. and R.P. Meyer, 1990. Observations of teleseismic shear-wave splitting in the basin and range from portable and permanent stations, Geophys. Res. Lett. 17, 21-24.

Savage, M.K., Peppin, W.A. and U.R. Vetter, 1989. Shear-wave anisotropy and stress direction in and near Long Valley caldera, California, 1979-1988, Jour. Geophys. Res., accepted.

Smith, K.W., Brune, J.N. and K.F. Priestley, 1989. Seismic energy spectrum, and the Savage and Wood inequality for complex earthquakes, Observatory Seismology, An Anniversary Symposium on the Occasion of the Centennial of the University of California at Berkeley Seismographic Stations, J.J. Litehiser, ed, University of California Press, 279-302.

Figure 1

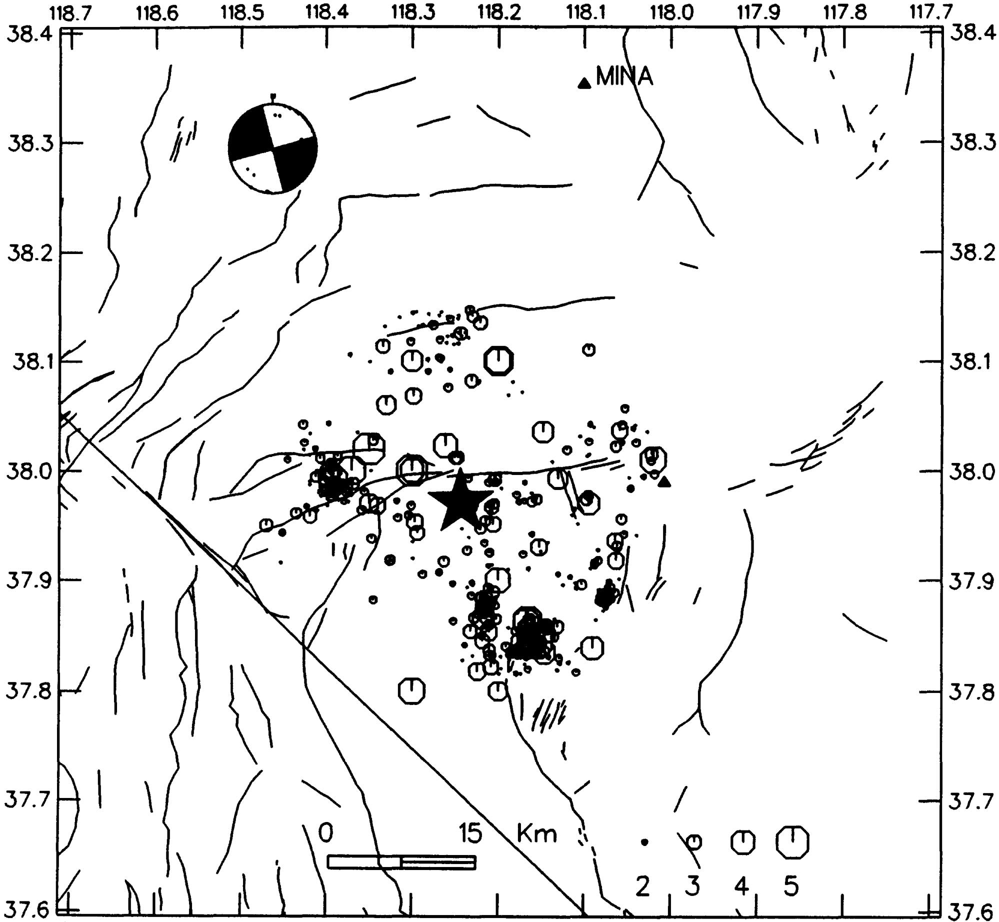
118.7
118.6
118.5
118.4
118.3
118.2
118.1
118.0
117.9
117.8
117.7
38.4
38.3
38.2
38.1
38.0
37.9
37.8
37.7
37.6
MINA
0
15
Km
2
3
4
5

Determination of Earthquake Hypocenters, Focal Mechanisms, and Velocity Structures in the Morgan Hill/Coyote Lake and Bear Valley/Stone Canyon areas of Central California through the use of Fast, Accurate Three-Dimensional Ray Tracing.

14-08-0001-G1697

Final Report

Steven W. Roecker
Department of Geology
Rensselaer Polytechnic Institute
Troy, New York 12180-3590
(518)-276-6773

Introduction

The objectives of this project were to (1) develop and test a new three-dimensional ray-tracing and tomography algorithm for locally recorded earthquake data, and (2) apply this method to data collected in the Morgan Hill/Coyote Lake and Bear Valley/Stone Canyon regions of California.

The first objective has been completed. In addressing the second objective, one of our principal aims in the year that we worked on this project was to demonstrate the necessity of three-dimensional ray tracing in structure with strong lateral heterogeneity. In this final report we summarize the major findings of our research, which center on new interpretations of earthquake locations, focal mechanisms, and velocity structure in the Morgan Hill area.

Data Selection and Initial Model

As a starting point we took the data selected by Michael (1987) in his study of Morgan Hill aftershocks. Our intention was to compare the results of a state-of-the-art inversion using approximate ray tracing (i.e., Michael's study) with our own application, and thereby establish the differences between techniques. Our only modification to the dataset was a parsing to reduce clustering with the idea that information in arrivals from these events would be largely redundant. By using the criterion that the distance between any two hypocenters be greater than 1 km, the total number of earthquakes was reduced from 271 to 154.

The area chosen for the study is an 80 x 80 km region centered on the Morgan Hill aftershock zone (figure 1). The grid mesh is rotated to the northwest to align with the general trend of the fault. Thirty-two stations are located within this model.

The three-dimensional model deduced by Michael was used as the initial model for much of this study. The three-dimensional mesh of grid points used in the analysis were assigned to five layers with depths of -1.2, 1.0, 3.0, 7.0, and 12.0 km. Within each layer the 13 x 9 mesh of points was assigned. In order to accommodate expected strong variations of lateral velocity near faulted areas, the grid points are denser in those regions.

Relocated Earthquakes

Michael's original hypocenters were relocated in a revised structure (described below) deduced with the same arrival time data. A comparison of the two shows that, in varying degrees, the 154 relocated epicenters are shifted to the northeast by 1 or 2 km. Cross sections of these locations taken perpendicular to the faults (figures 2a, 2b, and 2c) reveal that the amount of shifting is depth dependant. In cross-section bb' (figure 2a), it is clear that the trend of relocated seismicity is shifted to the northeast by about 1 km and the focal depths are mostly deeper in varying amounts than the originals. As a result, the dip angle of the seismicity in this cross-section has changed from 88° to 80°. Even so, the projection of the seismic zone to the surface still intersects the surface trace of the Calaveras fault.

The distribution of earthquakes in section cc' (figure 2b) is more complicated, but two main groups of earthquake (SW and NE) can be distinguished. For the SW group, also seen to the west of the Calaveras fault in figure 1 the hypocenters of the relocated earthquakes changed significantly. The locations shifted to the northeast by about 2.0 km and the focal depths generally increased by about 4 km. Thus, the angle of the seismic zone for the SW group appears to be dipping about 86° to the southwest and its projection to the surface is more closely aligned to the surface trace of the Calaveras fault. As for the NE group, also seen to the east of the Calaveras fault in Figure 2, the hypocenters of relocated earthquakes are shifted to the northeast by about 1 km and the focal depths generally increased by about 1 to 2 km . As a result, the earthquakes in the NE group appears to be more closely associated with the Modrone Spring fault than with the Calaveras fault.

As with the earthquakes to the north, the positions of relocated earthquakes in cross-section dd' (figure 2c) shifted to the northeast by about 1 km and the focal depths increased about 0.5 km. The dip angle of seismic zone changed from 85° to 76°. Although the dip angles of these seismic zones are different, the surface projections of both zones are very close to the surface trace of the Calaveras fault.

Ray Paths and Focal Mechanisms

One of the fundamental pieces of information we get from microearthquake recordings are focal mechanisms, the accuracy of which relies to some extent upon our ability to estimate ray directions at the source. In his study, Michael compared focal mechanisms deduced from a one-dimensional ray tracer and those deduced from an approximate three-dimensional ray tracer and concluded that there was little if any significant difference between the mechanisms produced by the two. To test whether or not real three-dimensional ray tracing made much difference, we produced plots of ray directions and focal mechanisms deduced from our model. A comparison of ray directions calculated in a true three-dimensional model those calculated in a "best average" one-dimensional model (figure 3) is revealing. Note that the differences in take off angle are generally not great, but that the differences in azimuth are impressive. The reason for this difference is clear: the "best-average" one-dimensional structure adequately takes into account the vertical variations which control the take-off angle, but are relatively insensitive to "out-of-plane" variations that control the azimuth. To see how these differences in ray direction affect our estimates of individual focal mechanisms, we plotted up the mechanism for three earthquakes which were published in Michael's study. These revised mechanisms show strikes and dips that are different from their original estimates by 10° to 15°. The dip angle for the more probable fault plane averages to the northeast at about 60° - 70°. The more probable fault plane for the main shock dips to the SW about 83°. The difference in focal mechanisms between the mainshock and aftershocks suggests that they have not occurred on the same fault.

Velocity structures

Generally stated, we find that while our estimates of absolute velocity are often significantly different from those in Michael study, the overall trends in structure (locations of highs and lows in velocity) generally follow his results. The significant differences are the following: (1) the width of the low velocity zone along the fault is somewhat narrower, and (2) the low velocity zones are shifted to the southeast and became somewhat deeper. We note that the latter trend is consistent with our inference that the fault dips to the southeast at about 80°.

After three iterations the standard deviation in the travel time residuals reduced to 0.03s, which is close to the estimated error in the readings. This final variance represents a

90% reduction in variance over the original fit, suggesting that we have interpreted all the available signal in the data with the model we have selected.

Summary and Discussion

To summarize, the main findings of our study are that we have demonstrated the usefulness of the three-dimensional ray tracing method employed in deducing the fine structure of fault zones. Hypocenters change locations and focal mechanisms are redefined in ways that effect the interpretation of how aftershocks relate to mainshocks and faulted structures. Velocity structures are also deduced to greater precision.

Due to the consistent evidence provided by seismicity distribution, velocity structures and focal mechanisms, we infer that the subsurface structures in this region might be mainly described by two faults: the Calaveras and Modrone Spring faults. For the Calaveras fault, the seismicity patterns and the well-defined low velocity zone imply that the fault dips to the southwest at about 85°. This result is consistent with the fault-plane solution of the 1984 mainshock. On the other hand, the evidence from seismic patterns and most of the fault-plane solutions of the aftershocks indicate that the eastern fault in this region (the Modrone) dips to the northeast at about 70 degrees. One possible explanation of these observations is that main shock of Morgan Hill earthquake occurred along the Calaveras fault and, in addition to the causing the aftershocks along the Calaveras, stressed the Modrone Spring fault, an older thrust fault dipping to the northeast at about 75 degrees, and triggered most of aftershocks along this feature.

Figure Captions

Figure 1. The initial epicenters taken from Michael (1987) (crosses) and the new epicenters (squares) relocated in a the final velocity structure.determined after a three iteration inversion. Locations of cross-sections bb', cc', and dd' are indicated. The left side of each section is indicated by "L" and the right by "R". The scale at edges of plot are distances in kilometers from the center of coordinates.

Figure 2. (a) Earthquakes in cross-section bb'. Meaning of symbols is the same as in figure 1. (b). Earthquakes in cross-section cc'. (c) Earthquakes in cross-section dd'.

Figure 3. Plot of Take off angles and Azimuths of rays determined in a "best-fit" one-dimensional model and those determined by the three-dimensional ray tracer in the three-dimensional model. Note the wide spread in azimuthal values.


morganhill
CST
CDV
CML
CAD
CMM
COS
CMH
CAO
CMP
JSJ
JSG
CCO
JLX
JST
JSS
HSP
HGS
HCP
JEC
JRR
HPL
HGW
HCA
HFE
HCR
HOR
-122.2
-121.2
36.8

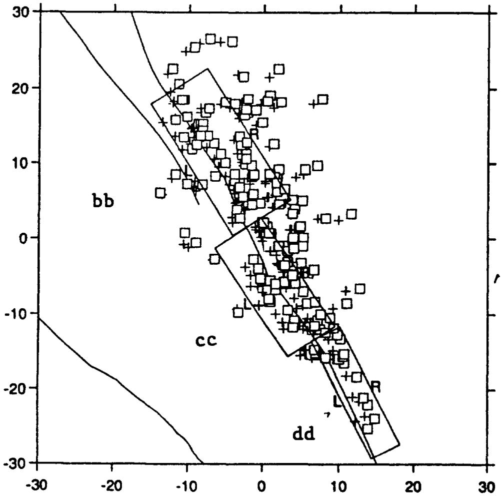
30
20
10
0
-10
-20
-30
-30
-20
-10
0
10
20
30
bb
cc
dd
R
L
R

Figure 1.

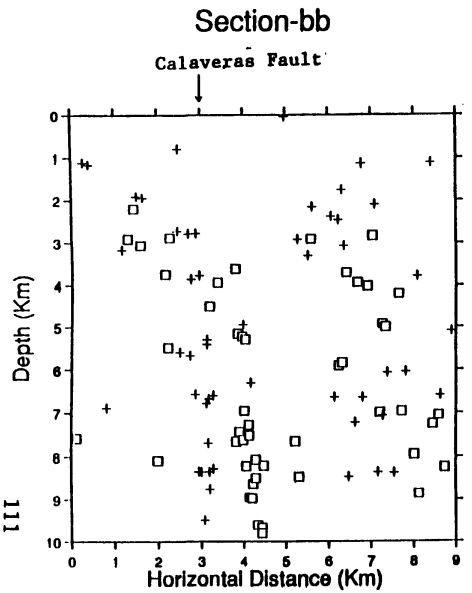

Figure 2a.

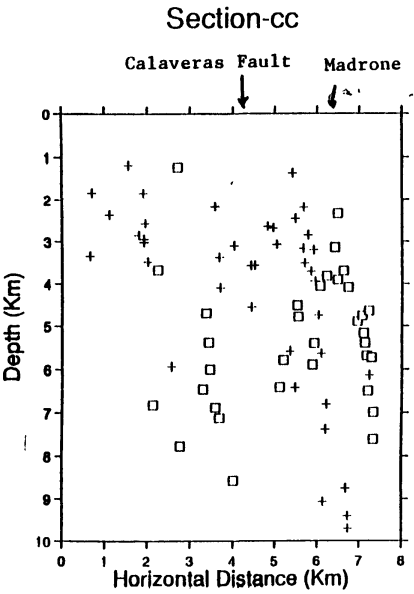

Figure 2b.

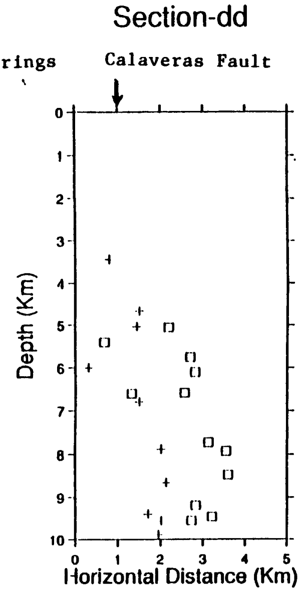

Figure 2c.

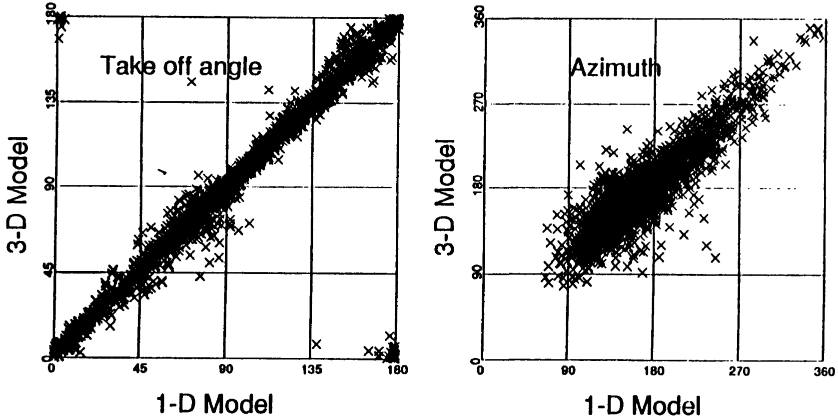

Figure 3.

Salton Trough Tectonics and Quaternary Faulting

9910-01292

Robert V. Sharp
Branch of Engineering Seismology and Geology
U.S. Geological Survey
345 Middlefield Road
Menlo Park, CA 94025
415/329-5642

Investigations

1. Post-seismic near-field deformation, 1989 Loma Prieta earthquake.
2. Normal faulting associated with the 1987 Superstition Hills earthquake.
3. Trenching study of a major fault near Bombay Beach, Imperial Valley (with M. Rymer).

Results

1. In order to monitor post-seismic deformation both vertically and horizontally within the zone of small surface breaks, an ~5 km-long array of survey marks was constructed along Summit Road a few days after the 17 October earthquake. Early indications from regional geodetic arrays and repeated slip measurements made at the surface breaks suggested that post-seismic deformation would be small to absent. Although remeasurement of the 5-km traverse has not yet been done, high-redundancy horizontal angle measurements have been repeated at a three point array straddling the Pink House fault on which the largest left-lateral coseismic slip was observed.

   As expected, the repeated horizontal measurements showed very little change over a 71-day lapse beginning on the 14th post-earthquake day. A 2.5 arc second angular shift, directionally consistent with continued left-lateral slip, is suggested by the data, but this apparent signal is too small relative to the angular resolution (± 5 arc seconds at 95 per cent confidence) to be accepted as real. If it were real, the angular change could be explained by a 2-4 mm leftward component of movement normal to Summit Road. On the pavement of Summit Road, however, no evidence of post-seismic growth of displacement has been observed at this site.

2. Normal faults within a 4 km-wide complex zone, striking north-northwestward on average and mostly dipping steeply

eastward toward the axis of the Salton Trough, have been identified and mapped between the Superstition Hills and the western edge of the agricultarally developed part of the Imperial Valley. This zone is now known to be at least 8 km but possibly as much as 22 km in length. The continuity and regional extent of the zone is obscured by agriculture north and south of the 22-km-span and by an 8-km-long area of dune sand in the central part.

In the course of mapping these structures with large-scale 1987 aerial photographs of the Superstition Hills region, discontinuous surface ruptures also were found along most of the traces within 10 km of the epicenter of the Elmore Ranch earthquake of 24 November 1987. Most of these surface ruptures were not reported in earlier publications. Where locational comparisons could be made, the new surface ruptures followed old fault traces. Although the preservation of the breaks ranged from severely degraded to nearly pristine, slip vectors, or at least vertical components of slip, were measureable at many locations. The largest vertical slip observed was nearly 8 cm, but typical movements on the new ruptures were less than 1 cm; at many locations the breaks were incipient extensional cracks.

These ruptures escaped earlier detection in the earthquake field investigation probably because little or no searching was made where they occur. Whether these breaks formed before or after the earlier field checks can be estimated now only by comparison of their states of preservation with those of ruptures of similar kind that were documented earlier. Reoccupation of one rupture in particular, near site 491 (Plate 1A of Sharp and others, 1989) indicated a similar range of degradation, so all are presumed to be of 1987 vintage. Inasmuch as earthquake epicenters before, during, and after the 1987 earthquake sequence do not delineate the zone of normal faulting in a convincing way, the ruptures of probable 1987 origin are interpreted to represent triggered movements.

Reference

Sharp, R.V., and others, 1989, Surface faulting along the Superstition Hills fault zone and nearby faults associated with the earthquake of 24 November 1987: Bulletin of the Seismological Society of America, v. 79, p. 252-281.

3. Two long trenches that were cut across northwest-trending faults about 3 km north of Bombay Beach show the zone to exceed 50 m in width. The principal and most continuous strand now recognized in this zone has an average orientation of N42^{o}W, nearly parallel to and about on strike with the southernmost mapped san Andreas fault, about 5 km

to the northwest. Small offsets within a thin superficial veneer of lake beds, presumably deposited about 300 year ago during the last high stand of Lake Cahuilla, suggest that creep,or small triggered displacements have occurred since that time. Three contiguous quadrilaterals spanning about 300 m across this zone have been constructed to verify the presence or absence of creep.

Reports

Sharp, R.V., 1989, Right-reverse faulting associated with the 7 December 1988 Armenia S.S.R. earthquake--an early reconnaissance [abs.]: EOS, Transactions of the American Geophysical Union, v. 70, p. 1199.

4/90

Seismotectonic Framework and Earthquake Source Characterization (FY90) Wasatch Front, Utah, and Adjacent Intermountain Seismic Belt

14-08-0001-G1762

R.B. Smith, W.J Arabasz, and J.C. Pechmann*
Department of Geology and Geophysics
University of Utah
Salt Lake City, Utah 84112-1183
(801) 581-6274

Investigations: October 1, 1989 - March 31, 1990

1. Left-lateral shear beneath the northwestern Colorado Plateau: The 1988 San Rafael swell and 1989 Southern Wasatch Plateau earthquakes.
2. The 1983 M_s7.3 Borah Peak, Idaho, earthquake: Stress tensor inversion of focal mechanisms for the main shock and 54 aftershocks.

Results

1. Two moderate earthquakes that occurred in the NW Colorado Plateau in central Utah on August 14, 1988, and January 30, 1989 (UTC), provide important new information on contemporary deformation and the state of stress at mid-crustal depths in this region. The first was an M_L 5.3 shock on the NW edge of the San Rafael swell, a broad Laramide anticlinal upwarp. The second was an M_L 5.4 earthquake located 70 km WSW of the first beneath the southern Wasatch Plateau, which rims the NW Colorado Plateau and forms part of a transition to the Basin and Range Province to the west. These earthquakes were the largest to occur within the Colorado Plateau since an M 5½ event near the Utah-Arizona border in 1959. Following each main shock, we supplemented the University of Utah's regional seismic network with 4-5 portable seismographs and later 2-4 telemetered stations in the epicentral areas. Each earthquake sequence was relocated with velocity models based on refraction studies and sonic logs of nearby oil wells; station delays were derived from well-located aftershocks. For the San Rafael swell sequence, the 66 best-located hypocenters define a 5-km-long aftershock zone extending from 11 to 18 km in depth and dipping 60° ± 5° ESE. P-wave focal mechanisms for the main shock and largest aftershock (M_L 4.4) both show oblique normal faulting, with the left-lateral nodal plane dipping E to SE in a direction similar to the dip of the aftershock zone. For the southern Wasatch Plateau sequence, the 32 best-located hypocenters define an 8-km-long aftershock zone between 20 and 25 km depth, striking NNE and dipping 90° ± 10°. P-wave focal mechanisms for the main shock and largest aftershock (M_L 4.2) both show strike-slip faulting with the left-lateral nodal plane striking NNE, parallel to the trend of the aftershock zone. The

---

*W.C. Nagy and S.J. Nava also contributed significantly to the work reported here.

T-axes for all four focal mechanisms are oriented between E-W and ENE-WSW, intermediate between the ESE-WNW extension direction of the Basin and Range—Colorado Plateau transition zone and the NE-SW extension direction of the interior of the Colorado Plateau. Our data suggest that both main shocks were caused by buried left-lateral or left-lateral and normal slip on Precambrian basement faults striking NNE. Active NNE left-lateral shear at depth may explain some enigmatic aspects of the surficial tectonics—including the right-stepping, en-echelon pattern of young, N-S-trending graben on the Wasatch Plateau.

2. Previous studies of aftershocks of the 1983 M_s7.3 Borah Peak, Idaho, earthquake and an analysis of the contemporary strain field from historical seismicity indicated NNE-SSW extension for central Idaho. However, the long-period focal mechanisms for the main shock and a study by Stickney and Bartholomew of Quaternary faulting and focal mechanisms for southwestern Montana and central Idaho suggest NE-SW extension. To investigate this apparent inconsistency, we applied the stress inversion algorithm of Gephart and Forsyth to P-wave first-motion focal mechanisms for 54 Borah Peak aftershocks of $2.3 \le M_L \le 5.8$ plus the main shock focal mechanism determined by Doser and Smith from moment-tensor inversion of long-period P waves. The inversion yielded a minimum principal stress (σ_3) direction that is horizontal and trends N 49° E, a maximum principal stress (σ_1) direction that trends S 41° E and plunges 81°, and a ϕ value of 0.65 (where $\phi = (\sigma_2 - \sigma_3)/(\sigma_1 - \sigma_3)$). The σ_3 axis is nearly parallel to the NE-SW extension directions inferred from T-axes of long-period focal mechanisms of the Borah Peak main shock and from analyses of Quaternary faulting and focal mechanisms in southwestern Montana and central Idaho. This stress field orientation would be expected to produce dominantly normal faulting along the Lost River fault with some left-lateral motion along the NNW-striking Thousand Springs segment and a small component of right-lateral motion along the WNW-striking Arentson Gulch fault.

Reports and Publications

Doser, D.I. and R.B. Smith (1989). An assessment of source parameters of earthquakes in the Cordillera of the western United States, *Bull. Seism. Soc. Am. 79,* 1383-1409.

McGuire, R.K. and W.J. Arabasz (1990). An introduction to probabilistic seismic hazard analysis, in *Geotechnical and Environmental Geophysics, Vol. 1: Review and Tutorial,* S.H. Ward, Editor, Society of Exploration Geophysicists, in press.

Pechmann, J.C. and B.S. Thorbjarnardottir (1990). Waveform analysis of two preshock-main shock-aftershock sequences in Utah, *Bull. Seism. Soc. Am.,* in press.

Shemeta, J.E. and J.C. Pechmann (1989). Source parameters of aftershocks of the 1983 Borah Peak, Idaho, earthquake, *EOS, Trans. Am. Geophys. Union 70,* 1188.

Shemeta, J.E. and J.C. Pechmann (1990). Source parameters of aftershocks of the 1983 Borah Peak, Idaho, earthquake, submitted to *J. Geophys. Res.*

Westaway, R. and R.B. Smith (1989). Source parameters of the Cache Valley (Logan), Utah, earthquake of 30 August 1962, *Bull. Seism. Soc. Am. 79,* 1410-1425.

Late Quaternary Recurrence Intervals on the Owens Valley Fault Zone, Lone Pine, California

14-08-0001-G1783

Paul Bierman and Alan Gillespie
Department of Geological Sciences, Mail Stop, AJ-20
Seattle, Washington 98195

<u>Objectives</u>: Our investigation is designed to constrain more tightly current estimates of recurrence intervals and fault slip rates for the Lone Pine fault (LPF), a subsidiary strand of the Owens Valley Fault Zone (OVFZ), and to test the hypothesis that earthquakes occur at regular and predictable intervals on the OVFZ. In addition to providing data for the refinement of risk estimates, our study provides information concerning the applicability and variability of different dating techniques.

In order to achieve these objectives, we are presently performing field and analytical work designed to answer the following specific research questions:

1. <u>What are the ages of alluvial fans deposited by Lone Pine Creek and ruptured by the LPF</u>?

2. <u>What are the ages of colluvial wedges recorded in the trench logs of Lubetkin and Clark (1988)?</u>

3. <u>What are the ages of varnish rings on large scarp boulders interpreted by Lubetkin and Clark as representing specific intervals of scarp lowering?</u>

4. <u>How and why do results obtained from different dating methods vary?</u>

<u>Results</u>:

1. <u>Mapping and dating of alluvial fan surfaces</u> -- During the past year, Bierman mapped the alluvial fans at Lone Pine delineating fan surfaces of at least four distinct ages (Bierman and Gillespie, 1989). He delineated fan units on the basis of relative weathering criteria, soil development, and surface morphology. In a distal portion of the youngest fan we collected two charcoal samples from fluvial sediments interbedded with debris flow diamictons. The dates for these samples were 4030 +/- 60 (TO-1666) and 610 +/- 70 (QL-4361). Samples were collected from each of the four fan surfaces for both rock varnish and cosmogenic isotope dating (^{3}He). Rock varnish analyses are ongoing and are being made using several different analytical techniques. Bierman

will perform the ^{3}He analyses in cooperation with J. Poths at the Los Alamos National Laboratory.

2. Results of trenching -- During March 1990 we opened seven trenches on the faulted Pleistocene alluvial fan 1 km west of Lone Pine. Two of the trenches were opened immediately below and normal to the scarp of the LPF. We logged both trenches and collected samples for both grain-size and thermoluminescence analyses. Our interpretation suggests four periods of surface stability are preserved in the southern trench and three in the northern trench. These interpretations are based on sedimentological criteria and the presence of buried Av horizons. Our interpretations are consistent with those of Lubetkin and Clark (1988). The thermoluminescence samples will be analyzed this summer by Bierman under the supervision of G. Berger (Western Washington University). No datable organic carbon was found in either trench.

3. Rock varnish dating -- To determine the applicability of varnish dating to neotectonic problems, we have made numerous measurements of rock varnish chemistry and rigorously considered the statistical constraints on the cation ratio method. Some of these data were presented in Bierman and Gillespie (1990) and will be considered in a paper we have recently submitted to *Geology.* The measurements and the statistical analysis we performed suggest that rock varnish cation ratio dating of neotectonic events will require chemical measurements to be made more precisely and with greater frequency than those made by previous investigators.

REFERENCES CITED

Bierman, P. and Gillespie, A., 1989, Rock varnish, alluvial fans, and tectonism in the southern Owens Valley, CA: Geological Society of America Abstracts with Programs, Vol. 21, No. 6, p. A343.

Bierman, P. and Gillespie, A., 1990, Varnish cation-ration ages - how precise can they be?: Geological Society of America Abstracts with Programs, Vol. 22, No. 3, p. A8.

Lubetkin, L. K. and Clark, M. M., 1988, Late Quaternary activity along the Lone Pine Fault, eastern California: Geological Society of America Bulletin, v. 100, p. 755-766.

Surface Faulting Studies

9910-02677

M.G.Bonilla
Branch of Engineering Seismology and Geology
U.S. Geological Survey
345 Middlefield Road, MS 977
Menlo Park, CA 94025
(415) 329-5615

Investigations

1. Loma Prieta earthquake
2. Geology of Marina District
3. Geodynamic map of Circum-Pacific region

Results

1. Following the October 17, 1989 earthquake, field examinations of dikes and broad artificial fills on the southwest fringes of San Francisco Bay found only a few minor ground cracks and no ground failures. Included in the examination were areas within Redwood City, Foster City, Palo Alto, Mountain View, and Alviso. The area near Laguna Salada (in Pacifica), known to include saturated clean sand, was examined independently by J.J. Lienkaemper and M.G. Bonilla, who found no evidence of liquefaction. Ground failures were recorded by K.R. Lajoie and M.G. Bonilla at the eastern approaches to the Bay Bridge, at Alameda Naval Air Station, and at the Oakland International Airport.

2. Maps dating back to 1851, archival materials including photographs, published reports, and logs of borings made from 1912 to 1990 were used to prepare a report on the geology, including the history of artificial fills, of the Marina District of San Francisco. Others in the study group are using the report to better understand what effect the artificial fills, Holocene and Pleistocene estuarine deposits, and bedrock configuration had on the severe earthquake damage in the Marina District.

3. Compilation and plotting of historical surface faulting was completed for the Arctic Sheet of the Geodynamic Map of the Circum-Pacific Region. This sheet covers most of western and northern North America, eastern and northern Asia, Greenland, and Iceland. Publication is expected in 1990.

Reports

Bonilla, M. G., and Lienkaemper, J. J., 1990, Visibility of fault strands in exploratory trenches and timing of rupture events: Geology, v. 18, no. 2, p. 153-156.

05/90

Northern San Andreas Fault System

9910-03831

Robert D. Brown
Branch of Engineering Seismology and Geology
U.S. Geological Survey
345 Middlefield Road, MS 977
Menlo Park, California 94025
(415) 329-5620

Investigations

1. Field reconnaissance in the epicentral region of the October 17, 1989, Loma Prieta earthquake and in lowland areas surrounding San Francisco Bay. Evaluated evidence for surface tectonic deformation in epicentral region and for liquefaction and amplified ground motions near present or historic bay margins.

2. Research and review of work by others on the tectonic setting and earthquake potential at Diablo Canyon Power Plant (DCPP), near San Luis, Obispo, California. Activities are in an advisory capacity to the Nuclear Regulatory Commission (NRC) and are chiefly to review and evaluate data and interpretations obtained by Pacific Gas and Electric Company (PG&E) through its long-term seismic program.

3. Serve as chairman of Policy Advisory Board, Bay Area Earthquake Preparedness Project (BAREPP). A joint project of the State of California and the Federal Emergency Management Agency, BAREPP seeks to further public awareness of earthquake hazards and to improve mitigative and response measures used by local government, businesses, and private citizens.

Results

1. No continuous or consistent zone of tectonic fractures marked the surface projection of the fault trace, although locally, on Madonna Road, the main break of the San Andreas fault exhibited right-lateral displacement of 1-2 cm. Liquefaction near San Francisco Bay was largely confined to historic marshlands and bay muds now chiefly fill-covered, on both sides of the bay and from 70 to 100 km distant from the epicenters.

2. Continued reviews of geologic and geophysical data related to DCPP and provided oral and written review comments to NRC. Coordinated USGS review and data acquisition efforts related to DCPP.

3. Provided informal oral and written data, analysis, and recommendations to BAREPP and other Policy Advisory Board members on geologic, seismologic, and management issues relating to earthquake hazard mitigation in California.

Reports

Brown, Robert D., 1990, Geologic hazard patterns for future earthquakes (abstract): American Association for the Advancement of Science, New Orleans, Annual Meeting.

Brown, R.D., Jr., 1990, Quaternary deformation, *in* Wallace, R.E., ed., San Andreas fault system: U.S. Geological Survey Professional Paper 1515, in press.

4/90

Seismic Hazards of the Hilo 7 1/2' Quadrangle, Hawaii

9950-02430

Jane M. Buchanan-Banks
Branch of Geologic Risk Assessment
U.S. Geological Survey
David A. Johnston Cascades Volcano Observatory
Vancouver, Washington 98661
(206) 696-7996

Investigations

Preparation of manuscript, Geologic Map of the Hilo 7 1/2' Quadrangle, Island of Hawaii.

Results

One month was spent revising the manuscript, and in checking all plates, tables, and figures for completeness and accuracy. The report was submitted through BGRA to BWTR in late December. Completion of this manuscript was deferred to permit full-time attention to project 9950-04073, Depth to bedrock map in the greater Tacoma area, Washington. This is the final product of this project.

Reports

Buchanan-Banks, J.M., Lockwood, J.P., and Ruben, Meyer, 1989, Radiocarbon dates for lava flows from northeast rift zone of Mauna Loa Volcano, Hilo 7 1/2' Quadrangle, Island of Hawaii: Radiocarbon, v. 31, no. 2, p. 179-186.

LATE QUATERNARY SLIP RATES ON ACTIVE FAULTS OF CALIFORNIA

9910-03554

Malcolm M. Clark
Branch of Engineering Seismology and Geology
U.S. Geological Survey
345 Middlefield Road
Menlo Park, California 94025
415/329-5624

Investigations

1. Recently active traces of Calaveras fault zone at Tres Pinos Creek and San Felipe Creek, California (K.J. Kendrick, J.W. Harden, M.M. Clark).

2. Recently active traces of Owens Valley fault zone, California (Sarah Beanland (NZGS), Clark).

3. Degradation of fluvial terrace risers along Lone Pine Creek, San Bernardino County. (Kendrick, in conjunction with J.B.J. Harrison, L.D. McFadden (UNM), and R.J. Weldon (University of Oregon)).

4. Revision of slip-rate table and map of late-Quaternary faults of California (Clark, Kendrick, J.J. Lienkaemper, K.R. Lajoie, C. Prentice, M.J. Rymer, D.P. Schwartz, R.V. Sharp, J.D. Sims, J.C. Tinsley, R.J. Weldon).

5. Geologic investigation of Loma Prieta earthquake (Clark).

Results

3. Many empirical models have been proposed to evaluate the rate of slope degradation; determination of the rate of slope processes will allow for estimating ages of landforms. For tectonic settings involving vertical separation, the degree of degradation of scarps may be one of the more useful tools for determining the most recent faulting event. Measurements made on a terrace riser and associated lower terrace tread in Cajon Pass allow us to evaluate one model of scarp degradation. Radiocarbon dates constrain the time of abandonment to approximately 8,350 years. We measured fourteen scarp profiles along this terrace riser and using the nonlinear diffusion equation of Hanks and Andrews (1988), estimated scarp age. There predicted ages ranges from 4,830 to 10,920 years. On three of these scarp profiles we described catenas of soils. This allowed us to compare the rate

of colluvial accumulation for different parts of the of the slope as determined from soil profiled with what is predicted by the model. We were also able to compare the variability of soil development with the variability of predicted scarp ages. previous studies in this area have shown that the most important factor affecting soil development is the influx of eolian dust, so that the profile mass of silt + clay is an adequate measure of degree of soil development. A parallel study of the soils on the terrace tread allows us to compare both the degree of soil development and the variability of the tread soils with the soils of the catenas. Soils below the inflection point were at least as strongly developed as the soils on the terrace tread, and the maximum soil development occurred at the base of the scarp. Most surprising is that the variation of soils on the terrace tread is greater than the variation of catena soils on the same geomorphic position. The variation of predicted ages based on the diffusion model was not reflected in variation of soil development. This would suggest imprecision in the model itself, rather than variation in slope processes.

4. We are in the process of revising, updating, and publishing (as a USGS Bulletin) the slip-rate table and map of late-Quaternary faults of California (USGS OFR 84-106). Our aim is to review all entries in OFR 84-106 and add all new data generated since its release. We welcome any relevant unpublished data from workers in this field.

5. Post earthquake investigation included search of the epicentral zone for tectonic ruptures, search of Calaveras fault with Peter Wood (NZGS) for triggered slip (none from Halls Valley to Coyote Reservoir), search for slip on range-front reverse faults in Los Gatos-Palo Alto, and mapping of extension fractures (with others) in Summit Road area of Santa Cruz Mountains.

Reports

Plafker, George, and Galloway, J.P., eds., 1989, Lessons learned from the Loma Prieta, California, earthquake of October 17, 1989: U.S. geological Survey Circular 1045, 48 p., (contribution by Clark).

U.S. Geological Survey Staff, 1989, Preliminary map of fractures found in the Summit Road-Skyland Ridge area during the Loma Prieta, California, earthquake of October 17, 1989: U.S. Geological Survey open-File Report 89-686, (Clark a co-author).

Ponti, D.J., Wells, R.E., Haugerud, R.A., Clark, M.M., and Hall, N.T., 1990, Surface rupture aspects, <u>in</u> Benuska, L., ed., Reconnaissance report on the Loma Prieta earthquake: Earthed., Reconnaissance report on the Loma Prieta earthquake, Earthquake Engineering Research Institute (EERI) Special

Report, in press.

U.S. Geological Survey Staff, 1990, The Loma Prieta, California earthquake: An anticipated event: Science, v. 247, p. 286-293, (contributions by Clark).

U.S. Geological Survey Staff, 1990, Surface fractures and ground failure associated with the Loma Prieta, California earthquake of October 17, 1989: American Geophysical Union, EOS, v. 71, p. 291, (Clark a co-author).

U.S. Geological Survey Staff, 1990, Apparent lithologic and structural control of surface fracturing during the Loma Prieta earthquake of October 17, 1989: American Geophysical Union, EOS, v. 71, p. 290, (Clark a co-author).

Kendrick, K.J., Harrison, J.B.S., McFadden, L.D., and Weldon, R.J., 1990, An evaluation of a non-linear diffusion model for determining the rate of scarp degradation in Cajon Pass, southern California (abs.): 1990 Mojave Desert Research Symposium, San Bernardino, California, in press.

TECTONICS OF CENTRAL AND NORTHERN CALIFORNIA

9910-01290

William P. Irwin
Branch of Engineering Seismology and Geology
U.S. Geological Survey
345 Middlefield Road
Menlo Park, CA 94025
415/329-5639

Investigations

Preparation and revision of manuscripts pertaining to the geology and tectonic of northern California and southwestern Oregon.

Results

The writing of a report describing the geology and tectonic development of the Klamath Mountains and adjacent regions continued during the report period and is planned for publication in the USGS Bulletin series. The Klamath Mountains province is of particular interest because it consists of an unusually large number and variety of accretionary terranes, and it documents a long history of tectonic development of the Pacific coastal region of North America. A geologic compilation of the Klamath Mountains province at a scale of 1:500,000 was revised and updates following review by the Geologic Map Editor and was approved for publication as a USGS I-series map. A review of paleomagnetic results from the Klamath Mountains, Blue Mountains, and Sierra Nevada, coauthored with E.A. Mankinen, was revised following technical and editorial review and is to be published in a symposium volume on Paleozoic and Early Mesozoic paleogeography.

Reports

Irwin, W.P., 1989, Cryptic tectonic domains of the Klamath Mountains, California and Oregon, in A.M. Johnson, C.W. Burnham, C.R. Allen,, and M. Muehlberger, eds., Richard H. Jahns Memorial Volume: Engineering Geology, v. 27, nos. 1-4, p. 433-448.

Irwin, W.P., in press, Geologic map of the Klamath Mountains, California and Oregon: U.S. Geological Survey, Miscellaneous Investigations Map I-2148, scale 1:500,000.

Mankinen, E.A., and Irwin, W.P., in press, Review of paleomagnetic data from the Klamath Mountains, Blue Mountains, and Sierra Nevada: Implications for paleogeographic reconstructions, in D.S. Harwood and M.M. Miller, eds., Paleozoic and Early Mesozoic paleogeography of the Klamath Mountains, Sierra Nevada, and related terranes: Geological Society of America, Special paper 255.

4/90

Very Precise Dating of Prehistoric Earthquakes in California using Tree-Ring Analysis

14-08-001G1329
EAR88-05058

Gordon C. Jacoby
Tree-Ring Laboratory
Lamont-Doherty Geological Observatory
Palisades, New York 10964
(914) 359-2900

A. SAN FRANCISCO BAY REGION (San Andreas fault)

From Fort Ross to near Point Arena, the San Andreas fault zone trends through open terrain and some extensive forests of coast redwood [*Sequoia sempervirens* (D. Don) Endl.]. A recent excavation-paleoseismic study of this region (Prentice, 1988) concluded that there were a minimum of five or six earthquakes in the last 2,000 years. The 1906 event produced 5 meters of slip at the excavation site and evidence from the offset of a buried channel indicated a slip rate of about 25 mm. per year (Prentice, 1988a). If there were a relatively consistent slip rate, 200 years would be enough to accumulate another 5 meters of potential release. This information encourages us to believe that we should have at least one, and very probably two, large events within the lifetime of the oldest trees we have found along the fault in the area. These estimated time intervals make this area very promising for application of tree-ring methods to paleoseismology.

We have found a redwood over 1,400 years in age and over 500 years is not unusual. Dating of coast redwoods is very difficult, especially near the base where the trunks are buttressed and irregular in form. Although most old growth redwoods have been cut in this area, the decay resistance of redwood has kept the stump wood in excellent condition since the logging days. The dating problem is being overcome in two ways. First, we are in the process of developing a master chronology from the same species sampled in the next major valley inland, away from the effects of coastal fog, where the growth rings tend to be more consistent and easier to crossdate. Analyses thus far indicate that the coastal trees do crossdate with the trees from the inland site. Second, our studies show crossdating between redwood and Douglas fir [*Pseudotsuga menziesii* (Mirb.) Franco] from the same area. Douglas fir have much better circuit uniformity and are readily dateable. With the kind permission of Mr. Larry Mailliard we have also sampled cross sections and cores of redwood and Douglas fir from the Mailliard Ranch, about 30 miles east of the coast. The inland redwood and the Douglas fir are serving as guides to the dating of the coastal samples from along the fault. We have already established crossdating in both cases and are making good progress in developing a basis for dating the old-aged stump samples from along the fault. We now have an absolutely-dated redwood chronology dating back to the late 1400's. Unpublished coastal redwood data from Schulman (1936) and ring-width data from other species in the northern California region are all being used to establish a network of crossdating relationships throughout the region.

The fault zone location was logged around 1900 but many stumps are intact today. From fire and decay of the sapwood, outer rings are gone but the remaining heartwood is solid in many of the stumps. We cored over 15 stumps and obtained ring counts of more than 500 annual rings in several of them. Adding the approximately 100 years accounting for decay and the logging date, we can expect to be obtaining information for the past 600 or 700 years. Sections were cut from several stumps but many more remain to be sampled. We traced the fault zone for two and one-half miles and noted many more sampling opportunities on or near the fault. There are several sag ponds and small linear scarps that delineate the fault zone. It is not a single continuous trace, there are subparallel traces and offset between traces. At one location there is an offset creek, a well-defined fault zone, and large redwood stumps on the immediate sides of the fault. This offset is about 10 meters and therefore must have been displaced by at least one other event in addition to the 1906 event. Dr. C. Prentice of the U.S.G.S. has aided us in locating the fault trace and making geological evaluations of the sample sites.

B. CASCADIA SUBDUCTION ZONE (CSZ)

The Late Holocene sediments along the margin of Humboldt Bay and the floodplain of Salmon and Little Salmon Creeks have been displaced by the Little Salmon Creek fault. Trenches across the fault at Little Salmon Creek have shown evidence of multiple slip events bracketed by periodic deposition of well stratified floodplain sediments during the late Holocene (Carver and Burke 1987a & b). The trench studies show that the west trace of the Little Salmon fault has experienced at least 33 meters of slip during the last 6200 years, and indicates the most recent event occurred more recently than 415 ±70 RYBP (Carver and Burke 1987a & b). The rate of fault displacement for the last 6,200 years corresponds well with the rate of sedimentation and scarp morphology measured at the site. The very youthful geomorphic expression of the fault, including numerous fault-line landslides, disrupted stream profiles, and mole-track scarps in late Holocene bay marginal marsh sediments support the radiocarbon dating of the last event as being less than 415 years B.P. The fault itself can be traced through formerly forested lands in the area.

Our sampling along the Little Salmon Creek fault itself produced a number of old-aged samples for processing. The oldest samples found thus far are exclusively redwood. All of the living Douglas fir and Grand fir [*Abies grandis* (Dougl. ex D. Don) Lindl.] encountered along the fault zone were too young (less than 150 years) to be of much use for our purposes. Old-aged redwood samples were obtained from two areas. Both areas were previously logged, most likely around the turn of the century, and the areas subsequently burned either naturally or deliberately. Considerable amounts of wood have been burned or lost from decay on the outer portions of some stumps. Some of the samples have 300 to over 500 annual rings and a few exhibit obvious trauma from disturbance and/or fire. With logging believed to have taken place around 1900, we can study a tree-ring record extending back about 400 to 600 years. Thus we have old trees along the fault that certainly extend back well past the estimated date of the most recent prehistoric event dated by carbon-14. Our sampling along the fault thus far has primarily been achieved using standard 5mm diameter corers. Although the fault sometimes can be traced in this area by geomorphology, only soil differences reveal its location at other sites. The soils in certain locations are distinct enough to mark the fault trace to within a meter.

We obtained tree sections from timber companies in the area in collaboration with Dr. G. Carver of the Geology Department of California State University at Humboldt. With the cooperation with the National Park Service, we sampled Grand fir and Douglas fir in Redwood National Park. That chronology extends back to the 1750's and crossdates with Schulman's redwood data. The successful crossdating of fir with redwood demonstrates that this fir chronology will be useful in dating the redwood samples with potentially 150 years of overlap with trees cut down around 1900. We also have developed a chronology based on Douglas fir from a timber operation that extends back to the early 1400's. This

Douglas fir chronology is from north of the Little Salmon Creek area. Whole sections were obtained from five old-aged trees and provide us with a good reference chronology to crossdate with our fault zone trees. With the above tree-ring data we are now ready to start dating the cores and other samples from the fault zone. We will compare the dating from the Little Salmon Creek fault region with the trees from the Gualala block zone as a means of cross-verification.

One intriguing result from our studies in this region is from Catfish Lake, north of the Little Salmon Creek and slightly east of the actual fault. The lake formed as a result of a large, prehistoric landslide in the hanging wall of the fault. The lake contains many submerged stumps of old trees. These trees were obviously killed as a result of the submergence, and dating the outer ring of each tree would effectively date the landslide. Assigning seismic origin to a landslide in the steep-sloped and rain-soaked coastal ranges of California is not justified unless there is some corroborative evidence. The large size of the landslide and its location relative to the fault allow for a seismic origin but we need confirmation from the fault zone trees or other sources before we can make any definitive interpretation. Dating the creation of the lake may merely date a geohazard event. Crossdating with other tree-ring data showed the most recent outermost ring is 1741. There is some loss of outer rings due to decay but judging from the configuration of the trunks sampled there are probably not many rings lost. We would estimate the event as occurring within a few years after 1741. Until there is other corroborative information, the date of 1741 must only be considered as the earliest date for a significant landslide event. It is considerably younger than the 415 yr. limit from Carver (1987). We will try to obtain samples with either bark or the outer rings present to enable us to absolutely date the year of the event.

We may precisely date at least the most recent large earthquake on the Little Salmon fault. We have a minimum age for a hazardous landslide. Dates from this region may be especially significant in comparison with dates for other possible paleoseismic events on the Washington and Oregon coast (Grant et al. 1989). The more recent carbon-14 dates from Grant et al. (1989) and tree-ring dates from Yamaguchi et al. (1989) show differences in dating of possible subsidence events in the CSZ. Problems in carbon-14 dating of young material from organically-active environments may partly account for some of the age discrepancies. As noted by Grant et al. (1989), earthquake hypotheses for the region can presently range from single 700 km events to smaller events distributed throughout several centuries. The convergence of dates indicating major events and the isolation of individual events related to the Cascadia Subduction Zone will all be important in assessing the seismic behavior and earthquake hazard potential.

Acknowledgement: This research was also supported by the Seismology Program of the Earth Sciences Division of NSF, Grant EAR88-05058

References:

Carver, G.A. 1987. Late Cenozoic tectonics in the Eel River basin region, coastal northern California. In: Schymiczek, H. and Suschsland, R.(eds.), Tectonics, Sedimentation and Evolution of the Eel River and Associated Coastal Basins of Northern California. San Joaquin Geological Society Misc. Pub. 37. pp. 61-71.

Carver, G.A. and R.M. Burke. 1987a. Late Holocene paleoseismicity of the southern end of the Cascadia Subduction Zone (abs). EOS 68(44):1240.

Carver, G.A. and R.M. Burke. 1987b. Late Pleistocene and Holocene paleoseismicity of Little Salmon and Mad River thrust systems, N.W. California--implications to the seismic potential of the Cascadia Subduction zone (abs). Geological Society of America, 26-29 October 1987, Phoenix, Arizona. p. 614.

Grant, W.C., Atwater, B.F., Carver, G.A., Darienzo, M.E., Nelson, A.R., Peterson, C.D., and Vick, G.S. 1989. Radiocarbon dating of Late Holocene coastal subsidence above the Cascadia Subduction Zone--Compilation for Washington, Oregon and northern California, EOS 70 (43) p. 1331.

Prentice, C.S. 1988a. Earthquake Geology of the Northern San Andreas Fault near Point Arena, California. PhD. Thesis. Calif. Inst. of Tech. Pasedena, Calif.

Schulman, E. 1936. unpublished data. Laboratory of Tree-Ring Research, Univ. of Arizona, Tucson, Arizona.

Yamaguchi, D.K., Woodhouse, C.A. and Reid, M.S. 1989. Tree-ring evidence for synchronous rapid submergence of the southwestern Washington coast 300 yrs. B. P. EOS 70 (43) p. 1332.

Coastal Tectonics

9910-01623

Kenneth Lajoie
Branch of Engineering Seismology and Geology
345 Middlefield Road, M/S 977
Menlo Park, California 94025
(415) 329-5641/5747

Investigations

1. Post-earthquake studies, Loma Prieta earthquake
2. ESR dating

Results

1. Loma Prieta Earthquake:

A. Surface Fractures: Field investigations immediately after the earthquake revealed that there were no primary surface fractures along the segment of the San Andreas fault that ruptured. However, there were many secondary surface fractures, especially in the Summit Road area. Many of these fractures apparently resulted from bedding-plane faulting within the folded Tertiary strata that underlie the area. Faulting within weak beds probably coincided with tectonic uplift and extension of the hanging-wall block, ridge-top spreading due to strong shaking, or both. Fractures commonly occur in laterally continuous NW-trending zones and have consistent displacement vectors, an observation suggesting that they are not related to near-surface slope failure. Most fractures are closely aligned to the strike of bedding, even in structural domains where bedding deviates from the overall trend. For some fracture sets, displacement vectors lie very close to bedding planes, and most of the fractures show downdip movement.

Most cracks are extensional, with a subordinate component of vertical displacement. Nearly two-thirds of the fractures have a component of left slip, whereas most of the rest exhibit right-lateral displacement; only 5% of measured cracks show pure extension. Physical models may explain sinistral lateral motion as due to anomalous shear stresses at the north end of the deep-seated rupture. However, lateral motion (both left and right slip) of most fractures can be adequately explained by considering the individual fracture orientations with respect to local bedding and topography.

Two different models can describe the sense of lateral movement on the fractures. In the first, pure dip-slip faulting occurs on underlying bedding planes. Lateral motion results if a crack trend deviates somewhat from the strike of bedding as it propagates through the overlying colluvium. If the deviation is in a clockwise sense, left-lateral displacement occurs on the surface fracture; counterclockwise deviations result in right-lateral displacements. This model predicts the proper sense of displacement for more than 60% of the fractures studied. The other model assumes that displacements are controlled only the local slope direction; lateral components of motion occur where fractures are oblique to the local slope. This model explains most observed lateral displacements on fractures with downslope displacement vectors. A combination of dip-slip faulting on bedding planes and downslope motion is probably all that is required to explain the orientation and sense of slip on surface ruptures in the Summit Road-Skyland Ridge area.

B. Liquefaction: In the San Francisco Bay area, where the water table is artificially depressed beneath most low-lying alluvial areas, liquefaction and associated ground failure occurred only in land fills that consist of hydraulically emplaced sand, such as those underlying the Marina District in San Francisco and the Alameda Naval Air Station in Alameda. All of these fills lie within the bay and are, therefore, water saturated. There is no surficial evidence that liquefaction occurred in alluvium, estuarine mud, or in land fills composed of hydraulically emplaced silt within the bay, such as those underlying Foster City and Redwood Shores in San Mateo County. All of the fills that liquefied lie in the central part of the Bay, between the Golden Gate and the San Mateo bridges, where there are extensive latest Quaternary sand deposits from which the fill was dredged. In the eastern part of the bay, along the shores of Oakland and Alameda, the source of the dredged fill was late Pleistocene Merrit sand and Holocene estuarine sand that was most likely reworked from the Merrit sand. Where the Merrit sand, a dune deposit that was largely submerged by the early Holocene rise in sea level, occurs above sea level it forms the low-lying areas of west Oakland, Alameda, and Bay Farm island. There is no evidence that undisturbed Merrit sand liquefied during the earthquake, suggesting that this loosely consolidated deposit had been compacted by shaking during many previous earthquakes. In the western part of the bay, along the northern and eastern shores of the San Francisco peninsula, the source of the dredged fill was most likely late Holocene littoral and estuarine sand most likely reworked from older dune deposits.

The most conspicuous surface manifests of the liquefaction that occurred during the earthquake were sand-blown deposits (mostly along the margins of and through cracks in large pavements), ground cracks (mostly in pavements), differential settlement (most beneath large pavements and residential buildings), and lateral spreads (mostly of earth-filled dikes). Liquefaction probably occurred in most water-saturated sand fills, but ground failure resulted mainly where the overburden loads of broad concrete and asphalt pavements and foundations increased fluid pressures sufficiently to produce vertical and lateral sand flows. However, in a few places, such as the Oakland International Airport, sand blows erupted in open areas away from pavements or building foundations.

2. Digitized and integrated ESR spectra provide more systematic results than the raw ESR data.

TL dosimeters at twelve sites along the California coast indicate that dose rates of gamma radiation (the source of most lattice damage in fossil carbonates) strongly reflect bedrock lithology (relatively high rates are associated with volcanic and plutonic rocks and low rates are associated with sedimentary rocks). These results indicate that dose rates will have to be measured at each fossil locality used for dating deformed marine strandlines.

Reports

Plafker, G., and Galloway, J.P., eds., 1989, Lessons learned from the Loma Prieta, California, earthquake of October 17, 1989: U.S. Geological Circular 1045, 48 p.

U.S. Geological Survey Staff, 1989, Preliminary map of fractures formed in the Summit Road-Skyland Ridge area during the Loma Prieta, California, earthquake of October 17, 1989: U.S. Geological Survey Open-File Report 89-686, scale 1:12,000.

U.S. Geological Survey Staff, 1990, The Loma Prieta, California, earthquake--An anticipated event: Science, v. 247, p. 286-293.

U.S. Geological Survey Staff, 1990, Apparent lithologic and structural control of surface fracturing during the Loma Prieta earthquake of October 17, 1989: EOS, v. 71, no. 8, p. 290.

U.S. Geological Survey Staff, 1990, Surface fractures and ground failure associated with the Loma Prieta, California, earthquake of October 17, 1989: EOS, v. 71, no. 8, p. 291.

Ponti, D.J., Wells, R.E., Haugerud, R.A., Clark, M.M., and Hall, N.T., Surface rupture aspects: EERI reconnaissance report on the Loma Prieta, California, earthquake of October 17, 1989: in press

Ponti, D.J., Wells, R.E., Origin of surface ruptures in the Santa Cruz Mountains, California, formed during the October 17, 1989, Loma Prieta earthquake: submitted to SSA for their Annual Meeting, May 1990.

Lajoie, K.R., Ponti, D.J., Powell, II, C.L., Mathieson, S.A., and Sarna-Wojcicki, A.M., Emergent marine strandlines and associated sediments, coastal California: DNAG Volume on Non-Glacial Quaternary Geology of the Western United States: in press.

TEMPORAL AND SPATIAL PATTERNS OF LATE QUATERNARY FAULTING, WESTERN UNITED STATES

NEW PROJECT

MICHAEL N. MACHETTE
Branch of Geologic Risk Assessment
U.S. Geological Survey, Box 25046, MS 966
Denver, Colorado 80225
(303) 236-1243

PURPOSE OF PROJECT

To define regional variations in the time-space partitioning of paleoseismic activity in the late Quaternary as a guide to understanding how strain accumulates and is released on faults in the Western United States. This project will serve as an umbrella for diverse but interrelated aspects of paleoseismicity in the western U.S. We will study selected faults that are critical to interpreting the paleoseismology and neotectonics in regions of active faulting. Our research will apply paleoseismologic studies to important problems at three different scales: (1) refine methodologies for dating fault movements that are applicable to a wide variety of tectonic problems and areas, (2) examine the long-term behavior and interaction of faults in a broad region (~20,000 km^2) that are exposed to the same regional stress field, (3) study the time-space distribution of strain accumulation and release in the upper crust on a regional (province-wide) scale.

INVESTIGATIONS

1. Bucknam, Machette, and Crone began analysis of data associated with Holocene faulting along the east flank of the Fish Springs Range in western Utah for which we have a set of high-quality scarp-morphology data.

2. Bucknam continued photographic monitoring of the natural (short-term) degradation of the 1983 Borah Peak fault scarps using precision close-range photogrammetry that was initiated in 1985. The continuation of this repeat photography will help quantify the rates and better understand the processes that contribute to the initial degradation of fault scarps.

3. Bucknam and Haller are completing work related to IGCP Project 206. They have partly revised the field trip guide (USGS Open-File Report 89-528) for submission as a USGS Bulletin. As editor, Bucknam has been ramrodding publication of tectonic atlas entitled "Geological Nature of Active Faults," a product of International Geologic Correlation Program (IGCP) Project 206 (Characteristics of active faults worldwide). The atlas is scheduled to be published by Cambridge University Press in 1992.

4. Crone and Haller (in collaboration with D.P. Schwartz, USGS, Menlo Park, CA) logged two trenches across the Lost River fault, Idaho, at the southeastern end of the Mackay segment.

5. Haller and Machette have started compiling a digital database of Quaternary faults in the Western United States; the first priority is to assemble data for a neotectonic transect of the northern Basin and Range province from the Wasatch fault zone (Provo, Utah area) to the Sierra Nevada frontal fault zone (Reno, Nevada area). This project is planned as an informal coop with personnel of the Nevada Bureau of Mines (John Bell and associates) and the Center for Neotectonics (Steve Wesnousky and associates). This aspect of the project will contribute to a broader compilation of neotectonics data, particularly Quaternary faulting data, for a large portion of the Western United States.

6. Bucknam, Haller, and Machette assisted in field investigations of surface deformation caused by the 1989 Loma Prieta, California earthquake.

7. Crone and Machette began preparation for their study of Australian Intraplate earthquakes as part of a USGS Gilbert Fellowship (FY 90/91). Field work is currently scheduled for July-September, 1990.

RESULTS

1. During earlier studies of Quaternary faulting in the Basin and Range province, Bucknam collected a high-quality data set on the morphology of the Fish Springs fault scarps. The utility of this data set was limited by the lack of information on the age of the scarps. In 1987, we obtained a well-constrained radiocarbon age from a sample collected during our trenching studies of the scarps. This radiocarbon sample indicates that the Fish Springs fault scarps are about 2,000 years old. This radiocarbon age now allows the morphologic data set to be used as a critically needed calibration point for morphometric analyses and theoretical models of scarp degradation that have been used for estimating the age of fault scarps the Western United States. In October, Bucknam and Machette completed field checking of surficial geologic mapping (1:24,000 scale) along the Fish Springs fault. As part of this mapping effort and field studies in Idaho (described in section 7), we conducted a one month training session on modern paleoseismologic techniques for Mr. Muhammed Muminullah (Geological Survey of Bangladesh). Crone's preliminary interpretations of the faulting events recorded in two trenches along the Fish Springs fault indicate a complex history of latest Pleistocene and Holocene surface faulting. Our favored interpretation of events recorded in the trenches indicates that Lake Bonneville may have had a major influence on the temporal distribution of surface-rupturing earthquakes on this fault during the latest Quaternary.

2. Analysis of digital elevation models of the Borah Peak, Idaho, fault scarp using an interactive surface-modeling program (ISM) maintained by the Branch of Petroleum Geology is providing a convenient means of measuring the geomorphic changes of the scarp that occur with time. The digital elevation models are derived from close-range photographs of the scarp taken with a calibrated mapping camera. Coordinates of points on the scarp have been digitized on a 10-cm grid by Jeff Coe and Gayle Culler (USGS Photogrammetic Laboratory) using a Kern DSR1 analytical plotter. Data is written to magnetic tape in a format directly readable by the ISM program.

John Michael and Bob Bucknam have used these data to compute the volumes of material removed from a section of the scarp face between successive surveys and, from this, calculated average rates of scarp retreat. Values determined between 1985 and 1989 are shown in the right-hand column. The methods used for collecting and analyzing the data appear to provide a reliable means of defining the changes occuring in morphology of the scarp against which possible variables, such as annual variations in local climate, can be evaluated. Variation in annual precipitation, paricularly that occurring in the late spring, is suspected to be an important variable. Except for the period of earliest surveys, the local climate has been dominated by unusually dry conditions. Thus, a greater variety of precipitation values will be needed to test this hypothesis.

Date of Survey	Average Retreat (mm)
10/85	
	42
05/85	
	6
09/86	
	5
06/87	
	4
04/88	
	14
10/89	

3. Continued editing manuscript on "Examples of active faults in the Western United States--A field guide." Bucknam and Haller will publish this comprehensive field guide (prepared for IGCP Project 206 Field Trip in July, 1989) as a USGS Bulletin. The field guide includes a 3000-km-long road log from San Francisco, CA to Salt Lake City, UT (via southern California), and narratives and site descriptions of the San Andreas and Garlock faults, the Sierra Nevada frontal (eastern) fault zone, and a selected faults across the Basin and Range province.

4. The trenches on the Mackay segment were excavated in alluvial gravel believed to have been deposited during the Bull-Lake glaciation (ending about 140 ka). Stratigraphic relations in the trenches indicate three surface-faulting events on this segment of the Lost River fault since deposition of the gravel. The most recent faulting event displaces Mazama ash (about 6,800 yr old). A pending radiocarbon date will establish a minimum age for this event. The next older event is believed to be latest Pleistocene in age on the basis of the faulting history interpreted from a trench at the northwestern end of this segment. The age of the oldest event is only known to be younger than 140 ka.

5. We have defined the limits of our neotectonic transect as the corridor between 39° and 41°N. and 111° and 120°W. This east-west strip allows us to build upon the Wasatch fault zone study and 1°x2° quadrangle mapping in Utah by BGRA personnel (Anderson, Barnhard, Bucknam, Machette, Nelson and Personius). Thus, our main concern for assembling a systematic fault data base is with Nevada; however, previous mapping by Barnhard (Elko 1°x2°), Wallace (Winnemuca 1°x2°), and Bell (Reno 1°x2°) can be used without major modifications. This leaves the

Ely, Lovelock, and Millett 1°x2° quadrangles as our main mapping objectives. During the first 6 months of the project, we have performed a search of literature on Quaternary basin-range faulting, obtained some aerial photography and topographic maps, and created a reference database using EndNote. In addition, Bucknam (in association with Paul Thenhaus) has digitized and updated the map of Quaternary faults in the Western United States (Nakata, Wentworth, and Machette; USGS Open-File Report 82-579) as part of our regional database.

REPORTS

Crone, A.J., and Haller, K.M., in press, Segmentation and the coseismic behavior of Basin-and-Range normal faults: Examples form east-central Idaho and southwestern Montana, U.S.A.: Submitted to the Journal of S tructural Geology, 24 ms. p., 7 figs.

Haller, K.M., 1990, Late Quaternary movement on basin-bounding normal faults north of the Snake River Plain, East-Central Idaho [part 4 of GSA field trip no. 1], *in* Roberts, Sheila, ed., Geologic tours of western Wyoming, Montana, and Utah: Geological Survey of Wyoming Public Information Circular 29, p. 41-54.

Machette, M.N., 1990, Slope morphometric dating *in* Forman, S.L., ed., Dating methods applicable to Quaternary geologic studies in the Western United States: Utah Geological and Mineral Survey Miscellaneous Publication 89-7, p. 30-42.

Machette, M.N., Nelson, A.R., Personius, S.F., Schwartz, D.P., and Lund, W.R., in press, Lengths of segments, earthquake recurrence intervals, and Holocene history of the Wasatch fault zone, Utah: Submitted to Journal of Structural Geology, 23 ms. p., 4 figs.

I.3

Latest Quaternary Surface Faulting in the Northern Wasatch to Teton Corridor (NWTC)

14-008-0001-G1396

James McCalpin
Department of Geology
Utah State University
Logan, UT 84322-4505
(801) 750-1220

Investigations

1. Trenching of late Quaternary fault scarps on the eastern Bear Lake, western Bear Lake (Utah and Idaho) and southern Star Valley faults (Wyoming).

2. Radiocarbon dating of the latest two to three surface-faulting earthquakes on these faults.

Results

1. Eastern Bear Lake fault -- the eastern Bear Lake fault is marked by a narrow zone of range-bounding fault scarps up to 30 m high. Based on stepovers and morphologic features of scarps, I postulate that three segments exist: the southern segment from Laketown, UT to the NE corner of Bear Lake (32 km), the central segment from Bear Lake to Montpelier, ID (26 km), and the northern segment north of Montpelier (at least 20 km).

   - six radiocarbon ages were received from two trenches excavated across 9 m- and 14 m-high fault scarps on the southern segment. Logs of these trenches, with locations of samples, were included in the previous NEHRP Summary (McCalpin, 1990). Ages indicate that about 10 m of vertical fault displacement has occurred since 12.7 ka. The most recent event occurred about 2.1 ka, but slip per event is unknown.

TABLE 1

Radiocarbon Dates From The Eastern Bear Lake Fault, Southern Segment

Trench	Sample No.	Lab. No.	Radiocarbon Age (yr. BP)	Significance
eastern	JM89-20	β-33403	12,780±140	predates latest two events
western	JM89-08	β-33400	9150±110	predates latest two events
"	JM89-11	β-33401	2130±80	closely dates latest event
"	JM89-13	β-33402	580±70	post-dates latest event
natural	JM89-01	β-33399	9100±90	predates latest two events
exposures	JM89-21	β-33404	12,700±130	predates latest two events

2. Western Bear Lake fault zone -- the western side of the Bear Lake graben is marked by a 3 km-wide zone of low horsts and grabens which displace the late Pleistocene/Holocene(?) lake floor. This wide zone of distributed Quaternary faulting was first identified in October, 1989, by V.S.

Khromovskikh (Institute of the Earth's Crust, USSR) while collaborating on this project. We interpret the zone as the surface expression of a complexly-faulted hingeline on the margin of an asymmetric graben.

- two trenches across 2.0-3.5 m-high fault scarps revealed faulted monoclines with displacements of about 1.6-2.0 m which we believe resulted from a single event. Larger scarps (up to 8 m high) exist on the western Bear Lake fault zone, and may be due to recurrent late Quaternary faulting or to shoreline modification. Four radiocarbon dates bracket the latest episode of faulting between 5.9 and 6.5 ka.

TABLE 2

Radiocarbon Dates From the Western Bear Lake Fault at Bloomington, ID

Trench	Sample No.	Lab. No.	Radiocarbon Age (yr. BP)	Significance
BLS	BLS-1	β-36674	5900±80	closely dates latest event
	BLS-2	β-36675	1890±70	post-dates latest event
	BLS-Aug. 1	β-36676	11,240±90	greatly pre-dates latest event
	BLS-Aug. 2	β-36677	6530±90	closely dates latest event

3. Star Valley fault -- Two or more trenches will be excavated near Afton, Wyoming in May 1990 across 11-12 m-high scarps which displace late Pleistocene alluvium.

4. Regional Tectonics of the NWTC
A comparison of the total Neogene throw with the late Quaternary slip on the major faults of the NWTC shows that faults are slipping in a non-uniform manner. Total Neogene throw estimates range from 3.4 km to 5.0 km, while late Quaternary (within last 12-15 ka) vertical slip rates range from 0.27 m/ka to 2.2 m/ka. The late Quaternary slip rates are greatest at the ends of the NWTC and smallest in the center (Fig. 1).

Extension

This contract was granted a 6-month no cost extension (until August 31, 1990) to allow trenching of the Star Valley fault in summer of 1990.

Reports

McCalpin, James, 1990, Latest Quaternary faulting in the northern Wasatch to Teton corridor (NWTC), in Jacobson, M.L. (comp.), Summaries of TEchnical Reports, vol. XXXIX, U.S. Geol. Survey Open-File Report 90-54, p. 140-143.

McCalpin, James, Zhang, Liren and Khromovskikh, V.S., in press, Quaternary faulting in the Bear Lake graben, Idaho and Utah: Geol. Soc. of America, Abstracts with Programs, v. 22, no. 5.

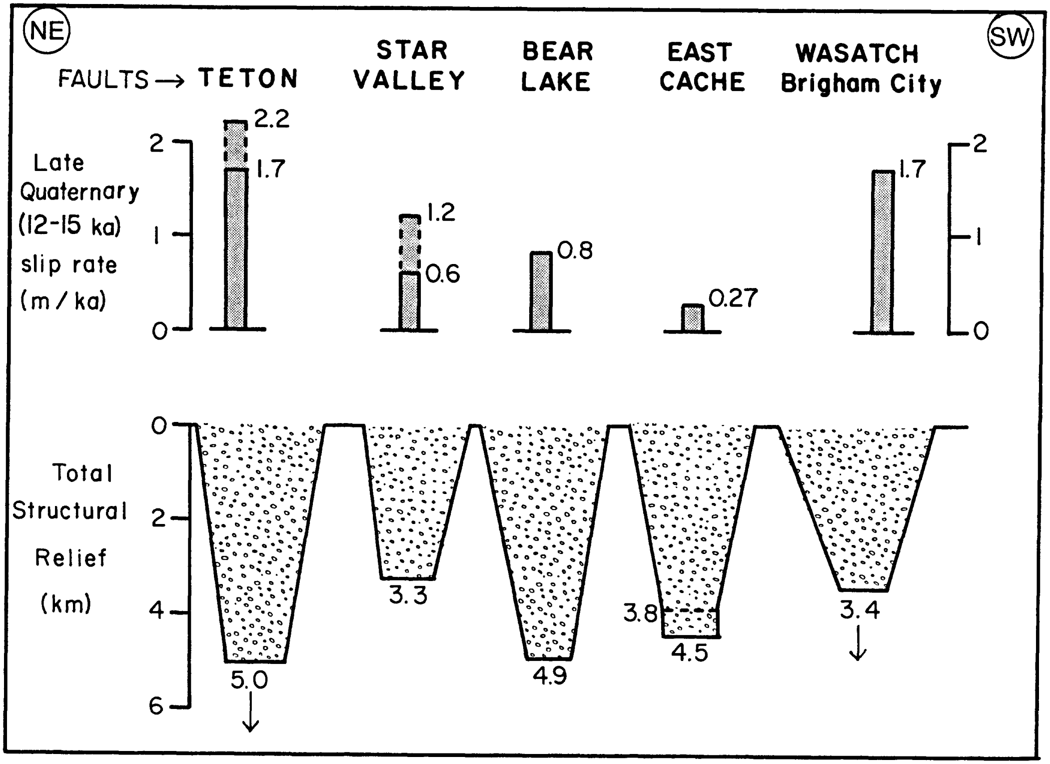

Figure 1. Diagram comparing the late Quaternary vertical slip rate within the last 12-15 ka (based primarily on fault scarp heights) to the total Neogene structural relief, for each of the major faults of the NWTC. Neogene vertical slip is estimated by combining the maximum depth of Neogene basin fill with the present maximum elevation of the mountain block above the valley floor; as such it does not include elevation removed from the mountain block by Neogene erosion. The low apparent late Quaternary slip rates of the central three faults are not compatible with the large amounts of Neogene structural relief. Several hypotheses exist to explain the disparity between late Quaternary and Neogene slip rates among the five faults: 1) long term rates are all similar, apparent differences in late Quaternary rates arise only from a short sampling period, 2)basins began forming at different times, or 3) during the late Quaternary slip rates on the central three faults have lagged behind the regionally-required slip, thus building up a "slip deficit" in the central NWTC.

ACTIVE MARGIN TECTONICS, PACIFIC NORTHWEST REGION

9910-04492

P. A. McCrory

Branch of Engineering Seismology and Geology
U.S. Geological Survey
345 Middlefield Road, MS 977
Menlo Park, California 94025
(415) 329-5677 or (FTS) 459-5677

Investigations

Document recent tectonic deformation in the vicinity of the Puget Sound metropolitan area and relate it to the earthquake potential in this region.

Results

1. FY90 research focuses on tectonically deformed sediments exposed along the coast of the Quinault Indian Reservation, Washington. Preliminary stratigraphy has been constructed for three key sedimentary sequences within the Quinault Formation: the Point Grenville, Taholah, and Duck Creek sections. The next task will be to determine the age of these sequences so as to understand the rates at which the sedimentary units are being compressed and tilted.

2. The last set of rock samples collected in FY89 are being processed for analyses of age and uplift data.

3. Analyses of rock samples collected in FY89 for age and uplift data are in progress.

Reports

None this reporting period.

Post Earthquake Investigations

9910-04428

Robert J. McLaughlin
Branch of Western Regional Geology
U.S. Geological Survey
345 Middlefield Road, MS 975
Menlo Park, California 94025
(415) 329-4945

For the last two years, geologic mapping in five 7.5 minute quadrangles has been conducted for the National Mapping Program, San Jose 1:100,000 sheet. These quadrangles straddle the San Andreas fault zone in the south San Francisco Bay region, in addition to poorly understood active thrust and reverse faults east of the San Andreas fault (the Sargent-Berrocal and Shannon fault systems). The quadrangles under investigation include Loma Prieta, Laurel, Los Gatos, Santa Teresa Hills, and Mount Madonna 7.5' quadrangles. On October 17, 1989, a magnitude 7.5 earthquake occurred off the San Andreas fault at a depth between 17 and 18 km; the epicenter was in the Laurel Quadrangle. Aftershock distributions and on-going field investigations following the earthquake indicate that the fault along which this event occurred did not rupture the surface, but that the rupture propagated up and northeastward to within a few kilometers of the surface beneath the Sargent fault. This blind thrust has a southwest dip of 60°-70°, based on aftershock depth distributions.

The present purpose of this mapping project is to focus on producing upgraded geologic maps and structure sections of the region of the Loma Prieta earthquake of October 17, 1989, which accurately depict the structure and stratigraphy of the region. In particular these maps should be important in determining the inter-relationships between the bedrock San Andreas fault, active reverse faults to the northeast, 1906 breaks along the San Andreas fault, and surface deformation which occurred in this region on October 17, 1989. We also are interested in determining the relationship of the rocks northeast of the San Andreas fault in this area, to possibly offset rocks east of the Calaveras-San Andreas fault zone in the southern Diablo Range.

We have so far published Loma Prieta (1988), and Laurel (1989) quadrangles as open-file maps and hope to complete Los Gatos Quadrangle in 1990. We also are in the process of digitizing these maps so that they may be published in the GQ or I-series as colored USGS maps.

STRUCTURAL FRAMEWORK OF THE PENINSULAR RANGES

9540-04040

Branch of Western Regional Geology
U.S. Geological Survey
University of California
Riverside, California 92521
(714) 276-6397

Investigations:

The project goal is to understand the geologic history of the northern part of the Peninsular Ranges Province and its interaction with the Transverse Ranges Province to the north with emphasis on the Neogene tectonic history. Field mapping was continued in the northern Perris Block and adjacent fault zone areas of the Peninsular Ranges. Morphometric measurements, at a scale of 1:24,000, were made on 10 fluvial basins which extend northeast from the Claremont fault into the San Timoteo Badlands. The Claremont fault is the sole active strand of the San Jacinto fault zone in this area northwest of the San Jacinto Valley.

Results:

Linear and areal parameters for the 10 fluvial basins located in the San Timoteo Badlands increase linearly from northwest to southeast along the Claremont fault. The area of the measured basins increases from 0.4 km^2 to 5.7 km^2 over a 8 km distance along the Claremont fault. The corresponding increase in length of the trunk streams is 1.3 to 6.8 km. These changes have shifted the crest of the badlands 0.5 km to 4.7 km east of the Claremont fault. Linear changes in basin lengths, areas, and trunk stream lengths suggest a constant rate of geomorphic development. The linear change of basin parameters with distance along the Claremont fault is most simply explained if the long-term slip rate for this part of the San Jacinto fault zone has also been constant.

Reports:

Morton, D. M. and Kennedy, M. P., 1989, A southern California digital 1:100,000 scale geologic map series: The San Ana Quadrangle, the first release: Geological Society of America Abstracts with Programs, v. 21, no. 6, p. A107.

Morton, D. M., Sadler, P. M., and Matti, J. C., 1990, Constant watershed growth and fault offset in the San Timoteo Badlands, southern California: Geological Society of America Abstracts with Programs, v. 22, no. 3, p. 70ty

DETECTION OF BLIND THRUSTS IN THE WESTERN TRANSVERSE RANGES AND SOUTHERN COAST RANGES

14-08-0001-G1687

Jay Namson and Thomas L. Davis

DAVIS AND NAMSON
CONSULTING GEOLOGISTS
1545 NORTH VERDUGO ROAD, SUITE 105
GLENDALE, CA 91208
(818) 507-6650

I. Objectives

A. Detection of seismically active blind thrusts in the western Transverse Ranges and southern Coast Ranges.

B. Determination of the geometry, kinematics, and slip rate of blind thrust faults.

C. Calculation of regional convergence rates across the western Transverse Ranges and southern Coast Ranges.

II. Approach: Compilation of surface and shallow subsurface geology using detailed maps and well data, regional seismicity, earthquake focal mechanisms and seismic reflection data for the construction of retrodeformable cross sections.

III. Results

A. A series of 9 cross sections and restorations across the western Transverse Ranges and southern Coast Ranges have been completed (Figures 1 and 2). The cross sections identify the major late Cenozoic anticlinoria which are interpreted to be caused by thrust faults (mostly concealed). The interpretations provide an estimate of slip on thrust faults as well as the regional shortening west of the San Andreas fault. The slip and shortening estimates are being integrated on maps to further understand the distribution of fault slip, slip rates, shortening and shortening rates in the region. Based on numerous geologic relationships, region-wide shortening began at ~2.0-4.0 Ma and is used to calculate the convergence rates below. The status of these cross sections are as follows:

1. Cross section 1 through the southern Coast Ranges near San Luis Obispo has been completed and accepted for publication (Namson and Davis, 1990). The cross section has 26.8 km of shortening from the edge of the continental margin to the San Andreas fault and yields a late Pliocene to Quaternary convergence rate of 13.4-6.7 mm/yr.

2. Cross section 2 extends across the western edge of the onshore Santa Maria basin and has been accepted for

Quaternary convergence across the onshore Santa Maria basin is 9.2 km and the convergence rate is 4.6-2.3 mm/yr.

3. Cross section 3 extends from the western Santa Barbara Channel near Point Conception to the San Andreas fault. The cross section and restoration are completed and indicate 30.4 km of late Pliocene and Quaternary convergence and a convergence rate of 15.2-7.6 mm/yr

4. Cross section 4 extends from the central Santa Barbara Channel to the San Andreas fault (Figure 3). The cross section and restoration are completed and indicate 57.1 km of late Pliocene and Quaternary convergence and a convergence rate of 28.6-14.3 mm/yr. These are the highest values for convergence and convergence rates in the western Transverse Ranges and could indicate this area is at the highest risk to moderate to large compressive earthquakes. The Santa Ynez Range anticlinorium and Coal Oil Point anticline are the southernmost structures on the transect and are caused by motion on the San Cayetano thrust which is shown as an active blind thrust beneath the cities of Goleta and Santa Barbara (Figure 3). The cross section also illustrates the thrust belt structural style of the area.

5. Cross section 5 extends from the eastern edge of the Santa Barbara Channel to the Big Pine fault and is a modified version of a previously published cross section (Namson, 1987). The interpretation shows 31.5 km of late Pliocene and Quaternary convergence and convergence rates of 15.7-7.8 mm/yr.

6. Cross section 6 extends from the coastline along the southwestern edge of the Santa Monica Mountains to the San Andreas fault. The cross section and restoration have been completed and indicate 33.2 km of late Pliocene and Quaternary convergence and a convergence rate of 16.6-8.3 mm/yr

7. Cross section 7 extends across the Ventura basin near the town of Filmore. The cross section and restoration have been completed and indicate 28.0 km of late Pliocene and Quaternary convergence and a convergence late of 14.0-7.0 mm/yr.

8. Cross section 8 extends from the coast near Santa Monica to the San Gabriel fault. The cross section and restoration have been completed and indicate 13.3 km of late Pliocene and Quaternary convergence and a convergence late of 6.7-3.3 mm/yr.

9. Cross section 9 extends offshore near Palos Verdes to the San Andreas fault and has been published (Davis et al., 1989). The cross section has 21.4-29.7 km of late Pliocene

and Quaternary convergence and a convergence rate of 3.8-13.5 mm/yr.

B. Published Papers 1989/90

1. Namson, J. and Davis, T.L., 1990, Late Cenozoic Fold and Thrust Belt of the Southern Coast Ranges and Santa Maria Basin, California: American Association of Petroleum Geologists Bulletin, v.74, n. 4.

2. Davis, T.L., Namson, J., and R.F. Yerkes, 1989, A Cross Section of the Los Angeles Area: Seismically Active Fold and Thrust Belt, the 1987 Whittier Narrows Earthquake, and Earthquake Hazard: Journal of Geophysical Research, v. 94, p. 9644-9664.

3. Namson, J., and T. Davis, 1989, Reply on Structural transect of the western Tranverse Ranges, Califronia: Implications for lithospheric kinematics and seismic risk evaluation: Geology, v. 17, p.670-671.

4. Namson, J., and T. Davis, 1989, Reply on Structural transect of the western Tranverse Ranges, Califronia: Implications for lithospheric kinematics and seismic risk evaluation: Geology, v. 17, p.672-673.

FIGURE 1

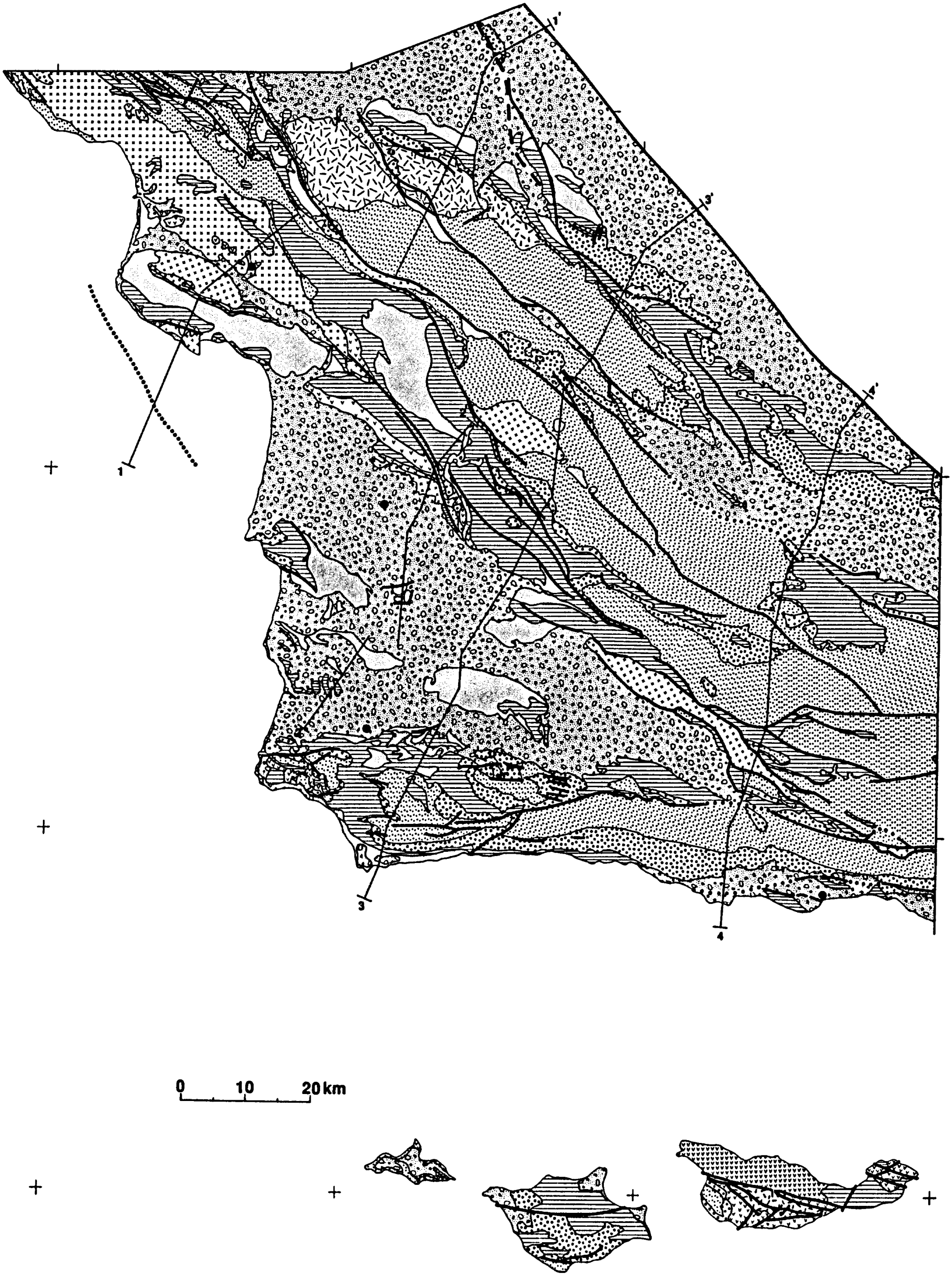

I.3 **FIGURE 2**

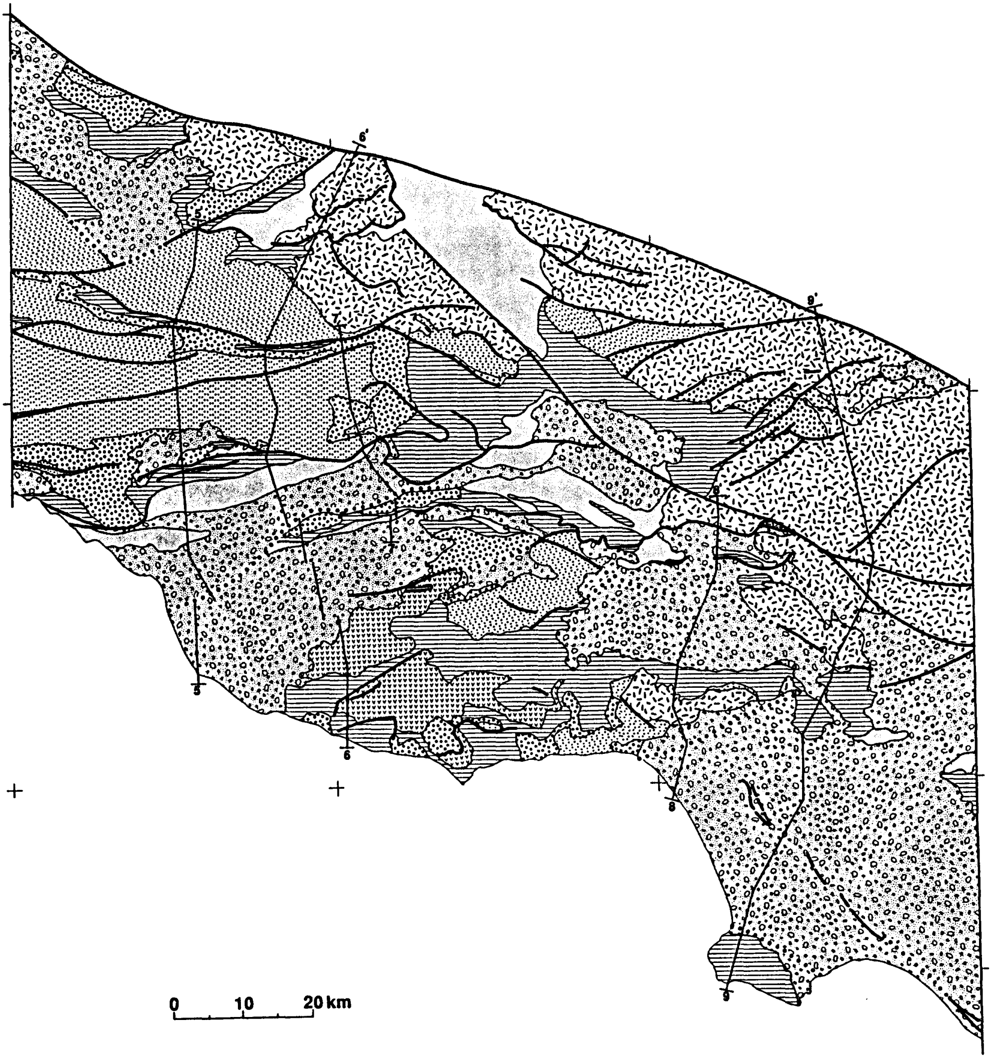

FIGURE 3

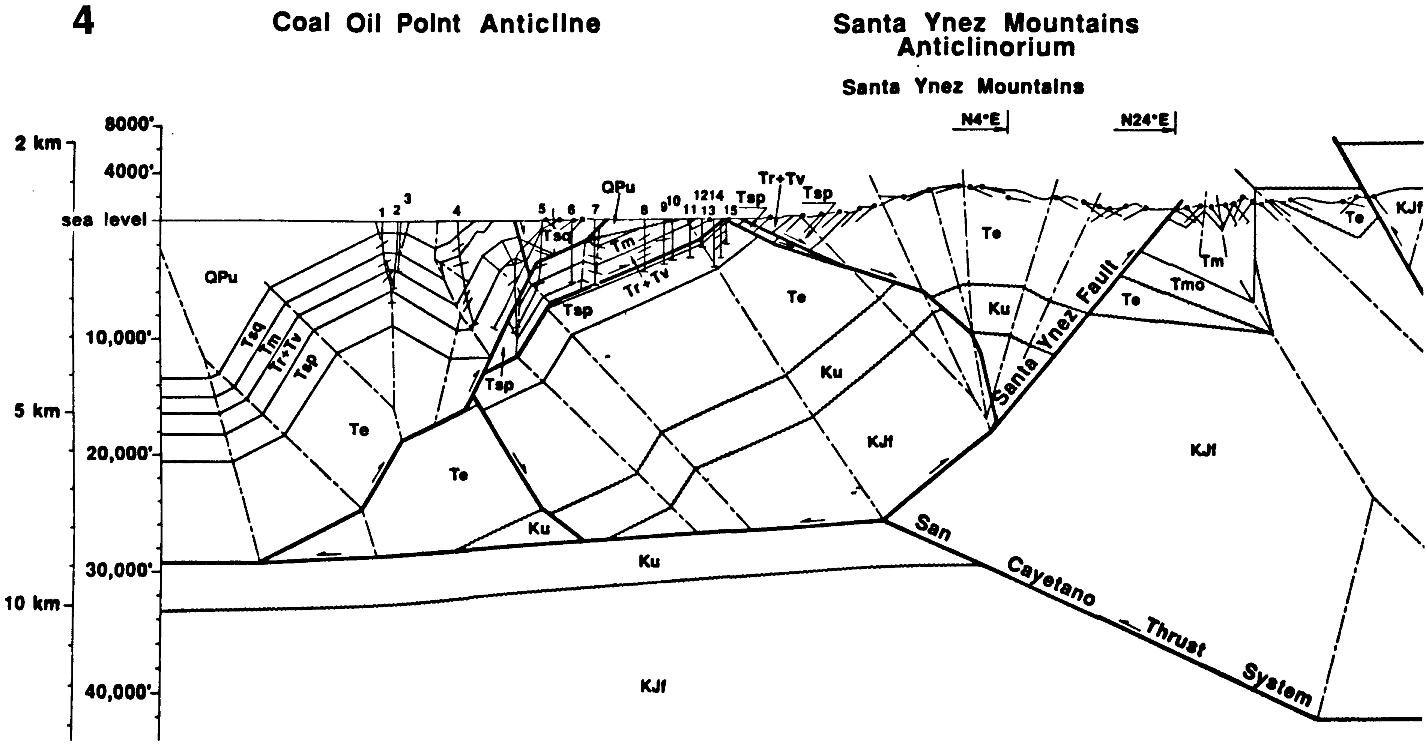
4
Coal Oil Point Anticline
Santa Ynez Mountains Anticlinorium
Santa Ynez Mountains
N4°E
N24°E
2 km
5 km
10 km
8000'
4000'
sea level
10,000'
20,000'
30,000'
40,000'
1
2
3
4
5
6
7
8
9
10
11
12
13
14
15
QPu
Tsq
Tm
Tr+Tv
Tsp
Te
Ku
KJf
Tmo
Santa Ynez Fault
San Cayetano Thrust System

NORTHERN SAN ANDREAS FAULT SYSTEM: PALEOSEISMIC AND SLIP RATE STUDIES IN NORTHERN AND CENTRAL CALIFORNIA

9910-04483

CAROL PRENTICE

BRANCH OF ENGINEERING SEISMOLOGY AND GEOLOGY
345 MIDDLEFIELD RD, MS 977
MENLO PARK, CA 94025
415-329-5690

Investigations

1) Investigations of the San Andreas and related faults in northern and central California to determine timing of prehistoric earthquakes and average Quaternary slip rates. 2) Investigations of the Loma Prieta earthquake.

Results

1) Studies of excavations at two sites are yielding paleoseismic data for faults of the San Andreas system in northern and central California: 1) on the Carrizo Plain along the San Andreas fault in central California, and, 2) along the Maacama fault near Ukiah, CA. An excavation site along the peninsular segment of the San Andreas fault is being evaluated for paleoseismic and slip rate potential. Results from the first two sites are summarized below:

An excavation across the San Andreas fault on the Carrizo Plain in central California has yielded evidence for at least six earthquakes. The most recent earthquake is known from historical records to have occurred in 1857. The penultimate earthquake occurred after the deposition of a unit with a corrected radiocarbon age of 1365 ± 165 AD. The third event back occurred before the deposition of a unit formed in 1190 ± 80 AD. The ages of the earlier seismic events will be constrained by the results of radiocarbon samples that are now being processed.

The excavation at the City of Ten Thousand Buddhas, in Talmage, near Ukiah, California, exposed a sequence of marsh, fluvial and lacustrine deposits overlying a paleosol developed on Pleistocene (?) gravel. The Maacama fault, clearly expressed in the older gravels, has not caused any brittle deformation of the overlying Late Holocene section. The section instead has been warped.across the fault zone. Relations indicate that only one warping event has occurred. Results of radiocarbon dating will provide information on the age of the Holocene section.

2) Investigations following the Loma Prieta earthquake of October, 1989, included mapping of ground fractures and study of the historical record to compare the effects of the 1906 earthquake along this segment of the San Andreas fault with the effects of the 1989 earthquake. In this region in 1906, as in 1989, many large ground cracks opened up in the Summit Road and Skyland Ridge areas. No surface rupture occurred along the San Andreas in 1989; it is not possible to determine from the report documenting the effects of the 1906 earthquake whether of not surface rupture occurred along the main trace of the San Andreas fault at that time. Left-lateral offset was documented in 1906 near the Morrell ranch; a smaller amount of left-lateral offset occurred on this same feature as a result of the 1989 earthquake.

Reports

Prentice, Carol S., and Sieh, Kerry E., 1989, A paleoseismic site along the Carrizo segment of the San Andreas fault, central California: [abs.] : EOS, Trans Am. Geophys. Union, v. 70, n. 43, p.1349.

U.S.G.S. Staff (including C.S. Prentice), 1989, Preliminary map of fractures formed in the Summit Road—Skyland Ridge area during the Loma Prieta, California, earthquake of October 17, 1989: U.S.G.S. Open-File Report 89-686.

Plafker and Galloway, eds., with contributions by U.S.G.S. Staff (including C.S. Prentice), 1989, Lessons Learned from the Loma Prieta, California, Earthquake of October 17, 1989: U.S. Geological Survey Circular 1045.

U.S.G.S. Staff (including C.S. Prentice), 1990, The Loma Prieta, California, Earthquake: an Anticipated Event: Science, v. 247, pp. 286-293.

Schwartz, D.P., and Prentice, C.S., 1990, Surface fractures in the Loma Prieta area, CA; 1906 & 1989: [abs.] Seismological Society of America, 1990, *in press*.

4/90

Determination of Slip Rates and Dating of Earthquakes for the Imperial and Cerro Prieto Fault Zones, Northern Baja California and Sonora, Mexico

14-08-0001-G1669

Thomas Rockwell
Andy Thomas
Dept. of Geological Sciences
San Diego State University
San Diego, CA 92182
(619) 594-4441

Objective: The primary purposes of this study are: 1) to date earthquakes along the Imperial and Cerro Prieto faults, where possible; and 2) to determine a slip rate across these two faults. These data will further our understanding on the timing of past earthquakes for two of the regions most prominent and seismically active faults and help resolve how slip is distributed in the southern San Andreas fault system.

Results: High ground water and agriculture have impeded preliminary work on the Cerro Prieto fault so our work has focused primarily on the Imperial fault. We excavated trenches across the fault at Tamalipas (Cucapa) and at the International Border. The proximity of the fault to buildings in Tamalipas precluded further work there at this time. The border site exposed the fault as a 2-4 m wide zone of rupture (consistent with historical accounts of the 1940 rupture) in stratified fluvial deposits. Work is now focusing on the resolution of slip for different stratigraphic units.

We have also begun study of the south end of the Imperial fault where the fault appears to express predominantly dip slip. Of interest is substantial recent (post 1984) dip slip that has occurred along the surface trace. Analysis of early aerial photography flown after the 1934 Cerro Prieto earthquake and the 1940 Imperial earthquake indicate that the southern end of the Imperial fault may have sustained surface rupture in both earthquakes. The recent slip, however, appears to be creep and may be either tectonic or induced by thermal well production in the nearby Cerro Prieto field. Individual buildings, roads or canals are vertically displaced by up to 30 cm, and a 50 cm high scarp in alluvium is locally present.

The Bootheel Fault, Southeastern Missouri, and Its Relationship to the New Madrid Seismic Zone

14-08-001-G1772

Eugene S. Schweig, III
Center for Earthquake Research and Information
Memphis State University
Memphis, TN 38152
(901) 678-2007

Objective:

Although the New Madrid seismic zone is the site of the greatest historical earthquakes in eastern North America, the surface expression of the causative fault(s) for these earthquakes has never been found. However, during a comprehensive remote sensing examination of the New Madrid seismic zone (Marple, 1989) a discontinuous linear feature was discovered that may be the surface expression of at least one of the coseismic faults of the New Madrid earthquakes of 1811 and 1812 (Figure 1). We now call this feature the Bootheel lineament. The objectives of this study are to demonstrate that the lineament is indeed a fault, to characterize it in terms of its length, geometry, and displacement, and to determine whether or not it has ruptured prior to 1811.

Results to date:

We are currently mapping the Bootheel lineament in detail and have excavated two trenches across it. Both trenches were in areas where the lineament is well-defined by linear sand bodies (Figure 1). The first was southwest of Hayti, Missouri. Here, the lineament is expressed as a shallow depression, with the area to the northwest of the depression about 0.5 m lower in elevation that the area to the southeast. A linear sand body runs along the depression. A portion of the trench log is shown in Figure 2a. A dike of liquefied sand, dipping 30° to the northwest, underlies the surface sand body. On the opposite side of the trench the dike is more steeply dipping. The modern plow zone obscures any possible offset of the pre-1811-12 ground surface. Also, the clayey sands into which the dike was intruded were massive, thus there was no opportunity to see offset horizontal bedding.

The second trench site was west of Steele, Missouri (Figure 1). There was no topographic expression of the lineament here, but again there was a well defined linear sand body. We had determined through hand augering that this site had vertical stratigraphic changes that would be useful in determining vertical offset. This was borne out in the excavation. The portion of the trench log near the trace of the lineament is shown in Figure 2b. Two nearly vertical dikes of sand are evident about 6 m apart. The block between the dikes has been down-dropped about one

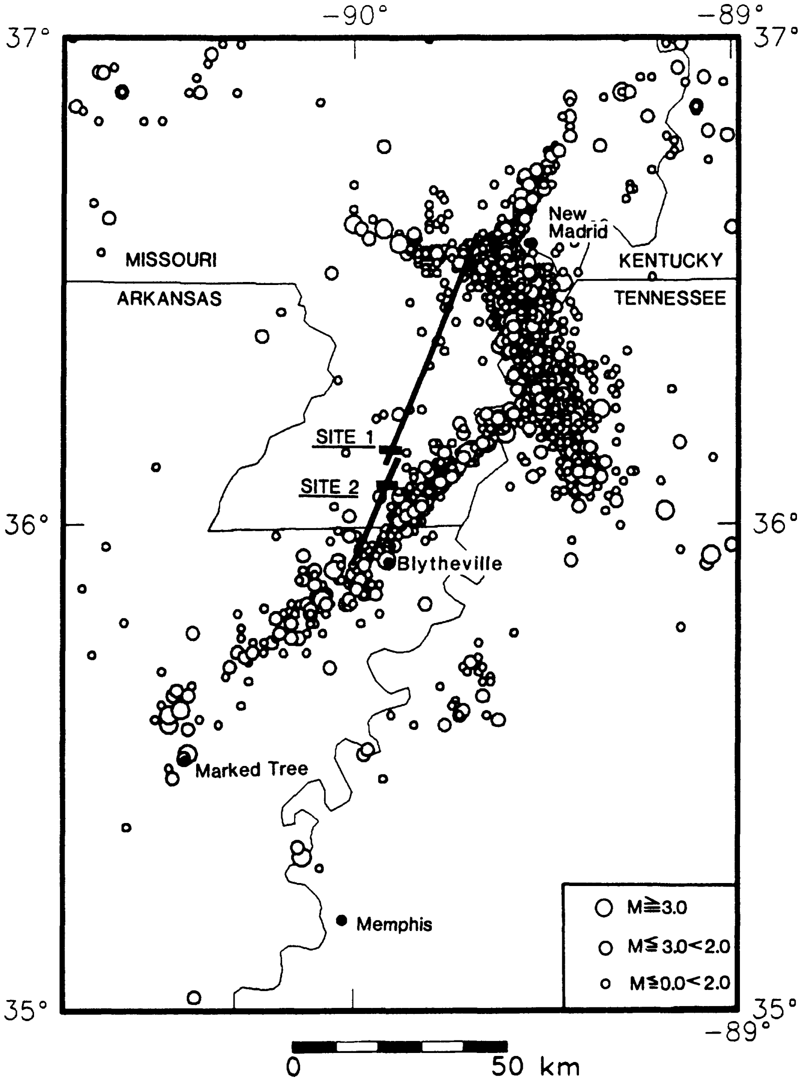

Figure 1: The Bootheel lineament shown in relation to the New Madrid seismic zone (1974-1987). The sites of the first two trenches are also shown.

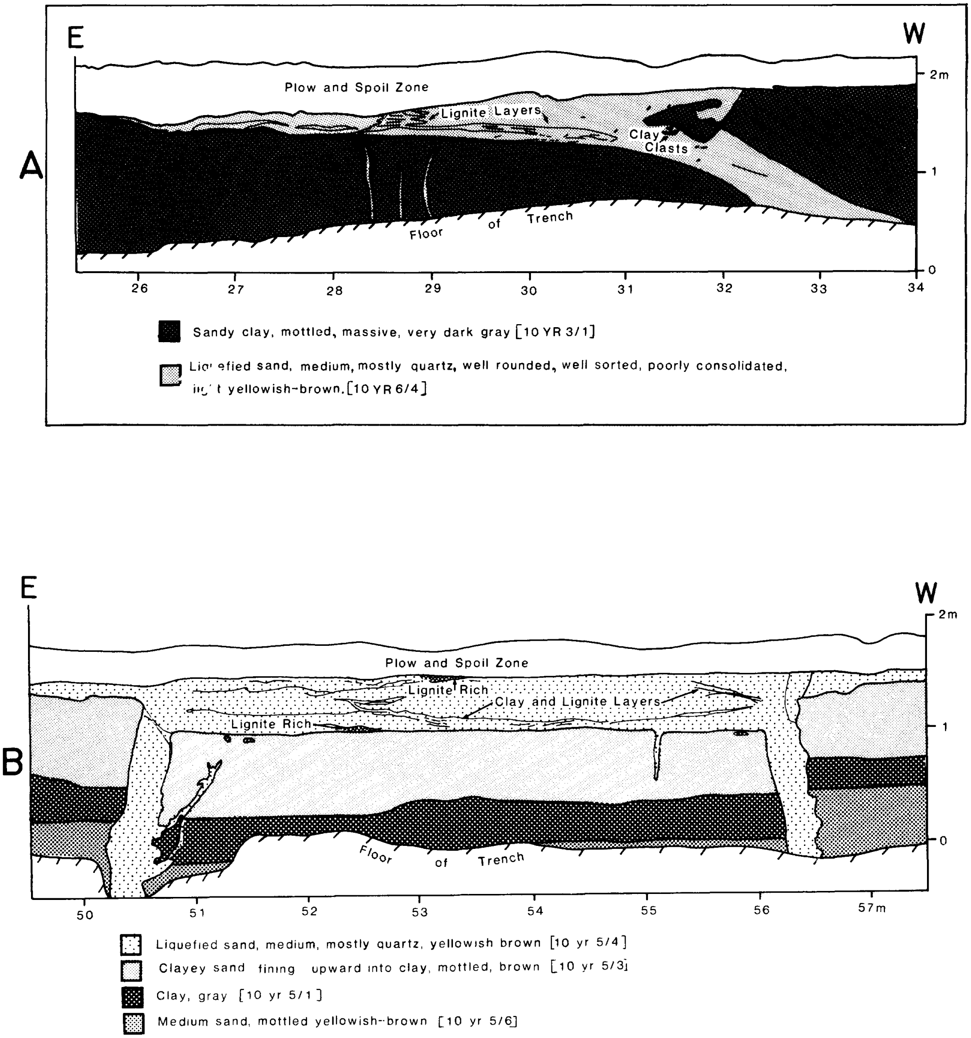

Figure 2: Logs of portions of trenches across the Bootheel lineament (see Figure 1 for locations). A: Trench site 1 southwest of Hayti, Missouri. The dike of sand underlies the trace of the lineament as identified from aerial photographs. B: Trench site 2 west of Steele, Missouri. The downdropped block between the two sand dikes underlies the trace of the lineament. Note that the clay unit (second from the bottom) appears to have different thicknesses on opposite sides of the dikes. Horizontal scale is meters from east end of trench.

half meter, with the fissure left at the surface having been filled by the liquefied sand erupted through the dikes. This down-dropped block may not be directly related to faulting, but may have dropped down to fill the space left by the erupted sand. In fact, this graben-like structure is probably very local; the dikes are not parallel to each other and, if planar, should intersect several meters south of the trench.

There was some circumstantial evidence of lateral displacement along the lineament at the second trench site. The thickness of a sandy clay unit was greater within the graben than to either side of it. This could either be due to lateral movement that juxtaposed different thicknesses of the unit or to growth faulting that led to a greater rate of deposition with the graben. The latter explanation seems unlikely because there is no other sedimentologic or geomorphic evidence (such as a colluvial wedge or eroded graben shoulders) that a graben existed at this location prior to the last movement. We plan to excavate at least two short trenches nearby and parallel to this trench to help resolve this question.

All geomorphic and pedologic data suggest that the liquefaction and movement documented in the first two trenches dates from 1811 and 1812. However, we collected wood from a tree stump buried by the liquefied sand in the graben area in the second trench and are having it carbon dated.

Reports:

Marple, R.T., 1989, Recent discoveries in the New Madrid seismic zone using remote sensing [M.S. thesis]: Memphis, Tenn., Memphis State University, 81 p.

Marple, R.T., and Schweig, E.S., III, 1989, Remote sensing of alluvial terrain in a tectonically active setting of the midcontinent: the New Madrid seismic zone: Geological Society of America Abstracts with Programs, v.21, p. A372.

Schweig, E.S., III, and Jibson, R.W., 1989, Surface effects of the 1811-1812 New Madrid earthquake sequence and seismotectonics of the New Madrid seismic zone, western Tennessee, northeastern Arkansas, and southeastern Missouri *in* Vineyard, J.D., and Wedge, W.K., eds., Geological Society of America 1989 Field Trip Guidebook: Missouri Division of Geology and Land Survey Special Publication 5, p. 47-67.

Schweig, E.S., III, and Marple, R.T., 1989, The Bootheel lineament in southeastern Missouri and northeastern Arkansas: a co-seismic fault of the New Madrid earthquakes?: Geological Society of America Abstracts with Programs , v. 21, p. A186.

Schweig, E.S., III, and Marple, R.T., 1990, The Bootheel lineament, northeastern Arkansas, and the New Madrid seismic zone, *in* Guccione, M.J., and Rutledge, E.M., eds., Field guide to the Mississippi alluvial valley, northeast Arkansas and southeast Missouri: Friends of the Pleistocene South-Central Cell, p. 265-277.

EARTHQUAKE GEOLOGY OF THE SAN ANDREAS AND OTHER FAULTS IN CALIFORNIA

Grant Numbers 14-08-0001-G1370
and 14-08-0001-G1789

Kerry Sieh
Division of Geological and Planetary Sciences
California Institute of Technology
Pasadena, CA 91125
(818) 356-6115

During the six month period ending April 1990, I and my graduate students, in collaboration with Carol Prentice of the U. S. Geological Survey, have made progress in several areas:

1) Bidart Site

Knowledge of the dates of the past few great earthquake ruptures in the Carrizo Plain would increase the likelihood of successful forecasts of future great earthquakes along the southern half of the San Andreas fault. Currently, intervals are believed to range from about 250 to 450 years, based upon our knowledge of the long-term slip rate and geomorphic evidence for the amount of slip during the past several earthquakes (Sieh and Jahns, 1984). This suggests that the Carrizo segment of the fault has a very low probability of rupturing in the next few decades. It also suggests that the next few Parkfield earthquakes are unlikely to trigger a great earthquake involving rupture of the Carrizo segment.

Unfortunately, the geomorphic basis of this important conclusion is tenuous. Thus, we have sought to date and characterize the past several earthquakes more convincingly. To this end, we excavated and logged one wall of a trench across the Carrizo segment of the San Andreas fault in May and July 1989. During March and April 1990 we reopened the trench and logged the opposite wall. This confirmed our earlier findings that several large rupture events are recorded by these sediments. These ruptures are clearly indicated by upward truncations of fault planes and facies variations in alluvial fan and pond deposits. The characteristics of the sediments are such that we are confident that we have a complete record of at least the latest three events. Within the past 6 months we received the results of radiocarbon analyses of samples collected from the trench. The radiocarbon dates indicate that two slip events have occurred at the Bidart site since about 1263 A.D. The carbon sample that was dated at 1263 A.D. was considerably below the horizon of the penultimate event. Thus the data are consistent with our earlier suspicions that the past three ruptures of the Carrizo segment of the San Andreas fault may correlate with ruptures documented at Pallet Creek that occurred around 1100 A.D., around 1480 A.D. and in 1857 A.D.

2) Van Matre Ranch Site

We have done no more field work at the Van Matre Ranch site in the past six months, but we have received the results of radiocarbon analyses of samples collected from that site. These analyses indicate that two slip events have occurred at this site (about 15 km southeast of the Bidart site) since the early 1400's A.D. This further supports the hypothesis that the past three ruptures of the Carrizo Plain segment correlate with ruptures at Pallet Creek that occurred around 1100 A.D., around 1480 A.D. and around 1857 A.D.

3) Phelan Site

Dextral offsets of small stream channels in the Çarrizo Plain occur in rough multiples of 10 meters (Sieh, 1978). This observation is the basis for the interpretation that 10 meters is the magnitude of slip associated with each large earthquake produced by this section of the fault. If this interpretation is correct, this section of the fault must rupture about every 250 to 450 years (Sieh and Jahns, 1984).

In order to test this interpretation, Lisa Grant and several other graduate students continued 3-D excavations of an alluvial fan/channel complex that crosses the Carrizo Plain segment of the San Andreas fault. During March 1990, Lisa excavated and logged two new trenches at this site. In combination with three trenches that were dug at this site earlier, the new trenches reveal two buried channels which are each offset 6.3 to 7.9 meters. Radiocarbon analysis of carbon samples collected from these channels is currently being performed and should bracket the age of the channels. Stratigraphic evidence for the number of slip events that produced the 6.3 to 7.9 m offset of the channels is inconclusive at this point and requires further investigation. If the offset occurred in one slip event then these data will basically confirm the hypothesis that the Carrizo Plain segment of the San Andreas fault ruptures in large-magnitude slip events spaced relatively far apart in time. If, however, the offsets occurred in two events, then the recurrence interval for rupture of the Carrizo segment may be shorter than previously believed. We expect that future work at the Phelan site will resolve this question.

4) Garlock fault

Graduate student Sally McGill has written the first draft of a paper that characterizes the most recent slip events along the eastern Garlock fault, based on offset geomorphic features. She has found that the most recent earthquake on the easternmost 90 km of the fault probably was produced by about 3 m of left-lateral slip. Furthermore, along part of this stretch, within Pilot Knob Valley, each of the past 5 earthquakes may have been produced by about 3 m of left-lateral slip. Farther west, near highway 395, the most recent event may have involved as much as 7 m of left-lateral slip. These data suggest that the Garlock fault is capable of producing earthquakes of M=7.3 to M=7.5. If the Holocene slip rate determined near Koehn Lake (Clark and Lajoie, 1974) is applicable to the entire eastern Garlock fault, then the recurrence interval for large earthquakes may be about 1000 years near highway 395 and may be as short as 430 years along the easternmost 90 km of the fault.

In order to determine the recurrence interval more directly, Sally has selected a site at which she will undertake paleoseismic excavations in May 1990. She has also begun mapping an offset shoreline of Searles Lake, from which she expects to determine a Holocene slip rate for the eastern Garlock fault.

Paleoearthquake Study in the New Madrid Seismic Zone

14-08-0001-G1791

Steven G. Wesnousky
Center for Neotectonic Studies
University of Nevada
Reno, Nevada 38152
702-784-6067

Objective: For purposes of flood control and land reclamation, the U.S. Army Corps of Engineers has recently reexcavated and widened an extensive set of drainage ditches within the Saint Francis drainage basin. The majority of the ongoing and planned excavations cut through the meisoseismal zone of the great 1811-12 New Madrid earthquakes. The 1811-12 earthquakes produced extensive liquefaction within the New Madrid Seismic zone at the time of the earthquakes. Evidence of that liquefactiction still exists in the geologic record. The ditches provide an excellent opportunity to systematically examine and document the geological record of liquefaction in the New Madrid Seismic Zone. The objective of this study is to document liquefaction phenomena exposed in the ditches and determine whether or not evidence for pre-1811-12 earthquakes exists.

Progress: Figure 1 shows where we concentrated our efforts during 1989. During 1988 and early 1989, the Corps completed the reexcavation of Buffalo Creek Ditch, Ditch No. 12, and Stateline Ditch No. 29. The contour and shading within the inset of Figure 1 shows the region where liquefaction deposits (i.e. extruded sands) attributed to the 1811-12 earthquakes still comprise greater than 1% and 25% of the ground cover, respectively. The ditches are situated on braided stream terrace deposits associated with the retreat of the last glaciation and, hence, on a surface that has been relatively stable during the last 6 thousand to 10 thousand years. The upper few meters of the stratigraphy of the braided stream terrace deposits and visible in the ditches is generally quite simple, consisting of very fine to fine sands overlain by a clay and silt-rich topstratum of low permeability. Toward identifying possible evidence of paleoliquefaction, we have walked the length of the reexcavated ditches in Figure 1 and searched for breaches in the clay-rich topstratum. In this manner, we systematically identfy sites of sandblows and sand dikes. Those sections of the ditches showing a greater concentration of liquefaction phenomena are later logged in greater detail. More specifically, we establish benchmarks that may later be reoccupied and use a *Total Station* to survey the upper and lower contacts of the clay-rich topstratum or 'clay cap'. The surveying serves to document the general character of liquefaction phenomena along the ditches and permanantly deocument their location for later study by ourselves and otheres in the future.. Sections of the ditches we have logged in this way are labeled Log 1, Log 2, and Log 3 in Figure 1. The pervasive nature of liquefaction is illustrated by the numerous breaches of the clay-rich topstratum by liquefied sands observed in the Log 2 pictured in Figure 2. Towards looking for evidence of pre-1811-12 liquefaction, ruptures or breaches in the 'clay cap' will be further cleaned off by hand shovel or backhoe to be photographed and logged in detail. Two sites selected for detailed logging are labeled Sites 1 and 2, respectively, in Figure 2. To date, no evidence of pre-1811-12 liquefaction has been recognized.

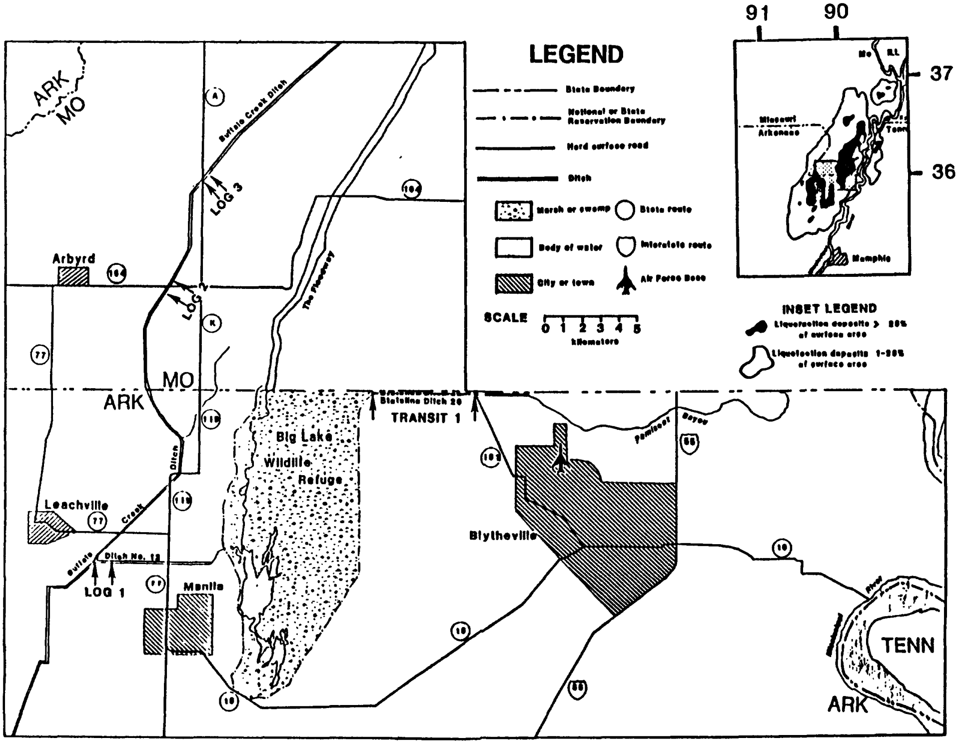

Figure 1.

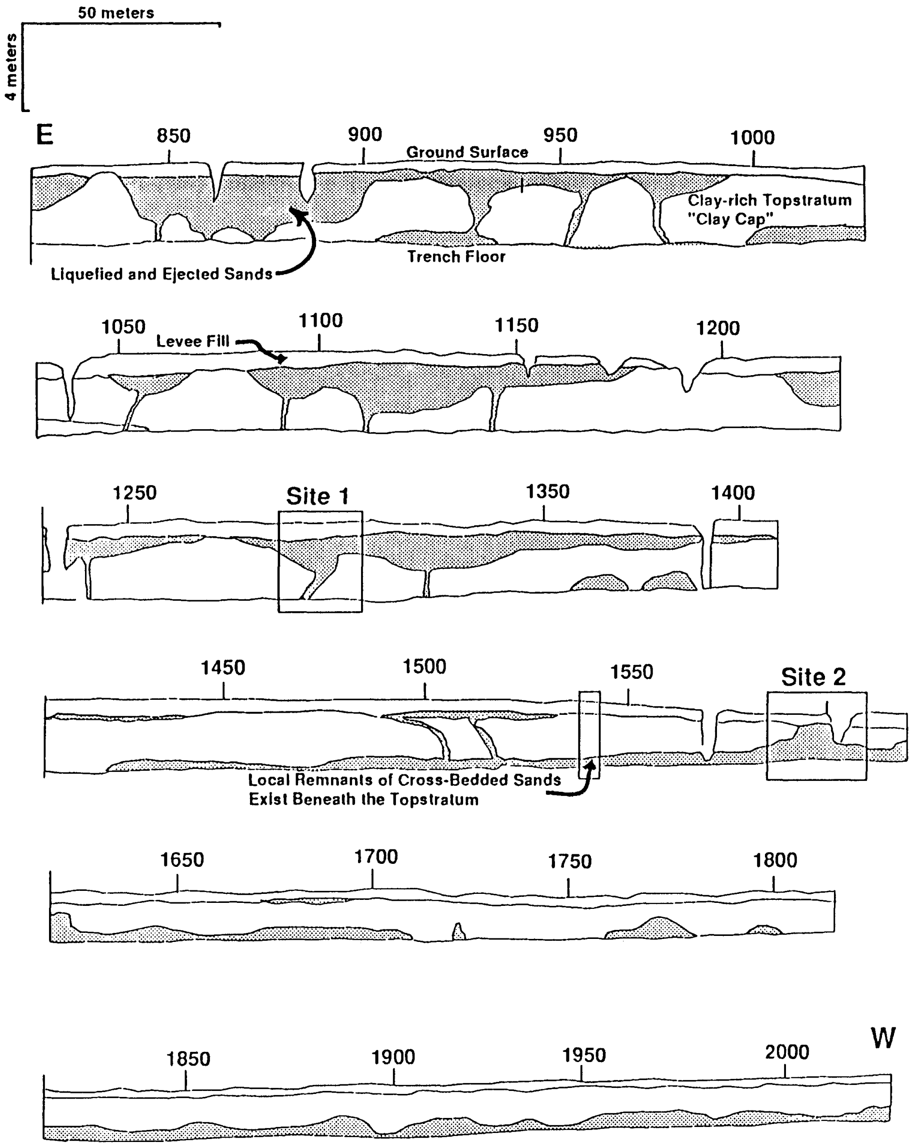

Figure 2. Log of the south side of Ditch No. 12. Locality shown in Figure 1.

Convergence Rates Across Western Transverse Ranges

14-08-0001-G1372 and -G1798

Robert S. Yeats and Gary J. Huftile
Department of Geosciences
Oregon State University
Corvallis, OR 97331-5506
(503) 737-1226

Investigations

Surface and subsurface geology of the Piru 7½-minute quadrangle (Figure 1) has been compiled, and the accompanying report is being written for submission as a USGS open-file report. The Piru quadrangle and the Val Verde quadrangle to the east, open-filed earlier (Yeats et al., 1985), comprise the displacement-transfer zone between the San Cayetano fault to the west and the Santa Susana fault to the east.

Prof. Lu Huafu of Nanjing University, China is constructing a regional cross section from the Simi fault through the San Cayetano-Santa Susana transfer zone to the San Gabriel fault. We are also starting a new cross section across the eastern lobe of the San Cayetano fault, part of which was included in a cross section by Yeats (1983, Figure 11).

Results

In the Piru quadrangle, the San Cayetano fault bifurcates into two strands (Figure 1), the Main and Piru strands. Both strands have evidence of late Quaternary displacement, offsetting alluvial-fan material. The southern, Piru strand offsets alluvium west of and in the town of Piru. The northern, Main strand offsets the alluvial fan at the mouth of Modelo Canyon; aerial photographs show that drainages in the fan are more incised northwest of the fault than they are southeast of the fault, suggesting uplift of the block northwest of the Main strand. Some drainages are offset left-laterally, suggesting that offset is oblique on this part of the fault as would be expected for a reverse fault that turns in the direction of stress shown by Mount and Suppe (1987) and dies out. The folds in the Modelo lobe (Figure 1), in the hanging-wall block of the San Cayetano fault, occur above a décollement in the lowermost Modelo Formation. The Oak Ridge fault (Figure 1) bifurcates into north, middle, and south strands, although the north strand is considered younger because it offsets folded Pleistocene Saugus Formation (Yeats, 1988). The Santa Clara syncline extends east to just southwest of Piru where a fold pair, the Piru anticline and Piru syncline trend N70°W and underlie the Santa Clara Valley at Piru. Much of the folding of the Piru syncline, between the San Cayetano and Oak Ridge faults in the Santa Clara Valley, was probably coincident with movement on the south strand of the Oak Ridge fault, thus predating movement on the north strand.

References Cited

Mount, V. S., and Suppe, J., 1987, State of stress near the San Andreas fault: Implications for wrench tectonics: Geology, v. 15-12, p. 1143-1146.

Yeats, R. S., 1983, Large-scale Quaternary detachments in the Ventura basin, southern California: Journal of Geophysical Research, v. 88-B1, p. 569-583.

Yeats, R. S., 1988, Oak Ridge fault, Ventura basin, California: Slip rates and late Quaternary history: U. S. Geol. Survey, Final Technical Report, Contract 14-08-0001-G1194, 33p.

Yeats, R. S., McDougall, J. W., and Stitt, L. T., 1985, Cenozoic structure of the Val Verde 7½-minute Quadrangle and south half of the Whitaker Peak 7½-minute Quadrangle, California: U. S. Geol. Survey Open-File Report 85-587, 23p., map scale 1:24,000.

Reports

Huftile, G. J., Thin-skinned tectonics and oil accumulation of the Upper Ojai Valley and Sulphur Mountain area, Ventura basin, California: submitted to American Association of Petroleum Geologists Bulletin.

Huftile, G. J., Displacement transfer between surface reverse faults and blind thrusts, central Ventura basin, California: to be submitted to Tectonics.

Huftile. G. J., and Yeats, R. S., in prep., Cenozoic structure of the Piru 7½-minute quadrangle, California: to be submitted to USGS as an open-file report.

Yeats, R. S., and Beall, J. M., in press, Stratigraphic controls of oil fields in the Los Angeles basin: A guide to migration history, in Biddle, K. T., and Phelps, D., eds., Los Angeles basin volume: American Association of Petroleum Geologists Petroleum Basin Series.

Yeats, R. S., and Taylor, J. C., in press, Saticoy oil field, Ventura basin, California, in Beaumont, E. A., and Foster, N. H., eds., American Association of Petroleum Geologists Treatise of Petroleum Geology.

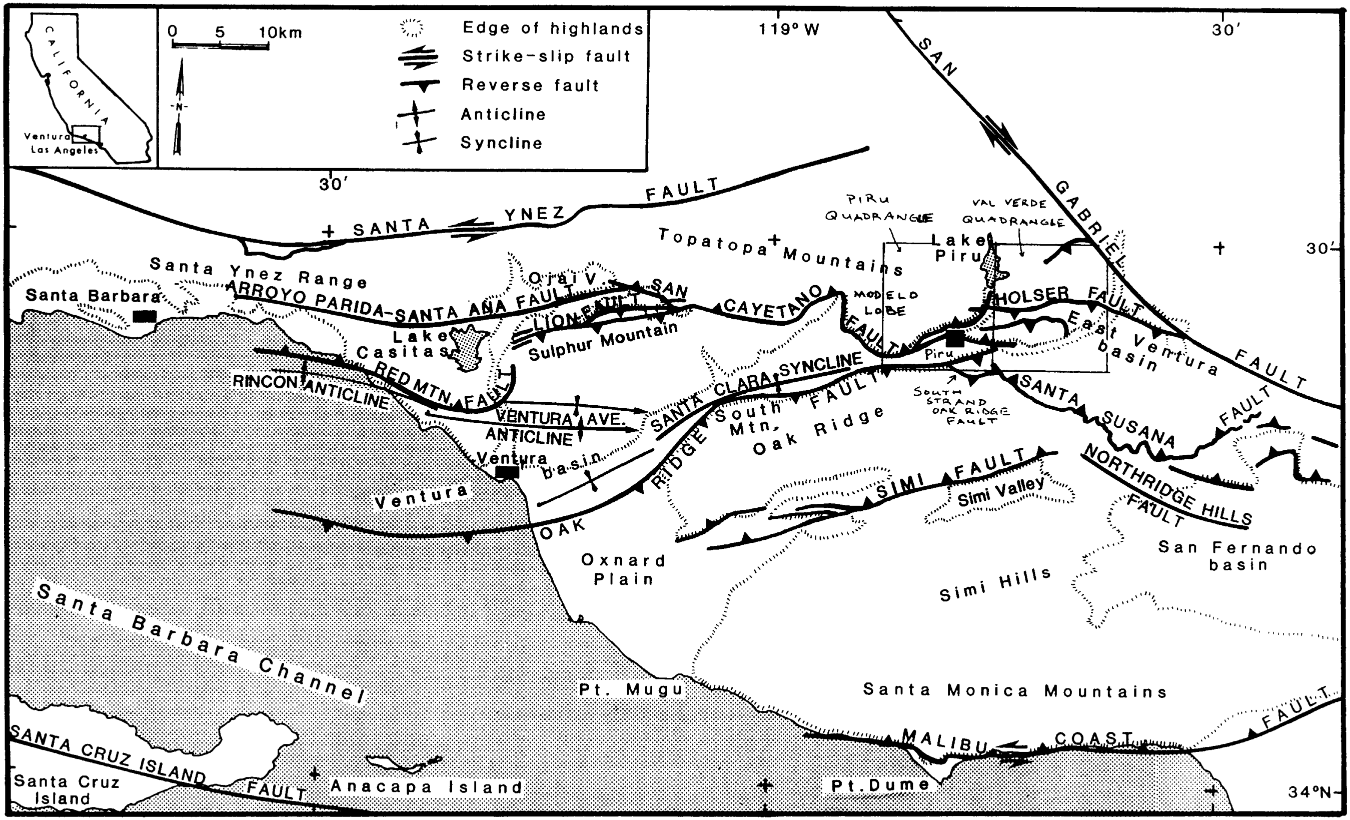
CALIFORNIA
Ventura
Los Angeles
0 5 10km
N
Edge of highlands
Strike-slip fault
Reverse fault
Anticline
Syncline
119° W
30′
30′
30′
34°N
SAN GABRIEL FAULT
SANTA YNEZ FAULT
Topatopa Mountains
Santa Ynez Range
Santa Barbara
ARROYO PARIDA-SANTA ANA FAULT
Ojai V.
SAN CAYETANO FAULT
LION FAULT
Sulphur Mountain
Lake Casitas
RINCON ANTICLINE
RED MTN. FAULT
VENTURA AVE. ANTICLINE
Ventura
Ventura basin
SANTA CLARA SYNCLINE
South Mtn.
Oak Ridge
OAK RIDGE FAULT
PIRU QUADRANGLE
VAL VERDE QUADRANGLE
Lake Piru
MODELO LOBE
Piru
HOLSER FAULT
East Ventura basin
SOUTH STRAND OAK RIDGE FAULT
SANTA SUSANA FAULT
SIMI FAULT
Simi Valley
NORTHRIDGE HILLS FAULT
San Fernando basin
Simi Hills
Oxnard Plain
Santa Barbara Channel
Pt. Mugu
Santa Monica Mountains
MALIBU COAST FAULT
Pt. Dume
Anacapa Island
SANTA CRUZ ISLAND FAULT
Santa Cruz Island

FIGURE 1

On-Line Seismic Processing

9930-02940

Rex Allen
Branch of Seismology
U.S. Geological Survey
345 Middlefield Road, MS 77
Menlo Park, California 94025
(415) 329-4731

Investigations and Results

Work has continued during this period at getting the RTP system running on INMOS transputer hardware. Progress on the software conversion has been slower than hoped, but no major difficulties have appeared. The principal bottleneck is getting used to the formalism of programming in OCCAM, the language of preference for INMOS equipment, and the one used in communicating between the various processors of a transputer multiprocessor.

The planned arrangement for outside design of the A/D converter did not work out as expected, and instead the A/D is being built in-house by Jim Ellis and Grey Jensen. They report satisfactory progress and no major known difficulties.

The Mk I RTP's at Menlo Park and the University of Utah have continued to operate satisfactorily, as have the Mk II's at Menlo Park and Caltech.

Long Baseline Tiltmeters: Southern California

14-08-0001-G1790

John Beavan
Lamont-Doherty Geological Observatory of Columbia University
Palisades, New York 10964
(914) 359-2900

Investigations

We operate a 535 m long-baseline half-filled water tube tiltmeter at Piñon Flat Observatory (PFO) in the San Jacinto Mountains of southern California. This is used in conjunction with a similar instrument operated by the University of California, San Diego (UCSD), to investigate:

(1) sources and magnitudes of noise affecting the tilt signal;
(2) water level sensor design and reliability;
(3) methods of referencing tiltmeter to depth;
(4) interpretation of tilt signal.

Results (April, 1990)

1. Tiltmeter Operation and Sensor Development

The LDGO tiltmeter continues to perform reliably, requiring little maintenance. Development of a simple absolute sensor (USGS Open File Report 90-54, pp 163-165, 1989) continues satisfactorily despite the departure of the engineer working on the project. A new engineer has been hired who brings highly relevant skills and enthusiasm to the task. The remainder of this report concentrates on analysis of data from the LDGO tiltmeter.

2. Tiltmeter Data Analysis

Tilt is monitored by measuring the height of the air-water interface at each end of a long horizontal pipe buried at ~2 m depth and half-filled with water. The water height is measured using a laser Michelson interferometer. Tilt is derived by differencing the two signals. The heights of the near-surface piers are also referenced to presumably more stable fiducial points at ~30 m depth using vertical strainmeters. The tilt measured between the (relatively unstable) surface piers is corrected using the vertical strain signals, so that the final estimate of tilt is from a long-baseline instrument that appears to be buried at ~30 m depth. Residual thermal signals can be removed by measuring the temperature of the sensors at each end and applying a correction to the resulting data.

The tilt data back through late 1984 have been analyzed, with corrections made for vertical displacements of the near-surface piers. Also, occasional micrometer measurements of water height have been used to adjust the datum of the water level series when it has been lost due to power outages or interferometer fringe counter failures. Results are presented in the Figures; data since November 1987 are superior due to more reliable fringe counters and to improved micrometer back-up measurements. The data presented here should not be regarded as final; the various edits and corrections applied are to be reviewed for accuracy, and the data analysis is to be extended back to 1983.

Figure 1a shows the water levels at the east and west ends of the tiltmeter as recorded by the occasional micrometer readings. Figures 1b and 1c show the difference between these

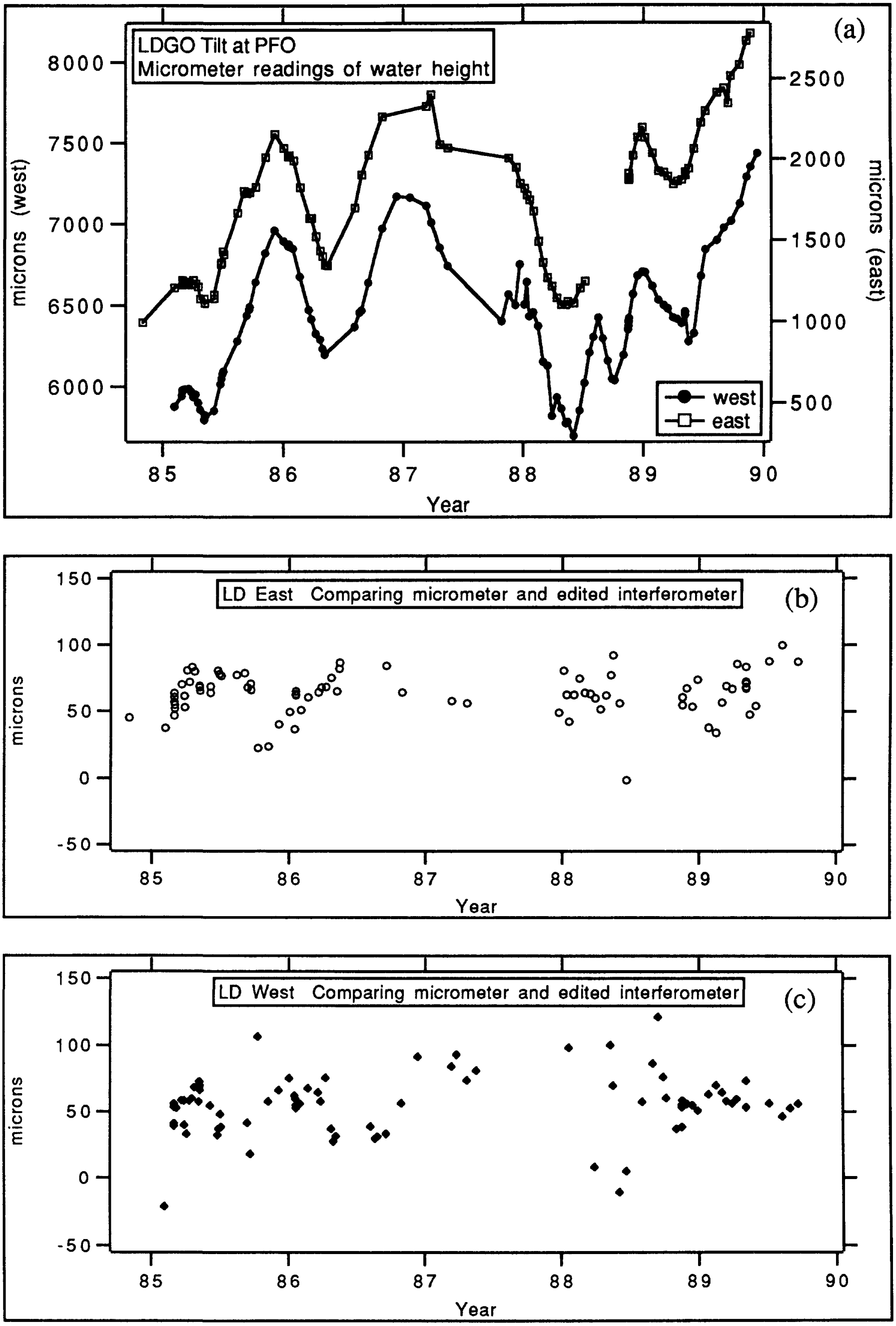
(a)
LDGO Tilt at PFO
Micrometer readings of water height
microns (west)
8000
7500
7000
6500
6000
microns (east)
2500
2000
1500
1000
500
west
east
85
86
87
88
89
90
Year
(b)
LD East Comparing micrometer and edited interferometer
microns
150
100
50
0
-50
85
86
87
88
89
90
Year
(c)
LD West Comparing micrometer and edited interferometer
microns
150
100
50
0
-50
85
86
87
88
89
90
Year

Figure 1.

micrometer readings of water height and the interferometer readings of water height, after the interferometer readings have been adjusted for datum shifts as described above. The residual scatter is less than ±20 μm. This is somewhat worse than the ±3 μm short-term reading repeatibility of the micrometers, and is probably due to differences in temperature response of the micrometer and the interferometer, and to temporal variations in surface cleanliness of the water in the micrometer chamber. Nevertheless, the micrometer readings assure the long-term accuracy of the water level difference to better than ±30 μm, which corresponds to ±0.05 μrad tilt.

Figure 2a shows the inferred tilt signal, after corrections for the micrometer readings and for vertical strain. Figure 2b shows the same signal with tides removed. These data have been independently analyzed by UCSD investigators (Wyatt, pers. comm., 1990), and the discrepancies between our respective residual signals are at most ~0.1 μrad; the discrepancies are largely confined to short sections of the data where there are obvious instrumental or other problems. The comparison between the independent analyses will be pursued in order to understand the source of the (small) differences. Our data suggest that the average 1984-89 tilt rate at PFO has been less than 0.01 μrad/yr, though there are more rapid fluctuations about this mean value.

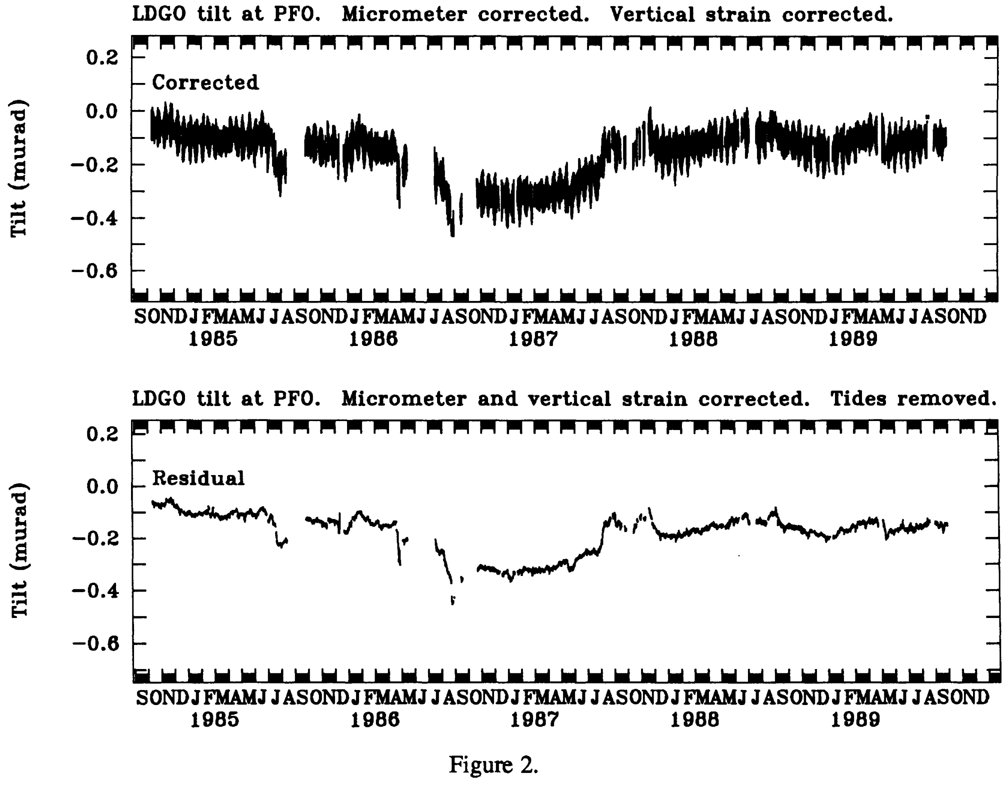

Figure 2.

In Figure 3, power spectral analysis of the LDGO tilt data is used to compare tilt noise levels with those expected from available and projected geodetic techniques. For signals that contain periods shorter than several years, this Figure demonstrates that long baseline tiltmeters provide far lower noise data than any available geodetic technique.

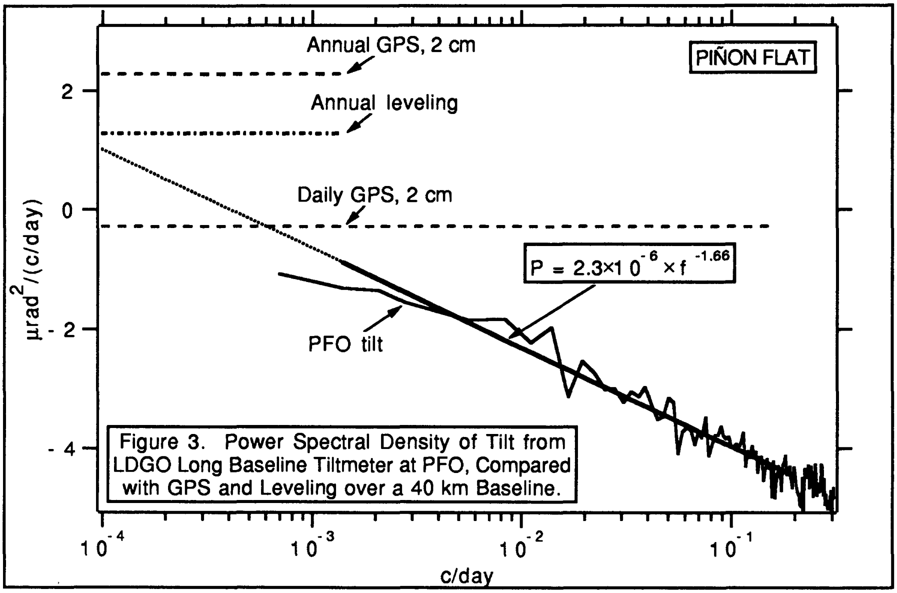

Figure 3. Power Spectral Density of Tilt from LDGO Long Baseline Tiltmeter at PFO, Compared with GPS and Leveling over a 40 km Baseline.

II.1

Crustal Deformation Measurements in the Shumagin Seismic Gap, Alaska

14-08-0001-G1792

John Beavan
Lamont-Doherty Geological Observatory of Columbia University
Palisades, NY 10964
(914) 359 2900

Investigations

1. Eleven short (~ 1 km) level lines are measured approximately annually within the Shumagin seismic gap, Alaska (Figure 1). Surface tilt data are interpreted in terms of tectonic deformation and earthquake hazard at the Pacific-North American plate boundary.
2. Six absolute-pressure sea-level gauges are operated in the Shumagin Islands in an attempt to measure vertical deformation associated with the Aleutian subduction zone.
3. The sea-level data are transmitted by satellite in near real time, and are examined for possible tectonic signals. Noise studies are used to determine the relative usefulness of different types of measurement, and to evaluate the minimum size of tectonic signal visible above the noise. Our data are compared with other crustal deformation data from the Shumagin gap.

Results (April 1990)

This report will deal principally with the sea level data. The leveling data are most recently described by Beavan (1989). As of this writing, three of our sea-level sites are still operating with three having failed during the winter. This is disappointing after a near-perfect performance during 1988-89. Some of the data may be recoverable from the backup recording described below, but most of the failures have occurred at sites not yet fitted with backup recording.

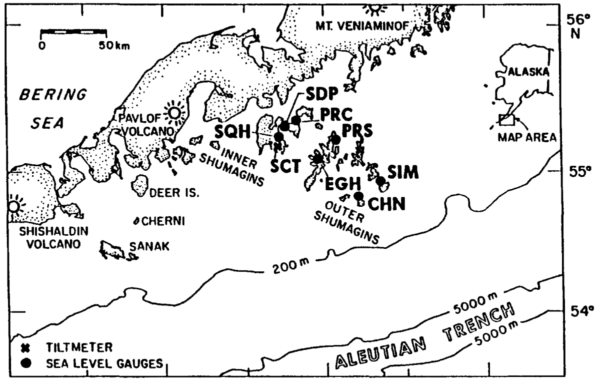

Figure 1. Location of the Shumagin Islands with respect to the trench and the volcanic arc. Depth contours are in metres. The seismic gap stretches from approximately Sanak Island in the west to about 30 km east of the Shumagin Islands. Also shown are the sites of six sea-level gauges operated by LDGO and one by the National Ocean Survey (at SDP). Level lines of approx. 1 km aperture are located on many of the Shumagin Islands, and on Sanak Is.

Backup Recording

During 1989, we installed solid-state backup recorders at three sites in order to protect against certain types of station failure. In 1990 we will upgrade the remainder of the sites: in some cases with backup recorders, in the more exposed sites with self-contained gauges that record more than a year of data in internal solid-state memory. These gauges will be far more robust because they will not require the cable linking the pressure sensor to shore. Their data will not be available in real time; however, some sites will continue to be transmitted in real-time so that detection of possible preseismic anomalies (see Beavan et al., 1984) will still be achievable.

Sea Level Data Analysis

The sea level gauge instrumentation and analysis techniques are described by Beavan et al. (1986) and Hurst and Beavan (1987). A suite of sea level difference data collected since 1976 is plotted in Figure 2. These plots show sea level difference with each trace labeled in the manner xxx_yyy, so that relative tectonic uplift of the second-named site (yyy) is indicated by an upward excursion of the graph. The gauges have been repeatedly tied to bedrock benchmarks in order to assure elevation control; none of these benchmarks has shown instability above the 1 mm level.

The three parts of the Figure require some explanation. Figure 2a includes the only 3 sites to have been operating during 1976: SDP and PRC in the Inner Shumagins, and SIM in the Outer Shumagins. The 1976 data were from a conventional NOS float gauge at SDP, and from mean-sea-level-indicators (msli; Bilham, 1977) at PRC and SIM. Before differencing, the NOS data were filtered with a long time-constant filter that approximated the operation of the msli.

The 1981-85 data are from gauges installed near lower low tide that used ceramic sensors to measure pressure. These gauges had significant long term instabilities. Empirical corrections of several cm have therefore been applied in order to make the SDP-PRC difference data approximately constant (because SDP and PRC are on the same island separated by only 15 km). The SDP gauge measures sea level, whereas the L-DGO gauges measure sea+air pressure. In order to difference these data correctly, an appropriate air pressure series is first added to the SDP data, assuming the usual 1 cm/mbar inverse barometer effect (see Beavan et al., 1986).

There is an offset between 1983 and 1984 that could coincide with the Valentine's Day earthquakes of 1983 which occurred just south-east of SIM (Taber and Beavan, 1986). This ~6 cm relative subsidence at SIM depends to some extent on the way corrections are made to the data, so we do not regard it as very persuasive. An offset this size could not have been coseismic because two sea-level gauges (SIM itself, and SAD near the S end of Nagai Is.) were running during the earthquakes and examination of their difference data excludes a sudden coseismic offset greater than ~3 cm. (It is difficult to make this estimate more precise because of a 10 cm seiche signal in the SIM data and the 12 min sample interval.) The horizontal deformation data show a displacement between SIM and sites to the NW of < 2 cm between Summer 1981 and Summer 1983 (Lisowski et al., 1988), which also suggests that a subsidence of 6 cm is too large.

The 1985-89 data are from quartz pressure gauges installed in a similar manner to the 1981-85 gauges. Some small corrections have been made to the raw data, based on calibrations of the gauges before installation and after removal. The noise levels are substantially reduced relative to earlier data. There is a positive trend on both the PRC-SIM and SDP-SIM plots between 1985-89. This represents relative uplift at SIM of ~3.2 mm/yr. The trend continues through several sensor changes (marked by dots in the Figure) so is most unlikely to be caused by sensor instability.

Despite the problems with the 1981-85 data there does appear to be a difference between the 1976 and 1985-89 relative elevations of SIM and PRC/SDP, with SIM having subsided 8±5 cm during that period (note that this is *not* significant at the 95% level). This subsidence would be explained in large part by the 1983 offset, if real.

A final result from Figure 2a is that the PRC-SIM relative elevation change between 1976-81 could not have been more than a few cm, say 10 cm at the most. Beavan et al.'s (1984) interpretation of the 1978-80 reverse tilting episode required uplift of SIM relative to PRC of ~25 cm between 1978-80. From the limited (1981/82 compared to 1976) differential sea level data

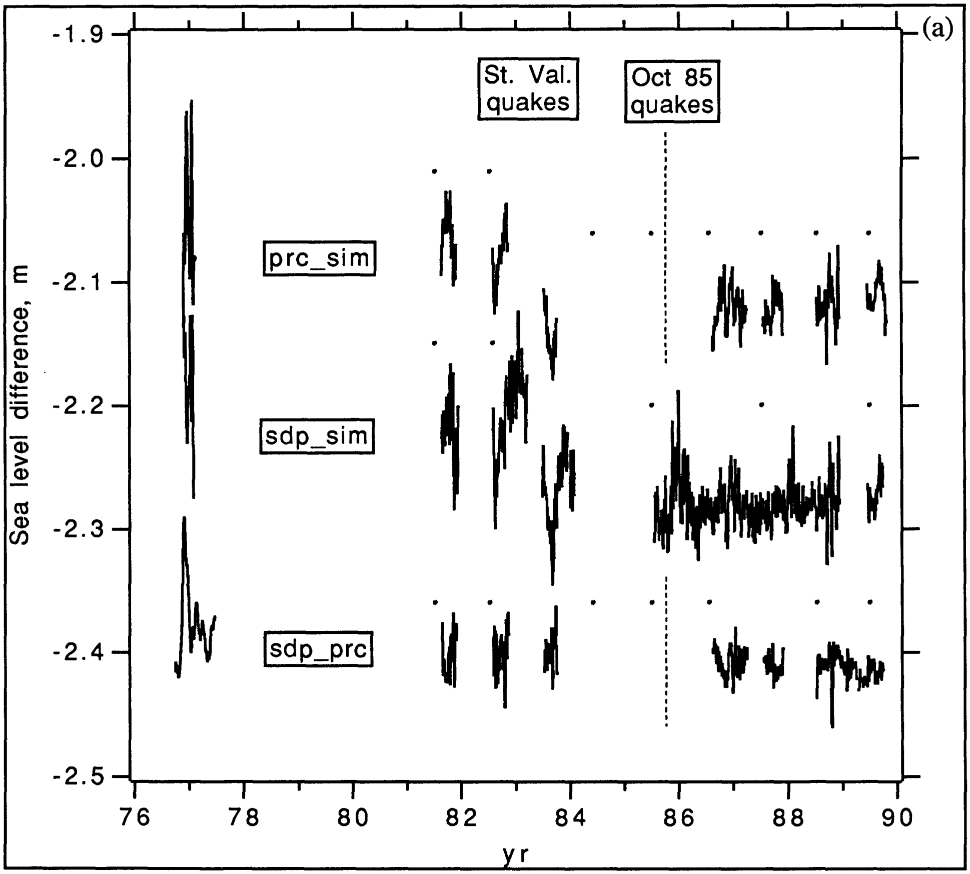

Figure 2. (a) Sea level differences from 1976 to 1989 at the three sites SDP and PRC (Inner Islands) and SIM (Outer Islands). The SDP data are from an NOS float gauge. The PRC and SIM data are from strongly filtered float gauges in 1976-7, ceramic pressure sensors in 1981-85, quartz pressure sensors since 1985. The post-85 data are by far the most reliable. The offset in 1983 may be caused partially by the 14 Feb 1983 earthquakes, but is probably partly due to gauge instability. The dots above the traces indicate when sensors were changed at one or both the sites. The fact that the 1985-89 positive trend on traces prc_sim and sdp_sim is independent of these changes leads us to believe that it is a real tectonic signal. The trend indicates emergence of the Outer Islands relative to the Inner Islands at ~3.2 mm/yr. See detailed discussion in text for more information.

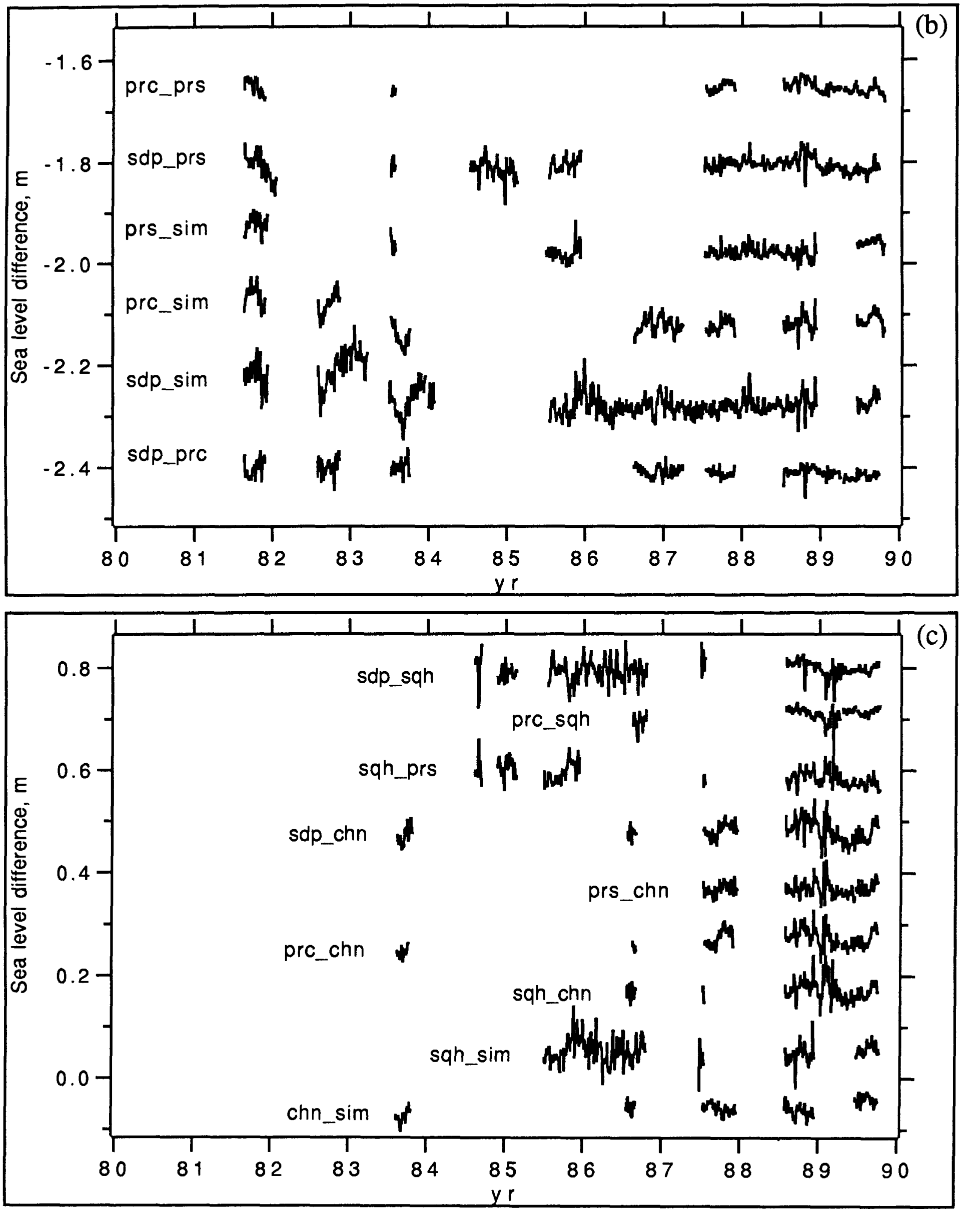

Figure 2 (contd.) (b) The lower 3 traces repeat the sea-level difference data of Figure 2a, from 1981 onwards. The top 3 traces are differences that include site PRS in the Central Islands - this is the only other site to have been operating since 1981. (c) Differences that include sites CHN and SQH, installed in 1983 and 1984. Sensor changes have also occurred frequently in these series, though they have not been marked as in Fig. 2a. Note the indications of slight submergence of the Central relative to the Inner Islands, e.g. trace sqh_prs, and the emergence of the Outer relative to the Inner Islands, e.g. traces prc_chn and sqh_sim.

available to them, Beavan et al. (1984) argued that the deformation in 1976-78 and 1980-81 might have partially masked this 25 cm signal, so that it might not be obvious in the differential sea level data. While this was a plausible explanation at the time, the continued measurement of <1 cm/yr deformation rates make it seem increasingly unlikely. Although the 1978-80 seismicity data, as well as the deformation data, show unusual behavior, we nevertheless now feel that the Beavan et al. (1984) interpretation of the 1978-80 reverse tilt episode is not supported by the sea level data.

Figure 2b repeats the 1981-89 data from (a), and adds data from the other gauge, PRS, installed in 1981. Looking in detail at only the post-1985 data, these plots suggest slow submergence of the Central Islands (PRS) relative to both Inner (PRC/SDP) and Outer (SIM) Islands. Note that these deformation rates are quite consistent with the sense and magnitude of our leveling data, which show tilting trenchward in the Inner and Central Islands and arcward in the Outer Islands. The combined data suggest a hinge line slightly trenchward of the Central Islands.

Figure 2c plots difference data that incorporate two additional gauges - CHN installed in 1983, and SQH in 1984. These data tend to support the above scenario, though there are some oddities such as the apparent motion between SIM and CHN; this, however, is not unexpected from the geology and geomorphology. Also, dislocation modelling of the Oct. 1985 earthquake sequence south of CHN predicts up to 1 cm subsidence at CHN, which is of the right sense, though rather too small, to explain the ~2 cm offset between the 1983 and 1986 CHN-SIM data.

The sea level data since 1985 are summarized in Table 1, where the rates are calculated by linear regression on all available post-1985 data. There are inconsistencies within these rates (e.g., SDP-PRS plus PRS-SIM does not add up to SDP-SIM), the reason being that the data sets are incomplete and the positions of the data gaps bias the derived rates. The mean values are also biased because there are 3 sites in the Inner, 1 in the Central, and 2 in the Outer Islands. Nevertheless, the tendency for submergence in the Central relative to both Outer and Inner Islands is apparent. The 1σ errors in these rates are on the order of 2 mm/yr, but we have not formally evaluated them. The data are also capable of interpretation as indicating zero vertical motion, in agreement with Lisowski et al.'s (1988) contention that deformation is currently taking place by steady aseismic slip.

Table 1. 1985-89 Differential Uplift Between Island Groups in mm/yr

Inner - Outer		Inner - Central		Central - Outer	
sdp-sim	+2.2	sdp-prs	-1.7		
prc-sim	+4.3	prc-prs	-3.9	prs-sim	+3.7
prc-chn	+0.5			prs-chn	+0.4
sqh-sim	-0.3	sqh-prs	-3.2		
sqh-chn	-0.1				
Mean	+1.3		-2.9		+2.0

Positive rate implies second-named site is uplifting relative to first.

The low measured deformation rates, both horizontal (Lisowski et al., 1988) and vertical, are in sharp conflict with the inferred seismic history (Boyd et al., 1988) if simple models of subduction (e.g., Savage, 1983) are assumed. One potential explanation is that the plate boundary is currently locked, yet the deformation rate is lowered by viscoelastic effects late in the interseismic cycle (Thatcher and Rundle, 1984). This possibility is considered by Lisowski et al. (1988), as is the possibility that the low rates may be the result of interaction with neighboring large quakes; they find that neither effect is large enough to explain the observations. However, recent finite-element modelling by Rice and Stuart (1989), which includes effects of mantle relaxation, re-opens the possibilty that relaxation effects are responsible for the discrepancy. The model predicts unusually low compressional (or even slightly extensional) horizontal strain rates during the latter part of the seismic cycle on the surface of the overriding plate somewhat inland of the down-dip end of the locked main thrust zone. This model also predicts reduced rates of vertical deformation in the same area, relative to the elastic model (Rice, pers. comm., April 1990). However, the model predictions do not match our observations of tilt and sea level in detail; in particular, the direction of tilting predicted by the models appears to be opposite to that observed.

A modification described by Beavan (1988), and also discussed by Lisowski et al. (1988) as the "Beavan" model, enables the predictions of the simple dislocation model to match the tilt and strain data about as well as they are matched by an aseismic deformation model. However, the model prediction of 0.5 - 1.5 cm/yr submergence of the Outer and Central relative to the Inner Islands is emphatically not matched by the sea level data (Table 1), so this model is now rejected.

References

Beavan, J., R. Bilham & K. Hurst, 1984. Coherent tilt signals observed in the Shumagin seismic gap; detection of time dependent signals at depth?, J. geophys. Res., 89, 4478-4492.

Beavan, J., K. Hurst, R. Bilham & L. Shengold, 1986. A densely-spaced array of sea-level monitors for the detection of vertical crustal deformation in the Shumagin seismic gap, Alaska, J. geophys. Res., 91, 9067-9080.

Beavan, J., 1988. Crustal Deformation Measurements in the Shumagin Seismic Gap, Alaska, USGS Open File Report, 88-673, 183-188.

Beavan, J., 1989. Crustal Deformation Measurements in the Shumagin Seismic Gap, Alaska, USGS Open File Report, 90-54, 166-169.

Bilham, R.G., 1977. A sea-level recorder for tectonic studies, Geophys. J. R. astr. Soc.

Boyd, T.M., J.J. Taber, A.L. Lerner-Lam and J. Beavan, 1988. Seismic rupture and arc segmentation within the Shumagin Islands seismic gap, Alaska, Geophys. Res. Lett., 88, 201-204.

Hudnut, K.W. and J.J. Taber, 1987. Transition from double to single Wadati-Benioff seismic zone in the Shumagin Islands, Alaska, Geophys. Res. Lett., 14, 143-146.

Hurst, K.J. and J. Beavan, 1987. Improved sea level monitors for measuring vertical crustal deformation in the Shumagin seismic gap, Alaska, Geophys. Res. Lett., 14, 1234-1237.

Lisowski, M., J.C. Savage, W.H. Prescott and W.K. Gross, 1988. Absence of strain accumulation in the Shumagin seismic gap, Alaska, 1980-1987, J. geophys. Res., 93, 7909-7922.

Rice, J.R. & W.D. Stuart, 1989. Stressing In and Near a Strongly Coupled Subduction Zone During the Earthquake Cycle (abstract), Eos, 70, 1063.

Savage, J.C., 1983. A dislocation model of strain accumulation and release at a subduction zone, J. geophys. Res., 88, 4984-4996.

Taber, J.J. & J. Beavan, 1986. 14 February 1983 earthquake sequence in the Shumagin Islands, Alaska, Bull. seism. Soc. Am., 76, 1588-1596.

Thatcher, W. & J.B. Rundle, 1984. A viscoelastic coupling model for the cyclic deformation due to periodically repeated earthquakes at subduction zones, J. geophys. Res., 89, 7631-7640.

Error Analysis and Network Design in GPS Measurement of Crustal Deformation

14-08-0001-G1335

Yehuda Bock
Institute of Geophysics and Planetary Physics
Scripps Institution of Oceanography
La Jolla, CA 92093
(619) 534-5292

Objectives:

Understanding the structure and geometry of seismogenic zones is a key element in the prediction of earthquakes. Geodetic measurements contribute to this understanding through the mapping of present-day crustal deformation. Three-dimensional relative-positioning using the Global Positioning System (GPS) is the most accurate and cost-efficient method for measuring crustal deformation over distances of tens to hundreds of kilometers. The objective of our research is to investigate sources of error and optimum analysis techniques for high-precision GPS measurements. Progress in these areas will lead directly to more accurate measurement of deformation in areas of high seismogenic potential.

Investigations undertaken:

Our investigations of the last six months have focused on two primary areas:

(1) continuously monitoring array of GPS observatories in southern California
(2) data analysis of the USGS Parkfield GPS network

Continuous Monitoring of Deformations with GPS

(1) Background

Investigators at four universities (Caltech, MIT, UCLA and UCSD) and JPL, in collaboration with USGS and NGS, are operating an array of continuously and remotely operating GPS receivers in southern California. In this concept, GPS observations are made continuously for an indefinitely long period of time in search of precursory deformation of some sort, particularly related to the earthquake cycle. If phase lock can be maintained, phase ambiguities on the network baselines need to be resolved only once and relative station positions can be constrained so that deformations can be analyzed continuously at temporal scales as short as several minutes (Bock and Shimada, 1989).

The scientific motivations for continuous monitoring are (1) establishing a reference network for rapid, frequent resurveys of dense networks in central and southern California; (2) detection and analysis of steady and transient strains; (3) studying strain over a broad spectrum of spatial and temporal scales; and (4) studying the three-dimensional strain tensor (horizontal and vertical). Ultimately, we seek to understand underlying physical phenomena, particularly the physics of the earthquake process.

The technical motivations for continuous monitoring are (1) determining the long-term positional accuracy of GPS geodesy; (2) understanding periodic, non-random signatures in GPS data; (3) determining the "instrument response" of GPS hardware (receivers and antennas); (4) improving the signal-to-noise ratio for baseline estimation; (4) developing optimal and rapid analysis techniques; and (5) studying monumentation and site stability issues. The overall goal is to separate the geophysical signal from the geodetic noise, rapidly and confidently.

The continuous array is meant to support the instrument and orbit tracking requirements of geophysical investigations using GPS. Any investigator will be able to do GPS surveys in central and southern California with as little as one receiver and know that there is a continuously recording station within 100 kilometers, and accurate satellite ephemerides available.

(2) Current Activities and Results

At present (April, 1990), three SNR-8 Rogue receivers are tracking at Scripps, Piñon Flat Observatory and Jet Propulsion Laboratory (Figure 1). For orbit tracking support, we are collecting, from the National Geodetic Survey, data from the U.S. CIGNET stations including Mojave (California), Westford (Massachusetts) and Richmond (Florida). In February and March, data were collected on the Scripps to Piñon baseline with Trimble 4000 SDT receivers. SNR-8 Rogue receivers were deployed in mid-March. The data collected through April 1990 are listed in Tables 1 and 2.

The continuous array data system under development at Scripps is illustrated in Figure 2. It includes collection, analysis, archiving, distribution and interpretation of data. The data from the array is available over Internet for all investigators using GPS measurements in California. At Scripps, we are currently processing the data collected in the array with the CIGNET data using analysis techniques described in Dong and Bock (1989). A byproduct of our analysis will be accurate satellite ephemerides to support GPS-based geophysical research in California.

We are currently analyzing 14 months of continuously monitored GPS observations collected at a ten station network in the Kanto-Tokai district in Japan by the National Research Center for Disaster Prevention [Fujinawa et al., 1989]. We have been using this data set as a basis for developing data processing, data handling and data archiving algorithms for use in the California network. The goal is to develop rapid and efficient techniques to handle large quantities of continuously monitored GPS data, and to be able to detect confidently any temporal strain events for time periods as short as several minutes.

Parkfield GPS data

(1) Background

We are currently analyzing the GPS time series collected by USGS since 1986 at four stations in the vicinity of Parkfield (Davis et al., 1990). The baselines are several kilometers in length, in a range where modeling of the ionospheric delay should be beneficial in more accurate monitoring of deformations. The baselines are too long to analyze using L1 and L2 frequency data independently (since residual ionospheric delays start becoming significant) and too short to optimally use the ionosphere-free linear combination (since amplification of the phase error in forming the linear combination is larger than the residual ionospheric delay). We are using hybrid observables [Schaffrin and Bock, 1988; Dong and Bock, 1989] which are a combination of L1, L2 observations and constraints on the ionosphere based on ionospheric models, available externally and/or derived from an internal calibration of the GPS data. The solutions using these observables will be compared to the L1 and L2 independent and ionosphere-free solutions, as well as to the solutions by Prescott's group at Menlo Park.

(2) Current Activities and Results

We have completed an analysis of 18 individual Parkfield GPS occupations from mid-1986 to early 1989. We have processed the data in two ways, using the L1 and L2 observations as independent observables, and using the ionosphere-free combination of phase. In both cases, phase ambiguities have been resolved. In general, the two solutions agree within 1 cm except for two occupations where the difference is several centimeters. As an example, we illustrate in Figures 3 and 4 the changing lengths of two baselines of the network, both spanning the fault, using both ways of processing. In general, the rate inferred from the L1 and L2 independent solutions (7.8 mm/yr for 10jdg to 33jdg) is almost 50% slower than the ionosphere-free solutions (14 mm/yr) although these differences may change as we refine our solutions and add additional data points. USGS investigators have published a rate of 9 mm/yr for 10jdg to 33jdg (Davis et al., 1989). The data from the ionosphere-free solutions more strongly support a linear rate of change (Figures 2 and 3). We are continuing our analysis of the remaining GPS occupations at Parkfield, testing hybrid observables, and ionospheric models.

References:

Davis J.L., W.H. Prescott, J.L. Svarc and K.J. Wendt (1989). "Assessment of Global Positioning System measurements for studies of crustal deformation," J. Geophys. Res., 94, 13635-13650.

Dong, D. and Y. Bock (1989). "Global Positioning System network analysis with phase ambiguity resolution applied to crustal deformation studies in California," J. Geophys. Res., 94, 3949-3966.

Fujinawa Y., S. Shimada, T. Kishii, S. Sekiguchi, T. Eguchi, Y. Okada and S. Watada (1989). "Some results in the preliminary data analysis of the fixed-point GPS baseline determination network in Central Japan," presented at International Association of Geodesy General Meeting, Edinburgh, Scotland, 3 to 12 August.

Schaffrin, B. and Y. Bock (1988). "A unified scheme for processing GPS dual-band phase observations," Bull. Geod., 62, 142-160.

Bock, Y. and S. Shimada, 1990: "Continuously monitoring GPS networks for deformation measurements," in Global Positioning System: An Overview, proc. IAG Symposium 102, Y. Bock and N. Leppard (eds.), Edinburgh, Scotland, August 7-8, 1989, Springer Verlag, in press.

Table 1: Permanent GPS Geodetic Array in Southern California — Tracking Log
February and March 1990

Date		Day	Start	Stop	GPS		SIO		Piñon		JPL	CIGNET			Comments
							1	2	1	2		M	W	R	
Feb	15	046	04:20	11:20	527	4	t	-	t	-	-	m	m	m	
	16	047	04:16	11:16	527	5	t	-	t	-	-	m	m	m	
	17	048	14:12	21:12	527	6	t	-	t	-	-	m	m	m	error in scenario
	18	049	04:08	11:08	528	0	t	-	t	-	-	m	m	m	Riverside Co. begin
	19	050	04:04	11:04	528	1	t	-	t	-	-	m	m	m	
	20	051	04:00	11:00	528	2	t	-	t	-	-	m	m	m	
	21	052	03:56	10:56	528	3	t	-	t	-	-	m	m	m	
	22	053	03:52	10:52	528	4	t	-	t	-	-	m	m	m	
	23	054	03:48	10:48	528	5	t	-	t	-	-	m	m	m	
	24	055	03:44	10:44	528	6	t	-	t	-	-	m	m	m	
	25	056	03:40	10:40	529	0	t	-	t	-	-	m	m	m	
	26	057	03:36	10:36	529	1	t	-	t	-	-	m	m	m	
	27	058	03:32	10:32	529	2	t	-	t	-	-	m	m	m	
	28	059	03:28	10:28	529	3	t	-	t	-	-	m	m	m	
Mar	01	060	04:20	10:24	529	4	t	-	x	-	-	m	m	m	no Piñon, late SIO
	02	061	03:20	10:20	529	5	t	-	t	-	-	m	m	m	
	03	062	03:16	10:16	529	6	t	t	t	t	-	m	m	m	SIO & Piñon ties
	04	063	03:12	10:12	530	0	t	t	t	t	-	m	m	m	" (Riverside Co, end)
	05	064	03:08	10:08	530	1	t	t	t	t	-	m	m	m	SIO & Piñon ties
	06	065	03:04	10:04	530	2	t	-	t	-	-	m	m	m	
	07	066	03:00	10:00	530	3	t	-	t	-	-	m	m	m	
	08	067	02:56	09:56	530	4	t	-	t	-	-	m	m	m	
	09	068	02:52	09:52	530	5	t	-	t	-	-	m	m	m	
	10	069	02:48	09:48	530	6	ti	t	t	-	-	m	m	m	NGS observes SIO 1
	11	070	02:44	09:44	531	0	-	t	t	-	-	m	m	m	SIO 2 observed
	12	071	02:40	09:40	531	1	t	-	t	-	-	m	m	m	
	13	072	02:36	09:36	531	2	t	-	t	-	-	m	m	m	
	14	073	02:32	09:32	531	3	t	-	t	-	-	m	m	m	
	15	074	02:28	09:28	531	4	t	-	t	-	-	m	m	m	Rogues installed
	16	075	02:24	09:24	531	5	-	t	-	t	-	m	m	m	Trimbles moved
	17	076	02:20	09:20	531	6	r	t	r	t	-	m	m	m	
	18	077	02:16	09:16	532	0	r	t	r	t	-	m	m	m	
	19	078	02:12	09:12	532	1	r	t	r	t	-	m	m	m	
	20	079	02:08	09:08	532	2	r	t	r	t	-	m	m	m	
	21	080	02:04	09:04	532	3	r	t	r	t	-	m	m	m	
	22	081	02:00	09:00	532	4	r	t	r	t	-	m	m	m	
	23	082	01:56	08:56	532	5	r	t	r	t	r	m	m	m	
	24	083	01:52	08:52	532	6	-	t	-	t	-	m	m	m	
	25	084	00:52	08:52	533	0	-	t	-	t	-	m	m	m	S. Calif. Expmnt.
	26	085	00:48	08:48	533	1	r	t	r	t	r	m	m	m	S. Calif. Expmnt.
	27	086	00:44	08:44	533	2	r	t	r	t	-	m	m	m	S. Calif. Expmnt.
	28	087	00:40	08:40	533	3	r	t	r	t	r	m	m	m	S. Calif. Expmnt.
	29	088	00:36	08:36	533	4	-	t	r	t	r	m	m	m	S. Calif. Expmnt.
	30	089	00:32	08:32	533	5	-	t	r	t	-	m	m	m	S. Calif. Expmnt.
	31	090	00:28	08:28	533	6	-	t	r	t	-	m	m	m	S. Calif. Expmnt.

t : Trimble 4000 SDT, r : SNR-8 ROGUE, m : Mini-Mac 2816 AT, ti : TI 4100, - : no data
CIGNET: M (Mojave, California), R (Richmond, Florida), W (Westford, Massachusetts)

Table 2: Permanent GPS Geodetic Array in Southern California — Tracking Log
April 1990

Date		Day	Start	Stop	GPS		SIO		Piñon		JPL	CIGNET			Comments
							1	2	1	2		M	W	R	
Apr	01	091	00:24	08:24	534	0	-	t	-	-	-	m	m	m	S. Calif. Expmnt.
	02	092	01:16	08:16	534	1	-	t	-	-	-	m	m	m	JPL GPS Workshop
	03	093	01:12	08:12	534	2	-	t	-	-	-	m	m	m	NASA CDP
	04	094	01:08	08:08	534	3	-	t	-	-	-	m	m	m	NASA CDP
	05	095	01:04	08:04	534	4	-	t	-	-	-	m	m	m	NASA CDP
	06	096	01:00	08:00	534	5	-	t	-	-	-	m	m	m	
	07	097	00:56	07:56	534	6	-	-	-	-	-	m	m	m	no array data
	08	098	00:52	07:52	535	0	-	-	-	-	-	m	m	m	no array data
	09	099	00:48	07:48	535	1	-	-	-	-	-	m	m	m	no array data
	10	100	00:44	07:44	535	2	-	-	-	-	-	m	m	m	no array data
	11	101	00:40	07:40	535	3	-	-	-	-	-	m	m	m	no array data
	12	102	00:36	07:36	535	4	-	-	-	-	-	m	m	m	no array data
	13	103	00:32	07:32	535	5	-	-	-	-	-	m	m	m	no array data
	14	104	00:28	07:28	535	6	-	-	-	-	-	m	m	m	no array data
	15	105	23:28	07:28	536	0	r	-	r	-	r	m	m	m	full Rogue tracking
	16	106	23:24	07:24	536	1	r	-	r	-	r	m	m	m	
	17	107	23:20	07:20	536	2	r	-	r	-	r	m	m	m	
	18	108	23:16	07:16	536	3	r	-	r	-	r	m	m	m	
	19	109	23:12	07:12	536	4	r	-	r	-	r	m	m	m	Piñon GPS survey
	20	110	23:08	07:08	536	5	r	-	r	-	r	m	m	m	
	21	111	23:04	07:04	536	6	r	-	r	-	r	m	m	m	
	22	112	23:00	07:00	537	0	r	-	r	-	r	m	m	m	
	23	113	22:56	06:56	537	1	r	-	r	-	r	m	m	m	
	24	114	22:00	09:00	537	2	r	-	r	-	r	m	m	m	
	25	115	21:56	08:56	537	3	r	-	r	-	r	m	m	m	
	26	116	21:52	08:52	537	4	r	-	r	-	r	m	m	m	
	27	117	21:48	08:48	537	5	r	-	r	-	r	m	m	m	
	28	118	21:44	08:44	537	6	r	-	r	-	r	m	m	m	
	29	119	21:40	08:40	538	0	r	-	r	-	r	m	m	m	
	30	120	21:36	08:36	538	1	r	-	r	-	r	m	m	m	

t : Trimble 4000 SDT, r : SNR-8 ROGUE, m : Mini-Mac 2816 AT, - : no data
CIGNET: M (Mojave, California), R (Richmond, Florida), W (Westford, Massachusetts)

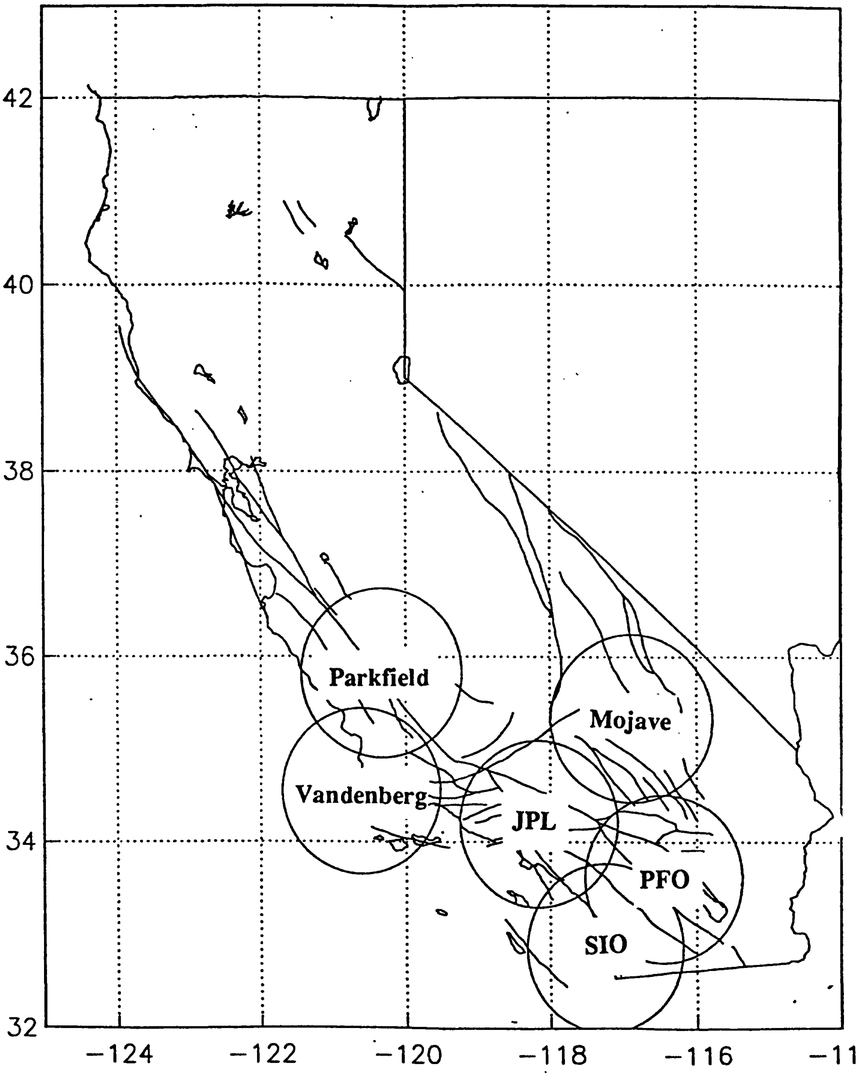

Figure 1: Stations of the Permanent GPS Geodetic Array in Central and Southern California and the CIGNET Mojave tracking station. SNR-8 Rogue receivers are deployed at SIO, PFO and JPL and a Mini-Mac 2816 AT receiver at Mojave. The stations at Vandenberg and Parkfield will be deployed in 1990. The circles have a radius of 100 km.

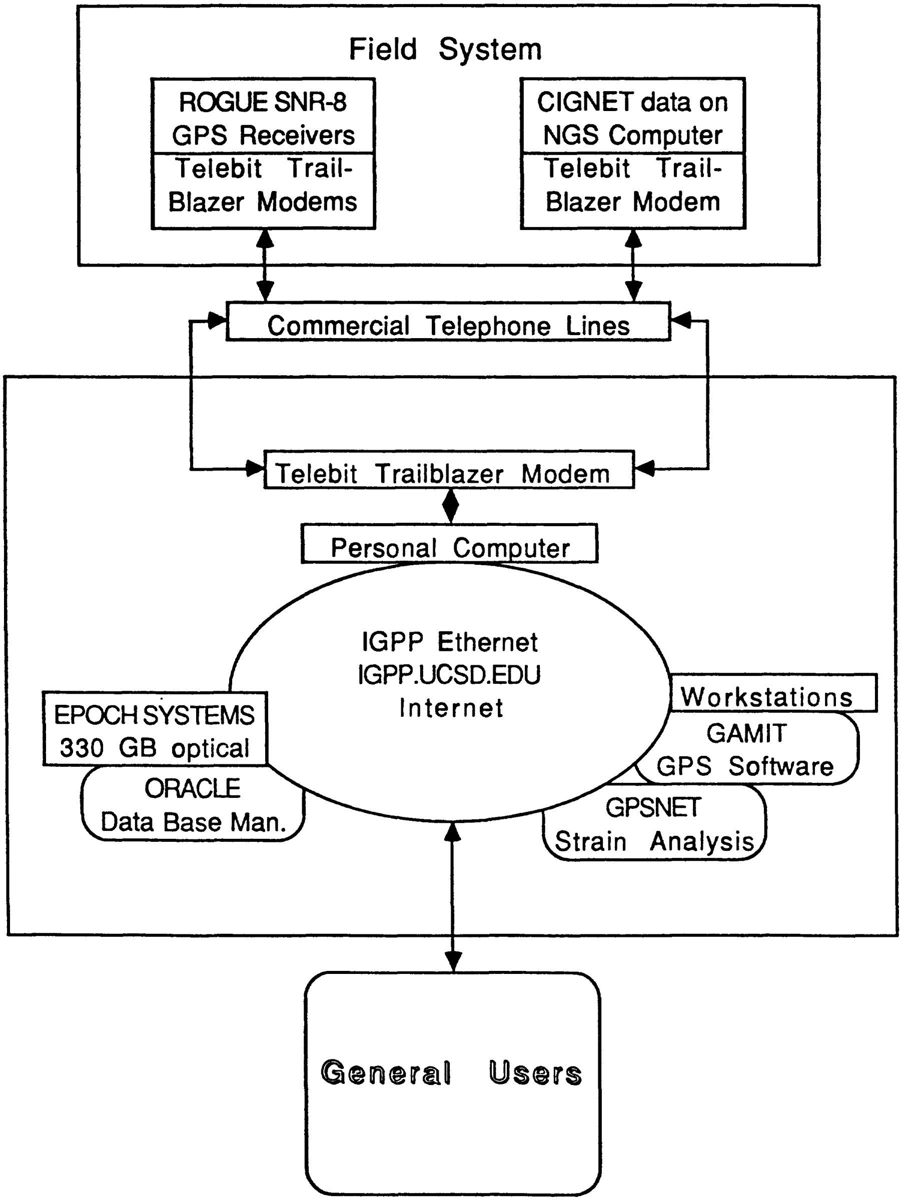

Figure 2: Data system under development at Scripps Institution of Oceanography to support the Permanent GPS Geodetic Array.

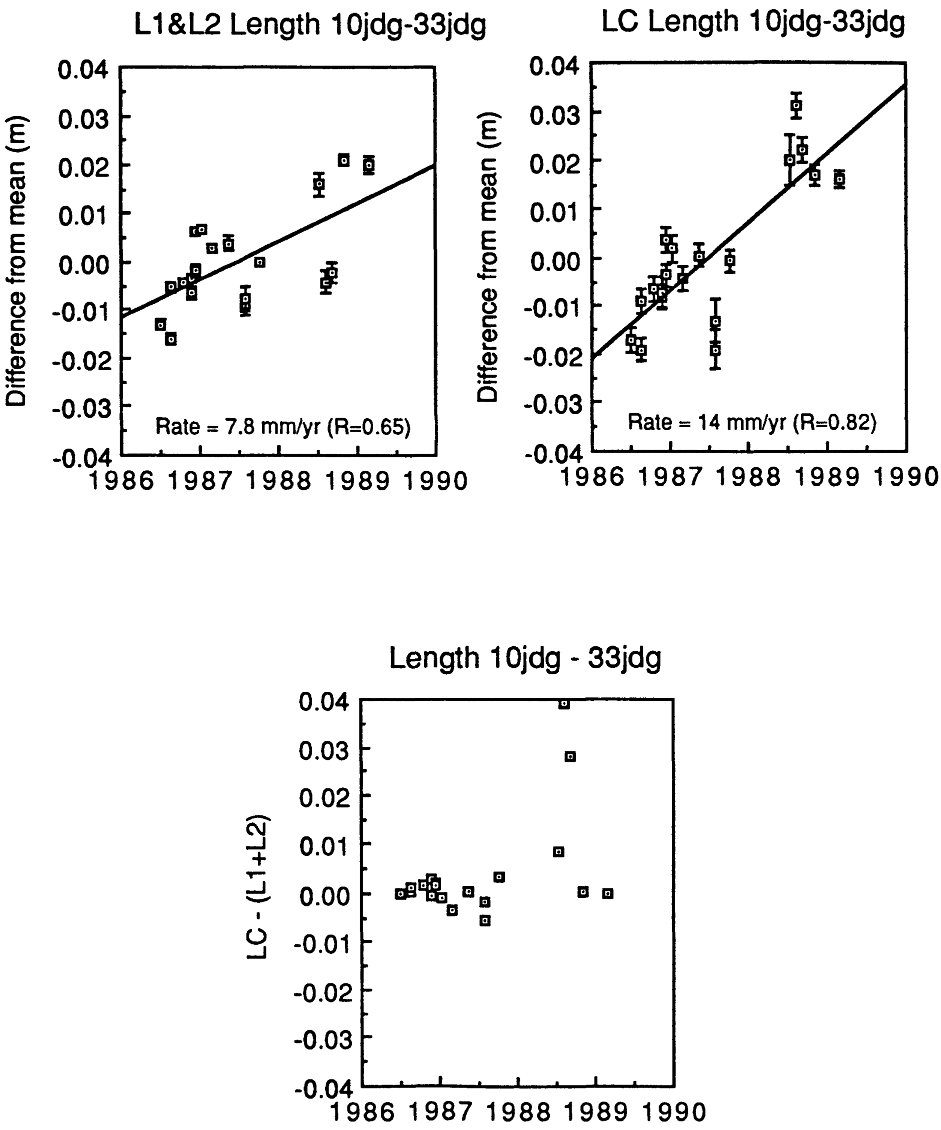

Figure 3: Rate of change of length of the Parkfield GPS baseline from station 10JDG to 33JDG based on 19 individual occupations from 1986 to 1989. The upper left plot shows the L1 and L2 independent solution, the upper right plot shows the ionosphere-free solution, and the lowe plot shows the difference between the two.

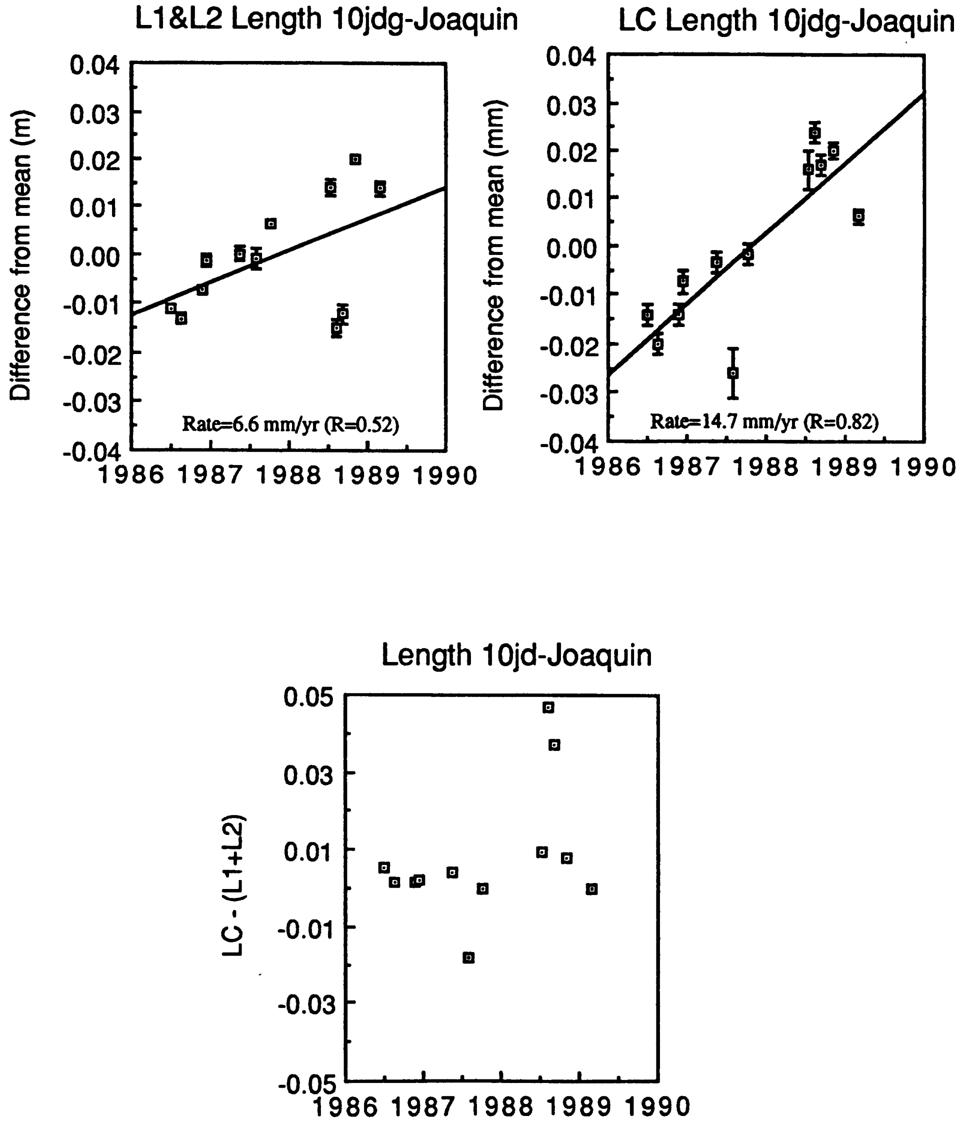

Figure 4: Rate of change of length of the Parkfield GPS baseline from station 10JDG to Joaquin based on 12 individual occupations from 1986 to 1989. The upper left plot shows the L1 and L2 independent solution, the upper right plot shows the ionosphere-free solution, and the lowe plot shows the difference between the two.

Remote Monitoring of Source Parameters for Seismic Precursors

9920-02383

George L. Choy
Branch of Global Seismology and Geomagnetism
U.S. Geological Survey
Denver Federal Center
Box 25046, Mail Stop 967
Denver, Colorado 80225
(303) 236-1506

Investigations

1. NEIC reporting services. Broadband data are used routinely to increase the accuracy of some reported parameters such as depth and to compute additional parameters such as radiated energy. These parameters are published in the Monthly Listing of the Preliminary Determination of Epicenters.

2. Rupture process of large- and moderate-sized earthquakes. We are using digitally recorded broadband waveforms to characterize the rupture process of selected intraplate and subduction-zone earthquakes. The rupture processes thus delineated are used to complement seismicity patterns to formulate a tectonic interpretation of the epicentral regions.

3. Teleseismic estimates of radiated energy and strong ground motion. On a world-wide basis, the relative paucity of near-field recording instruments hinders the prediction of strong ground motion radiated by earthquakes. We are developing a method of computing radiated energy and acceleration spectrum from direct measurements of teleseismically recorded broadband body waves. From our method, the maximum expectable spectral level of acceleration and lower bounds of stress drops can be made for any event large enough to be teleseismically recorded.

Results

1. Reporting services. The NEIC now uses broadband waveforms to routinely: (1) resolve depths of all earthquakes with $m_b > 5.8$; (2) resolve polarities of depth phases to help constrain first-motion solutions; and (3) present as representative digital waveforms in the monthly PDE's. In the Monthly Listings of the Preliminary Determination of Epicenters covering the interval April 1989-September 1990, depth phases from broadband data were computed for 59 earthquakes; radiated energies were computed for 55 earthquakes.

2. Rupture process of earthquakes. We have modeled the rupture process of three large earthquakes that occurred within an interval of 12 hours at Tennant Creek, Australia, on January 22, 1988, by using broadband data, strong constraints on earthquake location (provided by the Warramunga Array) and observed surface deformation. From the derived complexity of rupture and history of stress release, we conclude that the occurrence of multiple main shocks is not an uncommon mode of rupture in intraplate environments. A study of the Armenian earthquake of 7 December 1988, in collaboration with

the German Geological Survey, has been finished. The earthquake was a complex rupture; from the broadband data we can resolve the source functions of three subevents. From the distribution of aftershocks and the derived focal mechanisms, we infer that the causative faults have different strikes. The relative locations of these subevents indicate a fault zone that has a bend. Source characteristics of the Loma Prieta, California, earthquake of 18 October 1989 are being studied with global digitally recorded broadband data. Besides the static parameters such as focal mechanism and depth, we are deriving the rupture history, radiated energy, and associated stress drops. In addition to modeling displacement and velocity records in the time domain, we are analyzing acceleration in the frequency domain.

3a. Subduction-zone events. We have compiled the log-averaged P-wave acceleration amplitude spectra from teleseismic data for a set of large, shallow-focus subduction-zone earthquakes. The events range in size from the magnitude 6.2 to 8.1. The acceleration spectra, corrected for frequency-dependent attenuation and the modulation of depth phases, are approximately flat from 10 secs to 2-3 seconds, falling off somewhat at high frequencies. The radiated energies of these earthquakes are proportional to the seismic moments, but the high-frequency acceleration levels are more strongly proportional to the asperity areas than the seismic moments of the earthquakes.

3b. Intraplate events. We have applied our algorithm for the computation of acceleration spectra to a series of shallow intraplate earthquakes. Most of these events are characterized by a flat spectral level at high frequencies but an intermediate slope before an ω^2 falloff at low frequencies. The high-frequency spectral levels of these intraplate earthquakes are the same as the levels of subduction-zone earthquakes with the same seismic moments, although the spectral shapes are different.

Reports

Boatwright, J. and Choy, G. L., 1989, Acceleration spectra for subduction zone earthquakes: Journal of Geophysical Research, v. 94, p. 15541-15553.

Choy, G. L., 1990, Global digital data: Interpretation of the earthquake mechanism from broadband data: Proceedings of the PACRIM 90 Congress, Australia (submitted).

Choy, G. L. and J. Boatwright, 1990, Source characteristics of the Loma Prieta, California, earthquake of October 18, 1990 from global digital seismic data: Geophysical Research Letters (submitted).

Choy, G. L., Boatwright, J. and LaVonne, C. K., 1990, Teleseismic estimates of radiated energy from global seismicity of 1986-1988 [abs.]: EOS (American Geophysical Union, Transactions), v. 71, p. 258.

Choy, G. L. and Bowman, J. R., 1990, The rupture process of a multiple main shock sequence--Teleseismic, local and near-field analysis of the Tennant Creek earthquakes of 22 January 1988: Journal of Geophysical Research (in press).

Choy, G. L. and Kind, R., 1990, A preliminary broadband body-wave analysis of the Armenia S.S.R. earthquake of 7 December 1988: Geologisches Jahrbuch (submitted).

Analysis of Natural Seismicity at Anza

9910-03982

Joe Fletcher, Linda Haar, and Larry Baker
Branch of Engineering, Seismology, and Geology
345 Middlefield Road
Menlo Park, CA. 94025
(415) 329-5628

Investigations

The Anza project is based on the analysis of 3-component digital seismograms from an array of ten, short-period, broadband, high-dynamic-range stations distributed around the Anza seismic gap on the San Jacinto fault in southern California. The array has been in existence since 1982 and the data have been used to study such subjects as source scaling, attenuation of high-frequency seismic waves, and shear wave polarization.

Results

Several improvements were made to the array during the reporting period. Upgrades to the field instrumentation and to the data acquisition computer were accomplished this past fall. The RT-24 Data Acquisition Units, upon which the original field system was based, required that the digitizing parameters (*e.g.* sampling rates and gains) be hard-wired at each individual site. Each site, also, had its own clock which ran asynchronously. This has been changed with the substitution of RT-97s for the RT-24s. The RT-97s contain microprocessors. Now, timing and instrument parameters can be set remotely and the data are arranged and telemetered in packets. Along with the increased convenience, the upgrade has eliminated most of the telemetry glitches seen in previously recorded data.

The data acquisition system previously consisted of a DEC PDP 11/34 computer running software written by Larry Baker. The system required a special piece of hardware, called a TIU, which acted as an interface between the microwave telemetry system and the PDP 11/34. This past fall an RT-44 from Refraction Technology, was installed on Toro Peak. This module serves several functions including collating and packetizing the data from all of the field sites and transmitting the data on to San Diego *via* the microwave link. The RT-44 transmits data over the microwave telemetry to another RT-44 in San Diego, which then sends packets of data through a digital interface to a MICROVAX-II. This arrangement eliminated the TIU, which was difficult to maintain. The switch to a MICROVAX-II computer provides compatibilty across several projects all of which use the same computer and software for data acquisition. The MICROVAX II has a much larger address space which allows greater flexibility in building the data acquisition program. Although various aspects of using a virtual memory computer for a real-time application have presented problems, none of these problems have been insurmountable.

The array is generally set at gain levels that would cause the digitizer to clip on local events with magnitudes of 3.5 or larger. Since large events are not common in the gap, this is usually not a problem. However, since early December 1989, seismicity has increased dramatically and several magnitude 4+ events have occurred. Although there are several SMA-1 accelerographs in the area, few of these are co-located with Anza stations. To provide on-scale recordings for these larger events, we installed GEOS digital event recorders equipped with force-balance accelerometers at five sites (KNW, PFO, BZN, WMC, and CRY). Since their installation, a magnitude 4.1 event and a magnitude 3.2 event (both on February 18, 1990) have been recorded by the GEOS. Figure 1 shows a plot of the acceleration records obtained for the M 4.1 event.

Reports

none this reporting period.

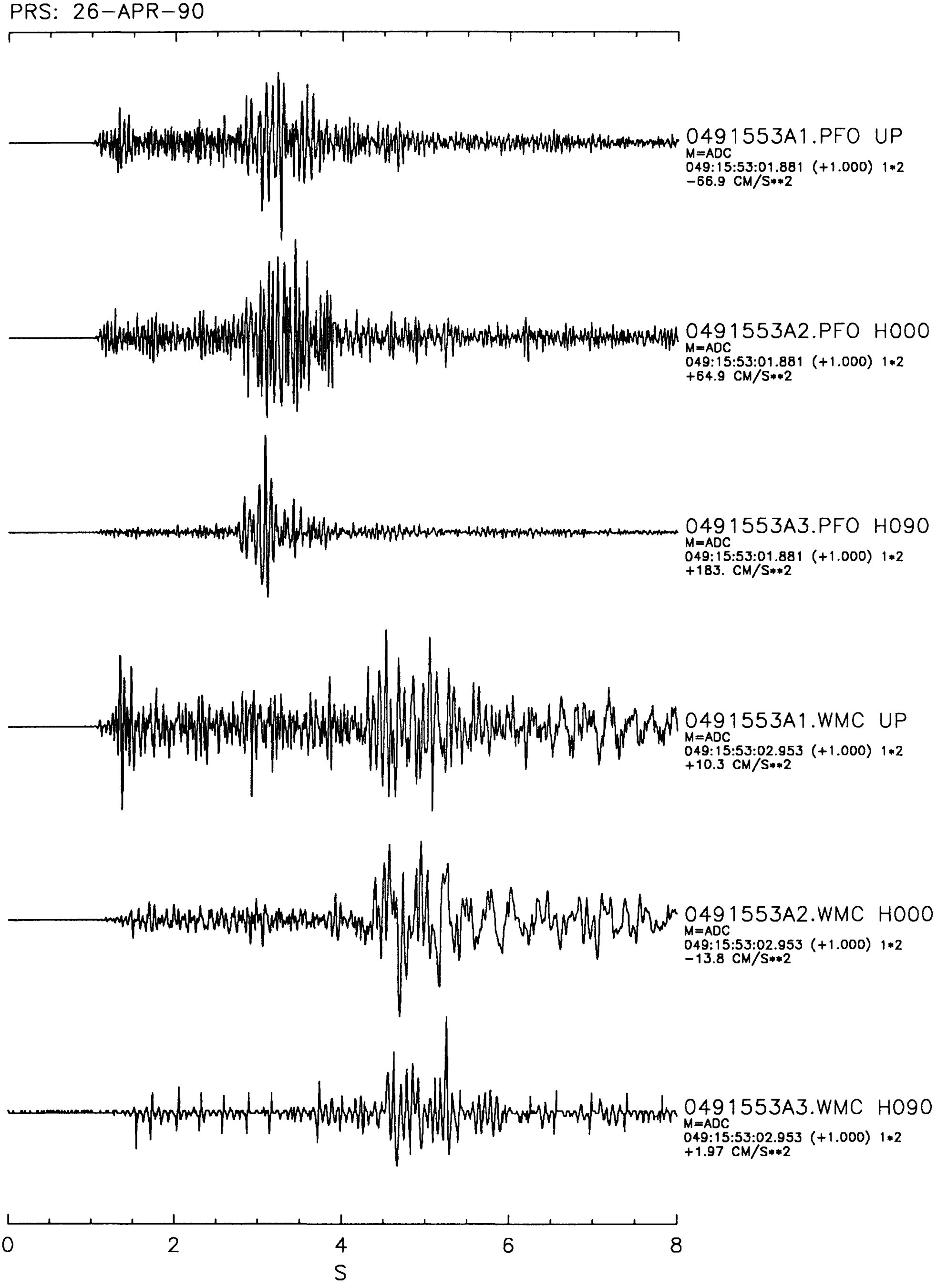
PRS: 26-APR-90
0491553A1.PFO UP
M=ADC
049:15:53:01.881 (+1.000) 1*2
-66.9 CM/S**2
0491553A2.PFO H000
M=ADC
049:15:53:01.881 (+1.000) 1*2
+64.9 CM/S**2
0491553A3.PFO H090
M=ADC
049:15:53:01.881 (+1.000) 1*2
+183. CM/S**2
0491553A1.WMC UP
M=ADC
049:15:53:02.953 (+1.000) 1*2
+10.3 CM/S**2
0491553A2.WMC H000
M=ADC
049:15:53:02.953 (+1.000) 1*2
-13.8 CM/S**2
0491553A3.WMC H090
M=ADC
049:15:53:02.953 (+1.000) 1*2
+1.97 CM/S**2
0
2
4
6
8
S

Figure 1

Southern California Earthquake Project

90-9930-01174

Thomas H. Heaton
Branch of Seismology
U.S. Geological Survey
525 S. Wilson Ave.
Pasadena, CA, 91106
FAX: 818-405-7827

Introduction

This project covers almost all of the activities of the Pasadena Office of the U.S. Geological Survey. This is a large and complex project that includes the operation of the 250-station Southern California Seismic Network (SCSN), response to major southern California earthquake sequences, and basic research in earthquake physics.

Investigations

1. Operation, maintenance, development and recording of the Southern California Seismic Network consisting of 220 U.S.G.S. telemetered seismometers and 66 seismometers telemetered from other agencies. All stations are recorded on the CUSP digital analysis system.

2. Routine Processing of Southern California Network Data. Routine processing of seismic data from stations of the cooperative southern California seismic network was continued for the period October 1989 through March 1990 in cooperation with scientists and staff from Caltech. Routine analysis includes interactive timing of phases, location of hypocenters, calculation of magnitudes and preparation of the final catalog using the CUSP analysis system. About 800 events were detected in most months with a regional magnitude completeness level of 1.8. The largest earthquake this recording period was the M_L=5.2 earthquake of February 28, 1990 near Upland in the San Gabriel Valley east of Los Angeles.

3. Development and testing of an automated real-time earthquake location capability that is fast, reliable, uses data from all network stations and is not dependent on exotic hardware.

4. Seismotectonics of Southern California. In 1985, a well recorded earthquake of M_L4.0 occurred at a depth of 30 km beneath the Ventura basin in the western Transverse Ranges. This earthquake was far deeper than any previously determined reliable earthquake depth in southern California. Subsequent analysis has shown that many microearthquakes have been recorded under the Ventura basin in the last two decades at depths between 20 and 30 km. Other analyses have shown that the Ventura basin is characterized by the lowest heat flow, deepest Quaternary sediments and one of the fastest rates of movement (as shown by geodetics) in California. We have ana-

lyzed the deep earthquakes under the Ventura basin to determine the cause of the deep events and their relation to the other anomalous phenomena in the Ventura basin.

5. Prediction Probabilities from Foreshocks. When any earthquake occurs, the possibility that it might be a foreshock increases the probability that a larger earthquake will occur at the same site within the next few days. It is intuitively obvious that the probability of a very large earthquake should be higher if the potential foreshock were to occur on or near a fault capable of producing that very large mainshock, especially if the fault is towards the end of its seismic cycle or if the background rate of seismic activity is particularly low. In this study, the probability of a major earthquake characteristic to a particular fault, given the occurrence of a potential foreshock near to that fault is analytically derived from basic tenets of probability theory.

6. Study of multiple P waves in the Imperial Valley. Continuing work was done on the multiple free-surface reflection of P waves which were observed in aftershock data of the 1987 Elmore Ranch and Superstition Hills earthquakes. Event record sections were formed from 39 aftershocks of the Elmore Ranch event and 29 aftershocks of the Superstition Hills event. These data were compared to synthetics calculated using flat-layered structures, to estimate the velocity gradient of the upper 5 km and the source depth of the aftershocks.

7. Teleseismic data recorded on the network. Record sections were constructed for teleseismic P waves which triggered the network.

8. Network recordings of sonic booms. We have examined the seismograms of the shock wave produced by the space shuttle as it passes over the Los Angeles area. We have estimated the direction and amplitude of the pressure wave produced by several supersonic sources.

9. Investigate the physics of the earthquake rupture process through the modeling of seismic waveforms.

Results

1. Operation and maintenance of field stations and recording systems continued with little failure during this reporting period. Time varying attributes of the system are completely recorded on a data base (DBASE III). Documentation of the system and changes to the system continued to be developed by the preparation of semi-annual network bulletins.

2. Routine Processing of Southern California Network Data. The projects to upgrade the southern California seismic network are continuing. To increase the accessibility and research potential of the seismic data, a series of semi-annual Network Bulletins have been issued since 1985. These bulletins pro-

vide information about how to access data from the network, problems with the data, details of the processing computer systems, and earthquakes in southern California. As part of this project, documentation of past and present station configurations has been compiled. Reconfiguration of station electronics to maximize the dynamic range and frequency response of the stations is continuing. The average dynamic range of most of the short period vertical seismometer stations in the network is now 40-50 dB. The gains on the stations are now staggered (some very high. others quite low) to maximize the overall dynamic range of the network. At the lowest gains, 7 force balance accelerometers are now being telemetered and digitized within the short period network. We have also completed installation of a system to digitize continuous FM-tape recordings of the network data. This system allows for the analysis of waveform data for times that were not contained in the normal online triggering process (e.g. teleseisms).

3. Development of Real-Time Analysis Systems. A software program (PICKLE) has been developed that runs in parallel with the existing online data aquisition system on a DEC MicroVAX computer. PICKLE was tested during the aftershock sequence of the M_L 5.2 Upland earthquake of 28 February 1990. During the two-week test, it picked and located 983 events. We have also installed a new MicroVAX 3200 online analysis system to phase out an obsolete PDP 11/34.

4. Seismotectonics of Southern California. Earthquakes at depths of 20-30 km occur beneath the Ventura Basin in southern California. The epicentral distribution of deep seismicity outlines an east-trending ellipse which corresponds closely with the mapped Santa Clara Syncline, the main structural element of the Ventura basin with 12 km thickness of sediments. Clear Pn and Pg phases are seen for even the deepest earthquakes which demonstrate that these earthquakes are occurring within the crust. Travel time curves from shallow and deep earthquakes in the western Transverse Ranges require that the depth to the Moho under the Ventura basin must be depressed by 5-7 km relative to the surrounding area. Other researchers have shown that the Ventura basin also has the lowest heat flow in California. Thus low heat flow, very deep (12 km) sediments, the deep earthquakes, and a depressed Moho all coincide within a small area, strongly suggesting a common cause for all four phenomena in the rapid shortening of the Ventura basin. The confinement of the deep earthquakes and depressed Moho to just the Ventura region suggests that the very rapid shortening of the Ventura basin is not representative of the rate of shortening across all of the western Transverse Ranges.

5. Prediction Probabilities from Foreshocks In this study, the probability of a major earthquake characteristic to a particular fault, given the occurrence of a potential foreshock near to that fault is analytically derived from basic tenets of probability theory. The data needed to compute this probabil-

ity are 1) the rate of background activity on that fault, 2) the long term probability of a large earthquake occurring on that fault, and 3) the rate at which foreshocks precede the large earthquakes. We compute the probability with an expression that includes the parameters of time, magnitude and spatial location. We assume that foreshocks to San Andreas earthquakes will follow the average properties of foreshocks to moderate earthquakes in California. We thus assume that 1) the rate of mainshock occurrence after foreshocks decays rapidly with a 1/t type behavior and that most immediate foreshocks occur within three days of their mainshock, 2) that foreshocks and mainshocks occur within 10 km of each other, and 3) that the percentage of mainshocks preceded by foreshocks increases linearly as the magnitude threshold for foreshocks decreases, with 50% of the mainshocks preceded by foreshocks with magnitudes within 3 units of the mainshock's magnitude within 3 days. This derivation is applied to the San Andreas, Hayward, San Jacinto and Imperial faults. We assume that at the scale at which we are examining the faults, all sections of the fault are equally likely to contain the epicenter of the mainshock (and thus the foreshocks). We use the long-term probabilities of a large earthquake from the Working Group on California Earthquake Probabilities (1988). The short-term probability that a M5.0 earthquake on the San Andreas fault will be followed by a large earthquake within 3 days ranges from a low of 0.2% from Point Arena to Cape Mendocino to a high of 24% in the Carrizo Plain (Figure). By comparison, the probability that any M5 in California will be followed by a M7.5 within 3 days is 0.08%. The rate of background activity along the major faults varies more than the long term probabilities and thus leads to greater variations in the short term probabilities.

6. Comparison of the synthetic seismograms with the data indicated that a linear velocity gradient with a surface velocity of 1.8 km/sec increasing to 5.8 km/sec at 5.5 km depth, could adequately model the arrival times of the multiple P waves. Using this velocity structure, the amplitudes of the arrivals were used to estimate source depths for the aftershocks. For both the Elmore Ranch and Superstition Hills aftershocks, the depth distribution were similar and ranged from about 5 to 10 km.

7. Plots of the teleseismic P waves recorded on 50-150 stations show coherent first arrivals and in some instances clear later arrivals, such as upper mantle triplications and PcP. Fig. 1 shows a record section formed by combining 4 events from Mexico with distances to the network stations that range from 15 to 30 degrees. Upper mantle triplications due to the 450 and 670 km discontinuities can be seen, with cross over points near 17 and 23 degrees, respectively. These data are being used to study upper mantle velocity structure.

8. A program was written to use shock wave arrival time data to estimate speed, direction and height of supersonic sonic

sources as they pass over the network. The program was used to determine the flight path of several space shuttle landings and the final SR-71 flight. The amplitude of the shock wave was used to estimate the air pressure at the recording site (about 0.7 to 2.2 millibars for a recent space shuttle landing).

9. Simultaneous and instantaneous changes in effective stress on a finite fault are shown to produce far-field body waves that have high-frequency spectral decays that depend upon the assumed geometry of the rupture surface and the location of the observer. For most assumed rupture geometries and physically plausible slip distributions, high frequency spectral decays are faster than inverse omega cubed. Brune (1970, JGR, 4997-5009) concluded that this class of rupture models should produce far-field high-frequency spectral decays proportional to the effective stress times inverse omega-squared, where effective stress is that stress that drives the inertia of the opposite sides of a fault. Therefore, it is incorrect to estimate effective stress from the level of high-frequency waves radiated during earthquakes.

Publications

Frankel, A., A. McGarr, J. Bicknell, J. Mori, L. Seeber, E. Cranswick, Attenuation of high-frequency shear waves in the crust: Measurements from New York State, South Africa and Southern California, submitted to J. Geophys. Res.

Heaton, T.H., 1990, Where does the inverse omega-squared come from in the Brune model?, submitted to Bull. Seism. Soc. Am.

Jones, L. M., K. E. Sieh, E. Hauksson, and L. K. Hutton, 1990, The December 3, 1988 Pasadena, California earthquake: Evidence for strike-slip motion on the Raymond fault, Bull. Seismol. Soc. Amer., 80, 474-482 Kanamori, H., J. Mori, T. Heaton, 1990, The 3 December 1988, Pasadena earthquake (M_L 4.9) recorded with the very broadband system in Pasadena, Bull. Seismol. Soc. Am., 80, P. 483-487.

Mori, J. and A. Frankel, 1990, Source Parameters for small events associated with the 1986 North Palm Springs, California earthquake determined using empirical Green functions, Bull. Seismol. Soc. Am., 80, p. 278-295.

Mori, J. and S. Hartzell, 1990, Source inversion of the 1988 Upland, California earthquake: Determination of a fault plane for a small event, Bull. Seismol. Soc. Am. (in press).

Mori, J., Estimates of velocity structure and source depth using multiple P wave from aftershocks of the 1987 Elmore Ranch and Superstition Hills, California, earthquakes (submitted for internal review).

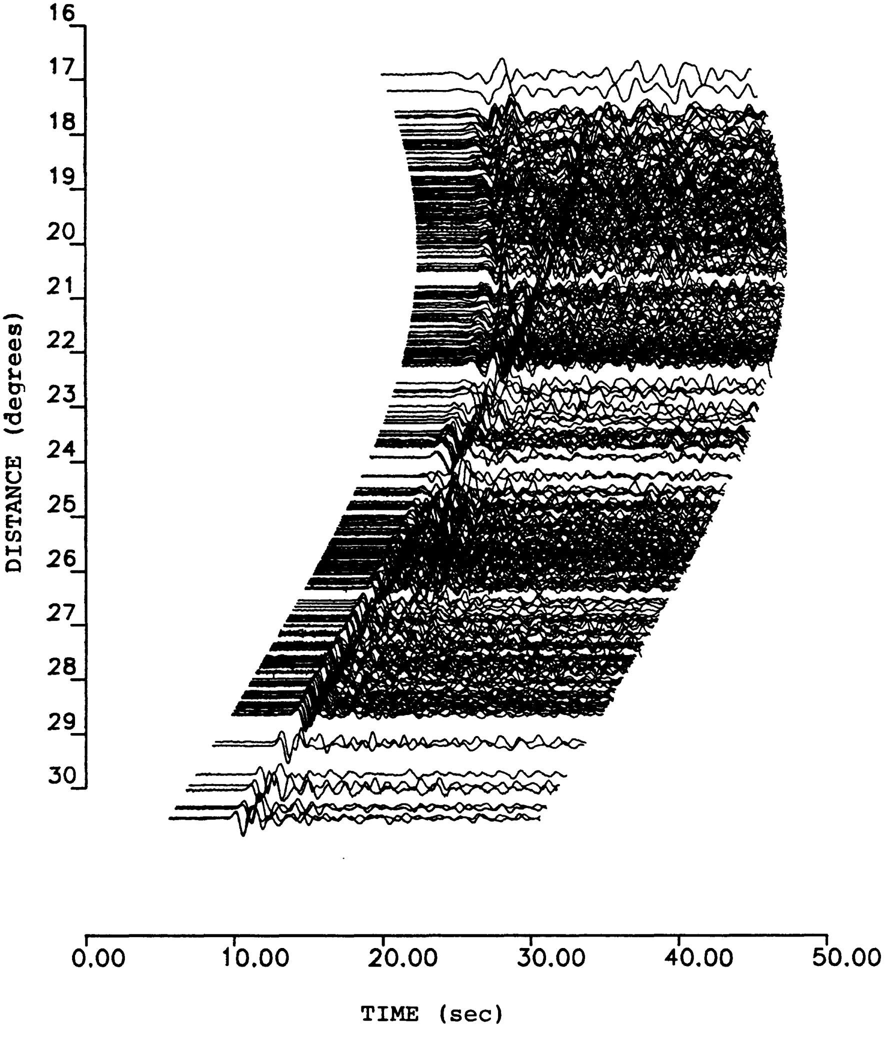

Figure 1. Record section formed by combining P-wave arrivals from 4 events in Mexico as recorded on the Southern California Seismic Network. The traces were initially lined up on the P wave arrival and then offset assuming a Herrin velocity structure. Note the triplications, caused by the 450 and 670 km upper mantle discontinuities, which have cross over points near 17 and 23 degrees, respectively.

Instrument Development and Quality Control

9930-01726

E. Gray Jensen
Branch of Seismology
U.S. Geological Survey
345 Middlefield Road - Mail Stop 977
Menlo Park, California 94025
(415) 329-4729

Investigations

This project supports other projects in the Office of Earthquakes, Volcanoes and Engineering by designing and developing new instrumentation and by evaluating and improving existing equipment in order to maintain high quality in the data acquired by the Office. Tasks undertaken during this period include activities related to the Loma Prieta earthquake (including an development of an aftershock alarm), modification of the SGR system and development of a new blaster and master clock combination, among other things.

Results

The Loma Prieta earthquake in October occupied much of our time early in this period. On the night of the 17th, project personnel maintained the continued operation of the main emergency generator which supplies power to all critical data acquisition operations. Additional power units and cabling were setup to permit use of lights, analysis computers, etc. For the following two weeks, technical personnel were on-site 24 hours daily to ensure prompt response to unforeseen problems.

During this time a new earthquake alarm system was developed in response to the need for early warning of aftershocks at such places as the I-880 Cypress structure. This unit was a variation of the multi-channel earthquake alarm developed previously for in-office use. For this version three low-gain seismic stations were installed at different locations in the epicentral region. These seismic signals were radioed directly to the Menlo Park office where a trigger circuit would trip if a signal amplitude equivalent to a magnitude 3.7 event in the epicentral region was detected on two or more sensors. The alarm output radioed a code via a mountaintop repeater to any of several receivers located in the Bay Area. The receivers emitted an audible alarm upon receiving the code. The receivers displayed a green light whenever they were in radio contact with the alarm system. This system provided about a 10 second (P-wave) or 20 second (S-wave) advance warning of Loma Prieta aftershocks greater than M3.7 to CalTrans operations in the I-880 Cypress area.

Microprocessor program code changes were made in the Seismic Group Recorder (SGR) timer boards and transfer clock units to implement improvements in operation. Changes were also made to the laptop computer software used to control the SGR's. The SGR's were used in Kenya in January and February as part of a multi-national cooperative refraction experiment (KRISP). This appears to have been quite successful although much of the data has yet to be processed.

A new blaster for firing explosives in refraction experiments was developed. Previously, blasting required a separate blaster, a master clock, a chart recorder and an interface unit. Eventually, this new device will incorporate all these elements in one case. Eight units with the new solid-state blaster circuitry have been built so far. These were used in the KRISP experiment in Kenya. Development of a new master clock based on the circuitry used in the SGR timer and an associated chart recorder is continuing.

A digital seismic station using a Nanometrics RD-3 digitizer was installed at Monument Peak in February. This station is telemetered using 9600 baud modems over the microwave system. The 3-component, 5 sample per second, 14-bit data is collected by a PC-AT compatible computer in Menlo Park. The signal is gain-ranged yielding a dynamic range as high as 124 dB. This is an experimental station and investigation into digitizer, radio and data receiver options is continuing.

Reports

Bakun, W. H., Fischer, F. W., Jensen, E. G., and Van Schaack, J., 1989, An early warning alert system for aftershocks, AGU , San Francisco, CA, December 1989.

State of Stress in the Rupture Zone of Large Earthquakes

Grant No. 14-08-0001-G1773

Hiroo Kanamori
Seismological Laboratory, California Institute of Technology
Pasadena, California 91125 (818) 356-6914

Investigations

1. Fault Parameters and Tsunami Excitation of the May 23, 1989 Macquarie Ridge Earthquake, Kenji Satake and Hiroo Kanamori.
2. Focal Mechanisms of the Spitak (Armenia) Earthquake of Dec. 7, 1988 Determined from Teleseismic Records, K. Satake, H. Kanamori, H. Kawakatsu and M. Kikuchi.

Results

1. Fault Parameters and Tsunami Excitation of the May 23, 1989 Macquarie Ridge Earthquake.

The Macquaire Ridge earthquake of May 23, 1989 is one of the largest events in the last decade. Furthermore, it is the largest strike-slip earthquake ever recorded instrumentally. We analyzed long-period surface waves and body waves recorded at global network (GDSN, IRIS, GEOSCOPE and IDA) to estimate the fault parameters and computed tsunamis from the estimated parameters. The Centroid Moment Tensor (CMT) solution from surface waves shows that the mechanism is almost pure strike-slip with one of the nodel planes parallel to the strike of the Macquarie Ridge. The seismic moment is 1.6×10^{21} Nm ($\times 10^{28}$ dyn·cm) and the corresponding moment magnitude is $M_W = 8.1$. Teleseismic P and S waves from 10 stations with good azimuthal coverage are used to model the temporal and spatial distribution of the subevents. Four subevents are located sequentially from south to north along the ridge system in about 30 sec. All of them have a mechanism similar to the CMT solution. The fault length is estimated to be about 120 km from the subevent and the aftershock distributions. The rupture propagates from south to north at a relatively high speed. The average slip on the fault depends on the estimate of the fault width, but it is probably in a range of 9 to 27 m. A large strike-slip earthquake like this event produces significant vertical displacements on the ocean bottom and excites tsunamis. Computation of tsunamis using the estimated fault parameters predicts that small tsunamis are expected at Australia and New Zealand. In fact, small tsunamis were observed at the southern coast of Australia.

2. Focal Mechanisms of the Spitak (Armenia) Earthquake of Dec. 7, 1988 Determined from Teleseismic Records

We determined the focal mechanism of the Spitak (Armenia) earthquake of December 7, 1988 using teleseismic surface and body waves. Time-domain Centroid Moment Tensor (CMT) inversion was made using long-period surface waves recorded at eight stations. Only those seismograms recorded by the Streckeisen (STS) seismometer were used because of their good signal-to-noise ratio at long period. The CMT solution gives T-axis of 1.2×10^{26} dyne·cm (pl 66°, az 240°), N-axis of 0.7×10^{26} dyne·cm (pl

21^o, az 90^o) and P-axis of 1.9×10^{26} dyne·cm (pl 11^o, az 356^o). Inversion of spectral data of Rayleigh and Love waves over a period range from 150 to 300 sec yielded an almost identical solution. This solution has a large non-double couple (non-DC) component (minor DC/major DC - 36%) and suggests complex faulting. The double couple soloution indicates a dip-slip fault striking roughly in an E-W direction. Body waves from this event show very complex waveforms. We used a revised version of multiple deconvolution technique by Kikuchi and Kanamori to obtain three major subevents with different mechanisms. The first two subevents are predominantely dip-slip type. The largest subevent occurred about 40 sec after the first one with strike-slip mechanism. This temporal change in mechanism causes an apparent large non-DC component in the CMT solution. The composite moment tensor obtained by tensorial summation of the sub-events is similar to the CMT solution and also has a large non-DC component.

Publications

Satake, K. and H. Kanamori, Fault Parameters and Tsunami Excitation of the May 23, 1989 Macquarie Ridge Earthquake, submitted to Geophys. Res. Lett. January, 1990.

Satake, K., H. Kanamori, H. Kawakatsu, and M. Kikuchi, Focal Mechanisms of the Spitak (Armenia) Earthquake of Dec. 7, 1988 Determined from Teleseismic Records, American Geophysical Union, Fall Meeting, San Francisco, California, December 4-8, 1989.

Kanamori, H. and D. V. Helmberger, Semi-Realtime Study of the 1989 Loma Prieta Earthquake Using Teleseismic and Regional Data, Special Session, American Geophysical Union, Fall Meeting, San Francisco, California, December 4-8, 1989.

FAULT MECHANICS AND CHEMISTRY

9960–01485

C.–Y. King
Branch of Tectonophysics
U.S. Geological Survey
345 Middlefield Road, MS/977
Menlo Park, California 94025
(415) 329-4838

Investigations

[1] Water temperature and radon content were continuously monitored at two water wells in Parkfield, California.

[2] Water level was continuously recorded at six other wells in central California.

[3] Water temperature and electric conductivity were periodically measured, and water samples were taken from most of these wells and two springs in San Jose for chemical analysis.

[4] Cumulative slip distribution for a long sequence of slip events along a laboratory fault is studied.

Results

[1] Geochemical Data Along Hayward Fault

Figures 1–4 show geochemical data measured at the four monitoring sites along the Hayward fault up to March 1990. The *in situ* data of temperature and conductivity beginning in the last quarter of 1989 are subject to larger experimental error due to instrumental problems and change of field persons. The anomalous increases of conductivity and sodium concentration at the Chabot well that began shortly before the 3 April 1989 earthquake of magnitude 4.9 about 55 km away persisted, and this finding is supported by the results of further analyses of the water samples for concentrations of calcium, magnesium, and potassium (Figures 5 and 6). However, an apparent conductivity increase that preceeded the October 17 Loma Prieta earthquake is not confirmed by the corresponding result of water–sample analyses, and it appears to be spurious. The Loma Prieta earthquake may have been followed by increases of flow rate at the two springs in the Alum Rock Park in San Jose, but the measurements were not made soon enough to catch the maximum rates. Other post–earthquake changes at the springs may possibly be spurious.

[2] Radon Data in Parkfield

Figure 7 shows radon concentrations with daily calibration pulses, temperature, water–flow rate through the instrument, and barometric pressure recorded at the Taylor well since the beginning of monitoring. The radon concentration is not significantly affected by the fluctuation in the flow rate (within allowance of instrumental design), except at times of power failures which interrupted water supply. The radon value shows a seasonal variation possibly as a result of variation in water degassing rate in the instrument caused by seasonal temperature and barometric–pressure changes.

Reports

King, C.–Y., 1989, Volume predictability of historical eruptions at Kilauea and Mauna Loa volcanoes, *Journal of Volcanology and Geothermal Research*, v. 38, p. 281–285.

King, C.–Y., Earthquake–prediction techniques, *Encyclopedia of Earth System Science*, Academic Press, Inc. (in press).

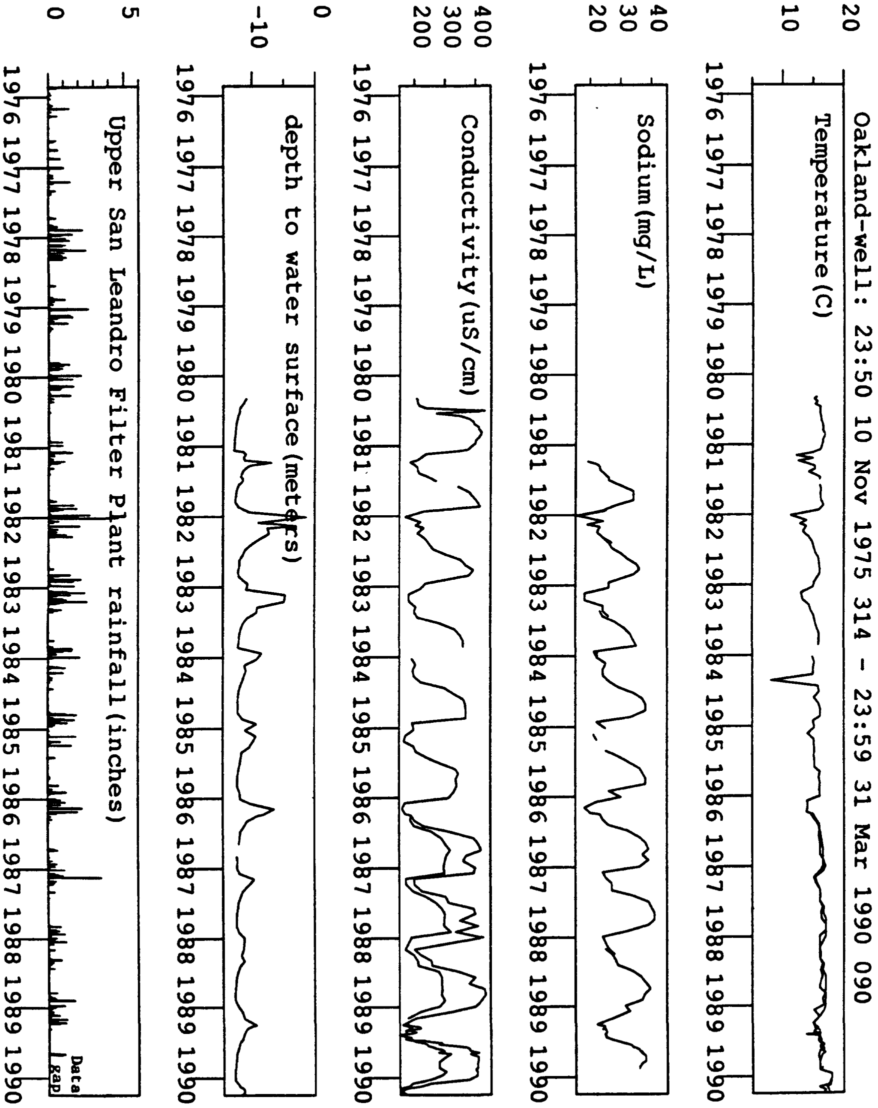
Oakland-well: 23:50 10 Nov 1975 314 - 23:59 31 Mar 1990 090
Temperature (C)
20
10
Sodium (mg/L)
40
30
20
Conductivity (uS/cm)
400
300
200
depth to water surface (meters)
0
-10
Upper San Leandro Filter Plant rainfall (inches)
5
0
Data gap
1976 1977 1978 1979 1980 1981 1982 1983 1984 1985 1986 1987 1988 1989 1990

FIGURE 1

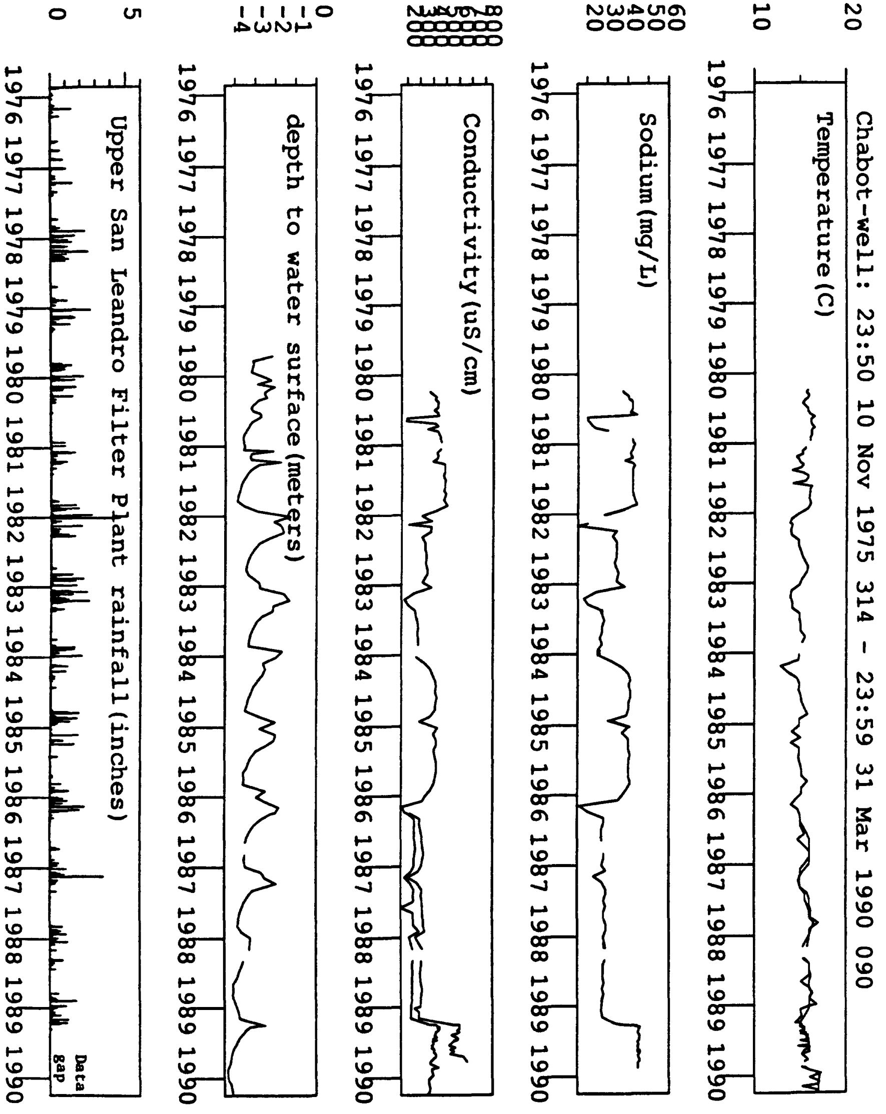
Chabot-well: 23:50 10 Nov 1975 314 - 23:59 31 Mar 1990 090
Temperature (C)
20
10
Sodium (mg/L)
60
50
40
30
20
Conductivity (uS/cm)
800
700
600
500
400
300
200
depth to water surface (meters)
0
-1
-2
-3
-4
Upper San Leandro Filter Plant rainfall (inches)
5
0
Data gap
1976 1977 1978 1979 1980 1981 1982 1983 1984 1985 1986 1987 1988 1989 1990

FIGURE 2

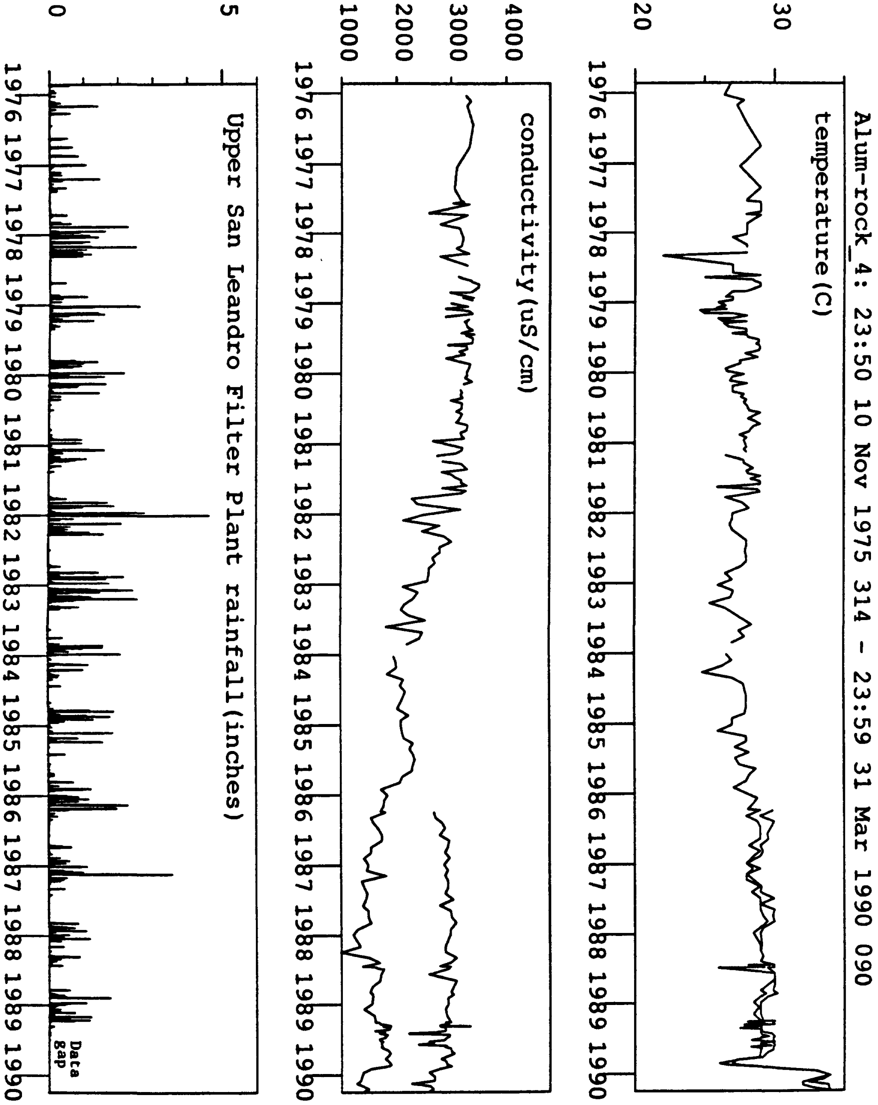
Alum-rock_4: 23:50 10 Nov 1975 314 - 23:59 31 Mar 1990 090
temperature(C)
20
30
conductivity(uS/cm)
1000
2000
3000
4000
Upper San Leandro Filter Plant rainfall(inches)
0
5
Data gap
1976 1977 1978 1979 1980 1981 1982 1983 1984 1985 1986 1987 1988 1989 1990

FIGURE 3

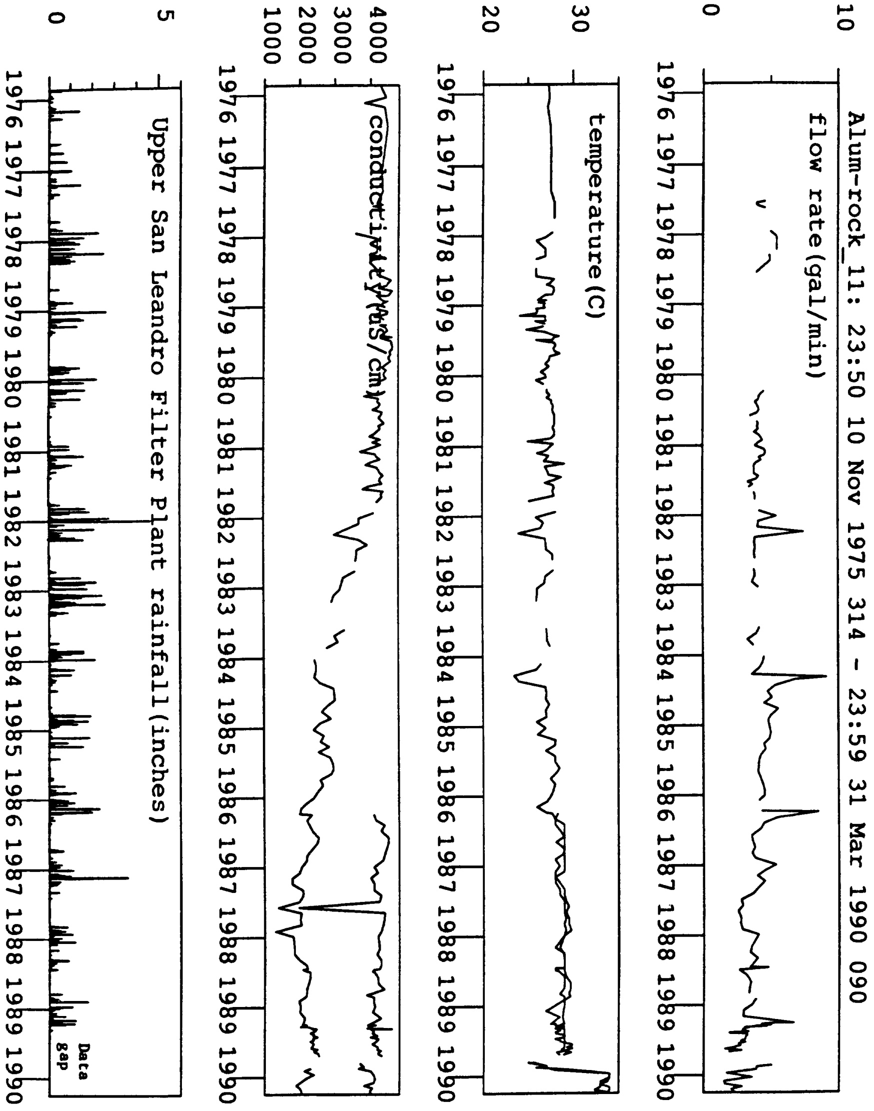
Alum-rock_11: 23:50 10 Nov 1975 314 - 23:59 31 Mar 1990 090
flow rate(gal/min)
10
0
temperature(C)
30
20
conductivity(uS/cm)
4000
3000
2000
1000
Upper San Leandro Filter Plant rainfall(inches)
5
0
1976 1977 1978 1979 1980 1981 1982 1983 1984 1985 1986 1987 1988 1989 1990
Data gap

FIGURE 4

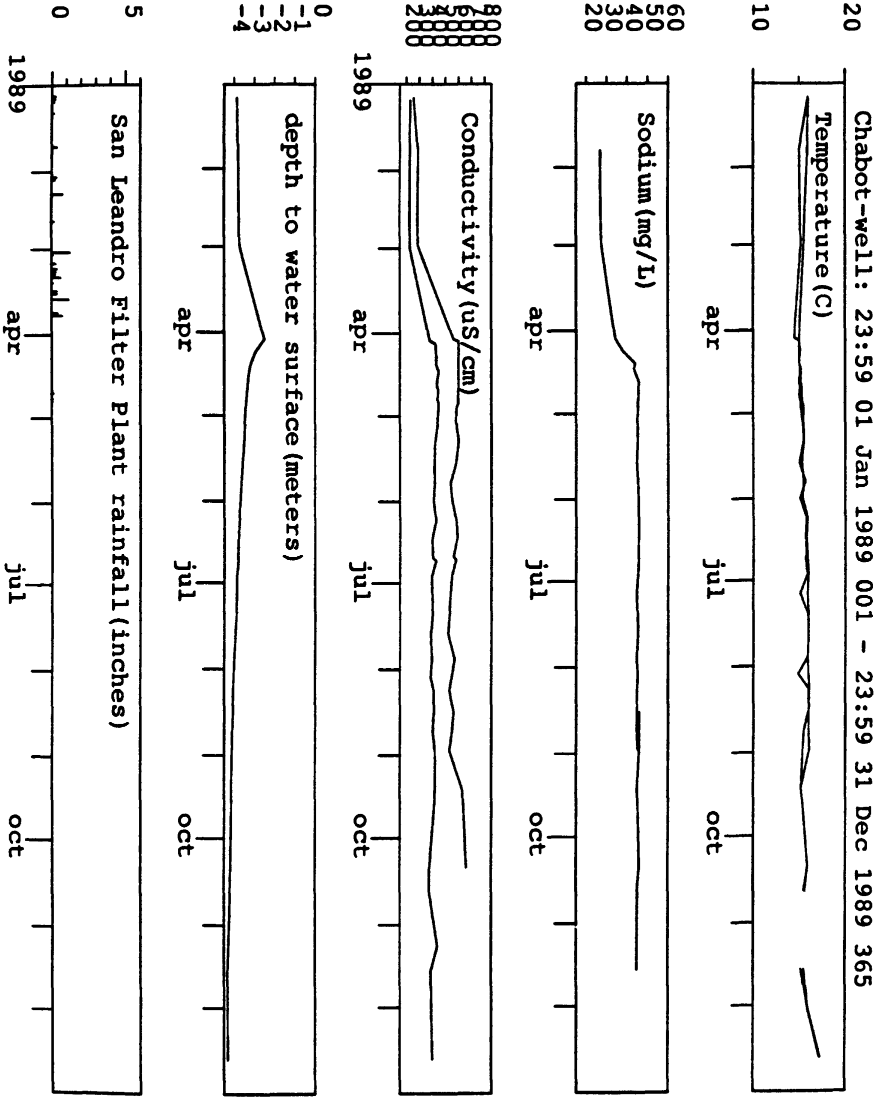
Chabot-well: 23:59 01 Jan 1989 001 - 23:59 31 Dec 1989 365
Temperature (C)
20
10
Sodium (mg/L)
60
50
40
30
20
Conductivity (uS/cm)
800
700
600
500
400
300
200
depth to water surface (meters)
0
-1
-2
-3
-4
San Leandro Filter Plant rainfall (inches)
5
0
1989
apr
jul
oct

FIGURE 5

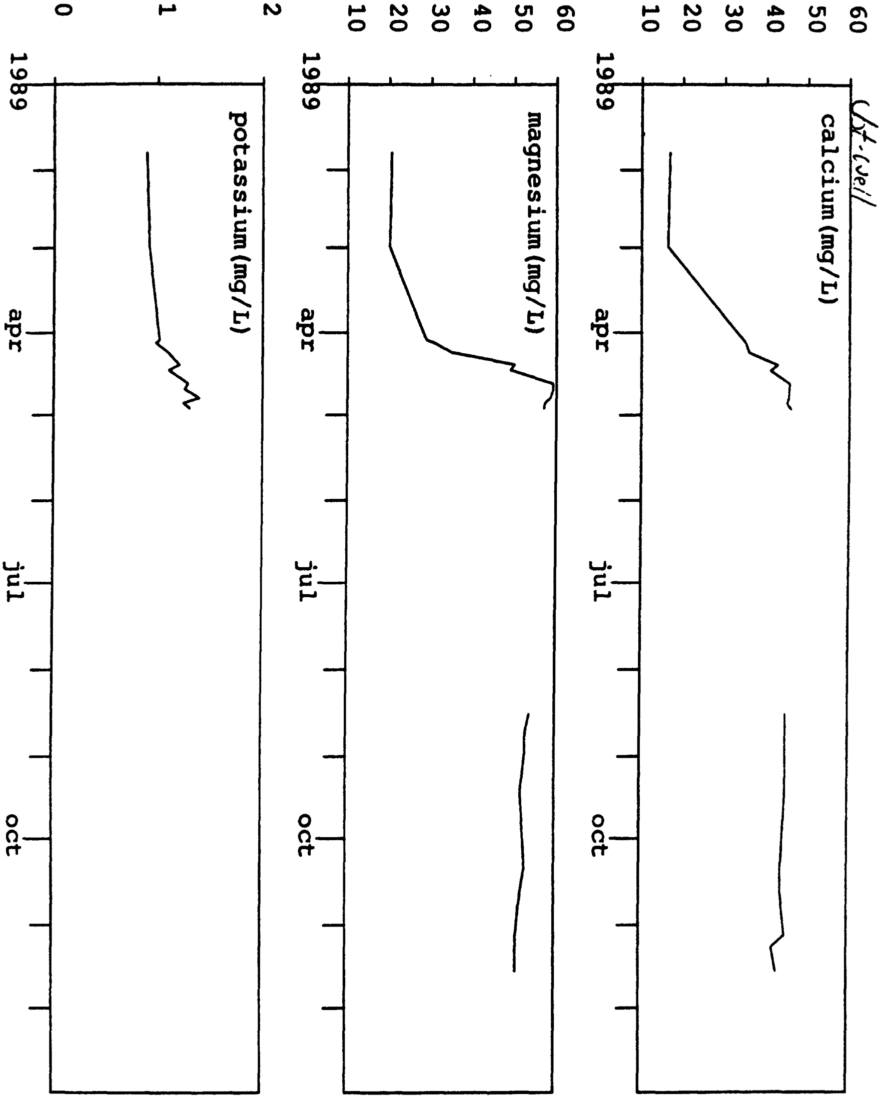
Wet-well
calcium (mg/L)
60
50
40
30
20
10
1989
apr
jul
oct
magnesium (mg/L)
60
50
40
30
20
10
1989
apr
jul
oct
potassium (mg/L)
2
1
0
1989
apr
jul
oct

FIGURE 6

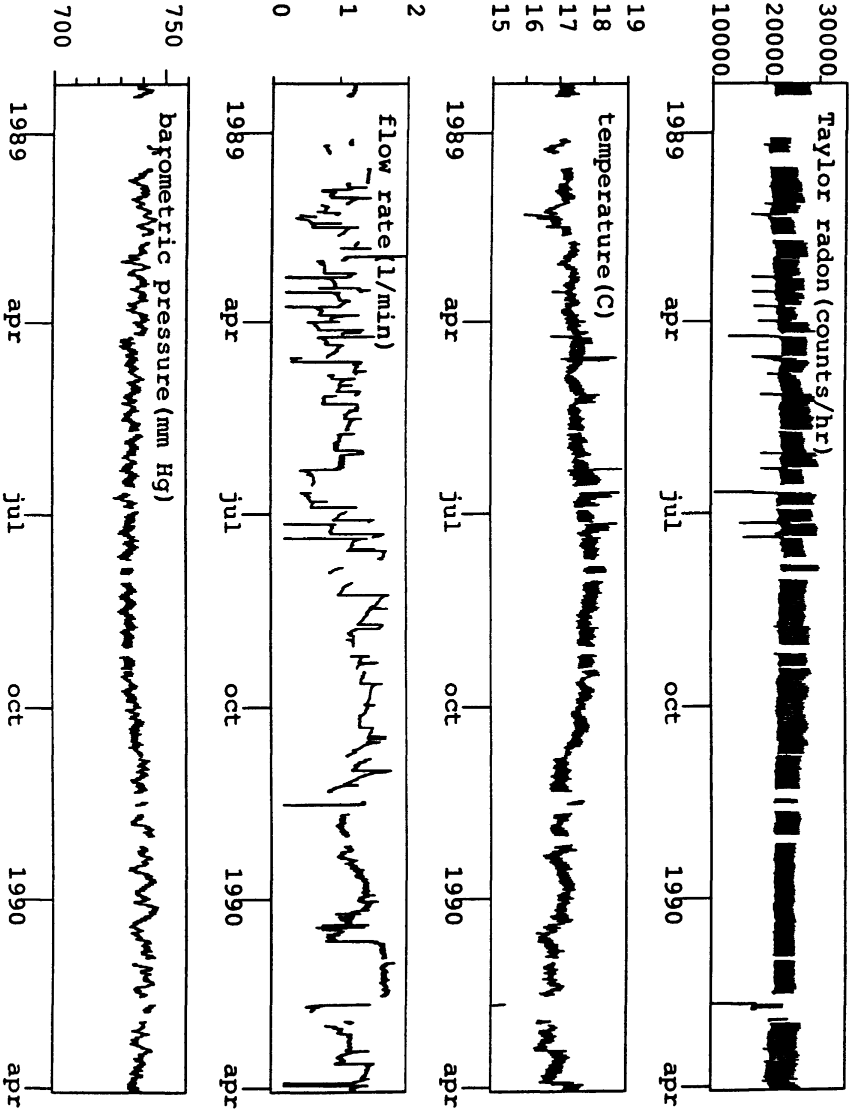
Taylor radon (counts/hr)
30000
20000
10000
temperature (C)
19
18
17
16
15
flow rate (l/min)
2
1
0
barometric pressure (mm Hg)
750
700
1989
apr
jul
oct
1990
apr

FIGURE 7

Operation of Borehole Tiltmeters at Pinon Flat Observatory, California and Analysis of Secular and Tidal Tilt

14-08-0001-G1765

Judah Levine
Joint Institute for Laboratory Astrophysics
Campus Box 440
University of Colorado
Boulder, Colorado 80309
(303) 492 - 7785

Objectives: To install borehole tiltmeters at Pinon Flat Observatory in Southern California; to compare the performance our instruments installed at three different depths; to analyze the data at secular and tidal periods; and to compare our results with those obtained from other instruments at the same site.

Results: We completed the installation of a third instrument in a borehole that is approximately 122 m deep. The installation was somewhat more difficult that expected because we first had to remove an accumulation of rust and metal chips from the bottom of the borehole. The new instrument uses a new alignment system. The azimuth of the instrument is fixed by two steel pins near that bottom of the casing that mate with two wedge-shaped slots attached to the tiltmeter capsule. The slots are tapered in such a way that the instrument is automatically rotated to the proper azimuth as it is lowered. The azimuth of the pins was determined using a rented gyro-compass that was mounted on a well-logging tool.

Although the newest instrument (named BOC) is somewhat noisier than its shallower cousins, we have found good agreement between it and the shallowest tiltmeter (which is installed at a depth of about 25 m and is named BOA). The discrepancy that we had previously found between BOA and BOB is thus peculiar to the intermediate depth at which BOB is installed (about 36 m). We have been able to model this discrepancy as a tilt-strain coupling effect. These very recent results were presented as a poster paper at the recent workshop in Moro Bay, California. Our conclusions so far are phenomenological -- we do not know if the coupling is a result of the change in the hydrostatic pore pressure below the water table that accompanies the strain tide cycle (and which has been observed as coherent changes in the heights of nearby wells) or whether some other strain-driven effect is responsible. We are continuing our study of this question.

We are also studying the usefulness of phenomenological models in explaining tilt fluctuations at intermediate periods ranging from a few hours to a few days. Our goal is to see by how much the sensitivity of existing instruments can be improved at intermediate-period using real-time adaptive digital processing.

We find significant coherence at these periods between barometric pressure and tilt, for example, although the admittances vary somewhat with time. We attribute this variation to changes in the wave-number spectrum of the barometric pressure. These changes would interact with the local topography to produce an apparent change in an admittance that was derived from only a single nearby barometer. Using an admittance to barometric pressure that changes slowly with time, we have had significant success in reducing the variance in the data recorded at other sites, and we are continuing this work using the data from PFO.

Summary of Data Collected: We acquire the data from our three instruments at PFO (2 channels/instrument) every 6 minutes. These same values are also transmitted to the PFO central recording trailer and are digitized and recorded there 12 times/hour.

CRUSTAL STRAIN

9960-01187

M. Lisowski, J.C. Savage, W.H. Prescott
Branch of Tectonophysics
U.S. Geological Survey
345 Middlefield Road, MS/977
Menlo Park, California 94025
(415) 329-4860

INVESTIGATIONS

The principal subject of investigation was the analysis of deformation in a number of tectonically active areas in the United States.

RESULTS

1. A Possible Geodetic Anomaly Observed Prior to the Loma Prieta Earthquake.

Monthly measurements since mid–1981 of distance from a geodetic station located 11 km from the epicenter of the Loma Prieta earthquake (M_s = 7.1; October 17, 1989) to three stations 30 to 40 km distant provides an unusually complete record of deformation in the epicentral region in the years prior to an earthquake. Roughly 1.3 years before the earthquake, at about the time of the first magnitude-5 foreshock, the rate of change in line length for two of the lines appears to change; the rate for the third line does not change. Other similar, though smaller, changes in rate are apparent in the eight-year record. Thus, there is marginal evidence for change in deformation rate about one year before the Loma Prieta earthquake, but that change need not be a precursor.

2. A Geodetic Estimate of Fault Slip During the Loma Prieta Earthquake.

Offsets in the relative positions of geodetic stations resulting from the Loma Prieta earthquake can be explained with a dislocation model that includes buried oblique slip on a rupture surface reaching 37 km along the strike of the San Andreas fault, dipping 70 to the SW, and extending from a depth of 5 to 17.5 km. Assuming uniform slip on this rectangular surface, the best fitting values for the slip vector components are 1.6 ± 0.3 m right-lateral strike slip and 1.2 ± 0.3 m reverse slip. The geodetic data clearly preclude rupture extending to near the surface. The uncertainties in the calculated slip values are scaled by the misfit of the model and include estimated uncertainty in the model geometry. Slip on an adjacent extension of the rupture to the southeast recorded in the aftershock sequence is not well constrained by the geodetic data, and across-fault extension observed in this area is not explained by the fault model.

3. Little Postseismic Deformation Detected After the Loma Prieta Earthquake.

In the interval from 3 to 140 days after the October 17, 1989, Loma Prieta earthquake (M_s = 7.1) we detected no significant postseismic change ($\sigma = \pm 7$ *mm*) in 7 Geodolite (EDM) line lengths observed from Loma Prieta and only marginally significant change in the relative positions of 13 GPS stations in a 90-km-long profile extending from Santa Cruz to the Central Valley. We surveyed the GPS profile 2, 6, 14, 49, 91, and 140 days after the main shock and used CIGNET tracking data to improve the satellite orbits for all but the last (3/05/90) survey. Fault parallel and perpendicular components of position change are shown in Figure 1. Component changes are nearly all less than 20 mm. There was no significant fault parallel displacement across the San Andreas fault, a possible 20 mm of right-lateral slip across the Calaveras fault (30 km NE of the San Andreas fault), and an apparent 30 mm of contraction across the San Andreas fault.

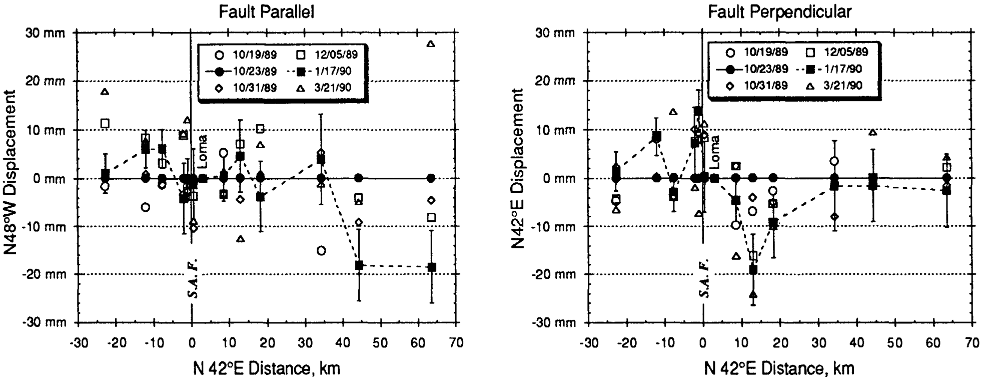

Figure 1. Plots of the fault parallel and perpendicular components of position change relative to the station on Loma Prieta (3.5 km NE of the San Andreas fault) with the second (20/23/89) survey taken as the base survey. The second survey was used as a base because only 8 of the 13 stations in the profile were occupied during the first (10/19/90) survey. Errors bars for the position change at the time of 1/17/90 survey are $\pm 1\sigma$ and are typical of the error in position change at the time of the other surveys.

4. Strain Measurements along the San Andreas Fault North of Los Angeles.

The Tehachapi and Palmdale trilateration networks have been surveyed repeatedly since the early 1970's. The lines in those networks that have been measured in each and every survey are shown to the left in Figure 2, 13 lines in the Tehachapi network and 31 lines in the Palmdale network. The uniform strain fields that best explain the line length changes observed in those two networks are shown to the right in Figure 2. The strains are referred to a coordinate system with the 1 and 2 axes directed parallel and perpendicular

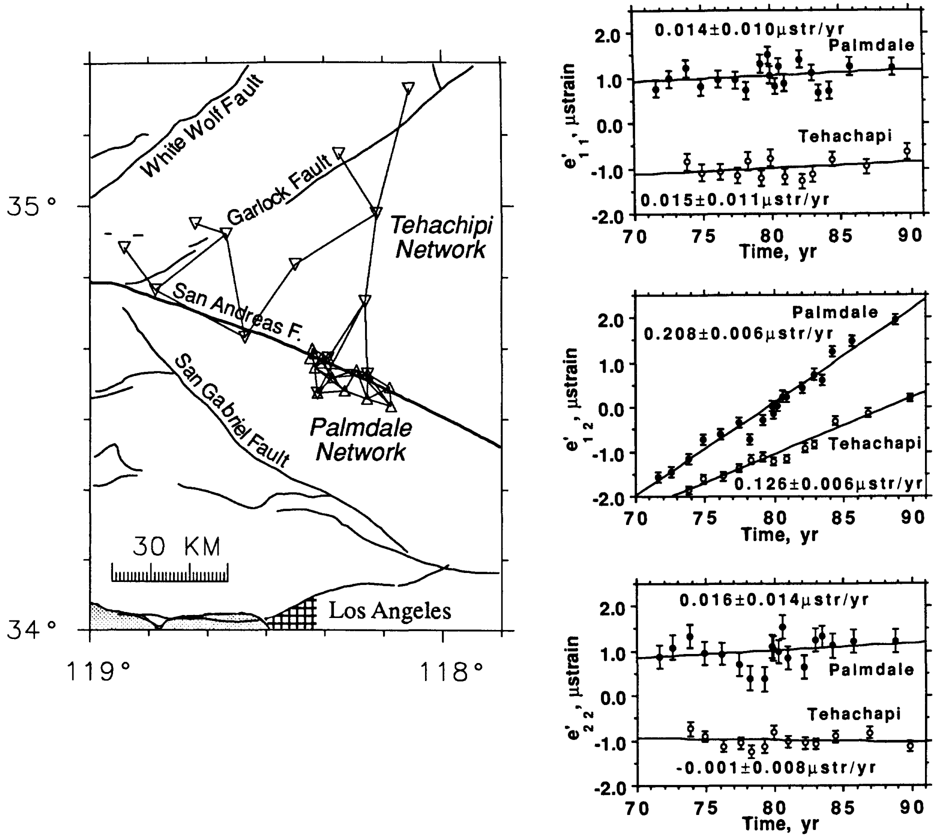

Figure 2. Lines in the Tehachapi and Palmdale trilateration networks measured in each and every survey (left) and strain components as a function of time for these parts of the Palmdale and Tehachapi networks (right). The 1 axis is directed S 65°E and the 2 axis is N 25°W. The error bars represent one standard error on either side of the plotted point.

to the local strike of the San Andreas fault. The accumulation of each component of strain for both networks has been approximated by a linear fit in the figure, and the average strain rate represented by the slope of that fit is shown. The only significant accumulation is in the shear component e'_{12}. Clearly, strain accumulates more rapidly close to the fault (Palmdale) than farther from it (Tehachapi) as one would expect if the slip at depth on the fault is the source of the strain accumulation concentration on a fault. Although at times data from one network may show marginally significant deviations from the linear trend, data from the other network does not show significant deviations at the same time. Thus, one is unable to demonstrate that significant deviations from uniform strain accumulation have been observed.

5. *Criticism of some Forecasts of the National Earthquake Prediction Evaluation Council*

The Working Group on California Earthquake Probabilities has assigned probabilities for rupture in the interval 1988–2018 to various segments of the San Andreas fault on the basis of the lognormal distribution of recurrence times of characteristic earthquakes postulated by Nishenko and Buland (1987). I question the validity of those probabilities on the basis of three separate arguments: 1) The distributions of recurrence times of the four, best-observed, characteristic-earthquake sequences are each only marginally consistent with the Nishenko-Buland lognormal distribution. 2) The range of possible 30-year conditional probabilities for many of the fault segments is so great due to uncertainty in the average recurrence time for that segment that the assigned probability is virtually meaningless. 3) The 1988 forecasts not subject to the foregoing objection are those in which there is a low probability of an earthquake in the near future (*e.g.,* only a 5% chance of rupture of the North Coast segment before the year 2049 and the Carrizo segment before the year 2018). However, the same reasoning would assign only a 5% chance of rupture before mid–1993 to the southern Santa Cruz Mountains segment, the segment that failed in October 1989.

Finally, the forecast of the next Parkfield earthquake (95% probability before 1993.0) by Bakun and Lindh (1985) depends upon an *ad hoc* explanation of the out-of-sequence 1934 earthquake. A less-contrived forecast would have assigned a conditional probability of about 60 ± 20% to the 1985.0–1993.0 interval and 30 ± 15% to the 1990.0–1993.0 interval.

6. *Strain Accumulation near the Mendocino Triple Junction, California.*

Measurements of the deformation of Geodolite trilateration networks near the Mendocino triple junction show a transition from northwest trending right-lateral shear associated with the San Andreas fault system to northeast trending contraction associated with the Cascadia subduction zone. Southeast of the triple junction, where the San Andreas fault is offshore, a broad zone of distributed right-lateral shear was observed. Near Round Valley, located 50 km southeast of Cape Mendocino and 60 km from the San Andreas fault, right-lateral shear strain accumulated at an average rate of 0.41 ± 0.07 μradian/yr across a vertical plane striking N33°W±4° in the 1985 to 1989 interval. This high rate of shear so far east of the fault indicates that about half of the estimated 34 mm/yr of relative plate motion across the San Andreas fault system is accommodated by the Garberville and Lake Mountain faults. Along the coast near Cape Mendocino, the average rate of right-lateral shear strain between 1981 and 1989 was 0.40 ± 0.04 μradian/yr across a vertical plane striking N44°W±4°, approximately parallel to the more westward trend of the San Andreas fault in this area. North of the triple junction, northeast and east-northeast directed contraction was observed. In the area between Cape Mendocino and Eureka, contraction at a rate of 0.20 ± 0.04 μstrain/yr in the direction N31°E±8° was calculated from 1981 to 1989 line length changes. In the area between Cape Mendocino and Trinidad Head an average shear rate of 0.26 ± 0.07 μradian/yr with the direction of maximum contraction N63°E±8° was calculated from the change in angles measured in 1941 relative to those deduced from a 1989 GPS survey.

7. Deformation in the Shumagin Seismic Gap, Alaska.

Sea level measurements at Sand Point, 200 km from the Aleutian trench, suggest uniform subsidence at a rate of 1.2 ± 1.1mm/yr during 1973–1988. Dislocation models of subduction predict uplift rates of 1 to 5 mm/yr. Strain accumulation in the eastern part of the Shumagin seismic gap has been monitored with biennial surveys of a Geodolite trilateration network since 1981. No significant strain accumulation was detected between 1981 and 1987 (the observed extension rate in the direction of plate convergence averaged -0.02 ± 0.03 μstrain/yr). A subset of this network was measured with GPS in 1987 and 1989. There is no significant difference in the lengths common to the 1987 Geodolite and GPS surveys, and the residuals from an adjustment for station position using both types of data are within the 0.2 ppm measurement uncertainty.

Reports

Dzurisin, D., J.C. Savage, R.O. Fournier, 1990, Recent crustal subsidence at Yellowstone caldera, Wyoming, *Bull. Volcanology*, **52**: 247–270.

Savage, J.C., 1990, Equivalent strike-slip earthquake cycles in half-space and lithosphere-asthenosphere earth models, *J. Geophys. Res.*, **95**: 4873–4880.

Davis, J.L., W.H. Prescott, J.L. Svarc, and K.J. Wendt, 1989, Assessment of Global Positioning System measurements for studies of crustal deformation, *J. Geophys. Res.*, **94**: 13,635–13,650.

Eberhart-Phillips, D., M. Lisowski, and M.D. Zoback, 1990, Crustal strain near the big bend of the San Andreas fault: Analysis of the Los Padres-Tehachapi trilateration networks, California, *J. Geophys. Res.*, **95**: 1139–1153.

Array Studies of Seismicity

9930-02106

David H. Oppenheimer
Branch of Seismology
United States Geological Survey
345 Middlefield Road - MS 977
Menlo Park, California 94025
415-329-4792

Investigations

1. Process, interpret, and disseminate Loma Prieta seismic data.
2. Continue consolidation and clean-up of phase data of central California Seismic Network (CALNET) from 1969 through present.
3. Investigate seismic gaps in San Francisco Bay region.

Results

1. The Loma Prieta earthquake of October 17, 1990 generated a tremendous volume of data concurrent with an immediate demand for its real-time interpretation. Efforts during the first several weeks of the sequence were devoted to processing the data and providing preliminary interpretations. These data enabled the USGS to assess the on-going hazard, advise public officials and the press of aftershock probabilities, and guide colleagues participating in aftershock studies on where to site instruments. As the aftershock sequence abated, attention was devoted to the following products:
   a. Dissemination of data. Online computer files of up-to-date earthquake locations were available to anyone that had access to communications over the Internet. Thus, scientists all over the world were able to examine the same data set we were collecting within a day of its creation. In addition, the corresponding phase data was available to scientists for special studies through tape distribution. Requests for data consumed approximately 20% of this project's effort.
   b. Aftershock focal mechanisms: Several manuscripts were prepared for a special issue on the Loma Prieta earthquake in Geophysical Research Letters. The first discusses an analysis of 745 aftershock fault plane solutions. At the northwestern end of the aftershock zone the earthquakes occurred off the fault with the mechanisms showing reverse slip on planes nearly parallel to the San Andreas fault. At the southeastern end the mechanisms show right-lateral strike-slip motion on near vertical planes suggesting that these aftershocks involve slip on the San Andreas fault. Few of the aftershock mechanisms in the central zone resemble the main shock mechanism (strike N50°W, dip 70°SW, rake 140°), but instead exhibit reverse, right lateral, left lateral, and normal motion on planes subparallel to the main shock rupture plane. The aftershock zone dips to the southwest, parallel to the main shock slip plane and includes the main shock hypocenter. However, the lack of agreement between of the main shock and the aftershock mechanisms suggests that few of the aftershocks occurred on the main shock slip plane. This behavior is consistent with observations of aftershock

sequences for other dip slip events and also with studies indicating that main shock rupture zones are at all other times aseismic. The variety of aftershock mechanisms can be explained in two ways. If the stress drop for the main shock relieved most of the tectonic stress, the mechanisms could reflect the heterogeneity of the near-field stress redistribution. Alternatively, the variety of the aftershock mechanisms reflects deformation by block rotation within a 1-3 km zone adjacent to the main shock rupture plane.

c. Seismic slip and segmentation: The second manuscript (in conjunction with project # 9930-02098) discusses how seismic data can be used to define main shock segment boundaries. We plotted the cumulative seismic slip projected onto a vertical plane for earthquakes occurring during the last 20 years along the 210 km of the San Andreas fault spanning the Loma Prieta earthquake. This technique illuminates differences in the depth and character of the seismicity between the locked and creeping portions of the San Andreas and clearly defines the segment upon which the Loma Prieta earthquake occurred. Working by analogy from the relation between pre-main shock microseismicity and presumed main shock slip regions at Parkfield and Loma Prieta, we identify a segment on the San Andreas peninsula upon which we believe the $M7$ 1838 earthquake occurred, and which we believe may have accumulated sufficient strain energy that rupture should be expected in the coming decades.

d. Coseismic stress changes: The third manuscript (in conjunction with project # 9930-02098) builds on the results of the focal mechanism study. The 1989 Loma Prieta, California earthquake is the best opportunity to date to infer the coseismic change in the stress field by comparing the locations and focal mechanisms of background seismicity with those of the aftershocks. We do this both by inspection and by using a stress inversion technique. This preliminary study shows that before the main shock the uniform component of the stress field was larger than the heterogeneities in the stress field and the uniform component had a vertical intermediate stress and a generally N-S most-compressional stress axis. After the main shock the area near, or within, the rupture zone has a very complex stress field with little or no spatially uniform component. This suggests that the main shock removed most of the tectonic stress from the region and perhaps all of the shear stress from its fault plane, making it a total stress drop event. South of the rupture area the stress field was distorted relative to its prior state.

e. Aftershock geometry: The fourth paper (in conjunction with project # 9930-02101) discusses the locations of aftershocks and their implications for fault structure. Well-constrained hypocenters of the Loma Prieta sequence form a southwest dipping zone that extends from the main shock hypocenter and is parallel with the main shock nodal plane. Most aftershocks cluster around the perimeter of the distribution and surround a relatively aseismic patch which we believe approximates with the extent of main shock rupture. In the southeast part of the aftershock zone the dipping zone warps into a vertical surface that corresponds with the San Andreas fault. In the central and northwestern parts of the aftershock zone and at depths above about 10 km the aftershocks define numerous disjoint fault structures. The large component of reverse-slip observed in this event agrees with a simple model for slip on a dipping plane within a compressional fault bend. We are unable to conclude, however, whether the fault activated by Loma Prieta earthquake was the principal plate boundary fault or a less-frequently active member of the San Andreas fault system.

2. Progress continues to be made in the collection, organization, relocation, archiving, and documentation of CALNET earthquake data since 1969 (see previous Semi-Annual Reports). Main efforts were directed toward merging RTP and CUSP data for the latter half of 1986, when the Chalfant Valley sequence occurred. Although the CUSP data was completed, the RTP data was never processed. We anticipate completion of this task by mid-year at which time the entire catalog from 1/69 through the present (with the exception of October, 1989) will be complete. At that time we will begin a quality check to remove systematic errors in magnitude determination and gross blunders.

3. One of the most striking features of the Loma Prieta seismicity is the imaging of the impending rupture zone by the pre-main shock seismicity. Although models of the main shock slip distribution are not yet available, the aftershocks fill in a gap in the pre-main shock seismicity and are assumed to be occurring along the slip region. Similar seismic behavior has been observed along the Calaveras fault in the vicinity of Morgan Hill, where the pre-main shock seismicity outlined aseismic regions at the base of the seismogenic zone that subsequently failed during main shocks. Whereas along the Calaveras fault the pre- and post-main shock seismicity occur directly on the fault and surround the main shock slip zone, on the Loma Prieta segment of the San Andreas fault the aftershocks occur adjacent to the slip region and off the fault. These results have prompted an investigation of other $M > 6$ seismic gaps in the San Francisco Bay region. Preliminary results show gaps on the San Andreas fault along the San Francisco Peninsula, Hayward fault, Rogers Creek fault, Green Valley-Calaveras-Sunol fault, and perhaps the Palo Colorado-San Gregorio fault (see Figures 1-3).

Reports

Oppenheimer, D.H., Aftershock slip behavior of the 1989 Loma Prieta, California earthquake, submitted to *Geophy. Res. Let.*

U.S. Geological Survey, Preliminary hypocentral locations from the Loma Prieta, California, earthquake of October 17, 1989, *U.S. Geol. Surv. Open-File Rep. 89-638*, 10 pp., 1989.

Dietz, L.D., and W.L. Ellsworth, The October 17, 1989 Loma Prieta, California, earthquake and its aftershocks: Geometry of the sequence from high-resolution locations, submitted to *Geophys. Res. Let.*

King, G.C.P, A.G. Lindh, and D.H. Oppenheimer, Seismic slip, segmentation, and the Loma Prieta earthquake, submitted to *Geophys. Res. Let.*

Michael, A.J., W.L. Ellsworth, and D.H. Oppenheimer, Coseismic stress changes induced by the 1989 Loma Prieta, California earthquake, submitted to *Geophys. Res. Let.*

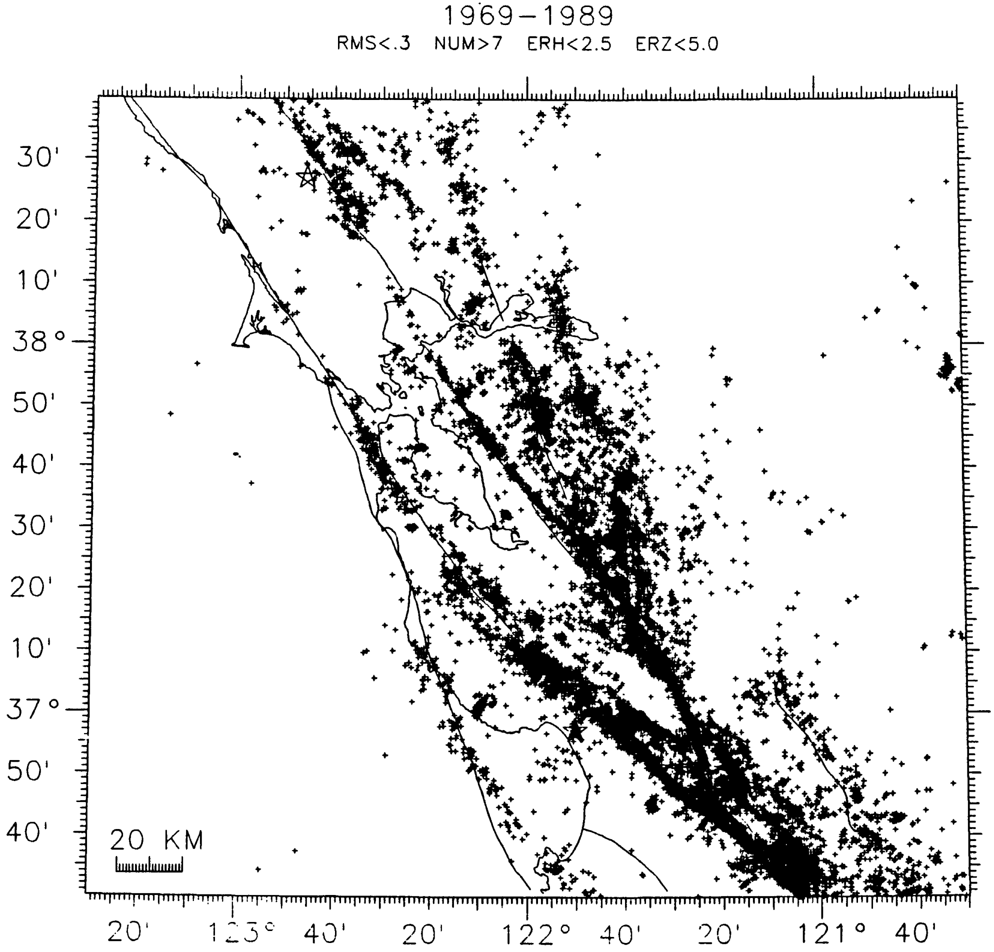

Figure 1. Map view of 20 years (1969–1989) of seismicity in the San Francisco Bay region. All solutions have at least 8 readings, an RMS < 0.3 sec, and horizontal and vertical uncertainties of 2.5 and 5.0 km.

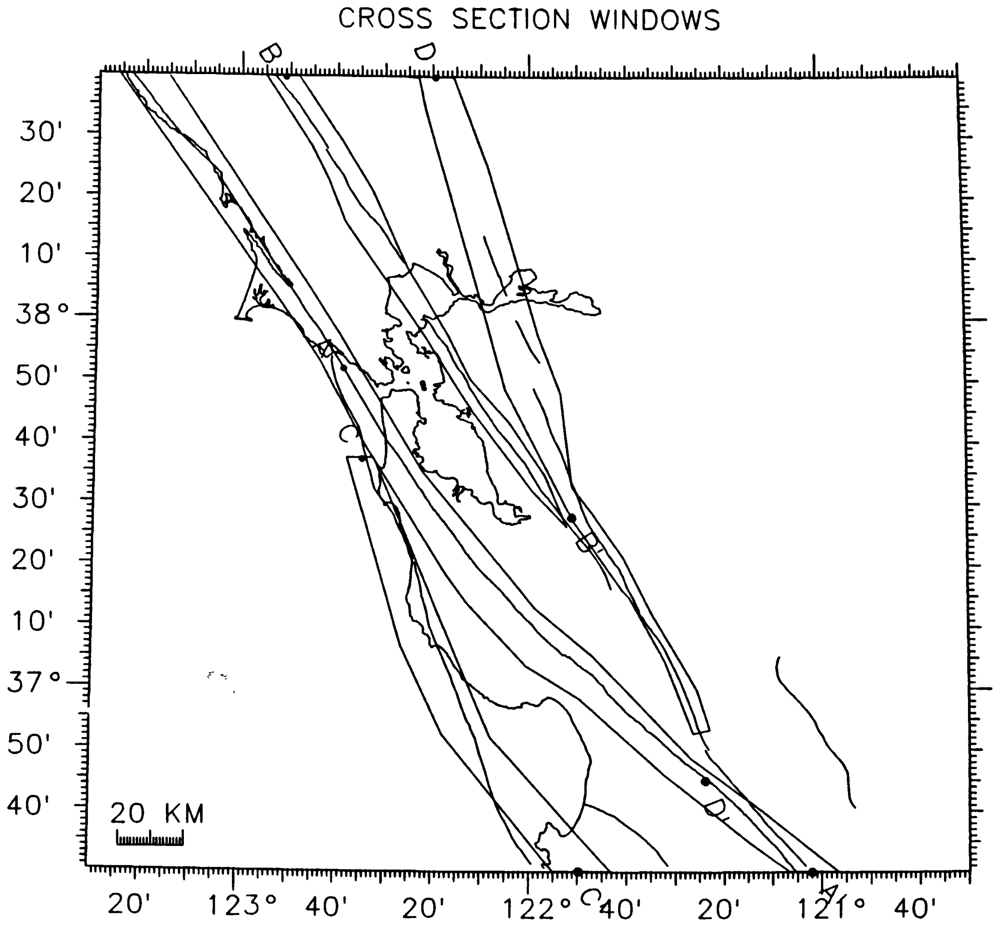

Figure 2. Cross section windows for Figure 3.

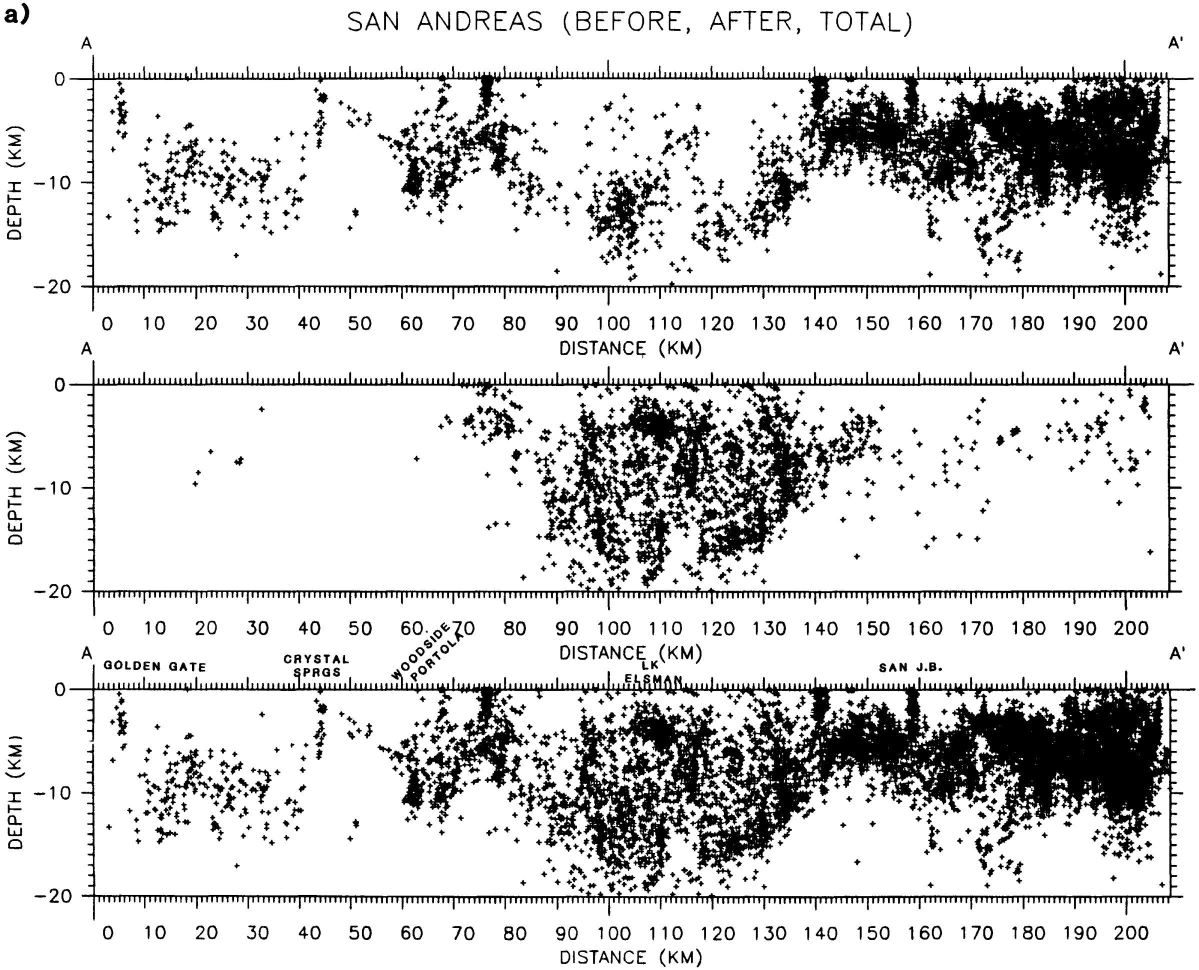

Figure 3. Fault-parallel cross sections corresponding to endpoints shown in Figure 2. a) San Andreas fault seismicity before, after and combined), b) Rogers Creek-Hayward-Mission faults, c) Seal Cove-San Gregorio-Palo Colorado faults, and d) Green Valley-Concord-Calaveras faults.

b)

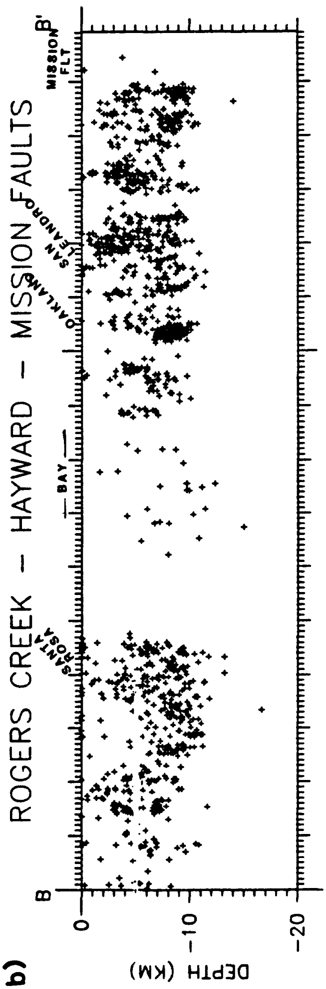
ROGERS CREEK – HAYWARD – MISSION FAULTS
B
B'
SANTA ROSA
BAY
OAKLAND
SAN LEANDRO
MISSION FLT
DEPTH (KM)
0
-10
-20
0
10
20
30
40
50
60
70
80
90
100
110
120
130
140
150

c)

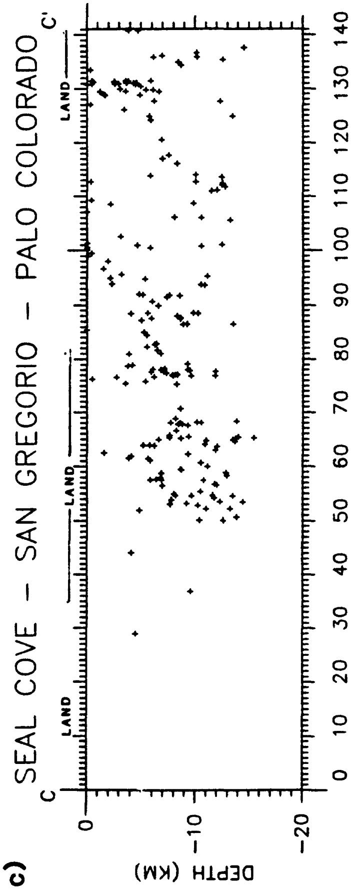
SEAL COVE – SAN GREGORIO – PALO COLORADO
C
C'
LAND
LAND
LAND
DEPTH (KM)
0
-10
-20
0
10
20
30
40
50
60
70
80
90
100
110
120
130
140

d)

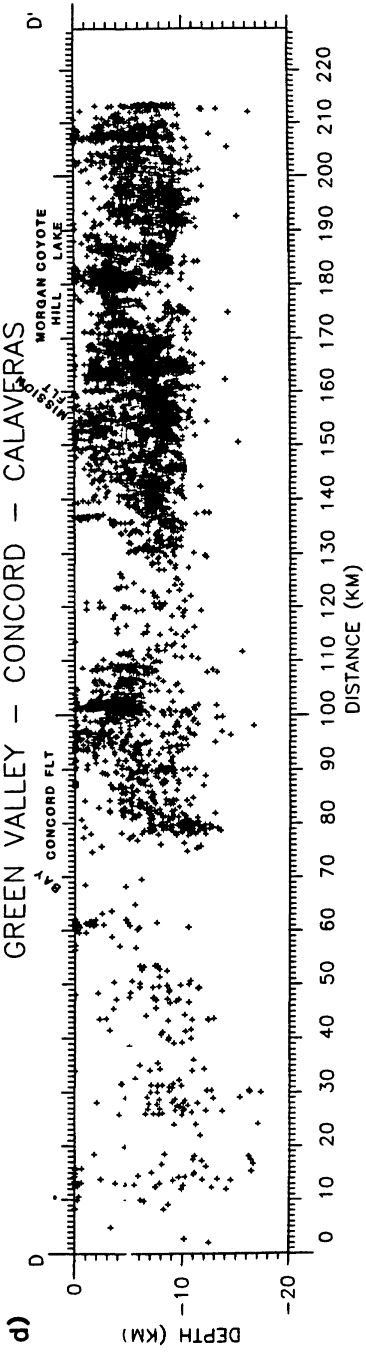
GREEN VALLEY – CONCORD – CALAVERAS
D
D'
BAY
CONCORD FLT
MISSION FLT
MORGAN HILL
COYOTE LAKE
DEPTH (KM)
0
-10
-20
DISTANCE (KM)
0
10
20
30
40
50
60
70
80
90
100
110
120
130
140
150
160
170
180
190
200
210
220

IGPP/UCR-90/9

Variations in Electrical Properties Induced by Stress Along the San Andreas Fault at Parkfield, California

Supported by the U.S. Geological Survey, Department of Interior
under award number 14-08-0001-G1357

Stephen K. Park
Tien Chang Lee
Institute of Geophysics and Planetary Physics
University of California
Riverside, California 92521

Introduction

We are monitoring fluctuations of resistivity with telluric currents in Parkfield. The array uses grounded telephone lines as dipoles (Figure 1). The analysis has been discussed in previous reports and will not be reviewed here. We look at daily fluctuations of the telluric coefficients relating Dipoles 1 through 6 to the reference dipoles of Dipoles 7 and 8. Thus, we are looking at relative variations, rather than absolute ones. Changes in the telluric coefficients are directly related, albeit through the response of a complex, heterogeneous earth, to changes of resistivity.

Discussion of Data

In previous reports, we have mentioned the variation seen on Dipole 2 between 9589 (Julian Day 95 in 1989) and 12589. This variation consisted of a 2% decrease followed by a 5% increase and then a return to the background level during that time. This occurred approximately one month before an M=3.7 earthquake just south of the array, and is much larger than the noise level on this dipole. We have found that this fluctuation corresponds to a change on a tensor strainmeter which is located at the midpoint of Dipole 2. However, the data from the strainmeter is suspect because an adjacent dilatometer recorded no change at that time. Precipitation also occurred during this time, but we do not see changes at other times during rain. We thus do not believe that the fluctuation we saw was induced by rain. We do not yet have a satisfactory explanation for the behavior of Dipole 2, but we believe it may be related to preparation for the earthquake. Lack of a coseismic change anywhere on the array leads us to discount any possible change of resistivity directly related to release of strain energy.

Results of the analysis for the past six months for Dipoles 1 through 6 are shown in Figures 2 through 4. We plot the projection of the daily fluctuation of the telluric coefficient onto the major and minor eigenvectors (upper and lower plots for each dipole, respectively) and the coherency as a measure of the data quality.

All of the major eigenvector projections are small (O(1%)), as are the minor projections for Dipoles 1, 3, 4, and 5. Dipoles 2 and 6 are showing variations of up to 7% on the minor projections. These dipoles, and Dipole 5, are traditionally our noisiest channels, so the large variations on them are suspect. However, we have not seen oscillations on Dipole 6 as large as these in the history of the array.

The variations on Dipoles 1 and 4 are probably of greater interest because the major projections have been very stable for two years. These projections vary usually by less than 0.5%. In December 1989, both of these changed by about 1% to new levels which have persisted into the first three months of 1990 (Figures 2 and 3).

A change of 2 to 3% on the minor projection on Dipole 5, which has also persisted into 1990. Coincident with this change is a marked drop in the cumulative seismic moment reported by Malin (personal communication, 1990). To date, that moment is continuing to drop.

Conclusions

We are beginning to see changes in the telluric coefficients that are above our noise level, although we cannot explain these changes at this time. Correspondence with other phenomena is intriguing, but is insufficient to help us explain the mechanism producing the changes of resistivity. We cannot locate where are the resistivity changes nor estimate their magnitudes because we have not yet run a 3-D inversion using the electrical structure of Parkfield. In any case, we suspect that our results will be nonunique.

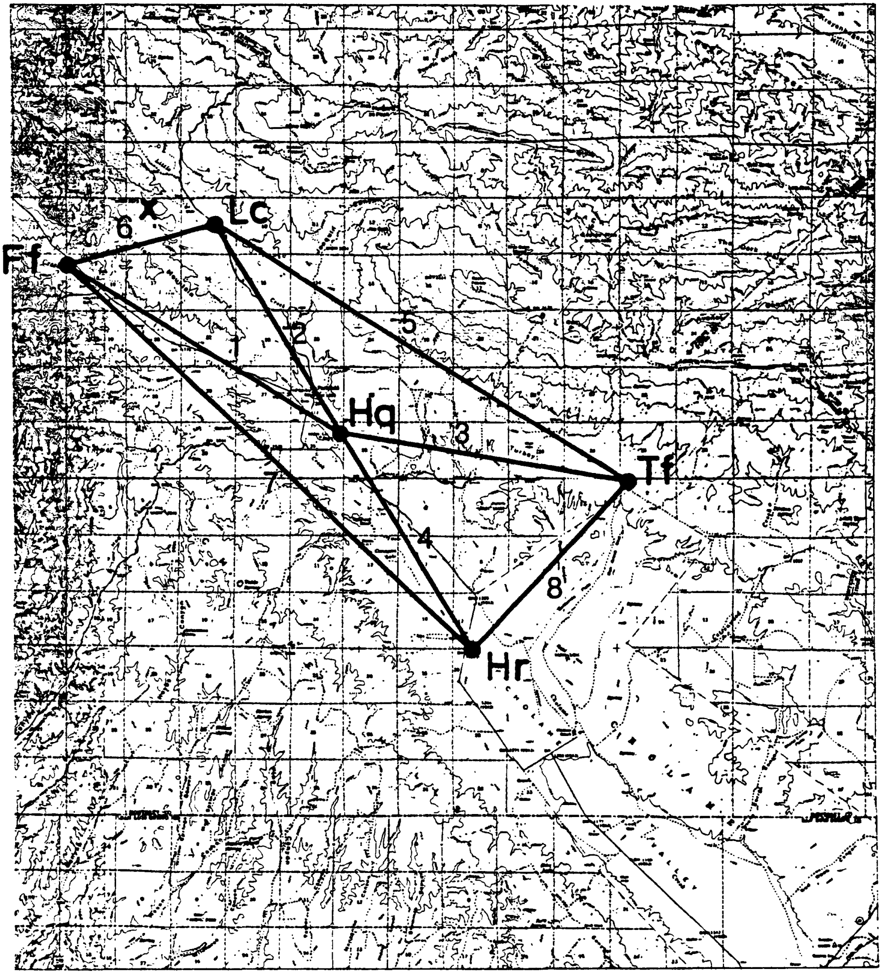

Figure 1 - Telluric monitoring array in Parkfield. Electrodes are marked with dots and eletronically created dipoles are shown with lines.

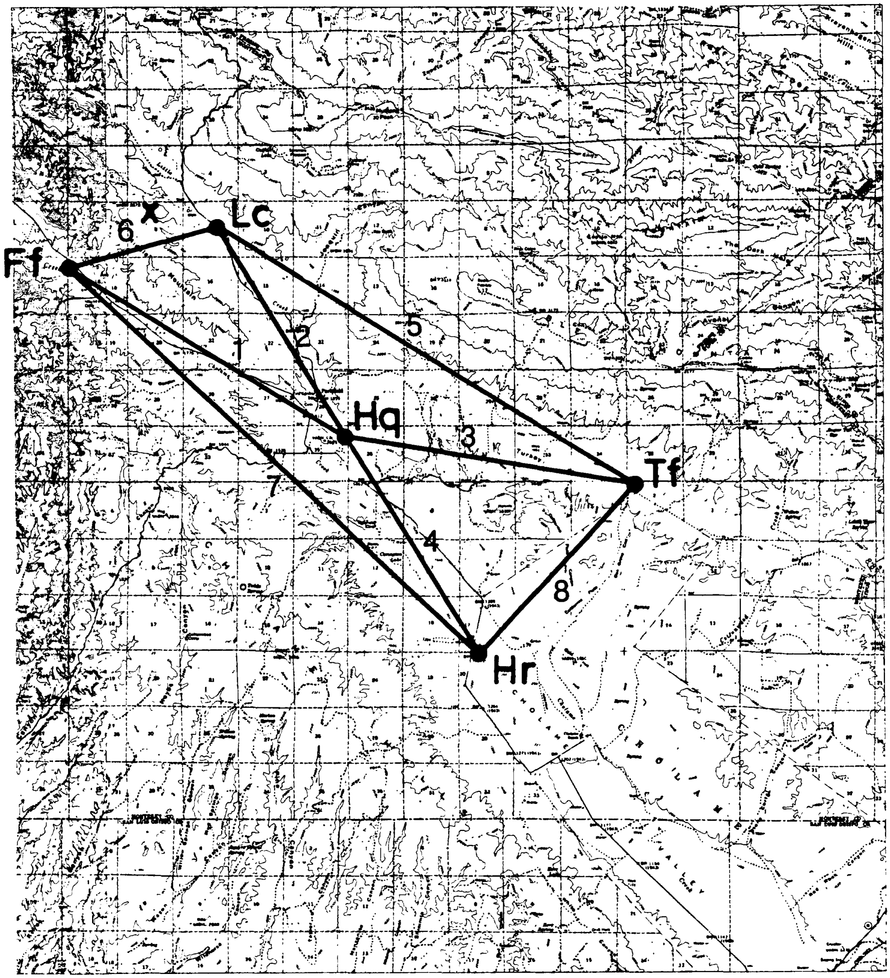

Figure 1 - Telluric monitoring array in Parkfield. Electrodes are marked with dots and eletronically created dipoles are shown with lines.

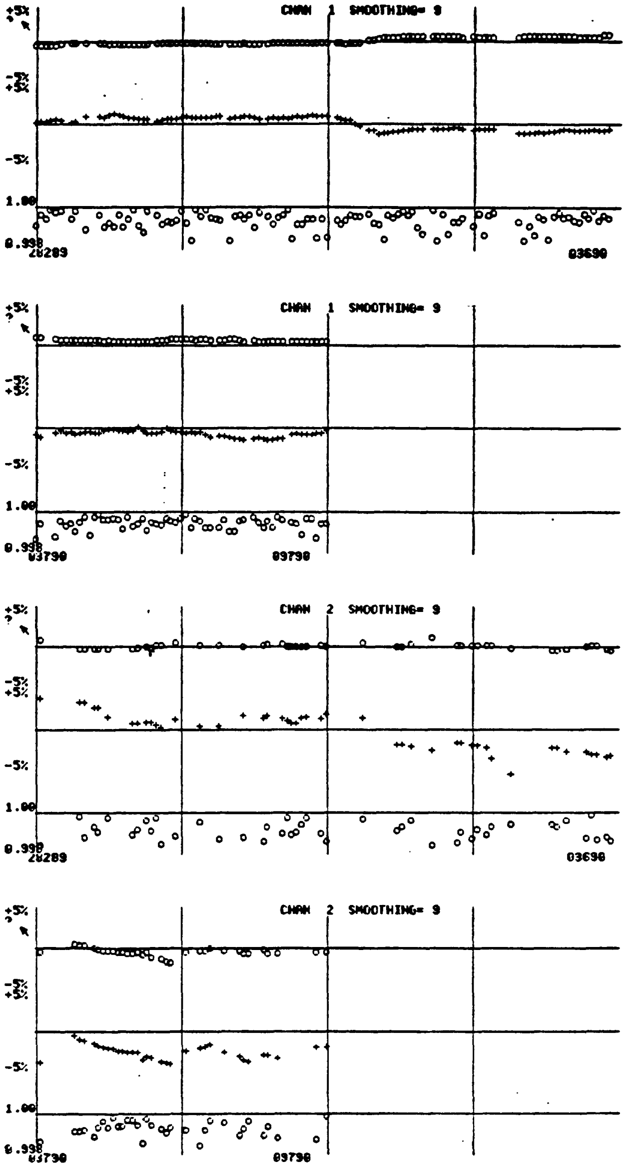

Figure 2 - Residual analysis for Dipoles 1 and 2 for the past six months. The first plot is the projection of the residual on the major eigenvector and the second is the projection on the minor eigenvector. Projections are shown with a scale of +5% to -5%. Coherencies are between the signal predicted using the telluric coefficients and the measured signalare shown between .998 and 1.000.

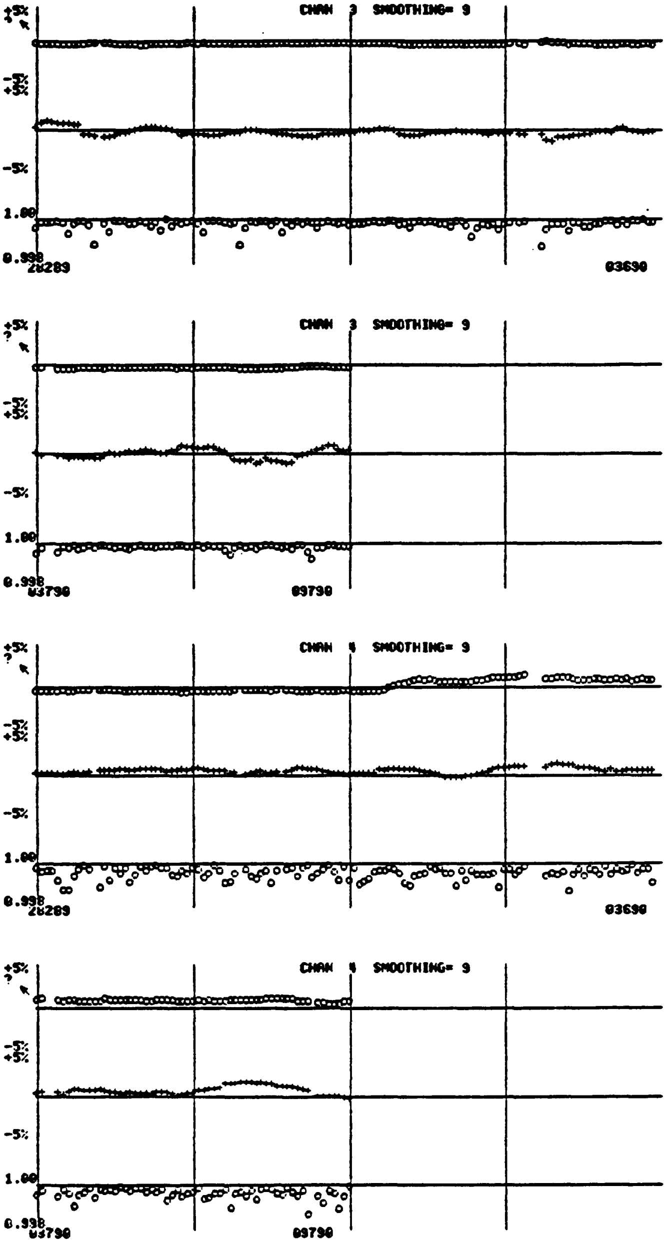

Figure 3 - Residual analysis for Dipoles 3 and 4 for the past six months. See caption of Figure 2 for explanation.

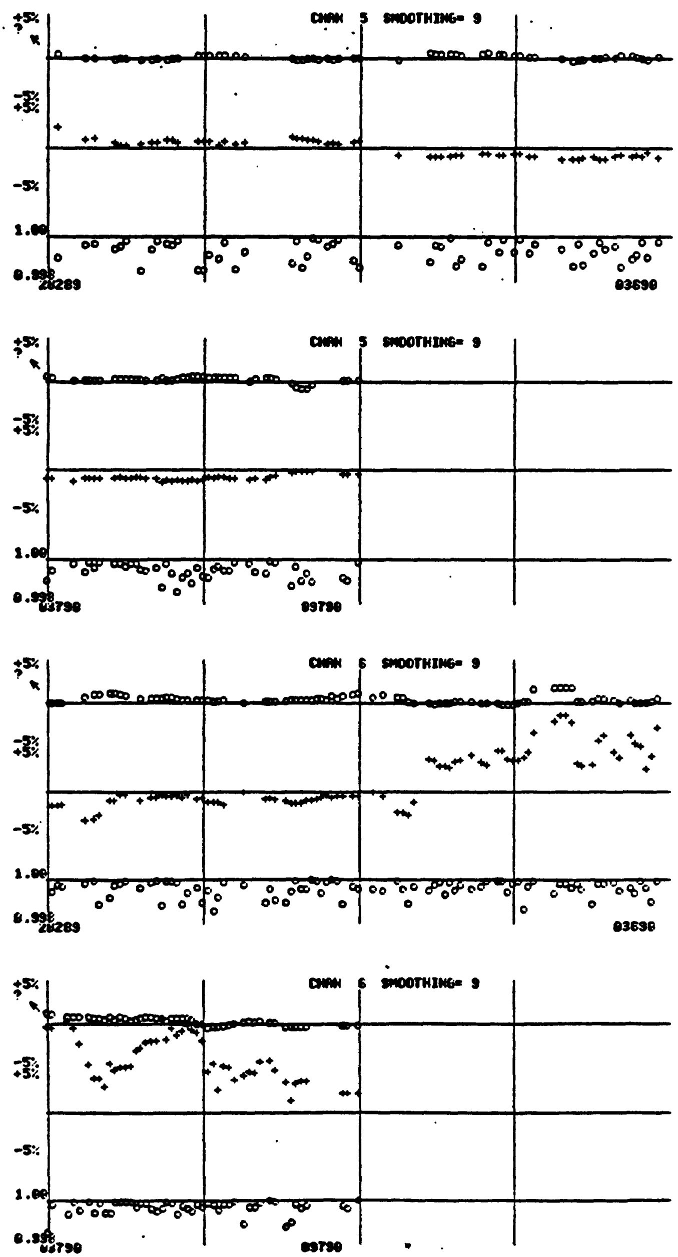

Figure 4 - Residual analysis for Dipoles 5 and 6 for the past six months. See caption of Figure 2 for explanation.

California Seismicity Studies

9930-02103

Paul A. Reasenberg
Donna Eberhart-Phillips
Mark V. Matthews

Branch of Seismology
United States Geological Survey
345 Middlefield Road - MS 977
Menlo Park, California 94025
415-329-5002

Investigations

1. Aftershock probability forecasts: applications.

The first practical application of our model for real-time probabilistic hazard assessment for earthquake sequences was provided by the 6 March, 1989 magnitude (M) 4.7 Obsidian Butte earthquake sequence in the northern Brawley Seismic Zone at the southern end of the Salton Sea, California. The earthquake sequence was initially very active and included a relatively high proportion of large-magnitude aftershocks ($a = -0.5$, $b = 0.6$). As a result, the model-estimated probability for a larger ($M \geq 4.7$) earthquake during the first week in the sequence was relatively high – on the order of 0.30. Some workers familiar with the seismicity of the Brawley Seismic Zone generally felt that this estimate was reasonable and compatible with the history of earthquake swarms in the region. We did find, however, that other factors, in addition to those considered in the model, also warranted consideration in assessing the post-mainshock hazard.

One factor was the proximity (18 km) of the Obsidian Butte earthquakes to the intersection of the Brawley Seismic Zone and the San Andreas fault and the possibility that a great ($M \approx 8$) earthquake on the southern San Andreas fault might be triggered by stress changes resulting from the Obsidian Butte sequence. The model estimate for the probability of a $M \geq 7.7$ earthquake during the first week of the sequence was 0.004. Subsequent discussion among scientists considered the fact that the southern San Andreas fault has accumulated significant strain and was recently assigned a (relatively high) 40% probability of producing a major earthquake in the next 30 years. The concensus was that the distance to the San Andreas fault was too great to warrant an upward revision of the model probability estimate for a great earthquake.

Another factor was the belief by some scientists that the Brawley Seismic Zone may not be capable of producing very large earthquakes because it is composed of numerous small faults, rather than a continuous fault long enough to produce a large shock. Our initial application of the model assumed that all earthquake magnitudes were possible. If, instead, we assume that the largest possible earthquake in the Brawley Seismic Zone is $M6.2$ (the magnitude of the largest known historic event), then the model-estimated probability of a $M \geq 4.7$ earthquake decreases from 0.30 to 0.26.

Loma Prieta Sequence. The USGS used the model to issue frequent public forecasts during the 17 October 1989 Loma Prieta earthquake sequence of probabilities of strong aftershocks within a day, a week, and 2 months. While this earthquake produced fewer aftershocks than expected for a generic M7.1 earthquake, the final model parameters determined for it ($a = -1.67$, $b = 0.75$, $p = 1.19$) all differ by less than 1 SD from their respective generic values. We reported 24 hours after the mainshock that the chance of a $M \geq 5$ aftershock in the next day was 0.13 (none occurred). One week later that probability had decreased to 0.05, while the probability of a ($M \geq 5$) aftershock over the next 2 months was 0.5 (none occurred). Forecasts were made first daily, and then less frequently, through 30 November 1989. These were issued to federal, state and regional government agencies and were widely reported by Bay Area printed and electronic media. Public demand for and interes in aftershock forecasts was greatest immediately after the earthquake and remained high for about 2 weeks, decreasing as the felt aftershocks subsided.

Some local and regional government agencies requested model results particular to their needs during the first week of the sequence. The Port of Oakland requested estimates of probabilites for strong aftershocks in order to decide whether and when to reoccupy a damaged structure. The San Francisco Fire Department requested probabilites of strong shaking in the Marina and China Basin districts to guide decisions about equipment deployment and staffing levels in these damaged areas. Within the USGS, scientists coordinating the regional deployment of strong motion portable seismographs frequently consulted model results in planning their experimental design and field strategy.

Our experience with the Obsidian Butte sequence and the Loma Prieta sequence has shown that the model can provide important information for real-time hazard assessment for earthquake sequences. Sensible real-time assessment of the seismic hazard during future earthquake sequences in California should take into account relevant regional factors, including proximity to stressed fault segments, fault complications or gaps, and possible regional limitation of the maximum possible earthquake size, in conjunction with the probabilities obtained from our model.

In the Loma Prieta sequence we found that regularly released short-term forecasts of expected aftershock activity were useful in meeting the high public demand for earthquake hazard information after a strong earthquake. We also saw that the press and public can easily misunderstand a probabilistic forecast; such public statements should be simple, clear and consistent. Overall, however, we feel that our use of model probabilites to forecast the continuing earthquake hazard after the Loma Prieta earthquake was generally understood and widely accepted by the public, the press, and other government agencies.

2. Aftershock probability forecasts: accuracy.

A technical comment by P. A. Rydelek criticising some aspects of our aftershock probability model was published in *Science* 19 January, 1990. Rydelek's main criticism concerned the formal uncertainties associated with the generic probability model. Because the *a priori* parameter distributions are fairly broad, he argued, the uncertainties in the model results are unacceptably high for use as a forecasting tool. Lucy Jones and I stated in our original report in *Science* that the initial uncertainty was high and decreased rapidly with time after the mainshock, but we did not have space there to give the uncertainties.

In response to Rydelek, Mark Matthews and I performed a Monte Carlo experiment to determine the model uncertainties both for the generic model and for the posterior values at varying times after the mainshock. The result contained no surprises, and confirmed that the uncertainties in interval probabilities for the generic model begin large and repidly decrease. For example, immediately after a M7 earthquake, the generic model probability of a $M \geq 6$ aftershock in the first week is 0.23, and the ±1 SD range is (0.07,0.59). The uncertainties drop precipitously with time due to the inclusion of aftershock data that helps define the model. After 1 day, the 1-week ($M \geq 6$) probability and ±1 SD range is 0.05 (0.034, 0.075). At 3 days after the mainshock, the corresponding result and ±1 SD range is 0.021 (0.015, 0.029).

3. Velocity structure of the San Andreas fault

The simultaneous inversion method for hypocentral and 3D velocity parameters that was developed to study the Coalinga area was applied to the Coast Ranges/Great Valley margin and the San Andreas fault (SAF). We have obtained a 3-D velocity model for the area surrounding the Parkfield segment of the San Andreas fault, which has been the site of five characteristic magnitude 6 earthquakes, and is the location of a M 6 event expected in the next few years. 100 km northwest of Parkfield the October 17, 1989, $M_s7.1$ Loma Prieta earthquake occurred in the southern Santa Cruz Mountains along another (previously) locked segment of the SAF. The Loma Prieta surface geology and fault traces are complex, suggesting that to fully understand the sequence we need to image the subsurface geology.

In the Parkfield study, the San Andreas fault is the primary feature in the velocity solution. The hypocenters follow the mapped fault trace except through the bend where the seismicity does not bend as sharply as the fault trace. Particularly in the 5- to 10-km depth interval, there is a strong lateral velocity gradient that follows the SAF trace through Parkfield and its bend into the Cholame Valley. Northeast of the fault velocities too low for typical Coast Range Franciscan rock are shown in the 3-D model below 4 to 5-km depth for a large area 50-km long and 10- to 15-km wide. In the shallower material there are two high-velocity features. The larger one, located on the northeast side of the fault near the bend, is a 10- to 20-km-long high-velocity body extending southeast from Gold Hill. The other is in the Salinian terrane southwest of Middle Mountain.

Preliminary 3D inversion results show that the velocity along the Loma Prieta segment is higher on the northeast side above 9 km and on the southwest side below this depth. Both the aftershock hypocenters and the velocity model show that the SAF changes from a southwest-dipping feature along the Loma Prieta segment to a vertical feature in the creeping section of the fault to the southeast. The across-fault velocity variation in the creeping section is also much simpler, with the southwest side having higher velocity at all depths.

The Loma Prieta velocity model can be compared to a resistivity model computed from a magnetotelluric sounding profile across the SAF. Between the San Andreas and Zayante faults a low-resistivity, low-velocity wedge is observed and is interpreted to be largely Tertiary marine sedimentary rocks. Between the SAF and the sub-parallel Sargent fault there is a roughly 20-km-long zone that shows high velocity and high resistivity and may represent largely mafic intrusive rocks. The strong agreement between independently developed velocity and resistivity models suggests that the combined use of magnetotelluric surveys and velocity inversions using local sources can be an important tool in understanding geologic structure along major faults.

Along both the Parkfield and Loma Prieta fault segments distinctive velocity variations are associated with variations in the seismicity and fault behavior. This suggests that the 3D velocity models are imaging fault zone heterogeneity that controls the rupture process.

Reports

Reasenberg, Paul A. and L. M. Jones, Earthquake Hazard After a Mainshock in California, *Science*, 243, 1173-1176 (1989).

Reasenberg, Paul A. and L. M. Jones, California Aftershock Hazard Forecasts, *Science*, 247, 343-346 (1990).

Reasenberg, Paul A. and Mark V. Matthews, California Aftershock Model Uncertainties (response), *Science*, 247, 343-345, (1990).

Hill, D.P., W.L. Ellsworth, M.J.S. Johnston, J.O. Langbein, D.H. Oppenheimer, A.M. Pitt, P.A. Reasenberg, M.L. Sorey, and S.R. McNutt, The 1989 Earthquake Swarm Beneath Mammoth Mountain, California, BSSA, 80, 325-339 (1990).

Eberhart-Phillips, D., Three-dimensional P- and S-velocity structure in the Coalinga region, California, submitted to J. of Geophys. Res., 1989.

Eberhart-Phillips, D., and A. J. Michael, Three-dimensional crustal velocity structure in the Parkfield, California, region from inversion of local earthquake and shot arrival times, EOS Amer. Geophys. Un. Trans., V. 70, p. 1203-1204, 1989.

Michael, A. J., and D. Eberhart-Phillips, Finding asperities without using seismicity patterns: results from Parkfield, California, EOS Amer. Geophys. Un. Trans., V. 70, p. 1233, 1989.

Eberhart-Phillips, D., and A. J. Michael, Preliminary views of three-dimensional crustal velocity structure in the region of the Loma Prieta, California, earthquake sequence, EOS Amer. Geophys. Un. Trans., V. 71, p. 288, 1990.

Ekstrom,G., R. S. Stein, J. P. Eaton, and D. Eberhart-Phillips, Seismicity and geometry of a 110-km-long blind fault, 1: the 1985 Kettleman Hills, California, earthquake, submitted to J. of Geophys. Res., 1990.

FLUID PRESSURE AND EARTHQUAKE GENERATION

Project #9960-04451

Evelyn Roeloffs, Eddie G. Quilty
Branch of Tectonophysics
U.S. Geological Survey
345 Middlefield Road, MS 977
Menlo Park, CA 94025
(415)329-4833

Investigations:

1. Real-time monitoring and processing of water level data from Parkfield, California as part of the Parkfield Prediction Experiment. Real-time monitoring of water level data from two sites near Palmdale, California. Water level data are processed in real time to remove tidal and barometric fluctuations, and the processed data are automatically screened for anomalous signals. A beeper monitoring system provides 24 hour a day automatic notification of water level anomalies.
2. Analysis of water level records and development of theoretical solutions to study response to fault creep, seismic waves, and barometric pressure. Searching of water level data for changes that may be related to to the earthquake generation process.

Results:

1. In cooperation with the USGS Water Resources Division, water level data from a network of 12 sites near Parkfield, California were collected throughout the reporting period. Water level data were also collected from two sites in the Mojave Desert. Site locations are shown in Figures 1a and 1b, and Raw water level, barometric pressure, and rainfall data are shown in Figures 2a-f.
2. Preliminary analysis of water level changes at Parkfield due to the Loma Prieta earthquake showed that the water level changes were, in general, too large to be explained either by the strain field of the earthquake or by the subsidiary strain field produced by triggered coseismic creep on the Parkfield segment of the San Andreas fault.

Reports:

No reports were produced during this reporting period.

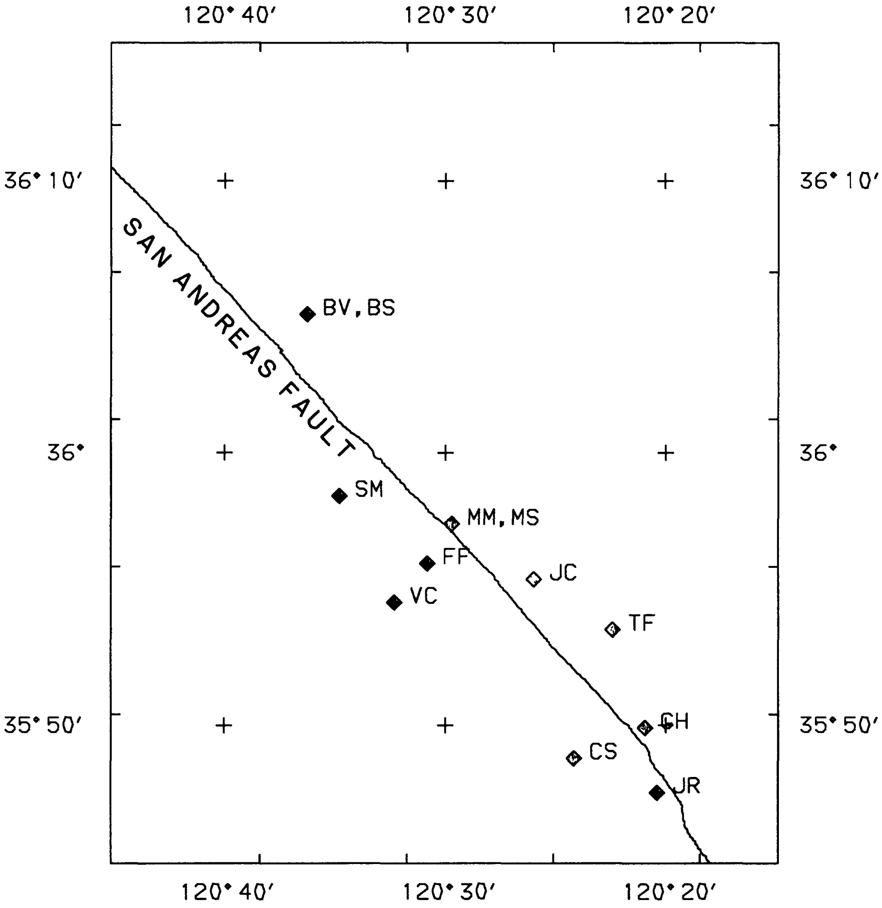

Figure 1. (a) Map showing water wells near Parkfield California, monitored as part of the Parkfield Earthquake Prediction Experiment.

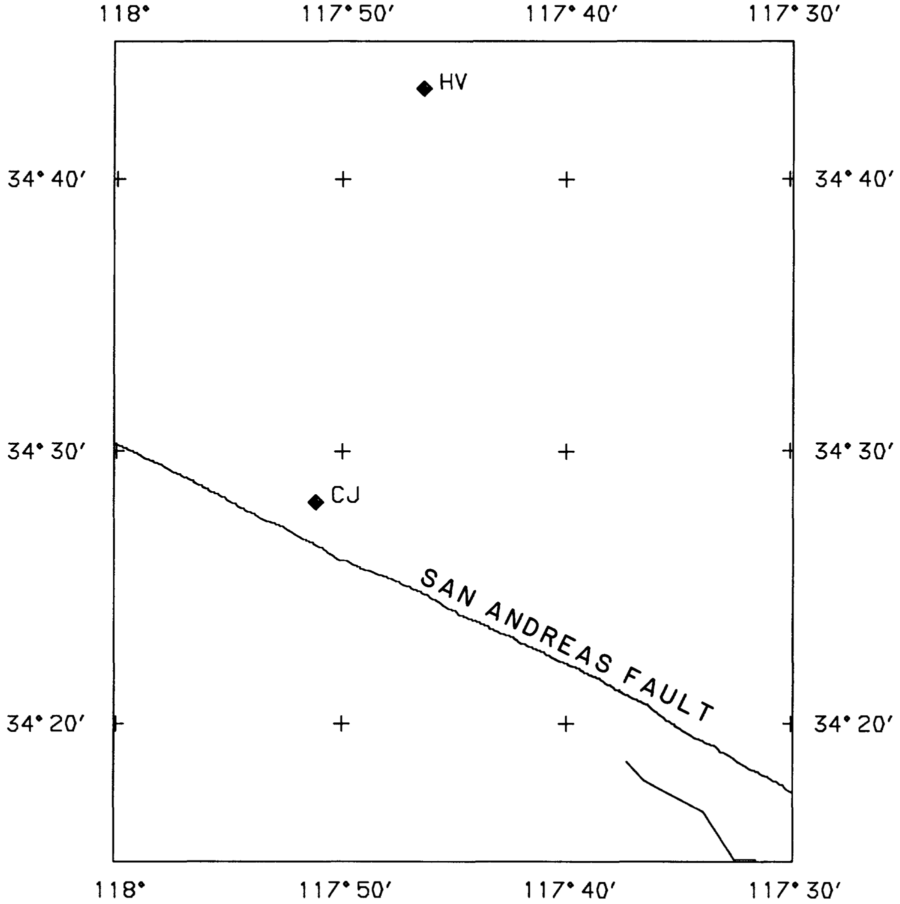

Figure 1. (b) Map showing wells HV and CJ near the Mojave segment of the San Andreas fault.

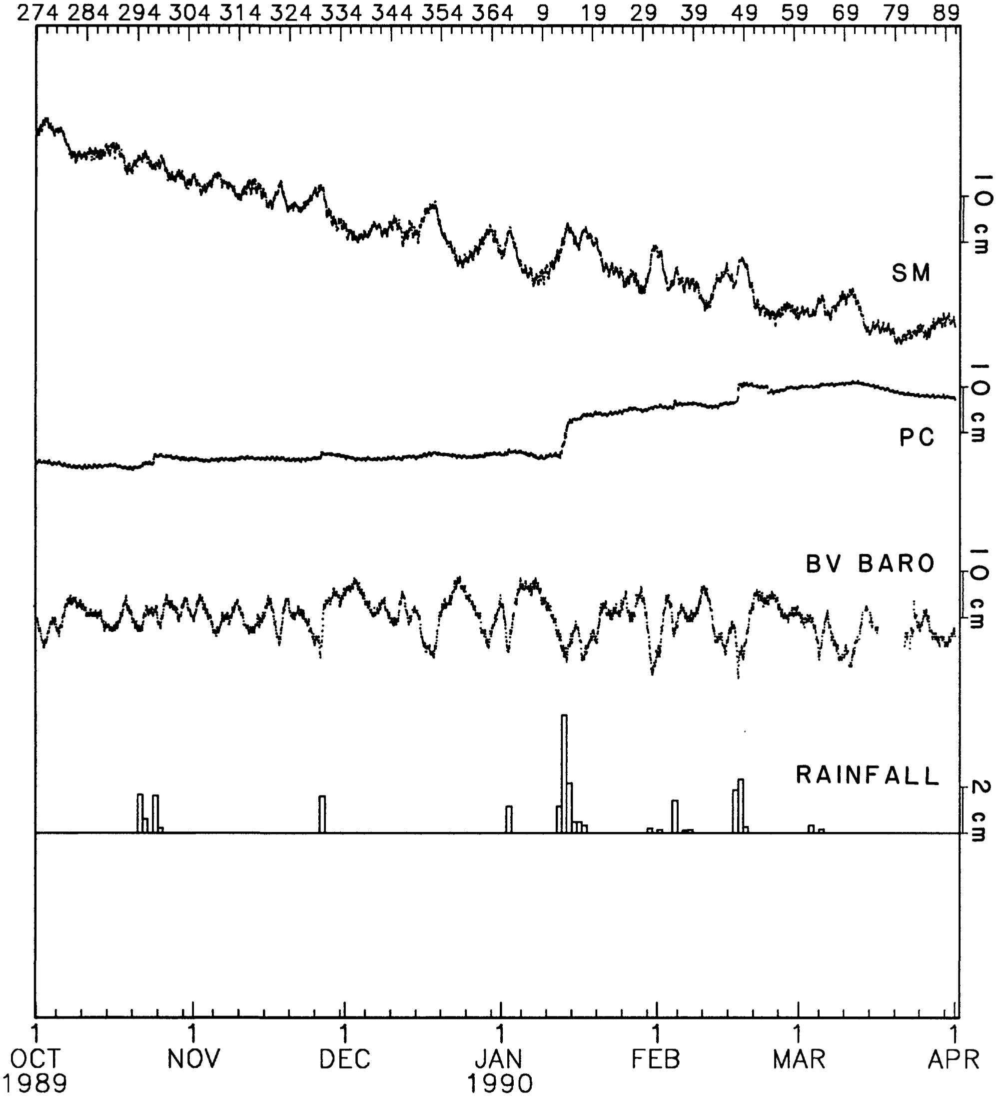

Figure 2. (a) Water level, barometric pressure, and rainfall records. Hourly values are plotted for water level and barometric pressure. Water level is in centimeters above an arbitrary datum. Barometric pressure is in centimeters of water with respect to an arbitrary datum. Bars indicate total rainfall in a 24 hour period. Site names are indicated at right.

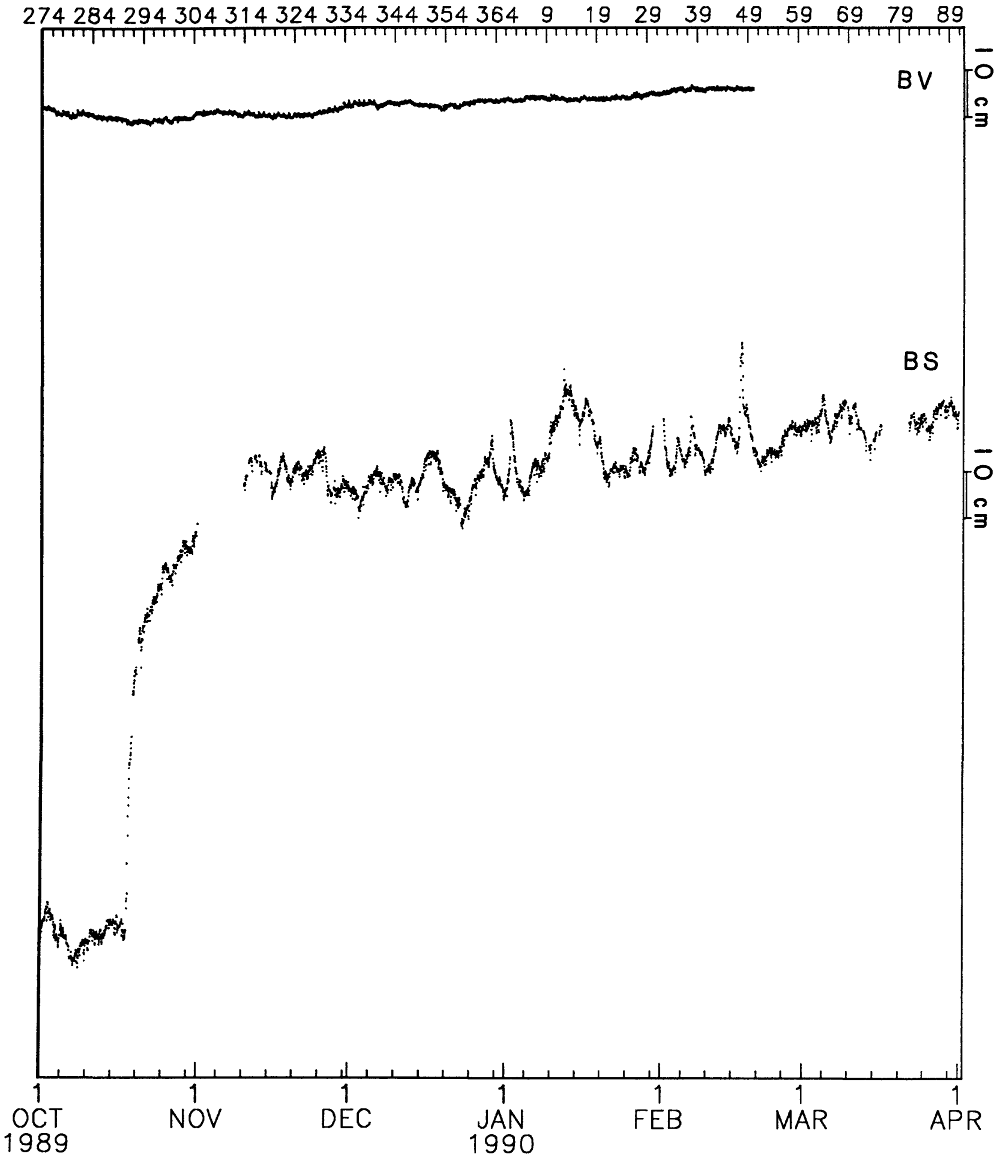

Figure 2. (b) Water level records plotted as in Figure 2(a).

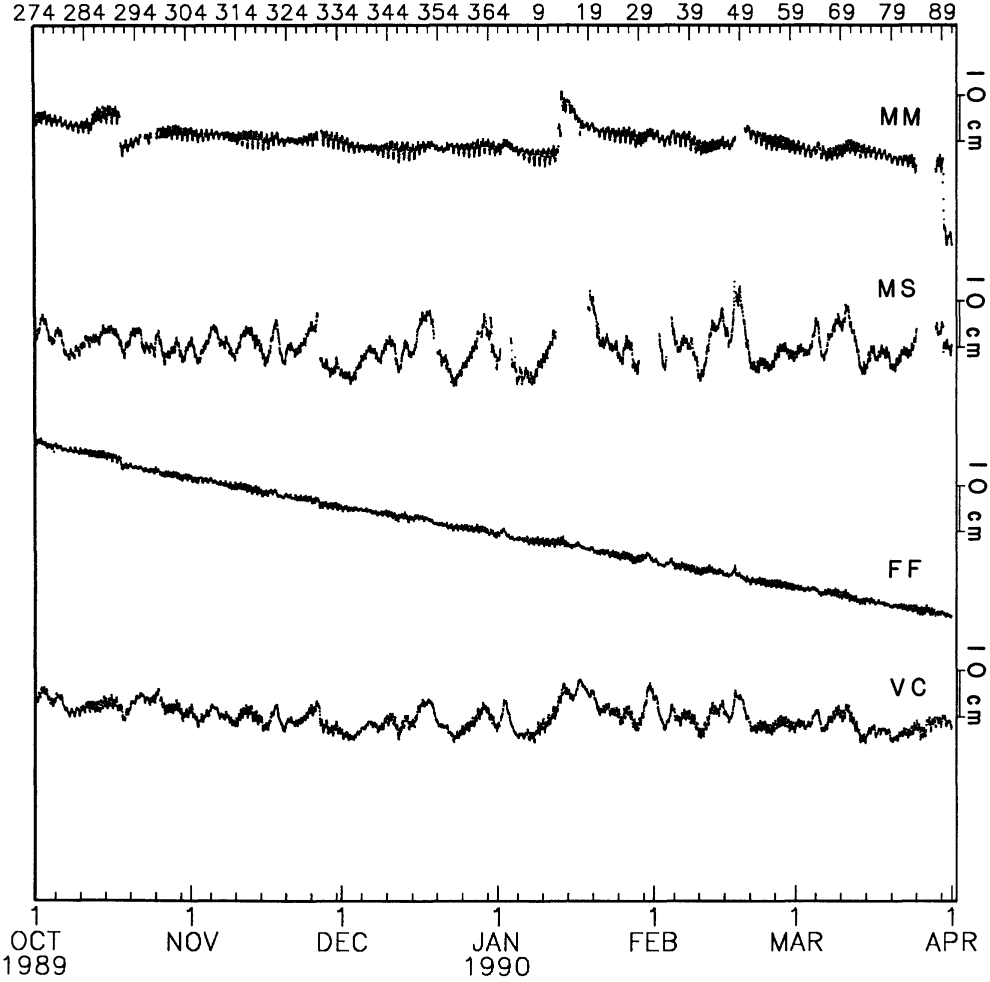

Figure 2. (c) Water level records plotted as in Figure 2(a).

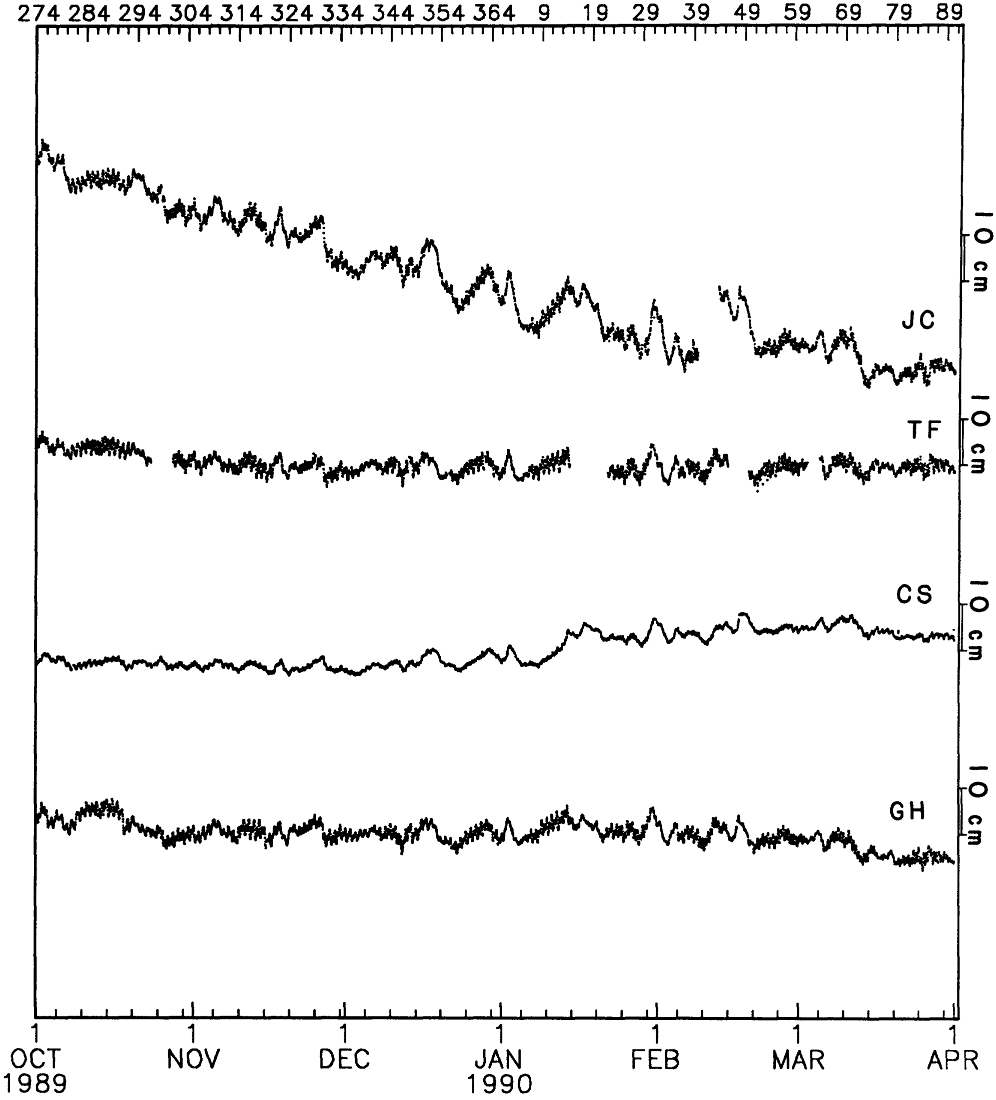

Figure 2. (d) Water level records plotted as in Figure 2(a).

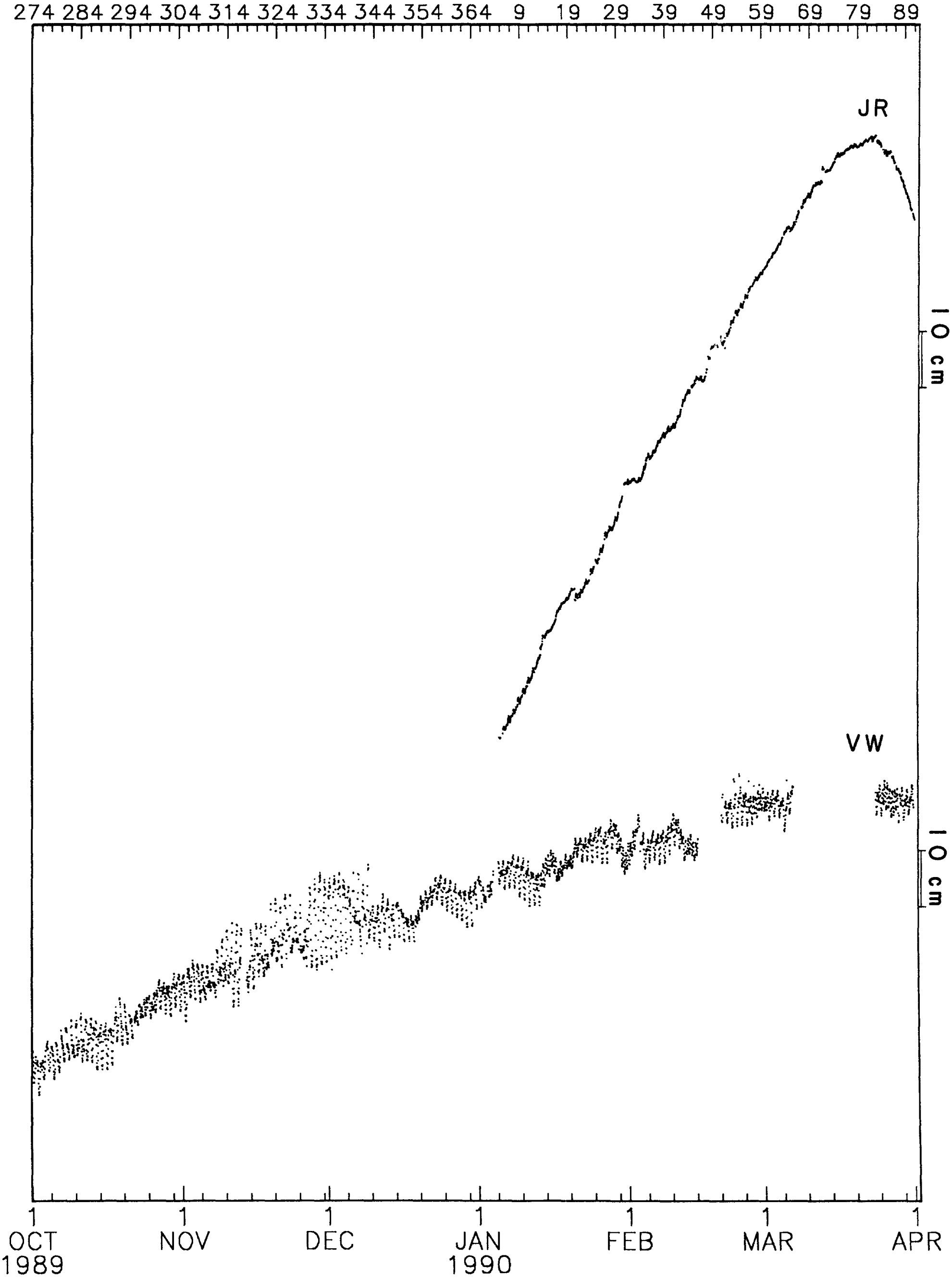

Figure 2. (e) Water level records plotted as in Figure 2(a).

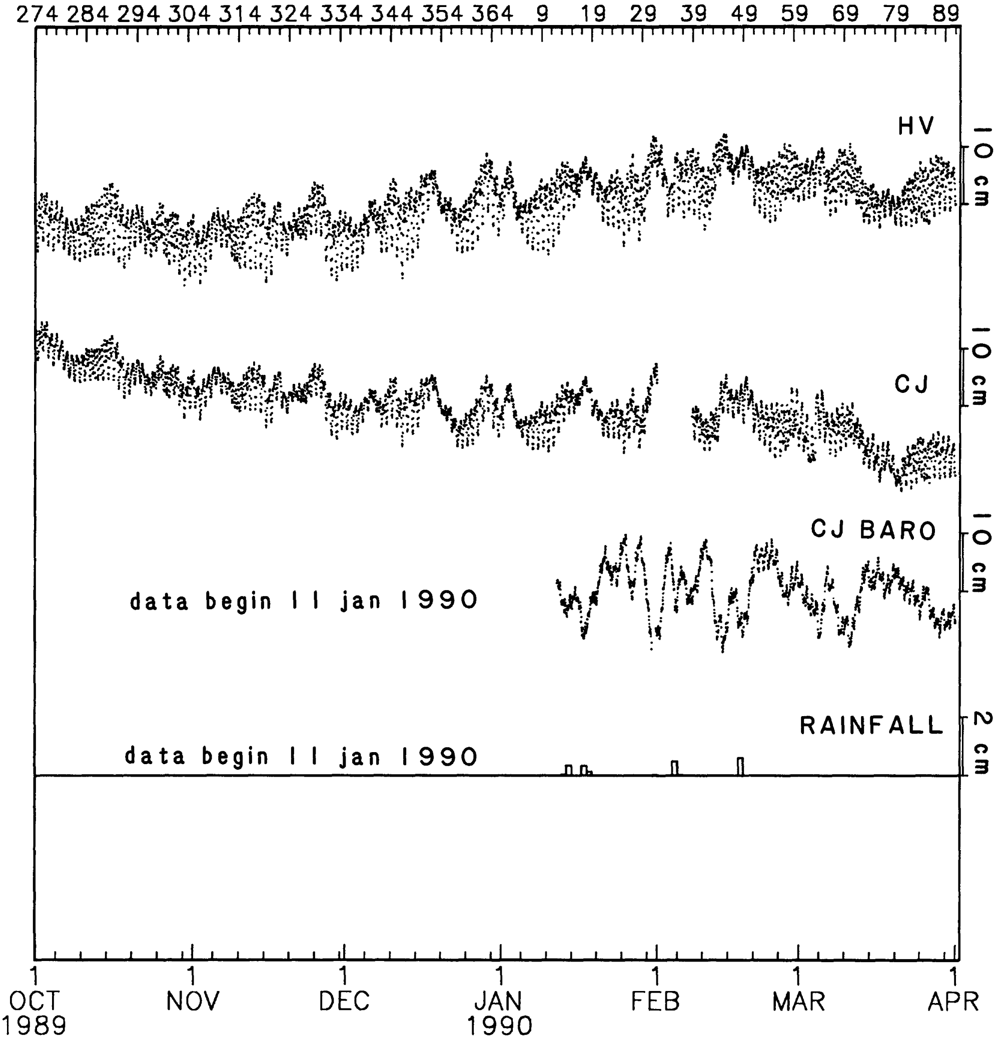

Figure 2. (f) Water level, rainfall, and barometer records plotted as in Figure 2(a).

Accurate Three-Dimensional Calculations for Advancing Slip Zones in the Earth's Crust

(Joint funding with NSF Grant EAR-8707392)

J. W. Rudnicki and L. M. Keer
Department of Civil Engineering
Northwestern University
Evanston, Il 60208
(708)-491-3411

(For period September 16, 1989 to April 15, 1990)

Objectives

Understanding the mechanism by which slip is transmitted from depth to the surface and along the strike of the fault from freely slipping to locked zones is of great importance for understanding the earthquake process and for possibly anticipating damaging events. A major impediment to more accurate and realistic analyses has been the difficulty of making calculations for three dimensional cracked bodies. We are doing three-dimensional analysis of slip zones (cracks) in an elastic half-space to determine stresses and surface deformations due to the advance of shear faults into locked, or more resistant, portions of the shallow crust. The goal of these studies is to understand three-dimensional geometric effects on the intensity of stressing near the edges of slip zones. Ultimately, we hope to develop theoretical models for the advance of slip zones into and around slip resistant portions of the fault, focussing particularly on the effects of nonuniformities in the advancing slip front.

Results

We are using the method of Lee et al. [1987], developed to analyze cracks in bimaterials. The method uses the integral representation for a distribution of body force and the elasticity solution for a point force near a bimaterial interface (free surface in the present application). The problem is then reduced to the solution of an integral equation for the unknown crack surface displacements over the two dimensional surface of the crack. Because the method uses the exact asymptotic form of the displacement field near the edge of the crack in discretizing the kernel of the integral equation, the results are accurate. In particular, we calculate the stress intensity factors (coefficients of the singular stress field at the edge of the slip zone) and energy release rate (per unit area of slip zone advance).

An auxiliary program uses the slip surface displacements to calculate displacements at the free surface since these are the quantities that are most easily observed. The method uses convolution of the displacements calculated for the slip surface with the Green's function for a unit point dislocation in a half space. The latter is calculated from Mindlin's solution for a point force in a half-space.

The effect of the free surface has been examined by comparing the computed stress intensity factors and energy release rates for various geometries, loadings and depths with those for shear cracks in infinite bodies. Two features are evident from this comparison. First, if the distance from the free surface to the fault center is greater than the vertical or downdip length of the fault, the difference between results for the half-space and for the full space are less than 10%. Second, for inclined faults near the free surface shear slip and relative normal displacement are coupled. More specifically, if the normal stress change on the fault is assumed to be zero, reverse dip-slip faults tend to interpenetrate and normal dip-slip faults tend to open. This effect has been noted previously in two-dimensional problems by Dmowska and Kostrov [1973] and has been discussed by Dmowska and Rice [1986].

As an application of these results, we have re-examined coseismic geodetic data from three earthquakes: 1966 Parkfield, 1983 Borah Peak and 1987 Whittier Narrows. The geometries inferred for these events are similar to those obtained by others. In constrast to models in which the slip is prescribed (kinematic models), our approach constrains the stress drop directly, by adjusting it to fit the observations, and determines the moment from the calculated slip distribution. In addition, we are able to calculate the energy release rate. If the slip zone is assume to propagate according to the critieria that the energy release rate equals a critical value, then the comparison with observations yields an estimate for the critical energy release rate at the termination of rupture.

The Whittier Narrows event is modeled as dip-slip of an inclined circular crack embedded in an elastic half-space. The shear stress drop is applied in the reverse sense. For the best model, which matches well the uplift data reported by Lin and Stein [1989] and is consistent with the aftershock locations, the radius is 3.0 km, the depth of the fault center is 14.2 km and the dip angle is 40 degrees. The total rms misfit is 5.8 mm, slightly larger than the rms pure error (4.9 mm). The stress drop and moment determined for the preferred model are 16 MPa and 10^{25} dyn cm, respectively. These values differ by less than 10% from the results of Lin and Stein. The energy release rate is approximately constant along the fault front and is essentially identical to that for a slip zone of the same size and stress drop in an infinite body. The value is approximately 2.0 x 10^{8} J/m^{-2}.

The coseismic line length changes for the 1966 Parkfield earthquake [King et al., 1987] are modeled using a vertical elliptical shear crack embedded in an elastic half-space. The shear stress drop is applied along the strike direction. The top, bottom and horizontal extent of the preferred model are 1.75, 15.75 and 50 km respectively. Although the area of the model fault plane is moderately larger than the region defined by the aftershocks, the mean misfit to the data is significantly smaller (by 20%) than for models having slip areas much less than the aftershock region. The mean misfit of the preferred model is 21.4 mm which is lower than the average standard deviation of the data (22.5 mm).

The stress drop and moment determined are about 1.43 MPa and 7.2×10^{25} dyn cm, respectively. Our estimated moment is larger than the 4.1×10^{25} dyn cm obtained by King et al. [1987] using the dislocation approach and the $0.9\text{-}2.1 \times 10^{25}$ dyn cm inferred from surface waves by Tsai and Aki [1969]. The maximum energy release rate occurs near the top of the slip zone and is estimated to be approximately 1.5×10^{6} J m^{-2}. This value is consistent with the 0.8×10^{6} J m^{-2} estimated by Aki [1978] as corresponding to arrest of this earthquake.

For the 1983 Borah Peak event, we use a dip-slip crack model to study the coseismic surface deformation. Because Borah Peak is a surface breaking event, the dip-slip zone is approximated by a semi-elliptical geometry. The strike (150^{o}) and inclination (50^{o}) of our best model are similar to those of Barrientos et al. [1987], but the surface center of the slip zone is 3 km SE of theirs. The horizontal extension of 36 km and width along dip of 18.5 km for our model are larger than but close to those (26 km and 18 km) for their best model. A normal dip-slip is required over the surface of the fault.

Overall, the predicted values roughly match the observations but the rms error of the fit to data is large, about 70 mm, six times the rms pure error. Comparison of the predicted and observed values suggests that the assumption of uniform stress drop needs to be relaxed in order to improve the fit to the data. The stress drop and moment determined by our best model are 1.8 MPa and 2.4×10^{26} dyn cm, respectively, smaller than the 3.0 MPa and 2.9×10^{26} dyn cm inferred by Barrientos et al. using a single plane model (No stress drop and moment values were reported for their two plane model). The maximum energy release rate occurs where the slip zone breaks the earth's surface and is estimated to be 1.2×10^{6} J m^{-2}.

Because this event breaks the surface, there is a strong coupling between slip and normal relative displacement. When the normal stress change on the fault surface is specified to be zero, a mode I stress intensity factor K_I is induced that has a maximum value slightly exceeding the larger of K_{II} and K_{III}. If the normal relative displacement is required to be zero, the maximum tensile stress required to close the crack is about 110% of the applied shear stress drop. Surprisingly, a small compressive stress (about 7% of the applied shear) is required on the deepest portions of the fault. Apparently, this occurs because closure of the crack near the surface tends to cause the deeper portions to interpenetrate.

References

Aki, K., Origin of the seismic gap: What initiates and stops a rupture propagation along a plate boundary?, Proceedings of Conference VI, Methodology for Identifying Seismic Gaps and Soon-to-Break Gaps, Convened under auspices of National Earthquake Hazards Reduction Program, 25-27 May, 1978 (USGS Open-File Report 78-943), pp. 3-46, 1978.

Barrientos, S. E., R. S. Stein, and S. N. Ward, Comparison of the 1959 Hebgen Lake, Montana and the 1983 Borah Peak, Idaho, earthquakes from geodetic observations, Bull. Seismol. Soc. Am., **77**, 784-808, 1987.

Dmowska, R. and B. V. Kostrov, A shearing crack in a semi-space under plane strain conditions, Arch. Mech., **25**, 421-440, 1973.

Dmowska, R. and J. R. Rice, Fracture theory and its seismological applications, in **Continuum Theories in Solid Earth Physics** (ed. by R. Teisseyre), Polish Scientific Publishers, Warsaw, pp. 187-255, 1986.

Lee, J.C., Farris, T. N. and L.M. Keer, Stress intensity factors for cracks of arbitrary shape near an interfacial boundary, Engn. Frac. Mech., **27**, 27-41, 1987.

Lin, J. and R. S. Stein, Coseismic folding, earthquake recurrence, and the 1987 source mechanism at Whittier Narrows, Los Angeles Basin, California, Journal of Geophysical Research, **94**, 9614-9632, 1989.

King, N. E., P. Segall and W. Prescott, Geodetic measurements near Parkfield, California, 1959-1984, J. Geophys. Res., **92**, 2474-2766, 1987.

Tsai, Y.-B. and K. Aki, Simultaneous determination of the seismic moment and attentuation of seismic surface waves, Bull. Seismol. Soc. Am., **59**, 275-287, 1969.

Publications

Kuo, C., M. Wu, J. W. Rudnicki, and L. M. Keer, Intepretation of coseismic deformation data using three dimensional crack (stress drop) models (Abstract), presented at NSF/USGS Workshop on Crustal Deformation Measurement and Earthquake Mechanics, Morro Bay, California. March 18-22, 1990.

Wu, M., C. Kuo, J. W. Rudnicki, and L. M. Keer, Modeling of coseismic surface deformation using non-kinematic approach (Abstract), for presentation at the 1990 SSA Meeting.

Wu, M., J. W. Rudnicki, C. Kuo, and L. M. Keer, Surface deformation and energy release rates for constant stress drop slip zones in an elastic half-space, draft manuscript.

Interpretation of Slip-Induced Water Well Level Changes at Parkfield

14-08-0001-G1691

J. W. Rudnicki
Department of Civil Engineering
Northwestern University
Evanston, Il 60208
(708)-491-3411

(For period September 16, 1989 to April 15, 1990)

Objective

Properly calibrated water wells can function as inexpensive and sensitive strainmeters. Solutions predicting water well level changes due to slip are needed to infer fault slip history and distribution from observed water well level changes. Recent solutions for pore pressure changes induced by fault slip have demonstrated that the coupling between deformation and pore fluid diffusion can strongly affect the response of the well to slip, particularly if the well is close to the fault, and, consequently, the inference of fault slip from water well level changes. The objective of this study is to assess effects of coupling between deformation and diffusion on the inference of fault slip from observed water well level changes and to include these effects in the analysis of observed water well level changes at Parkfield.

Results

We have been using the model of Rudnicki and Hsu [1988] to investigate coupled deformation - diffusion effects in ten creep-related water level changes observed since January, 1987 in the well at Middle Mountain near Parkfield. Because the original calculations of Rudnicki and Hsu assume a ramp time function for the introduction of slip, we have modified the calculations to include an exponential time function and a slip function suggested by Wesson [1988] as a good model of near-surface creep. The latter appears to describe well the observed creep near Middle Mountain.

Preliminary comparisons of the calculated water level changes with those observed suggest that the coupling between deformation and diffusion plays a limited role in these observations. There appear to be at least two reasons for this. The first is that the rise times of the slip events are very short. Thus, as indicated by the analysis of Rudnicki and Hsu [1988], even though the Middle Mountain well is quite close to the fault (460 m), the response approaches that of an ordinary elastic solid with the undrained constants. Furthermore, for some events, the observed water level changes are sharper (shorter rise time) than the slip. This cannot be explained by simple coupling of deformation and diffusion, but could occur because of differences in the slip at depth and at the surface.

A second reason for the discrepancy between calculations and observations is that decay of the water well change appears to be dominated by vertical flow to the free surface. Because the coupled-deformation diffusion solutions are for infinite bodies, this effect is not included. Consequently, we are concentrating on attempting to determine the portion of the decay in the deep segment of the well [Roeloffs et al., 1989] that can be attributed to deformation coupled with horizontal flow.

References

Roeloffs, E.A., S.S. Burford, F.S. Riley and A. W. Records, Hydrological effects on water level changes associated with episodic fault creep near Parkfield, California, J. Geophys. Res., 94, 12,387-12,402, 1989.

Rudnicki, J. W. and T.-C. Hsu, Pore pressure changes induced by slip on permeable and impermeable faults, J. Geophys. Res., 93, 3275-3285, 1988.

Wesson, R. L., Dynamics of fault creep, J Geophys. Res., 93, 8929-8951, 1988.

Use of Stress Drop Models to Interpret Geodetic Measurements at Loma Prieta

14-08-0001-G1847

J. W. Rudnicki, M. Wu and L. M. Keer
Department of Civil Engineering
Northwestern University
Evanston, IL 60208-3109
(708)-491-3411

(For period January 1, 1990 to April 15, 1990)

Objective

Surface deformation due to slip in the earth's crust is typically interpreted using the well-known dislocation method. Here, we employ an alternative approach in which slip regions are approximated by planar zones of prescribed stress drop (rather than relative displacement, i.e., dislocation). By applying this approach to the observed coseismic geodetic data associated with the 1989 Loma Prieta, California, earthquake, we are able to obtain estimates for the slip induced stress drop and moment, and the critical energy release rate at the termination of rupture.

Results

The Loma Prieta event is modeled as shear slip of an inclined elliptical crack embedded in an elastic half-space. The shear stress drop is assumed to be uniform with a component $\Delta\tau_s$ along the strike and a component $\Delta\tau_d$ along the dip direction of the fault. The resulting slip is calculated using the method of Lee et al. [1987]. Normal relative displacement over the fault plane, which tends to occur because of the free surface, is constrained to be zero. A fairly large set of forward searches was performed to find the model parameters that give a best fit to the observed coseismic geodetic data [Prescott, personal communication, 1990] subject to the constraint that the fault geometry agrees roughly with the aftershock locations [USGS staff, 1990].

Except for two lines lpl - lp2 and lpl - brush 2, most of the data are consistent with a right-lateral slip. In addition, a reverse dip slip is required. The fit of the preferred model to the geodetic data without these two lines is provided in Table 1. The mean misfit is 57 mm. The mean misfit to all data (including lpl - lp2 and lpl - brush 2) is 91 mm, 40% larger than for the case excluding these two lines. We suspect that these two lines are affected by local surface cracking and they are neglected in this study. The surface center of the best model is at x = 121° 48′ 30″ longitude and y = 37° 3′ 10″ latitude, about 5 km east of the main shock location. The inclination angle (downdip), the depth of the fault center, the fault length, and the fault width are about 72°, 11 km, 55 km, and 20 km, respectively. The shear stress drops determined by minimizing the difference between the observed and predicted surface deformation are $\Delta\tau_s$ =

1.1 MPa and $\Delta\tau_d$ = 1.4 MPa. The calculated geodetic moment is 2.5 x 10^{19} Nm. The maximum energy release rate (energy released per unit area of fault advance) occurs near the top of the fault and is estimated to be 5.5 x 10^6 Jm^{-2}. If it is assumed that the slip propagated according to the criterion that the energy release rate is equal to a critical value, then the estimated value is the critical energy release rate corresponding to arrest of the earthquake. The slip over the fault surface is distributed approximately elliptically . The average slips in the strike and (reverse) dip directions are $[\bar{U}_s]$ = 1.0 m and $[\bar{U}_d]$ = 0.8 m, respectively.

The geodetic moment, the dipping angle, and the ratio between strike and dip slip are very close to those (3.5 x 10^{19} Nm, 70°, and 1.3) reported by Savage (cited by McNally et al. [1989]). The magnitudes of our strike and dip slip are smaller than Savage's (1.7 m and 1.3 m) because our best model prefers a fault geometry having a larger area. If we use the geometry suggested by Savage, the mean misfit to data is increased to be 84 mm. The mean misfit to all data for this geometry is 99 mm.

References

Lee, J. C., Farris, T. N. and L. M. Keer, Stress intensity factors for cracks of arbitrary shape near an interfacial boundary, Engn. Frac. Mech., 27, 27-41, 1987.

McNally, K. C., Lay, T., Protti-Quesada, M., Valensise, G., Orange, M., and R. S. Anderson, Santa Cruz mountains (Loma Prieta) earthquake, EOS, Trans. AGU, 70, 1463-1467, 1989.

USGS Staff, The Loma Prieta, California, earthquake: An anticipated event, Science, 247, 286-293, 1990.

Table 1. Fit of Model to Geodetic Data

STATION - STATION		Observed (mm)	Calculated (mm)	Residual (mm)
<u>Line Length Changes</u>				
american	loma use	-76.5	9.8	-86.3
biel	loma use	231.6	154.2	77.4
fair	lp1	-290.0	-273.5	-16.5
llagas	lp1	-53.0	-22.6	-30.4
allison	loma use	109.3	119.2	-9.9
eagle rk	loma use	265.1	170.1	95.0
hamilton	loma use	21.8	71.6	-49.8
lp1	vargo	-198.4	-273.1	74.7
lp1	lp4	-203.8	-259.6	55.8
lp1	pr 6	-274.1	-245.3	-28.8
p4	p5	47.0	13.2	33.8
p5	chamb 6	-24.0	5.2	-29.2
p5	chamb 2	-40.0	0.0	-40.0
p5	p6	93.0	-3.7	96.7
hat crk	brush 2	-50.0	-43.8	-6.2
mojave	brush 2	0.0	14.8	-14.8
lp1	allison	17.2	100.4	-83.3
lp1	eagle rk	220.3	169.4	51.0
lp1	hamilton	-13.6	55.4	-69.0
<u>Relative Elevation Changes</u>				
lp1	allison	-149.0	-129.3	-19.7
lp1	eagle rk	-225.0	-170.3	-54.7
lp1	hamilton	-146.5	-119.9	-26.6
lp1	brush 2	-47.0	-132.9	85.9

Total Mean Misfit ------- (rms) = 57.0 mm

Observed Changes are given with the conventions: Post-Seismic value - Preseismic value, and Station B - Station A.

Hydrogen and Other Non-Radon Geochemical Monitoring

Project #9980-02773

Motoaki Sato* and J. Michael Thompson**
Branch of Igneous and Geothermal Processes
U.S. Geological Survey
* MS-959, Reston, VA 22092; ** MS-910, Menlo Park CA 94025
(703) 648-6766, FTS 959-6766

INVESTIGATIONS

We continuously monitor soil hydrogen at 1.5 m depth along the San Andreas and Calaveras faults in central California. There are 4 telemetered monitoring sites in the Hollister area, and 7 sites in the Parkfield area (Fig. 1). Five sites in the Parkfield area are now equipped with duplicate sensors installed 17 m apart.

We also continuously monitor water conductivity, dissolved CO_2, and dissolved H_2 of pumped water from two wells, one drilled into the San Andreas fault zone and the other about 500 m from the fault (filled triangles in Fig. 1).

RESULTS

Soil Hydrogen

1. Hollister Area

Telemetered data from 4 sites (Shore Road, San Juan Bautista, Cienega Winery, Melendy Ranch) are shown in Fig. 2. There are no duplicate sensors at these sites. During the semi-annual maintenance visit in mid-November, two sites were found to be malfunctioning.

The sensor at San Juan Bautista site, which was refurbished in June 1989 and recorded distinct precursory changes prior to the Los Gatos earthquake of 8/08/89 (NEHRP Tech. Rpts, XXIX, p.226), was destroyed in late August by modernized farming operation that tilled the ground much deeper than in previous 7 years. The sensor was repaired and relocated to a safer location on 11/15. There was an abrupt decrease on 2/17.

Cienega Winery site was planned to be renovated in November upon the completion of the sensor duplication work in the Parkfield area. The old sensor was not equipped with an in-situ feeder for the calibration gas, and could not be tested in situ. It was rebuilt and installed with a feeder on 11/20. This site had a 100-ppm peak followed by a complex changes between 2/04 and 3/17.

Melendy Ranch site recorded pronounced increase in diurnal changes in mid-September and a very brief (2 hours) but moderately large (600 ppm) peak on 10/10/89, 8 days prior to the Loma Prieta earthquake. This site recorded an abrupt increase in H_2 activity on 1/19/89 after a 6-month period of quiescence (Fig. 3). The H_2 changes subsided by mid-November. If H_2

anomalies, which are not generally coincident to meteorological factors except for diurnal emission (much data available on request), are considered to be intermediate-term tectonic precursors, the recorded changes may be recognized as precursory to the Loma Prieta earthquake. The lack of supporting data from San Juan Bautista and Cienega Winery make the correlation less pursuasive, though the latter sites were proven to be malfunctioning at the crucial time. A 50-ppm peak was recorded at Melendy Ranch on 1/15.

2. Parkfield Area

Telemetered data from 7 sites (12 sensors) are shown in Figs. 4A (Slack Canyon, Middle Mountain, Parkfield), 4B (Work Ranch, Gold Hill), and 4C (Taylor Ranch, Twisselman Ranch, and rain data from Vineyard Canyon).

Slack Canyon had a 200-ppm peak in mid-January, and small complex changes between 2/17 and 2/25. A sharp decrease occurred on 3/26, which returned to the baseline by 3/28.

Middle Mountain #1 started showing an increased diurnal emission on 3/18. The increase continues to April as shown in the figure. The second sensor started showing a steady drift to more negative voltages for an unknown cause. An instumental cause is strongly suspected. The data for this sensor is not shown in Fig. 4A.

Parkfield #1 started showing increased diurnal emission on 12/24. The increase continues to April, though it is not monotonous. Parkfield #2 seems to be suffering from an electronic problem since 12/23, although we had suspected failure of the voltage regulator.

Work Ranch site showed distinct H_2 activity on 3/19/90 for the first time since the installation of this site in May 1986. At least 6 sharp peaks up to 250 ppm H_2 were recorded concurrently by both sensors between 3/19 and 3/26, although air-zinc battery started expiring on 3/24, disrupting the records (Fig. 4B, also see Fig. 5 for details). Upon replacing the battery on 3/29, it became clear that diurnal emission definitely started at this site.

Gold Hill site, which had become dormant in the spring of 1989 after one and a half years of large changes, started showing increased diurnal emission almost constantly since mid-December. Even the baseline started to go up in early Aparil.

Taylor Ranch site was off power prior to 11/16. Taylor Ranch #1 recorded a complex pattern (Fig. 4C), which resembles that of dissolved H_2 monitored at Miller Ranch (Fig. 7). Taylor Ranch #2 seems to be reversely connected somewhere. When the data are inversely plotted (Fig. 4C), the data shows a general match with that of #1. The sensitivity of #2 is very low. The #2 sensor system will be scrutinized in the next visit.

Twisselman Ranch site had a loose solar panel connection and the battery went dead in early October. We resoldered the connection and replaced the battery in mid-November. Diurnal emission began increasing at this site in late March like other sites in the Parkfield area.

The duplicatability of soil hydrogen pattern at 50-feet separation was well demonstrated at Work Ranch and Gold Hill (Fig. 5). Although there were some differences in absolute values, the patterns were beautifully duplicated. Parkfield #2 and Middle Mountain #2 are suffering from diurnal changes of the signal due to solar-power supply voltage fluctuations (voltage regulator not functioning), which are larger than the true diurnal emission signal of the sensor.

Dupliation of H_2 pattern does not seem to be limited to a distance of 50 feet. In Fig. 6, dissolved H_2 in pumped water at Miller Ranch, soil H_2 based on solar-panel operation (sensor #1 with functioning voltage regulator) at Parkfield, and soil H_2 based on power-line operation at Taylor Ranch are compared for a period of no rain (3/05 -4/01). Barometric pressure recorded at Middle Mountain is also shown. There seem to be a general resemblance of the H_2 pattern among the three adjacent sites, and the general pattern is not clearly correlatable to barometric pressure changes. Furthermore, there appears to be a general trend of increassing hydrogen emission throughout the Parkfield area at the end of this reporting period.

Water Geochemistry

1. Miller Ranch

Water conductivity, dissolved CO_2, and dissolved H_2 data recorded at this site are shown in Fig. 7. Conductivity showed an abrupt decrease of about 400 micro-Siemens on 10/18/89, 10 minutes after the Loma Prieta earthquake. It returned to the normal level by 12/01. Dissolved CO_2 was high immediately after the servicing on 11/17, but it decreased irregularly until 1/08/90 and then settled on the pre-service baseline. So far we have not been able to determine the cause for the behavior. An instrumental problem is strongly suspected. Dissolved H_2 did not show abrupt changes. Its pattern resembled those of soil H_2 recorded by Parkfield #1 and Taylor Ranch #1.

2. Taylor Ranch

The recorded data are shown in Fig. 8. Because of breakdown of metering pump on 8/02/89, the power for the monitoring system was turned off by local personnel prior to the maintenance service performed on 11/16. The system worked well until 1/22/90, when the main pump stopped due to the area-wide power failure. This produced a domino effect on the metering pump, which subsequently failed due to the clogging of the bubbler by iron oxides in the stagnant degassing chamber. A design modification to avoid the problem will be made in the next maintenance visit.

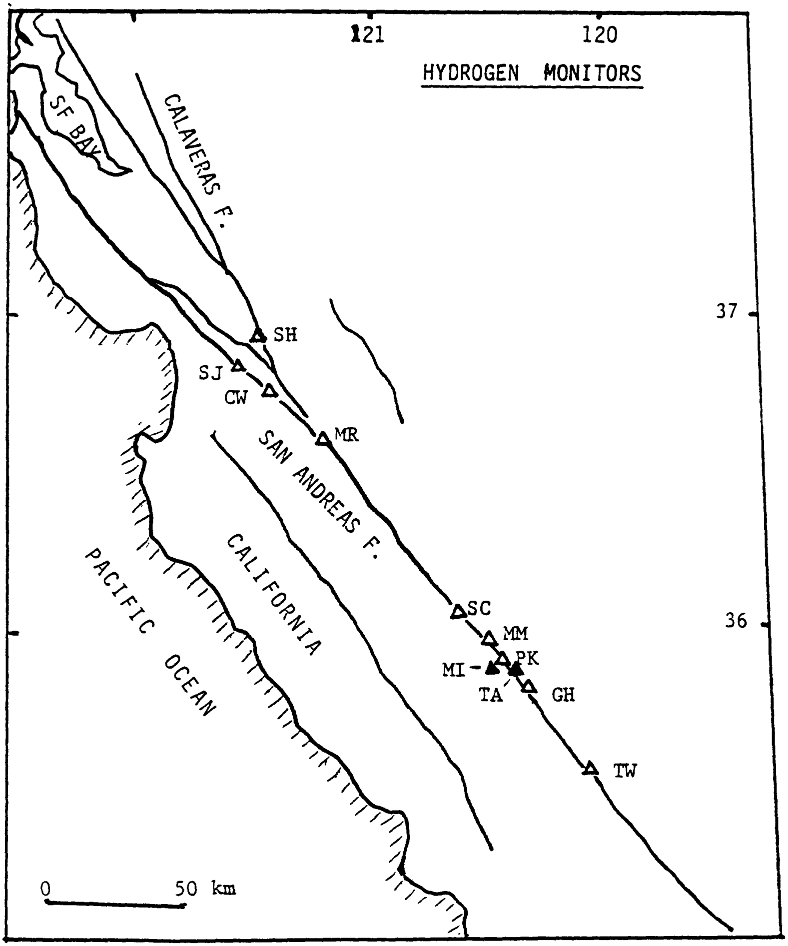

(Fig. 1) Location map for the hydrogen monitoring sites in central California. The sites marked with filled triangles also have other monitors for pumped water.

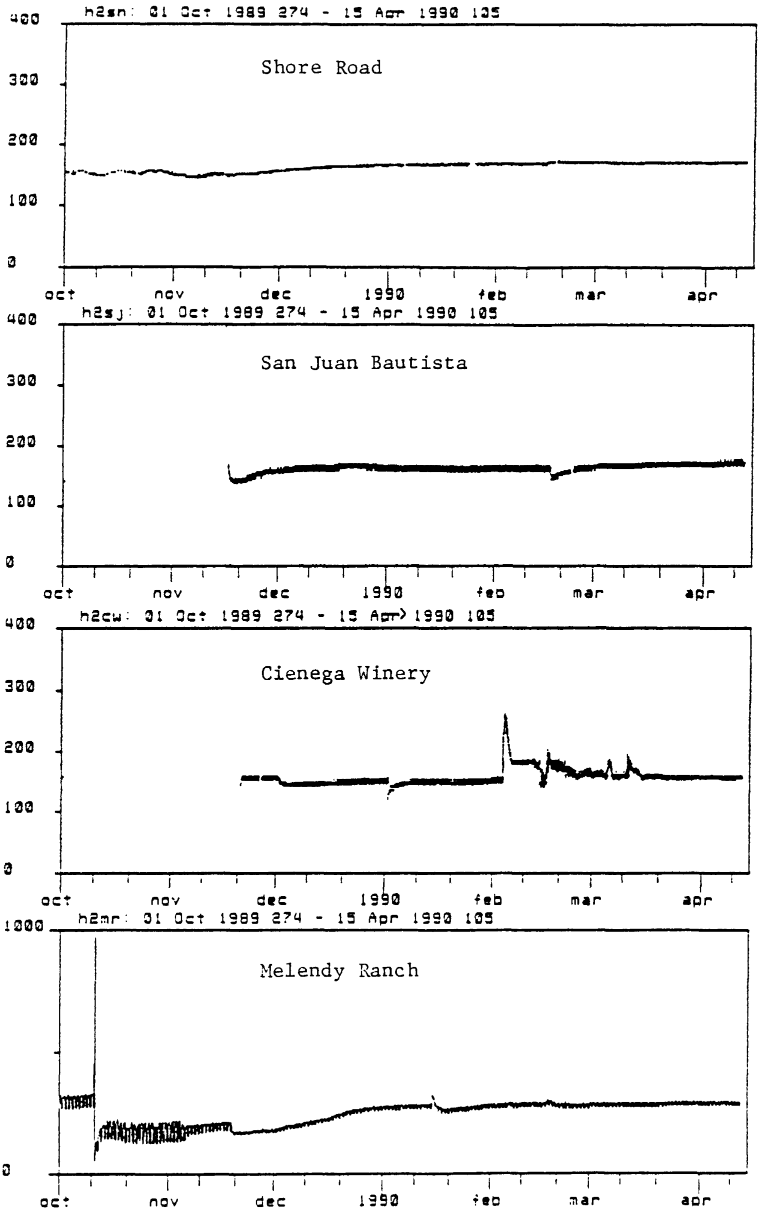

(Fig. 2) Soil hydrogen data recorded in the Hollister area. The vertical axis is H_2 concentration in ppm.

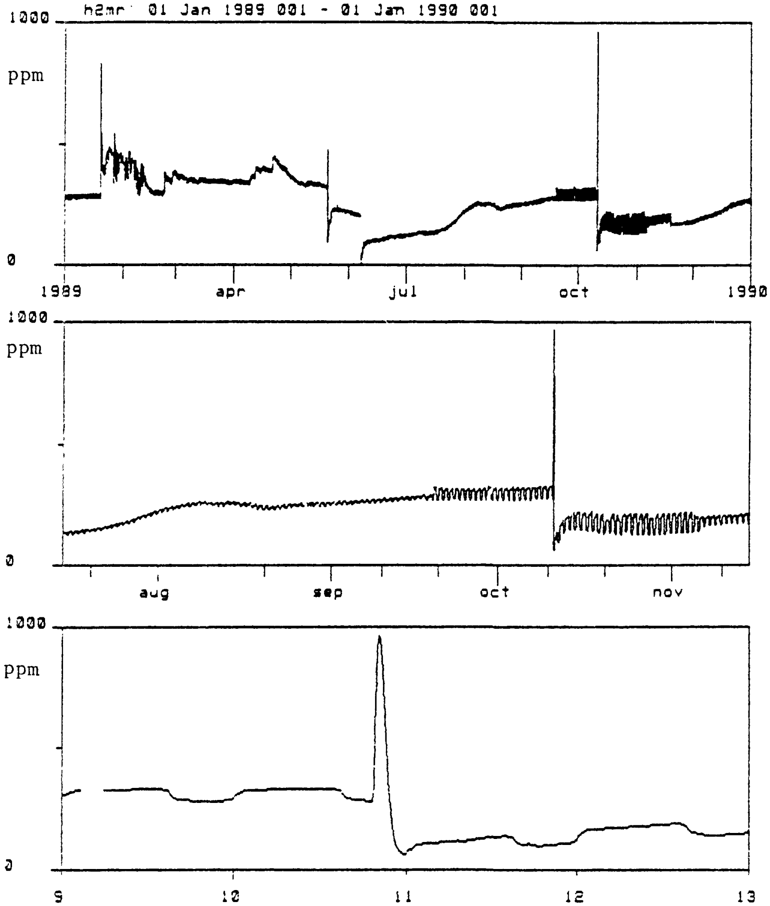

(Fig. 3) Soil hydrogen data recorded at Melendy Ranch prior to and around the time of the Loma Prieta earthquake of 18 October 1989.

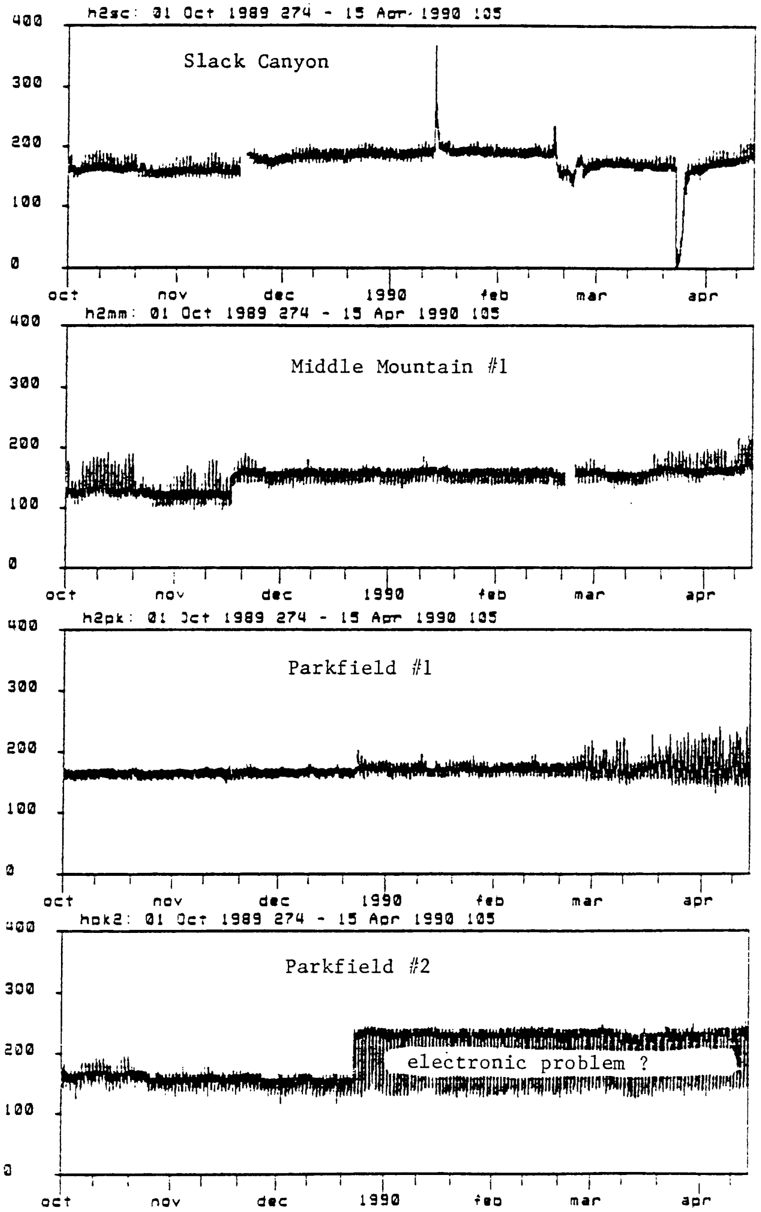

(Fig. 4A) Soil hydrogen data recorded in the Parkfield area. The vertical axis is H_2 concentration in ppm.

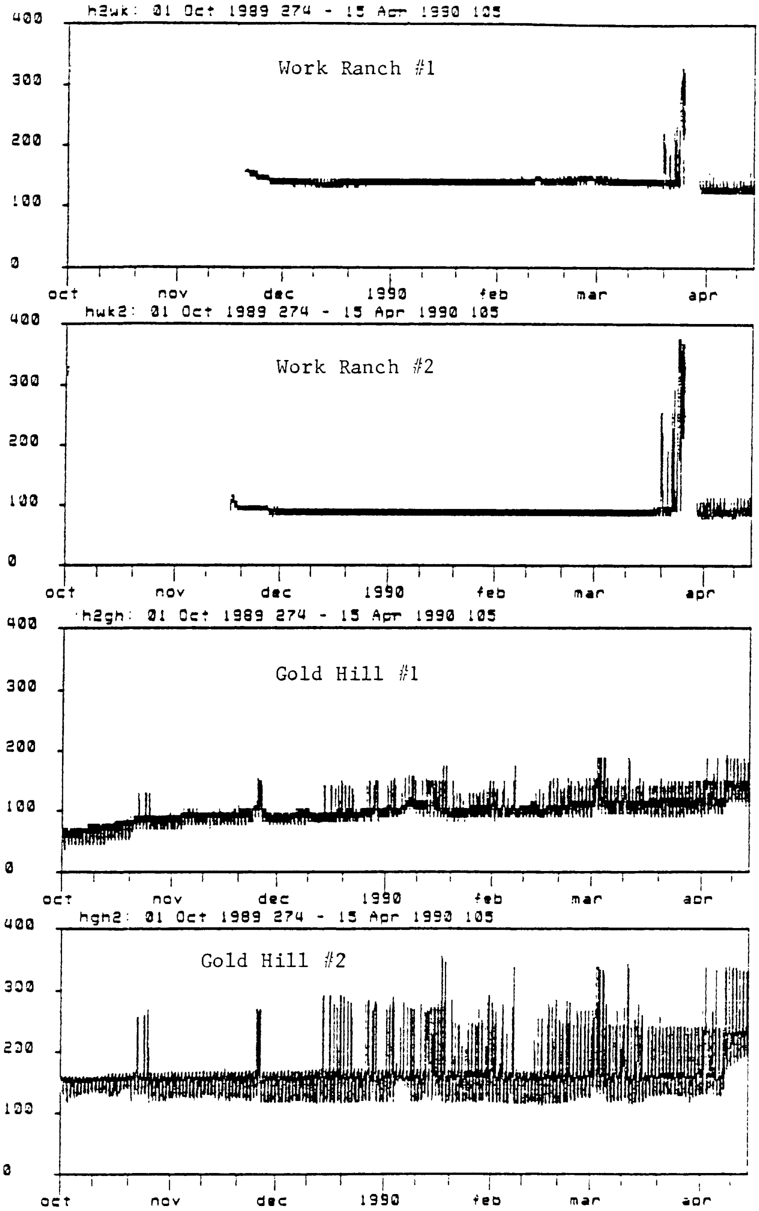

(Fig. 4B) Soil hydrogen data recorded in the Parkfield area.

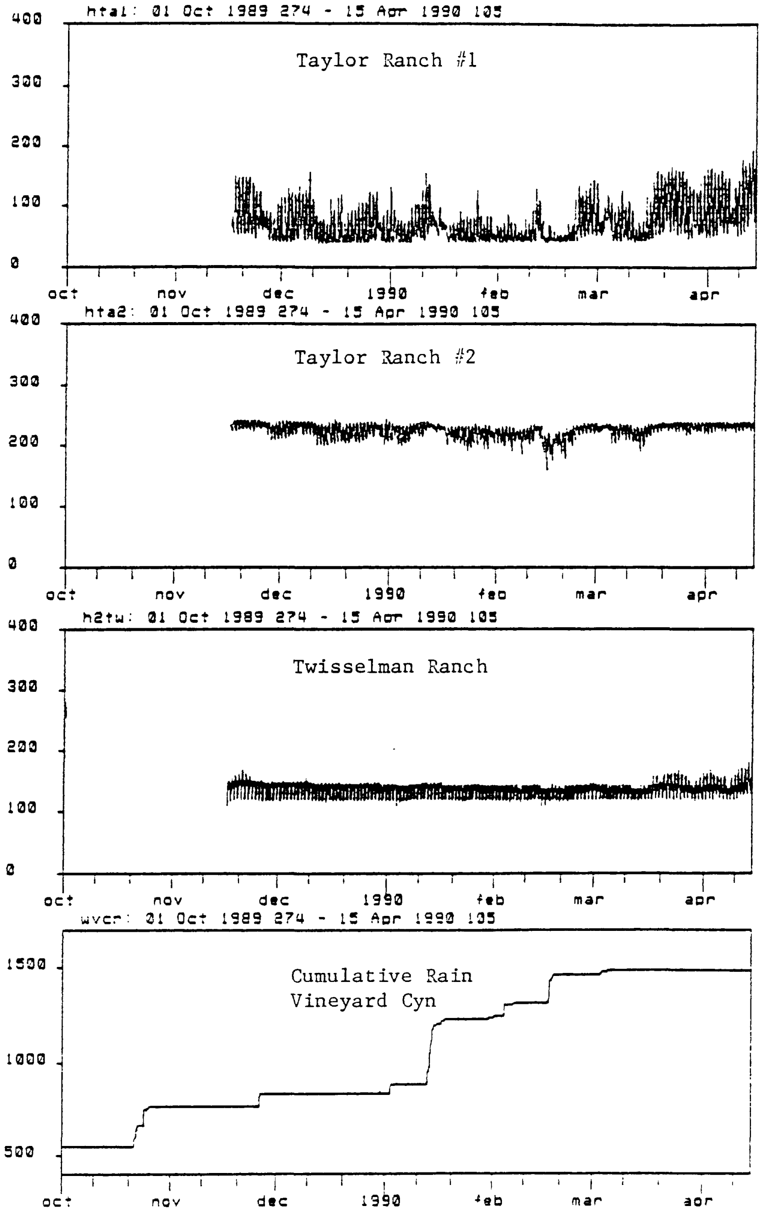

(Fig. 4C) Soil hydrogen data recorded in the Parkfield area and cumulative rain.

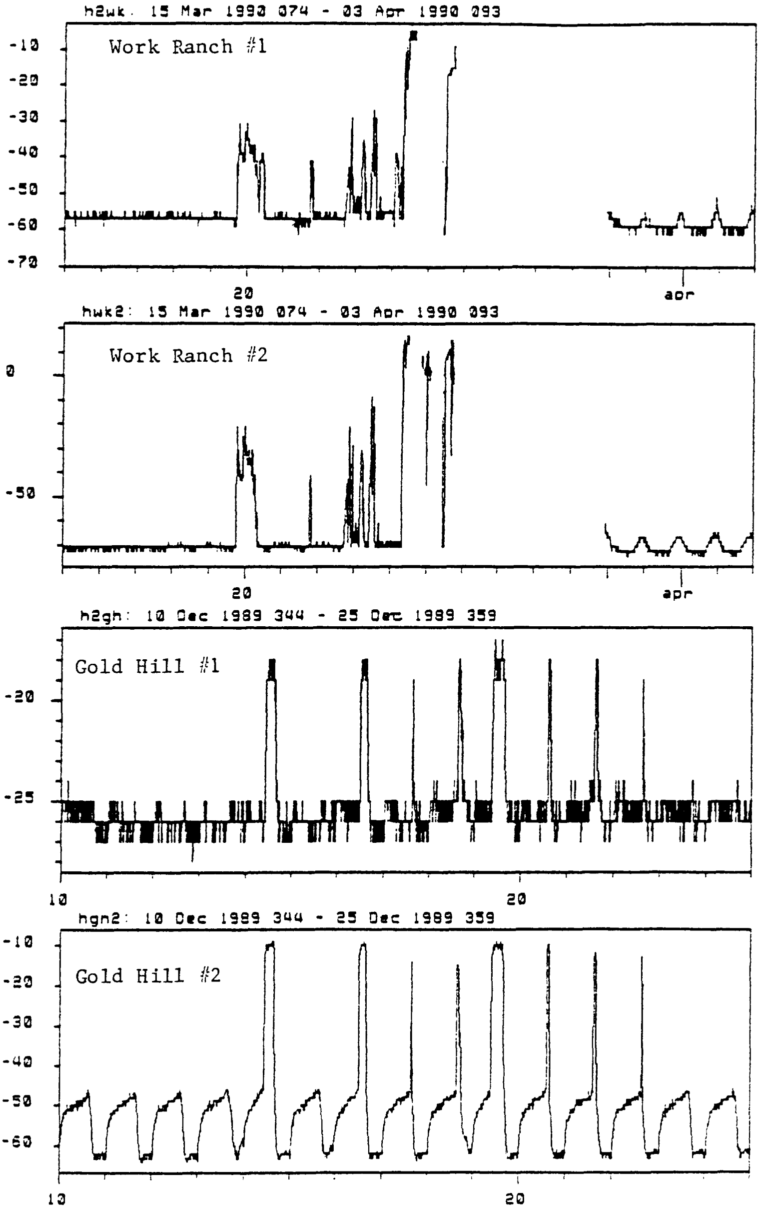

(Fig. 5) Soil hydrogen data recorded by duplicate sensors 50 feet apart. The vertical axis is H_2 sensor signal in telemetry counts.

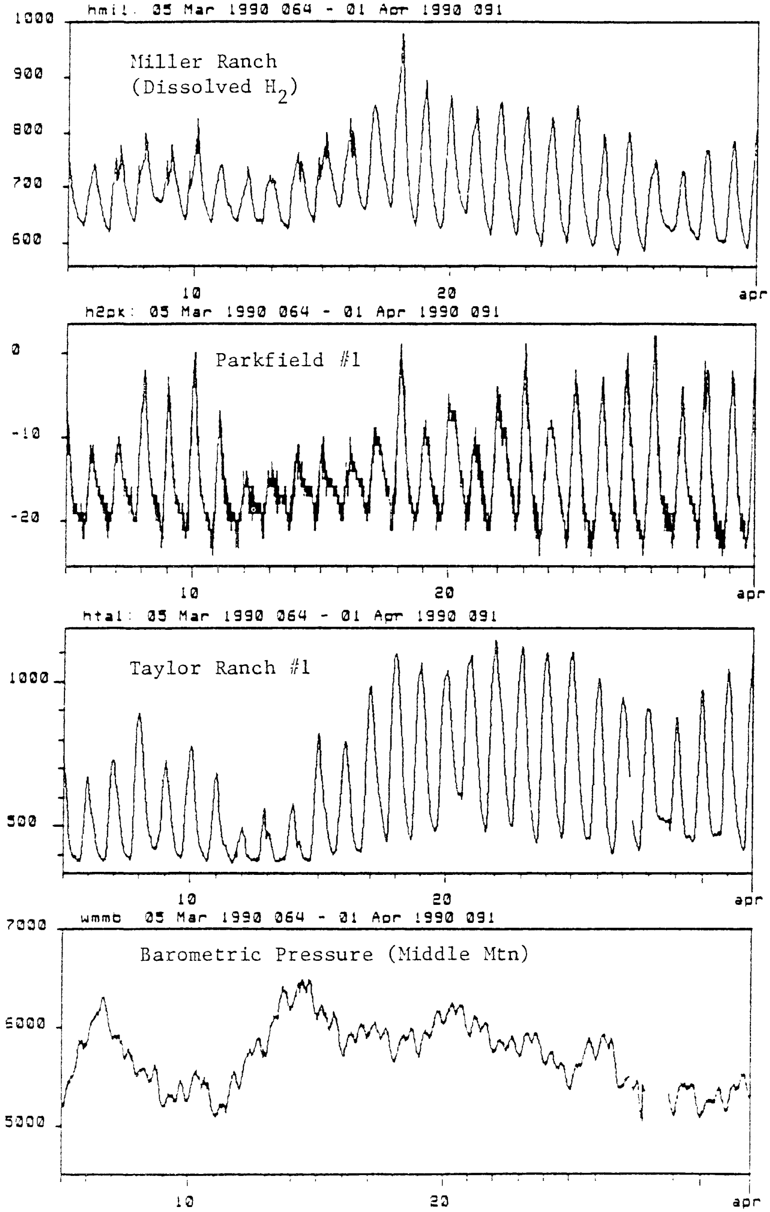

(Fig. 6) Comparison of hydrogen data and barometric pressure in the vicinity of Parkfield.

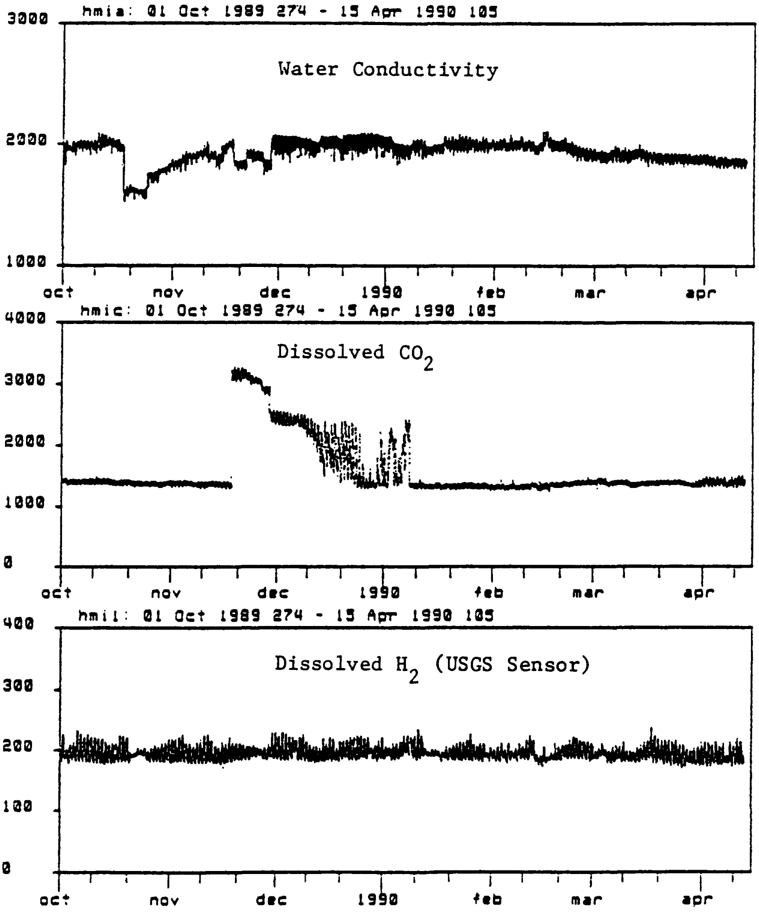

(Fig. 7) Water conductivity, dissolved CO_2, and dissolved H_2 monitored at Miller Ranch, about 500 m from the San Andreas fault in the Parkfield area.

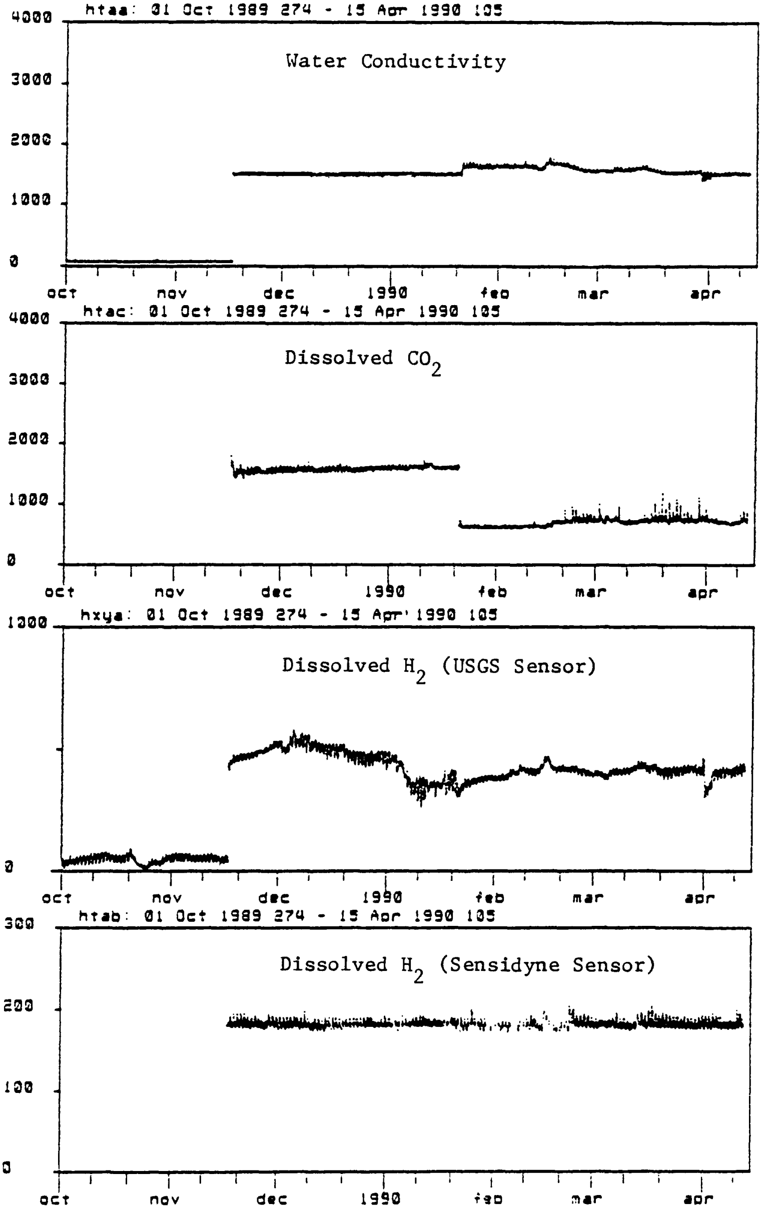

(Fig. 8) Water conductivity (in micro-Siemens), dissolved CO_2, and dissolved H_2 data recorded at Taylor Ranch.

Quantitative Analyses of Shear-wave Polarizations and Inversion for Shear-wave Splitting Parameters

14-08-0001-G1767

Peter M. Shearer
Institute of Geophysics and Planetary Physics
Scripps Institution of Oceanography
University of California, San Diego
La Jolla, CA 92093
(619) 534-2260

Investigations

Our research in the last six months has focused on developing quantitative methods for analyzing shear-wave polarizations, applying these techniques to data from three-component seismic arrays, and evaluating recent claims that temporal changes in polarizations caused by shear-wave splitting may be useful in predicting earthquakes. Results of this work are described in detail in Aster et al. (JGR, in press, 1990), a brief summary follows.

Results

Several recent studies have claimed to observe temporal changes in shear-wave splitting delay times as seen by three-component recordings of local earthquakes (e.g., Peacock et al., *JGR* **93**, 3339-3356, 1988), and in some cases a correlation has been claimed between these changes and earthquake occurrence (e.g., Crampin et al., *JGR*, in press, 1990). The observational evidence for temporal changes in shear-wave splitting is based on the picking by eye of the shear-wave arrival and the onset of non-linear motion from polarization plots in the horizontal plane. This procedure, while suitable for preliminary observations, has several significant drawbacks: (1) the measurements are subject to possible subjectivity and observer bias, (2) measurements are time consuming for large data sets, (3) error bounds are lacking, and (4) motion out of the horizontal plane is not considered. In order to address these difficulties, we have developed quantitative methods for objectively measuring the polarization of three-component records, and have applied these techniques to the problem of estimating the degree and direction of polarization and the duration of the linearity interval for three-component recordings of local earthquakes.

We used these methods to examine hundreds of seismograms from the Anza Seismic Network in southern California. Our analysis shows that initial shear-wave polarizations at several Anza stations are aligned, regardless of the azimuth of the event. In order to test whether this might be a source effect, we calculated the S-wave polarizations predicted at individual stations using focal mechanisms obtained from P-wave polarity data. A comparison between these predicted polarizations and those actually observed (Fig. 1) shows that the alignment in the S-wave polarizations is not a source effect, and is most likely caused by shallow crustal anisotropy.

Plots of linearity interval vs. time show a great deal of scatter with no clear long term trends (Fig. 2). No evidence is found to support the assertion of Crampin et al. that temporal changes in shear-wave splitting delay time at station KNW are correlated with the occurrence of the North Palm Springs earthquake. A striking feature of these plots is the large amount of scatter in the observed linearity intervals. A simple model of shear-wave splitting due to an anisotropic layer beneath the stations cannot explain this scatter since it would predict nearly constant linearity intervals (i.e. shear-wave splitting delay times) for the data at each station. We believe that near-receiver scattering is the source of the variations in the observed linearity intervals, and that this scattering severely limits the accuracy with which shear-wave splitting delay times can be measured at these surface sites. We were able to identify a slight correlation between our measured linearity intervals and earthquake moment, presumably reflecting the longer source time functions for the larger events.

Much of the scatter in these measurements which is not associated with moment is probably due to path and source mechanism variations. In an attempt to find a subset of the data which might contain earthquakes with more repeatable properties, we searched the KNW seismograms for events with nearly identical waveforms. The similarity criteria used was $C3_{max}$, the maximum of the three-component circular cross-correlation function. We have identified 22 event pairs that were separated in time by more than 30 days and had values of $C3_{max}$ of 0.8 or better. Although these seismograms are not exact wiggle-for-wiggle duplicates (Fig. 3), they have higher values of $C3_{max}$ than 99% of all seismogram pairs considered and are the best available examples of repeated shear-wave sources recorded at KNW. Due to the waveform similarity in these seismogram pairs, we were able to use cross-correlation techniques for these events to obtain accurate measures of possible temporal variations in waveforms. In particular, we examined the possibility of time shifts between waveforms in the "slow" horizontal direction (H_2) relative to waveforms in the "fast" horizontal direction (H_1) which might be influenced by temporal variations in the shear-wave splitting delay time. To within 1 sample (0.004 s), however, the best lags for the H_2 and H_1 components are in agreement for all pairs, even those separated in time by more than 5 years. This result argues strongly for stability of the earth response over this approximately 7 year period. By extension, the large scatter in linearity times at KNW for the complete data set (Figure 2) must be due to source and ray path differences between earthquakes rather than to temporal changes in material properties along ray paths.

Reports

Aster, R., Shearer, P., Berger, J., Seismic polarizations at the Anza seismic array, southern California, *Seism. Res. Lett.*, **60**, no. 1, 11-12, 1989.

Aster, R., Shearer, P., Berger, J., Compressional- and shear-wave polarizations at the Anza seismic array, *Proc. 11th Annual AFGL/Darpa Seism. Res. Symp.*, **8**, 1989.

Aster, R., Shearer, P., Berger, J., Shear-wave polarizations at the Anza seismic array, *EOS Trans. AGU*, **70**, 15, 395, 1989.

Aster, R., Shearer, P., Berger, J., Shear-wave anisotropy at the Anza seismic network, *EOS Trans. AGU*, **70**, 43, 1211, 1989.

Aster, R., Shearer, P., Berger, J., Seismic polarizations observed with borehole instruments in the Anza seismic gap, *Seism. Res. Lett.*, in press, 1990.

Aster, R., Shearer, P., Berger, J., Quantitative measurements of shear-wave polarizations at the Anza Seismic Network, Southern California — implications for shear-wave splitting and earthquake prediction, *J. Geophys. Res.*, in press, 1990.

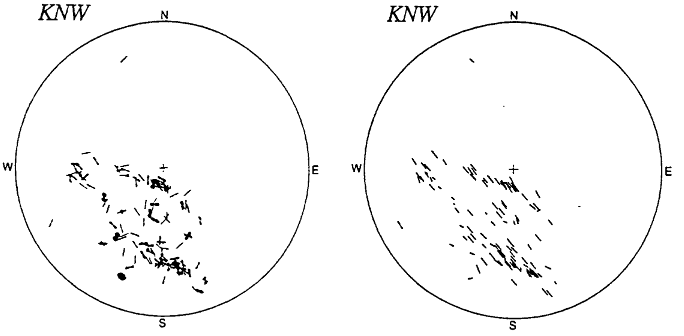

Figure 1. Initial shear-wave particle motion directions predicted from focal mechanism analysis (left) compared with those actually observed (right) for station KNW. Only the horizontal components are considered in these plots. The predicted alignments were obtained by ray tracing allowed source polarizations to the station for each earthquake. The plots at the right depict vector linearities obtained from 20 samples of the initial shear-wave arrival for each event. Notice that the observed alignments are not predicted by the scattered orientations obtained from the focal mechanisms.

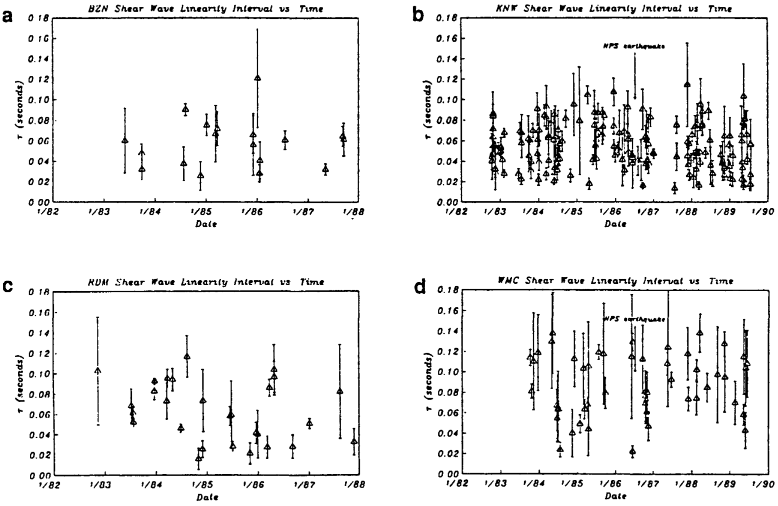

Figure 2. Linearity interval vs. time for events within the 45° shear-wave window for four Anza stations. The time of the North Palm Springs earthquake is indicated. Notice the large scatter in these times and the lack of any clear temporal trends.

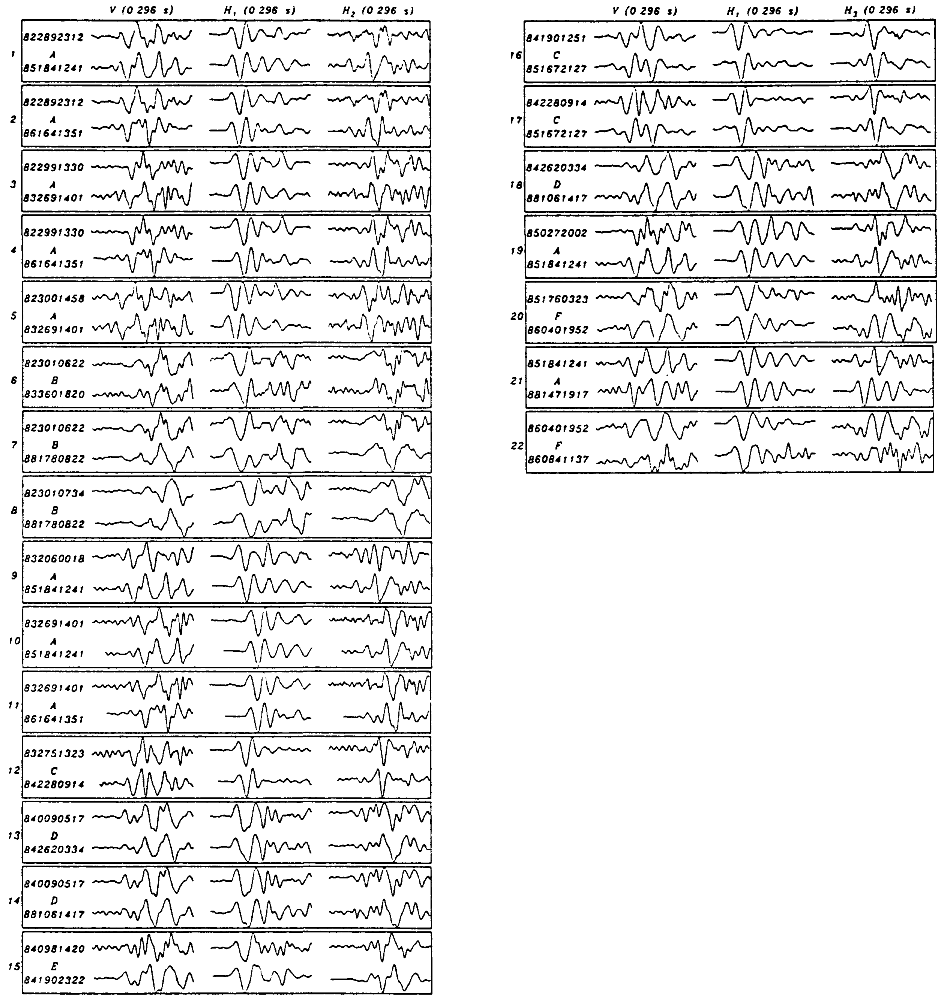

Figure 3. 74 samples (0.296 s) of the shear wave seismogram for similar pairs of events recorded at KNW. All traces have been aligned on the maximum of the 3-component cross-correlation function. Note that there are no large changes in the character of the waveforms or time shifts of the components for these pairs, which are separated by up to approximately 5.5 years.

An Absolute Long-Base Tiltmeter with Vertical Anchoring

14-08-0001-G1336

Frank K. Wyatt, Hadley O. Johnson,
Mark A. Zumberge, and Duncan Carr Agnew
Institute of Geophysics and Planetary Physics
University of California, San Diego
La Jolla, California 92093-0225
(619) 534-2411

This grant supports work on the design and construction of a long baselength tiltmeter intended for use in crustal deformation studies, and for the monitoring and evaluation of this instrument against existing systems at Piñon Flat Observatory (PFO). For long-base tiltmeters to be useful in crustal deformation measurement, they must be exceptionally stable, engineered for general use, and suitable for installation in a wide variety of locations. For the past few years we have been working toward these ends with much of the emphasis on design and testing of the equipment. We recently completed construction of a new 550-m instrument which fulfills most of these wants.

Figure 1 presents data collected from the new north-south tiltmeter — from the first day of operation to the present. (Our target date for instrument completion had been January 1, 1990; a date we missed by a mere month.) Owing to continued work on the instrument vaults this record is gappy, but none-the-less tells an interesting story. The long-term tilt rate, at 0.35 μrad/yr down to the south, is some three times larger than the tilt observed by the perpendicular long-base tiltmeters at the site, and so roughly equal to the maximum deformation rates expected directly over an active fault, slipping at depth. This may be real, as it generally matches the ground slope across Pinyon Flat. An important virtue of the new generation of deformation monitors — to some degree offsetting their cost and the effort involved in constructing them — is the immediate constraint they provide on the rate of secular deformation. Even over longer baselines, say 10 km, it would take many years of leveling to get similar results, and for GPS measurements it would take longer still.

It is possible that the magnitude of the observed signal is instrumental in origin. At this stage, the most likely source of error is from the optical-fiber anchoring system used to measure and correct for end-monument instability. So far the total deformation we have observed amounts to no more than 50 μm of differential motion, and all anchoring schemes must be viewed with suspicion at this level, at least until they have been given a chance to settle in. Because our optical-fiber anchoring system is a new technology we are especially uncertain of its quality. The redundancy of measurements at PFO provides us with a check on this. Secondary fibers are being monitored at the ends of the new instrument and will soon be edited and evaluated. Also, the north end of the new instrument shares a vault with an extension of the original east-west tiltmeter, allowing us to contraint its end-monument motion independently of the fiber measurements. Two other explanations for the larger-than-expected signal stem from the possibility that the tiltmeter's communicating fluid may not be in thermal equilibrium, because (1) so far only one end of the tiltmeter is air conditioned (though initial experiments indicate this is not a problem), and (2) we recently discovered that a remote section of the tiltmeter conduit is still unburied. Additional observations and further study should clarify the outstanding issues, and give us better confidence in the results.

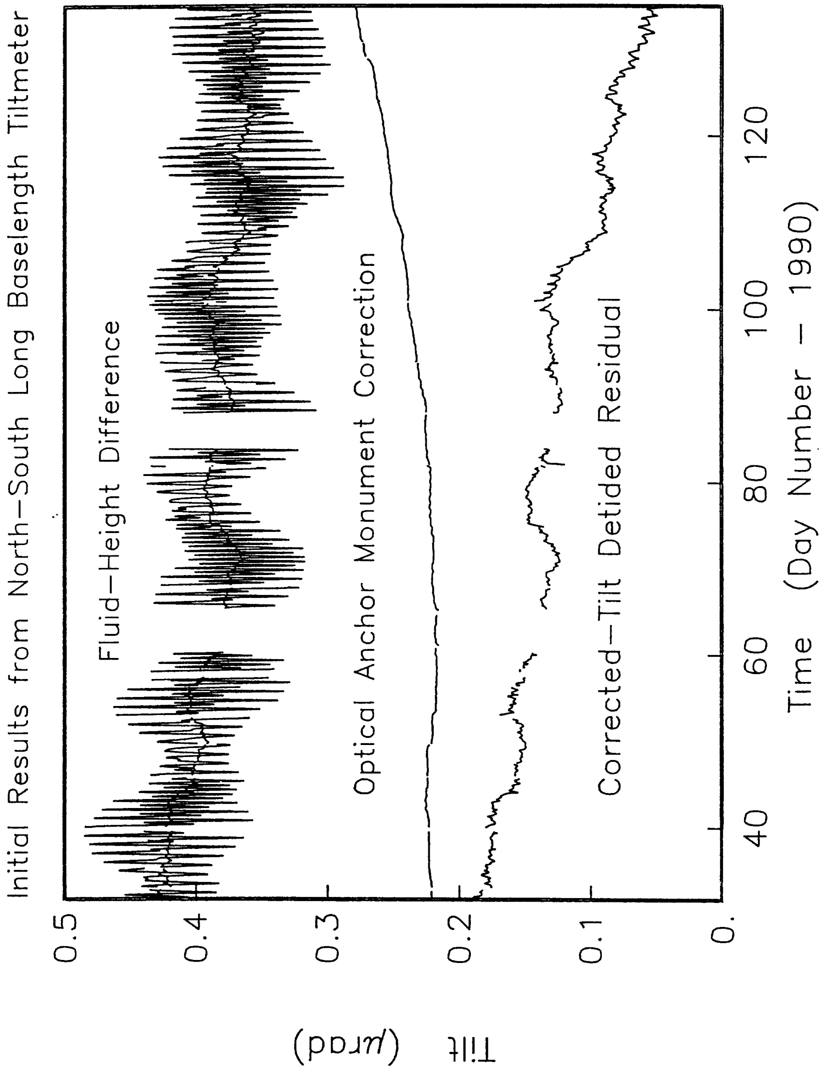
Initial Results from North–South Long Baselength Tiltmeter
Fluid–Height Difference
Optical Anchor Monument Correction
Corrected–Tilt Detided Residual
Tilt (μrad)
0.5
0.4
0.3
0.2
0.1
0.
40
60
80
100
120
Time (Day Number – 1990)

Figure 1.

Piñon Flat Observatory: Comparative Studies and Geophysical Investigations

14-08-0001-G1763

Frank K. Wyatt, Duncan Carr Agnew,
and Hadley O. Johnson
Institute of Geophysics and Planetary Physics
Scripps Institution of Oceanography
University of California, San Diego
La Jolla, CA 92093
(619) 534-2411

This grant provides support for our collaborative studies with those investigators conducting research at Piñon Flat Observatory (PFO) under the auspices of the U.S. Geological Survey. The main purpose of this work is to evaluate instrumentation developed for the measurement of ground deformation, the idea being to simultaneously operate a number of continuously recording sensors, and small geodetic arrays, and thereby to identify the merits and limitations of the various techniques. Good progress has been made by evaluating the instruments in a common setting.

Many research groups sponsored by the USGS NEHRP are currently active at the site. This report describes a few of these projects in detail.

Tilts from Parallel Long-base Tiltmeters

Particularly since its refurbishment in late 1987, Dr. John Beavan's 535-m Michelson-Gale water-tube tiltmeter has produced excellent data. The middle panel of Figure 1 shows the latest results. At this stage of its development this instrument runs nearly without maintenance, but is visited weekly for manual, absolute readings of the fluid height at the two ends. These observations are forwarded to Dr. Beavan, providing him with an independent measure of the secular tilt, and the means to evaluate the long-term stability of the tiltmeter's sensors. The original UCSD long-baseline tiltmeter at PFO has continued to operate well, though with some recent perturbations caused by temperature changes in the end-vaults because of utility problems (Figure 1, middle panel). The top panel of Figure 1 presents the corrected UCSD tilt record since fall 1982, when the end-monuments for this instrument were anchored.

Both long-base tiltmeters have shown remarkable stability. For the UCSD instrument, the long-term tilt rate is about 0.085 μrad/yr down to the west. The most conspicuous signal in this record is the large and long-lasting artifact produced when a 115-m extension tube was added in late 1986. This extension contained fluid of a slightly different density and the very slow mixing of these two fluids caused a transient ''tilt'' lasting nearly a year. Other variations are limited to amplitudes of roughly 0.1 μrad about the mean trend, and might very well be real. Further comparison with

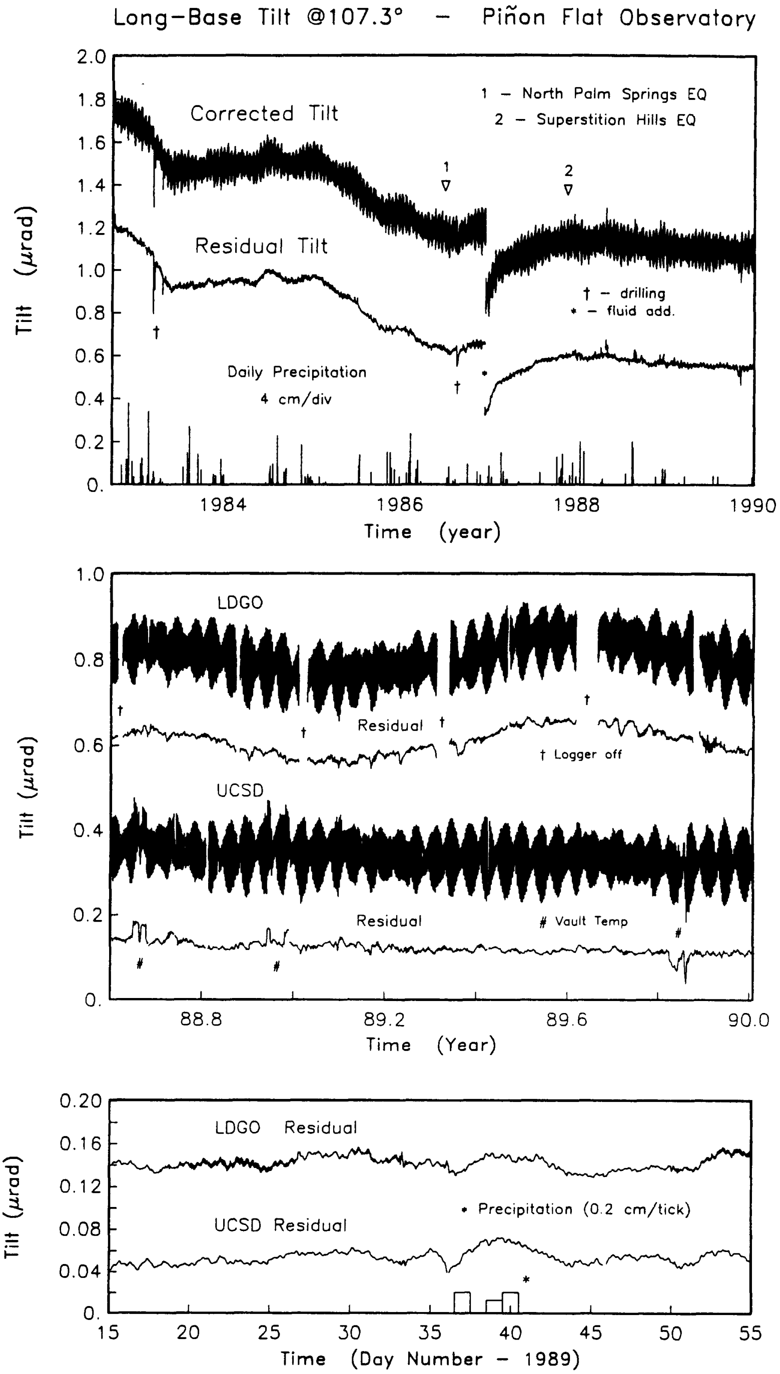
Long-Base Tilt @107.3° – Piñon Flat Observatory
Corrected Tilt
Residual Tilt
1 – North Palm Springs EQ
2 – Superstition Hills EQ
1
2
† – drilling
* – fluid add.
†
†
*
Daily Precipitation
4 cm/div
Tilt (µrad)
2.0
1.8
1.6
1.4
1.2
1.0
0.8
0.6
0.4
0.2
0.
1984
1986
1988
1990
Time (year)
LDGO
Residual
† Logger off
UCSD
Residual
Vault Temp
Tilt (µrad)
1.0
0.8
0.6
0.4
0.2
0.
88.8
89.2
89.6
90.0
Time (Year)
LDGO Residual
UCSD Residual
* Precipitation (0.2 cm/tick)
Tilt (µrad)
0.20
0.16
0.12
0.08
0.04
0.
15
20
25
30
35
40
45
50
55
Time (Day Number – 1989)

Figure 1.

the Lamont-Doherty instrument records will help clarify this (we have just completed editing all the data), but it is worth noting that both instruments showed the same high tilt rate (0.2 μrad/yr) in 1985-1986 and now show a rate near zero (about 0.02 μrad/yr). Of course the two 535-m long instruments, being separated by only 15 m, might be reacting to very localized effects, such as ground-water level changes, but we can test for this in a number of ways: the many well-level records at the site allow us to check for such correlations, the addition to the UCSD instrument of a 115-m-long extension (done in 1986) provides an independent measurement of EW tilt (albeit over a shorter baseline), and the NS instrument we have just completed should produce correlated records if the signals we are recording are due to broad scale deformation.

We have examined the long-period tilt records for signals possibly related to the 1986 North Palm Springs earthquake and the 1987 Superstition Hills earthquakes and do not find anything obvious. Figure 1 (upper panel) indicates the times of these events. On a much finer scale the permanent coseismic deformations associated with these earthquakes appear as large signals. Because even the coseismic signals are inconspicuous on Figure 1, we probably should not expect to detect any aseismic component for these events. In contrast, for nearby faulting on the San Jacinto and San Andreas faults, permanent coseismic tilts could amount to 10 μrad, or five times the full range in the long-term tilt plot of Figure 1; this is the magnitude of the deformation that we suspect has accumulated.

The middle and bottom panels of Figure 1 indicate just how well the LDGO and UCSD tiltmeters are currently tracking. Outside of a small cycle-per-year component in the LDGO instrument these sensors appear to have reached the same level of performance; the annual cycle is, we suspect, caused by the LDGO instrument vaults not being air-conditioned, as the UCSD vaults are. This annual cycle was not so evident in the earliest records from the LDGO instrument, perhaps because of the initial gappiness of the data; now that we are aware of it, we will be examining the records from all parts of this, including the hydraulic ties to the UCSD instrument, to isolate the source of this noise.

Deep Borehole Tiltmeters

The two ~30-m-deep borehole tiltmeters run by Dr. Judah Levine and Mary Holt (in boreholes BOA and BOB) functioned well from their installation in early 1986 until November 1987, when a lightning strike destroyed their electronics (and almost all other electronics in the immediate area). Two new sensors were reinstalled in late spring 1988, with one of these needing further replacement in the spring of 1989. Figure 2 presents the records from the first and second installations on the same time scale. The data from these installations and the Askania tiltmeter show a surprising scatter in their earth-tide response; the earth tides, being roughly the same amplitude as the anticipated annual crustal tilt signal near a fault zone, though of shorter period, give us an important ''calibration'' signal which is worth understanding fully.

We also operate an Askania tiltmeter, lent to us by Dr. Walter Zürn of the University of Karlsruhe. The instrument was first installed in late 1985 in a 25 m deep borehole (KUA), and produced excellent records until it was damaged by the lightning strike mentioned above. Figure 2 shows these results. With advice from Dr. Zürn we were able to dismantle, repair, and reinstall this instrument; it was put back into borehole KUA in summer 1988. In the summer of 1989 we removed the instrument once again for more work on its electronics and cabling, and to prepare for the deep deployment.

During 1987-1988 we drilled, cased, and grouted a deep borehole for this Askania tiltmeter. This deeper installation was planned to see how much improvement would be made by going into more solid material. Dr. Levine has made a parallel installation, using a different sensor. Owing to a lack of funding for this JILA project in 1989, along with other difficulties, instrument installation was not attempted until late 1989. Our own progress on a deeper installation has been slower than we expected. We have however learned a number of lessons about such deep installations that should be useful for any future attempts to install deformation sensors (of whatever type) in cased holes. These lessons fall into two areas: instrument alignment and down-hole debris. The tiltmeter was aligned by having a "muleshoe" at the bottom of the hole to guide the tiltmeter into a definite orientation; the orientation of this fixture is determined using a gyrocompass survey before the tiltmeter is put in the hole. In such a survey, the gyro is aimed at a known surface azimuth and uncaged; it retains this direction as the tool is lowered. At the bottom of the hole, the outer casing of the tool locks into the muleshoe, and a camera records the angle between this outer part and the gyro. In our final three measurements the scatter observed was ±2°. But doing this turned out to be much more difficult than was expected; it required considerable technical expertise (3–4 weeks of effort). In the future we would have the whole survey done commercially rather than renting the tool.

Our second lesson was that corrosion and scaling of the casing in a deep hole creates serious problems at its bottom. Lowering anything down the hole generates a substantial collection of debris at the bottom, as whatever is lowered scrapes against the inside of the casing, creating a shower of fine metal particles. Our bottom fixture was deliberately designed to have a large "sump" for debris to fall into; but even so, the deposits of dust on the bearing surfaces were too large to be acceptable. We therefore had to design and build a series of downhole cleaning tools. Even now, both the Askania and JILA tiltmeters are showing residual signals whose character we attribute to the remaining layer of debris. (This was not a problem in the shallower holes, since their verticality can be much better and the casing's internal surface area is much less.)

Gravity Changes

With NSF and AFGL funding, Drs. G. Sasagawa and M. Zumberge have continued to make absolute gravity measurements at PFO. These have shown no significant trend during the 4.5 years of measurement. A linear fit to the data gives a gravity change of 0.9 ± 1.5 μGal/yr or an equivalent elevation change of -3 ± 5 mm/yr.

However, these gravity data do show an interesting pattern of variation. The bottom panel of Figure 3 shows two "geodetic" series that indicate height changes at

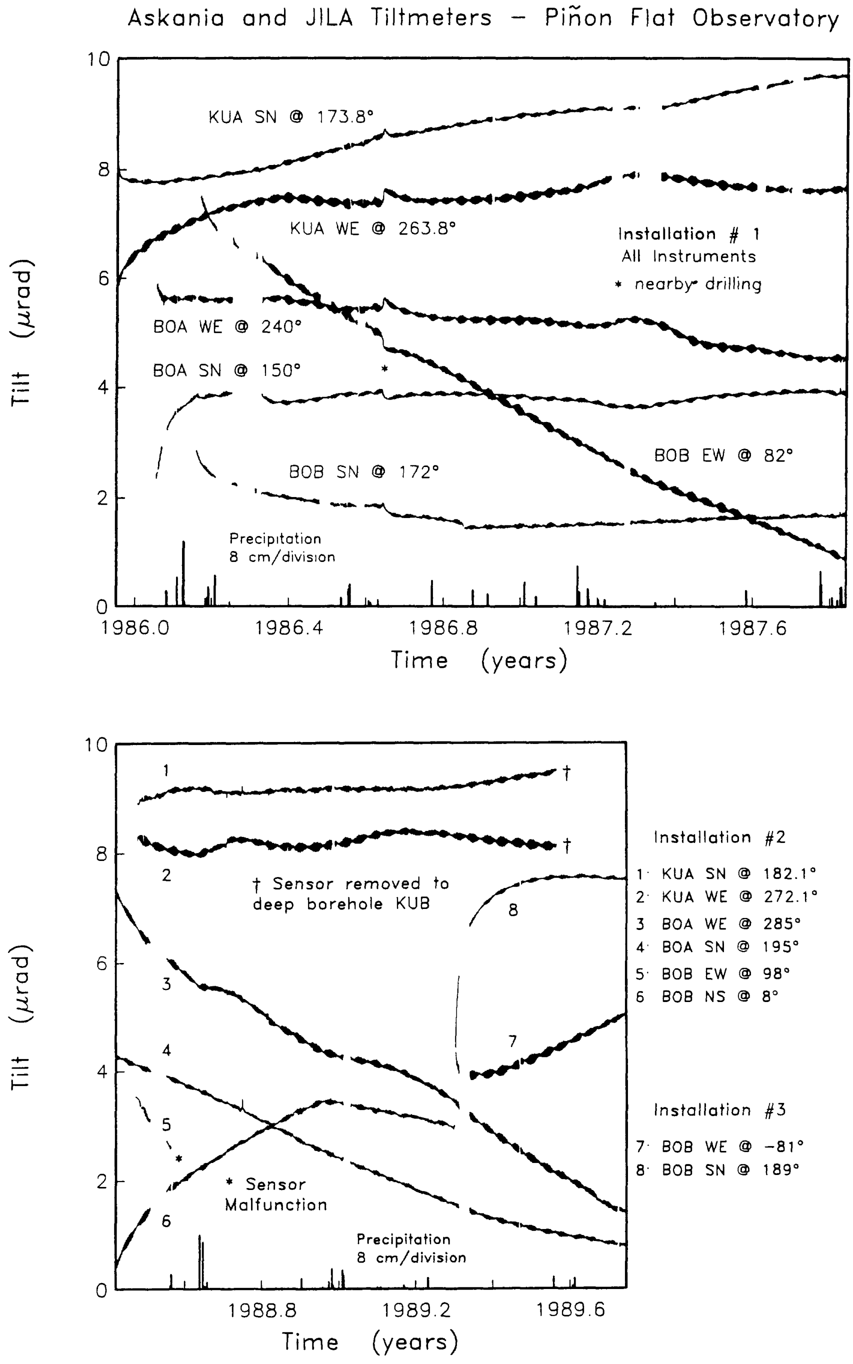
Askania and JILA Tiltmeters – Piñon Flat Observatory
Tilt (μrad)
10
8
6
4
2
0
KUA SN @ 173.8°
KUA WE @ 263.8°
Installation # 1
All Instruments
* nearby drilling
BOA WE @ 240°
BOA SN @ 150°
*
BOB EW @ 82°
BOB SN @ 172°
Precipitation
8 cm/division
1986.0
1986.4
1986.8
1987.2
1987.6
Time (years)
Tilt (μrad)
10
8
6
4
2
0
1 †
2 †
† Sensor removed to
deep borehole KUB
3
4
5
*
* Sensor
Malfunction
6
7
8
Precipitation
8 cm/division
1988.8
1989.2
1989.6
Time (years)
Installation #2
1 KUA SN @ 182.1°
2 KUA WE @ 272.1°
3 BOA WE @ 285°
4 BOA SN @ 195°
5 BOB EW @ 98°
6 BOB NS @ 8°
Installation #3
7 BOB WE @ -81°
8 BOB SN @ 189°

Figure 2.

PFO. One is gravity measurements made at PFO with the IGPP absolute gravimeter, corrected for ocean loading, barometric pressure, polar wander, and water table variations, and converted to elevation change by applying the reciprocal free air gravity gradient (–0.325 cm/μGal). The other is mobile VLBI vertical component estimates, for the baseline PFO to MOJAVE. since this baseline is only 195 km long, the baseline vertical is close to the local vertical. Within the limits of experimental uncertainty, both sets of data can be interpreted as showing no significant deformation. There is, however, an intriguing correlation between the VLBI data and gravity, beginning in 1986. Since there is no obvious signal in the data from the long-base tiltmeters during this time (Figure 1), we know that if vertical motion did occur, it must have had a very long wavelength–or else PFO was at a local maximum. However, since the strain record (in the top panel of Figure 3) shows no significant variations, we would prefer to regard the signal in the bottom panel as a coincidental instrument artifact.

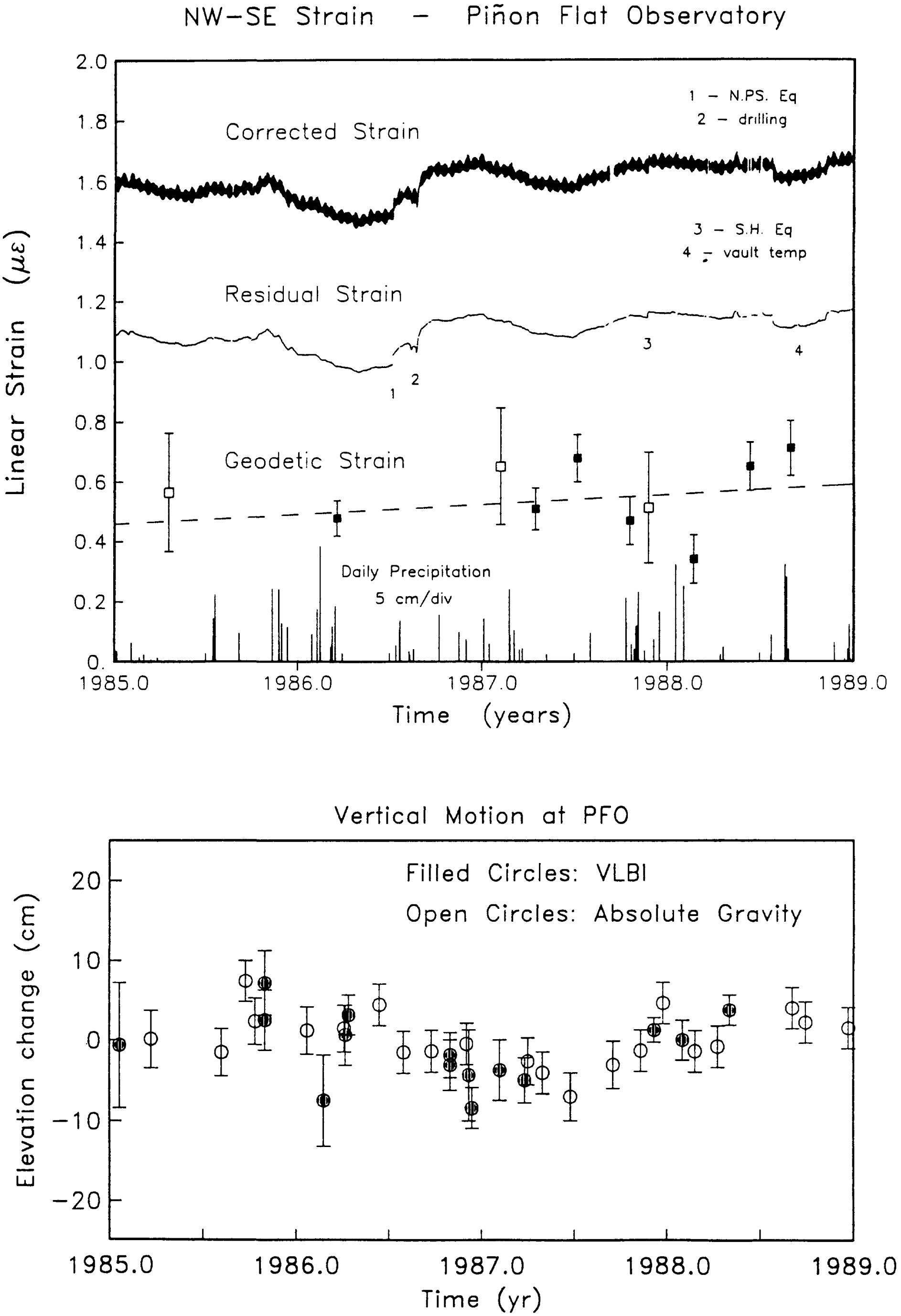
NW–SE Strain – Piñon Flat Observatory
Corrected Strain
1 – N.PS. Eq
2 – drilling
3 – S.H. Eq
4 – vault temp
Residual Strain
Geodetic Strain
Daily Precipitation
5 cm/div
1
2
3
4
Linear Strain ($\mu\varepsilon$)
2.0
1.8
1.6
1.4
1.2
1.0
0.8
0.6
0.4
0.2
0.
1985.0
1986.0
1987.0
1988.0
1989.0
Time (years)
Vertical Motion at PFO
Filled Circles: VLBI
Open Circles: Absolute Gravity
Elevation change (cm)
20
10
0
−10
−20
1985.0
1986.0
1987.0
1988.0
1989.0
Time (yr)

Figure 3.

Piñon Flat Observatory: A Facility for Studies of Crustal Deformation

14-08-0001-G1764

Frank K. Wyatt, Duncan Carr Agnew,
and Hadley O. Johnson
Institute of Geophysics & Planetary Physics
Scripps Institution of Oceanography
University of California, San Diego
La Jolla, CA 92093
(619) 534-2411

This grant supports the operation of Piñon Flat Observatory (PFO) as a research center for the study of crustal deformation in an area of active faulting. Through this grant, the U.S. Geological Survey provides 50 percent of the funding needed both for running the 160-acre facility and for maintaining the reference-standard instruments there. Matching funds are provided by a grant from the National Science Foundation. The work done at PFO includes establishing the accuracy of instruments designed for measuring various geophysical quantities by comparing results from them with data from the best available continuously recording deformation monitors. Such comparison then provides for an accurate record of strain and tilt changes in the area near the observatory, between the active San Jacinto fault and southern San Andreas fault systems. All of this effort is intended to foster development of precision instrumentation and from this an improved understanding of the earth. Particularly for crustal deformation studies, more accurate measurements are needed for a better understanding of the mechanics of faulting. The site continues to be utilized by roughly 20 different research teams, the most recent efforts focusing on GPS and seismic correlation/waveform studies.

This semi-annual report covers our response to a recent surge of activity on the San Jacinto fault, which prompted genuine concern that we might be seeing the prelude to a moderate to large earthquake in the area. Figure 1 (courtesy of Dr. Lucile Jones, USGS-Pasadena) shows the seismicity of this fault zone during December 1989 (and early 1990). During this month there were eight earthquakes of magnitude 3 or more, with two exceeding magnitude 4—a much higher level of activity than usual. Concern over the possibility that this might have been a response to deep aseismic slip led us to examine carefully the records from PFO. Figure 2 shows the strain on two of the instruments: the NW-SE laser strainmeter (the most accurate of the long-base strainmeters) and the Carnegie borehole dilatometer. Neither record has been detrended, and it should be noted that while the long-term trend of the Carnegie data (0.5 $\mu\varepsilon$/yr) is very likely due to local effects, the much lower trend seen on the NW-SE strainmeter (0.17 $\mu\varepsilon$/yr) appears to be the true measure of secular strain at that azimuth. Neither record shows any obvious "events" during this time. (The slight excursion in the NW-SE record at the start of December is probably the result of imperfections in the laser-frequency correction.)

If we are prepared to make an assumption about what kind of deep slip might have occurred, we can of course put bounds on it using this data. For uniform right-lateral slip along the fault over the distance covered by the December earthquakes (from 0 to 130 km along the profile in Figure 1), the NW-SE strainmeter has a response of $10^{-25}\varepsilon$/N-m. The total strain accumulated during December 1989 (after subtracting out the trend from the previous two months) is less than 3 nε, giving a bound of 3×10^{16} N-m in moment release. The seismic moment release from the earthquakes shown in Figure 1 is about 6×10^{15} N-m, about one fifth of this bound. If deep slip triggered this burst of activity, it could not have been much larger than the results it produced. Without these data—available in few other places—speculation on such an aseismic slip episode would be extremely hard to avoid.

Figure 3 gives another perspective on the pattern of seismicity in the area—and further reason to pay close attention to the San Jacinto fault. The upper panel shows the depth distribution of seismicity along the San Jacinto fault for roughly the same section as outlined in Figure 1 (data from USGS-Caltech Southern California Seismographic Network). The lower two panels are the now familiar seismic distribution plots for the San Andreas fault, before and after the Loma Prieta earthquake (The Loma Prieta, California, Earthquake: An Anticipated Event, U.S. Geological Survey Staff, *Science*, **247**, 286-293, 1990). All three plots are identically scaled. The similarity of the pre-earthquake seismicity for the Loma Prieta area and the Hemet/Anza area of the San Jacinto fault is most striking. Coupled with the generally high level of activity on the San Jacinto fault in historic times, we are well warned as to the seismic potential of this area (e.g., State of Stress in the Seismic Gaps Along the San Jacinto Fault, Hiroo Kanamori and Harold Magistrale, in Observatory Seismology, edited by J.J. Litehiser, University of California Press, Los Angeles, 1989).

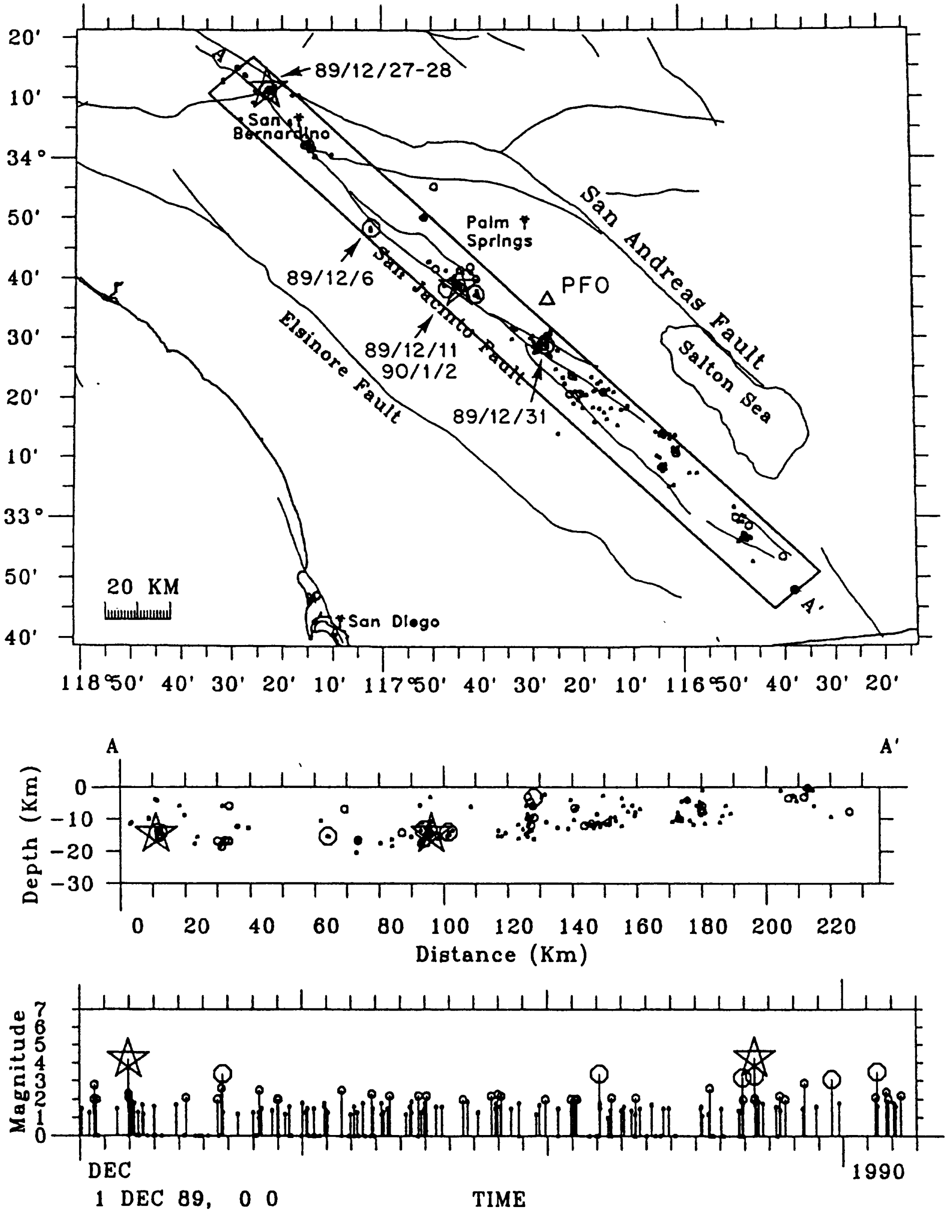

San Jacinto Fault
December 1, 1989 - January 3, 1990

Figure 1.

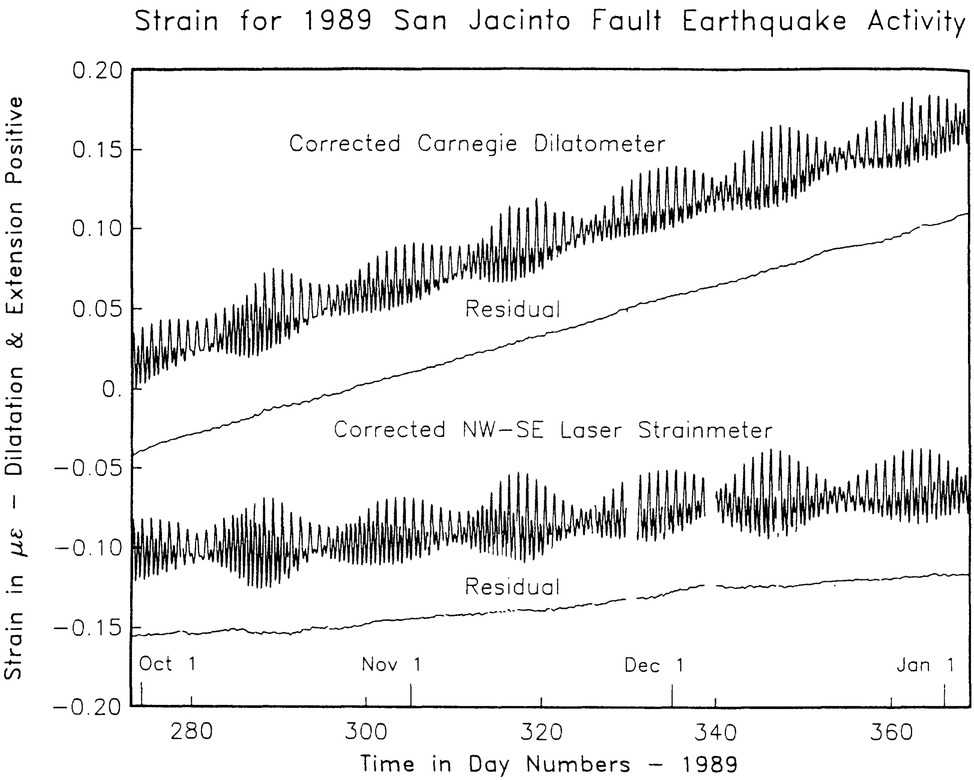
Strain for 1989 San Jacinto Fault Earthquake Activity
Strain in $\mu\varepsilon$ - Dilatation & Extension Positive
0.20
0.15
0.10
0.05
0.
−0.05
−0.10
−0.15
−0.20
Corrected Carnegie Dilatometer
Residual
Corrected NW−SE Laser Strainmeter
Residual
Oct 1
Nov 1
Dec 1
Jan 1
280
300
320
340
360
Time in Day Numbers − 1989

Figure 2.

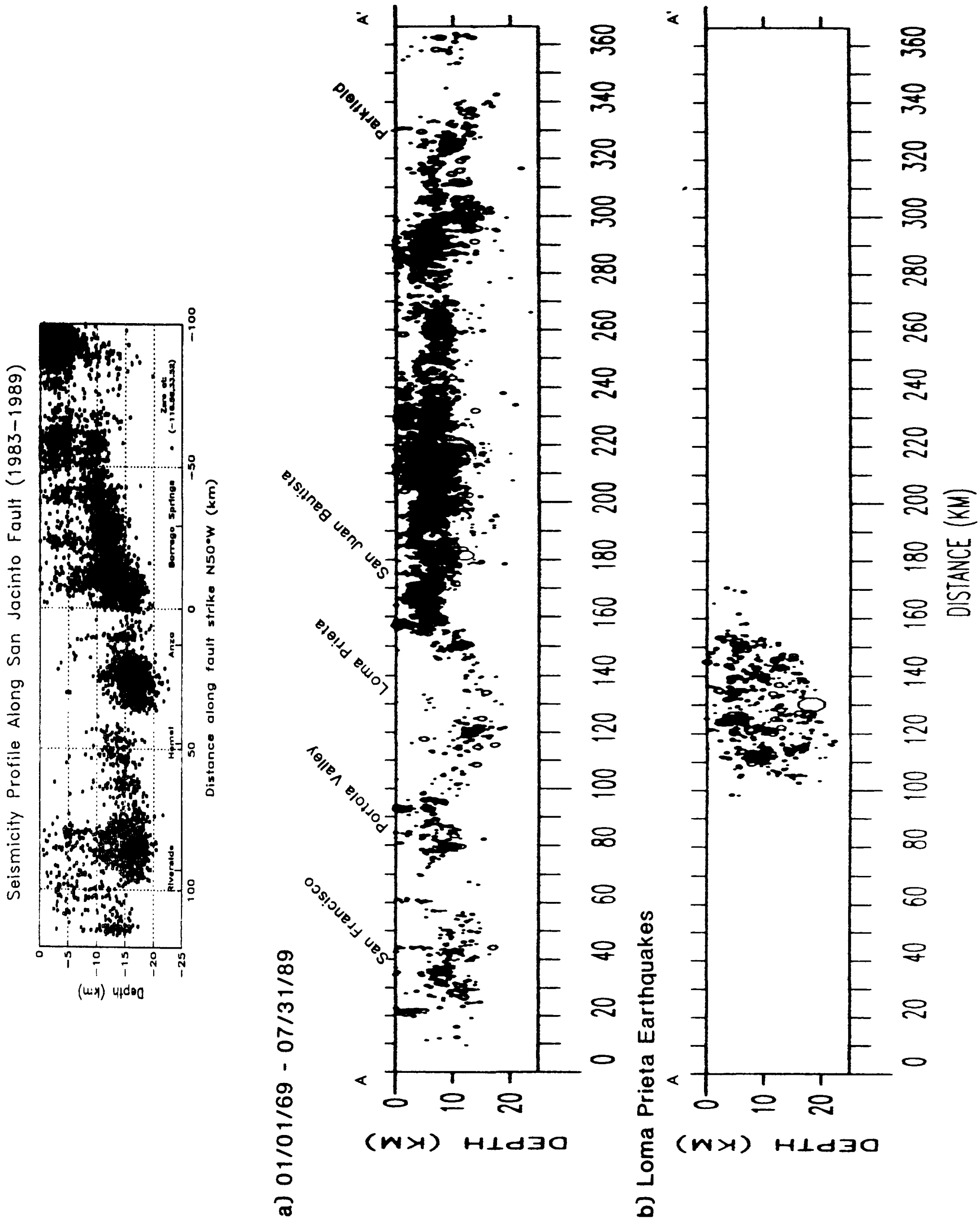
Seismicity Profile Along San Jacinto Fault (1983–1989)
Depth (km)
0
−5
−10
−15
−20
−25
Riverside
Hemet
Anza
Borrego Springs
Zero at (−116.58,33.32)
100
50
0
−50
−100
Distance along fault strike N50°W (km)
a) 01/01/69 - 07/31/89
San Francisco
Portola Valley
Loma Prieta
San Juan Bautista
Parkfield
A
A'
DEPTH (KM)
0
10
20
b) Loma Prieta Earthquakes
DISTANCE (KM)
0
20
40
60
80
100
120
140
160
180
200
220
240
260
280
300
320
340
360

Figure 3.

Creep and Strain Studies in Southern California

Grant No. 14-08-0001-G1666

Clarence R. Allen and Kerry E. Sieh
Seismological Laboratory, California Institute of Technology
Pasadena, California 91125 (818-356-6904)

Investigations:

This semi-annual Technical Report Summary covers the six-month period from 1 October 1989 to 31 March 1990. The grant's purpose is to monitor creepmeters, displacement meters, and alignment arrays across various active faults in the southern California region. Primary emphasis focuses on faults in the Imperial and Coachella Valleys.

During the reporting period, alignment arrays were resurveyed as follows: across the Superstition Hills fault at IMLER ROAD; across the Imperial fault at HIGHWAY 80, WORTHINGTON ROAD, and ALL-AMERICAN CANAL; across the Coyote Creek fault at BAILEYS WELL; across the unnamed fault at DIXIELAND; across the San Andreas fault at NORTH SHORE, DILLON ROAD, and INDIO HILLS; and across the Mission Creek fault at THOUSAND PALMS CANYON. The nail-file array across the Imperial fault at ANDERHOLT was remeasured, although the similar array at ROSS ROAD had recently been destroyed by repaving. Creepmeters were serviced at ROSS ROAD (4 times), SALT CREEK, MECCA BEACH, HEBER ROAD (twice), TUTTLE RANCH (twice), and HARRIS ROAD.

Although we had been planning to place a fourth satellite-telemetered creepmeter across the San Andreas fault near Indio (in addition to those at NORTH SHORE, SALT CREEK, and ROSS ROAD), the landowner decided at the last minute to develop a golf course across the proposed locality. We are now tentatively planning instead to place the creepmeter near Devers Hill (12 km north of Palm Springs), a locality where only minor creep has been observed heretofore, but where a significant creep episode could be ominous in terms of the potential for a large earthquake on the Coachella Valley-Bombay Beach segment of the San Andreas fault.

Results:

The reporting period was one of little activity. Shortly after the close of the period, on April 3rd and 4th, a classic 7-mm creep event took place on the Imperial fault at ROSS ROAD, with most of the slip occurring in 3 episodes of 2-3 hours each. A very similar event had occurred one year earlier.

Southern San Andreas Crustal Deformation

14-08-0001-G1809

John Beavan
Lamont-Doherty Geological Observatory of Columbia University
Palisades, New York 10964
(914) 359-2900

Investigations

1. Historical water level recordings from three sites around the Salton Sea are being investigated to determine tectonic tilting, taking account of as many noise and error sources as possible.
2. The tectonic tilt so derived is being carefully compared with leveling data from the area.
3. LDGO-designed pressure-sensor gauges at five sites around the sea are being used to measure water level continuously, to investigate noise sources, to determine the level of detectability of tectonic tilt signals in the data, and to measure tectonic tilting.
4. A dense network of sites near the Southern San Andreas and northern Imperial Valley Faults is being surveyed approximately annually to cm-level horizontal accuracy, using Global Positioning System (GPS) techniques (in cooperation with Dr. R. Reilinger of MIT and others).

Results (April, 1989)

1. Four of the GPS stations are close to our water level sites (Figs. 1 and 2). We are hoping to enhance the vertical accuracy of the GPS survey by introducing the 1 cm accurate inter-site height differences obtained from the water level data into the GPS analysis. The success of this effort will depend on being able to define the local geoid with sufficient accuracy. We have begun the task of analyzing GPS, water level and gravity data with this objective in view.

A major GPS campaign was carried out during February and March 1990, involving MIT, Lamont, CalTech, NGS and Riverside County, as well as several other institutions. Lamont provided 3 Trimble 4000ST dual frequency receivers and 3 operators for this experiment. The survey greatly improved the station coverage in the vicinity of the southern San Andreas fault (Fig. 2), and generated a third epoch of GPS observations at some of our water level sites.

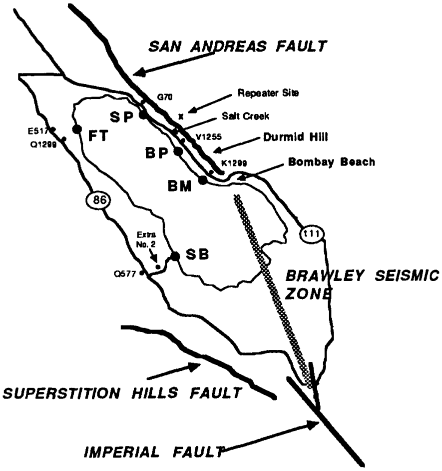

Figure 1. Map of the study region, showing the tectonic setting and the sea-level gauge network. Historical sea-level data have been collected at FT and SB since 1950, and at SP since 1970. Continuous recording pressure gauges have operated at SP since May 1985, at SB since January 1986, at BP since December 1986, and at BM and FT since May 1987. The pressure gauge data are digitally telemetered, via the repeater site shown, to SP. There they are stored on disk, and can be accessed by modem. Datum control of the sea level gauges has been provided by leveling them to nearby NGS benchmarks; clockwise from SP, these are G70, V1255, K1299, Extra No. 2 and Q1299. P. Williams' trenching site across the San Andreas is at Salt Creek. The SB to FT baseline length is 35 km, FT to SP is 14 km. Gauge BP has been out of operation since April 1989 due to silting at the site.

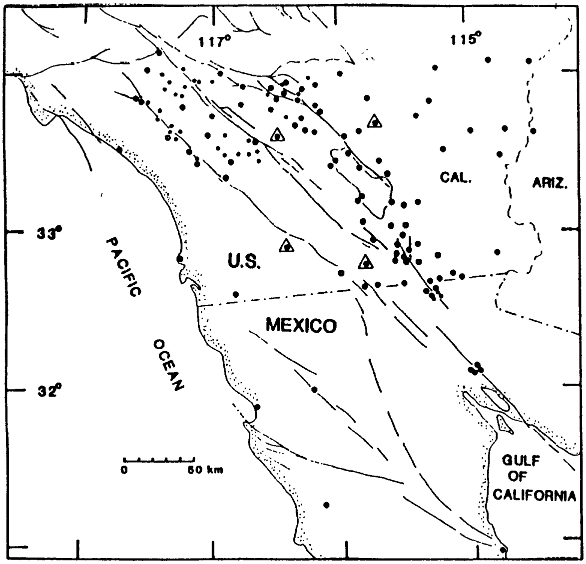

Fig. 2. Imperial Valley/Southern San Andreas/Riverside County GPS network measured during February and March 1990 by MIT, L-DGO, CalTech, Riverside County, NGS, UT Dallas and Mexican collaborators. The large dots represent sites occupied for 3 sessions, while the smaller dots show Riverside Co. sites occupied for a single session or with kinematic surveying. Triangles are VLBI sites used for control of the GPS survey.

2. Data from the L-DGO water level sites (Fig. 1) continue to be collected. We do not plot the original data from the pressure-sensor water level gauges since they are all basically similar, showing a ~40 cm annual cycle and a number of gaps due to vandalism, silting of the gauge site, and other problems. (See Open File Report 89-453, p 278 for examples.) Only a very small fraction of the gaps are due to data transmission link failures or to central computer problems; however, since such failures could be catastrophic, we have now installed solid-state back-up recorders at the 3 operating remote sites. It is also planned to back-up the gauge at the SP central recording site, and at the BP site when it is reinstalled.

A complete suite of differences between the observed water level series is plotted in Figure 3, after low-pass filtering at 4 day periods. These differences may be converted to apparent ground tilt (i.e., true ground tilt plus measurement noise of various sorts) by dividing by the distance between the gauges. The rms value of these difference series is close to 1 cm, and our estimated error in referencing the gauge datum to the nearby benchmark array is ±0.5 cm. All but one of the differences show rates that are less than 5 mm/yr, and our estimate of the accuracy in these rates is ±5 mm/yr. Hence we presently see no significant long term tilt at any site, though there is a suggestion of down-to-the-south tilting on the SB-SP baseline, at least through the Fall of 1989. The apparent change in tilt direction since Fall 1989 was investigated during a brief field trip in February 1990. There are no obvious problems in the calibration of the pressure sensors, so the possibility that this is a real signal remains open. Alternative explanations include an unusual salinity change (possible) or a local instability (unlikely, but this will be tested by leveling in the near future). There are short term (weeks - months) variations in several of the difference series, with peak-peak amplitudes as high as 4 cm; we expect that these are due to temperature or salinity variations, but there is also the possibility of barnacles fouling the gauge inlet in some cases. Higher frequency noise (days - weeks) is due to wind and to temperature changes in the sea. Despite these various problems, our difference data are quieter than the data obtained from the staff and float gauges used historically.

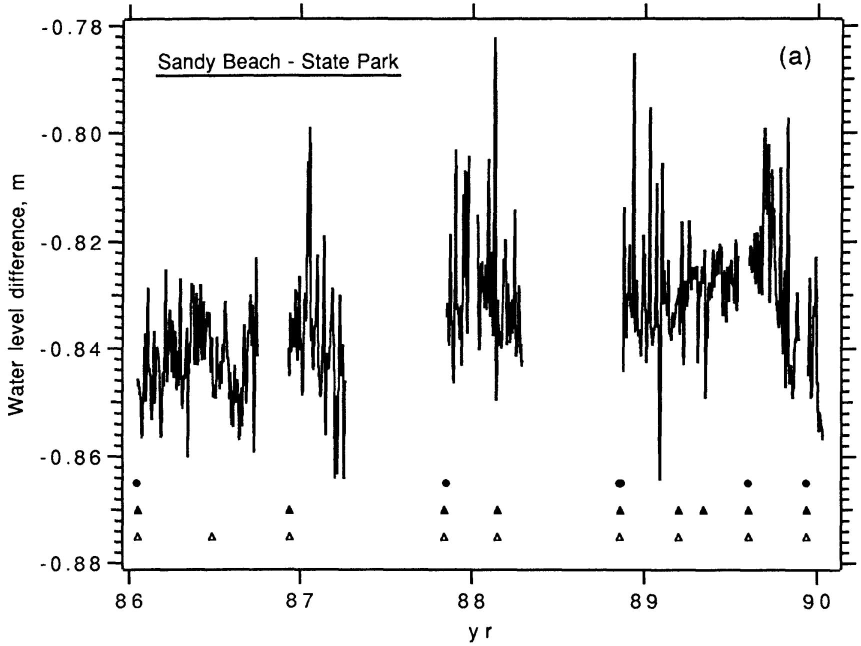

Figure 3. Differences between water level series after low-pass filtering at 4 day period. These differences may be converted to apparent ground tilt (i.e., true ground tilt plus measurement noise of various sorts) by dividing by the distance between the gauges. The rms value of these difference series is close to 1.0 cm. Positive trends on the plots indicate ground uplift of the second-named site relative to the first. All trends are within the estimated noise level of 5 mm/yr. Gaps are due to vandalism and other problems at one or both sites. 1989 has been our best year so far for data continuity, with the unfortunate exception that BP had to be removed because of severe silting at the site.

(a) shows SB-SP water level differences since January 1986. SP apparently uplifted relative to SB at 3.6 mm/yr between Jan 1986 and Fall 1989 (i.e., down-to-south tilting). Our estimate of the error in this rate is about ±5 mm/yr - the error will decrease as the data length increases since the referencing of the gauge pressure datum to nearby benchmarks is a primary source of error, and is independent of data length. The dots below the data indicate times that a sensor was exchanged at one or other of the sites; since the trend continues through these changes we suspect it is not due to sensor instability. The triangles (filled=SB, open=SP) indicate times that staff gauges adjacent to the pressure sensors were read manually as a check on gauge stability; generally the agreement is 5 mm or better. The gauges have also been leveled annually to nearby arrays of benchmarks; their stability has been at the mm level. During Fall 1989 there is an apparent change in the direction of tilting. Since the change coincides with a sensor exchange we hesitate to claim that it is tectonic; also, strainmeters at Piñon Flat have showed nothing unusual over the past several months to suggest a regional strain event (Wyatt, pers. comm., 1990). Tests during a February 1990 field trip found no problems with gauge calibrations, so the possibility that the change repesents a real signal remains open.

(b), (c), (d) (overleaf). These plots show many additional pairs of differences that include the other three gauges, BP, BM and FT. These gauges are also regularly checked for stability with staff readings and leveling; we have not, however, marked the plots as in Figure 3a. See text for more discussion.

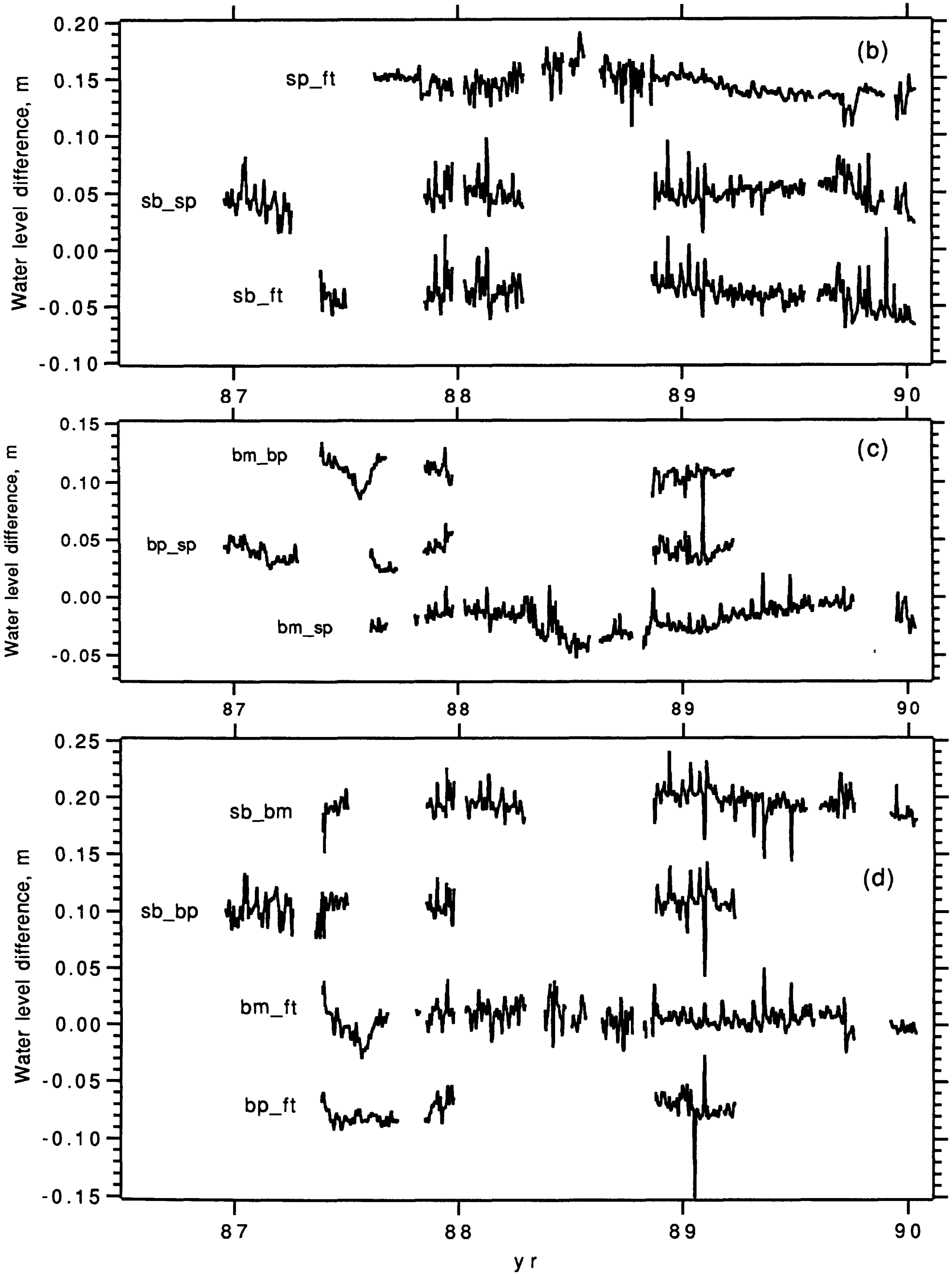

Figure 3 (b), (c), (d). See caption on previous page.

Figure 4 shows spectra of apparent tilt derived from our water level data compared to tilt derived from GPS and leveling measurements. We may use linear fits to these spectra, and Agnew's (1987) formalism, to estimate the period of a signal at which either repeated leveling or GPS measurements become the technique of choice, rather than differential water level measurements.

Agnew's method works by comparing noise levels in the frequency domain, and its specific importance is its applicability to data both from continuously monitoring instrumentation and from survey techniques such as leveling and GPS. Assuming that leveling or GPS errors are uncorrelated between surveys, these data have a flat ("white") power spectrum, whose power spectral density is given by $P_0 = \sigma^2/f_n = 2\sigma^2 t$ where σ is the rms error in each survey, and f_n is the Nyquist frequency corresponding to the time interval between surveys, t. Instrumental spectra are often "red" and can often be modelled as a straight line of log power versus log frequency, $P(f) = K/f^{\alpha}$. The survey data become quieter than the instrumental observations at periods longer than that period, T, at which these two lines cross; they are therefore superior for detecting signals whose period is greater than T. T is given by: $T = (2\sigma^2 t/K)^{1/\alpha}$. An important point to note about the survey errors is that more frequent repeats of the survey (smaller t) decreases the noise level even at very long periods, provided the errors remain uncorrelated between consecutive surveys.

In the Figure, the water level difference power spectra, calculated by conventional section-averaging techniques, are plotted in terms of equivalent tilt over a 40 km measurement baseline, using units of μrad for tilt, and days for time. These spectra are band-limited at long periods by the available length of data, so they have been extrapolated (dotted lines) assuming a linear relation between log power and log frequency.

Also plotted in the Figure are spectra of: (i) annually repeated leveling measurements over a 40 km baseline, assuming a 1 mm/km$^{1/2}$ standard error, (ii) annually repeated GPS over a 40 km baseline, assuming a vertical baseline accuracy of 2 cm, (iii) *daily* repeated GPS over a 40 km baseline, assuming a 2 cm standard error as above, and that these errors are uncorrelated between consecutive measurements (this may be a poor assumption).

40 km is the maximum baseline that is likely to be useful for plate boundary monitoring; for parts of California 10 km, or even less, would be more appropriate. As the baselines get shorter, all the spectral levels in Figure 4 will rise. For a factor of 10 decrease in baseline, the spectral level for GPS and differential sea level will rise by up to 2 units; that for leveling will rise by 1 unit.

It is clear that annual GPS surveys will perform better than sea-level only at periods greater than several decades. However, daily (i.e., effectively continuous) GPS will equal or outperform sea-level differencing at all periods of interest, provided that uncorrelated daily GPS data are attainable. In order to validate this conclusion, more work needs to be done on vertical errors in GPS over relatively short baselines. Annual leveling is superior to differential water level for periods greater than a few years; but leveling is progressively favored as baselines become shorter.

Reference

Agnew, D.C., On noise levels in deformation measurements: comparison in the frequency domain, USGS Open File Report, 87-591, Vol II, pp 838-844, 1987.

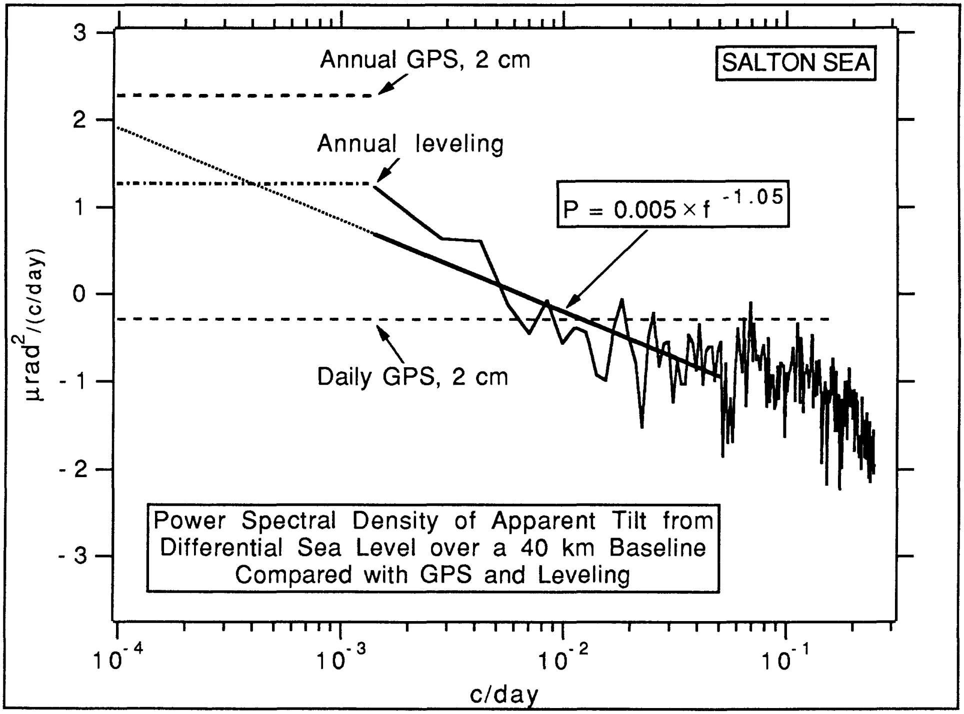

Figure 4. Apparent tilt spectrum derived from Salton Sea differential water level, compared to predicted spectra for GPS and leveling over 40 km baselines. The "water level" spectrum has been linearly extrapolated to lower frequencies by fitting a straight line to the spectrum between 2 year and 50 day periods.

Acceleration, Velocity, and Volumetric Strain from Parkfield GEOS Network

9910-02089

Roger D. Borcherdt, Malcolm J. Johnston, C. Dietel, and Allan Lindh
Branch of Engineering Seismology and Geology
345 Middlefield Road, MS 977
Menlo Park, California 94025
(415) 329-5619

Investigations

- Maintain GEOS array near Parkfield, CA to serve as a strong-motion array to provide broad-band, high-resolution measurements of the mainshock as well as an array to provide measurements of pre-, eo-, and post-seismic strain and displacement field pertubations for purposes of earthquake prediction.
- Maintain up-to-date archive of all events recorded in anticipated rupture zone.
- Develop theoretical basis and models to interpret colocated measurements of volumetric strain and seismic displacement fields.

Results:

- An array of 15 stations has been maintained at 95 percent or greater reliability since July, 1987. An up-to-date digital data archive is being maintained and summarized in monthly internal USGS reports. (See previous reports for detailed description of the array.) Events recorded along Parkfield segment of study zone during time interval are summarized according to magnitude and depth (Table 1). Examples of colocated measurements of volumetric strain (Figures 1 and 2; traces 1, 2, and 3), ground velocity (Figure 1, traces 4, 5, and 6), and ground acceleration (Figure 2; traces 4, 5, and 6) for a magnitude 4 event are shown.

Reports

Borcherdt, R.D., Johnston, M.J.S., and Glassmoyer, G., 1989, On the use of volumetric strain-meters to infer additional characteristics of short-period seismic radiation: *Bulletin of the Seismological Society of America*, v. 79, p. 10,106-10,230.

(See projects (Borcherdt, 9910-02689 and 9910-03009) and Johnson for related reports.)

4/90

TABLE 1

HYPO-71 LISTING: PARKFIELD EARTHQUAKES RECORDED ON ONE OR MORE GEOS STATIONS FROM MAY 1 TO FEBRUARY 10, 1990.

```
89 5 5  229 47.76 35 58.14 120 31.55  11.06   1.83 35  73  2.9 0.13  0.3  0.3 S
89 525 1240  9.47 35 51.94 120 24.58   9.39   3.70 54  43  2.0 0.15  0.2  0.4 S
89 527 1016 36.61 36  7.33 120 40.47   7.76   2.16 36  42  4.5 0.10  0.2  0.4
89 630  135 17.36 35 59.63 120 33.30   5.51   2.11 41  65  4.3 0.10  0.2  0.3 S
89 7 5 1648 22.15 36  2.31 120 35.85   4.90   1.91 31  58  3.5 0.10  0.3  0.4 S
89 7 8  756 15.51 35 59.01 120 32.76   4.10   1.97 34  68  5.0 0.10  0.2  0.5 S
89 728  4 2 24.83 36  0.87 120 33.61   3.91   1.01  8 179  4.9 0.06  0.6  2.5 S
89 729  039 55.67 35 49.65 120 22.22   7.29   1.47 35  53  1.6 0.14  0.3  0.5 S
89 8 2  742 58.85 35 55.53 120 29.07   5.15   1.44 15  99  2.2 0.06  0.3  0.6 S
89 8 6 21 0 34.51 36  0.25 120 33.97   5.32   2.40 38  34  3.8 0.10  0.2  0.4
89 8 7  354 50.96 36  0.11 120 33.84   5.30   2.11 32  62  3.9 0.08  0.2  0.3 S
89 8 8  119  7.07 35 55.49 120 29.30   4.80   1.23 10 160  1.9 0.03  0.5  0.6 S
89 810 16 0 34.08 35 55.89 120 28.60   5.18   1.74 22 122  2.9 0.08  0.3  0.4 S
89 823  557 31.64 35 57.39 120 30.99   2.71   1.34 15  65  1.7 0.05  0.3  0.5
89 825  747 59.39 35 55.46 120 28.72   4.99   1.21 16 101  2.7 0.08  0.3  0.5 S
89 9 4 1212 36.34 36  2.47 120 36.37   5.89   2.06 23 165  6.2 0.07  0.3  0.3 S
89 9 6 1838  4.22 35 58.17 120 31.51   7.79   1.77 15 167  2.9 0.06  0.6  0.5
89 921 13 5 50.60 35 51.47 120 24.40   5.81   2.38 33  79  2.5 0.12  0.2  0.3
8910 9 15 0 18.54 36  3.36 120 34.41   5.06   1.91 16 139  8.2 0.21  0.8  1.2
891025  229 12.06 36  0.64 120 33.60   5.17   1.98 10 189  4.7 0.03  0.5  0.6
891025 1621 45.62 35 47.83 120 21.00  11.13   2.82 37  54  6.1 0.11  0.3  0.5 S
8911 3  758 28.85 36  0.07 120 32.97   3.17   1.98 11 175  5.0 0.02  0.6  0.7
8911 4 1329 31.68 35 52.50 120 25.61   9.06   1.36 12 107  2.5 0.04  0.5  0.6
891112  553 13.45 35 47.67 120 21.04  10.02   2.05 28  66  6.3 0.09  0.3  0.6
891214 1227 28.07 35 31.15 120  4.69  12.40   2.05 29 129  6.6 0.11  0.3  0.4
891215 1311 28.21 35 58.00 120 31.04  11.43   1.74 21 135  2.1 0.05  0.5  0.4 S
891216  3 1  4.61 35 31.37 120  4.36  12.79   2.46 29 133  6.2 0.07  0.3  0.4
891223 2213 54.39 35 46.17 120 18.54   5.02   2.21 29  61  6.8 0.08  0.2  0.4
90 125  838 16.12 35 57.59 120 29.86  11.55   1.85 19 138  0.4 0.05  0.4  0.3
90 131 1033  1.96 35 55.34 120 28.22   5.46   1.68  9 157  3.5 0.03  0.5  1.0
90 131 1052 43.04 35 55.33 120 28.30   5.37   1.69  9 155  3.4 0.02  0.5  1.0
90 210  856 53.87 35 44.61 120 17.57  13.75   1.89 25  48  4.1 0.06  0.3  0.4
```

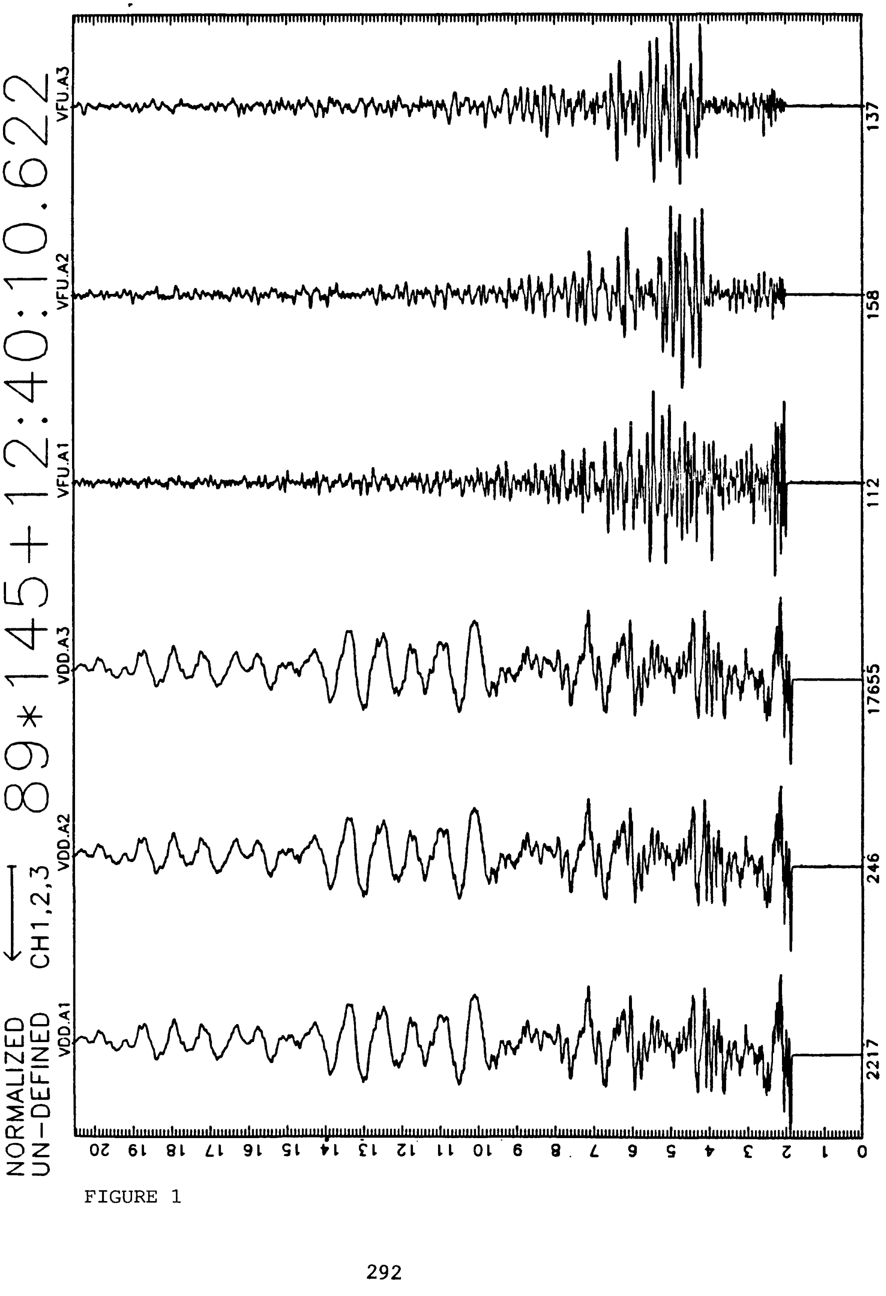
NORMALIZED
UN-DEFINED
← CH1,2,3
89*145+12:40:10.622
VDD.A1
VDD.A2
VDD.A3
VFU.A1
VFU.A2
VFU.A3
2217
246
17655
112
158
137
0
1
2
3
4
5
6
7
8
9
10
11
12
13
14
15
16
17
18
19
20

FIGURE 1

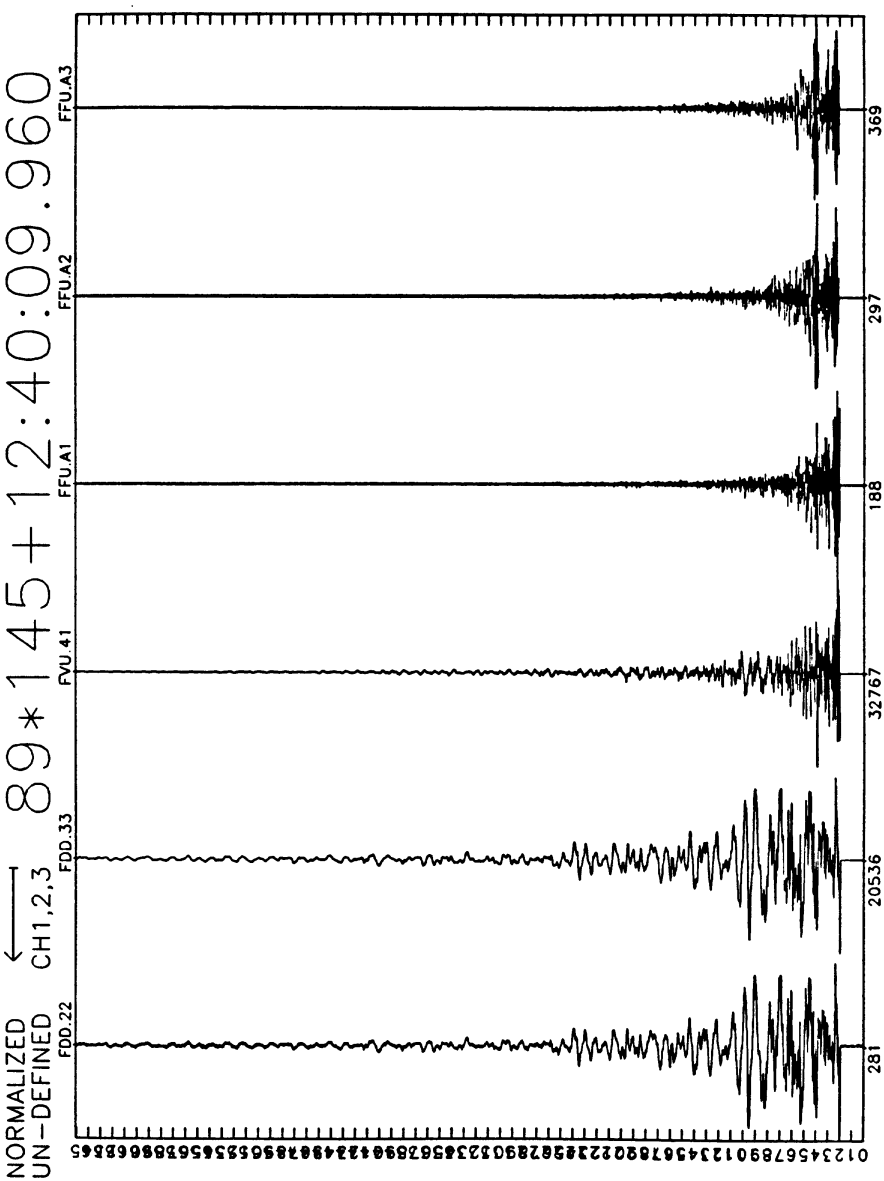
NORMALIZED
UN-DEFINED
CH1,2,3
89*145+12:40:09.960
FDD.22
FDD.33
FVU.41
FFU.A1
FFU.A2
FFU.A3
281
20536
32767
188
297
369

FIGURE 2

Seismic Studies of Fault Mechanics

9930-02101

William L. Ellsworth
Lynn Dietz and Randall White

Branch of Seismology
U.S. Geological Survey
345 Middlefield Road - MS 977
Menlo Park, California 94025
415-329-4784

Investigations

1. Aftershocks of the M_S 7.1 Loma Prieta earthquake sequence.
2. Variation in seismic noise in the frequency band from 0.1 to 20 Hz immediately preceding the Loma Prieta earthquake.
3. Loma Prieta earthquake response.

Results

1. The October 17, 1989 Loma Prieta earthquake (0004 UTC on October 18) occurred beneath one of the most densely instrumented portions of the Calnet, and provides an unusual opportunity to analyze the "complete" aftershock sequence of a major event. Our work to date has concentrated on the geometry of the Loma Prieta earthquake sequence. We calculated station delays and 1-dimensional velocity models to improve the locations over those determined by routine procedures. To model the contrasting surface geology across the San Andreas fault, we derived a separate velocity model for each side using a simultaneous inversion of the mainshock and aftershock traveltimes. The resulting locations (figure 1) are more precise in relation to each other (±0.3 km) than in an absolute sense (± 1 km based on relocations of shots).

   Well-constrained aftershock hypocenters of October 18-31, 1990, form a 60 km long zone with the mainshock at its base. Most aftershocks cluster around the perimeter of the distribution and surround a relatively aseismic patch (~15×30 km) which we believe approximates the extent of main shock rupture. In the central and northwestern parts of the zone, earthquakes at depths above about 10 km define numerous disjoint fault structures. The earthquakes deeper than 10 km define a plane dipping 65°±5°SW and striking N51°W±2°, consistent with the mainshock focal mechanism. In the southeastern 15 km of the aftershock zone the dipping zone warps into a vertical surface that corresponds with the San Andreas fault.

   The large component of reverse-slip observed in this event agrees with a simple model for slip on a dipping plane within a compressional fault bend. We are unable to conclude, however, whether the fault activated by Loma Prieta earthquake was the principal plate boundary fault or a less-frequently active member of the San Andreas fault system.

2. The detection of unusual ULF radio signals preceding the Loma Prieta earthquake, reported by A.C. Frasier-Smith and his colleagues at Stanford, raises the issue of concurrent variations in seismic noise within the epicentral region. To examine this question, we are studying the ambient seismic noise using continuous recordings from the 7 hours immediately preceding the main shock, as recorded on the Calnet. The seismograms are analyzed by computing the power spectral density from long records (160 s), and yield useful measurements of ground motion between 0.1 and 20 Hz (figure 2).

   No unusual variations in seismic noise were detected during the 7 hours before the earthquake. Ground noise levels at Calnet station (JBZ) nearest, located 1.5 km to the west of the Stanford ULF receiver, are indistinguishable from noise levels measured well before and after the earthquake (figure 3). The seismograms at this station, however, contain long sections of high-amplitude cultural noise during the three hours immediately preceding the event, generated by a half-track truck used to load crates during the apple harvest. Other nearby stations display normal ground-motion noise levels and did not detect this cultural noise.

3. Response activities to the earthquake ranged from crisis management of information and reporting to the public during the days immediately following the event, to testimony at a Congressional Field Hearing, to the editing of a report on the earthquake published in Science within 3 months of the event.

Reports

Dewey, J.W., Hill, D.P., Ellsworth, W.L., and Engdahl, E.R., 1989, Earthquakes, faults, and the seismotectonic framework of the contiguous United States: Geological Society of America Memoir 172, p. 541-575.

Dietz, L.D., and Ellsworth, W.L., in press, The October 17, 1989 Loma Prieta, California earthquake and its aftershocks: geometry of the seqence from high-resolution locations: Geophysical Research Letters, 4 p.

Ellsworth, W.L., 1990, Future Earthquakes: Lecture notes for the American Geophysical Union Lecture, National Science Teachers Association 38th National Convention: American Geophysical Union, 4 p.

Hill, D.P., Ellsworth, W.L., Johnston, M.J.S., Langbein, J.O., Oppenheimer, D.H., Pitt, A.M., Reasenberg, P.A., Sorey, M.L., and McNutt, S.R., 1990, The 1989 earthquake swarm beneath Mammoth Mountain, California: an initial look at the 4 May through 30 September activity: Bulletin of the Seismological Society of America, V. 80, P. 325-339.

Michael, A.J., Oppenheimer, D.H., and Ellsworth, W.L., in press, Coseismic stress changes induced by the 1989 Loma Prieta, California earthquake: Geophyiscal Research Letters, 4 p.

U.S. Geological Survey Staff, 1990, The Loma Prieta, California earthquake: an anticipated event: Science, v. 247, p. 286-293.

White, R.A., and Ellsworth, W.L., in press, Seismic signals (and the lack thereof) immediately preceding the Loma Prieta earthquake (abs.): Seismological Research Letters.

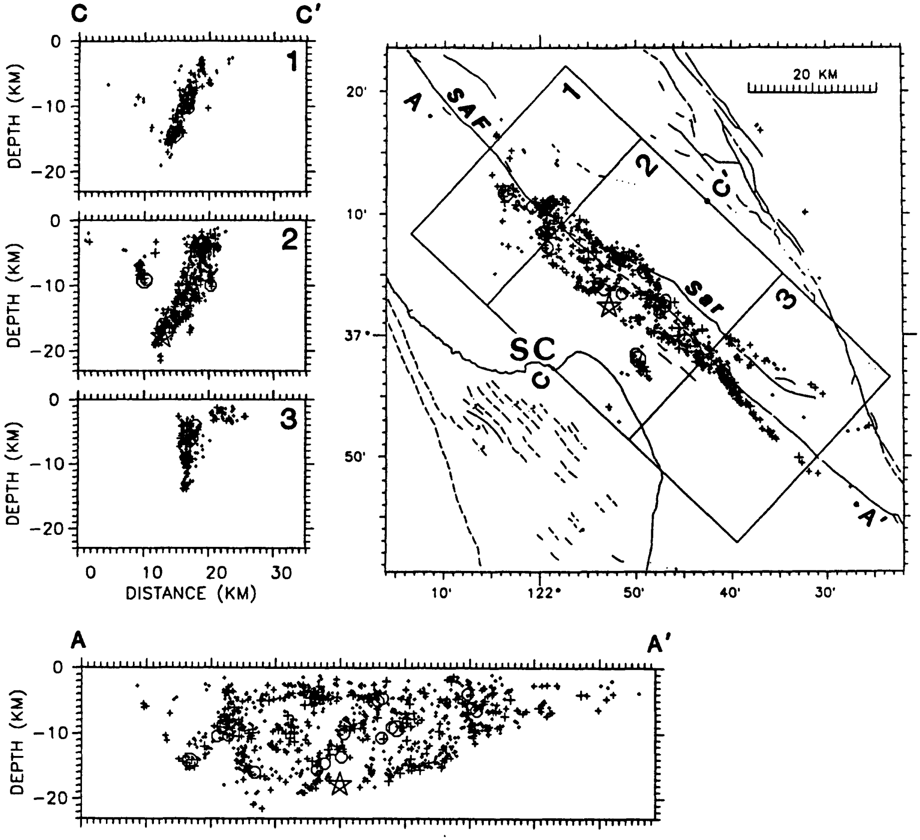

Figure 1. Well-constrained aftershock hypocenters, October 18-31, 1989. Main shock denoted by star.

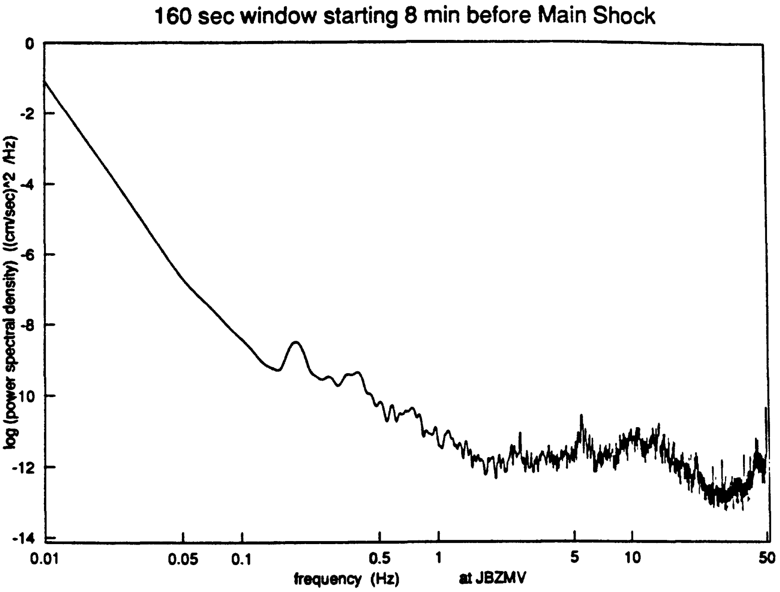

Figure 2. Power spectral density of seismic noise at station JBZ 6-8 minutes before Loma Prieta earthquake.

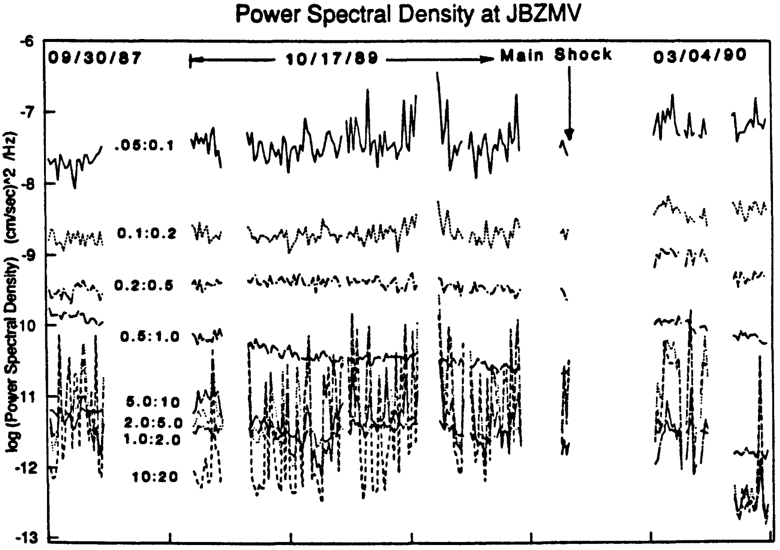

Figure 3. Time variation of seismic noise at station JBZ in frequency bands shown for September 30, 1987, seven hours preceding the Loma Prieta earthquake and March 4, 1990.

Dense Seismograph Array at Parkfield, California

9910-03974

Joe Fletcher, Paul Spudich, Larry Baker, and Margaret Hellweg
Branch of Engineering Seismology, and Geology
345 Middlefield Rd., MS 977
Menlo Park, California 94025
(415) 329-5628, 5654, and 5608

Investigations

The Parkfield Dense Array is a 14 element, short-baseline seismic array situated on the Work Ranch near Parkfield, California. Each site has 6 channels of data including a three-component velocity transducer and a three-component accelerometer which will provide on-scale recordings from the smallest local microearthquakes to the expected main shock. Each channel is digitized at 200 samples/s with a 16 bit A/D and data is stored in local memory and then telemetered to a central recording site.

The 14 stations are irregularly spaced along a serial coaxial line with a total length of about 8,000 ft. Arbitration of the coaxial line is handled using ARCNET protocols. The ARCNET controllers drive the coaxial line through Computrol modems which operate between 3.25 and 6.75 MHz. Using high-quality cable these modems can drive a network with a total length of about 32,000 ft. Time synchronization signals and power are also provided at each site through their own cabling system. In continuous mode the rate of data acquisition of the Parkfield Dense array is more than double that of the Anza array.

Results

While we have been recording data since April, 1989, several timing problems were discovered in the early data. These were mostly fixed in two stages. During the first stage we replaced the GOES receiver with a GOES receiver/clock that would provide meaningful time codes even when GOES reception was not good. At the same time software was installed in each field unit that prevents the internal clock from being reset unless it is sure that it has received uncontaminated time code. Time code is judged to be good if no parity errors are detected during transmission and several consecutive time codes are received in a row, each new one predictable from the previous. This upgrade to the timing system occurred at the end of August, 1989.

The second stage involves the circuitry in each field unit designed to phase-lock the time code so that digitization is synchronous across the array. It was discovered during December, 1989 that the circuitry that accomplishes this function was miswired. This was fixed. Whereas we were detecting 2,000 timing errors/day before the wiring errors were discovered, we now log only 20 timing errors/day. A timing error occurs when a packet is received with a time tag that is beyond limits set by the data acquisition system. We now feel most of our hardware is functioning as designed.

At present we are turning our attention to processing the data which has accumulated since late August, 1989. When we have calibrated the array for events recorded since the timing problems have been corrected, we will be able to correct the timing errors on the data recorded prior to August, 1989, and will include this data in the analysis. We are currently designing a data base to keep track of event files, archival volumes, parameters that describe the data, the associated earthquake parameters, and seismologically interesting parameters such as coda-Q that can be derived from the data. We have chosen Sybase as our data base. Since it resides on a VAX with the data, the data base can interact with the processing or analysis programs, either as a 'driver' providing queried information or as an immediate receiver of parameters for storage.

Reports

Fletcher, J.B., Spudich, P., MacDonald, T., Sembera, E., Miller, D., and Baker, L.M., 1989, The Parkfield, California, dense seismograph array: *EOS*, v 70, 1224.

Fletcher, J.B., Baker, L., Spudich, P., and Goldstein, P., 1989, The Parkfield, California, dense seismograph array: *Bulletin Seismological Society Amerioa, submitted.*

Theodolite Measurements of Creep Rates on San Francisco Bay Region Faults

14-08-0001-G1676

Jon S. Galehouse
Department of Geosciences
San Francisco State University
San Francisco, CA 94132

(415) 338-1204

We began to measure creep rates on San Francisco Bay region faults in September 1979. Amount of slip is determined by noting changes in angles between sets of measurements taken across a fault at different times. This triangulation method uses a theodolite to measure the angle formed by three fixed points to the nearest tenth of a second of arc. Each day that a measurement set is done, the angle is measured 12 times and the averaged determined. The amount of slip between measurements can be calculated trigonometrically using the change in average angle.

We presently have theodolite measurement sites at 22 localities on active faults in the San Francisco Bay region (see Figure 1). Most of the distances between our fixed points on opposite sides of the various faults range from 50-275 meters. The precision of our measurement method is such that we can detect with confidence any movement more than a millimeter or two between successive measurement days. We remeasured most of our sites about once every two to three months prior to the 17 October 1989 Loma Prieta earthquake. Following the quake, we established new Sites 22 and 23 on the San Andreas fault northwest and southeast of the epicentral area (see Figure 1). We also began more frequent measurements on sites on the San Andreas fault (14, 10, 22, 23), on the Hayward fault (17, 13, 12, 2, 1), and on the Calaveras fault in the Hollister area (6, 4). These more critical sites are now being measured about every six to seven weeks. The following is a brief fault by fault summary of our movement measurements through 26 April 1990. Included are brief discussions regarding the effect of the Loma Prieta earthquake on creep rates at each measurement site.

SAN ANDREAS FAULT (See Figure 2) - We have been measuring horizontal slip on the San Andreas fault at Site 10 in South San Francisco for about ten years and at Site 14 at the Point Reyes National Seashore Headquarters for about five years. Both sites have shown virtually no net slip over the years and neither was affected by the 17 October 1989 earthquake thus far.

In November 1989, we began measuring a USGS site (our Site 22) in Woodside that had not been remeasured for several years. Our preliminary results compared to unpublished USGS measurements in 1977 show that virtually no surface slip occurred between 16 February 1977 and 4 November 1989. About 4 millimeters of right slip has occurred, however, between 4 November 1989 and 20 April 1990.

We also established in November 1989 a new measurement site (23) on the creeping segment of the San Andreas fault near the southeastern end of the aftershock area near San Juan Bautista. We intend to compare the post-earthquake slip rate at this site with the pre-earthquake rate of about 6 to 8 mm/yr determined by USGS creepmeter and theodolite measurements in the San Juan Bautista area.

Our Site 18 (not shown on Figure 1) in the Point Arena area has averaged less than a millimeter per year of right slip since January 1981.

HAYWARD FAULT (see Figure 3) - We have been measuring horizontal slip at five sites along the Hayward fault for about the past ten years and have determined that the right-lateral creep rate is about 4 to 5 mm/yr. Although the creep characteristics (steady, episodic, or seasonal) differ from site to site, the ten-year rates are similar. None of our five sites on the Hayward fault showed any unusual movement either before or after the 17 October 1989 earthquake.

CALAVERAS FAULT (See Figure 4) - We have been measuring horizontal slip at two sites on the Calaveras fault in the Hollister area for more than ten years. Slip at both sites has been rather episodic with intervals of relatively rapid right slip typically lasting a couple months or less alternating with longer periods of time when little net slip occurs. More specifically, Site 4 along Seventh Street in Hollister has had ten episodes of relatively rapid right slip of about 5 millimeters or more since September 1979. Alternating with these times of relatively rapid movement are intervals of little net movement typically lasting about 8 - 12 months with one lasting two years between January 1986 - January 1988. The Loma Prieta earthquake occurred during an interval of slower movement that had persisted for about a year. The earthquake apparently triggered up to 14 millimeters of right slip at Seventh Street. Total cumulative right-lateral displacement went from about 67 millimeters to about 81 millimeters (see Figure 4). Overall the rate of right slip at Seventh Street is about 7 mm/yr for the past 10.5 years.

Slip at Site 6 along Wright Road just 2.3 kilometers northwest of Site 4 has included 12 episodes of relatively rapid right slip of about 5 millimeters or more since October 1979. Intervals of little net movement typically last about 3 - 12 months with one lasting about a year and a half between June 1985 - December 1986. The Loma Prieta earthquake occurred during an interval of slower movement that had persisted for about a year at Wright Road (similar to the situation at Seventh Street). The earthquake apparently triggered up to 12 millimeters of right slip and cumulative displacement went from about 119 millimeters to about 131 millimeters. The overall rate of right slip at Wright Road is more than 12 mm/yr for the past 10. 5 years. This rate is the fastest of any of our sites in the San Francisco Bay region and is about 5 mm/yr faster than the rate at nearby Seventh Street. It is possible that undetected surface movement may be occurring outside our 89.7 meter-long survey line at Seventh Street.

Our theodolite data alone cannot prove coseismic slip on the Calaveras fault due to the Loma Prieta earthquake on the nearby San Andreas fault. Our last measurement in the Hollister area before the earthquake was on 19 August 1989 and our first measurement after the quake was on 21 October 1989. Strictly speaking, we can only say that the 12-14 millimeters of right slip in the Hollister area occurred between these two measurement days. Other evidence, however, does indicate that the 12 - 14 millimeters of displacement was at least partially coseismic. We detected fresh en echelon cracks on Highway 25 near Hollister on 21 October 1989. The cracks extended from the asphalt into the dirt shoulder of the road. In addition, a USGS creepmeter detected coseismic slip of about five millimeters on the Calaveras fault about eight kilometers northwest of Hollister (S. Schulz-Burford, personal communication, 1989). Since 21 October 1989, both of our Hollister sites have returned to a slower phase of movement.

In contrast to our sites in the Hollister area, Site 19 in San Ramon near the northwesterly terminus of the Calaveras fault was not affected by the Loma Prieta earthquake. It remained virtually locked as it has been throughout our 9.4 years of measurements. It has also been unaffected by the recent (April 1990) swarm of earthquakes near Alamo.

CONCORD - GREEN VALLEY FAULT (see Figure 5) - We began our measurements at Site 3 and Site 5 on the Concord fault in the City of Concord in September 1979. We measured about one centimeter of right-lateral slip at both sites during October and November 1979. Following this, both sites showed relatively slow slip for the next four and one-half years at a rate of about a millimeter per year. In late Spring-early Summer 1984, both sites again moved relatively rapidly, slipping about seven millimeters in a right-lateral sense in a few months. The rate again slowed to about a millimeter per year for about the next three years, beginning in late August 1984. Between late November 1987 and late February 1988, the Concord fault moved about eight millimeters right-laterally. Between late February 1988 and April 1990, the fault at Site 3 has moved about a centimeter, somewhat faster than its ten-year average rate. The fault at Site 5, however, has moved at about its overall average rate. If thus appears that typical movement characteristics on the Concord fault since at least 1979 are intervals of relatively rapid right slip of about 7-10 millimeters over a period of a few months alternating with intervals of relatively slower right slip of about a millimeter or two a year over a period of several years. An exception to this pattern is the relatively average rate of movement of the Concord fault since late February 1988.

It appears that the Loma Prieta earthquake and the recent (April 1990) swarm of earthquakes near Alamo had no affect on the Concord fault at our measurement sites in the City of Concord.

We began measuring Site 20 on the Green Valley fault in Cordelia in June 1984. Large variations tend to occur at this site between measurement days, possibly because logistical considerations resulted in our survey line being particularly long (335.8m). However, our results suggest that the Green Valley fault behaves similarly to the Concord fault which is along trend to the southeast, i.e., relatively rapid right slip in a short period of time (months) alternating with relatively slower slip over a longer period of time (years). The Green Valley fault was in a period of relatively slow movement for the first 20 months of our measurements, averaging a few millimeters per year of right slip. In early 1986, however, the fault slipped right-laterally more than a centimeter. This was followed by about three years in which the net slip was less than a millimeter per year. Preliminary results indicate that sometime after 6 August 1989, the Green Valley fault entered into another phase of relatively rapid right slip that is still continuing. Four measurements since then indicate slip of about 15 millimeters. It is tempting to suggest that shaking from the Loma Prieta earthquake triggered the onset of this relatively rapid displacement. However, the measurement intervals are too far apart to lend much credence to this hypothesis and as far as we know, there is no additional evidence suggesting a relationship between the two. It is probably a coincidence that the Green Valley fault began a period of rapid movement at a time that could be related to the Loma Prieta earthquake. Nevertheless, the movement characteristics of the Green Valley fault do suggest a relationship with the

Concord fault. Even though the episodes of relatively rapid slip and relatively slower slip on the Green Valley and Concord faults occur at different times, they are similar in amount of slip and duration of the intervals. Although future measurements may suggest otherwise, at the present time we consider the Concord and Green Valley faults to be different names for southeastern and northwestern segments of the same fault. The overall average rate of about 5 to 6 mm/yr of right slip on the Green Valley fault for the past 5.9 years is higher than the rates determined for the Concord fault. This may be because of the shorter duration of measurements and because of the fact that the Green Valley fault is still in its second relatively rapid phase of movement since we began our measurements.

OTHER FAULTS - Seasonal and/or gravity controlled mass movement effects are present at Site 21 on the Rodgers Creek fault and Site 15 on the West Napa fault. Both sites show large variations from one measurement day to another and both show virtually no net slip since September 1986 and July 1980 respectively.

Not much, if any, net slip appears to have occurred at our two sites along the Antioch fault since 1980 and 1982. However, much subsidence and mass movement creep occur both inside and outside the Antioch fault zone and it is probable that these nontectonic movements obscure any tectonic slip that could be occurring.

The Seal Cove-San Gregorio fault has shown virtually no net slip since November 1979 and May 1982 respectively.

The Loma Prieta earthquake appears to have had no noticeable effect on the rate of movement at our sites on the Rodgers Creek, West Napa, Antioch, and Seal Cove-San Gregorio faults. All these faults have remained virtually locked thus far.

Publications

Galehouse, J.S., Baker, F.B., Graves, O., and Hoyt, T., 1989, San Francisco Bay region fault creep rates measured by theodolite: in Sylvester, A.G. and Crowell, J.C., editors, The San Andreas Transform Belt , Field Trip Guidebook T 309, 28th International Geological Congress, American Geophysical Union, Washington, D.C., p. 45-48.

Galehouse, J.S., 1990, Effect of the Loma Prieta earthquake on fault creep rates in the San Francisco Bay region: EOS, Transactions American Geophysical Union, v. 71, p. 288.

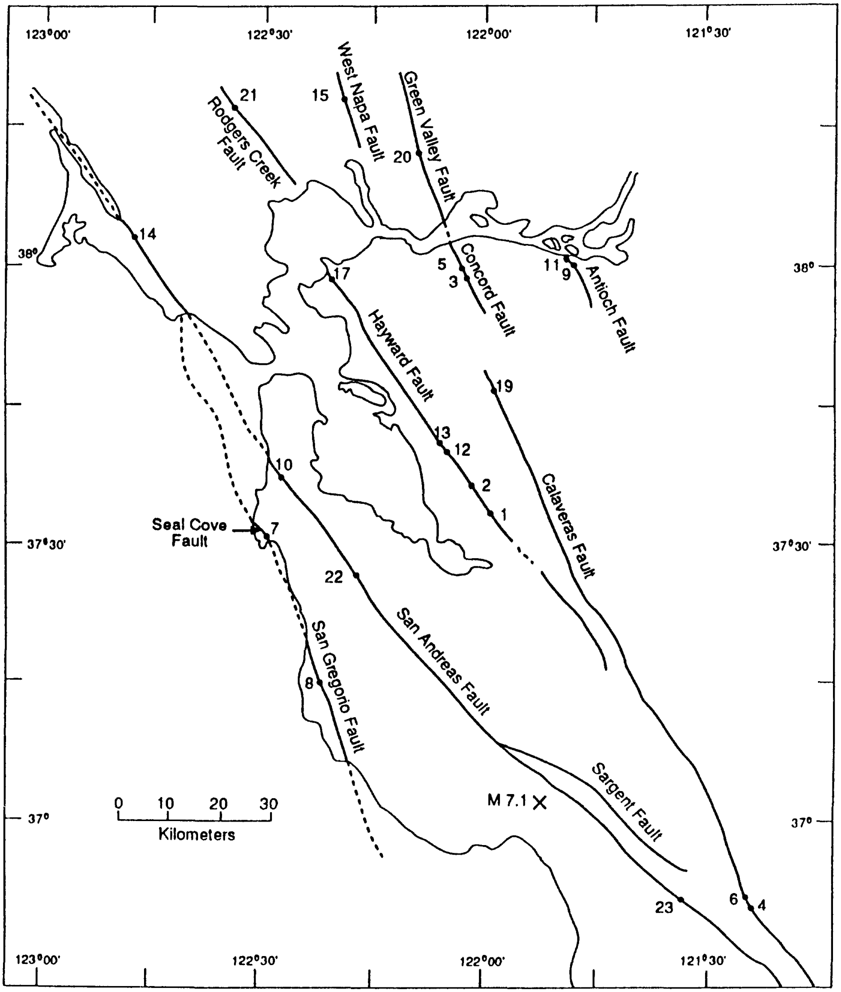

Figure 1. San Francisco State University Theodolite Measurement Sites

SAN ANDREAS FAULT

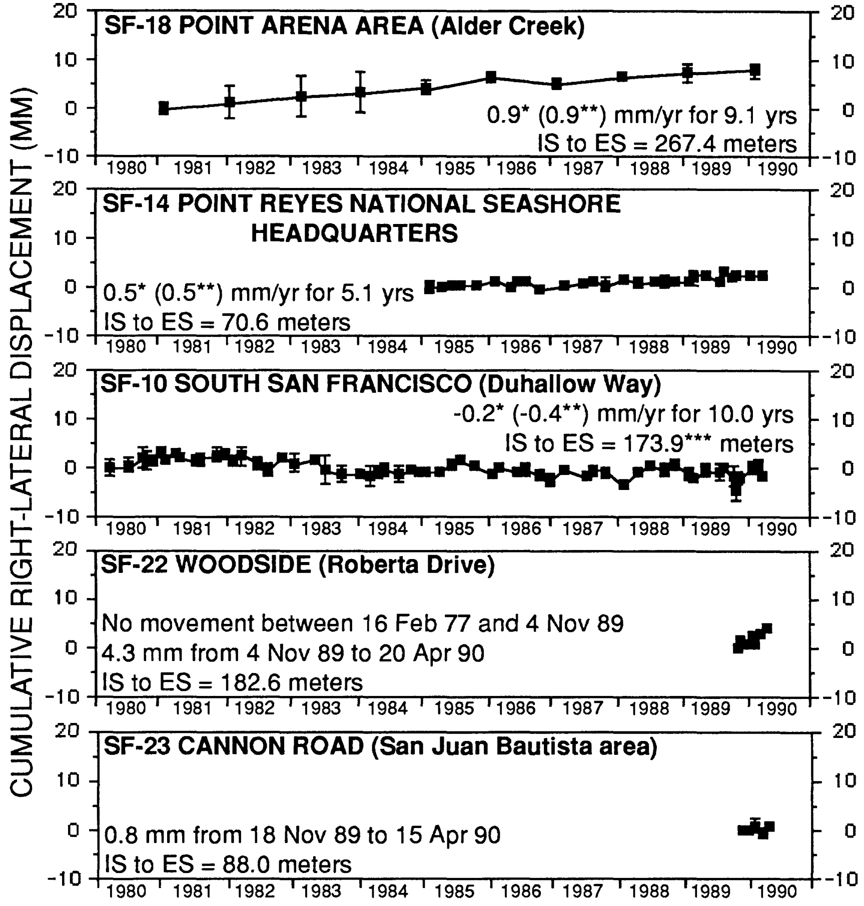

* Simple average ** Least-squares average
*** Extended to 207.5 meters on 15 Nov 89

Figure 2. San Andreas Fault Displacement

HAYWARD FAULT

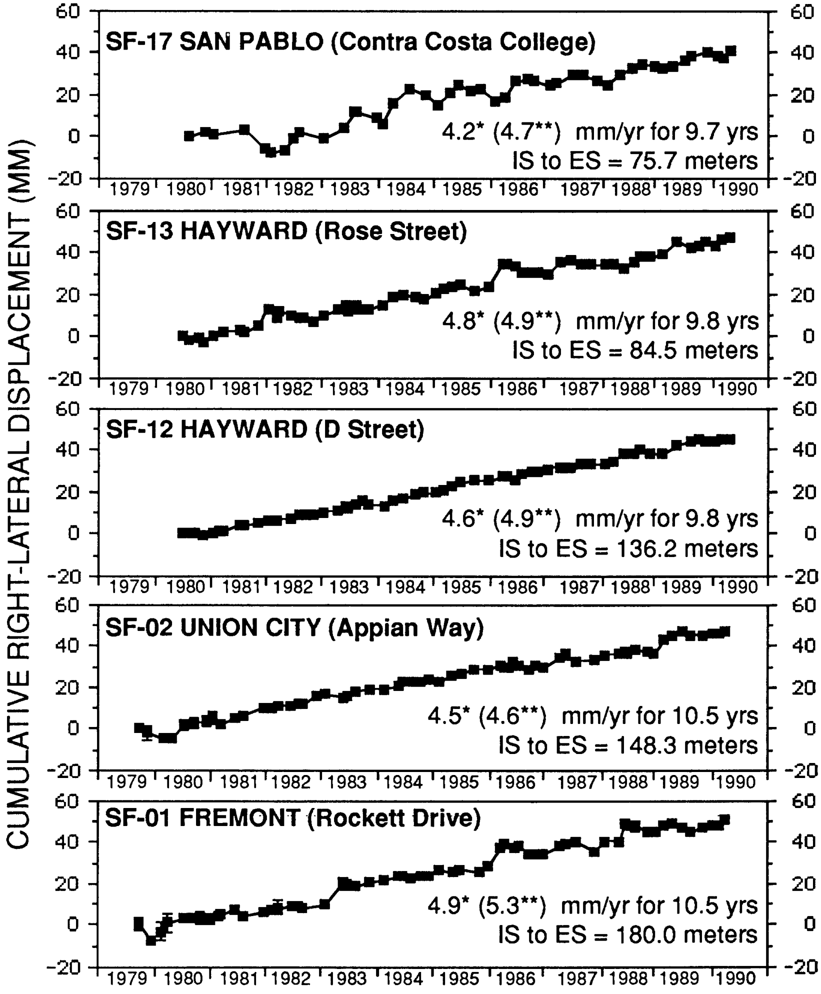

* Simple average ** Least-squares average

Figure 3. Hayward Fault Displacement

CALAVERAS FAULT

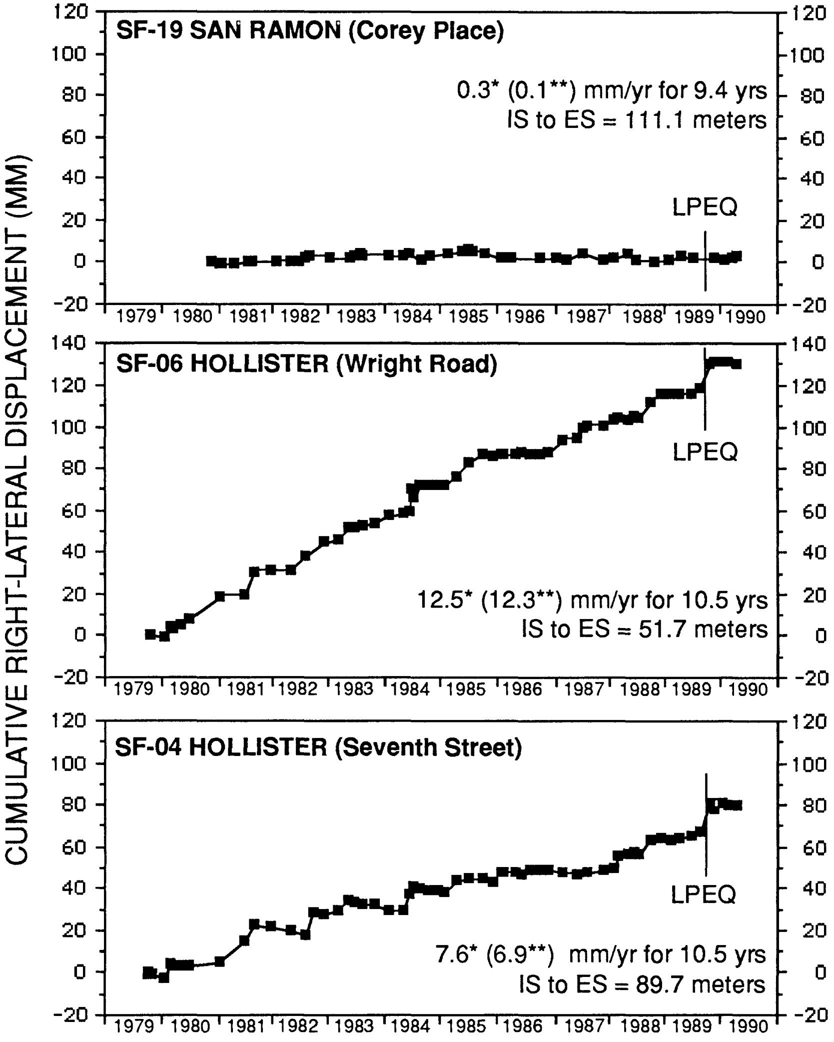

* Simple average   ** Least-squares average

LPEQ = Loma Prieta Earthquake of 17 Oct 89

Figure 4. Calaveras Fault Displacement

CONCORD - GREEN VALLEY FAULT

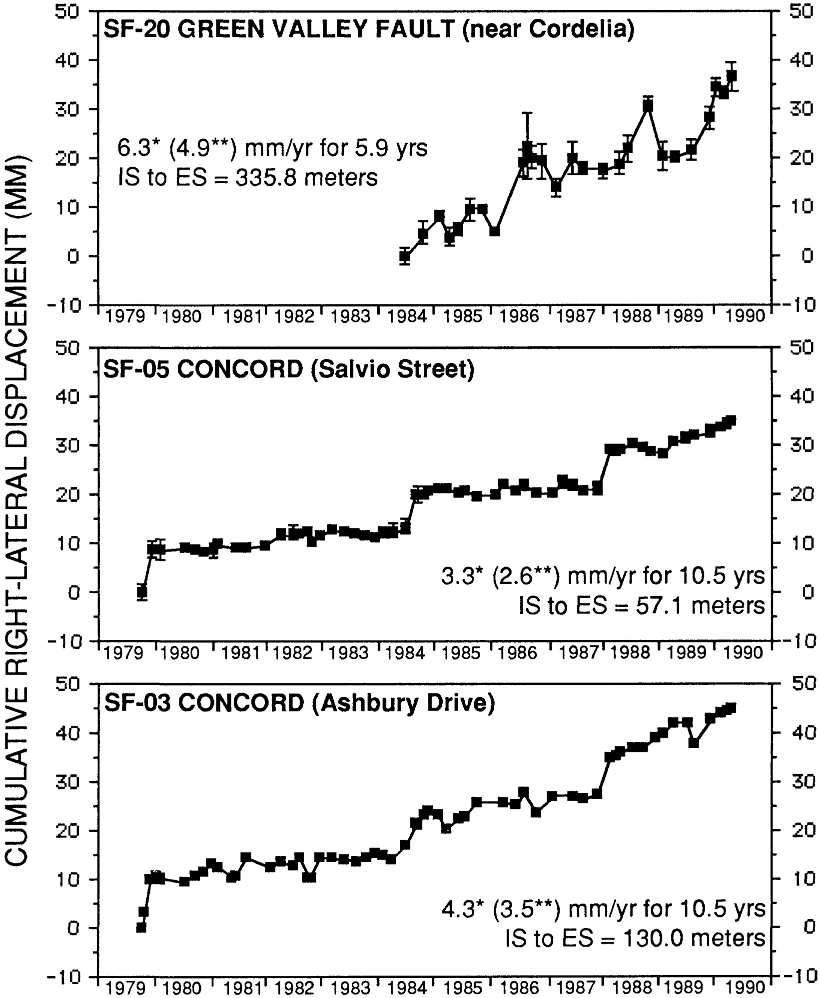

* Simple average ** Least-squares average

Figure 5. Concord-Green Valley Fault Displacement

DEEP BOREHOLE PLANE STRAIN MONITORING

14-08-0001-G1376

Michael T Gladwin,

Department of Physics
University of Queensland
St.Lucia, 4067
AUSTRALIA.

ACTIVITIES

1.Detailed investigation of the long and short term strain data associated with the Loma Prieta earthquake of October 17, 1989 has been carried out.

2. Necessary conditions for the establishment of a full scale strain instrumentation array in an earthquake-prone region such as the San Francisco Bay area were investigated, and the results presented at the USGS/NSF Workshop on Crustal Deformation and Earthquake Mechanics at Morro Bay in March, 1990.

3. Progress has been achieved in developing tidal calibration procedures based on comparison of borehole tensor strain data with data from the Pinon Flat Laser strainmeter. However further development of this procedure is necessary.

4. Retrieval and processing of data from the five borehole tensor strain instruments in California (at San Juan Bautista, Pinon Flat and three near Parkfield) has continued. Regular reports have been presented to the monthly Parkfield review meetings, including comments on any significant signals. In particular a number of strain signals coincident with nearby creep events have been observed.

RESULTS

1. The Loma Prieta earthquake of 17 October 1989 provided the first opportunity in California to observe the near field of a magnitude 7 earthquake with borehole tensor strainmeters. No short term (seconds to days) precursors were identified at the 1 nϵ level. The medium term data at the San Juan Bautista tensor strainmeter site, 30 km to the south of the epicentre, where the strain rate had been constant at the 20nϵ level since 1986, showed a clearly anomalous change in strain rate of approximately 200nϵ/year established in late 1988, a year before the event, in the fault parallel shear $\Gamma_1 = (e_{xx}-e_{yy})/2$. The areal and Γ_2 (e_{xy}) shear strain rates remained constant over this period. These data are shown in the accompanying figure, which contains areal strain and shear strains Γ_1 and Γ_2 in nanostrain. Two simple exponentials have been extracted from the data to account for grout cure (approximately 100 days time constant) and non elastic long term hole recovery (approximately 1000 days time constant).

This signal is compatible in sense of shear and order of magnitude with a change in strain rate of 300 nϵ/year implied from changes of line length of the Loma Prieta - Allison geodetic record. These observations seem to indicate a broad regional change of strain rate about one year before the event acting to increase the shear stress across the fault and the probability of failure. With such limited spacial sampling of the region it is impossible to model the tectonic processes occurring in the region and so determine whether there is a causal link useful for prediction between this observation and the Loma Prieta earthquake.

2. Presentation at the Morro Bay workshop developed the concept of an instrument cluster to provide a coherent observatory type data base for geodetic, seismic and borehole strain instruments for a region scaled appropriately for a magnitude 7+ event. Typically a cluster would cover an area of about 150 by 50 km, and include sites instrumented with borehole strain monitors, seismometers and accelerometers.

It was demonstrated that for reasonable borehole strain coverage of such an area, a minimum of 25 sites would be necessary. The sites would be located not nearer than 5 km from the fault trace, and be operated at a precision of 0.1 nanostrain for frequencies below 10 Hz. This will provide useful co-seismic data for all events above M=4, and for larger events permit monitoring of longer period precursive strain fluctuations larger than 0.1% of the event. The strain cluster should be a 50-50 mix of dilatometers and tensor strain meters because of their complementary characteristics.

PUBLICATIONS

Gladwin, M. T., High Precision multi component borehole deformation monitoring. *Rev.Sci.Instrum.*, *55*, 2011-2016, 1984.

Gladwin, M.T., Gwyther, R., Hart, R., Francis, M., and Johnston, M.J.S., Borehole Tensor Strain Measurements in California. *J. Geophys. Res. 92.* B8 pp7981-7988, 1987.

Gladwin, M. T. and Hart, R. Design Parameters for Borehole Strain Instrumentation. *Pageoph.,123,* 59-88, 1985.

Gladwin, M. T., Hart, R., and Gwyther, R. L. Tidal Calibration of Borehole Vector Strain Instruments.*EOS, (Trans. Am. G. Un.) 66,* 1057, 1985.

Gladwin, M.T., and Johnston, M.J.S. Coseismic moment and total moment of the April 24, 1984, Morgan Hill and the January 26, 1986, Quiensabe earthquakes. *EOS,(Trans.Am.G.Un.), 67, R 308, 1986.*

Gladwin, M. T. and Wolfe, J. Linearity of Capacitance Displacement Transducers. *J.Sc.Instr. 46,* 1099-1100, 1975.

Johnston, M.J.S., Gladwin, M.T., and Linde, A.T. Preseismic Failure and Moderate Earthquakes. *I.A.S.P.E.I.* , Tokyo, August 19-30, S7-65, 35 , 1985.

Johnston, M. J. S., Linde, A.T., Gladwin, M.T., and Borcherdt, R.D. Fault Failure with Moderate Earthquakes. *Tectonophysics.* 144, 189-206, 1987.

Johnston, M.J.S., Borcherdt, R.D., Glassmoyer, G., Gladwin, M.T., and Linde, A.T. Static and Dynamic Strain during and following January 26, 1986, Quiensabe, California, Earthquake. *EOS,(Trans. Am. G. Un.), 67,* 16, 308, 1986.

Johnston, M.J.S., Borcherdt, R.D., Gladwin, M.T., Glassmoyer, G., and Linde, A.T. Static and Dynamic Strain during the M_L 5.9 Banning, California Earthquake on July 8, 1986. *EOS,(Trans. Am.G.Union),68,* 44, 1244 (1987).

Myren, G.D., Johnston, M.J.S., Linde, A.T., Gladwin, M.T. and Borcherdt, R.D. Borehole Strain Array near Parkfield, California. *EOS (Trans. Am.G.Union), 68,* 44, 1358 (1987).

Gladwin, M. T., Hart, R., and Gwyther, R. L. Continuous Regional Deformation Measurements Related to the North Palm Springs Earthquake of July 8, 1986.*EOS, (Trans. Am. G. Un.) 69* 1432, 1988.

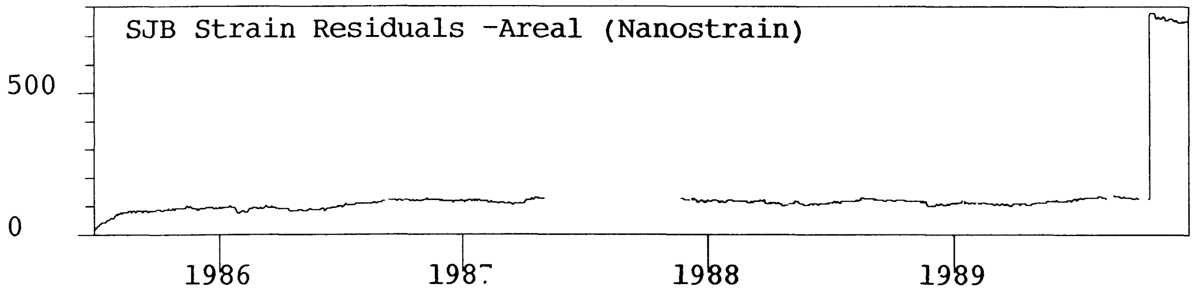
SJB Strain Residuals -Areal (Nanostrain)
500
0
1986
1987
1988
1989

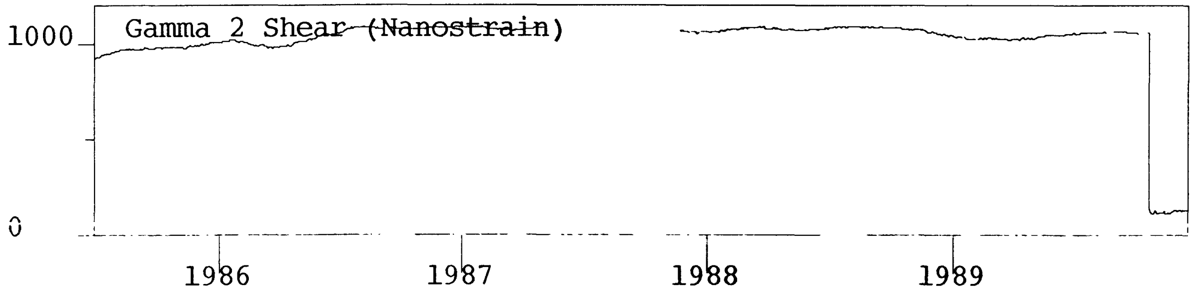
Gamma 2 Shear (Nanostrain)
1000
0
1986
1987
1988
1989

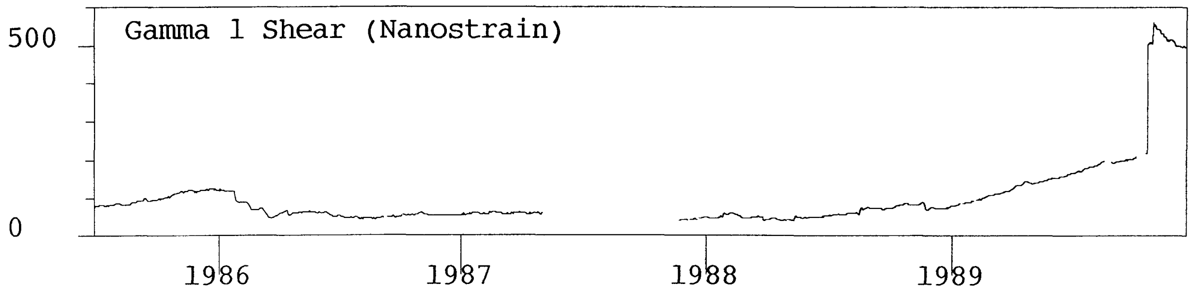
Gamma 1 Shear (Nanostrain)
500
0
1986
1987
1988
1989

Geodetic Measurement of Coseismic Slip and Block Rotation in Southern California

Contract # 14-08-0001-G1805

Ken Hudnut and Kerry Sieh
Caltech; Geology 170-25; Pasadena, CA 91125
(818) 356-6271 // hudnut@legs.gps.caltech.edu

Introduction

This project is primarily a data collection effort, the short-term aim being to increase the density of geodetic monumentation and measurement along the southern San Andreas fault. Longer-term goals are to accomplish this along other segments of surficial faults in southern California as well, and to initiate a detailed study of block rotation in the Salton Trough. Proposed for 1991 is the integration of this project with two other Caltech projects; the long-standing Creep and Strain study, and the recently completed GPS survey and future monitoring of crustal deformation in the Los Angeles Basin, which is being done in collaboration with the City and County of Los Angeles.

We have accomplished two GPS surveys since early February, when this project's funding began. The first was a cooperative survey involving a large group, organized primarily by Rob Reilinger of MIT, which is described below. Our participation in this survey involved site selection and reponsibility for adding eleven new stations to the network in the Coachella Valley. Second was a kinematic GPS survey of the UCSB monument array at Painted Canyon, combined with static measurements between this array, the Durmid Hill array, and the fiducial station at Black Butte. In addition to descriptions of these data collection projects, this report briefly describes work in the past six months that is scientifically related but funded by other sources to date. The following section lists data collected since the fall of 1989, in chronological sequence. Thus, work directly funded by the USGS comes towards the end of the following section.

Results

1. December 1989 Kinematic GPS Surveys:

Two arrays across the San Andreas fault, one at Durmid Hill (the UCSB array) and one at Cholame (southeast of Parkfield; the USGS "FMK" level line) were surveyed by kinematic GPS. Results to date are all from processing of the GPS data by M. Jackson (UNAVCO). Information on these data is available by requesting a copy of the paper presented at the Morro Bay workshop. Baselines have now been processed from the array at Cholame as well. A manuscript is in preparation by M. Jackson and others regarding accuracy of kinematic GPS, and results from these December 1989 surveys will be incorporated in this manuscript.

Funding for these surveys in Dec. 1989 was not provided by the USGS, but the Durmid Hill array survey in particular is encompassed by the present USGS project for FY1990. Using our USGS funding, we anticipate adding new monuments near this array, and directly tying it to the adjacent USGS small trilateration array at Durmid Hill (M. Lisowski, written comm.).

2. 1990 Salton Trough GPS Campaign (Static GPS Survey of 11 new stations in the Coachella Valley):

This survey, primarily organized by Rob Reilinger, was important to our geodetic densification project in the Coachella Valley. In order to provide a good distribution of new primary GPS stations in the Coachella Valley, Caltech worked with Riverside County to select sites and install several new GPS monuments. Furthermore, field reconnaissance of a large number of existing monuments led to incorporation of a total of eleven new monuments in the Coachella Valley during this year's major Salton Trough campaign. Establishment of these will help us by providing coordinates for relatively nearby control points for our kinematic GPS surveys. We are also initiating occasional GPS monitoring of a subset of these primary points; so far Black Butte has been reoccupied since the main campaign in February.

Following our work on the planning and reconnaissance, Caltech fielded our two Trimble 4000SST GPS receivers and two operators (Hudnut and Larsen) in the campaign. Our USGS funds supported the field expenses for only one of us, as had been requested in our 1990 budget - for 1991, we hope to support operators for both of our recievers during the resurvey of this network. We thank Reilinger for support of this initiative in the Coachella Valley, and Mike Lisowski for sending unpublished information on USGS trilateration stations in the area.

3. 1990 Los Angeles Basin GPS Campaign (Static GPS survey of 23 stations across the San Fernando Valley and LA Basin):

This survey was organized and operated by Caltech, and was funded by the City and County of LA Survey Divisions - most of the field personnel were professional surveyors from these offices. Although not funded by the USGS in FY1990 because it was not written into our original proposal, this project is strongly related to the NEHRP goals of assessing hazard in the Los Angeles area. Our proposed work for FY1991 includes processing of the data from this survey and analysis for strain since the historic surveys in 1933 and 1979 there. We anticipate presenting initial results at the 1990 Fall AGU meeting. Station descriptions and all information on the experiment have already been distributed to other groups conducting GPS research in southern California.

4. April 1990 Kinematic GPS Survey:

Twelve of the monuments in UCSB's Painted Canyon array, in addition to two monuments farther from the fault, were surveyed using kinematic GPS. In addition, a baseline from this array to the Durmid Hill kinematic array (done in Dec. '89) was measured by static GPS. Both were observed synchronously with the Black Butte fiducial station. UCSD's Trimble at the Pinon Flat station was running for part of our survey, and the Rogue receivers in the permanent array were also operating during our survey.

We have primarily operated using one roving kinematic receiver per reference receiver, obtaining two measurements per night to each kinematic point. We have also now attempted operating two roving kinematic receivers using just one as a reference. Processing of these data from the five receivers will be done next month.

Acknowledgements: We are grateful to UNAVCO and to the M.I.T. group, who have allowed us to use their GPS receivers on the projects described here. We also thank Riverside and Los Angeles Counties and the City of Los Angeles for their substantial support of the data collection efforts described in this report.

A Vertical Deformation Sensor on the Southern San Andreas Fault

14-08-0001-G1786

Hadley O. Johnson, Frank K. Wyatt,
and Duncan Carr Agnew
Institute of Geophysics and Planetary Physics
University of California, San Diego
La Jolla, California 92093-0225
(619) 534-2019

This grant supports the construction of a fiber-optic anchoring system near the Coachella segment of the San Andreas Fault—specifically, on the western flank of Durmid Hill, near the termination of this fault and its junction with the Brawley Seismic Zone. This area has been identified as one of the more likely initiation points for a great earthquake during our lifetimes. The experiment involves measuring the relative vertical motion of several points in the ground down to a depth of 50 m. The goal of this temporary (two year) installation is to study the stability of the near-surface material in the region to determine if it is stable enough to support precise measurements of strain and tilt. Efforts at Piñon Flat Observatory have shown that observatory-based instruments can give data up to one thousand times more precise than geodetic surveying techniques in the period range of months to minutes, while accurately recording the secular accumulation of deformation—provided that the instruments are adequately anchored to depth. Determining what depth is adequate in this area—as a first step toward consideration of more extensive instrumentation—is the main goal of this project.

Over the course of several trips to the area our opinion on where to site this experiment changed a number of times, based primarily on logistics considerations as the geology is fairly uniform over broad areas. We came to feel that our best possibility of getting good data would be to seek an agreement with a private land owner—this despite the consistent helpfulness shown by public-lands representatives in the area. Indeed, our initial choice for siting was on Salton Sea State Park land, and we pursued permitting for this, but due to the remote yet frequented nature of the area we came to feel that building on private land, where we will have relatively easy access to electric power, phone lines, and most importantly, security and ready assistance, would be better. Toward this end we have recently come to an agreement on a privately owned site approximately 1 km west of the surface trace of the San Andreas Fault (see figure). We have also made arrangements to use part of an out-building on the property to house a small data-recording computer. This computer will allow us access (via modem) to the data from our lab in San Diego, and provide an on-site display of the displacement sensor's health.

The installation itself will be made underground, to get away from some of the daily temperature fluctuations, and housed inside two connected sections of drainage culvert tipped on-end. One of these sections will serve as the entrance way, extending from the surface down to about 2½ meters depth. A "window" between this section and the instrument section will provide access to the optical and electronic components and to the optical fiber sensors which will extend down the vault's borehole. The instrument half of the vault will be buried under approximately 1 meter of dirt. Installation of our low cost vault is awaiting borehole drilling and fiber installation. Other boreholes which have been drilled in the area have had problems with side-wall cave-ins due to the very weak nature of the surface material; we see successful completion of the borehole work as the most difficult task remaining.

The displacement sensors themselves will be un-equal arm Michelson interferometers using as light paths single-mode optical fibers which extend to different depths. By monitoring the differential displacement between pairs of these fibers we hope to measure a vertical profile of the ground's deformation rate. We expect to find relatively small differential motions between the deeper fibers, indicating that the material at depth is deforming very little. It is this "bedrock" material to which long-base surface instruments need to be "anchored" and that we would like to locate with this experiment.

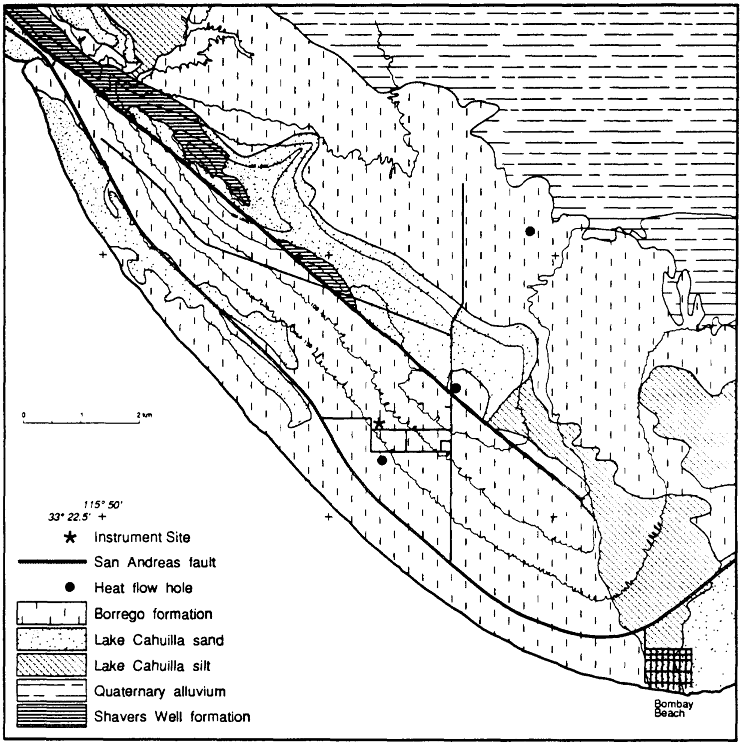

Figure 1.

TILT, STRAIN, AND MAGNETIC FIELD MEASUREMENTS

9960-2114

M. J. S. Johnston, R. J. Mueller, G. D. Myren
Branch of Tectonophysics
U. S. Geological Survey
Menlo Park, California 94025
415/329-4812

Investigations

[1] To investigate the mechanics of failure of crustal materials using data from both deep borehole tensor and dilational strainmeters and near surface strainmeters, tiltmeters, and arrays of absolute magnetometers.

[2] To develop physical models of incipient failure of the earth's crust by analysis of real-time records from these instruments and other available data.

Results

[1] SEISMOMAGNETIC EFFECT GENERATED BY THE OCTOBER 18, 1989, M_L 7.1 LOMA PRIETA, CALIFORNIA, EARTHQUAKE.

A differentially connected array of proton magnetometers operated within the eventual epicentral region of the October 18, 1989, M_L 7.1 Loma Prieta earthquake for 10 years from 1976 to 1986. Following the earthquake, the magnetometers were reinstalled with sensors replaced in the original undisturbed sensor holders. Comparison of data obtained during the weeks following the earthquake with the earlier data indicates offsets of about 1 nT may have been generated at some of the sites. The measurement error in these data ranges from 0.1 nT to 0.4 nT. The offsets can be generally, but not perfectly, fit with a simple seismomagnetic model of the earthquake for which 1.9 m of right lateral and 1.3 m of dip slip (south-west side up) occurred on a fault patch between 6 km and 18 km deep and 45 km long. The total rock magnetization is assumed to be 1.0 A/m. An alternate explanation in terms of electokinetic effects is possible since some ground water flow occurred following the earthquake.

[2] NEAR-FIELD HIGH PRECISION STRAIN PRIOR TO THE OCTOBER 18, 1989, LOMA PRIETA M_L 7.1 EARTHQUAKE?

High resolution strain recordings were made throughout California prior to, during, and following, the October 18, 1989, M_L 7.1 Loma Prieta earthquake. These recordings were made in deep boreholes with both dilational strainmeters (sensitivity 10^{-11}) and 3-component tensor strainmeters (sensitivity 10^{-9}). The nearest instruments, a dilatometer and a tensor strainmeter near San Juan Bautista, California, are about 40 km to 45 km, respectively, to the south-east along strike from the epicenter of the earthquake but only about 10 km and 15 km, respectively, from the probable southern end of the final rupture. All instruments remained on scale during the earthquake and all instruments recorded strain offsets generated by the earthquake. The data have been searched for indications of short, intermediate, and long term strain redistribution and/or fault slip that might have indicated imminent rupture. Changes in both dilational and tensor strain during the months to minutes before the earthquake are about 1000 times smaller than the strain offset generated on these nearby instruments by the earthquake. This constrains preseismic slip at the nucleation point of the earthquake, if the form is similar to that during the earthquake, to be less than 0.1% of the earthquake rupture. In other words, slip equivalent to that expected for a M 5 earthquake could have occurred in the hypocentral region without the strainmeters (or the geodetic instruments over the hypocenter), detecting it. Some hints of intermediate term strain changes occurred in mid-1988 and mid-1989. These changes were both followed by M_L 5 earthquakes in the hypocentral region on June 27, 1988, and August 8, 1989, respectively, and correspond approximately in time with minor indications of changes in geodetic strain rate over the epicenter.

[3] REVIEW OF CONTINUOUS HIGH PRECISION STRAIN MEASUREMENTS NEAR THE LOCKED AND CREEPING SECTIONS OF THE SAN ANDREAS FAULT

Deep-borehole strainmeters have been operating since 1984 at sites near the northern and southern creeping/locked transition zones and in the "Big Bend" region of the San Andreas fault in northern and southern California, respectively. These instruments resolve strain changes to better than 1 part per billion (ppb) over periods of months to minutes. The last five years of strain data show long periods of uniform crustal strain, infrequent episodes of aseismic strain sometimes resulting from aseismic fault creep, and high frequency straingrams and strain field offsets generated by local earthquakes. Whereas simple views of the earthquake rupture process have suggested that: 1) substantial non-linear deformation occurs prior to rupture, 2) the scale of this deformation exceeds the eventual earthquake rupture dimensions, and 3) the properties of near-fault materials may vary with time and location, these high resolution borehole strain recordings indicate: 1) minimal short-term non-linear precursive strain occurs, 2) the size of fault patches that initiate failure are probably less than a few hundred meters in size while the eventual earthquake rupture dimensions can be several tens of kilometers, 3) no evidence of variations in near-field material properties, and 4) strain offsets from local earthquakes that are largely transmitted elastically despite complex geology and fault geometry. In the case of the recent October 18, 1989, M_L 7.1 Loma Prieta earthquake, strain data from two instruments near San Juan Bautista, 5 km to 10 km southeast of the final southern extent of the rupture, indicate that any precursive failure in the hypocentral region (with a form similar to that during the earthquake) was at least a 1000 times smaller in the minutes to months before the earthquake. This, in turn, constrains the maximum amount of horizontal or vertical displacement in the hypocentral region to be, at most, a few millimeters, if any occurred at all. As more borehole strainmeters are installed, these data will continue to place increasingly tighter constraints on physical processes that occur at the earthquake source.

[4] STRAIN AND MAGNETIC FIELD CHANGES ON THE RED RIVER FAULT SYSTEM NEAR DENGCHAUN AND LIANTE, YUNNAN, CHINA: 1980-1990.

Arrays of differential magnetometers and intermediate-baseline geodetic nets have been installed and surveyed since 1980 at the northern end of the Red River fault in Yunnan Province. The primary features of the geodetic data are a non-uniform, but net negative dilation of 0.3 μ strain/a and a maximum shear increase of 0.2 μ strain/a in a direction N60W. Test line data indicate repeatibility in distance measurements during this time to better than 3 mm on a 734 m line. Magnetic measurements in the region of high magnetization on the west side of the fault at Dengchaun show an increase in local magnetic field of up to 1 nT/a over sites on the east side of the fault. In contrast, no significant magnetic changes have occurred in the Liante array. This result is in accordance with tectonomagnetic theory since the absence of regional magnetic anomalies indicate remanent and induced rock magnetization of less than 0.001 A/m.

[5] BOREHOLE STRAIN ARRAY IN CALIFORNIA

A network of 15 borehole strainmeters along the San Andreas fault zone and in the Long Valley Caldera continue to be monitored and maintained (Figure 1). All instruments are installed at depths between 117-m and 324-m and all are between 1-km and 5-km from the the surface trace of the fault. High frequency dilatometer data in the frequency range 0.005 Hz to 100 Hz are recorded on 16-bit digital recorders with least count noise less than 10^{-11}. Low frequency data from zero frequency to 0.002 Hz are transmitted through the GOES satellite to Menlo Park, CA, using a 16-bit digital telemetry system. At the USGS in Menlo Park the data are displayed in "almost real time" and are continuously monitored with detection algorithms for unusual behavior. The data for the past 6 months are shown in Figures 2a, 2b, 2c. Least-count noise is about $5*10^{-12}$ for the on-site digital recordings, and about $2*20^{-11}$ for the satellite telemetry channels. Earth strain tides, strain transients related to fault creep and numerous strain seismograms from local and teleseismic earthquakes with magnitudes between -1 and 6 have been recorded on these instruments. Static moments and total earthquake moments are determined from the co-seismic strains and total strain changes observed with the larger events.

[6] CROWLEY LAKE AND SAN ANDREAS LAKE WATER LEVEL MONITORING

Water level monitoring sites have been installed on Lake Crowley in the Long Valley/ Mammoth Lakes region and San Andreas lake on the San Andreas fault just south of San Francisco. These data provide differential water level measurements (tilt) with a measurement precision of less than 1 mm on baselines of 5 to 8 kilometers. Monthly averages of the data from San Andreas lake between 1979 and 1989 indicate a tilt rate of 0.02 ± 0.08 microradians/yr (down S34°E). The data for the past 6 months are shown in Figure 3.

[7] DIFFERENTIAL MAGNETOMETER ARRAY IN CALIFORNIA

We continue investigations of local magnetic fields and relationships to crustal strain and seismicity in the Parkfield region and in southern California (Figure 4). The network consists of 9 stations which are all sampled synchronously every 10 minutes and transmitted with 16-bit digital telemetry to Menlo Park, CA through the GOES satellite. Data are monitored daily with particular attention to the seven stations operating in the Parkfield region of central California. The data for the past 6 months are shown in Figure 5a, 5b, 5c, 5d.

Reports

Mueller, R. J., and M. J. S. Johnston, 1989. Large scale magnetic field perturbation arising from the May 18, 1980, eruption from Mount St. Helens, Washington, Physics Earth Planet. Int. v57, 23-31.

Davis, P. M., M. J. S. Johnston, J. Dvorak, and D. Dzurisen, 1989. Electric and Magnetic Field Measurements on Mount St. Helens Volcano at Times of Eruptions 1980-1985, J. Geomag. Geoelec., v41, 783-796.

Johnston, M. J. S., 1989. Review of magnetic and electric field effects near active faults and volcanoes in the U.S.A., Physics Earth Planet. Int., v57, 47-63.

Myren, D. and M. J. S. Johnston, 1989. Borehole dilatometer installation, operation and maintenence at sites along the San Andreas fault, California, U. S. Geological Survey Open File Report 89-349.

D. P. Hill, W. L. Ellsworth, M. J. S. Johnston, J. O. Langbein, A. M. Pitt, P.A. Reasenberg and M. L. Sorey, 1989. Mammoth Mountain Earthquake Swarms, Long Valley Caldera, California, Trans. Am. Geops. Un., v 70, 1190.

M. J. S. Johnston, A. T. Linde, and S. Schulz, 1989. Transient Earth Strain Associated with Near-Surface Creep Near Parkfield, California. Trans. Am. Geops. Un., v 70, 1354.

G. Glassmoyer, R. D. Borcherdt, M. J. S. Johnston, and T. Noce, 1989. Local Dilatometer and Seismometer Recordings of the $M_L = 4.0$ Parkfield Earthquake of 25 May, 1989. Trans. Am. Geops. Un. v70, 1218.

Prescott, W. H., M. Lisowski, M. J. S. Johnston, S. S. Burford, J. C. Savage, and T. A. Clark, 1990. Deformation Before, During, and After the Loma Prieta Earthquake of October, 1989. Trans. Am. Geops. Un., v71, 291.

Mueller, R. J. and M. J. S. Johnston, 1990. Seismomagnetic Effect generated by the October 18, 1989, Loma Prieta, California, Earthquake. Trans. Am. Geops. Un., v71, 289.

Johnston, M. J. S., A. T. Linde and M. T. Gladwin, 1990. Did Preseismic Slip Occur During the Months to Minutes before the October 18, 1989, Loma Prieta Earthquake? Trans. Am. Geops. Un., v71, 288.

D. P. Hill, W. L. Ellsworth, M. J. S. Johnston, J. O. Langbein, A. M. Pitt, P.A. Reasenberg and M. L. Sorey, 1989. The 1989 Earthquake Swarm beneath Mammoth Mountain, California: An Initial Look at the 4 May through 30 September Activity. BSSA (in press).

Johnston, M. J. S. 1990. Review of high precision continuous strain measurements near the locked and creeping sections of the San Andreas fault. Joint NSF/USGS Workshop on Crustal Deformation Measurement and Earthquake Mechanics. Morro Bay, California, March, 1990

Johnston, M. J. S., A. T. Linde, and M. T. Gladwin, 1990. Near-Field High Precision Strain Prior to the October 18, 1989 Loma Prieta M_L 7.1 Earthquake. *Geophys. Res Lett.*, (in press).

Lisowski, M., W. H. Prescott, J. C. Savage, and M. J. S. Johnston, 1990. Geodetic Estimate of Coseismic Slip During the 1989 Loma Prieta Earthquake.

Geophys. Res. Lett., (in press).

Mueller, R. J. and M. J. S. Johnston, Seismomagnetic Effect Generated by the October 18, M_L 7.1 Loma Prieta, California, Earthquake. *Geophys. Res. Lett.*, (in press).

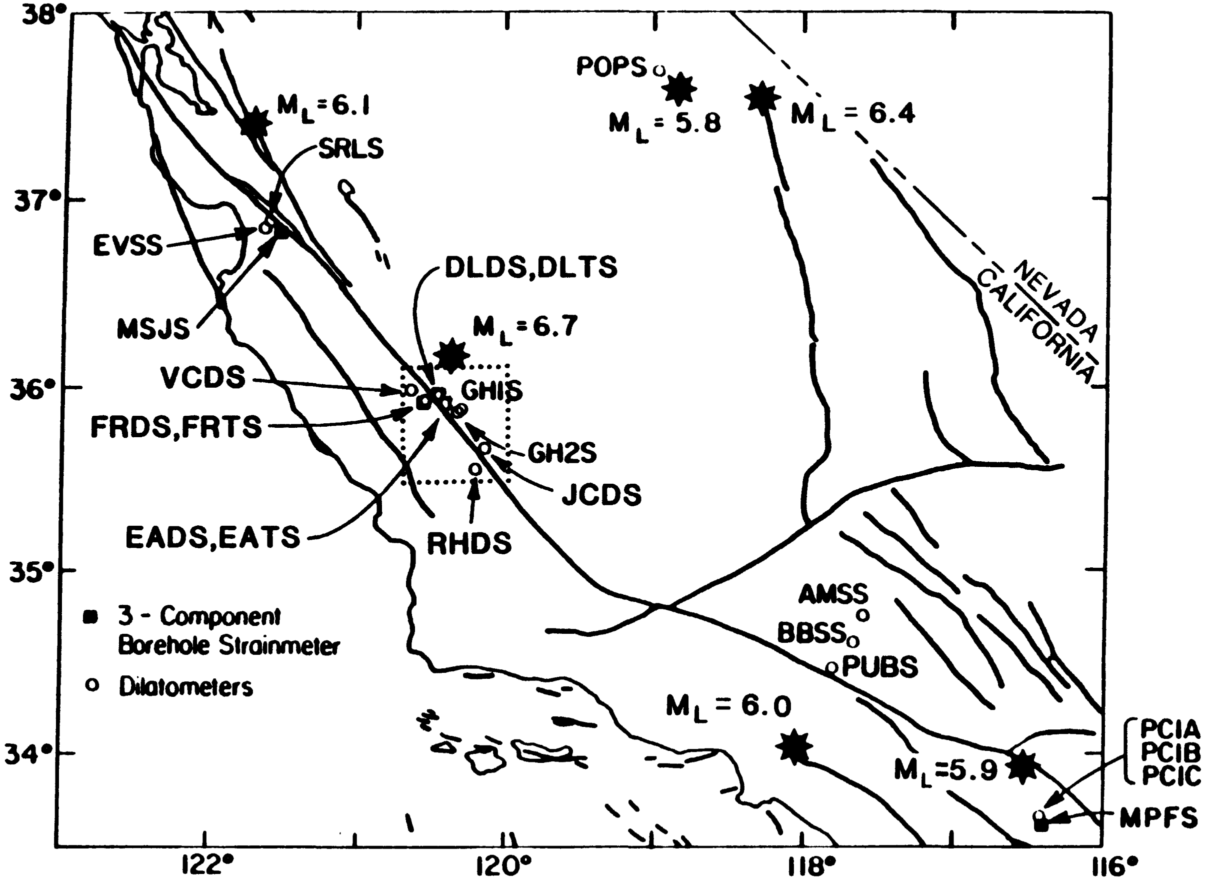
38°
37°
36°
35°
34°
122°
120°
118°
116°
POPS
$M_L = 5.8$
$M_L = 6.4$
NEVADA
CALIFORNIA
$M_L = 6.1$
SRLS
EVSS
MSJS
DLDS,DLTS
$M_L = 6.7$
VCDS
GHIS
FRDS,FRTS
GH2S
JCDS
EADS,EATS
RHDS
AMSS
BBSS
PUBS
$M_L = 6.0$
$M_L = 5.9$
PCIA
PCIB
PCIC
MPFS
■ 3 - Component Borehole Strainmeter
○ Dilatometers

FIGURE 1.

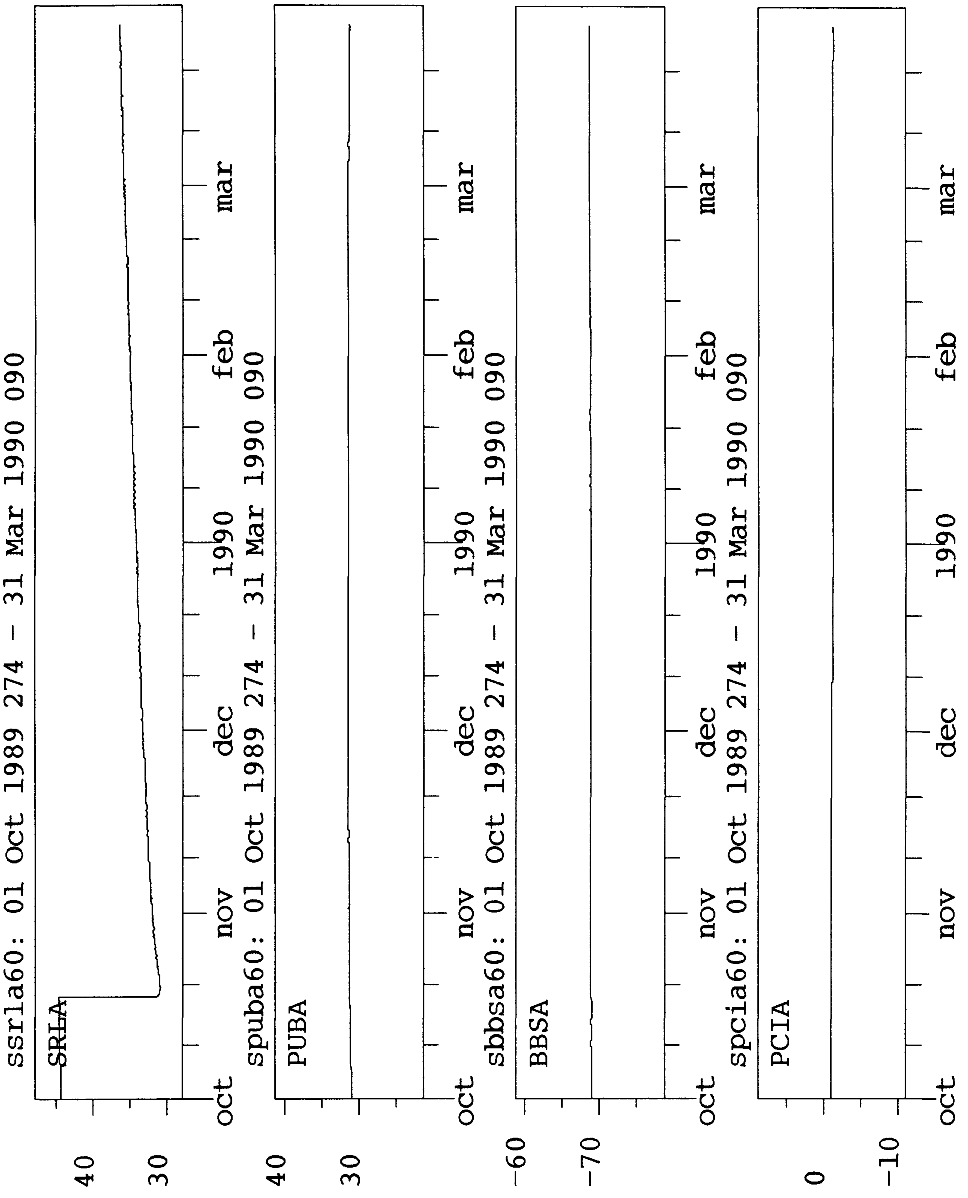
ssrla60: 01 Oct 1989 274 - 31 Mar 1990 090
SRLA
40
30
spuba60: 01 Oct 1989 274 - 31 Mar 1990 090
PUBA
40
30
sbbsa60: 01 Oct 1989 274 - 31 Mar 1990 090
BBSA
-60
-70
spcia60: 01 Oct 1989 274 - 31 Mar 1990 090
PCIA
0
-10
oct
nov
dec
1990
feb
mar

FIG 2a

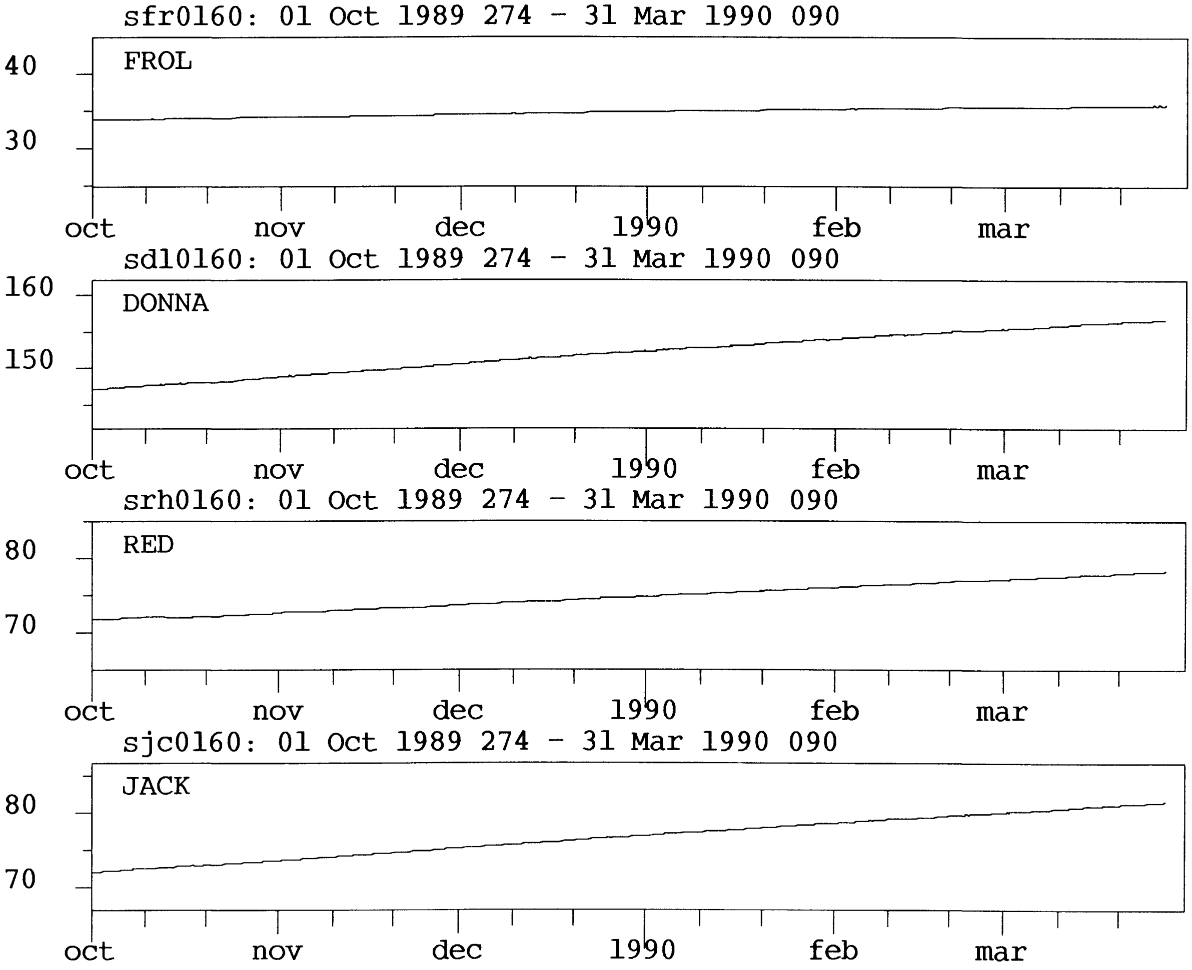
sfr0160: 01 Oct 1989 274 - 31 Mar 1990 090
FROL
40
30
sd10160: 01 Oct 1989 274 - 31 Mar 1990 090
DONNA
160
150
srh0160: 01 Oct 1989 274 - 31 Mar 1990 090
RED
80
70
sjc0160: 01 Oct 1989 274 - 31 Mar 1990 090
JACK
80
70
oct
nov
dec
1990
feb
mar

Fig 2b

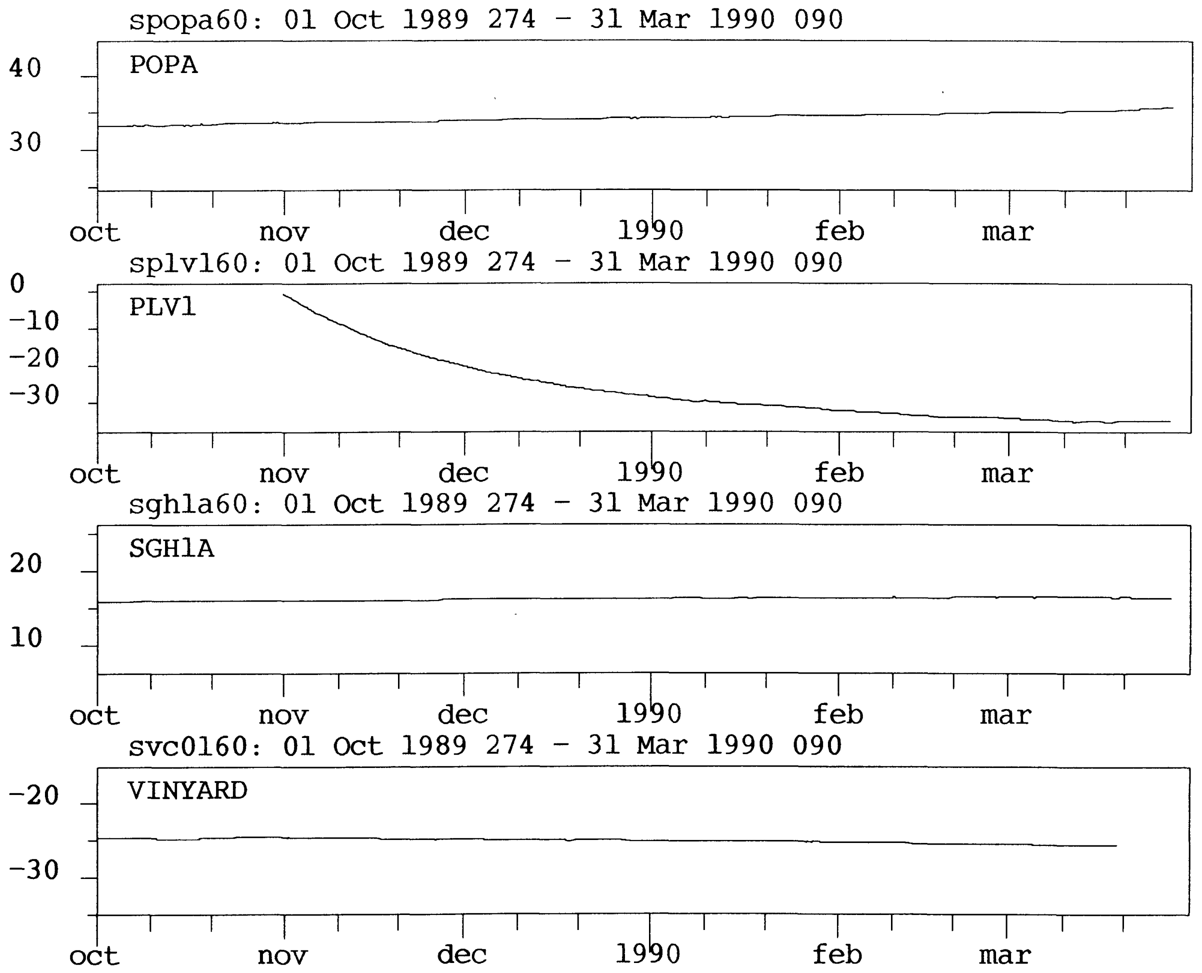
spopa60: 01 Oct 1989 274 - 31 Mar 1990 090
POPA
40
30
splvl60: 01 Oct 1989 274 - 31 Mar 1990 090
PLV1
0
-10
-20
-30
sghla60: 01 Oct 1989 274 - 31 Mar 1990 090
SGH1A
20
10
svc0160: 01 Oct 1989 274 - 31 Mar 1990 090
VINYARD
-20
-30
oct
nov
dec
1990
feb
mar

FIG 2e

FIG 3a

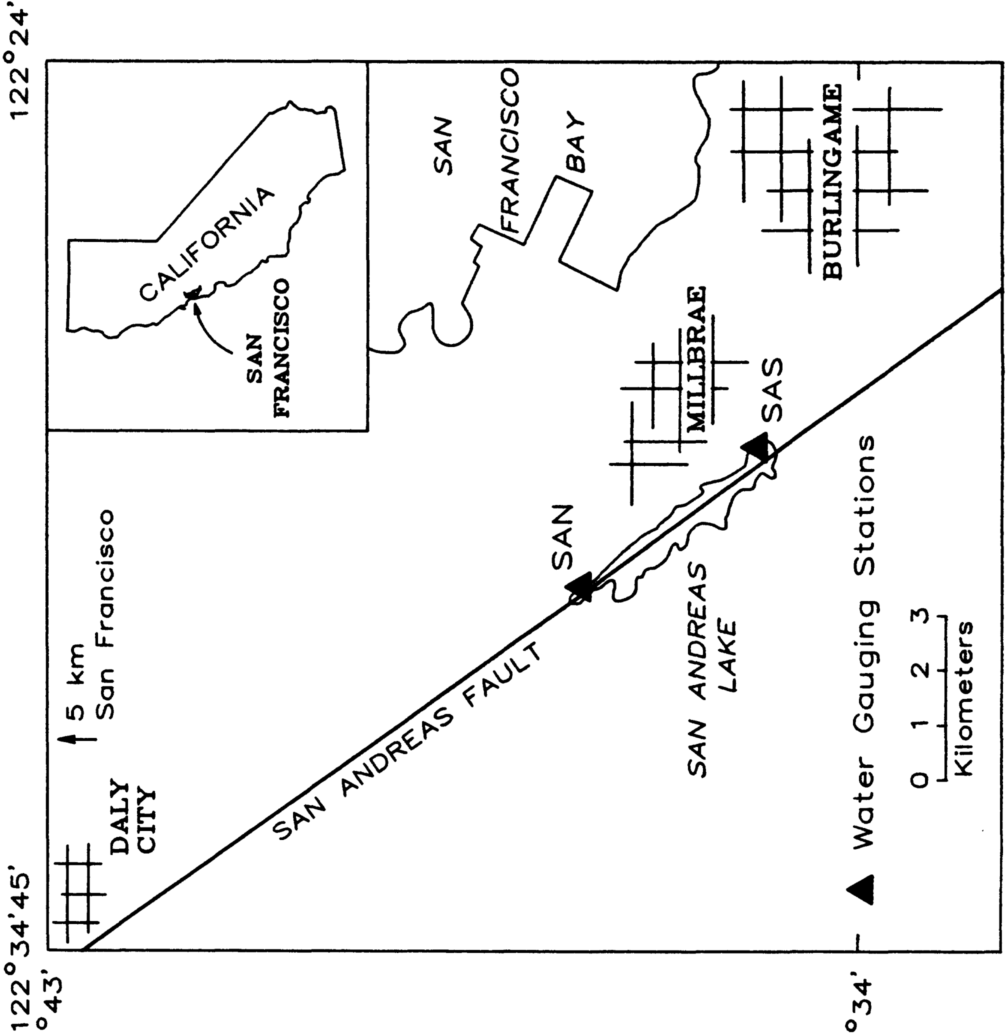
122°24'
122°34'45'
37°43'
37°34'
CALIFORNIA
SAN FRANCISCO
SAN FRANCISCO BAY
BURLINGAME
MILLBRAE
SAS
SAN
SAN ANDREAS LAKE
SAN ANDREAS FAULT
5 km San Francisco
DALY CITY
▲ Water Gauging Stations
0 1 2 3
Kilometers

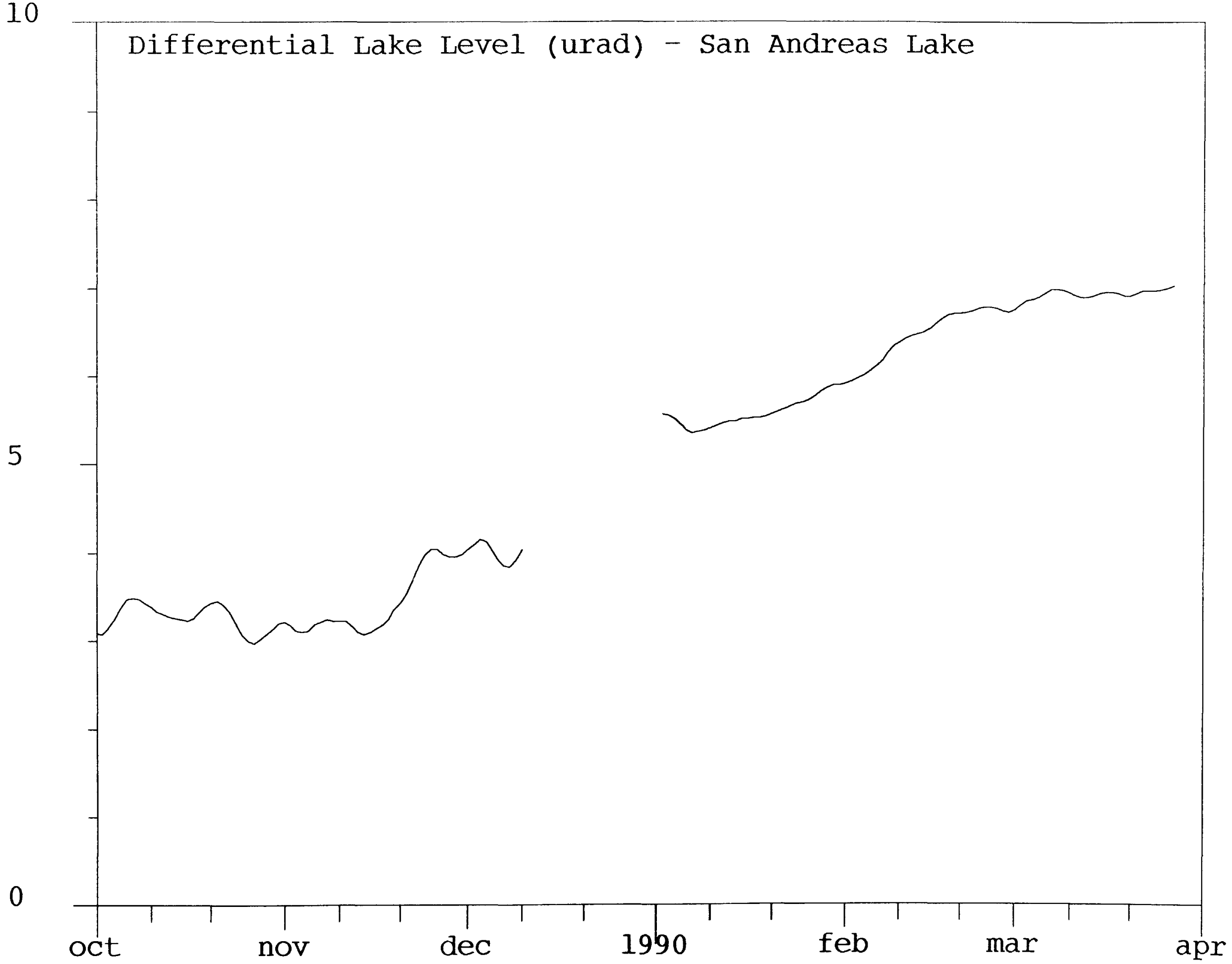
Differential Lake Level (urad) - San Andreas Lake
10
5
0
oct
nov
dec
1990
feb
mar
apr

FIG 3 f

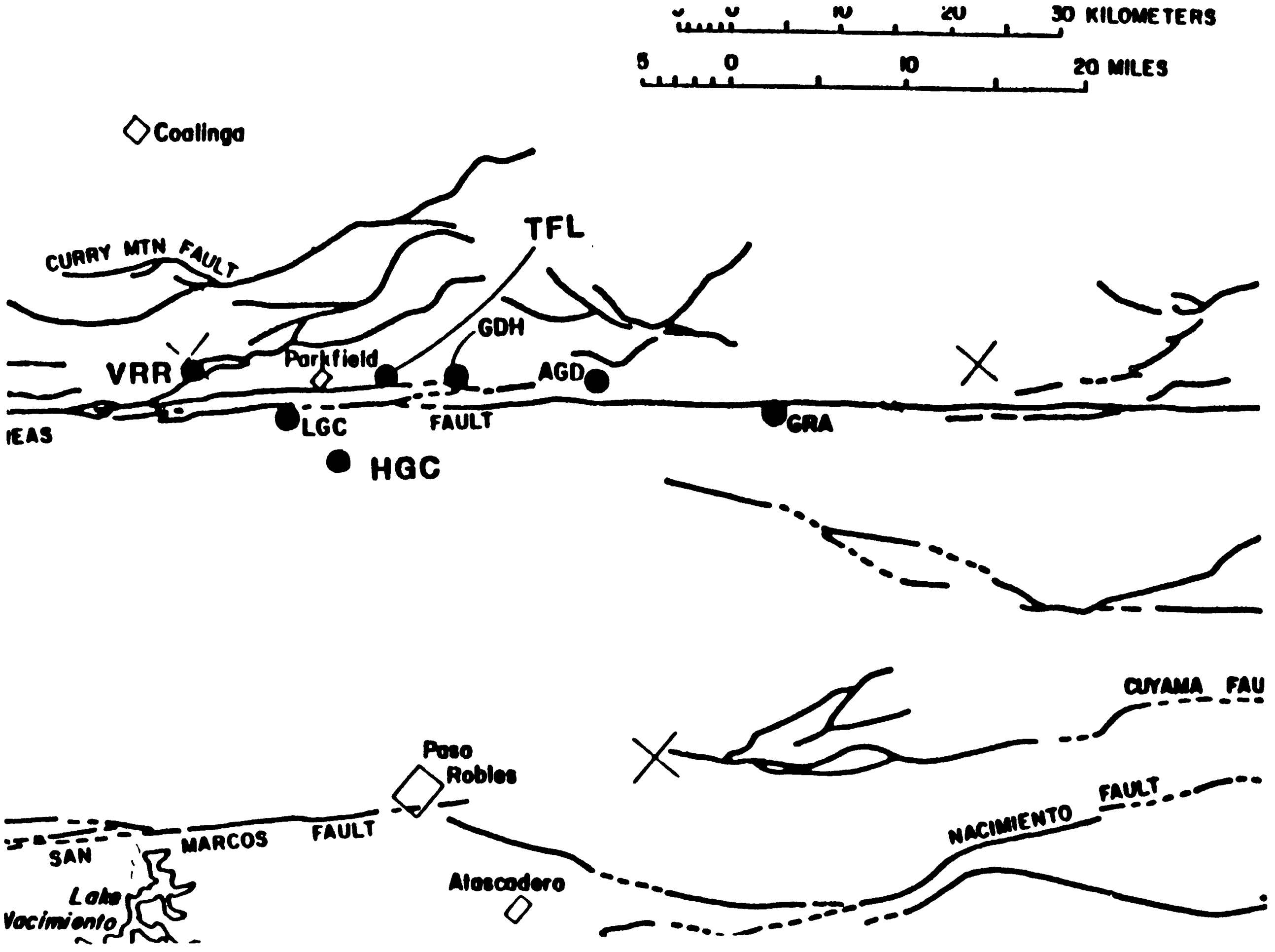
5 0 10 20 30 KILOMETERS
5 0 10 20 MILES
Coalinga
CURRY MTN FAULT
TFL
GDH
VRR
Parkfield
AGD
IEAS
LGC
FAULT
HGC
GRA
CUYAMA FAU
Paso Robles
SAN MARCOS FAULT
Lake Vacimiento
Atascadero
NACIMIENTO FAULT

FIGURE 14a

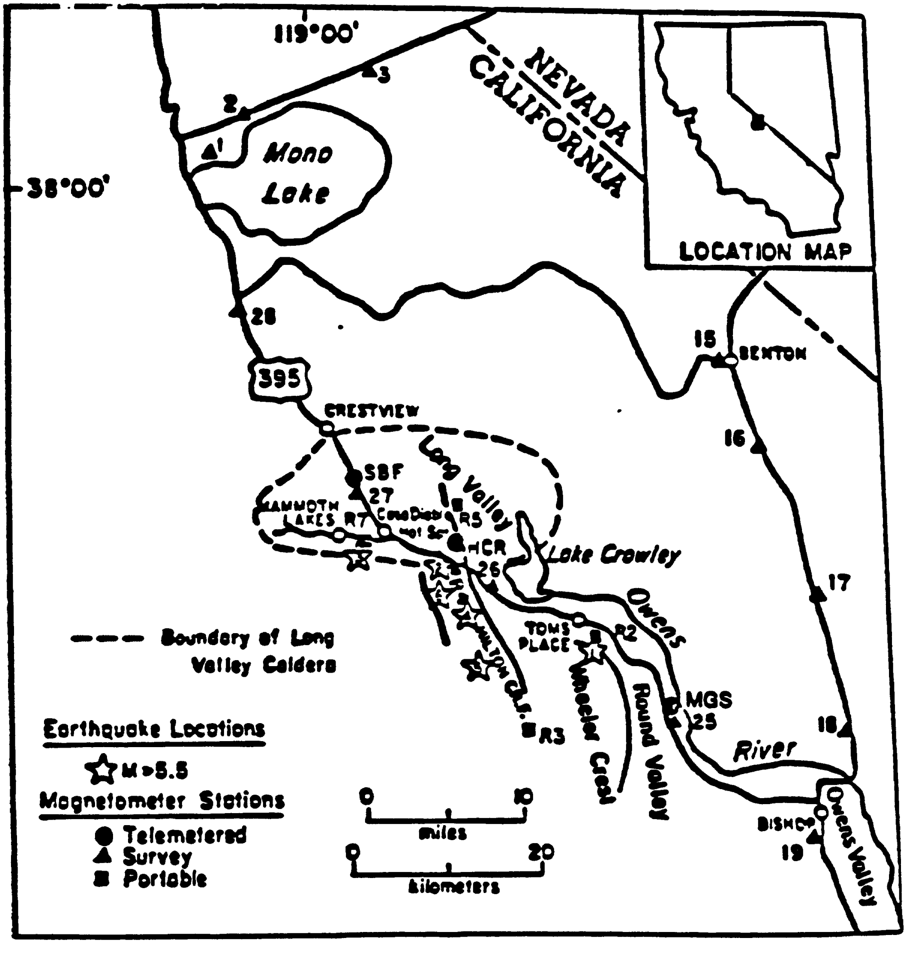
119°00'
38°00'
NEVADA
CALIFORNIA
LOCATION MAP
Mono
Lake
1
2
3
28
395
15
BENTON
16
17
18
19
CRESTVIEW
SBF
27
MAMMOTH
LAKES
R7
Casa Diablo
Hot Sp.
R5
HCR
26
Long Valley
Lake Crowley
Owens
TOMS
PLACE
R2
Hilton Crk. F.
R3
Wheeler Crest
Round Valley
MGS
25
River
BISHOP
Owens Valley
Boundary of Long
Valley Caldera
Earthquake Locations
M>5.5
Magnetometer Stations
● Telemetered
▲ Survey
■ Portable
0
10
miles
0
20
kilometers

FIGURE 4 b

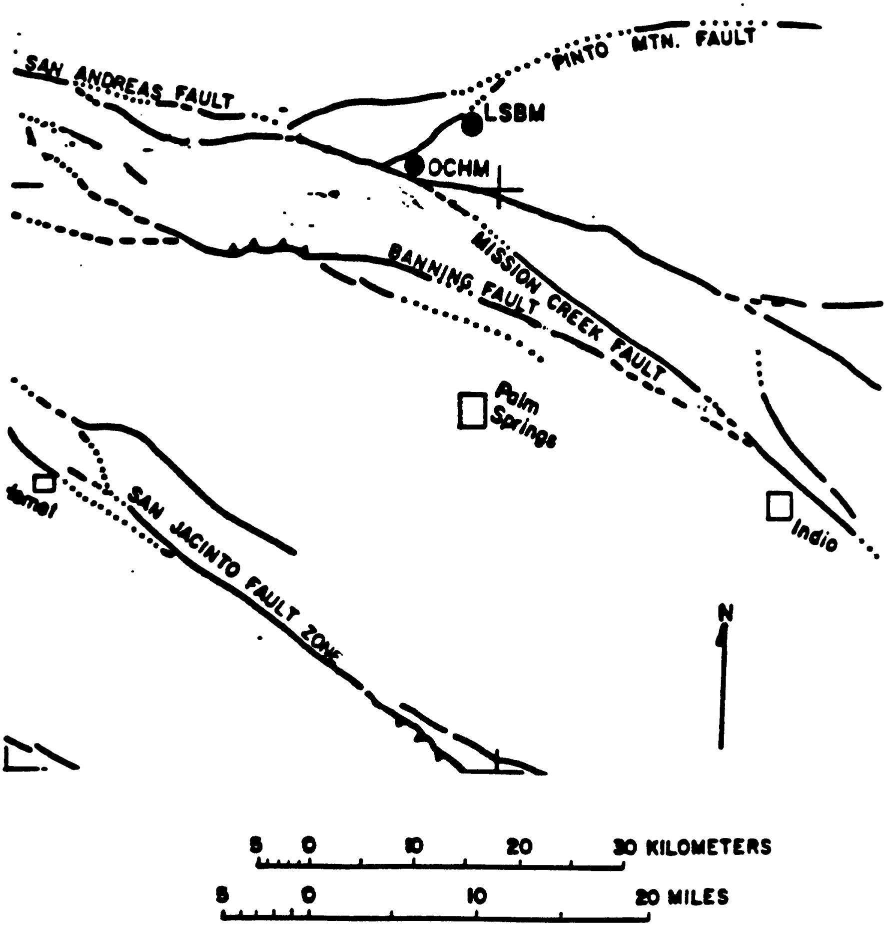
SAN ANDREAS FAULT
PINTO MTN. FAULT
LSBM
OCHM
MISSION CREEK FAULT
BANNING FAULT
Palm Springs
Indio
Hemet
SAN JACINTO FAULT ZONE
N
5 0 10 20 30 KILOMETERS
5 0 10 20 MILES

FIGURE 4c

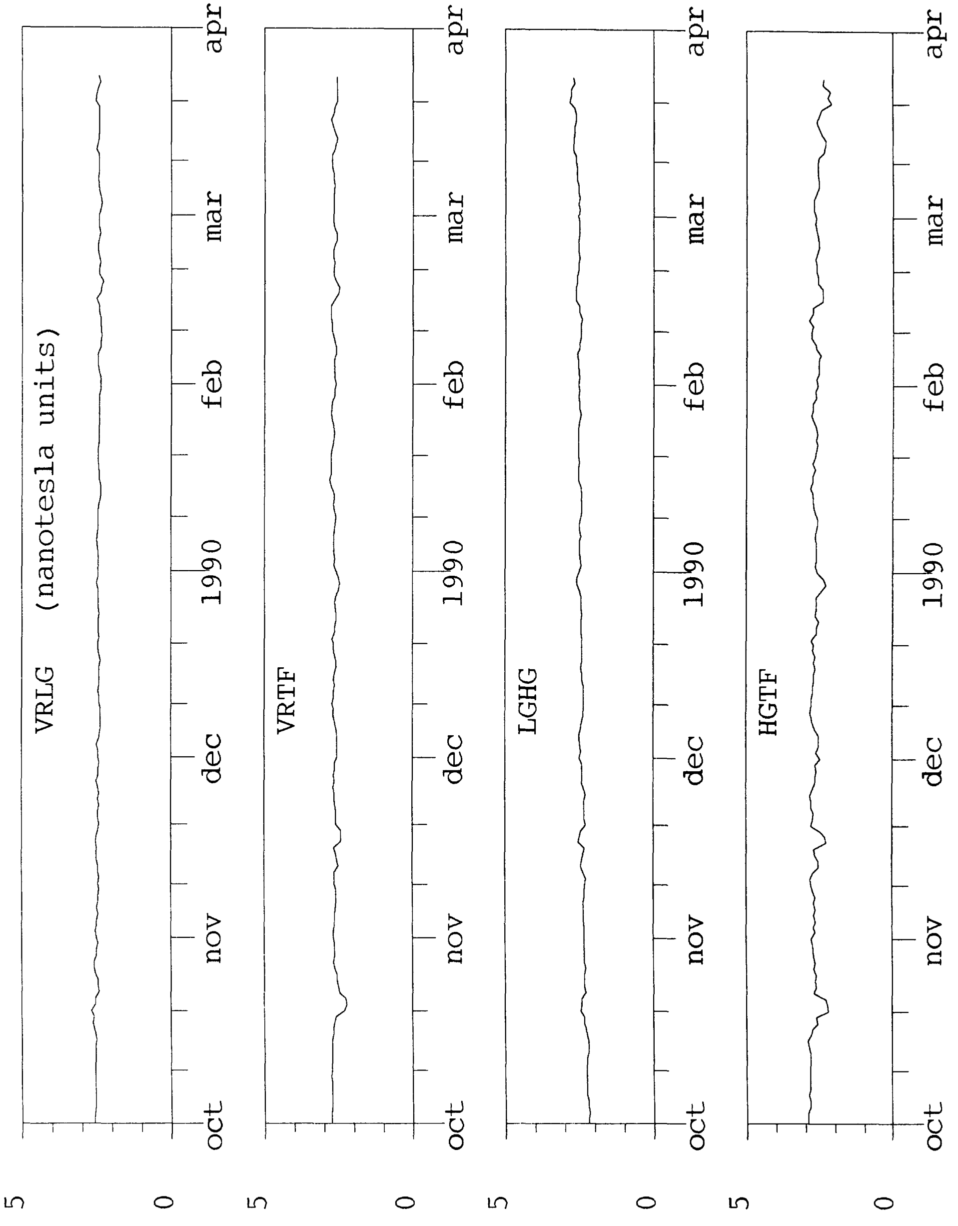
VRLG (nanotesla units)
VRTF
LGHG
HGTF
5
0
oct
nov
dec
1990
feb
mar
apr

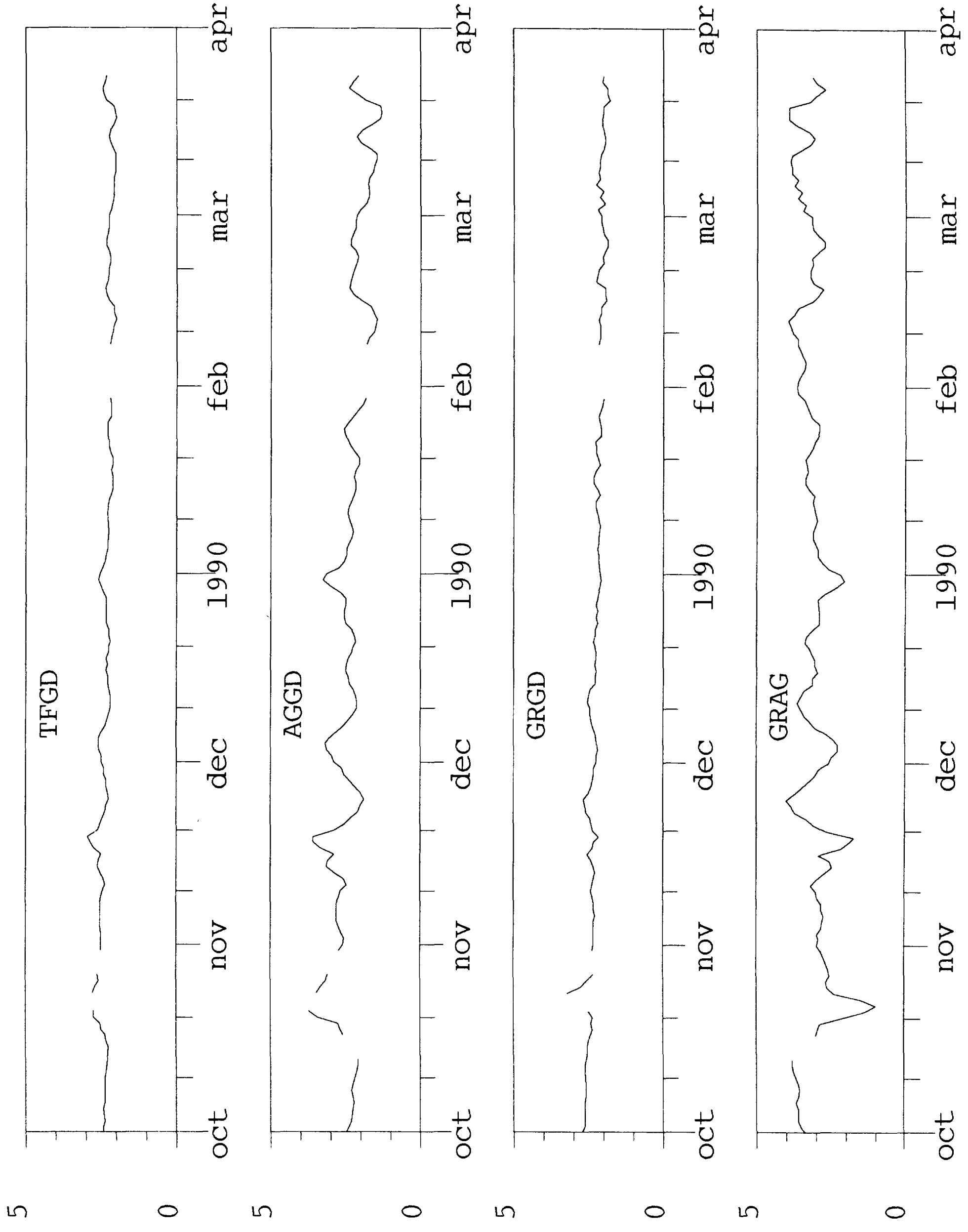
TFGD
AGGD
GRGD
GRAG
oct
nov
dec
1990
feb
mar
apr
5
0

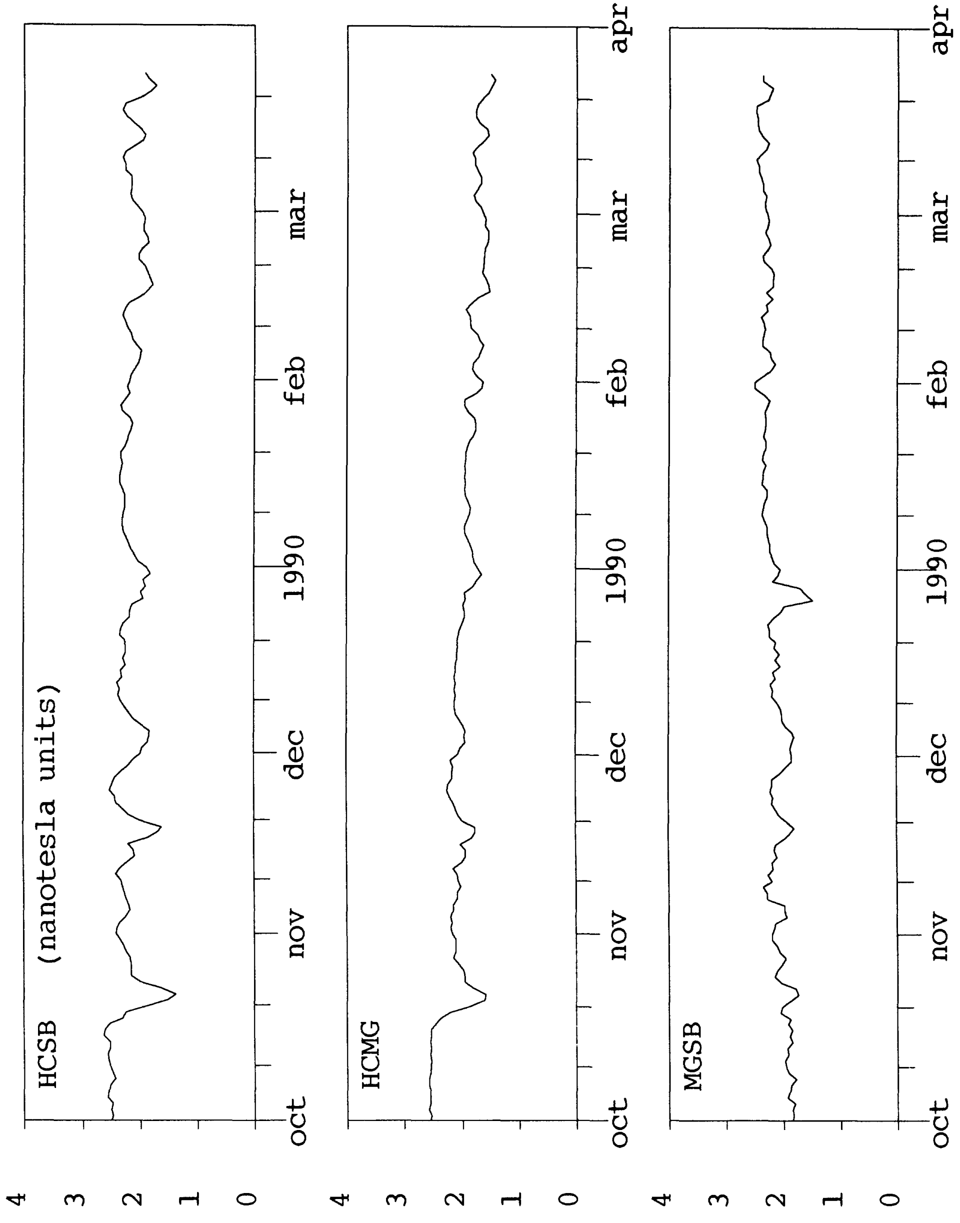
HCSB (nanotesla units)
HCMG
MGSB
oct
nov
dec
1990
feb
mar
apr
0
1
2
3
4

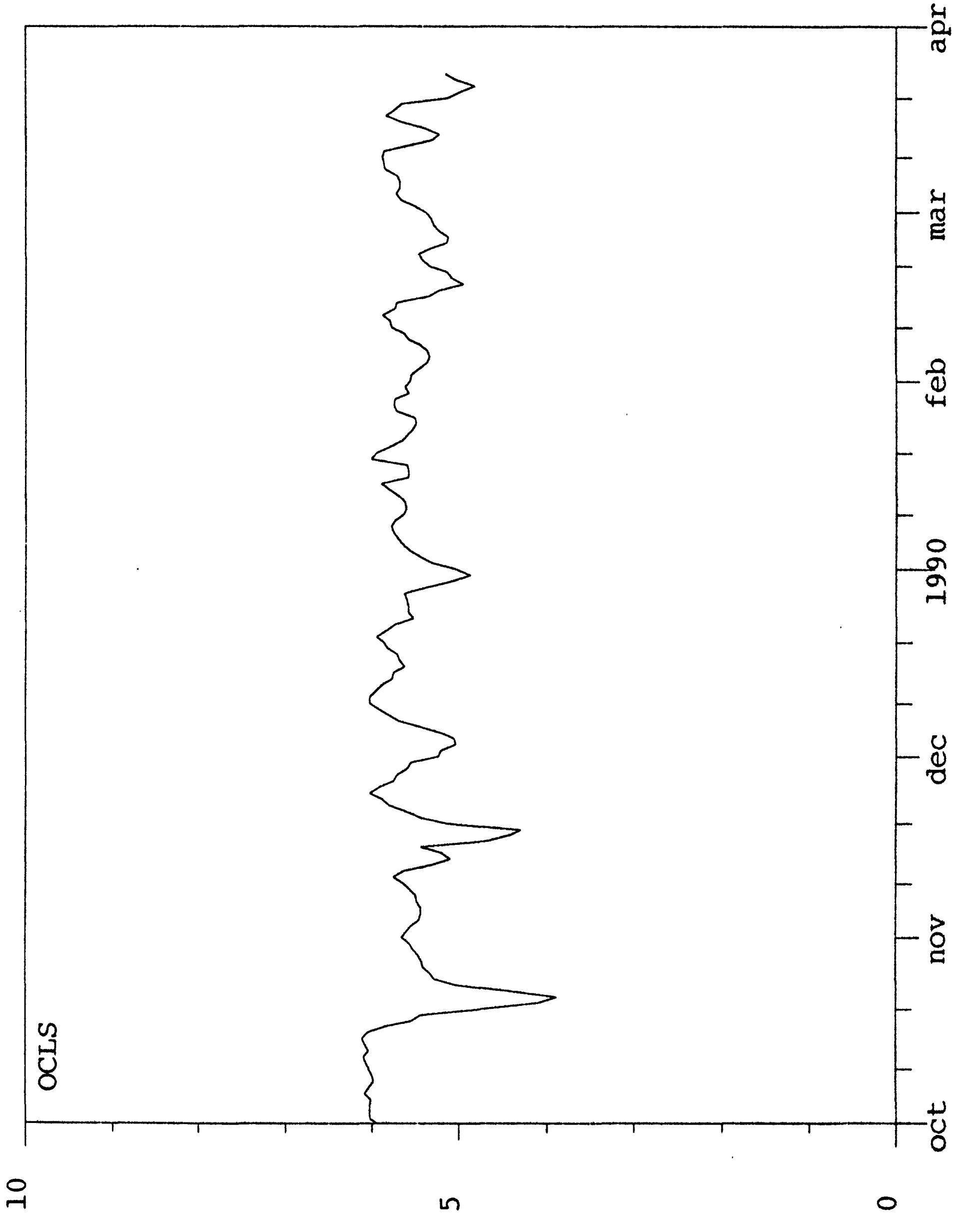
OCLS
10
5
0
oct
nov
dec
1990
feb
mar
apr

GEODETIC STRAIN MONITORING

9960-02156

John Langbein
Branch of Tectonophysics
U.S. Geological Survey
345 Middlefield Road, MS/977
Menlo Park, California 94025
(415) 329-4853

Investigations

Two-color geodimeters are used to survey, repeatedly, geodetic networks within selected regions of California that are tectonically active. This distance measuring instrument has a precision of 0.1 to 0.2 ppm of the baseline length. Currently, the crustal deformation is being monitored within the south moat of the Long Valley caldera in eastern California, near Pearblossom, California on a section of the San Andreas fault that is within its Big Bend section and on Middle Mountain near Parkfield, California. Periodic comparisons with the prototype, two-color geodimeter are also conducted near Parkfield, California. These intercomparison measurements serve as a calibration experiment to monitor the relative stabilities of the portable and prototype geodimeters.

Results

1. Post-seismic slip following the 1989 Loma Prieta Earthquake

A small geodetic network was installed and measured 7 days, 78 days and 158 days following the October 17, 1989 Loma Prieta $M7.1$ earthquake. This network straddles the northwestern end of the rupture plane defined by the locations of numerous aftershocks. In the initial 70 day interval, the measured line-length changes revealed that 5.6 ± 0.6 mm of slip occurred within the network. However, during the later 80 day interval, an insignificant, -0.6 ± 0.6 mm of right lateral slip could be detected. Thus, it appears that the measured slip is a typical response of the fault following a major shock in that the rate of slip decreases in time. However, the magnitude of the post-seismic slip is less than 0.5% of the inferred co-seismic slip at depth and that the observed rate decrease in post-seismic slip is faster than the usual inverse-time rate decay observed for post-seismic slip.

2. Long Valley Caldera

We have two dramatic results to report. The most dramatic observation is that since late September through the present, the resurgent dome in the Long Valley caldera has started to reinflate after several years of quiescence. Shown in Figures 1, 2, and 3 are the location of the CASA sub-network and the line-length changes measured from CASA.

are made very frequently and can be interpreted as a linear combination of fault slip on the San Andreas near the central station at CARR, a shear strain parameter, and areal dilatation. The shear strain accounts for the unknown spatial distribution of slip on the San Andreas fault which is not included in the local slip parameter. The areal dilatation is a combination of tectonic dilatation plus any drift in the instrument. The result of estimating these parameters as a function of time is shown in Figure 4. In computing this result, I have tried to estimate the parameters for times when "most" of the 15 baseline network was measured. Although the results plotted in Figure 4 show some very interesting variations in slip and strain, I will focus on the apparent variations in dilatation. As mentioned above, the data show an apparent 1 ppm areal compression on the network in April 1989. In the following month, several large fluctuations (again 1 ppm) occurred. During the past 6 months, these fluctuations have continued. These high peak–to–peak fluctuations of 1.6 ppm should be compared with the relatively small fluctuations (0.6 ppm) that were observed before April 1989.

To determine whether these variations in areal dilatation are either tectonic or instrumental, I have been periodically measuring a large subset of the Parkfield baselines using the portable, two–color geodimeter. These measurements are made simultaneously with the observatory based instrument. By tracking the differences in the distances recorded with both instruments, I can check stability of one instrument relative to the second. The bottom trace in Figure 4 shows the variations of the length scale of the observatory based instrument relative to the portable instrument. To first order, the variations in length scale mimic the apparent areal dilatation estimated from the observatory based instrument. Hence, I conclude that most of the dilatational signal is instrumental in origin.

As a rough check on the stability of the portable instrument, I have been conducting an experiment at Mammoth using both of the USGS's portable instruments. The second instrument only became operational again in February 1990. For a period of about 2 months, we have been measuring the lengths of 7 baselines from CASA using both instruments. The measurements are not made simultaneously, but are separated by about 2 to 3 hours which cause us to use slightly differing meteorologic corrections. These sets of measurements have been repeated 15 times. Using the same analysis technique that I applied to the differential Parkfield measurements, I found that the standard deviation of the inferred length scale changes came to 0.06 ppm which if doubled to equate to apparent areal dilatation yields 0.12 ppm. To compare this value with the peak–to–peak scatter of areal dilatation at Parkfield, I multiply the Mammoth result by a factor of 4 which implies that the recent Parkfield dilatation is at least a factor of 3 noiser than predicted.

Reports

Langbein, John O., Post–seismic slip on the San Andreas fault at the northwestern end of the 1989 Loma Prieta earthquake rupture zone, submitted to *Geophys. Res. Let.*, 1990.

The rates measured on the few baselines for which data exist from mid 1983 indicate that the current strain rates are as high now as they were in mid 1983. The two examples come from the baselines LO/NU–MIKE and JCM/SEWER. Furthermore, the baseline to KRAKATAU (Figure 3) shows the highest rate, approximately 0.15 ppm/week. This baseline spans the resurgent dome (Figure 1) and is sensitive to inflation sources at depth. I have attempted to model the line–length changes using the same types and locations of deformation sources discussed in *Langbein* [1989]. Using this model with a deep point source of inflation at 10 km and a shallow point source at 5 km beneath the resurgent dome plus dextral slip in the south moat, I have adequately fit the data. The results indicate that during the 6 month interval, the deep inflation source increased its injection rate from nearly 0 to 0.0392 ± 0.0012 km^3/yr, no change in the volume of the shallow source, and left–lateral slip in the south moat of 10 ± 8 mm/yr. By using the deep inflation source, an uplift rate for a point along the leveling route on highway 395 can be predicted. Using this model, I predict a 80 mm/yr rate of uplift for the segment of Rt 395 that crosses the resurgent dome. This inferred uplift rate exceeds the observed average rate between the leveling surveys in 1976 and 1980 and the current rate is nearly equal to the rate obtained between 1982 and 1983. As reported by *Hill* [this volume], the seismicity in the caldera had been relatively quiet through mid November 1989. After then, there have been a number of swarms of M1 and M2 earthquakes.

As noted in the previous Semi–annual report, we installed a small geodetic network southeast of Mammoth Mountain and centered around MILL (Figure 1). This network is designed to monitor possible deformation associated with the earthquake swarm detected beneath Mammoth Mountain during the summer of 1989. From early September through mid November 1989, we made 3 measurements of the 8 baseline network. By fitting a spatially uniform strain model to the data, the results indicated 8.4 ± 2.0 ppm/yr of nearly uniaxial extension oriented N45° W. This axis is perpendicular to the alignment of the earthquake epicenters and the axis formed by the location of Mammoth Mountain and the Inyo Domes. Encouraged by this result, I used the dense pattern of earthquake hypocenters [*Hill et al.* 1990] to define the location of possible dike injection under Mammoth Mountain. Relative to the uniform strain model, the use of the dike yielded smaller misfits. My initial dike used a length of 2.1 km, a width of 3.0 km centered at 7.5 km beneath Mammoth Mountain. These numbers are taken from the figures of *Hill et al.* By least squares fitting, the estimated dike opening comes to 8.8 ± 1.4 m or a volume change of 0.055 km^3. By changing the location of the dike along the initial plane, I could further reduce the misfits yielding a dike that is 1.5 km long, 3.0 km wide, centered at 5.5 km depth and opening by 4.3 m or an equivalent volume change of 0.019 km^3.

3. Parkfield deformation

During the past year, I have been tracking the performance of the two–color geodimeter instrument at Parkfield. I initiated this practice when it came to our attention that the network appeared to compress uniformly in mid April, 1989. The obvious question was whether the event was tectonic or instrumental in origin? To answer this, I relied upon two data sets. The first set consists of line–length measurements made using the observatory based, two–color geodimeter which resides in Parkfield. These measurements

Hill, D.P., W.L. Ellsworth, M.J.S. Johnston, J.O. Langbein, D.H. Oppenheimer, A.M. Pitt, P.A. Reasenberg, M.L. Sorey, and S.R. McNutt, The 1989 earthquake swarm beneath Mammoth Mountain, California: An initial look at the 4 May through 30 September activity, *Bull. of Seismol. Soc. of America*, in press, 1990.

Langbein, John, Testing for long-term stability of two-color geodimeters; January 1986 to August 1989, *U.S. Geological Survey Open File Report*, 90-91, p. 23, 1990.

Figure Captions

Figure 1. Map showing the location of the two-color network within the Long Valley caldera. During this 6 month period, only the baselines with stations common to either CASA or MILL were measured.

Figure 2. Plot of the changes in length of all of the baselines using CASA as a common station. The vertical bars represent ±1 standard deviation of the measured distance. The distance changes have been normalized by the nominal baseline length. Hence, the length changes are plotted in units of part per million (ppm). The vertical line in mid 1986 designates the time of the 21 July earthquake in Chalfant Valley.

Figure 3. Plot of the changes in length of the 7 frequently measured baselines using a CASA as a common station. The vertical scale represents length change in millimeters (mm). To accentuate the observed rate change associated with reinflation of the resurgent dome, I have only plotted the observations between January 1989 and April 1990.

Figure 4. The variation of fault slip on the San Andreas fault at the center of the Parkfield two-color network at CARR, shear strain, areal dilatation, and twice the inferred variations in length scale of the observatory based instrument relative to the portable, two-color geodimeter. Since slip as a function of time is only determined for the central part of the network, slip along the other portions of the San Andreas fault gets lumped into the shear strain parameter, thus this parameter should not be used to estimate the load on the fault due to very long wavelength sources such as plate tectonics. Of interest is the large fluctuations in dilatation and its coherence with the calibration results.

LONG VALLEY NETWORK

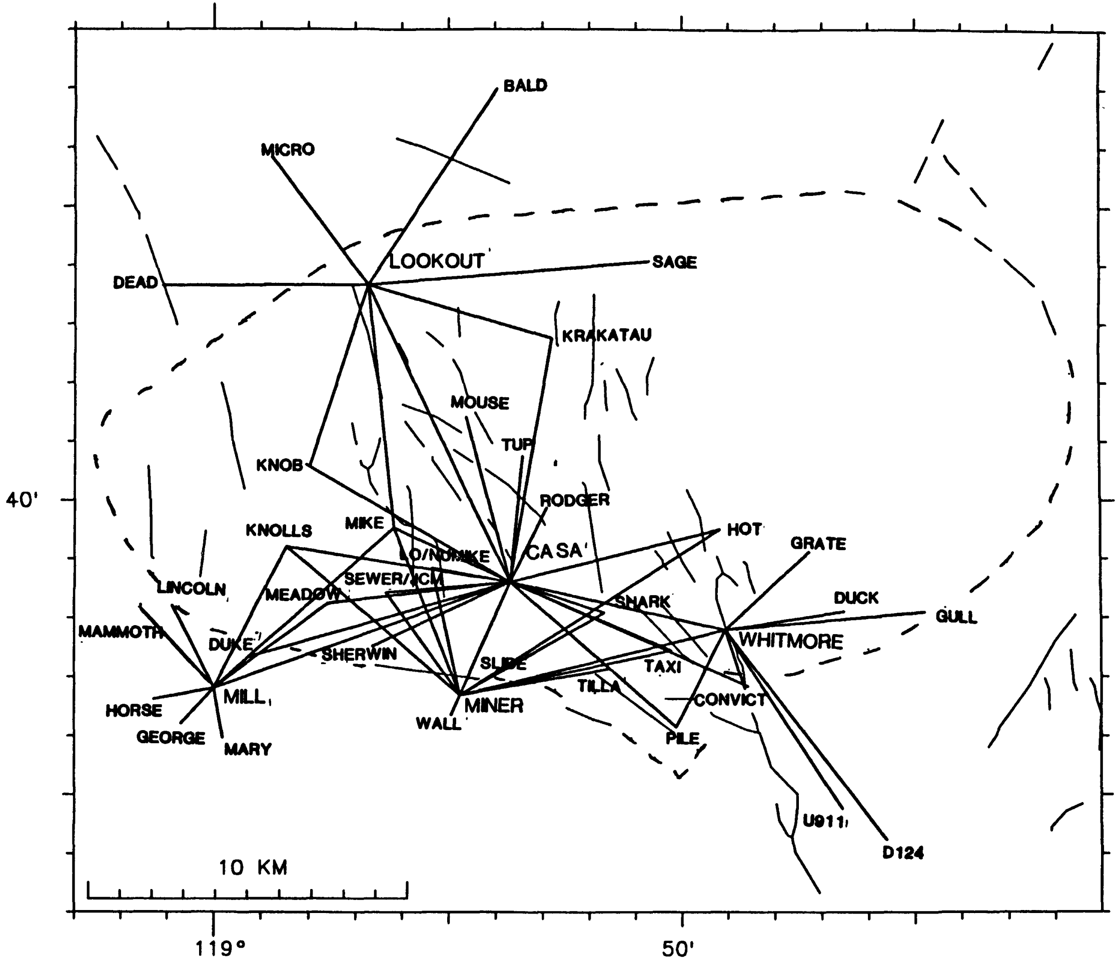

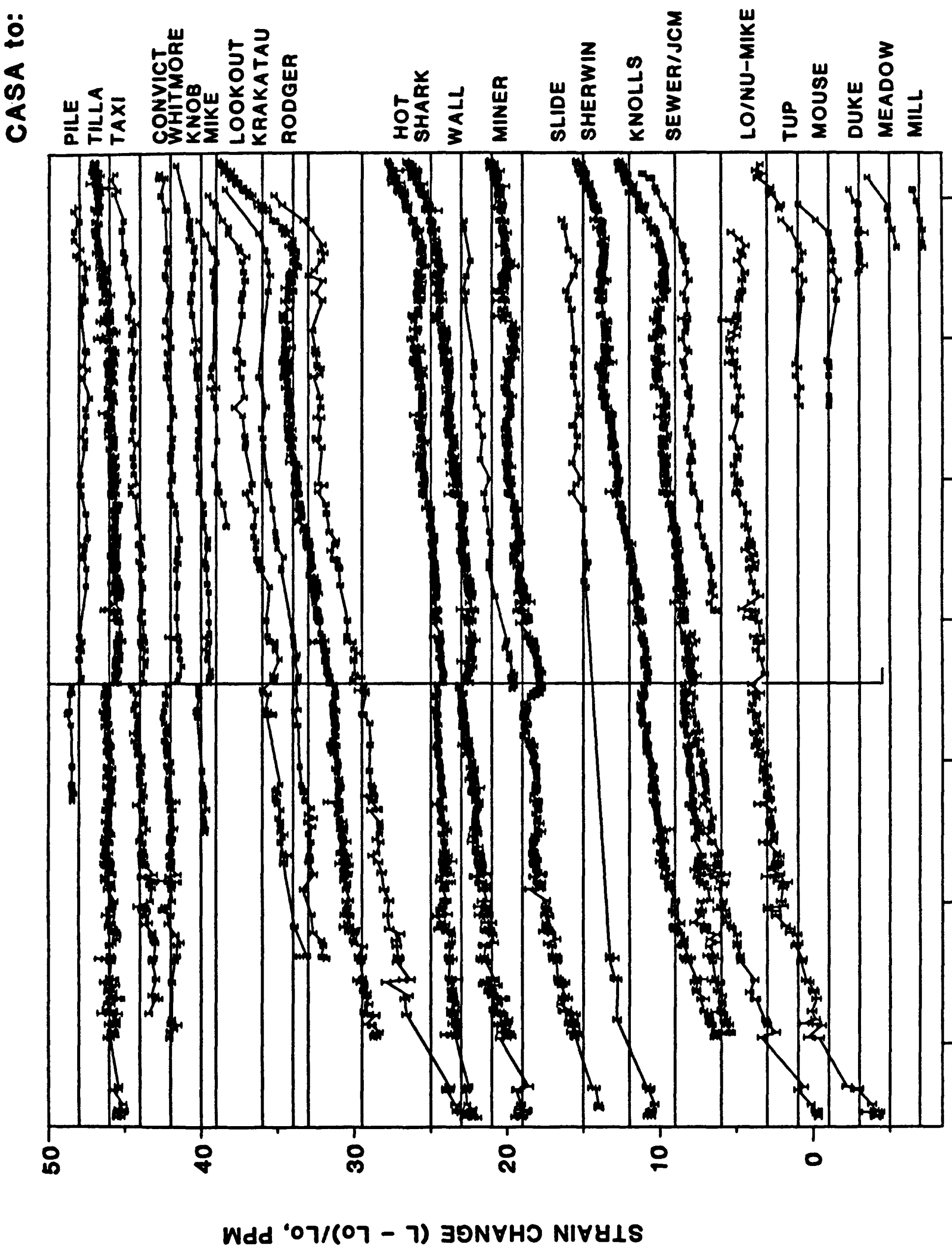
CASA to:
PILE
TILLA
TAXI
CONVICT
WHITMORE
KNOB
MIKE
LOOKOUT
KRAKATAU
RODGER
HOT
SHARK
WALL
MINER
SLIDE
SHERWIN
KNOLLS
SEWER/JCM
LO/NU-MIKE
TUP
MOUSE
DUKE
MEADOW
MILL
50
40
30
20
10
0
STRAIN CHANGE (L - Lo)/Lo, PPM
1984
1985
1986
1987
1988
1989
1990

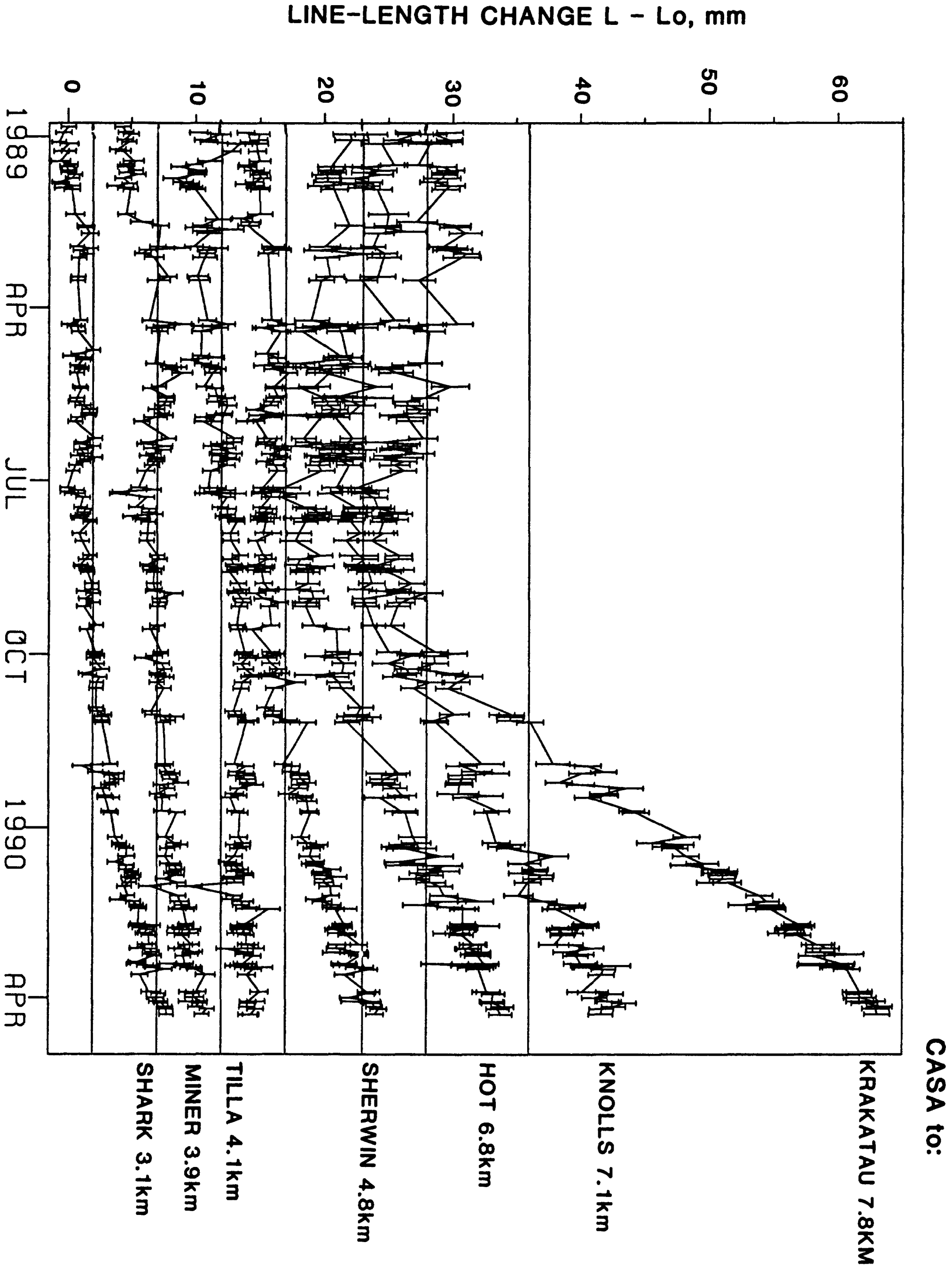
LINE-LENGTH CHANGE L - Lo, mm
0
10
20
30
40
50
60
1989
APR
JUL
OCT
1990
APR
CASA to:
KRAKATAU 7.8KM
KNOLLS 7.1km
HOT 6.8km
SHERWIN 4.8km
TILLA 4.1km
MINER 3.9km
SHARK 3.1km

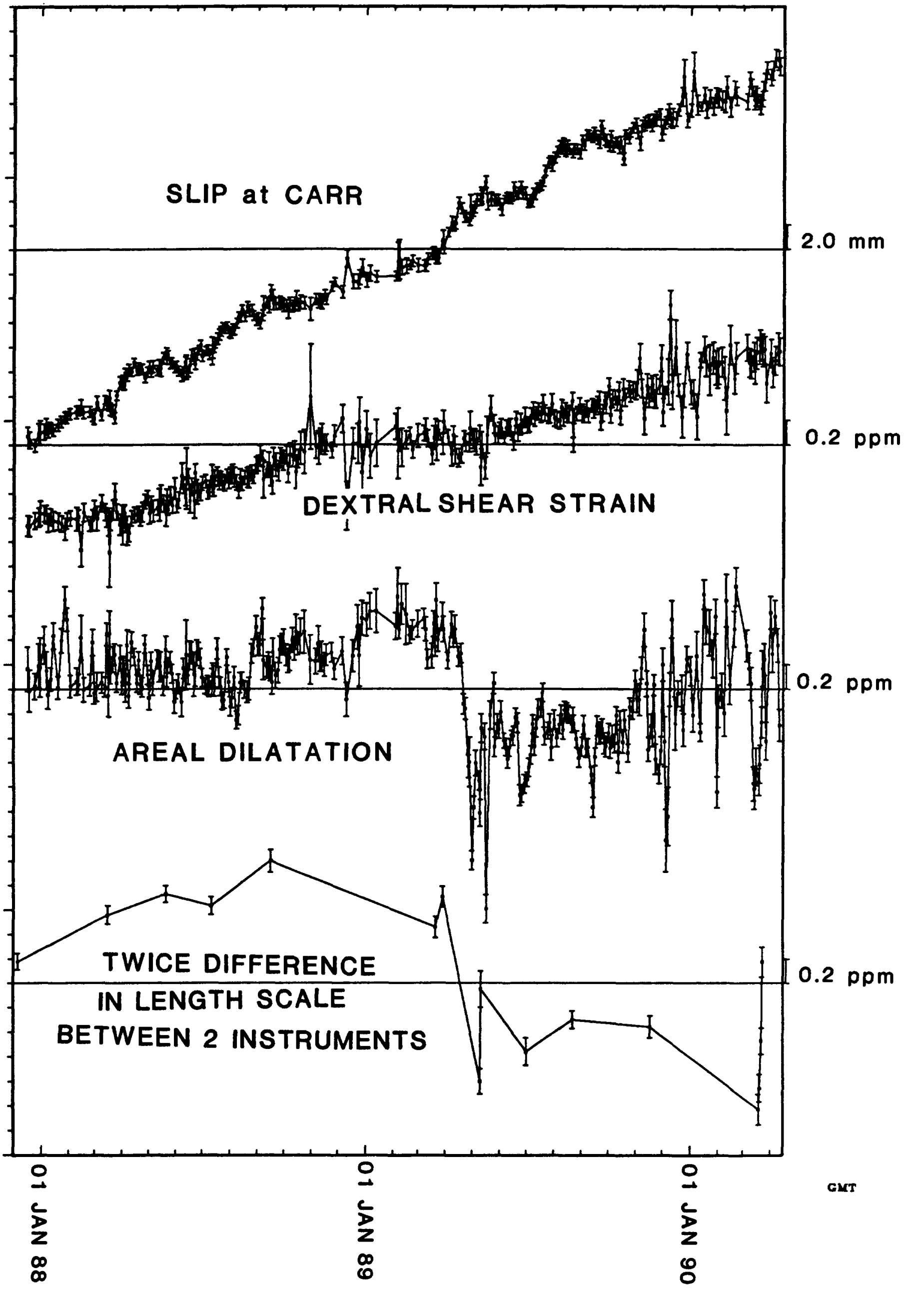
SLIP at CARR
2.0 mm
0.2 ppm
DEXTRAL SHEAR STRAIN
0.2 ppm
AREAL DILATATION
TWICE DIFFERENCE
IN LENGTH SCALE
BETWEEN 2 INSTRUMENTS
0.2 ppm
01 JAN 88
01 JAN 89
01 JAN 90
GMT

Microearthquake Data Analysis

9-9930-01173

W.H.K. Lee
U.S. Geological Survey
Branch of seismology
345 Middlefield Rd., MS 977
Menlo Park, CA 94025
(415) 329-4781

Investigations

The primary focus of this project is the development of state-of-the-art computation for analysis of data from microearthquake networks. For the past six months I have been involved in:

(1) A continued seismic study of explosive sources.

The depth effects of explosive source were investigated by spectral analysis of seismograms recorded in the near-field of three single explosions at depths of 138, 353, and 712 feet. The spectral amplitude of the deeper shots at 30 Hz is about an order of magnitude higher than that at 5 Hz. On the other hand, the spectral amplitude of the shallow shot at 30 Hz is about the same as that at 5 Hz. Using this spectral ratio technique, it is easy to discriminate a quarry blast from a single explosion at depth of over 300 feet if near-field seismograms are available.

(2) Loma Prieta Earthquake Sequence

A low-cost 128-channel PC data acquisition and recording system was implemented with the off-the-shelf hardware and a proto-type multiplex designed by Jim Ellis. It became operational just a few hours before the Oct. 18, 1989 Loma Prieta earthquake, and recorded the main shock for about 20 seconds. The system was shut off because the electric power supply failed in Menlo Park. At about 10 p.m. local time, the PC system was connected to emergency power and recorded about 30 aftershocks before its 30-megabyte hard disk was full and stopped. I had to transfer the digitized data and re-started the system several times a day to keep the system operating. This situation was greatly improved 1 day later when another PC was networked to it to off-load the data. Since then the system has performed reliably and has recorded over 3,000 aftershocks. Some preliminary analysis was performed on selected aftershocks to check the system performance. Occasionally, the digitized channels were shifted and this problem was caused by an improper timing of the proto-type multiplex. A circuit correction implemented by John Rogers has solved this problem.

(3) Armenia Seismic Studies

I have also been involved in planning and preparing seismic studies to be carried out in Armenia in June, 1990. In brief, some techniques for processing and analysis of data recording by GEOS were ported from the VAX computer to PC under my supervision.

Reports

Tottingham, D. M., Ellis, J. O., and Lee, W. H. K., 1989. A low-cost 128-channel seismic data acquisition and recording system (abstract), EOS, v. 70, p. 1189.

Lee, W. H. K., Gibbs, J. F., Criley, E. E., 1989. A seismic study of explosive sources (abstract), EOS, v. 70, p. 1189.

Harlow, D. H., Lee, W. H. K., Chouet, B., and Gil, F., 1989. Seismic monitoring of volcanic ash emissions at Galeras Volcano, Colombia using a PC-based data acquisition and analysis system (abstract), EOS, v. 70, p. 1194.

Yerkes, R. F., Oppenheimer, D. H., and Lee, W. H. K., 1989. Elsinore fault zone--seismicity vs. age of surface faults (abstract), EOS, v. 70, p. 1363.

Lee, W. H. K., and Stewart, S. W., 1989. Large-scale processing and analysis of digital waveform data from the USGS Central California Microearthquake Network, in "Observatory Seismology" edited by J.J. Litehiser, University of California Press, p. 86-98.

Parkfield Seismicity Project

0-9930-02098

Allan G. Lindh
Branch of Seismology
U.S. Geological Survey
345 Middlefield Road, Mail Stop 977
Menlo Park, California 94025
(415) 329-4778

Investigations: An Interpretive Seismic History of the San Francisco Bay Area

During the nineteenth century, almost all of the large earthquakes in the San Francisco Bay area occurred in two short time periods in the 1830s and 1860s (Figures 1 and 2); both intervals included pairs of M6.5-7 earthquakes on the San Andreas and Hayward faults. Since 1979 there have been three M6 earthquakes in the same general area, and now a M7.1 earthquake on the San Andreas (Figure 4); this activity resembles in some respects the pattern of seismicity observed from 1858 to 1865, which was followed by the M7 1868 earthquake on the Hayward fault (Figure 2). The question of whether this similarity is sufficient to significantly increase the probability of a M7 earthquake on the Hayward fault cannot be answered objectively with such a sparse data set, but a very subjective, back-of-the-envelope calculation suggests that the probability of a M7 earthquake in the Bay area may be as high as 20% in the next 5 years. This represents a factor-of-two probability gain above the long-term estimates in Agnew et al. (1988); other lines of reasoning suggest that this may not be unreasonable.

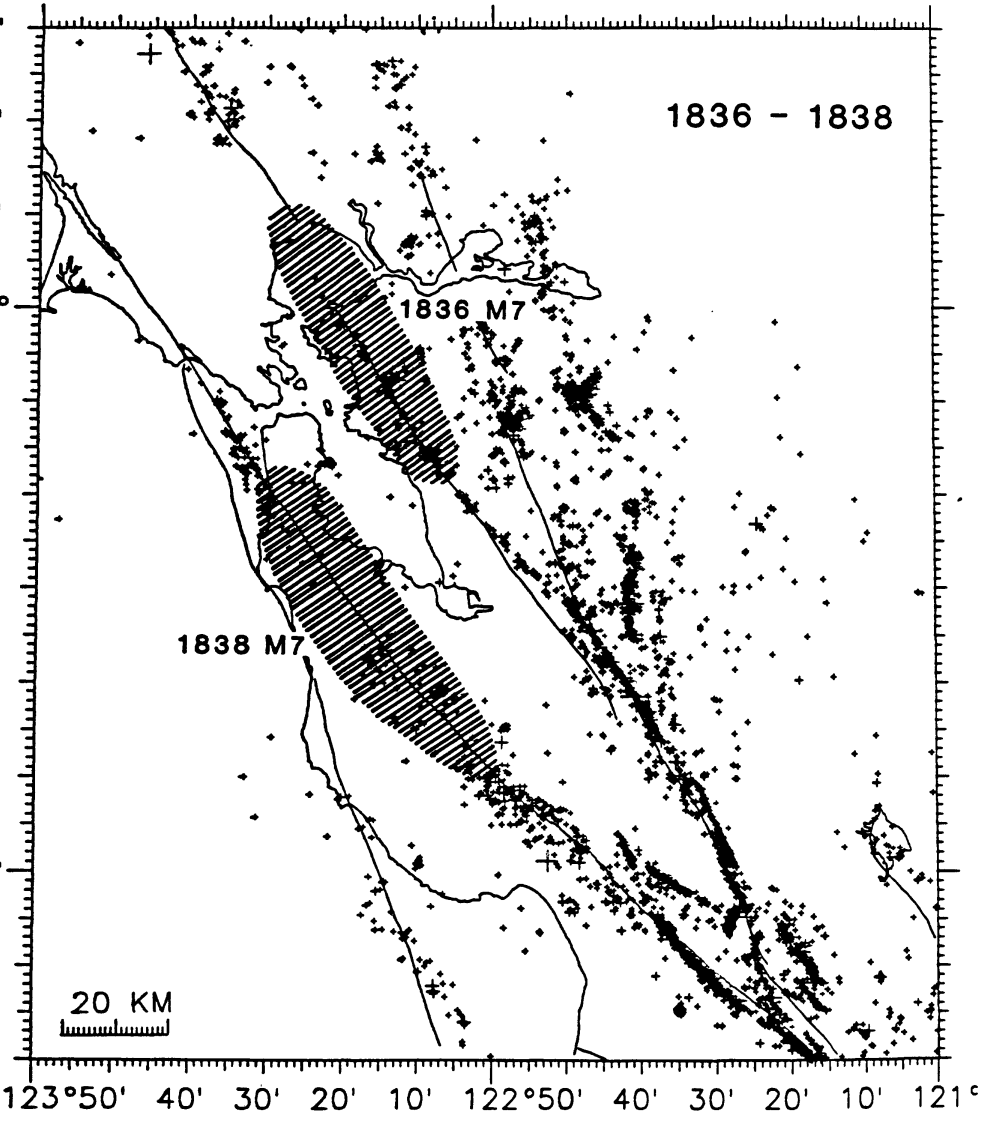
1836 - 1838
1836 M7
1838 M7
20 KM
30'
20'
10'
38°
50'
40'
30'
20'
10'
37°
50'
40'
123°50'
40'
30'
20'
10'
122°50'
40'
30'
20'
10'
121°

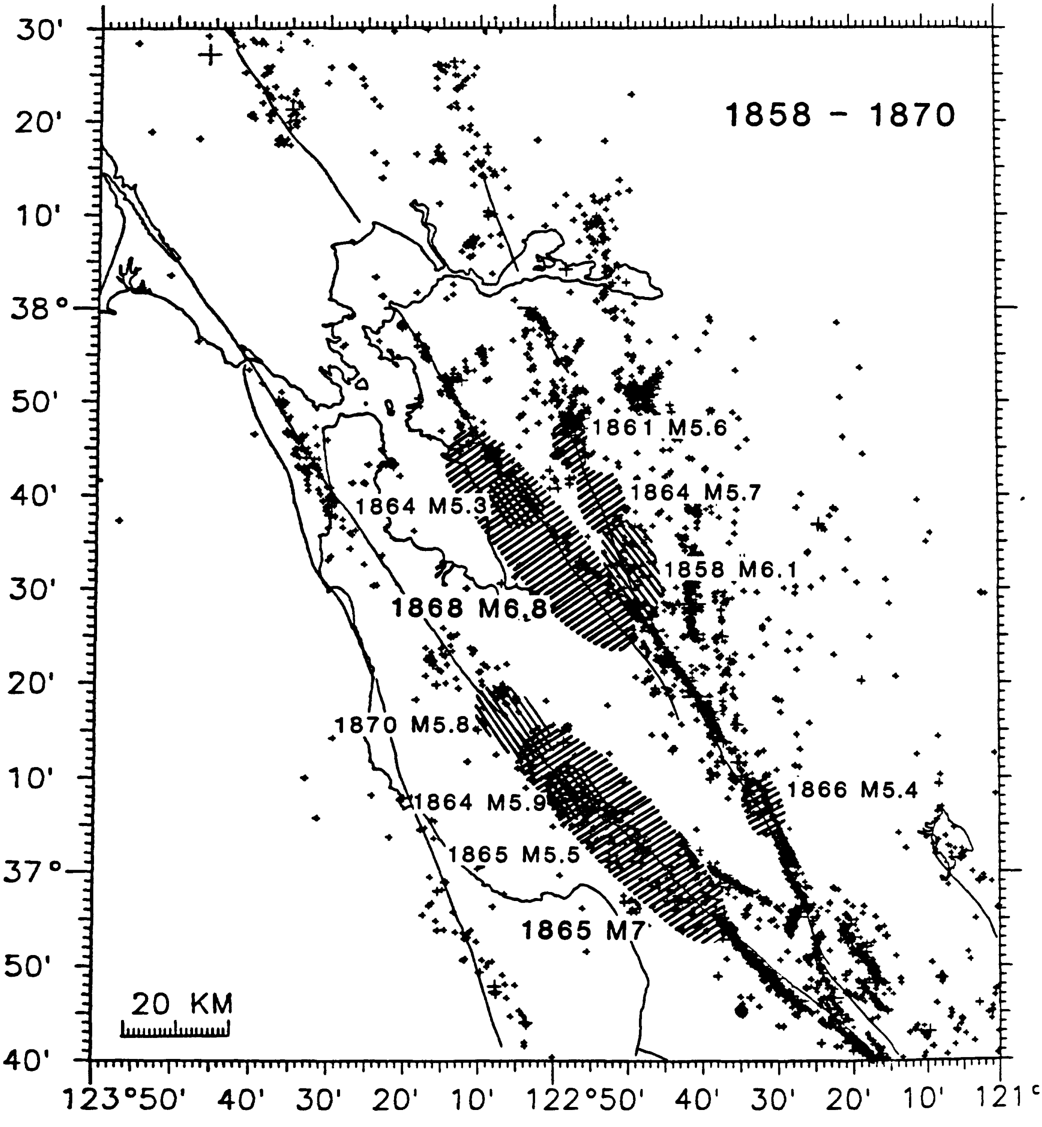
1858 - 1870
1861 M5.6
1864 M5.7
1864 M5.3
1858 M6.1
1868 M6.8
1870 M5.8
1866 M5.4
1864 M5.9
1865 M5.5
1865 M7
20 KM
30'
20'
10'
38°
50'
40'
30'
20'
10'
37°
50'
40'
123°50'
40'
30'
20'
10'
122°50'
40'
30'
20'
10'
121°

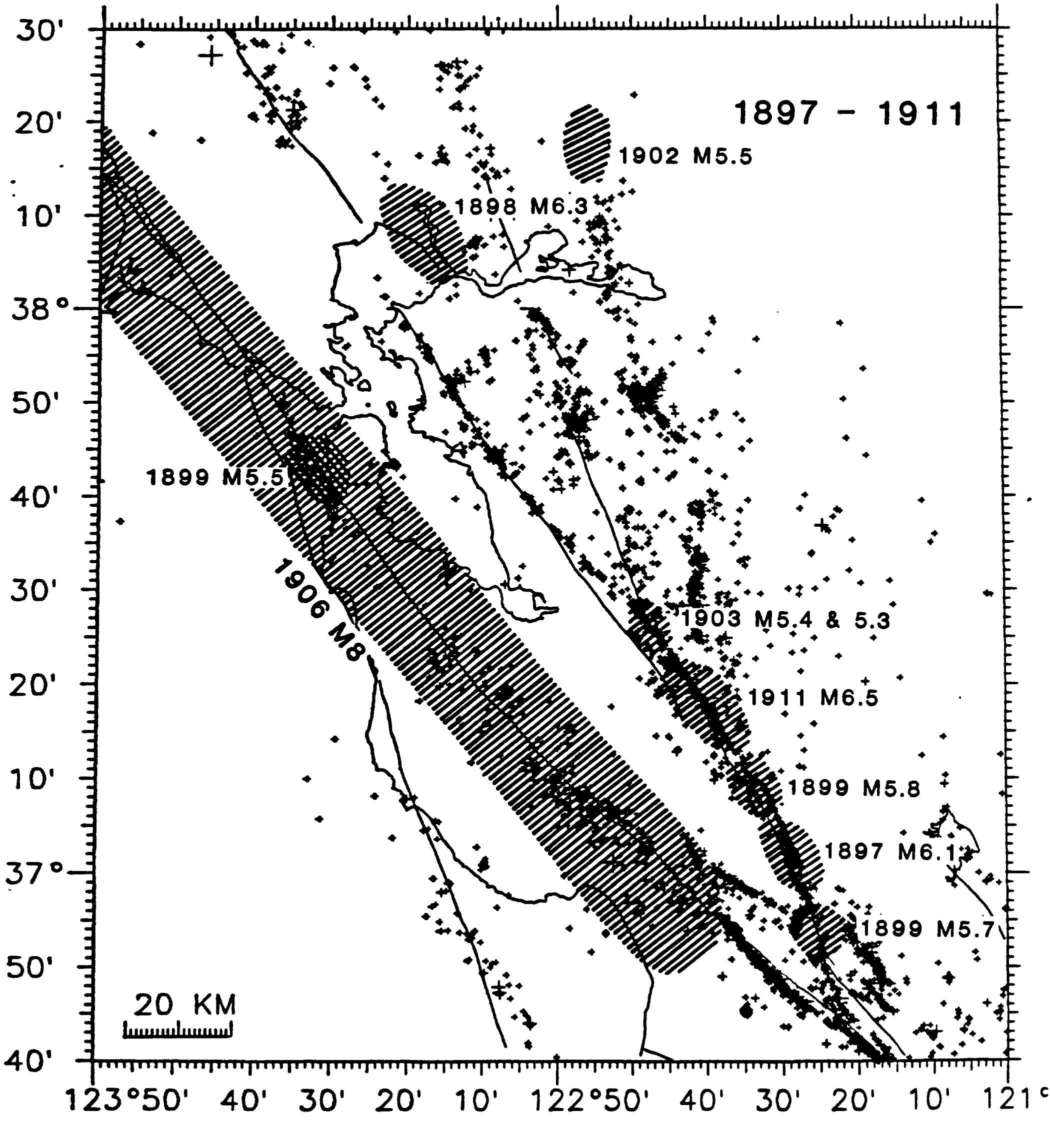
1897 - 1911
1902 M5.5
1898 M6.3
1899 M5.5
1906 M8
1903 M5.4 & 5.3
1911 M6.5
1899 M5.8
1897 M6.1
1899 M5.7
20 KM
30'
20'
10'
38°
50'
40'
30'
20'
10'
37°
50'
40'
123°50'
40'
30'
20'
10'
122°50'
40'
30'
20'
10'
121°

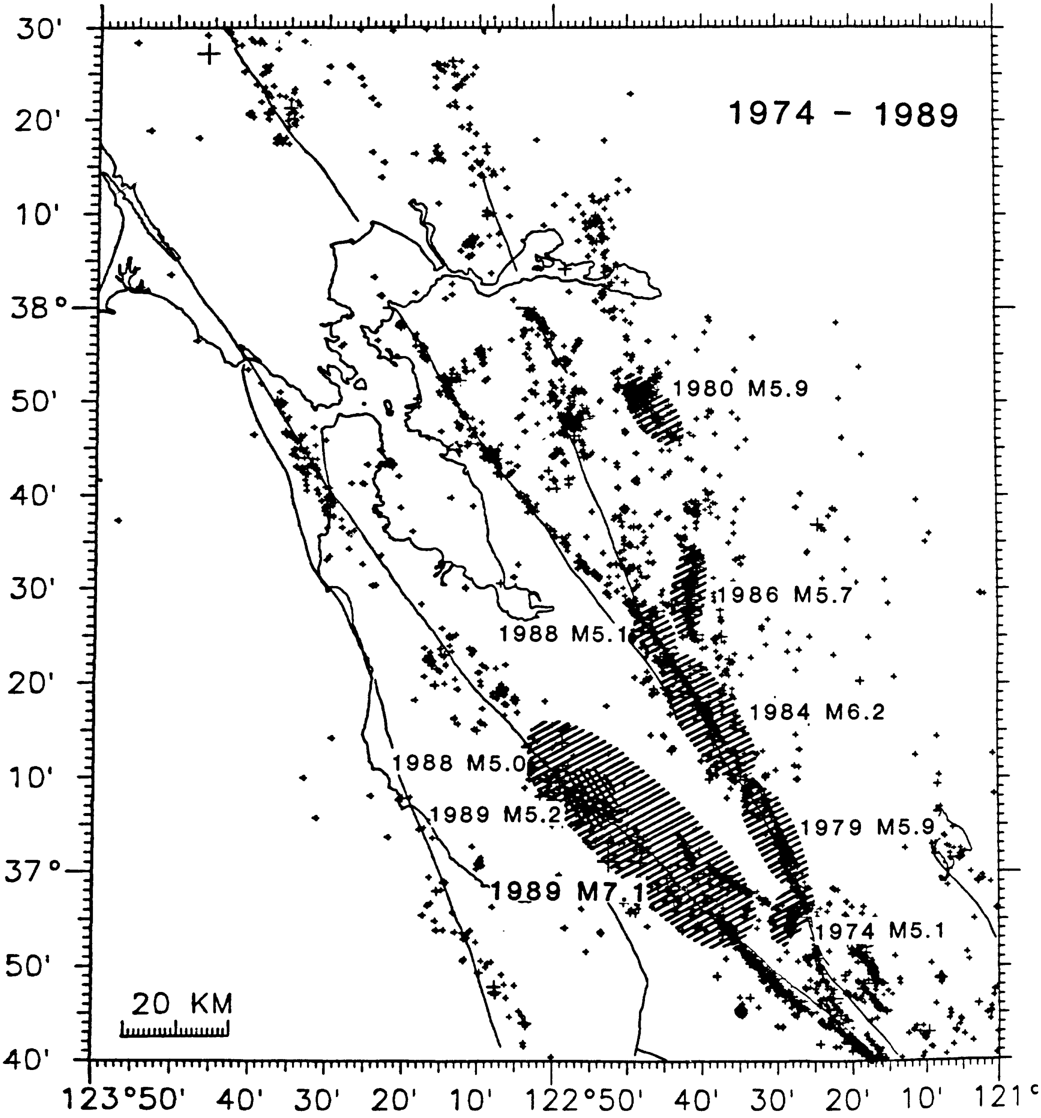
1974 - 1989
1980 M5.9
1986 M5.7
1988 M5.1
1984 M6.2
1988 M5.0
1989 M5.2
1979 M5.9
1989 M7.1
1974 M5.1
20 KM
30'
20'
10'
38°
50'
40'
30'
20'
10'
37°
50'
40'
123°50'
40'
30'
20'
10'
122°50'
40'
30'
20'
10'
121°

SEISMIC WAVE MONITORING AT PARKFIELD, CALIFORNIA

14-08-0001-G1703

T.V. McEvilly, R. Clymer, T. Daley, W. Foxall, E. Karageorgi, A. Michelini
Seismographic Station
University of California
Berkeley, CA 94720

INTRODUCTION

Three programs of seismic wave measurements continue: Earthquake recording with the high-resolution seismic network (HRSN), begun in December, 1986; controlled-source monitoring with HRSN begun in June, 1987; and controlled-source monitoring with the Varian well vertical array (VWVA), begun in November, 1987.

The HRSN (Figure 1) consists of ten, 3-component, borehole seismometers surrounding the 1966 Parkfield epicenter. Data-acquisition features digital telemetry with 125-Hz bandwidth and 16-bit resolution, and can operate in external-trigger *(i.e.,* controlled-source) or event-trigger (earthquake) modes.

The VWVA extends to 1400-m depth at a site 2 km from the San Andreas fault (Figure 1), close to the nucleation zone of the expected magnitude 6 Parkfield earthquake. While tests done shortly after installation indicated that the entire array was functioning, failure of deep connecting cables soon eliminated sensors below 968m. There is some indication of further degradation. The original November, 1987 tests provide a 'benchmark' vertical seismic profile (VSP) using the full string. The remaining instruments are adequate to proceed with all the proposed uses of the VWVA. The array is recorded on a Sercel 338 96-channel reflection system.

INVESTIGATIONS

1) Earthquakes. Local microearthquakes of magnitude about -1 to about +2 are continuously recorded on scale. A 3-D velocity model and a high-precision hypocenter location procedure have been developed, which will allow high-resolution analysis of all earthquakes in this area. Relocated events are being used to study failure processes, fault zone structure, and material properties within the Parkfield nucleation zone.

2) Controlled-source monitoring with HRSN. From June, 1987 through March 1990, the HRSN has been illuminated 27 times with S-waves of three polarizations at eight source positions throughout the study zone, using a shear-wave Vibroseis source, in an on-going monitoring program. The resulting data contain a temporal record of wave propagation characteristics throughout the nucleation zone. Albeit complexly encoded, the wave fields recorded contain the evidence for any nucleation-induced changes in velocities, attenuation or anisotropy, along with the ubiquitous seasonal effects of varying moisture content at the vibrator sites. Data reduction is accomplished at the University of California's Lawrence Berkeley Laboratory (LBL).

3) Controlled-source monitoring with VWVA.

- Analysis of local anisotropy and velocity structure using short-offset VSP's.
- Monitoring of seismic parameters by occasional illumination from at least the four closest HRSN source sites plus an additional near-offset site.

RESULTS

1) Data collected.

- Full-time, triggered recording of earthquakes has continued in the past six months. Local Parkfield events have been picked and relocated with the 3-D model through December, 1989.
- Five vibrator data sets have been collected and the data reduced.
- At VWVA, a detailed multi-azimuth VSP survey was collected in December, 1989, to be used in modeling material properties in the vicinity of the well. In addition, three monitoring data sets have

been recorded.

2) *Earthquakes.*

We have completed the development of a three-dimensional model for P and S velocity in the Parkfield area, a model that capitalizes in its resolution on the bandwidth and dynamic range of the HRSN data, and provides the necessary framework for on-going and subsequent studies. A discussion of the modeling process and results have been submitted for publication (Michelini and McEvilly, 1990). A cubic B-spline parameterization was used to produce optimally smooth velocity distributions suitable for generating, using dynamic ray tracing (Cerveny, 1985), the 3-D Green's functions needed for studying the earthquake sources and rupture processes. These velocity models still retain some small-scale features. A result of particular interest is a zone of high Vp/Vs ratio (1.9) in the vicinity of the hypocenter of the 1966 earthquake.

These models form the basis for several studies:

- The three years of earthquakes recorded on HRSN have been relocated using the new model, and spatial clusters of events producing very similar waveforms are being defined.
- Very precise relative locations of clustered events are being used to study fine-scale structure of the fault zone.
- Event clusters whose members occur over a significant time span are being used to search for temporal variations in fault-zone properties. Preliminary results show stability of travel-times near the 1966 epicenter on Middle Mountain.
- Comparison of results of ray-tracing through the 1-D Parkfield model and the new 3-D model shows suprisingly little difference between ray take-off angles at the source in the two models. Therefore, it appears that although the smooth 3-D model is suitable for dynamic ray-tracing it may not adequately account for effects produced by the strongly laterally heterogeneous fault zone, such as laterally refracted head waves and fault-zone trapped modes. We are presently examining ways to incorporate first-order lateral discontinuities into the smooth 3-D model so we can model these effects.
- Green's functions will be calculated for moment tensor inversions for equivalent point sources of Parkfield microearthquakes.

3) Controlled-source studies - HRSN.

The final working data sets for analysis are "time gathers": one source into one receiver gathered across calendar time, producing 720 files, each containing, at present, 27 similar traces. An example is shown in Figure 2. To analyze these gathers, several data manipulation methods have been developed to display waveform properties of 1) windowed phases, 2) for whole traces, and 3) for entire time gathers. Simple techniques displaying various properties in short time windows centered on particular phases produce interesting results, but present only a small fraction of the information available in the waveforms. In recent months, our primary effort has been development of color-graphics displays of trace amplitude, frequency content, travel-time changes, and instantaneous trace attributes (signal strength and instantaneous frequency) of whole traces or entire gathers.

The figures illustrate this development with an example of particular present interest. Most displays to date show only the seasonal variations (we are presently working on procedures to reduce their effect), however, two paths (all we have analyzed to date) from source site 2 show a significant travel-time anomaly at late travel times. The grey-scale display of relative travel-time change in a moving window shown in Figure 3 does not contain the richness of information of the equivalent color plot, but the anomaly clearly shows as the dark zone from 6-8 sec. Figure 4, showing windowed travel-time changes for two phases, shows that the advance does not appear on early arrivals, and is thus not a near-surface, seasonal effect as usually observed. The phases used are identified on the trace gather in Figure 2.

There are similar large late variations on paths 1-MMN and 7-JCN, though in zones of relatively poor correlation.

We are now searching for the effect on many more paths and source orientations, and are attempting to identify the wave types involved with particle motion and frequency analyses.

Two further methods are under development. We are developing 3-component, particle-motion techniques to study S-wave anisotropy. Finally, using a Stardent computer system, we are extending the 3-parameter color displays to 4-parameter, 3-D displays of cubes of data that can be viewed in perspective, rotated, sliced, *etc.*

The tools discussed here are a beginning; the task ahead is their application to the efficient reduction of a massive data set to a few displays of key waveform parameters. These, in conjunction with the high-precision HRSN microearthquake observations, will be the basis of active programs of 1) prediction monitoring, and 2) high-precision interpretation of changes in physical properties observed in the nucleation of Parkfield earthquakes.

4) Controlled-source studies - VWVA.

The analysis of the initial VSP studies, showing up to 10% anisotropy in the vicinity of the well, has been submitted for publication (Daley and McEvilly, 1990).

The present recording system, on loan to LBL/UCB, was placed in service in November, 1989. The system has proven difficult to operate and maintain, and we have decided to reduce our data gathering to three to four month intervals.

The development of 3-D, generally anisotropic models continues, in cooperation with V. Cerveny, I. Psencik, and D. Gajewski. The results will be used in modeling of material properties with the data set discussed above.

References

Cerveny, V., 1985. The application of ray tracing to the propagation of shear waves in complex media, in *Seismic Shear Waves, Part A: Theory,* Gerhard P. Dohr, editor, Geophysical Press, London and Amsterdam, 1-124.

Papers submitted for publication

Daley, T.M., and T.V.McEvilly, 1990. Shear Wave Anisotropy in the Parkfield Varian Well VSP, submitted to *Bull. Seis. Soc. Am.*

Michelini, A., and T.V.McEvilly, 1990. Seismological studies at Parkfield: Simultaneous inversion for velocity structure and hypocenters using cubic B-splines parameterization, submitted to *Bull. Seis. Soc. Am.*

Presentations, Seismological Society of America annual meeting, May 4, 1990

Foxall, W., A. Michelini, and T.V.McEvilly, Effects of three-dimensional velocity structure on focal mechanism solutions of Parkfield earthquakes.

Karageorgi, E.D., R.W. Clymer, and T.V.McEvilly, Seismic Monitoring at Parkfield: Variations in controlled-source parameters.

Michelini, A., and T.V.McEvilly, Seismic monitoring at Parkfield: Search for temporal variations through successive joint hypocenter and velocity inversion for fault zone properties.

All in *Seismological Research Letters, 61,* 49.

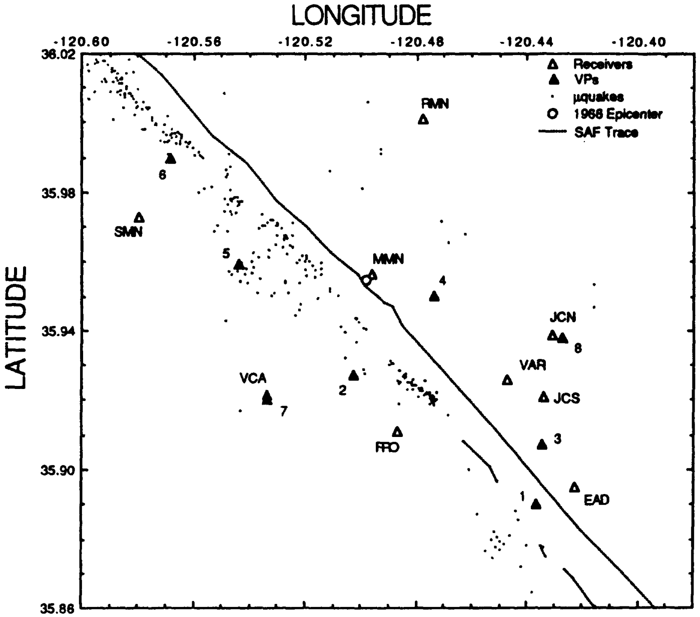

Figure 1. Parkfield location map, showing the High-Resolution Seismic Network, controlled-source (vibrator) points, and 6/87-12/89 seismicity as relocated through the 3-D model.

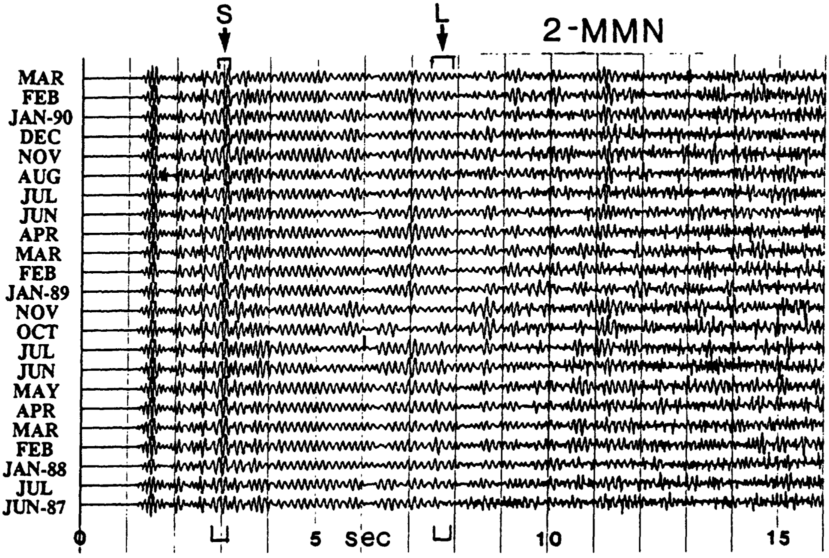

Figure 2. Twenty-three trace time gather for one source polarization at source site 2 and the MMN (Middle Mountain) H1 receiver. The indicated windows (S and L) refer to the travel-time analysis shown in Figure 4.

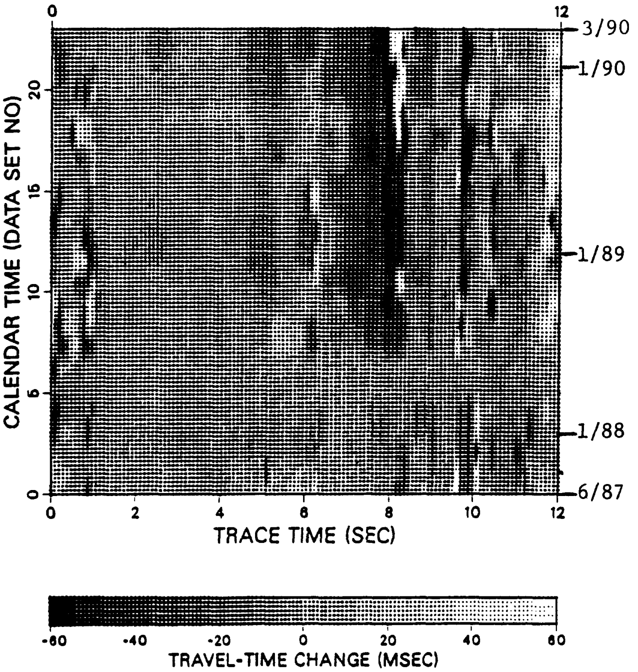

Figure 3. Travel-time change relative to a reference trace (here trace 6, Figure 2) by cross-correlation in a moving time window. Note the 50-60 msec anomaly from 6-8 sec.

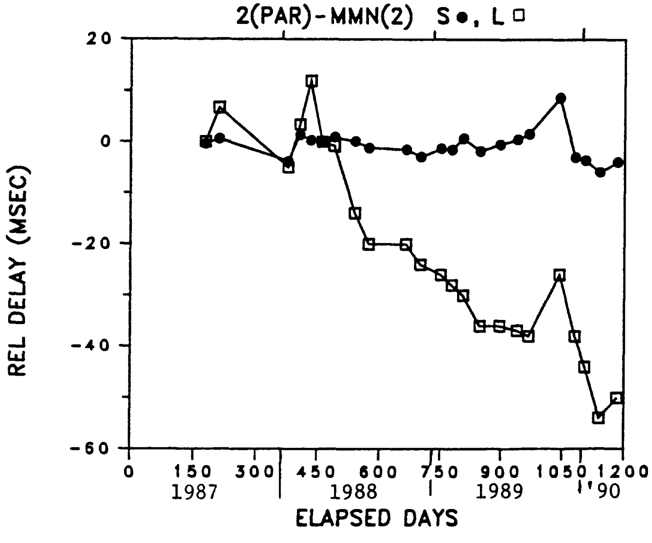

Figure 4. Travel-time change (relative to trace 6, Figure 2) of two windowed phases by a cross-correlation, cross-coherence technique. Note the large variation in the late phase.

EXPERIMENTAL TILT AND STRAIN INSTRUMENTATION

9960–01801

C.E. Mortensen
Branch of Tectonophysics
U.S. Geological Survey
345 Middlefield Road, MS/977
Menlo Park, California 94025
(415) 329–4856

Investigations

1. There are currently 134 Data Collection Platforms (DCP's) that transmit a variety of data through the GOES–6 spacecraft to the Direct Readout Ground Station (DRGS) in Menlo Park. Fifty–four of these DCPs transmit data at 10–minute intervals on an exclusively assigned random channel, which is being utilized under a special agreement with NESDIS. This system transmits data from all types of low–frequency instruments including dilatometers, creepmeters, strainmeters, water–level meters, magnetometers, tiltmeters, and related instruments.
2. A system to backup the satellite telemetry with non-volatile, solid–state memory and dialup or dedicated telephonic communications path has been developed. Included in this system is the capability to lock the DCP timing to a radio time standard. This feature will enable more efficient utilization of the assigned satellite bandwidth. This system is known as the Companion because of its interfacing role with satellite DCP's. The first five production models have been delivered and are currently being tested prior to field deployment.
3. A system has been developed that utilizes the emergency interrogate capability of GOES to switch the Sutron 8004 DCP to rapid reporting at random, frequent intervals. This adaptive random reporting system is being interfaced with the Parkfield alert systems to test the feasibility of utilizing adaptive random reporting in earthquake prediction monitoring applications.
4. Networks of tiltmeters, creepmeters and shallow strainmeters have been maintained in various regions of interest in Califorina. A network of tiltmeters monitors crustal deformation within the Long Valley caldera. Roger Bilham of the University of Colorado and Jon Beavan of Lamont–Doherty installed a very long baseline tiltmeter in Long Valley. This project provided three DCP's to collect the data from that instrument and return it to Menlo Park via the GOES satellite. We also monitor the data received to keep track of deformation within the caldera, comparing results frequently with the USGS tiltmeter array. Other tiltmeters are located in the San Juan Bautista and Parkfield regions. Creepmeters located along the Hayward, Calaveras and San Andreas faults between Berkeley and the Parkfield area are maintained in cooperation with the Fault Zone Tectonics project. A shallow strainmeter is located near Parkfield, while observatory type tiltmeters and strainmeters are sited at the

Presidio Vault in San Francisco, and a tiltmeter is installed in the Byerly Seismographic Vault at Berkeley. Data from these instruments are telemetered to Menlo Park via the GOES satellite.

5. A low–cost, short–haul digital telemetry system utilizing UHF radios, packet controllers and off–the–shelf digital data converters has been developed, tested, and is currently in use in Parkfield monitoring the tilt of monuments that support the reflectors that constitute the 2–color laser network. This system, components for which cost less than $1500 per site, automatically polls the remote sites and transfers the data to a computer file, calculating the mean and standard error in the process. The system, including the tiltmeters, can easily be removed and transported to other locations.

Results

Strainmeters and tiltmeters having short base lengths and installed at shallow depths have been known for years to be sensitive to very local perturbations caused by surface soil conditions, meteorological events, thermoelastic effects and other sources of spurious noise. Because of this, these instruments usually display poor long–term stability and can respond wildy at times, especially to episodes of heavy rainfall. From extensive arrays of these instruments installed years ago, most have been removed; just a few that perform especially well, or are located in critical spots, remain. Despite the inherent disadvantagess of these instruments, they are highly sensitive and are capable of detecting deformational changes that occur over short time spans such as solid earth tides, signals that are associated with propagating creep events (see for example, *Mortensen, et al.*, BSSA, 1977) or volcanic intrusions (see, for example, *Mortensen and Hopkins*, JGR, 1987). When associated with data from other sensors, these instruments can constrain source mechanisms of such signals and make a contribution to a regional monitoring effort.

Plotted in the figures that follow are data from most of the shallow borehole tiltmeter and strainmeter sites. In each figure the part labeled ‘a’ is the raw data for the period 1 October, 1989, through 31 March, 1990. In part ‘b’ of each figure the data have been high pass filtered using a Butterworth digital filter having a cutoff period at 48 hr. The plots in the ‘b’ part of each figure roughly demonstrate the instrumental performance at each site in the frequency range of interest for these instruments. For example, tidal modulations dominate the instrument responses at most sites, and increased noise can be seen during the winter periods of rainfall (around February). Each tiltmeter is identified by a three letter code followed by an ‘n’ or ‘e’ for the north or east component, respectively. The sites are plotted on the map in Figure 1. Movement of the record trace in the positive sense represents tilt down to the north or east. On the strainmeter records movement in the positive sense is extension. Units are all ppm – microradians or microstrain.

These records have been “cleaned” using an automatic cleaning algorithm. The data have not been reviewed for spurious effects of instrumental or metorological origin. Instruments sited at the San Francisco Presidio (pdo...etc....) and UC Berkeley (brk..) are installed in temperature–stable vaults, the Harris Ranch tiltmeter (har..) is installed in a mine shaft (giving very good results), and all other instruments are installed in shallow boreholes.

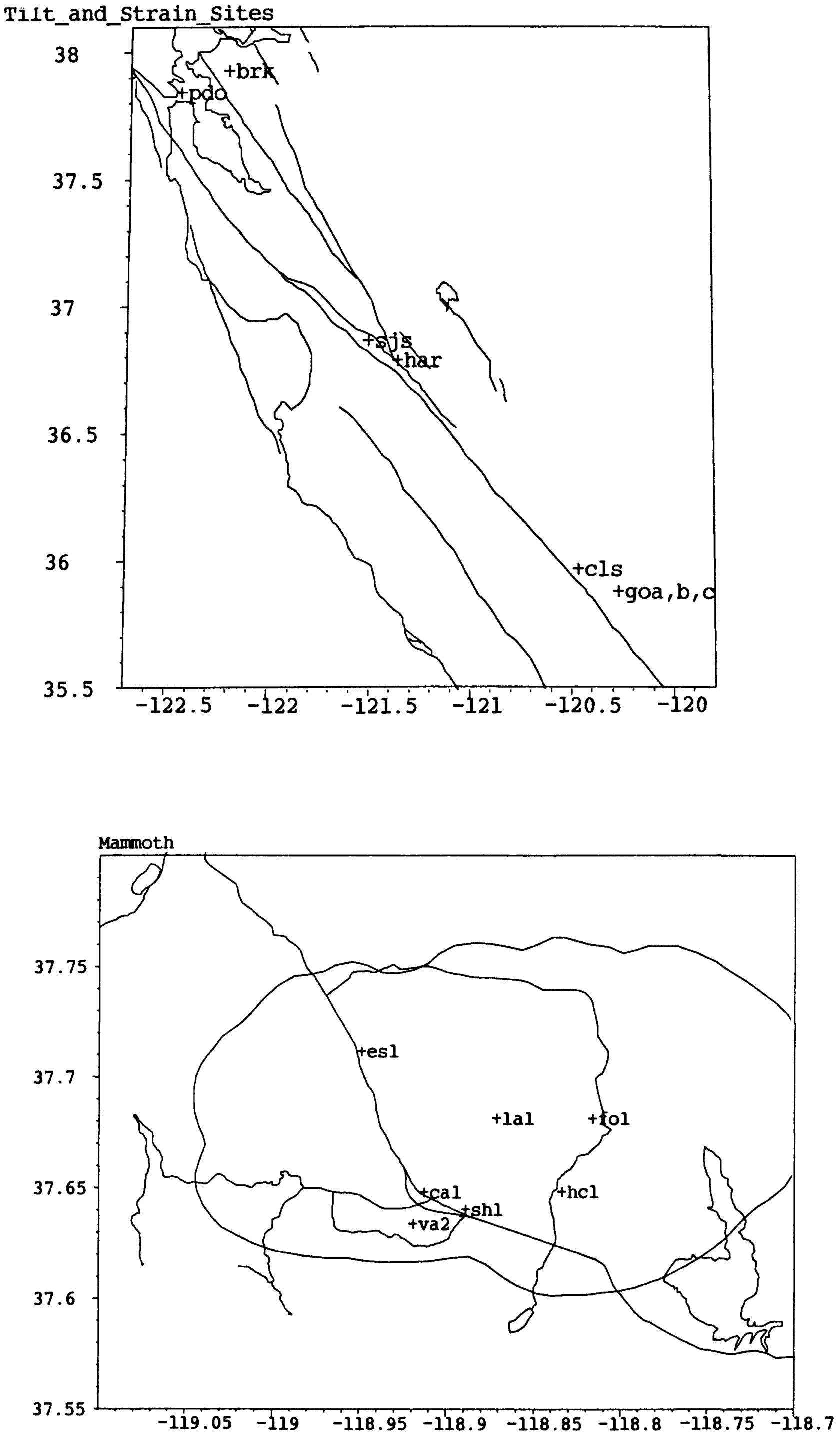
Tilt_and_Strain_Sites
38
37.5
37
36.5
36
35.5
-122.5
-122
-121.5
-121
-120.5
-120
+brk
+pdo
+sjs
+har
+cls
+goa,b,c
Mammoth
37.75
37.7
37.65
37.6
37.55
-119.05
-119
-118.95
-118.9
-118.85
-118.8
-118.75
-118.7
+esl
+lal
+fol
+cal
+shl
+va2
+hcl

Figure 1.

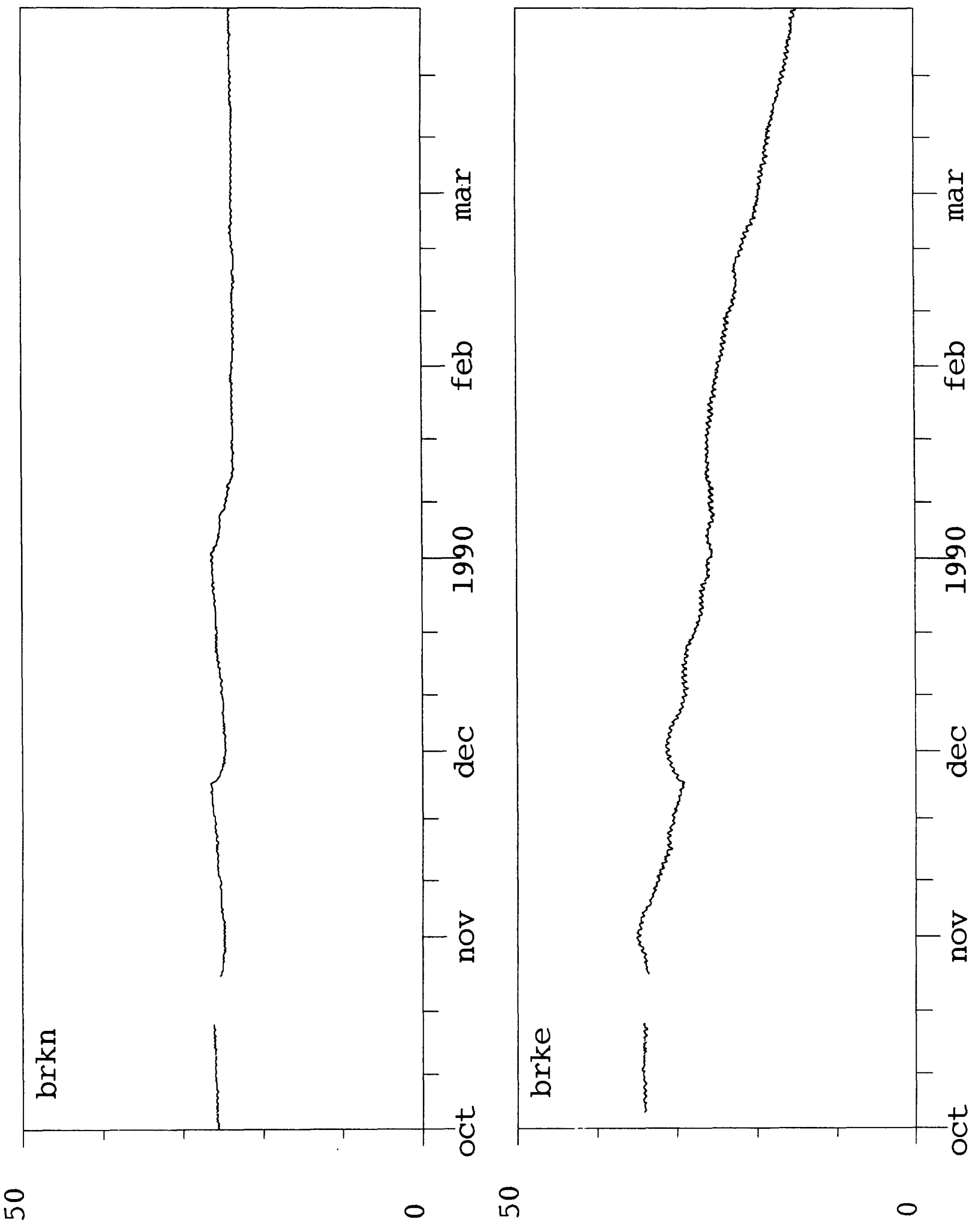

Figure 2a.

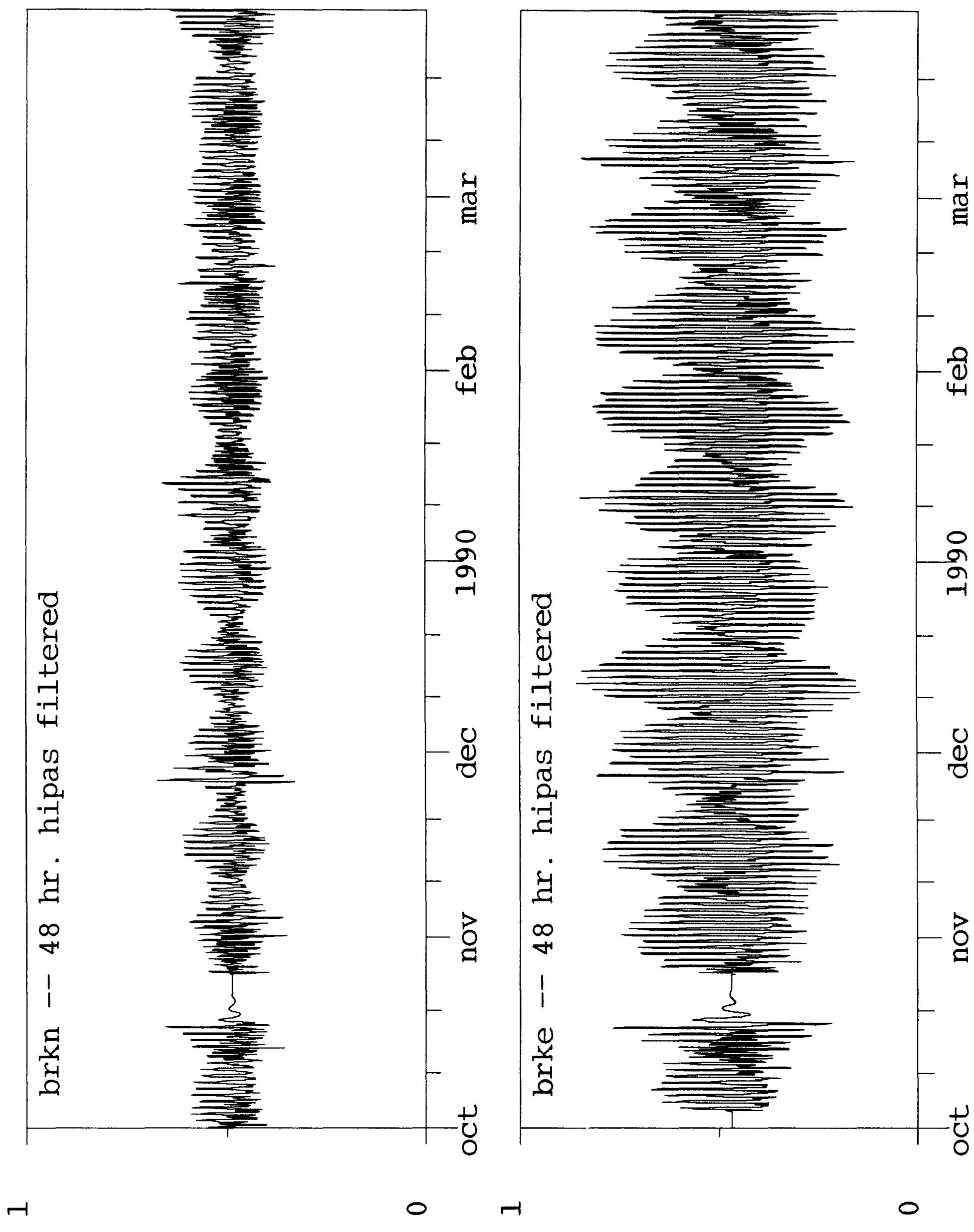
brkn -- 48 hr. hipas filtered
brke -- 48 hr. hipas filtered
oct
nov
dec
1990
feb
mar
oct
nov
dec
1990
feb
mar
1
0
1
0

Figure 2b.

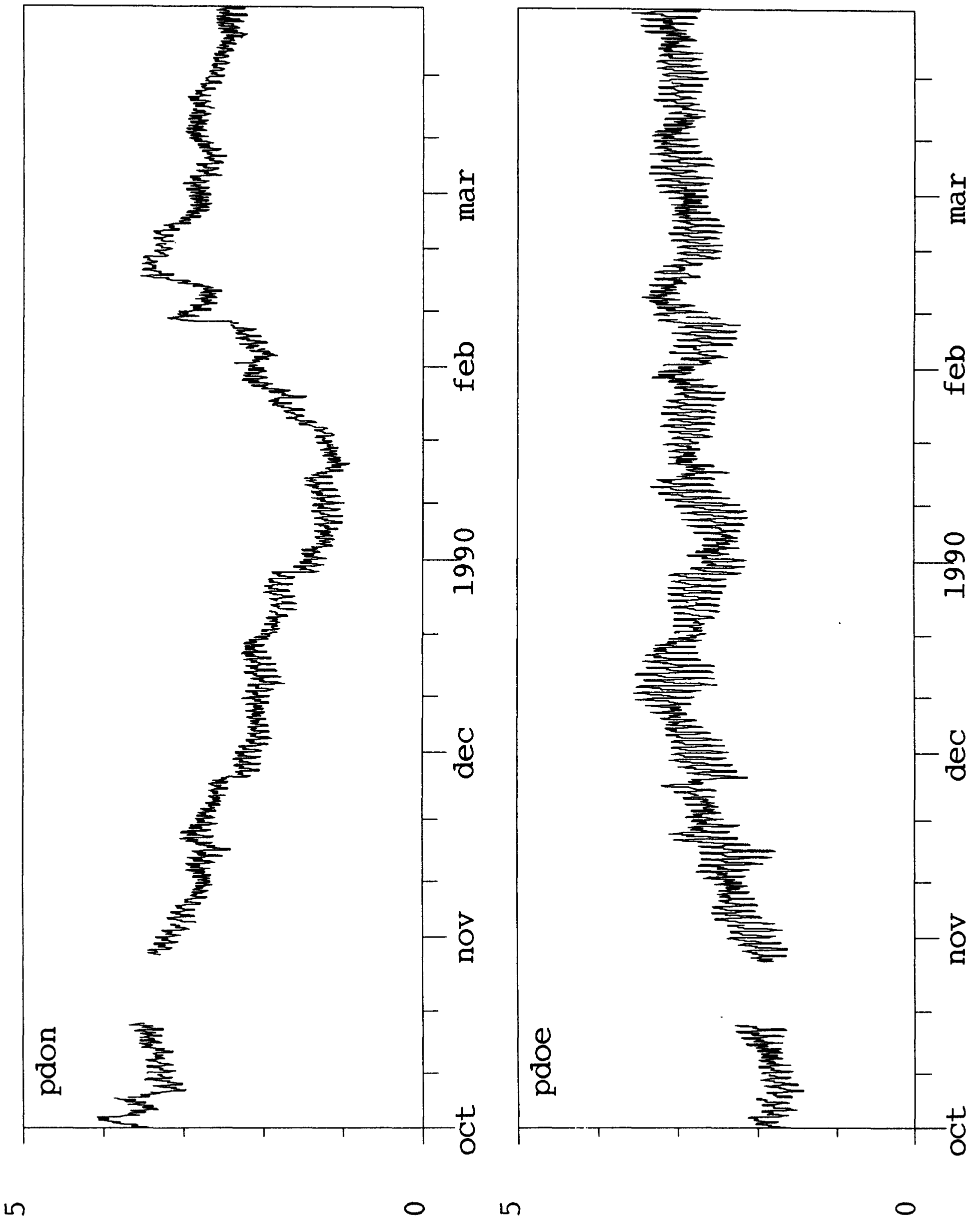

Figure 3a.

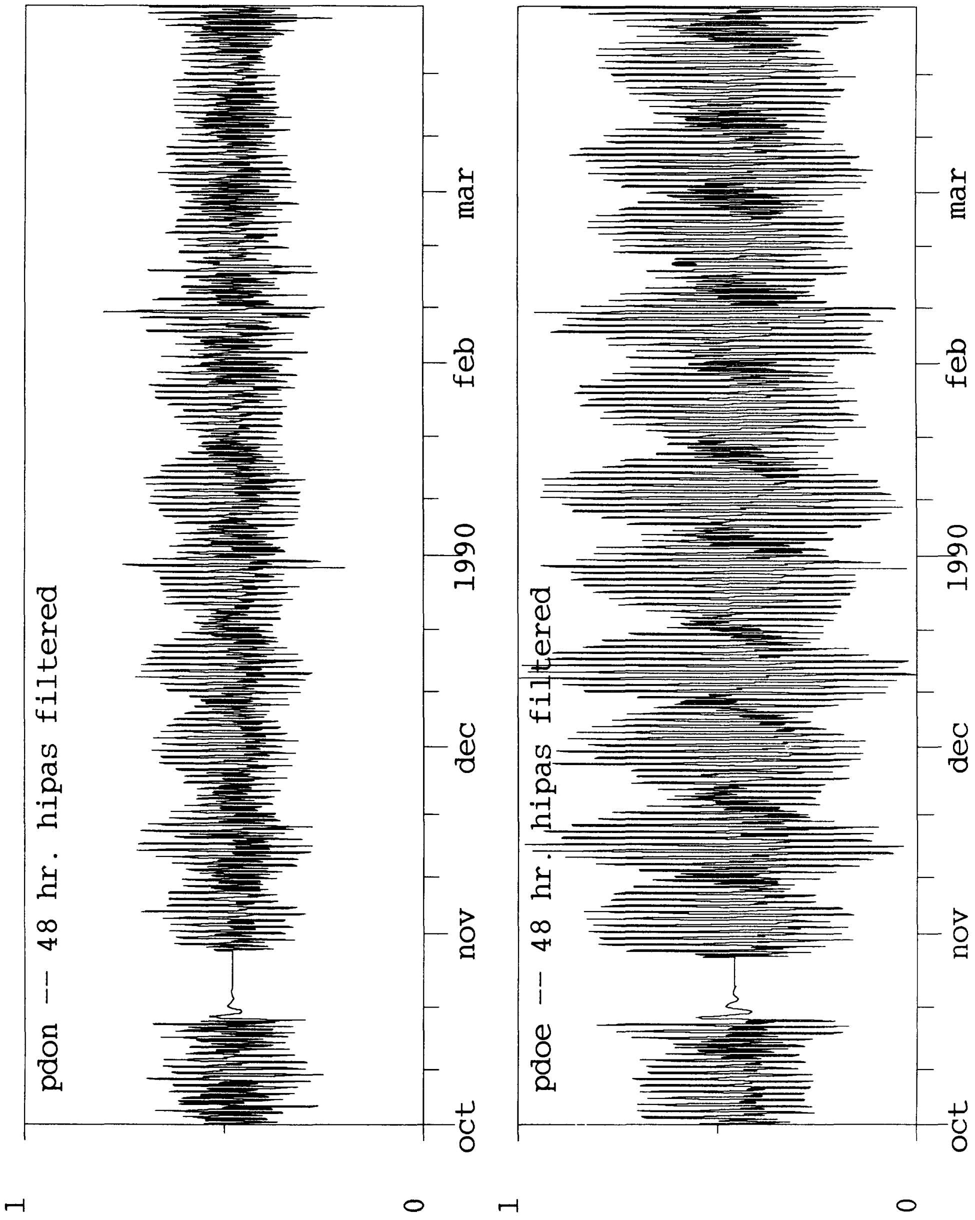
pdon -- 48 hr. hipas filtered
pdoe -- 48 hr. hipas filtered
oct
nov
dec
1990
feb
mar
1
0
1
0

Figure 3b.

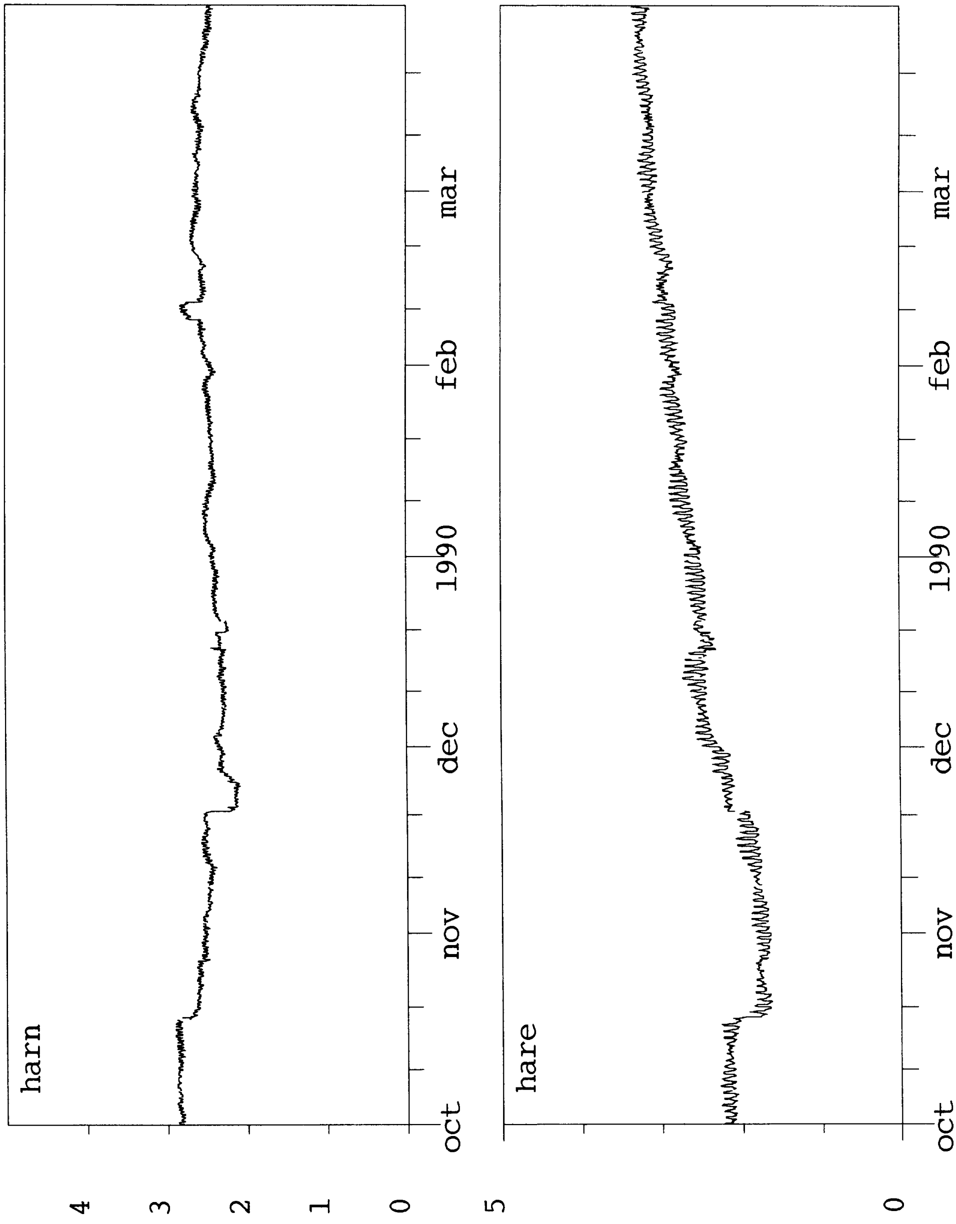

Figure 4a.

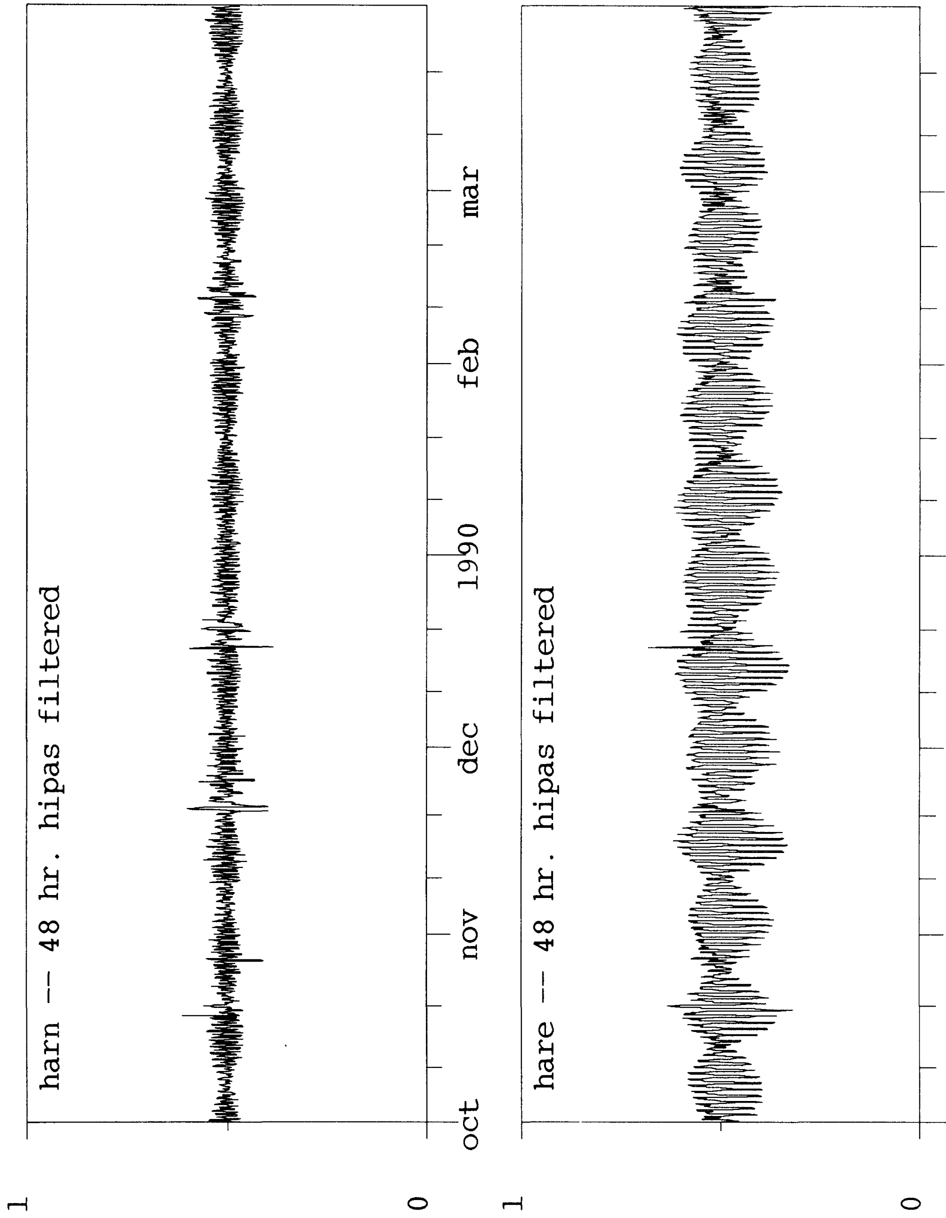
harn -- 48 hr. hipas filtered
hare -- 48 hr. hipas filtered
oct
nov
dec
1990
feb
mar
1
0
1
0

Figure 4b.

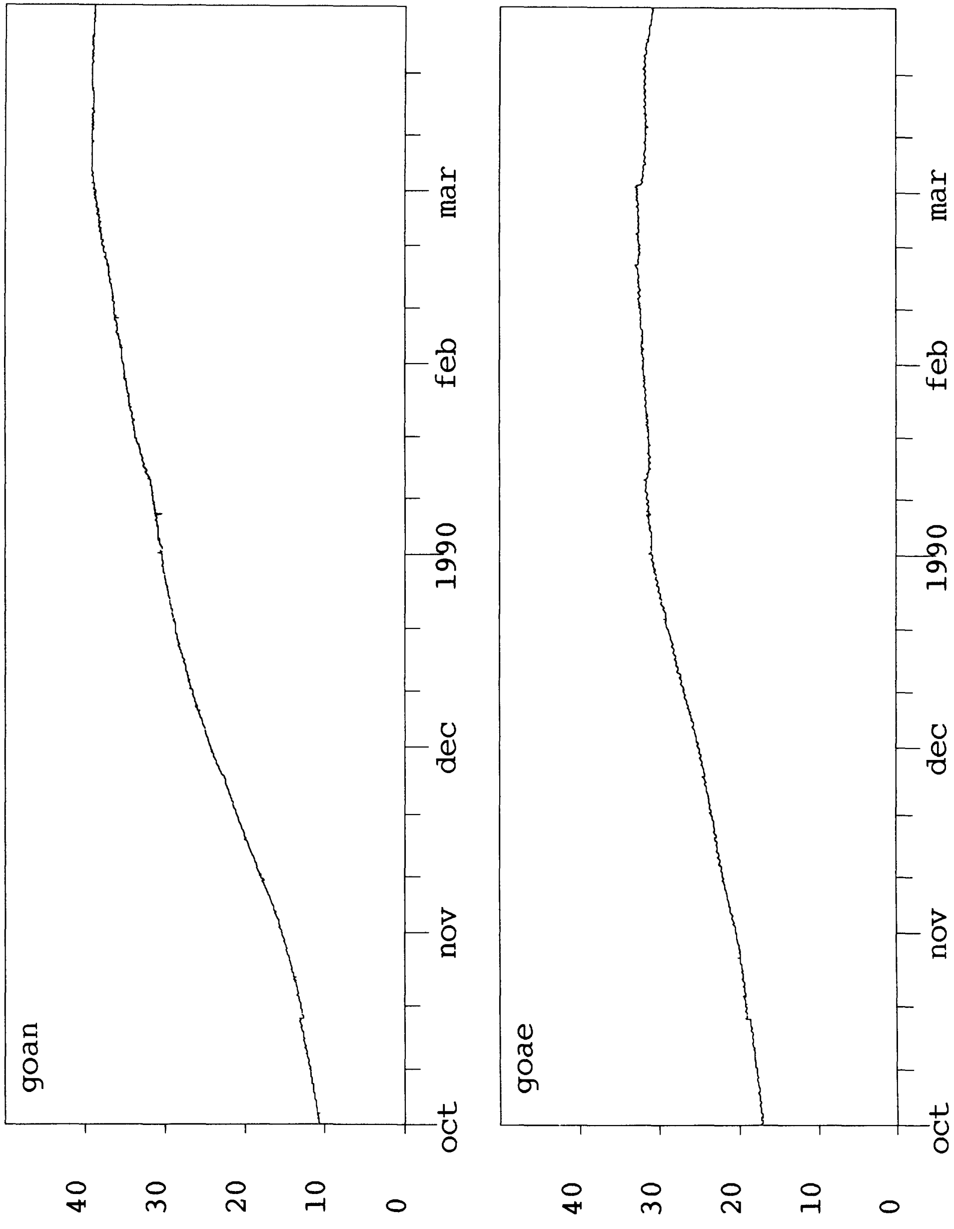

Figure 5a.

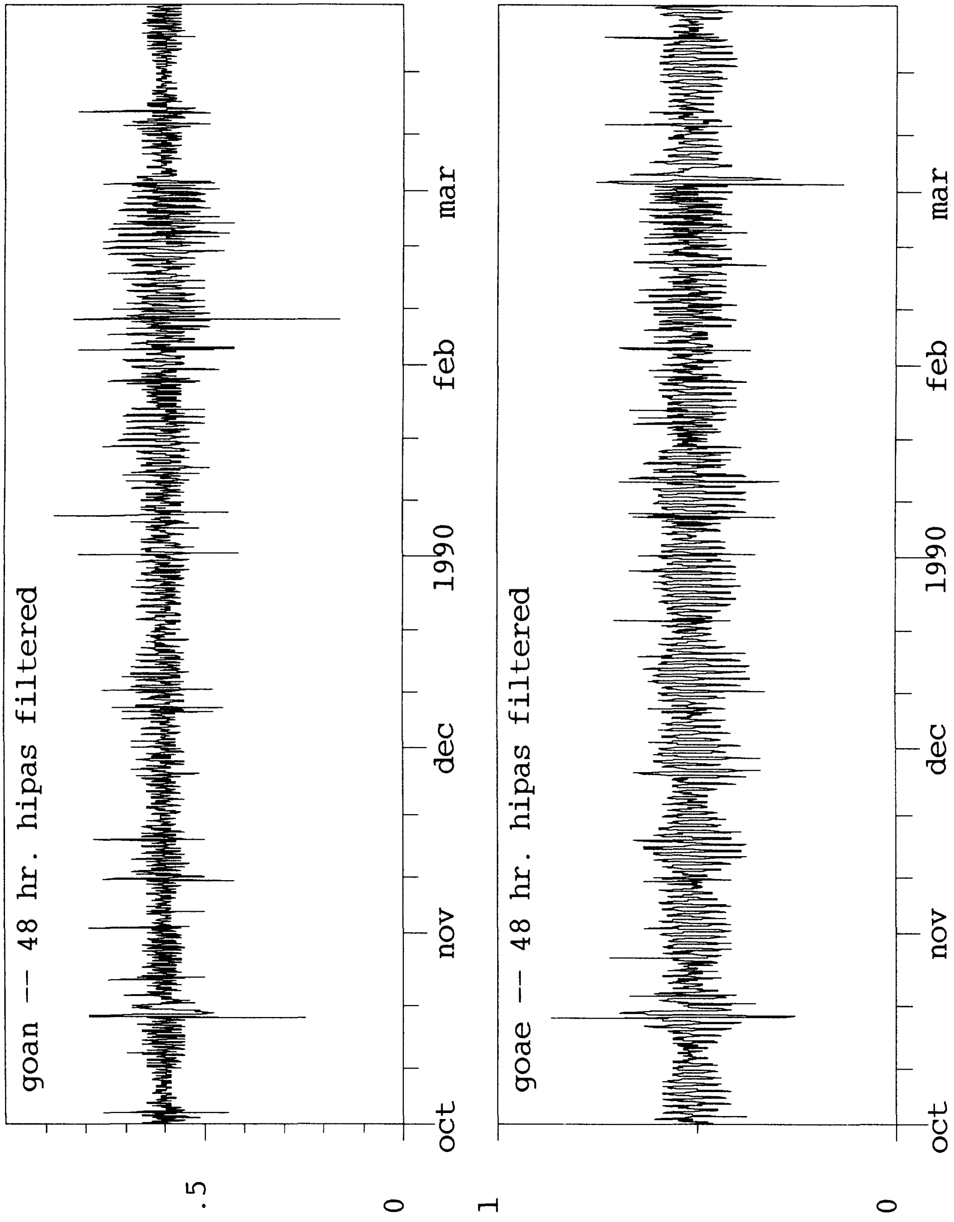
goan -- 48 hr. hipas filtered
goae -- 48 hr. hipas filtered
oct
nov
dec
1990
feb
mar
oct
nov
dec
1990
feb
mar
.5
0
1
0

Figure 5b.

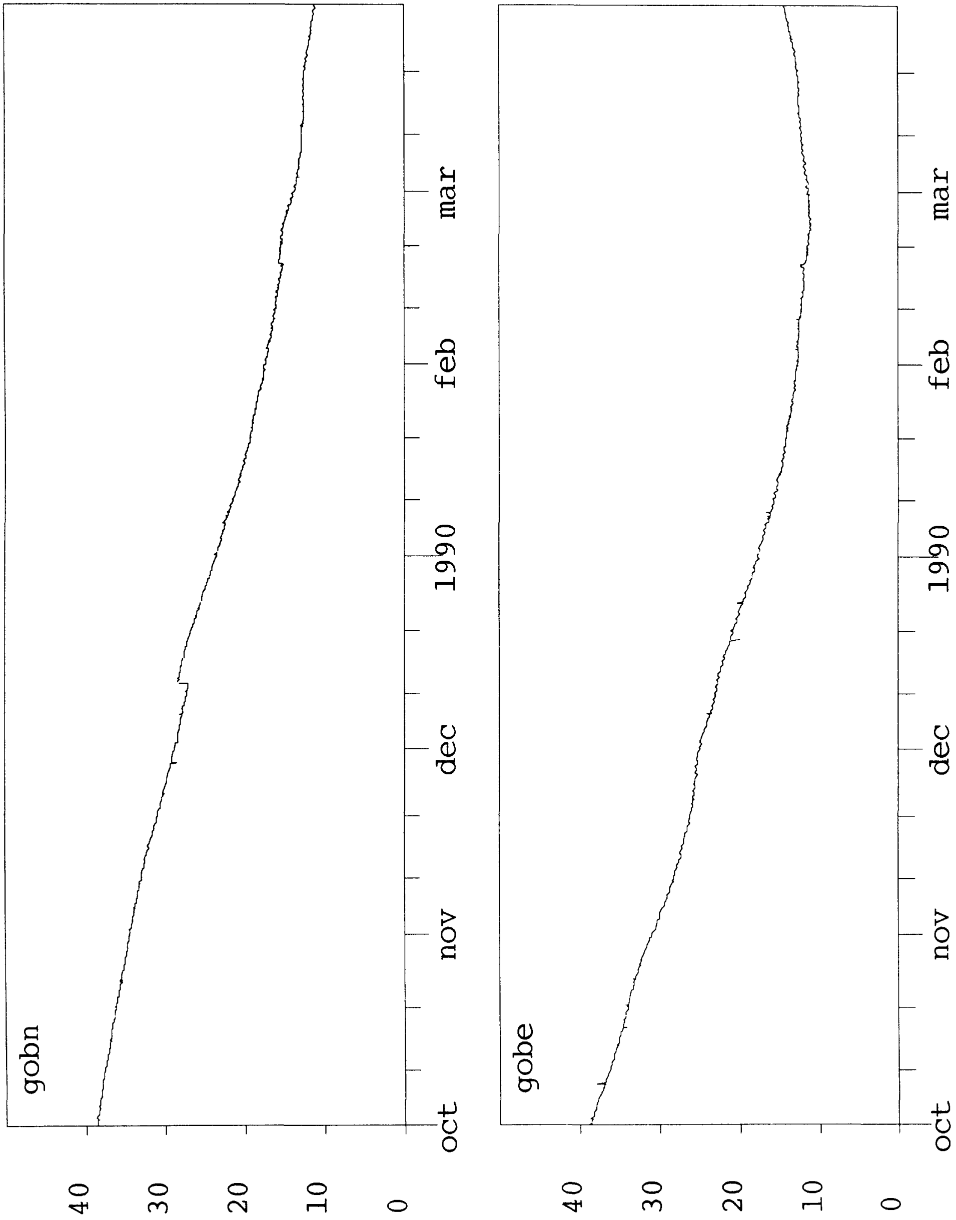

Figure 6a.

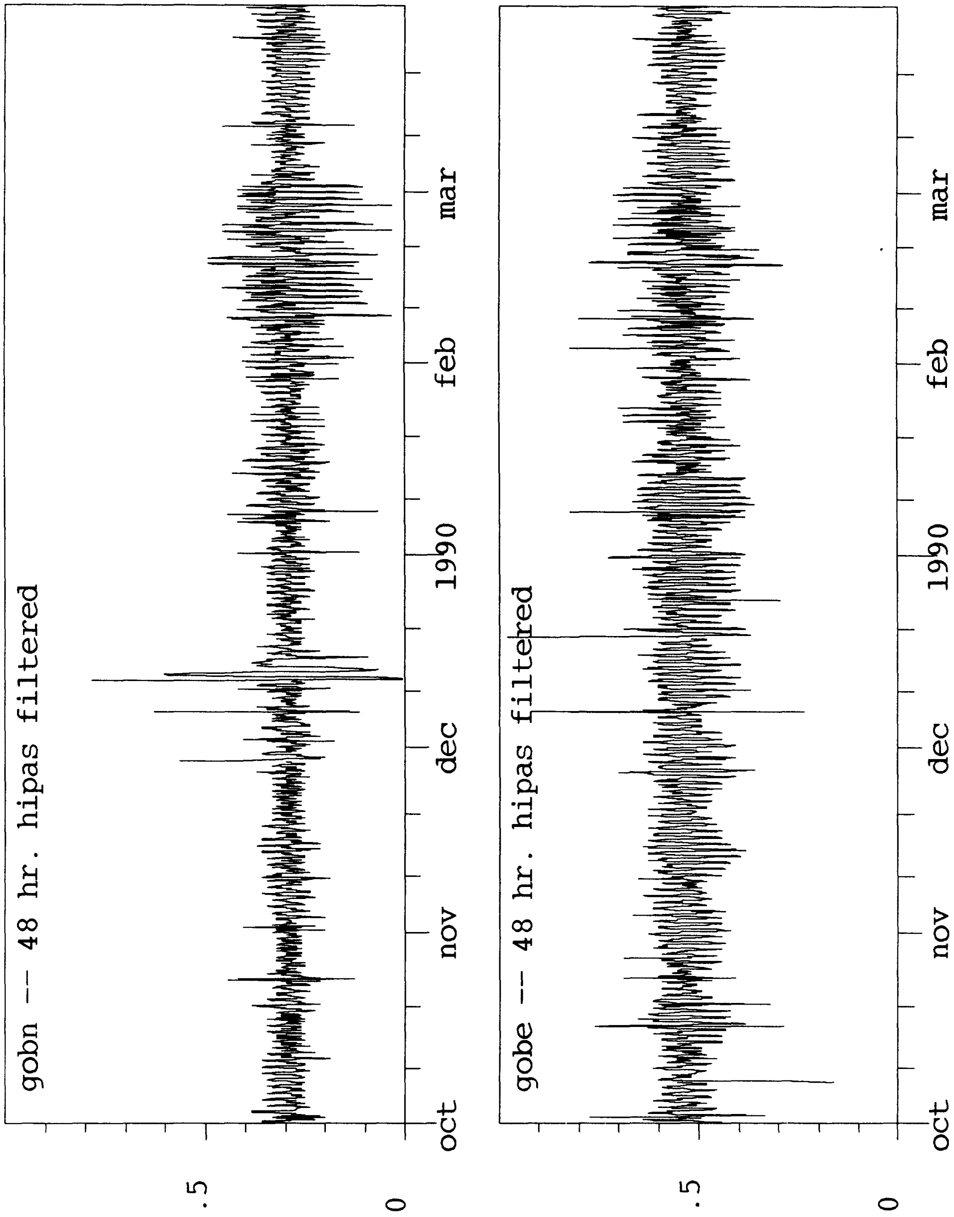
gobn -- 48 hr. hipas filtered
gobe -- 48 hr. hipas filtered
.5
0
.5
0
oct
nov
dec
1990
feb
mar
oct
nov
dec
1990
feb
mar

Figure 6b.

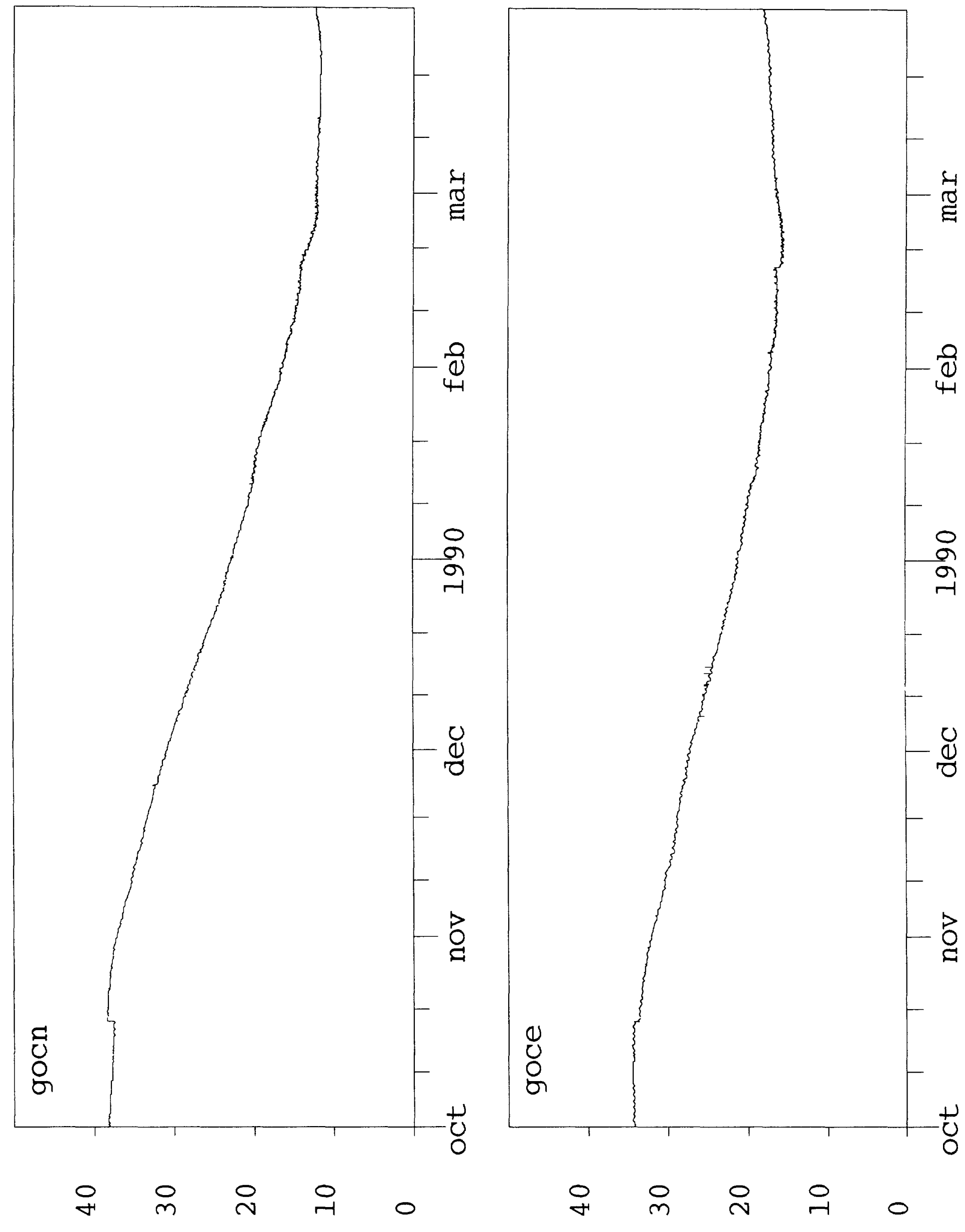
gocn
40
30
20
10
0
oct
nov
dec
1990
feb
mar
goce
40
30
20
10
0
oct
nov
dec
1990
feb
mar

Figure 7a.

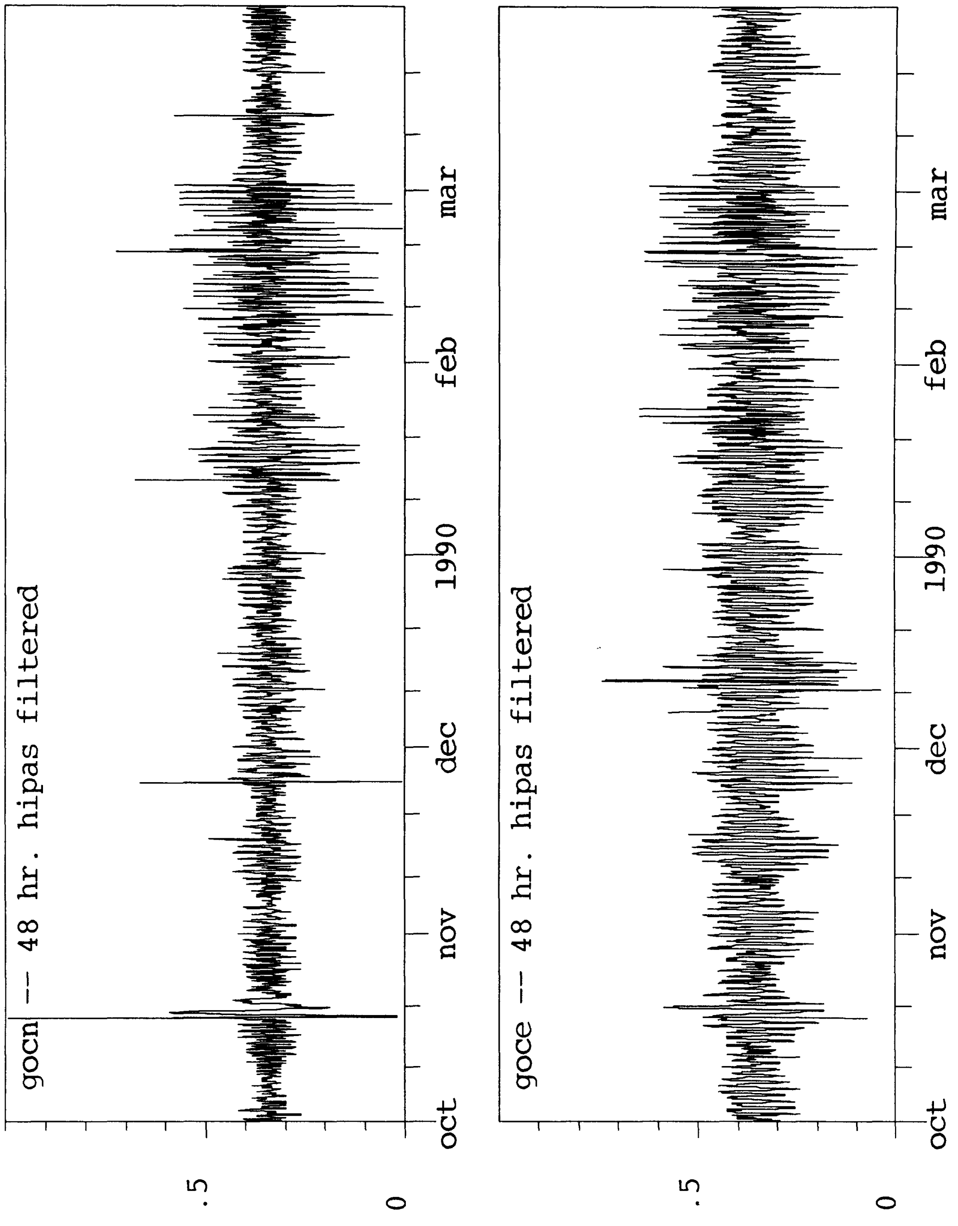
gocn -- 48 hr. hipas filtered
goce -- 48 hr. hipas filtered
oct
nov
dec
1990
feb
mar
.5
0

Figure 7b.

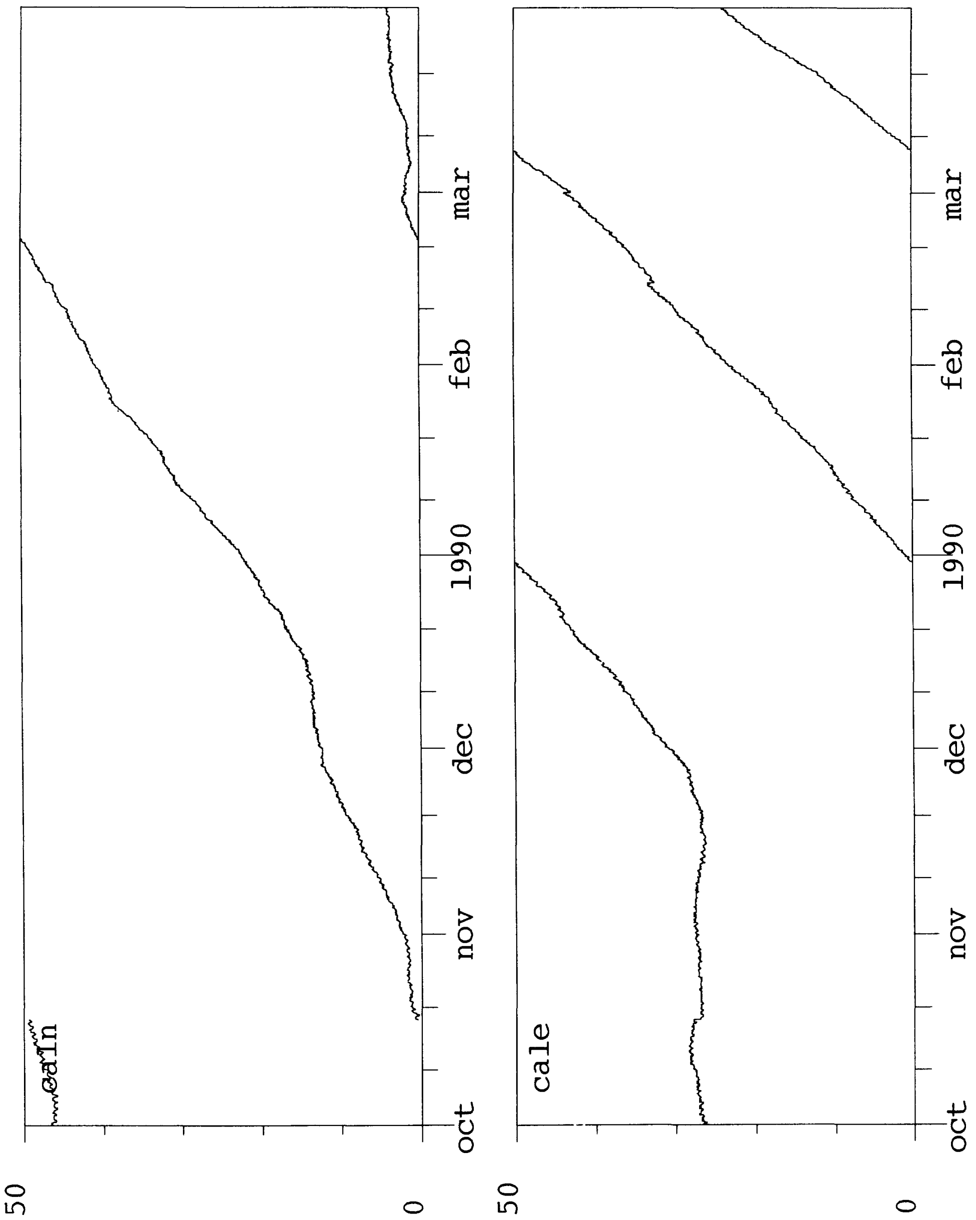
caln
cale
50
0
50
0
oct
nov
dec
1990
feb
mar
oct
nov
dec
1990
feb
mar

Figure 8a.

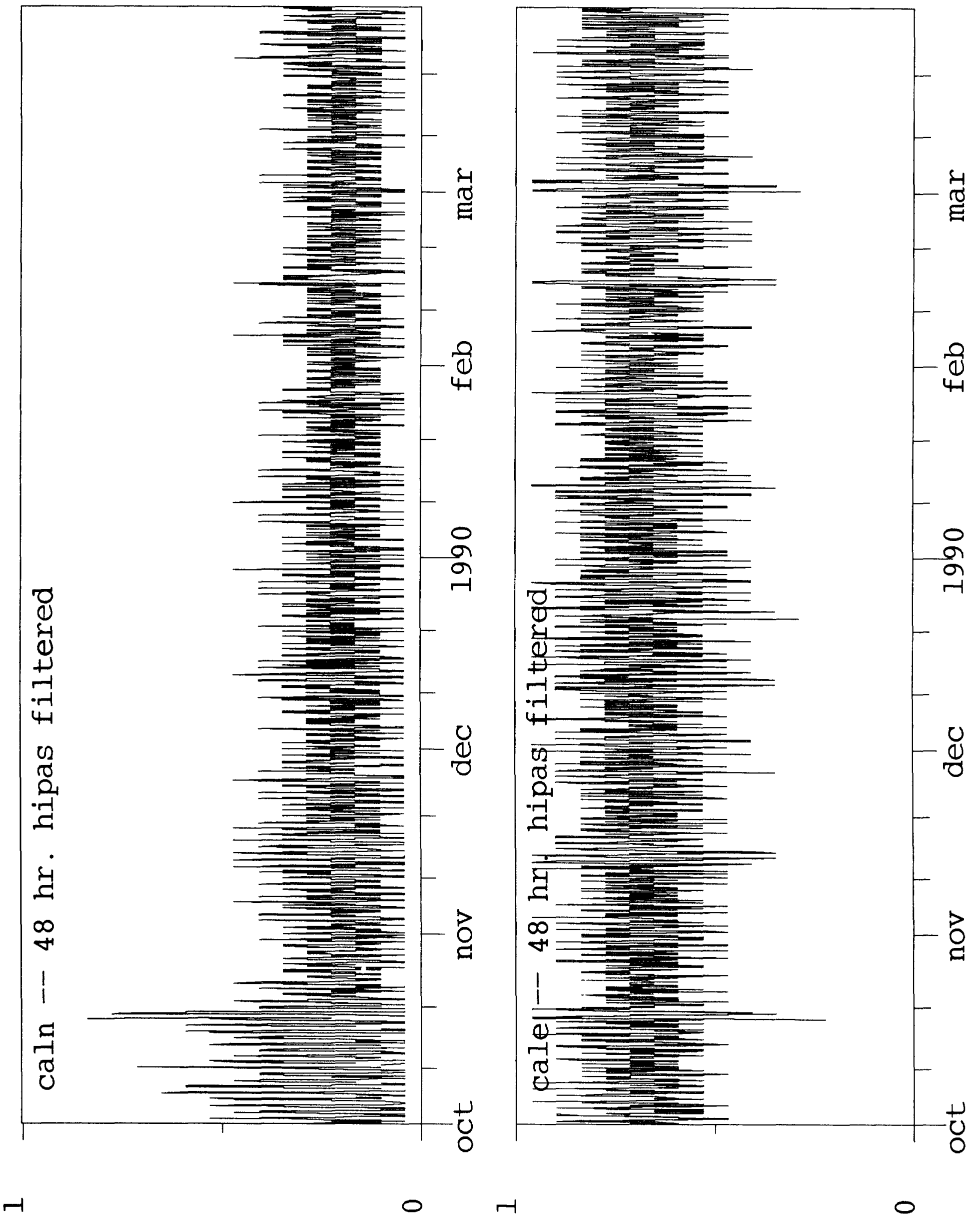
caln -- 48 hr. hipas filtered
cale -- 48 hr. hipas filtered
oct
nov
dec
1990
feb
mar
1
0
1
0

Figure 8b.

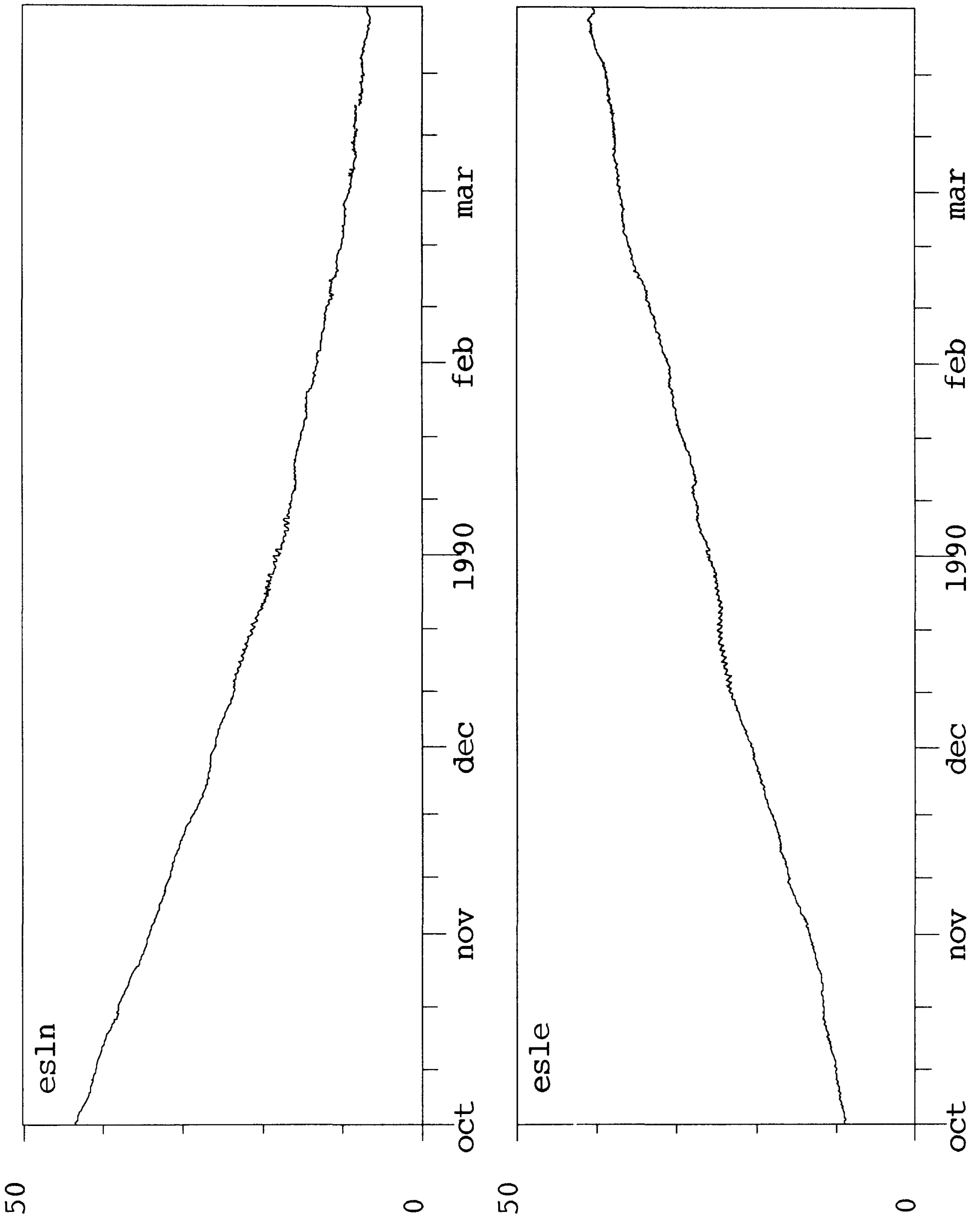
esln
esle
50
0
50
0
oct
nov
dec
1990
feb
mar
oct
nov
dec
1990
feb
mar

Figure 9a.

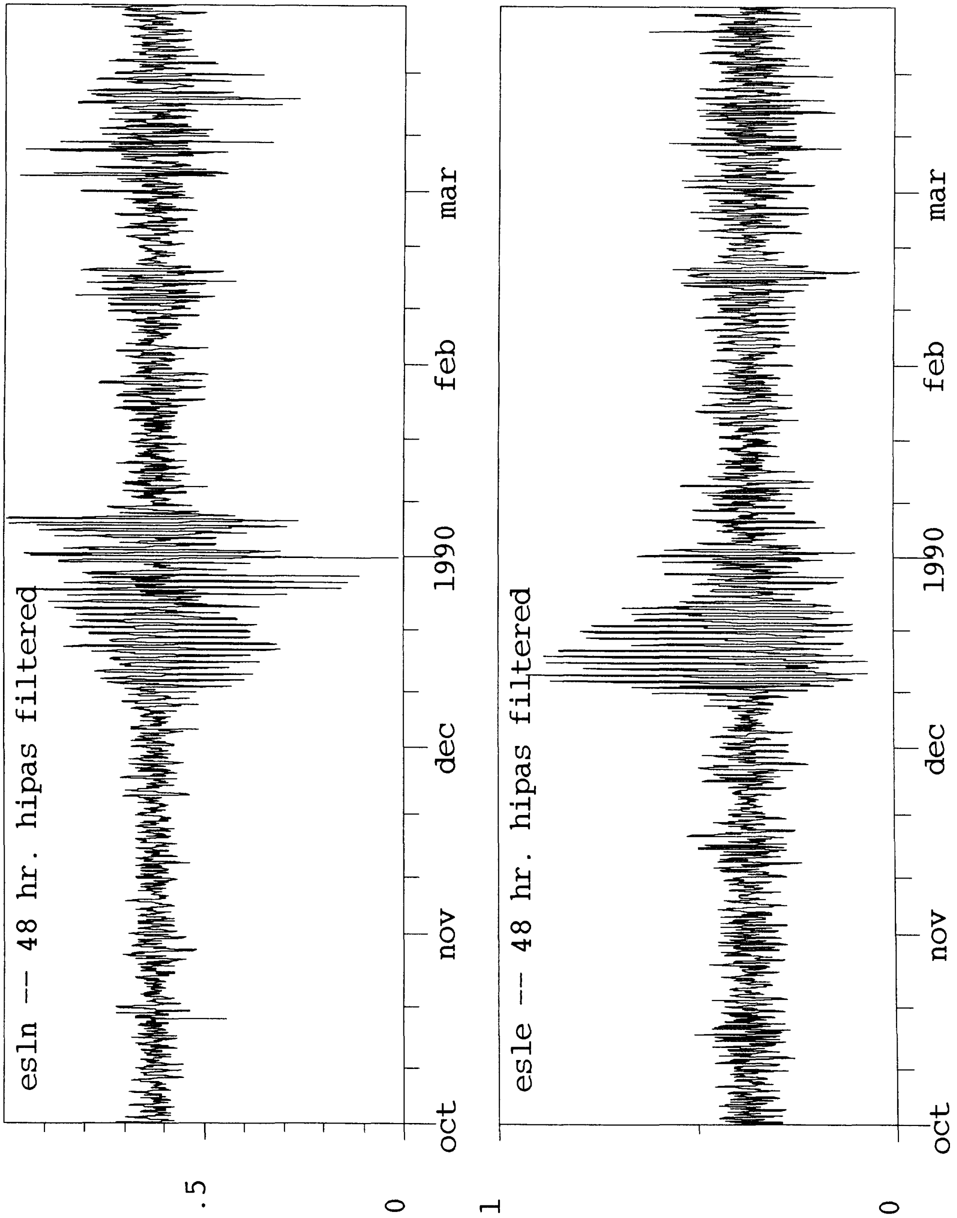
esln -- 48 hr. hipas filtered
esle -- 48 hr. hipas filtered
oct
nov
dec
1990
feb
mar
.5
0
1
0

Figure 9b.

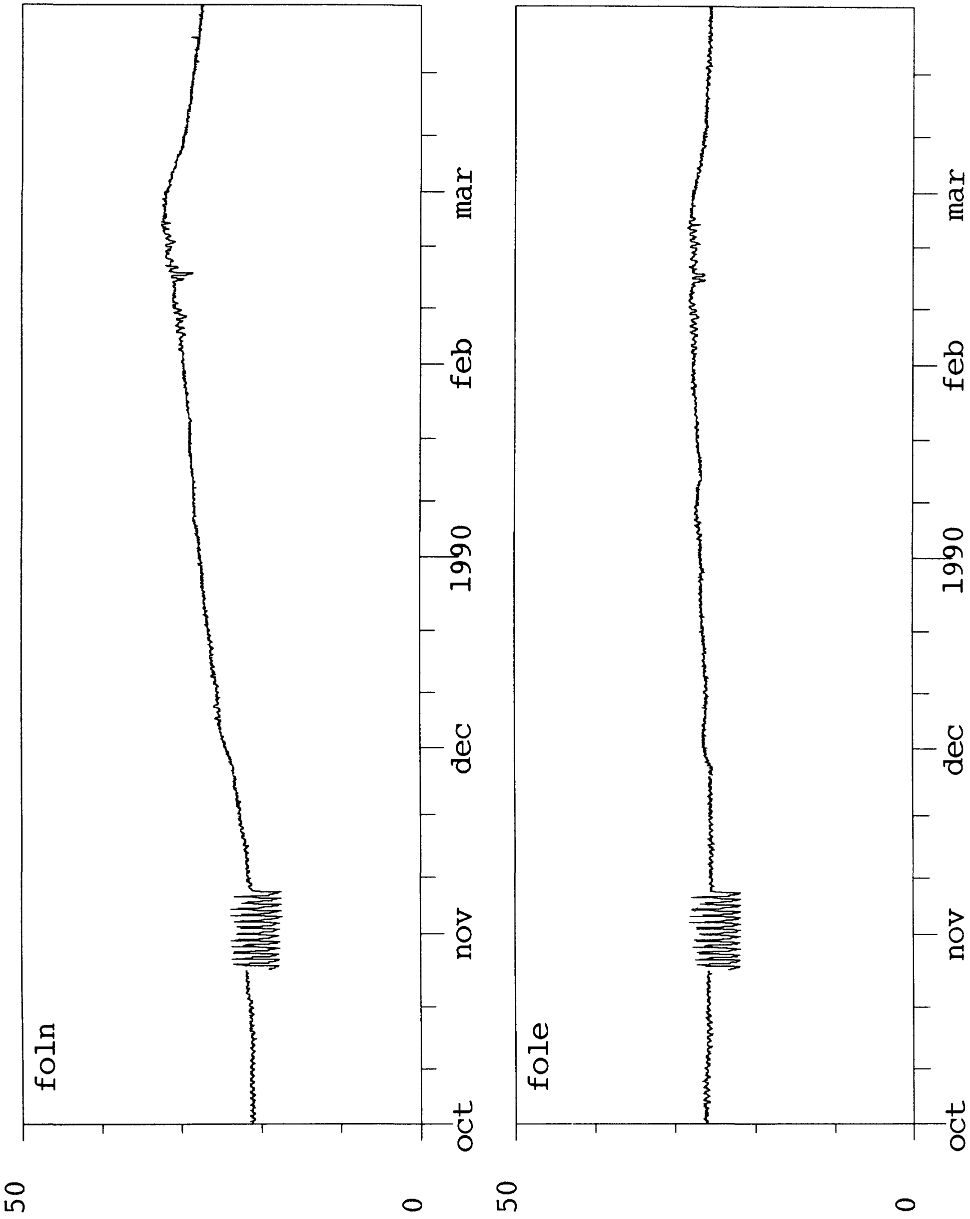
foln
fole
50
0
50
0
oct
nov
dec
1990
feb
mar
oct
nov
dec
1990
feb
mar

Figure 10a.

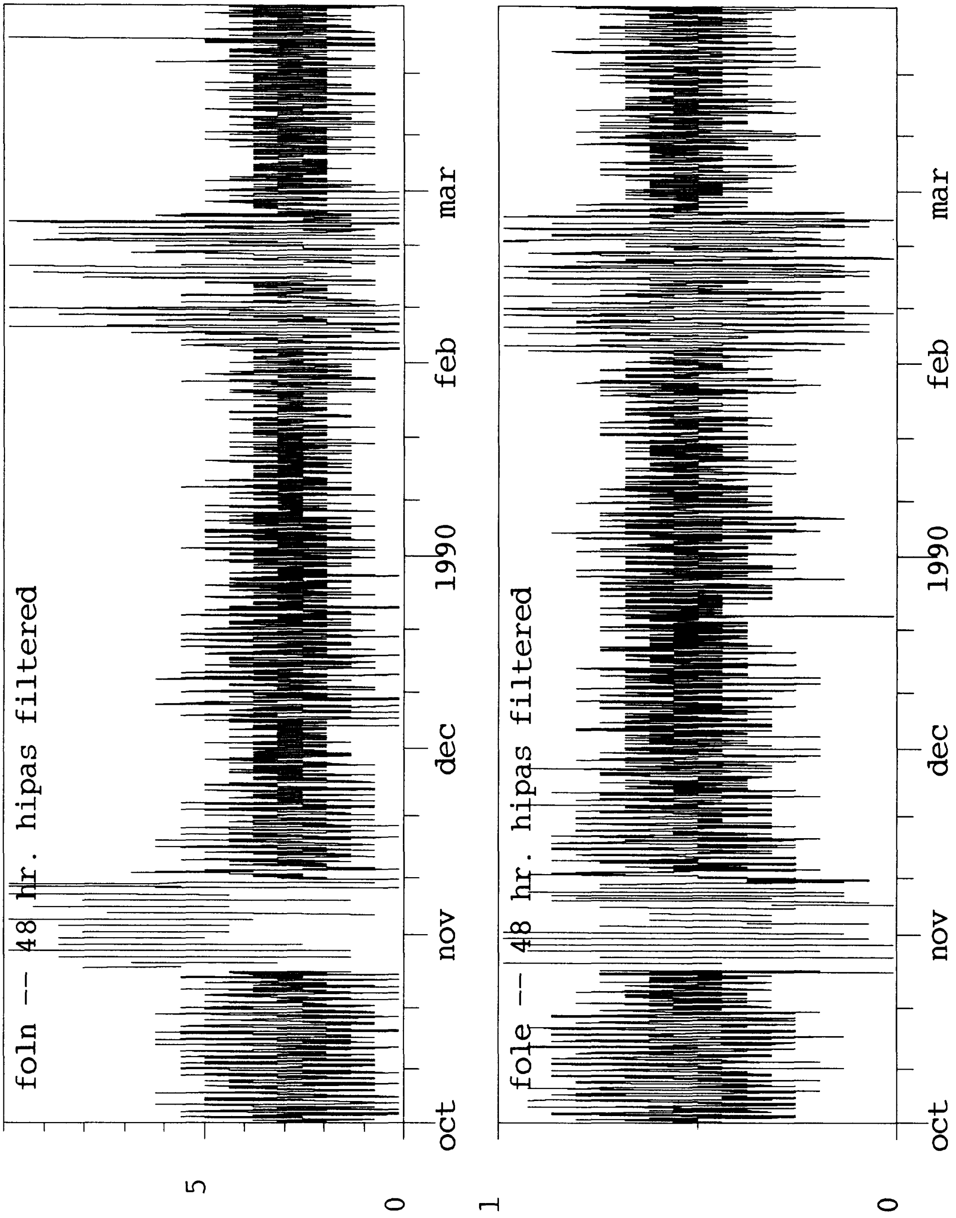
foln -- 48 hr. hipas filtered
fole -- 48 hr. hipas filtered
oct
nov
dec
1990
feb
mar
5
0
1
0

Figure 10b.

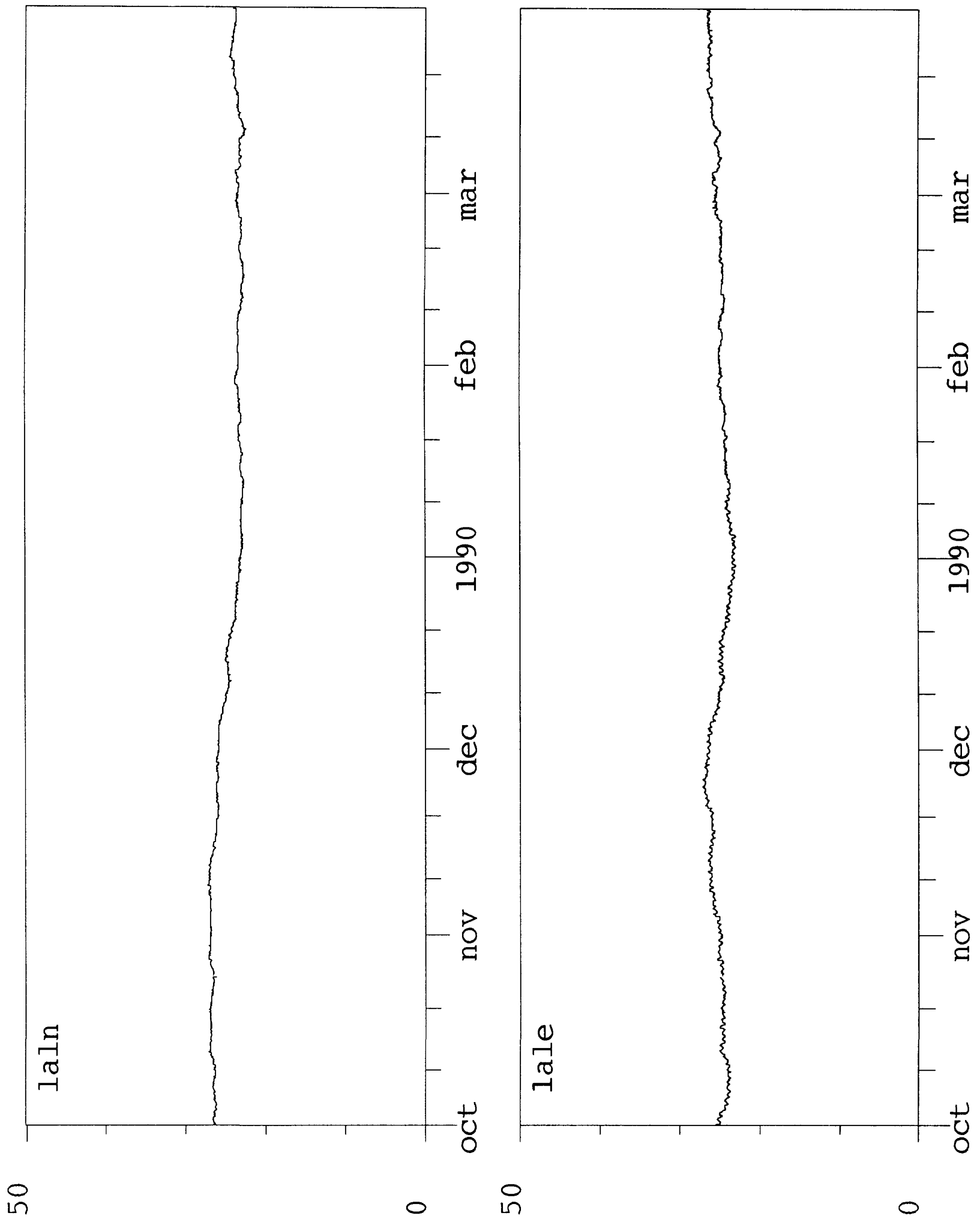

Figure 11a.

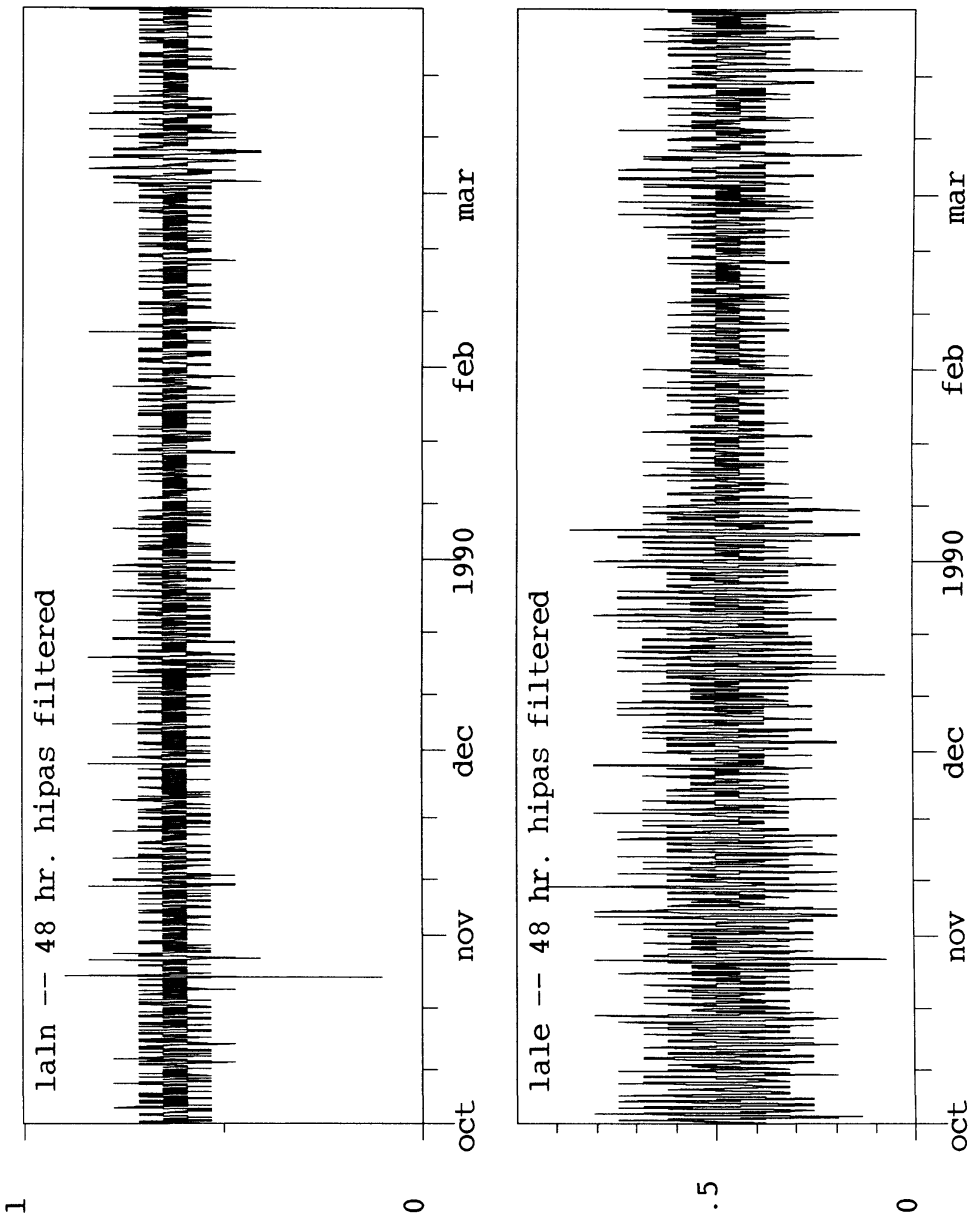
laln -- 48 hr. hipas filtered
lale -- 48 hr. hipas filtered
oct
nov
dec
1990
feb
mar
1
0
.5
0

Figure 11b.

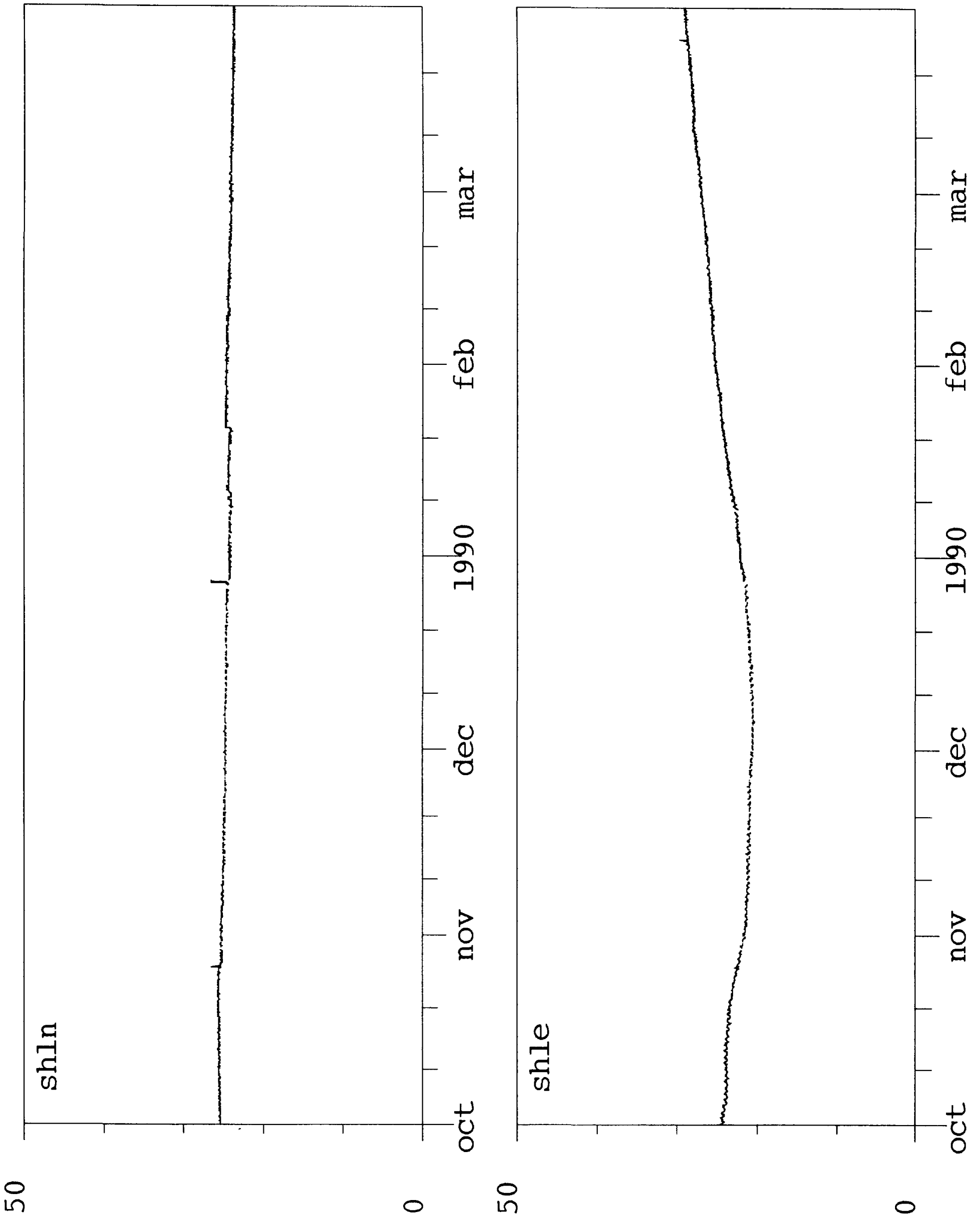

Figure 12a.

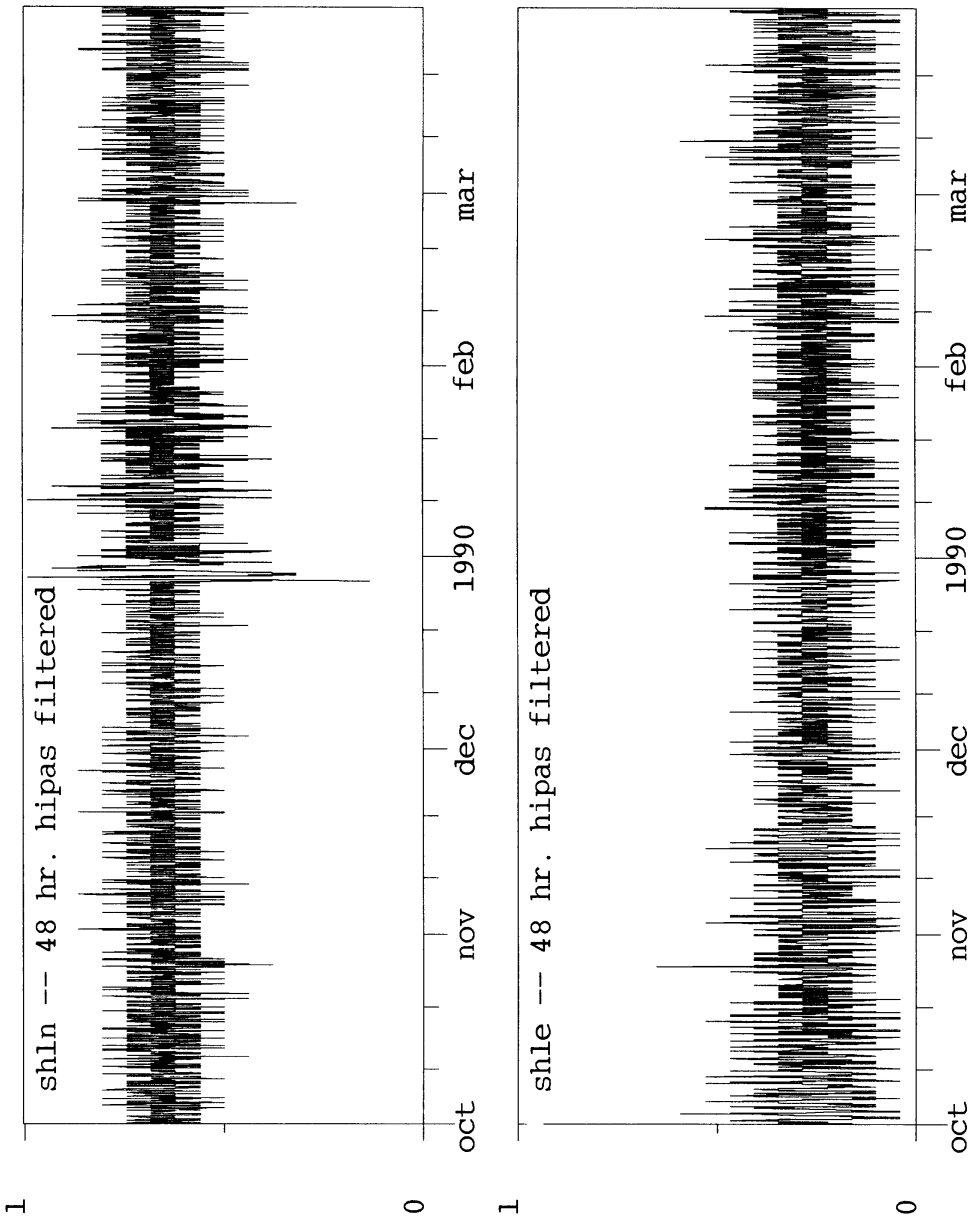
shln -- 48 hr. hipas filtered
shle -- 48 hr. hipas filtered
oct
nov
dec
1990
feb
mar
1
0
1
0

Figure 12b.

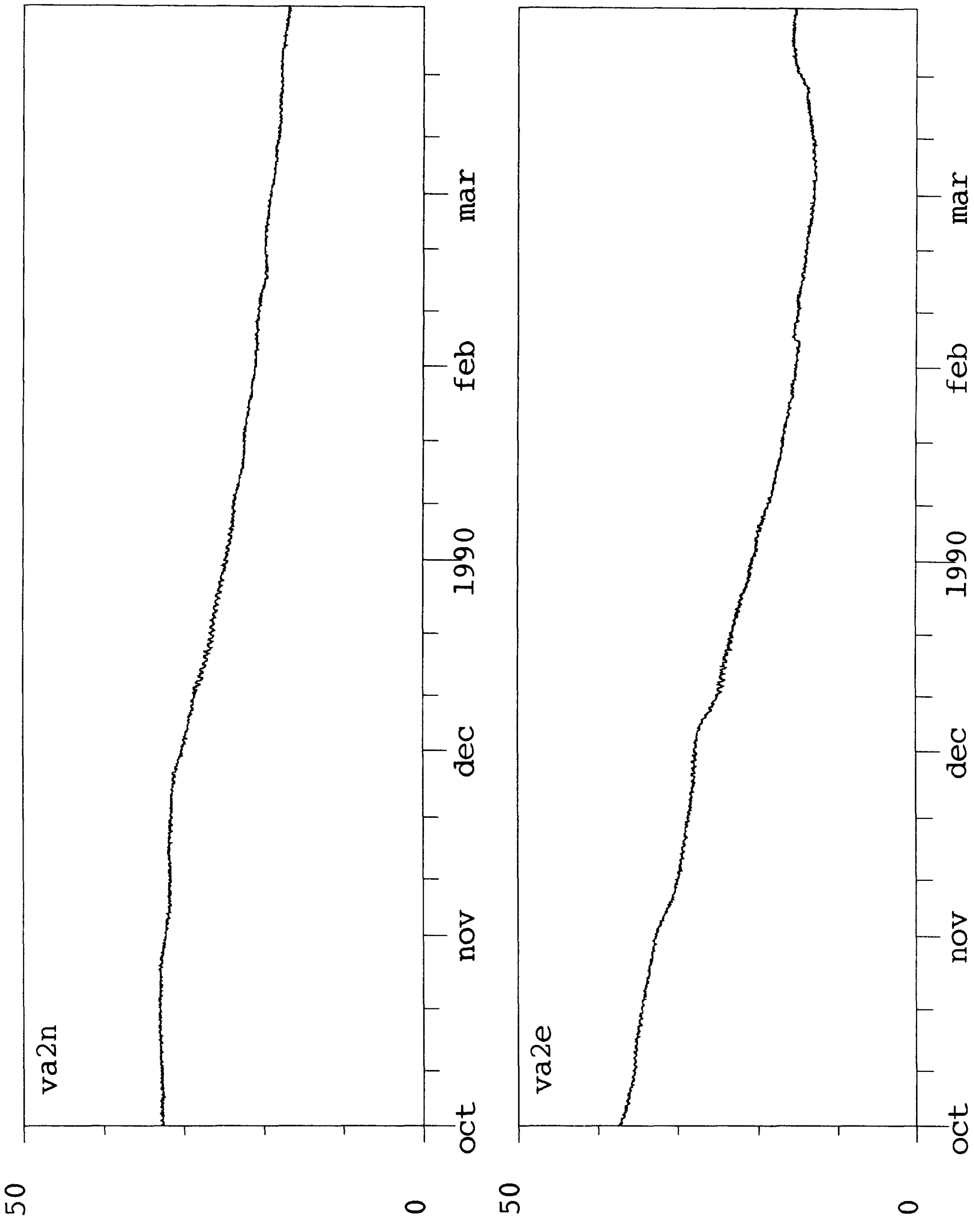

Figure 13a.

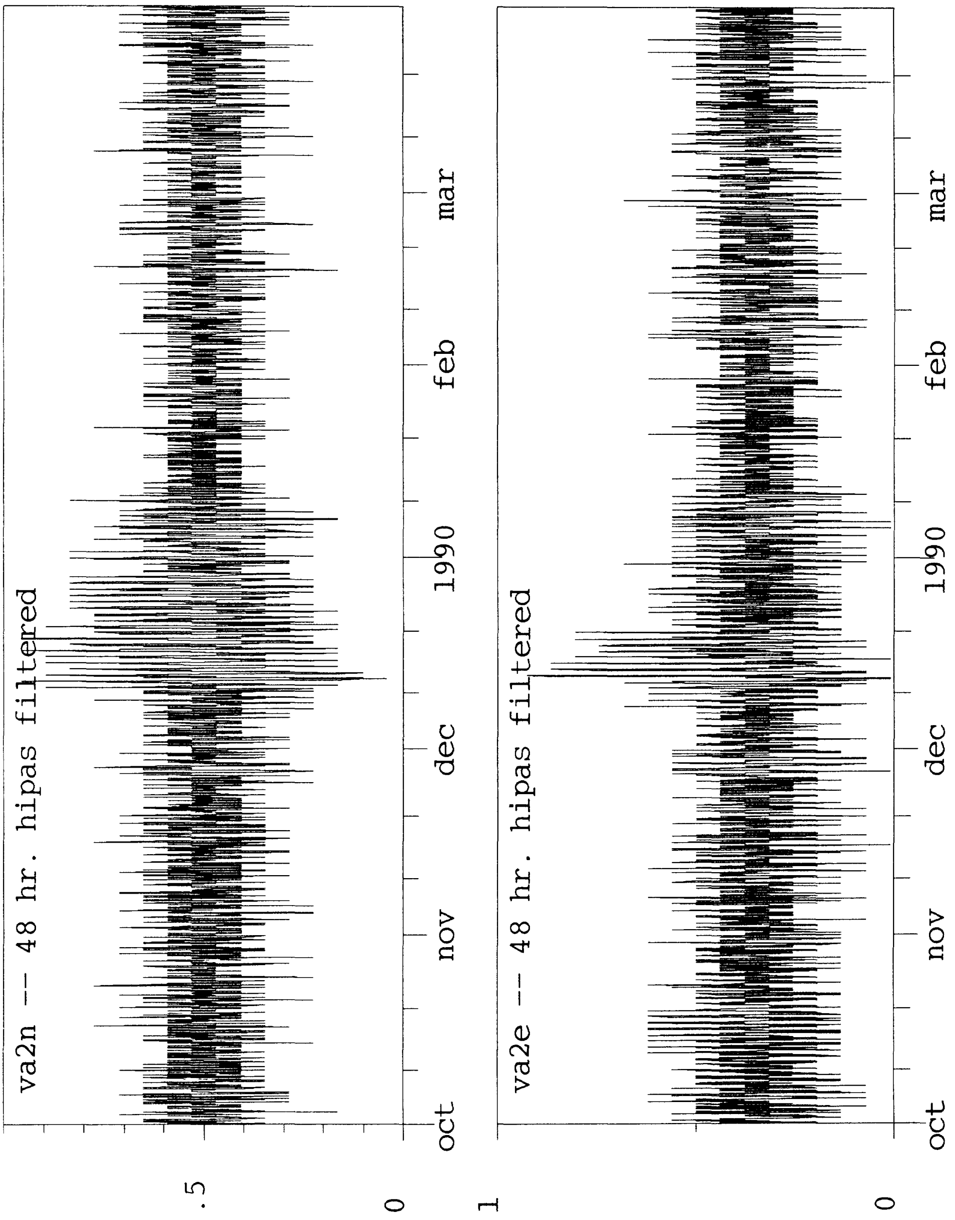
va2n -- 48 hr. hipas filtered
.5
0
1
oct
nov
dec
1990
feb
mar
va2e -- 48 hr. hipas filtered
0
oct
nov
dec
1990
feb
mar

Figure 13b.

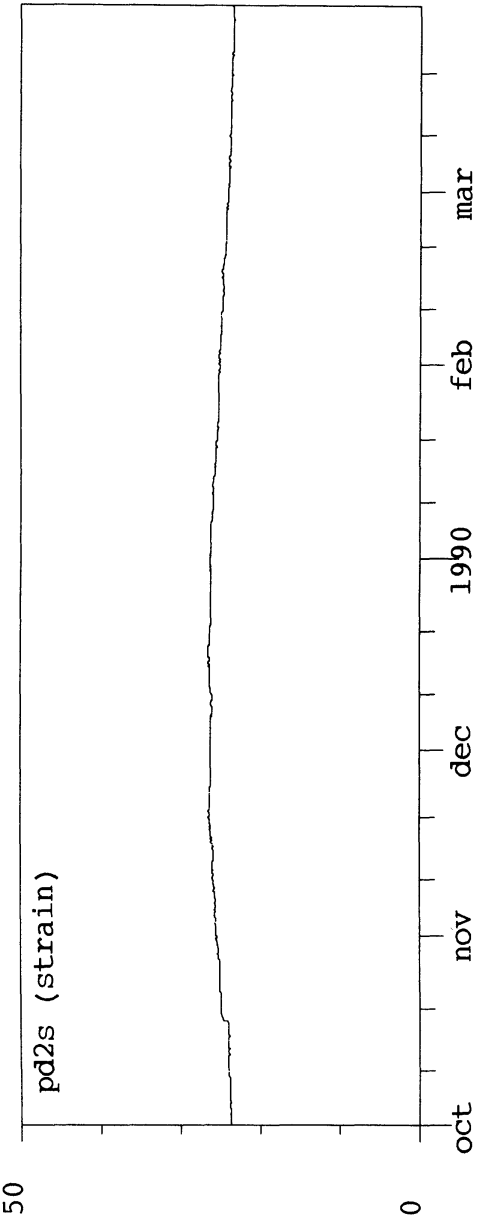

Figure 14a.

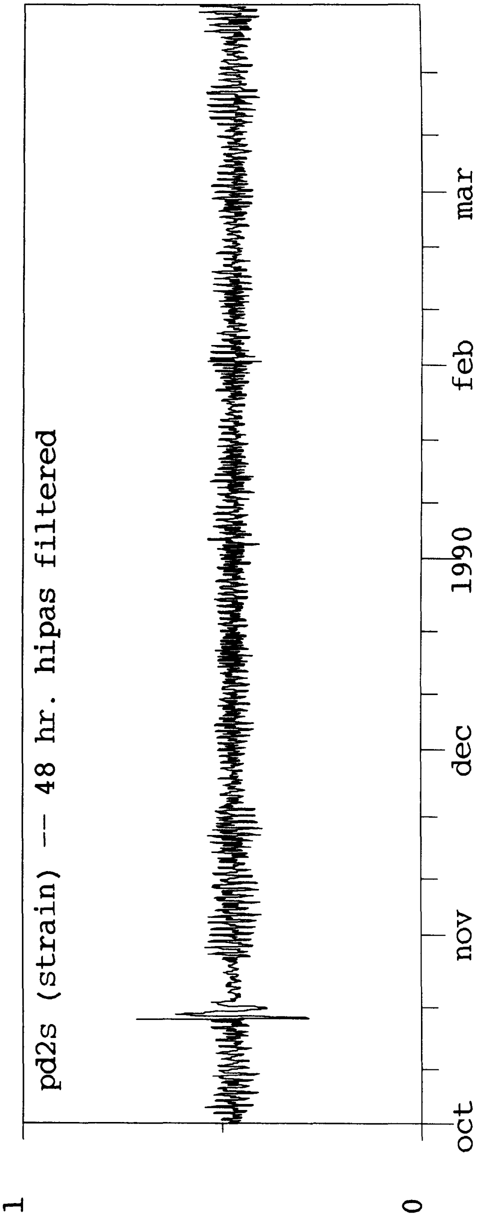

Figure 14b.

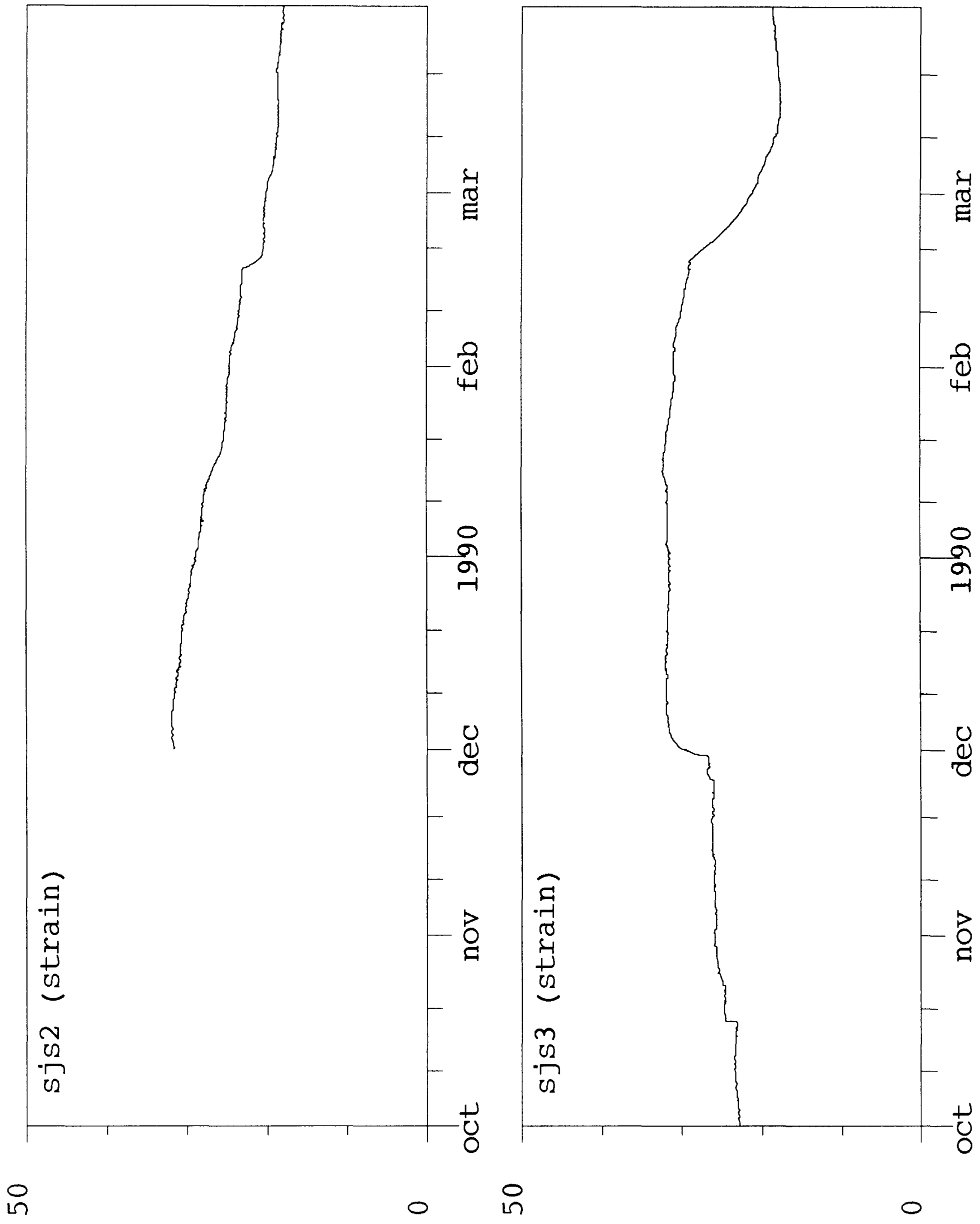

Figure 15a.

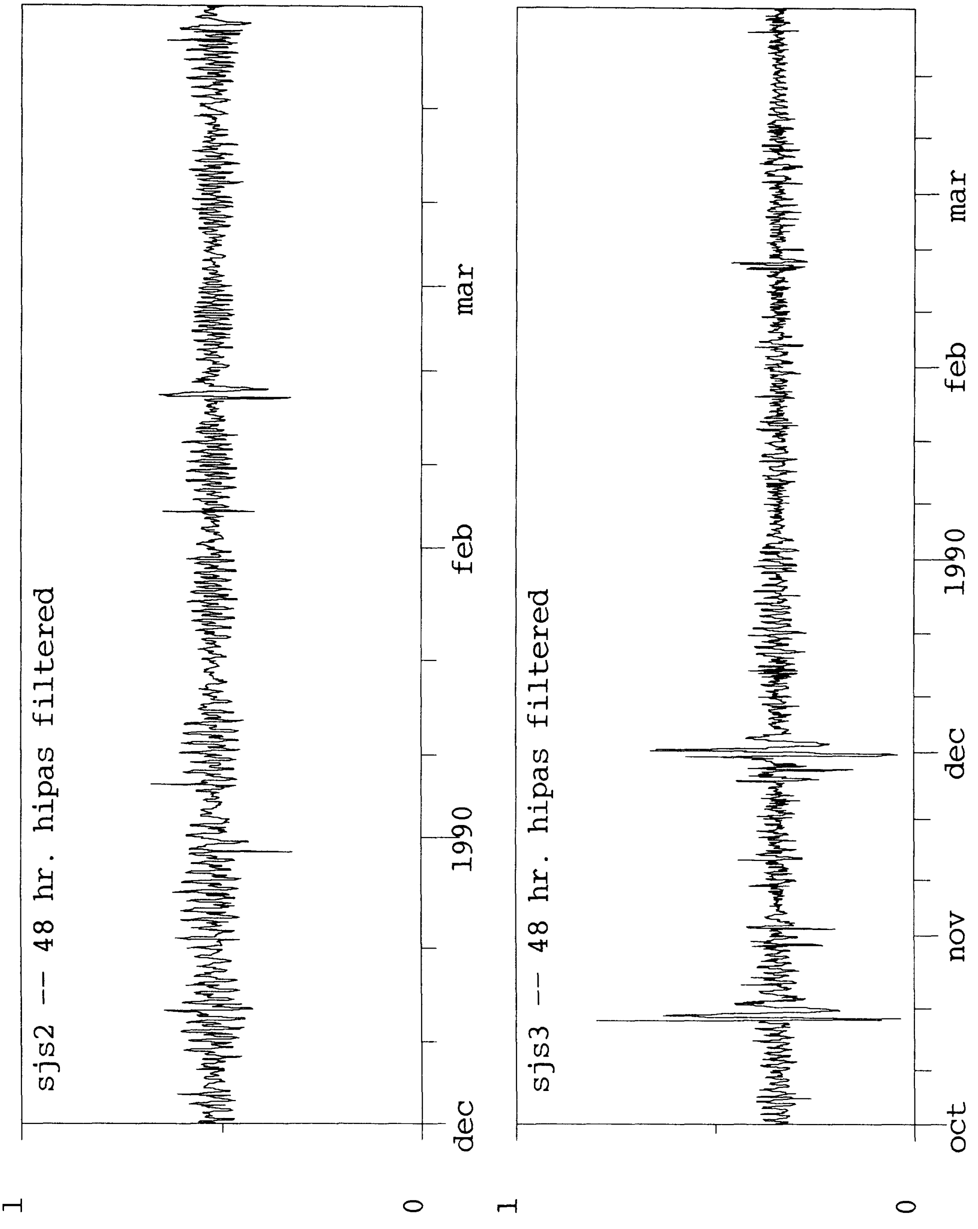
sjs2 -- 48 hr. hipas filtered
dec
1990
feb
mar
1
0
sjs3 -- 48 hr. hipas filtered
oct
nov
dec
1990
feb
mar
1
0

Figure 15b.

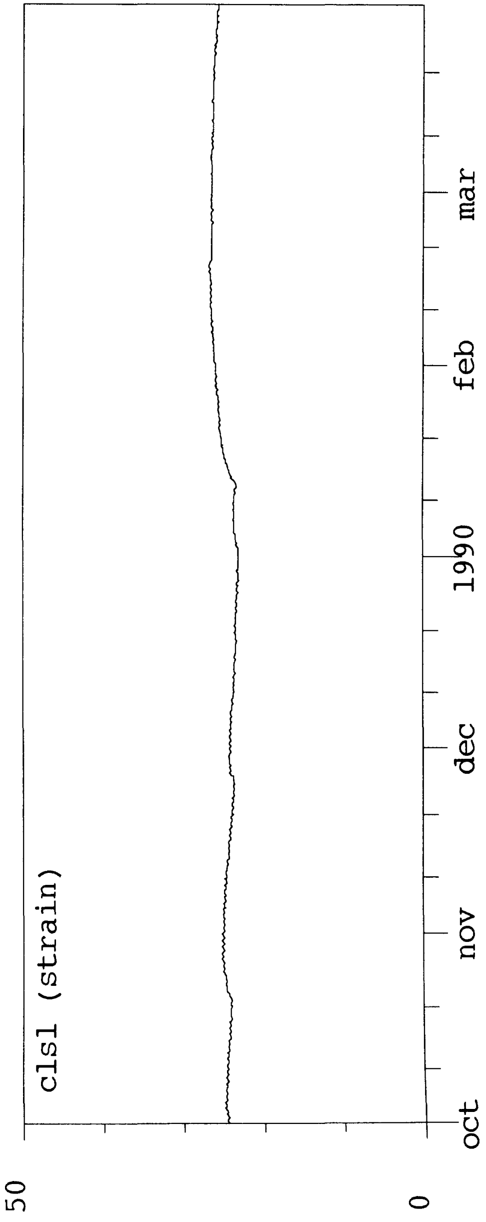

Figure 16a.

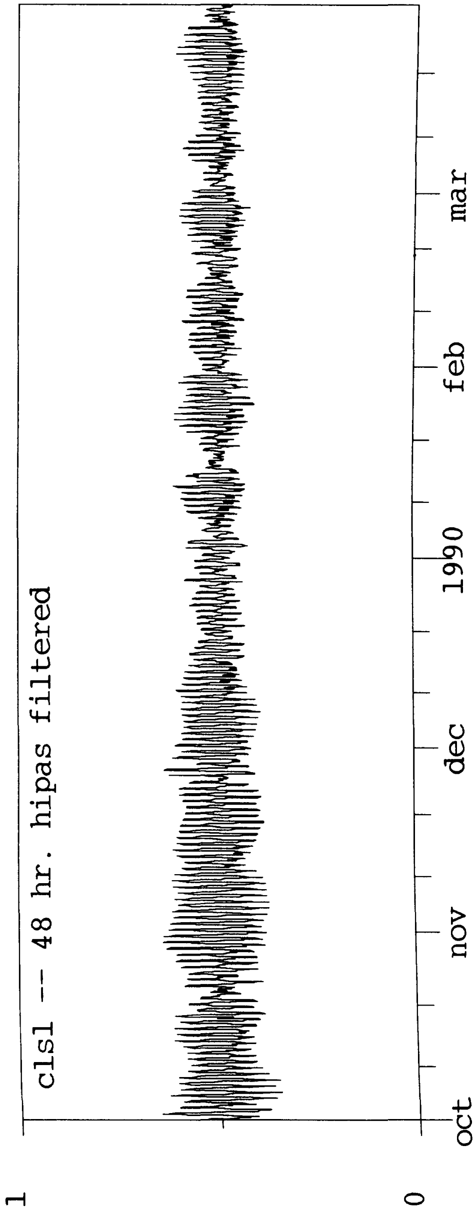

Figure 16b.

Analysis of Crustal Deformation Along the Southernmost Segment of the San Andreas Fault System, Imperial Valley, California: Implications for Earthquake Prediction

14-08-0001-G1679

R.E. Reilinger
Earth Resources Laboratory
Dept. of Earth, Atmospheric, and Planetary Sciences
Massachusetts Institute of Technology
Cambridge, Massachusetts 02142
(617) 253-7860

INVESTIGATIONS

This project involves using geodetic observations in conjunction with other geophysical and geological information to investigate contemporary tectonic processes along the southernmost segment of the San Andreas fault system. Our primary efforts during the present contract period include:

1. Planning and carrying out (February-March 1990) a Global Positioning System survey in the Salton Trough-Riverside County region (Figure 1).
2. Continuing analysis and interpretation of 1986, 1988 and 1989 GPS measurements in the Imperial Valley-Salton Trough with emphasis on regional strain accumulation and strain release associated with the 1987 Superstition Hills earthquakes (Larsen/Reilinger/Strange/Naugebauer).
3. Comparison of geodetic and geologic deformation in the Imperial Valley to investigate the age of the present style of deformation and the mechanics of the transition from rifting/ocean formation in the Gulf of California to strike-slip faulting along the San Andreas fault system (Larsen/Reilinger).

RESULTS

1. From February 18 through March 9, 1990 a high precision GPS network was established along an approximately 400 km segment of the Pacific-North American plate boundary from the Gulf of California in Northern Mexico to just south of the junction of the San Andreas and San Jacinto faults (~34°N). Participating institutions in the field campaign included: Caltech, CICESE, L-DGO, MIT, NGS, Riverside County, UNAVCO, U. of Mexico, U.T., Dallas, and U. of Nevada. A total of 103 primary stations were observed, most for 2 to 3 days. In addition half sessions (~3–4 hours) were observed at 31 sites near the San Andreas (Banning-Mission Creek segments), San Jacinto and Elsinor faults, and 5 sites were observed in a kinematic survey within a pre-existing EDM network straddling the Imperial fault in Northern Mexico (2 of these kinematic sites were also observed statically). Dense coverage (~5–10 km site

spacing) was also established along the southernmost San Andreas and Imperial faults in S. California. Coverage extends to 150 km from the active fault systems.

A total of 23 dual frequency GPS receivers were fielded, with continuous GPS observations at 3 VLBI stations located within the network (Pinyon Flat, Black Butte, Ocotillo). Observations at Pinyon Flat were made with a remotely operated Trimble 4000ST receiver (courtesy of Yehuda Bock and Duncan Agnew, UCSD). Many of the sites observed in the Coachella Valley and Riverside County have a history of GPS observations dating from 1988, and all sites in the Imperial Valley date back to 1986. Overlap was established with 1989 GEOMEX GPS sites, and new GPS sites were established along the Imperial-Cerro Prieto faults in Northern Mexico.

2. Shawn Larsen has completed initial reduction of the 1988 and 1989 static GPS observations made with TI-4100 receivers using the Bernese 3 software at Caltech (reduction of 1989 Trimble data has been hampered by severe ionospheric disturbances during the campaign). Preliminary strain maps (Figures 2 and 3) show large deformations associated with the 1987 Superstition Hills earthquakes and right-lateral strain accumulation. Reduction, analysis and interpretation of these data and the new 1990 observations is continuing.

3. Releveling and other geophysical data for the Imperial Valley of Southern California suggest the northern section of the Imperial- Brawley fault system, which includes the Mesquite Basin and Brawley Seismic Zone, is much younger than the 4 to 5 million year age of the valley itself. A minimum age of 3000 years is calculated for the northern segment of the Imperial fault from correlations between surface topography and geodetically observed seismic/interseismic vertical movements. Calculation of a maximum age of 80,000 years is based upon displacements in the crystalline basement along the Imperial fault, inferred from seismic refraction surveys. This young age supports recent interpretations of heat flow measurements, which also suggest that the current patterns of seismicity and faults in the Imperial Valley are not long lived. The current fault geometry and basement morphology suggest northwestward growth of the Imperial fault and migration of the Brawley Seismic Zone. We suggest this migration is a manifestation of the propagation of the Gulf of California rift system into the North American continent.

PUBLICATIONS

Reilinger, R.E., J. Beavan, L. Gilbert, S. Larsen, K. Hudnut, C. Aiken, D. Ziegler, W. Strange, M. de la Fuente, J. Gonzalez, J. Stowell, W. Young, G. Doyle, G. Stayner, 1990 Salton Trough-Riverside County GPS Network, *EOS, Trans. Am. Geophys. Union,* in press, 1990.

de la Fuente, M., J.J. Gonzalez, D. Ziegler, C. Aiken, The Northern Baja California GPS Campaign: First Epoch, *EOS, Trans. Am. Geophys. Union,* in press, 1990.

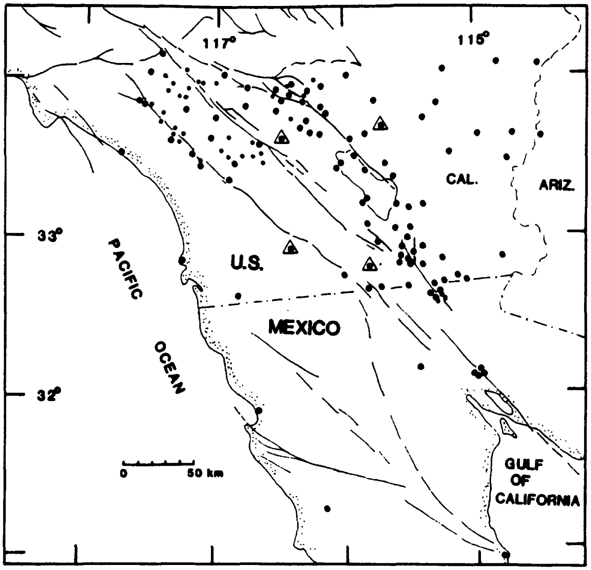

Figure 1. GPS stations observed during the 1990 Salton Trough-Riverside County campaign. Large dots show primary stations, small dots half-session and kinematic sites.

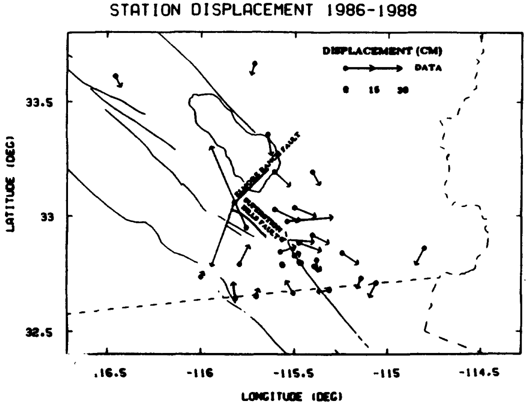

Figure 2. Observed station displacements derived from GPS surveys in 1986 and 1988. Large movements southwest of Salton Sea due to 1987 Superstition Hills earthquake.

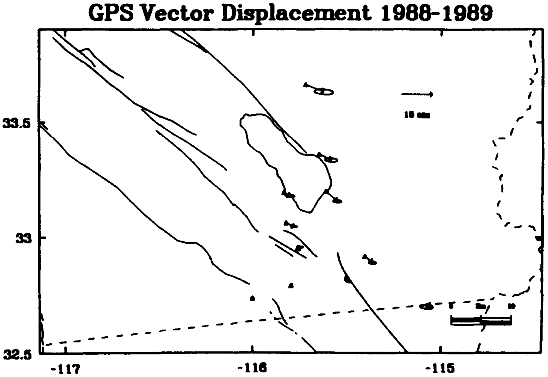

Figure 3. Observed station displacements derived from GPS surveys in 1988 and 1989 showing right-lateral strain accummulation.

Implacement of Alignment Arrays Across the Elsinore and San Jacinto fault zones in southern California

14-08-0001-G1771

Thomas Rockwell
Dept. of Geological Sciences
San Diego State University
San Diego, CA 92182
(619) 594-4441

Objective: To emplace alignment arrays across strands of the southern San Jacinto and Elsinore fault zones and associated NE-trending cross faults for the purposes of: 1) measurement of creep or triggered slip, should it occur; and 2) measurement of coseismic fault slip should rupture occur on one of the fault segments under study.

Results: To date, nine lines have been built. Along the San Jacinto fault zone, three are across the southern Clark fault in Clark Valley, one is across the Superstition Mountain fault, and one is across the Dixieland fault (in the same vicinity as the Caltech array). Along the Elsinore zone, two lines have been emplaced across the southern Elsinore fault, and one each across the Laguna Salada and Yuha Wells faults.

MECHANICS OF FAULTING AND FRACTURING

9960-02112

Paul Segall
Branch of Tectonophysics
U.S. Geological Survey
345 Middlefield Road, MS/977
Menlo Park, California 94025
(415) 329-4861

Investigations

1. Geodetic Displacements in the San Francisco Bay Area Due to the 1906 Earthquake.

2. Comparison of the 1934 and 1966 Parkfield Earthquakes (with Wayne Thatcher and Yijun Du, Purdue University).

3. Analysis of deformation and slip on the San Andreas Fault near Parkfield, California (with Mark V. Matthews).

Results

1. The October 1989 Loma Prieta Earthquake has focused attention on deformation in the San Francisco Bay region. We have recomputed the surface displacements due to the 1868 and 1906 earthquakes as determined by repeated triangulation measurements. This calculation was (to our knowledge) last done by Hayford and Baldwin in 1910, and used by H. F. Reid in his classic report on the 1906 earthquake. There are two limitations to Hayford and Baldwin's solution. First, in order to overcome the non-uniqueness inherent in these calculations, they arbitrarily held stations Diablo, Mocho, and Santa Ana fixed. Secondly, they did not compute uncertainties in the the displacement vectors. We overcome the non-uniqueness using the "model-coordinate" solution of Segall and Matthews (1989, J.G.R.) and fix the null space component of the solution (rigid body motions and uniform dilatation) using a simple dislocation model of the 1906 earthquake. Note in Figure 1 that the data include angle changes between the 1850's and 1906 and the 1880's and 1906, the error ellipses are 95% confidence intervals, and the data has been assumed to be independent.

2. Bakun and McEvilly (Science, 1979; J.G.R., 1984) showed that waveforms of the 1922, 1934 and 1966 earthquakes are remarkably similar, particularly at teleseismic distances. This observation requires that the three earthquakes have comparable moment, source mechanism, and location. This result, in combination with intensity data indicating similar sized events in 1857, 1881, and 1901, led to the now famous forecast of a "characteristic" Parkfield earthquake in 1988, with some uncertainty.

Given that the last three Parkfield mainshocks have inter-event times of 12 and 32 years, the question remains: Just how similar were these earthquakes? We report here on the slip distributions for the 1934 and 1966 earthquakes determined from the inversion of geodetic measurements. Previously, Segall and Harris (J.G.R., 1989) inverted changes in the lengths of 15 geodimeter lines measured before and after the 1966 earthquake. To this data set we add triangulation data from an arc that crosses the San Andreas Fault near the southeastern end of the 1966 rupture. This network was surveyed in 1932, 1951, 1962, and 1966 (post-earthquake).

As noted by Savage and Burford (B.S.S.A, 1970), the 1966-62 angle changes show relaxation of the fault-parallel shear strain, demonstrating that the 1966 rupture passed as far southeast as the triangulation arc. Simultaneous inversion of the geodimeter and triangulation data confirms that the 1966 earthquake slipped the San Andreas Fault about 10 km southeast of the prominent right-step in the fault trace. The magnitude of the slip at seismogenic depths southeast of the step was comparable to that northwest of the step.

In contrast, the 1951-32 angle changes show an increase in fault-parallel shear strain. If the 1951-32 changes are dominated by the 1934 earthquake, it must have stopped northwest of the triangulation arc (Savage and Burford, 1970). We use the Harris and Segall (J.G.R., 1987) model of inter-seismic slip to subtract out the effects of inter-seismic deformation between 1932 and 1951. With this model, or indeed any reasonable model that locks the Parkfield segment between earthquakes, we conclude that the shear strain due to the 1934 earthqauke increased at the latitude of the triangulation net.

Inversions of the 1934 coseismic slip distributions, were done employing the best-fitting 1966 slip pattern as an *a priori* model and positivity constraints. Even trying to force the 1934 earthquake to look like the 1966 earthquake we see that the maximum slip is considerably farther northwest in 1934 than it was in 1966. It is possible that there was deep slip southeast of the step in 1934. The data seem to prohibit shallow slip there. We conclude that the 1934 and 1966 earthquakes could not have been the same, unless the 19 years of interseismic deformation between 1932 and 1951 were *very* different from the 18 years of interseismic deformation between 1966 and 1984. Either way the earthquake cycles were different.

3. Crustal deformation around active faults is commonly measured by various techniques. From both historic and current surface deformation data, we would like to know as much as we can about fault behavior at depth. Elastic dislocation models sometimes furnish a useful relationship between observable surface deformation and slip at depth, but the problem of inverting dislocation models to estimate slip is generally ill-posed. There are usually many hypothetical slip distributions that satisfactorily fit available data. In order to address the problem of nonuniqueness, we have proposed finding slip distributions that fit the available data and minimize a measure of elastic strain energy.

Let $\mathbf{s}$ be an unknown slip distribution on a fault surface, Σ, and let $\tau_i(\xi; \mathbf{s})$, $\xi \in \Sigma$, be the components of traction on the fault surface due to $\mathbf{s}$. The τ_i are the *self-tractions* of $\mathbf{s}$, and the *self-energy* is given by

$$E_{\mathrm{self}}(\mathbf{s}) = \frac{1}{2} \int_\Sigma s_i(\xi)\tau_i(\xi; \mathbf{s}) d\Sigma(\xi).$$

Self-energy is a good candidate for minimization because it depends only on slip, not on an unknowable absolute stress state, and because under certain assumptions the self-energy of coseismic slip equals the energy available for seismic radiation. We are able to show that when a deformation measurement is related to slip by

$$d = \int s_i(\xi) w_i(\xi) d\Sigma$$

we can *minimize self-energy by finding the slip distribution with traction on the slipping part of the fault matching the weight function multiplying slip to produce the measured datum.* We call this the *traction-matching condition* (TMC). It says, for instance, that we get least self-energy for a given *moment* from a slip distribution with constant stress change in the slipping region.

We have been experimenting with energy-minimizing slip inversions in certain antiplane slip models that are of interest because of their computational tractability and because of their use in describing deformation around long strike-slip faults such as the San Andreas. We have simulated the process of observing deformation at the free surface of a half-space and inverting for slip, and we are now working on applying our techniques to real data. The first application will be to estimate coseismic slip at the northern end of the the 1906 rupture by inverting triangulation measurements made near Point Arena. Subsequently, we will construct a time-varying estimate of interseimic slip for the segment of the San Andreas near Parkfield. The first step in constructing this estimate involves using the TMC to determine the energy minimizing slip distribution corresponding to the slip functional measured by each station in the instrumental network. These energy-minimizing distributions are taken to be basis functions with time-varying coefficients, and the coefficients are estimated using recursive linear filters which also try to remove noise due to measurement errors and benchmark motion.

Figure 1. 1906 Displacements in the San Francisco Bay Region.

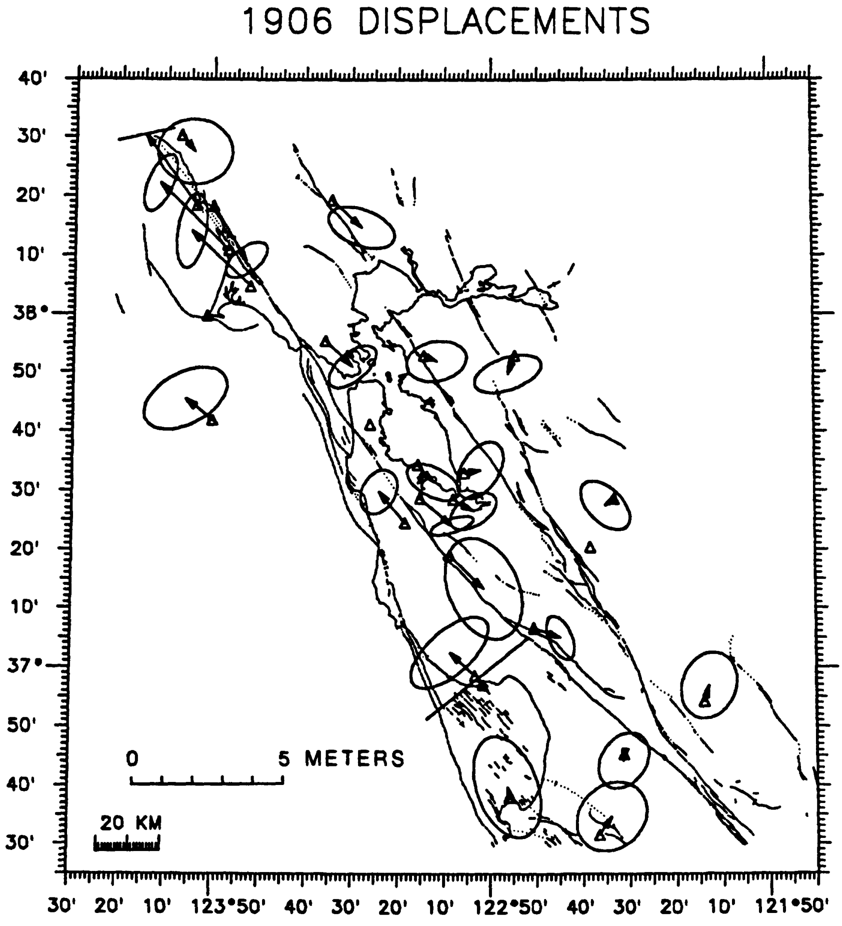

Reports

Segall, P., Earthquakes triggered by fluid extraction **Geology**, v. 17, p.942-946., 1989.

Du, Yijun, A. Aydin, and P. Segall, Comparison of various inversion techniques applied to the 1983 Borah Peak earthquake, **EOS**, v. 70, p. 1363, 1989.

Martel, S.J., P. Segall, E.H. McKee, and B.D. Turrin, Late Cretaceous faulting in the Sierra Nevada Batholith, **EOS**, v. 70, p. 1310, 1989.

Kronenberg, A.K., P. Segall, and G. Wolfe, Hydrolitic weakening and penetrative deformation within a natural shear zone, in Brittle-Ductile Deformation of Rock, the Heard Volume, Geophysical Monograph (AGU), in press 1990.

Segall, P., E.H. McKee, S.J. Martel, and B.D. Turrin, Late Cretaceous faulting in the Sierra Nevada Batholith, submitted to **Geology**, 1990.

Segall, P., and D. Richards, Displacements in the San Francisco Bay Area, California due to the 1906 earthquake, **EOS**, Spring AGU, 1990.

Matthews, M.V. and P. Segall, Minimum strain energy inversions for fault slip, **EOS**, Spring AGU, 1990.

Segall, P., Y. Du, and W. Thatcher, Were the 1934 and 1966 Parkfield earthquakes similar? **Seismological Society of America Meeting**, Santa Cruz, May, 1990.

Segall, P., Earthqaukes induced by hydrocarbon production, **AAPG Annual Convention**, San Francisco, May 1990.

LOW FREQUENCY DATA NETWORK

9960–01189

S. Silverman, K. Breckenridge, J. Herriot
Branch of Tectonophysics
U.S. Geological Survey
345 Middlefield Road, MS/977
Menlo Park, California 94025
(415) 329-4862

Investigations

[1] Real–time monitoring, analysis, and interpretation of tilt, strain, creep, magnetic, and other low frequency data within the San Andreas fault system and other areas for the purpose of understanding and anticipating crustal deformation and failure.

[2] Enhancements to satellite–based telemetry system for reliable real–time reporting and archiving of crustal deformation data.

[3] Development and implementation of backup capabilities for low frequency data collection systems.

[4] Specialized monitoring, including automated alerts, and display of data relevant to the Parkfield region.

Results

[1] Data from low frequency instruments in southern and central California have been collected and archived using the Low Frequency Data System. In the six months over eight million measurements from over 100 satellite platforms have been received via satellite telemetry and subsequently archived by Low Frequency Network computers for analysis.

[2] The project has operated a configuration of an Integrated Solutions (ISI) V24S computer running under the UNIX operating system, with another ISI serving as data storage backup. In addition, after the Loma Prieta earthquake, a Sun 3/280 was also used as a backup for the collection and storage of low frequency data. This backup was added due to the importance of maintaining operations and problems with maintence of the ISI systems. Data from the Network are made available to investigators in real–time and software for data display and analysis is readily available. Tectonic events, such as creep along the fault, can be monitored while still in progress. Also, periodic reports are produced which display data collected from various groups of instrumentation.

[3] The project continues to use a five meter satellite receiver dish installed in Menlo Park for retrieval of real–time surface deformation data from California and South Pacific islands. The GOES geostationary satellite together with transmit and receive stations make possible a reliable real–time telemetry system. Further expansion of the number of platforms monitored is ongoing.

[4] The project continues to take an active part in the Parkfield Prediction activities. Software has been written to provide scientists with automated alerts for signals which may indicate anomalous tectonic activity. Kate Breckenridge is the monitor for Parkfield creep events, which includes contact via paging system during periods of increased activity. Stan Silverman is the alternate monitor for Parkfield strainmeter data, which also includes contact via paging system alerts. Also, data collection and computer operations are automatically monitored for abnormal activity and project members are paged in event of problems with either.

[5] The project has continue to provide real–time monitoring of designated suites of instruments in particular geographical areas. Terminals are dedicated to real–time color graphics displays of seismic data plotted in map view or low frequency data plotted as a time series. During periods of high seismicity these displays are particularly helpful in watching seismic trends. The system is used on an ongoing basis to monitor seismicity and crustal deformation in central California and in special areas of interest.

[6] Data collection, storage and analysis were performed before and after the Loma Prieta earthquake of October 17, 1989, without loss of data. Use of backup power at the Menlo receive site and transmission of redundant data samples from field sites provided uninterrupted coverage of satellite telemetry. During the last quarter of 1989, operations of the low frequency computer were switched to a loaner system while the Survey computer was removed from the building for repairs. During this period, complete satellite telemetry was available from either the loaner system or backup computer facilities. Aside from short interruptions for system operations, users of the low frequency computer system were provided with a working system during this repair period.

Parkfield Area Tectonic Framework

9910-04101

John D. Sims
Branch of Engineering Seismology and Geology
U.S. Geological Survey
345 Middlefield Road, MS 977
Menlo Park, California 94025
(415) 329-5653

Investigations

1. Field investigations of structural and stratigraphic relationships between late Cenozoic sedimentary units and underlying Franciscan and granitic basement in central California with emphasis on the Parkfield-Cholame area.

2. Field investigations of late Holocene and historic slip rates in the Parkfield and Carrizo Plain segments of the San Andreas fault.

3. Post-earthquake investigations of the 1989 Loma Prieta, California earthquake.

Results

1. Geologic mapping progressed and the Parkfield and Cholame 7½-minute quadrangles have been completed. The Parkfield Quadrangle was and the Cholame Quadrangle is now at Menlo-BTR. Work is progressing on the Stockdale Mountain and Orchard Peak 7½-minute quadrangles.

   These quadrangles along with those already publish delineate the complexities of the San Andreas fault zone in the Parkfield segment. The San Andreas is shown to be composed of three segments that have been occupied as the "main" trace over the past 18-20 Ma. Preliminary conclusions derived from mapping in the Orchard Peak and Cholame quadrangles suggest multiple phases of uplift sine late Cretaceous time. Each period of uplift is followed by transgression of the seas and inundation of the southern Diablo and northern Temblor Ranges. Major unconformities separate late Cretaceous Maastrichtian, late Oligocene to Early Miocene, and middle Miocene deposits in this area.

2. A network of surveyed quadrilaterals, established on the San Andreas, White Canyon, Red Hills, Gold Hill, and Gillis Canyon faults in the Parkfield-Cholame area, totals 19 quadrilaterals. Fifteen quadrilaterals lie across the San Andreas, 2 on the White Canyon, and one each on the Red Hills and Gold Hill faults. These quadrilaterals are resurveyed every 2 months to gain background information on the sites prior to the next Parkfield earthquake.

3. We excavated 10 additional trenches (~165 m total length) in November 1989 to search for more offsets, evidence of individual events, and additional study of the process of stream abandonment at the Phelan Site on the Carrizo Plain. The fault trace at the site is easily identified by geomorphic features. The site is characterized by a pair of offset modern streams, an older abandoned and infilled stream channel, and a pair of beheaded streams. Off-sets of the modern streams were measured by high precision surveys of their thalwegs. The thalweg of the SE larger stream is offset 17.4 ± 1.6 m, and the offset of the NW smaller stream is 15.8 ± 0.6 m. Excavations in the alluviated abandoned channel reveal that it is offset 101.9 ± 1.4 m from the smaller stream, its probable parent stream. Offset of the stream lengthened the channel without significantly altering its base level, and aggradation proceeded. Filling of the channel occurred in four phases, the last ending just prior to establishment of the present pair of stream courses. One or two older abandoned and filled channels were revealed by the excavations NW of the younger abandoned channel.

   The 1857 break varies from a single fracture with horizontal slickensides, to multiple vertical faults with gouge zones of 2 to 25 cm, to an indistinct zone of distributed shear up to 2 m-wide. Conjugate faults of the San Andreas fault have both normal and reverse sense and occur in groups which alternate in sense of movement along strike of the SAF. Deposits in the modern channels show evidence for 2 events; the 1857 and the penultimate event. Identification of events older than the penultimate event is uncertain. Detrital charcoal for C-14 dating is abundant in the sediments excavated; more than 320 samples were collected. All sedimentary units contained multiple charcoal samples and potentially can be dated. Initial radiocarbon dates were received in December and suggest a slip rate of 32.0 and 35.6 mm/yr for the past 4645 yr. This is based on a single date from Trench I that dates the abandonment of the large stream at the site. The date is 4645 ± 205 CAL BP. Other dates received in December require substantiation by dating in progress.

4. Following the 17 October 1989 Loma Prieta earthquake I set out a large quadrilateral across the San Andreas at the intersection of Mount Madonna and Hazeldell Roads. The quad is about 160 by 45 meters and consists of 6 monuments. We have been resurveying the quad since 1 day after the earthquake. Thus far the quad records ambiguous surface slip.

Reports

Sims, J.D., 1989, Chronology of displacement on the San Andreas fault in central California: Evidence from reversed positions of exotic rock bodies near Parkfield, California: U.S. Geological Survey Open File Report 89-571, 39 p.

Sims, J.D., Ito, Tanio, Hamilton, J.C., and Meier, D.B., 1989, Late Holocene Record of Earthquakes and Slip on the San Andreas Fault in Excavations on the Carrizo Plain, Central California: American Geophysical Union, EOS, v. 70,no. 43, p. 1349.

Sims, J.D., 1990, Geologic map of the San Andreas fault zone in the Parkfield 7½-minute quadrangle, Monterey and Fresno Counties, California: U.S. Geological Survey Miscellaneous Field Studies Map MF-2015, scale 1:24,000.

Sims, J.D., and Hamilton, J.C., 1990, Geologic map of the San Andreas fault zone in the Cholame Quadrangle, San Luis Obispo County, California: U.S. Geological Survey Miscellaneous Filed Studies Map MF-*xxxx*, scale 1:24,000.

McLaughlin, R.J., Sliter, W.V., Elder, W.P., McDougall, K., Russel, P.C., Sorg, D.H., Sims, J.D., and Blake, M.C., 1990, 190-Km post-middle Miocene offset on the Tolay-Hayward-Calaveras fault system superposed on large-scale Late Cretaceous to Early Eocene translation: Geological Society of America Abstracts with Programs, v. 22, no. 3, p. 67.

27 April 1990

Semi-Annual Technical Report XXX

Modeling and Monitoring Crustal Deformation
9960-01488

Ross S. Stein, Wayne Thatcher, and Grant Marshall
Office of Earthquakes, Volcanoes, and Engineering
345 Middlefield Road, MS 977
Menlo Park, California 94025

415/329-4840
FTS 459-4840

Investigations.

1. STUDY OF THE CONTEMPORARY, HOLOCENE AND LATE QUATERNARY DEFORMATION OF THE ASAL RIFT, DJIBOUTI, AND ITS IMPLICATIONS FOR THE MECHANICS OF MID-OCEAN RIDGES. The Asal rift in Afar is one of the few segments of the world ocean rift system to stand above water, affording detailed measurement of its deformation. The only other equally accessible site is Iceland, which is complicated by its position over a hot spot. The Asal Rift is the most active spreading center of the Nubia-Arabia plate system in Afar, opening at 18 mm/yr, and propagating inland from the Gulf of Aden at 30 mm/yr. Because of Djibouti's hyper-arid climate, there is virtually no erosion and little deposition on to the rift features, which means that a topographic surface is also a structural datum. In addition, shoreline markers of the highstand of Lake Asal furnishes a precise measure of Holocene deformation. The lake level stood 160 m above sea level 8,600-6,000 yrs ago and dropped precipitously 300 m 6,000-5,000 yrs ago. Some 85 14^C dates on 100 surveyed highstand sites provide an unparalleled index of Holocene vertical deformation of a rift system. Finally, deformation associated with a seismovolcanic crisis in 1978 was measured by precise leveling and electronic distance measurement by Ruegg et al (in progress by R. Stein, Pierre Briole, Jean-Claude Ruegg, and Paul Tapponnier from Institut de Physique du Globe de Paris).

2. STUDY OF COSEISMIC AND POST-SEISMIC DEFORMATION AT COALINGA IN CONTEXT OF THE 110-KM-LONG NEW IDRIA-COALINGA-KETTLEMAN-LOST HILLS FOLD CHAIN. (Part 1 submitted; Part 2 in progress; R. Stein & G. Ekström, Harvard Univ.)

3. STUDY OF THE RECURRENCE CHARACTERISTICS OF LARGE EARTHQUAKES AND THE INFLUENCE OF COSEISMIC SLIP DISTRIBUTION ON MECHANICS OF RECURRENCE. Investigations include survey and synthesis of existing historical, seismological and paleoseismic information on earthquake recurrence. Geologic, geodetic and seismologic estimates of earthquake slip distribution are integrated with recurrence data whenever possible. Assessments of the precision and resolution of fault slip estimated by these different methods are needed both to evaluate the methods themselves and to judge the reliability of individual slip determinations (in progress, W. Thatcher and G. Marshall).

4. STUDY OF THE STATIC DEFORMATION FIELD OF THE 17 OCTOBER 1989 LOMA PRIETA, CA, EARTHQUAKE. In cooperation with the National Geodetic Survey and Santa Cruz County, 400 km of 1st Order leveling is being conducted by NGS crews to measure the coseismic elevation changes. The pre-earthquake surveys were conducted by the NGS, USGS, Santa Cruz County, and CalTrans to 1st-3rd Order standards. These pre-

earthquake surveys are quite variable in quality and date from 1908 to 1988. The post-earthquake surveying spans February-May 1990. Installation and reoccupation of a tidal gage at the Santa Cruz warf is also in progress. Reprocessing of the pre-earthquake surveys has just begun (G. Marshall, R. Stein & W. Thatcher).

Results.

1. ASAL RIFT. We seek to determine the time when rifting commenced at Asal, which is known only to have formed during the past 1 million years. In addition, we seek to find out whether active faulting becomes progressively less active with distance from the axis, is distributed across the 10-km-wide rift, or migrates around the rift with time. Finally, we wish to learn how the spreading, fault slip, and rift subsidence rates are related. We find that one quarter of the deformation has occurred during the past 6,000 yrs; thus the rift is likely to be just 25,000 years old. Faulting has been uniformly distributed across the entire rift. All faults within the rift flanks are similarly active; only one out of 13 has ceased during the Holocene. The subsidence rate of the rift, as well as the summed fault slip rate, are found to be equal to the spreading rate.

2. NEW IDRIA-COALINGA-KETTLEMAN-LOST HILLS FOLD. We argue that the New Idria-Coalinga-Kettleman-Lost Hills chain of en echelon folds marks the leading edge of a continuous segmented thrust fault, the 3 northern segments of which ruptured in three $5.5 \leq M_W \leq 6.5$ earthquakes in less than 3 years. The earthquakes ruptured from north to south and the sequence may continue. The southernmost Kettleman South Dome-Lost Hills segment is the longest in the chain, and thus may be capable of generating an earthquake of $6.5 > M_W > 7.0$. The main shocks and nearly all well-constrained aftershocks exhibit compressional mechanisms perpendicular to the fold axes, suggesting that the blind fault undergoes pure dip slip and accommodates contraction normal to the San Andreas fault, which strikes parallel to the fold chain and lies 30 km to the east. The master fault appears to lie at a depth of 14-15 km at the north end, shallowing to perhaps 5 km at the southern extremity. Relocation of the seismicity reveals that the aftershock zones abut at en echelon offsets in the fold axes. We interpret the fold offsets to overlie tears, offsets or step-ups in the fault below, and suggest that offsets along youthful folds elsewhere can be used to deduce the plausible segmentation on blind faults, which are otherwise inaccessible for assessment. The large earthquakes also provide evidence that the blind fault is propagating away from the San Andreas fault at a rapid rate of about 2 mm/yr. The Kettleman main shock and center of coseismic uplift are displaced 5-7 km basinward of the Quaternary fold axis, the New Idria main shock is displaced 2 km, and the postseismic deformation at Coalinga is displaced 2 km from the coseismic deformation, all suggesting that the fault is propagating into the undeformed Great Valley sediments.

A common feature of the large earthquakes is their diffuse pattern of aftershocks, with the shallowest events locating in the core of the anticlines. We argue that this pattern is a fundamental feature of seismicity on blind faults that contrasts with events on strike-slip or normal faults, and corresponds to secondary faulting on associated fractures, and to small adjustments in the highly deformed and strained anticlinal cores. Background seismicity during the 12 years before the New Idria-Coalinga-Kettleman sequence began is concentrated at the offsets and ends of fold axes, and also in the cores of the anticlines. A feature unique to the Kettleman Hills event among the 3 earthquakes is its slow rupture speed, resulting in a long-period and geodetic moment 10 times larger than the moment estimated from short-period seismograms, and delayed triggering and late peak amplitudes in the strong ground motion. Whether other historical earthquakes beneath the fold—several of which predate the seismic network—also ruptured slowly is unknown.

3. FAULT SLIP HETEROGENEITY AND PATTERNS OF EARTHQUAKE RECURRENCE. The existence of an upper failure threshold for fault slip is a central axiom of earthquake mechanics and a common feature of concepts as diverse as Ried's elastic rebound model and modern laboratory-based constitutive laws of fault behavior. This axiom is also closely related to the time predictable model of Shimazaki and Nakata, which postulates that earthquake interevent time is determined by the ratio of slip in the most recent event to longterm fault slip rate. Applying this prescription to simple patterns of slip heterogeneity results in a wide range of permitted recurrence behavior. If slip rate is constant along fault strike and earthquake slip is not, then cycle-to-cycle variability in the rupture lengths and magnitudes of successive events is required. Overlap of rupture zones during a single strain release cycle is also common. Provided slip on specific subsegments of plate boundary does not vary from event to event, interoccurrence times on these may be constant even though different combinations of them may rupture in each cycle. However, interaction between adjacent subsegments can significantly perturb these patterns. If slip on each subsegment depends on total rupture length then interevent times will become nonuniform. Occurrence time will also be influenced by the slip history of the adjacent regions through the timing of their events, the resulting dynamic and quasistatic stress transfer that accompanies them, and the existence of locked or freely sliding zones. Downdip variations in earthquake slip distribution would produce further complications. Given these expectations it is surprising that observed recurrence behavior shows as much order as it does. Rupture zones of circum-Pacific earthquakes tend to abut without significant overlap, and in a number of regions rupture characteristics vary from cycle to cycle, but events are clustered in time and cycle duration is relatively uniform. These features might be rationalized if subsegments (asperities?) are largely isolated from the perturbing effects of their neighbors (by aseismic slip zones?). On some plate boundary segments recurrence behavior is apparently less ordered and some of the permitted effects of slip heterogeneity may be responsible.

Reports published or submitted during this period (excluding abstracts):

Ekström, G., R. Stein, J.P. Eaton, and D. Eberhart-Phillips, Seismicity and geometry of a 110-km-long blind fault, 1, The 1985 Kettleman Hills, California, earthquake, 49 p., submitted to *J. Geophys. Res.*, 1990.

Thatcher, W., Earthquake recurrence and risk assessment in circum-Pacific gaps, *Nature*, *341*, 432-434, 1989.

Thatcher, W., Order and diversity in the modes of circum-Pacific earthquake recurrence, *J. Geophys. Res.*, *95*, 2609-2623, 1990.

Thatcher, W., Precursors to eruption (News & Views article), *Nature*, *343*, 590-591, 1990.

Northeast Striking Cross Faults, Detachments, Crustal Blocks and Strain Partitioning in Southern California: A Search for Changes in Seismicity and Focal Mechanisms Precursory to Major Earthquakes

USGS 14-08-0001-G-1688

Lynn R. Sykes and Leonardo Seeber
Lamont-Doherty Geological Observatory of Columbia University
Palisades, New York 10964

Objective:

For the past 5 years we have been studying the detailed distribution of earthquakes, focal mechanisms, rotations of small crustal blocks, N.E. striking cross-faults, the existence of shallow-angle detachment faults and premonitory changes before large earthquakes along the southern San Andreas and San Jacinto faults in southern California. Major emphasis has been given to the large tectonic knot centered near San Gorgonio Pass and to 2 recent earthquakes near the southern end of the Salton Sea. Little of the present seismic activity occurs on the major throughgoing faults themselves. Instead much of it is situated on secondary faults and detachments. Seismicity in the months before the 1986 North Palm Springs earthquake appears to be concentrated on a detachment fault that determined the lower limit of the rupture. Secondary cross-faults at the two ends of the rupture were active during the aftershock sequence. The purpose of this study is to use relocated hypocenters and single-event focal mechanisms to examine precursory changes in three regions near the San Jacinto and southern San Andreas faults that contain prominent cross-faults and detachment faults. One includes small earthquakes associated with a magnitude 6 event on a cross-fault near the southern end of the Salton Sea that was a short-term precursor to a larger event in 1987 on the Superstition Hills fault. A temporal sequencing of activity along NW and NE trending conjugate faults of the Brawley zone has been identified and is being examined in detail. Future changes in activity on the next cross fault to the north of the one that ruptured in 1987 could be a precursor to a larger event that would rupture the southern San Andreas. We have developed computer programs to automatically determine hundreds of focal mechanism solutions of high quality so as to examine in detail the hypothesis that the San Andreas is a weak fault. Moderate earthquakes prior to the 1989 Loma Prieta earthquake in central California, most or all of which are outside the ensuing rupture zone, show a pattern of accelerating moment release. In light of this precursory change in seismicity in a region of complex fault interaction, we have begun re-examining seisimicity of moderate-to-large earthquakes in southern California to establish if such changes also occur before large earthquakes on the San Andreas system in southern California.

Results:

Two large strike-slip ruptures 11.4 hours apart occurred on intersecting, nearly orthogonal, vertical faults during the November 1987 Superstition Hills earthquake sequence. This rupture was investigated in the paper "Cross-fault triggering in the November 1987 Superstition Hills Earthquake Sequence, Southern California" that was published in Geophysical Research Letters in February, 1989 by Hudnut, Seeber, and Pacheco. They show evidence that this sequence is the latest in a northwestward progression of earthquakes (1979, 1981, and 1987) rupturing a set of parallel left-lateral cross-faults that trend northeast between the Brawley seismic zone and the Superstition Hills fault. It is inferred that the observed northwestward progression of ruptures on cross-faults may continue. The next cross-fault expected to rupture intersects both the San Andreas fault and the San Jacinto fault zone. They hypothesize that slip on the cross fault decreased normal stress on the main fault and triggered main strand rupture after a delay that was caused by fluid diffusion.

The preprint "The interaction between secondary and master faults within the southern San Jacinto fault Zone, southern California" by Petersen, Seeber, Sykes, Nabelek, Hudnut and Armbruster shows evidence that a third of the moment radiated from the April 9, 1968 Borrego Mountain earthquake came from a subevent that occurred on a secondary fault. In addition, the April 28, 1969 Coyote Mountain earthquake may have occurred on a northeast cross-fault instead of along the mainstrand fault as was previously thought. They relocate seismicity (1981-1986) and identify a secondary fault (the Palm Wash fault) that is parallel to the mainstrand fault and appears to be activated by regional large earthquakes. Increased seismic activity in a location well off the master fault occurs in a three-month time window both subsequent and prior to activity on the master fault and may signal increased stress in the region.

An abstract "Stress orientation inferred from the kinematics of secondary faults within the San Andreas fault zone at Parkfield" by Seeber and Armbruster demonstrates the use of the focal mechanism program that automatically determines hundreds of mechanisms from the most well-constrained phase data. They show that near Parkfield almost half of the focal mechanisms have nodal planes that are not parallel to the San Andreas fault and are not ruptures on a master strand. They infer these ruptures to be on minor faults confined to the fault zone. If these faults are randomly oriented, their combined slip geometry define the direction of maximum compression on the San Andreas fault in the seismogenic depth range. The compression axis lies at about 55° with the San Andreas fault. This angle is consistent with friction laws derived from laboratory experiments.

An abstract "Seismicity changes in the San Francisco Bay region before the Loma Prieta earthquake of 1989" by Jaumé and Sykes establishes a pattern of accelerating moment release prior to 1989 Loma Prieta earthquake. Most, if not all, of the $M \geq 5.0$ earthquakes in the 35 years prior to this earthquake are outside the ensuing rupture zone. In the preprint "Long-term seismic precursors to three large earthquakes, greater San Francisco Bay area, California" Sykes and Jaumé show that accelerating moment release has occurred before three large earthquakes in central California and also before the 1948 Desert Hot Springs earthquake in southern California.

Publications:

Hudnut, K.W., L. Seeber, and J. Pacheco, Cross-fault triggering in the November 1987 Superstition Hills earthquake sequence, southern California, *Geophys. Res. Lett.*, *16*, 199-202, 1989.

Jaumé, S.C., and L.R. Sykes, Seismicity changes in the San Francisco Bay region before the Loma Prieta earthquake of 1989 (abstract), *EOS, Trans. AGU, 71*, 288, 1990.

Nicholson, C., L. Seeber, P. Williams, and L.R. Sykes, Seismicity and fault kinematics through the eastern Transverse Range, California: Block rotation, strike-slip faulting and shallow-angle thrusts, *J. Geophys. Res.*, *91*, 4891-4908, 1986.

Nicholson, C., L. Seeber, P.L. Williams, and L.R. Sykes, Seismic deformation along the southern San Andreas fault, California: Implications for conjugate slip and rotational block tectonics, *Tectonics, 5*, 629-649.

Pacheco, J., and J. Nabelek, Source mechanisms of three moderate southern California earthquakes of July 1986, *Bull. Seismol. Soc. Amer., 78*, 1907-1929, 1988.

Petersen, M.D., L. Seeber, J. Nabelek, and K. Hudnut, The interaction between secondary and master faults within the southern San Jacinto fault zone, southern California, (abstract), *EOS, Trans. AGU, 70*, 1211, 1989.

Seeber, L., and C. Nicholson, Block/fault rotation in geologic and interseismic deformation, *U.S. Geol. Surv. Open File Report, 86-850*, 185-203, 1986.

Seeber, L., J.G. Armbruster, P. Williams, and L.R. Sykes, Faults antithetic to the San Andreas delineated by seismicity in the San Gorgonio Pass of southern California (abstract), *EOS, Trans. AGU, 67*, 1200 1986.

Seeber, L., J.G. Armbruster, M. Tuttle, Secondary faults associated with the 7 July, 1986 Palm Springs earthquake rupture on the San Andreas fault (abstract), *Seismol. Soc. Am. Abstracts with Programs*, pp. 20, 1987.

Seeber, L., and J.G. Armbruster, Secondary faults as agents for segmentation of the master strands in southern California (abstract), *IUGG Conference*, Vancouver, Canada, Aug. 17-22, 1987.

Seeber, L., and J.G. Armbruster, Stress orientation inferred from the kinematics of secondary faults within the San Andreas fault zone at Parkfield (abstract), *EOS, Trans, AGU, 69*, 1456, 1988.

Sykes, L.R., and S.C. Jaumé, Long term seismic precursors to three large earthquakes, greater San Francisco Bay area, California, preprint, 1990.

Sykes, L.R., and L. Seeber, Great earthquakes and great asperities, San Andreas fault, southern California, *Geology, 113*, 835-838, 1985.

Williams, P., S. Fagerson, and K. Sieh, Triggered slip of the San Andreas fault after the July 8, 1986 North Palm Springs earthquake (abstract), *EOS, Trans. AGU, 67*, 1090, 1986.

Williams, P.L., L.R. Sykes, C. Nicholson, and L. Seeber, Seismotectonics of the easternmost Tranverse ranges, California: Relevance for seismic potential of the southern San Andreas fault,*Tectonics, 9*, 185-204, 1989.

Nearfield Geodetic Investigations of Strain across Faults in Southern California

14-08-0001-G1690

Arthur G. Sylvester
Department of Geological Sciences, and
Marine Science Institute
University of California
Santa Barbara, California 93106
(805) 961-3156

OBJECTIVE

The long-term, fixed purpose of this investigation is to search for and monitor the spatial and temporal nature of nearfield displacement across active and potentially active faults. Thus, we document pre-, co- and post-seismic displacement and aseismic creep, if any, especially where seismographic, paleoseismic and geomorphic evidence indicates current or recent fault activity. The geodetic arrays range in length from 300 m to 7000 m and are intermediate in scale, therefore, between the infrequent, regional geodetic surveys traditionally done by the National Geodetic Survey, and point measurements by continually recording instruments such as creepmeters, tiltmeters, and strainmeters. All leveling is done according to First Order, Class II standards, and horizontal surveys are done to First Order standards.

RESULTS

LOMA PRIETA EARTHQUAKE: The only geodetic arrays we had near the meisoseismal area of the 17 October 1989 Loma Prieta were a 978 m-long level line and two nail lines across the San Andreas fault at San Juan Bautista. We resurveyed the level line 10 weeks before the earthquake, two days afterward, and then again 10 weeks after the earthquake. We measured the nail lines in December 1988, then 3 days after the earthquake, and then again 10 weeks after the earthquake. We found that the San Andreas fault at San Juan Bautista was hardly affected by the Loma Prieta earthquake, and the earthquake did little to terminate the six year-long episode of horizontal and vertical creep retardation there. Resurveys of cross-fault nail lines, each 1 km NW and SE, respectively, of San Juan Bautista showed that 15 mm of right slip occurred between December 1988 and October 20, 1989. Some of that slip may have been coseismic, however, because creepmeter XSJ2 southeast of the town recorded 5.18 mm of coseismic, right-lateral creep, which decayed left-laterally in the two days after the earthquake to yield net right slip of 4.05 mm. First-order surveys of bench marks in the leveling array revealed 25 mm of vertical separation occurred across the fault between 1974 and 1983, but no change occurred from 1983 to 1990, corresponding approximately in time to the period of horizontal creep retardation that commenced in early 1984. This leads to a conclusion that the vertical displacement across the San Andreas fault at San Juan Bautista represents tectonic creep rather than non-tectonic subsidence related to withdrawal of groundwater for agriculture in San Juan Valley. Moreover, the lack of significant, triggered, nearfield surficial slip at the time of the Loma Prieta earthquake means that a strain deficit still remains at San Juan Bautista, a deficit which will require a M 4.9 ± 0.3 earthquake to resume the average horizontal strain rate of 7 mm/yr observed there over the past 20 years. These results were reported in a poster session at the Annual Fall Meeting of the American Geophysical Meeting by Sylvester, Burford and Schulz (1989).

SAN JACINTO FAULT: The increased seismic activity along the northern reach of the San Jacinto fault in December, 1989, prompted us to resurvey nearfield geodetic arrays across the fault near Anza and on the campus of San Bernardino Valley College in January 1990. Horizontal displacement was not detected to a precision of ± 5 mm along the main strand of the San Jacinto fault in the Anza area between mid-1988 and mid-January, 1990, based on comparison of two incomplete EDM-resurveys of small aperture trilateration arrays across the fault at trench sites north of 3 km north of Anza and 1 km northwest of Hog Lake. Resurveys of short level lines across the fault, however, reveal 10 mm (± 0.4 mm) at the San

Bernardino site, and 1.5 mm (± 0.5 mm) at Anza in the same time period. The vertical displacement in San Bernardino occurred across a horst where 6 previous levelings of the same line of permanent bench marks revealed less than 4 mm of displacement from 1985 to 1988, northeast side-down relative to the southwest side. That displacement was previously attributed to withdrawal of groundwater, only because the San Jacinto fault is an aquiclude in San Bernardino damming groundwater northeast of the fault. The abrupt displacement across the fault coincides temporally not only with nearby seismic activity in December 1989, but also with the southern California drought. Water pumping records and more frequent surveys are required to determine whether the displacement is tectonic or due to subsidence. At Anza, a height change of 1.5 mm (± 0.5 mm), mountain side-up, from July 1988 to January 1990, occurred across a 100 m-wide zone that coincides with the trace of a subsidiary strand of the fault, whereas no displacement occurred across the main fault. Repeated annual levelings of the array from 1984 to 1988 yield a displacement rate of 0.5 mm/yr across the subsidiary fault, but the rate doubled to 1 mm/yr from mid-1988 to January 1990. The surveys demonstrate that vertical displacements have occurred across widely separated parts of the San Jacinto fault, but they are not sufficiently frequent, laterally extensive, or temporally lengthy to determine whether the displacements represent coseismic slip or aseismic creep, or if they have non-tectonic causes. These results were reported at the 1990 Annual Meeting of the Seismological Society of America by Sylvester, Helm, Hitchcock, and Howe (1990).

GRAND TETON PROJECT: The 22 km-long line across the Teton fault in Grand Teton National Park (Fig. 1) was resurveyed during the last few days of August and the first week of September. The line was established and first surveyed in August, 1988 in cooperation with the University of Utah and the National Park Service. The observed misclosure for the 1989 survey is 12.25 mm, compared with 12.44 mm for the 1989 survey. The standard deviation, after the data were adjusted by the National Geodetic Survey for misclosure, rod error, atmospheric effects, and refraction effects, in both surveys is 0.4 mm. Displacement across the east-dipping fault from 1988 to 1989 was 8 mm, footwall down relative to the hanging wall (Fig. 2). No earthquakes > M 2.5 occurred during that time period. This means that aseismic reverse slip occurred on a normal fault by means of one or a combination of the following mechanisms: 1) interseismic, east-west regional crustal shortening; 2) complex tectonic interaction with the seismically active Gros Ventre Range, 25 km southeast of the Teton Range; 3) hanging wall dilation prior to an impending earthquake; and 4) poroelastic strain of glacio-fluvial sediments beneath Jackson Valley due to refilling of Jackson Lake. We are performing elastic dislocation modeling to evaluate these possibilities more fully. These results were reported at the 1990 Cordilleran Section Meeting of the Geological Society of America by Sylvester, Byrd, and Smith (1990).

COACHELLA VALLEY: We resurveyed our 2.2 km-long level line across Bat Caves Buttes, the Extra fault, and Kane Spring fault in March 1990. The height differences between bench marks in the Bat Caves lines in 1990 are virtually identical to those we observed in 1989, which means that no vertical displacement has occurred across the San Andreas fault there since the 3 mm we observed within 3 weeks of the 1987 Superstition Hills earthquake. Also in March 1990 we resurveyed alignment arrays EXTRA, KANE SPRING, and CORVINA BEACH.

PARKFIELD: We resurveyed our 7 km-long line across Cholame Valley in January 1990. Comparisons with previous surveys reveal continued vertical displacement across the San Andreas fault at a rate of 3 mm/yr, valley side down relative to Gold Hill.

Reports

Sylvester, A. G., R. O. Burford, and S. S. Schulz, 1989. Almost no surface displacement occurred at San Juan Bautista as a result of the Loma Prieta earthquake. EOS 71 (8), 290.

Sylvester, A. G., J. O. D. Byrd, and R. B. Smith, 1990. Aseismic (?) reverse creep across the Teton fault, Wyoming, with implications for interseismic strain. GSA Abstracts with Programs, (86th Cordilleran Section Meeting, Tucson, Arizona), v. 22 (3), p. 88.

Sylvester, A. G., J. Helm, C. Hitchcock, and N. Howe, 1990. Minor vertical, but no horizontal nearfield displacement across the San Jacinto fault at Anza and San Bernardino, California, from 1988 to 1990. Annual Meeting, Seismological Society of America, Santa Cruz.

GRAND TETON LEVEL LINE

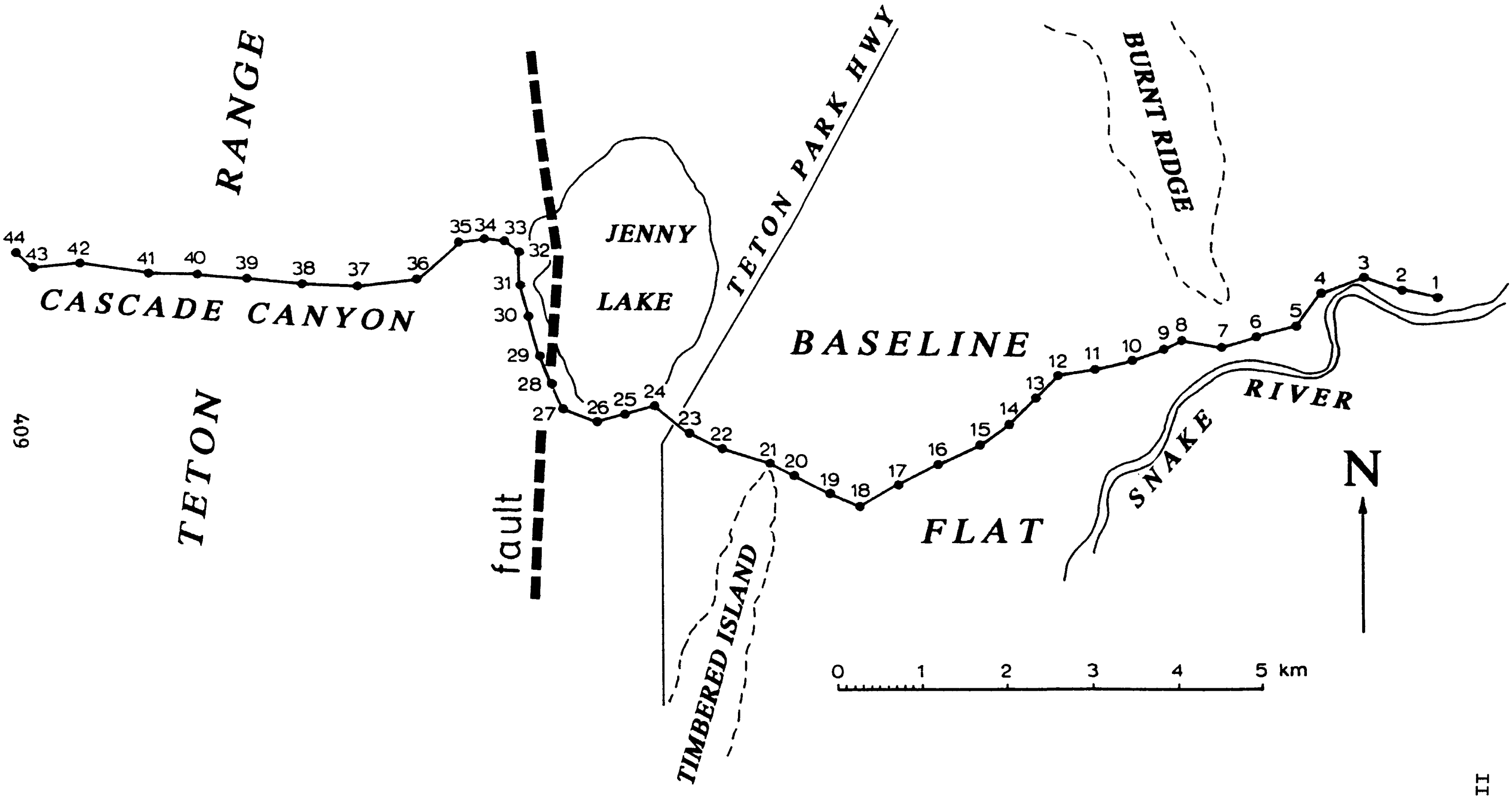

Fig. 1. Sketch map of the UCSB/U of Utah first order level line across the Teton fault, Grand Teton National Park, Wyoming

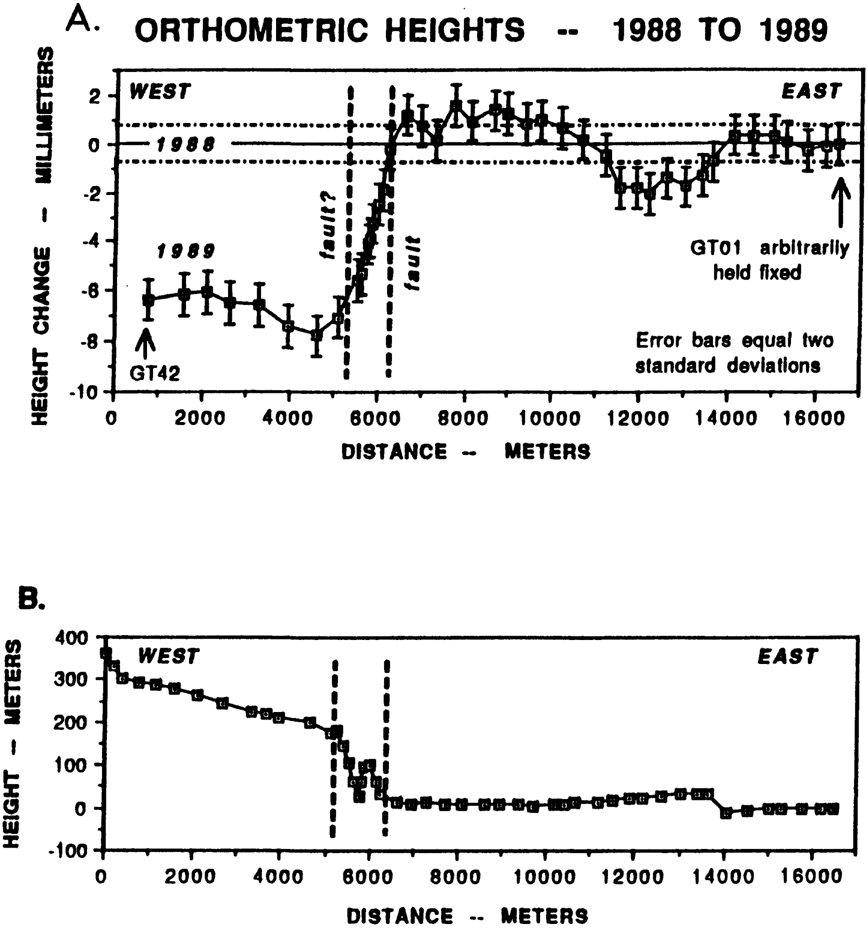

Figure 2. Height changes of bench marks across the Teton fault west of Jenny Lake, Grand Teton National Park, from 1988 to 1989.

A. Height changes plotted *versus* distance, where the distance is the straight line distance from GT01 at the east end of the line to GT42 at the west end. Error bars for the 1989 survey are two standard deviations. Dashed lines on each side of the solid, straight line that represents the 1988 datum are also error limits that correspond to two standard deviations. Both surveys have been adjusted by the National Geodetic Survey for misclosure, rod error, and refraction.

B. Topographic profile of the level line.

ROCK MECHANICS

9960–01179

James Byerlee
U.S. Geological Survey
Branch of Tectonophysics
345 Middlefield Road, MS/977
Menlo Park, California 94025
(415) 329–4841

Investigations

Laboratory experiments are being carried out to study the physical properties of rocks at elevated confining pressures, pore pressure and temperature. The goal is to obtain data that will help us to determine what causes earthquakes and whether we can predict or control them.

Results

Friction experiments have been conducted in a triaxial press on 2.4 mm–diameter cylindrical granite samples containing simulated faults. Fault surfaces were sawcuts included 30° to the sample axis and contained ridges and grooves oriented perpendicular to the direction of slip. A layer of wet montmorillonite clay of thickness comparable to the ridge heights was used to separate the fault surfaces. A single pair of ridges sliding past each other resulted in a strength transient whose magnitude and shape depended on the dimensions of the ridges and the thickness of the clay layer. A variety of more complex geometries was also studied. In one example, surfaces with regularly spaced ridges and grooves were used to produce a strength function which varied cyclically with displacement. This geometry was used to investigate the dependence of fault stability on machine stiffness, which was varied in two ways: first, stiffness was reduced by placing a chamber of compressed gas between the ram and the piston used to apply load to the sample. In the second method, stiffness reduction was accomplished electronically by adding a signal proportional to the axial load to the servo feedback loop controlling sample displacement. In both cases, samples which slid stably at normal stiffness were observed to slide unstably when stiffness was reduced.

The effective stress law relates the total stress acting on a material to the difference between the confining and fluid pressures. The effective stress law for frictional sliding has been shown to hold for a variety of rock types and gouges, but has not been studied for clays. Because clay gouges are common in fault zones such as the San Andreas, we have studied the effective stress law for representative expanding and non–expanding clays that are likely to exist to seismogenic depths. Frictional sliding experiments were performed on pure montmorillonite, illite and mixed montmorillonite/illite gouges with effective pressures ranging from 2 to 300 MPa. The data show that the shear strength of both montmorillonite and illite vary as a function of effective pressure, independent of confining and fluid pressures, verifying that the effective stress law holds. We also found that pure montmorillonite gouge showed the lowest strength at all effective pressures, with shear strength increasing in proportion to illite content. Dry gouge was consistntly stronger than wet gouge for all sample compositions. The coefficient of friction of both dry and wet montmorillonite gouge increased with increasing effective pressure, whereas the illite gouge showed significantly less dependence upon effective pressure. The low strength of expanding clays has been related to the presence of loosely bonded interlayer water. Our results for montmorillonite suggest that with increasing pressure, fewer layers of water are retained by the gouge, thus the coefficient of friction increases.

To look for differences in the style of fault zone deformation between stick–slip and stable sliding, cylinders of intact granite were loaded in triaxial testing equipment until they failed in compression, and deformation was continued by sliding along the resulting breaks. The experiments were conducted at room temperature on dry or fluid–saturated granite cylinders. At confining pressures between 40 and 120 MPa, the samples slid stably following the initial break, and at confining pressures between 150 and 600 MPa they showed stick–slip motion. Deformation maps were prepared from thin sections of the faulted samples. The deformation maps vary widely in appearance, reflecting sample–to–sample variations in the initial breaks, but the paths along which shear was concentrated could be identified. In the low–pressure, stably sliding samples, shear was accommodated in zones as much as 1.5 mm wide, which are characterized by a pronounced fabric of deformed opaque and phyllosilicate grains and a moderate reduction in grain size compared to adjoining areas that were fractured but not sheared. In contrast, shear in the high–pressure, stick–slip samples were localized in zones that are roughly 0.2 mm or less in width. These zones, in turn, contain as many as four, 0.005 to 0.010 mm wide, sub–parallel shear bands that consist of extremely fine–grained gouge. Each shear band may represent a single episode of slip; thus, successive slip events in the stick–slip cycle may occur as fresh breaks in the same part of the fault. The observed textural differences emphasize the correlation between stick slip and the localization of shear. Repeated slip events along nearly the same path, similar to those occurring in the stick–slip samples, are also characteristic of natural faults such as the San Andreas of California.

We have completed a suite of hot isostatic pressing experiments using fine grained (5–10 μ m) quartz powders saturated with water at 700°C. Pore fluid pressures ranged from 30 to 200 MPa; confining pressures ranged from 200 to 370 MPa; initial porosity varied from 35–47%. After hot pressing under effective pressures of 170 MPa for several days, the final porosities were from 20% to as low as 7%. As is common in compaction experiments, the volumetric strain rate is quite rapid at first ($\sim 10^5$/s), decreasing with time ($\sim 10^8$/s). Under these conditions, densification rates appear to depend on the pore fluid pressure as well as the total effective pressure. The electrical conductivity of the compact also falls steadily with time. After the initial rapid compaction, the conductivity of the compact may be represented by a power law relation between porosity and electrical conductivity similar in form to Archie's law. However, the empirical values of the exponent range widely from experiment to experiment, varying from 0.8 to 2.8. The exact form of the relation between porosity and conductivity are probably related to changes in average particle size, size distribution, and packing geometry which occur during compaction.

A plane–strain multiple crack interaction model is presented in which finite difference quasi–static equilibrium equations are solved to examine multiple crack interactions. A multi–scaling approach is used to achieve solutions for large crack populations. The model includes frictional strength for crack surfaces and time–dependent sub–critical crack growth. Many features of laboratory experiments are duplicated. These include dilatency, Mohr failure envelope, acoustic emission and acoustic wave velocity. In the multi–scaling approach, the sample is divided into small cells which are analyzed individually to determine local average elastic properties. A new system, constructed of these cells of averaged properties, is itself subdivided, this time on a coarser scale than the scale of the original system. The new system, in turn, is analyzed for average elastic properties. This procedure is continued, increasing in scale, until a single set of average properties for the entire system is determined. Desired boundary conditions are then applied to the coarsest scale system and average displacements are computed. These displacements are used as boundary conditions for each cell at the next finer scale and interior displacements are computed cell by cell. This procedure is continued until displacments and stresses are determined for the original system. Finally, crack growth is precribed based on the local stress conditions and a critical stress intensity criterion. The entire process is then repeated with the new crack population.

Reports

J. Byerlee and D. Lockner, (1989), Strength and stability of faults containing surface structure, *Trans. Am. Geophys. Union* (EOS), v. **70**, No. 43, p 1303.

B. Radney, C. Morrow and J. Byerlee, (1989), Effective stress law for montmorillonite and illite clays, *Trans. Am. Geophys. Union* (EOS), v. **70**, No. 43, P. 1303.

D. Moore, R. Summers, and J. Byerlee, (1989), Localization of deformation during stick–slip and stable sliding in granite, *Trans. Am. Geophys. Union* (EOS) v. 70, No. 43, p. 1303.

D. Lockner and T. Maddon (1989), Crack interaction simulation using a multi–scaler approach, *Trans. Am. Geophys. Union* (EOS) v. **70**, No 43, p. 1304.

B. Evans and D. Lockner (1989), Densification and electrical properties of hot pressed quartz aggregates, *Trans. Am. Geophys. Union*, v. **70**, No. 43, p. 1323.

D. Moore and J. Byerlee (1989), Variations in fault zone geometry along the San Andreas fault, California, *Geol. Soc. Am.* Abstracts with program v. **21**, p. 1766.

C. Morrow, and J. Byerlee, Permeability of core samples from Cajon Pass scientific drill hole: Results from 2100 to 3500m depth, *J. Geophys. Res.* (in press).

D. Lockner, J. and Byerlee, (1990), An example of slip instability resulting from displacement varying strength, *PAGEOPH* (in press).

D. Moore, and J. Byerlee, (1990), Geometrical segmentation of the San Andreas fault between Point Arena and Cajon Pass, California, *Geol. Soc. Am. Bulletin* (in press).

D. Moore and J. Byerlee, (1990), Textural development of clayey and quartz feldspathic fault gouge relative to their sliding behavior, *Phys. and Chem. of the Earth*, (in press).

D. Moore, and J. Byerlee (1989), Geometry of recently active breaks along the San Andreas fault, California, *U.S. Geological Survey* Open–File Report, 89–347, 72 p.

D. Moore and J. Byerlee, (1990), Textural development of clayey and quartzo–feldspathic fault gouge relative to their sliding behavior, *J. Struct. Geol.*, v. **11**, p. 329–342.

Friction Constitutive Behavior of Saturated Faults at Hypocentral Conditions

USGS 14-08-0001-G1768

Frederick M. Chester*

Lamont-Doherty Geological Observatory, Palisades, NY 10964; (914)359-2900.
(*Permanent address: Department of Earth & Atmospheric Sciences, St. Louis University,
3507 Laclede, St. Louis, MO 63021; (314)658-3124.)

Investigations

The goal of the project is to determine the friction constitutive behavior of water saturated faults at hypocentral conditions through experimentation and constitutive modeling. Specifically, we are conducting triaxial friction experiments on wet and dry quartz gouge at normal stresses to 100 MPa and temperatures to 250 °C. Methods of testing include velocity stepping, slide-hold-slide and temperature stepping. Through such experiments we will determine the trade-off between slip rate and temperature, and the form of temperature dependence in rate and state dependent friction constitutive laws. Experiments are being conducted at water saturated and nominally dry conditions to determine the effects of water on frictional behavior, and in particular, to search for evidence of solution transfer at elevated temperatures and low sliding velocities.

Mounting geologic evidence suggests that solution transfer is an important mechanism of deformation in natural faults at seismogenic depths. It has been suggested repeatedly that solution transfer could be an important process for fault healing during interseismic periods, and promote creep at low shear stresses. It is well known that the mechanisms of solution transfer are favored in fine grain materials at low deformation rates, and have strain-rate/temperature relationships described by relatively low activation energies (Rutter 1983). Consequently, it is very difficult to study these mechanisms in the laboratory. Some of the best evidence indicating that solution transfer can be studied in experimental faults is provided by stress relaxation (hold) tests because these achieve low deformation rates (e.g. Rutter & Mainprice 1978). To date, analyses of this type of experiment have generally assumed that the specimen relaxes at steady state even though the fault continues to slip at continuously varying velocities, and accordingly, under a changing state. Moreover, the experiments show frictional behavior, yet the constitutive laws utilized are not friction laws. Thus, with our present state of knowledge, these analyses are no longer entirely satisfying.

Part of our work under this contract has been to analyze relaxation experiments using the framework of the rate and state dependent friction laws. This is important ground-work for analysis of our experiments utilizing the slide-hold-slide mode of testing. Our findings show that stress relaxation experiments on simulated faults can be used to investigate friction behavior at low velocities and at conditions favorable for the operation of solution transfer. This work also has been useful to reanalyze previous experiments on faults containing quartz gouge at elevated temperatures and pressures by Nigel Higgs (Higgs 1981, Higgs & Logan 1981). Although Higgs' data are sparse, we are able to infer the rate and temperature dependence of friction from his slide-hold-slide tests, and delineate friction behavior at low sliding velocities where solution transfer is thought to dominate. We summarize this analysis in the following, and will report on our findings at the Spring Meeting of the AGU (Chester & Higgs 1990).

Results

The experiments by Higgs involved shear of thin layers of ultra-fine grained quartz gouge along 35° sawcuts in a triaxial rock deformation apparatus. Experiments were conducted at both water saturated and nominally dry conditions at an effective pressure of 150 MPa and temperatures of 25, 300, 450 and 600 °C. Higgs performed slide-hold-slide tests in which he closely monitored the stress relaxation as a function of time during the hold periods, and the transient friction strength versus displacement upon resuming the sliding after the holds. Hold times varied up to 10^5 seconds. Based on the microstructures produced during the shearing experiments, Higgs identified two deformation regimes. The regime characterized by fairly typical cataclastic microstructures and relatively high porosity occurs at all temperatures under dry conditions and at temperatures below 300 °C for wet tests. The other regime is characterized by relatively low porosities, preferred crystallographic orientations in the quartz shear zone, and fractures cemented with quartz. Higgs (1981) and others (Power & Tullis, 1989) have interpreted these features as indicative of solution transfer. The two deformation regimes also are distinguished on the basis of the relaxation response during the hold tests. The wet experiments at elevated temperatures produced rapid stress relaxation relative to the stress relaxation observed at dry, and low temperature, wet conditions (Fig. 1). Higgs' data indicate that the onset of rapid stress relaxation in the wet tests is itself a function of temperature, indicating a trade-off between temperature and deformation rate.

We have simulated Higgs' experiments numerically to infer friction constitutive properties. Our simulations utilize a spring-slider model of the triaxial apparatus. The friction law is based on the rate and state dependent law formulated by Ruina (1981), with assumptions regarding normal stress dependence following Rice and Gu (1983), and addition of temperature dependence as suggested by Chester (1988). The single state variable law is given by:

$$\mu = \tau/\sigma = \mu^* + a[\ln(V/V^*) + Q_a/RT] + b\Theta$$

and

$$d\Theta/dt = (-V/L)[\Theta + \ln(V/V^*) + Q_b/RT],$$

where a and b are the friction parameters describing the direct and evolution effect, and Q_a and Q_b are the apparent activation energies for these effects.

The relationship between velocity and stress for the spring slider model of the triaxial apparatus is given by:

$$d\mu/dt = k_\tau[(1-\mu\tan\alpha)^2/P_c](V_o-V) - [\mu(1-\mu\tan\alpha)/P_c]dP_c/dt,$$

where V_o is the load point velocity resolved onto the shear plane, α is the angle of the shear plane with the cylinder axis, k_τ is the stiffness of the apparatus in units of shear stress and shear displacement, and P_c is the effective confining pressure of the experiment. We solve this system of equations numerically using a Runge-Kutta integration scheme.

The transient frictional response observed in Higgs' dry and low-temperature, wet slide-hold-slide tests are sufficient to define approximately the friction parameters a, b and L. The data are described satisfactorily with a single state variable friction law. The analysis suggests that the ultra-fine quartz is slightly rate-strengthening at room temperature for both wet and dry conditions. At elevated temperatures and dry conditions the gouge is rate-weakening.

To fit both the microstructure observations and mechanical data from Higgs' wet experiments requires a two-mechanism constitutive law (Fig. 1 and 2). In this case we let $\mu = \mu^1 = \mu^2$ and $V = V^1 + V^2$ where superscripts represent the two mechanisms, and the behavior of each mechanisms is described with a friction law as shown above. The relaxation and transient friction behavior for experiments at 300, 450 and 600 °C are adequately described by this formulation. We find that the behavior of the cataclastic mechanism (dominant at lower temperatures and higher velocities) is rate weakening with $a-b = -.005$; this is similar but greater in magnitude than what we find for the dry, high temperature tests. The solution transfer mechanism (dominant at lower velocities and higher temperatures) is strongly rate-strengthening with $a-b = .03$. The apparent activation energy for the solution transfer mechanism as determined through this analysis is approximately 44 kJ/mol. This value is similar to that suggested by Rutter (1983) for pressure solution in quartz, and determined from experiments on diffusional crack healing in quartz by Brantly et al. (1990).

The findings from this phase of our project emphasize that frictional behavior in fault systems at water saturated and elevated temperature conditions is substantially different than at room temperature conditions. Our analysis suggests frictional behavior of quartz is most rate weakening at moderate temperatures, wet conditions, and at higher velocities. At lower velocities the quartz layers are strongly rate strengthening, and the absolute velocity at which the transition from weakening to strengthening occurs depends on the temperature.

Although Higgs' experiments can be modeled successfully using the temperature dependent friction law formulated previously by Chester (1988), the experiments are not sufficient to verify if this formulation is correct. Our current experiments involving temperature and rate stepping will address this question. We also will use stress relaxation experiments, as this can be a useful technique to investigate friction at low rates where solution transfer is promoted.

Reports

Chester, F. M. and N. G. Higgs, Friction constitutive behavior of wet and dry ultra-fine grained quartz gouge at elevated temperatures, AGU Spring Meeting, Baltimore, 1990.

References

Brantly, S. L., B. Evans, S. H. Hickman, and D. A. Crerar, Healing of microcracks in quartz: implications for fluid flow, Geology, 18, 136-139, 1990.

Chester, F. M., Temperature and rate dependence of friction for faults, EOS Trans. Am. Geophys. Union, 69, 471, 1988.

Higgs, N. G., Mechanical properties of ultra-fine quartz, chlorite and bentonite in environments appropriate to upper-crustal earthquakes, unpublished Ph.D. dissertation, Texas A & M Univ., College Station, TX, 1981.

Higgs N. G., and J. M. Logan, Frictional properties of ultrafine quartz in upper-crustal earthquake environments, EOS Trans. Am. Geophys. Union, 62, 1037, 1981.

Power W. L., and T. E. Tullis, The relationship between slickenside surfaces in fine-grained quartz and the seismic cycle, J. Struct. Geol., 11, 879-894, 1989.

Rice, J. R., and Gu, J. C., Earthquake aftereffects and triggered seismic phenomena, Pure Appl. Geophys., 121, 187-219, 1983.

Ruina, A. L., Slip instability and state variable friction laws, J. Geophys. Res., 88, 10,359-10,370, 1983.

Rutter, E. H., Pressure solution in nature, theory and experiment, J. Geol. Soc. London, 140, 725-740, 1983.

Rutter, E. H., and D. H. Mainprice, The effect of water on the stress relaxation of faulted and unfaulted sandstone, Pure Applied Geophys., 116, 634-654, 1978.

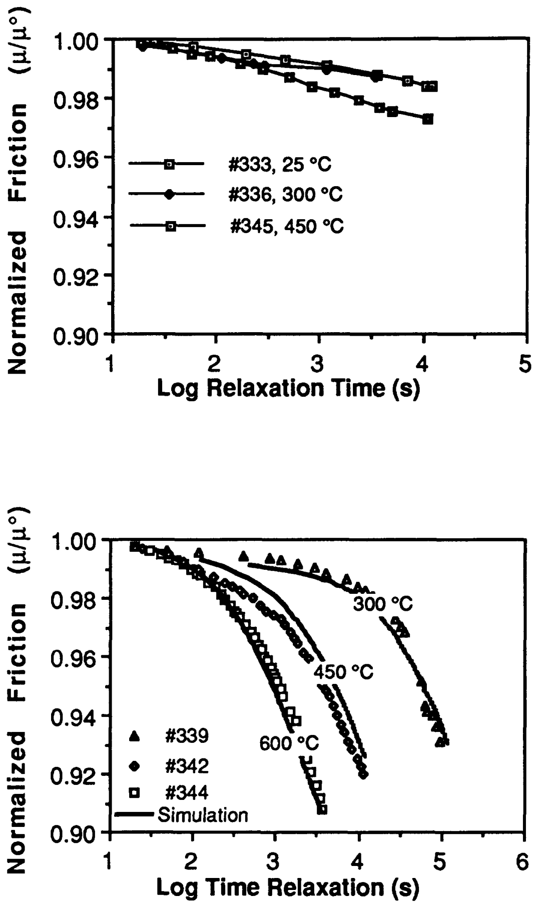

Fig. 1. Stress relaxation response for a) dry and b) wet ultra-fine grained quartz gouge as a function of temperature. Dry experiments show relaxation response for the cataclastic mechanism. The relatively greater relaxation seen in the wet tests at long hold times and high temperatures reflects the operation of an additional mechanism involving solution transfer. Simulation of relaxation in wet tests based on our friction constitutive model for the simultaneous and independent operation of the two mechanisms (see text) is shown by the solid lines.

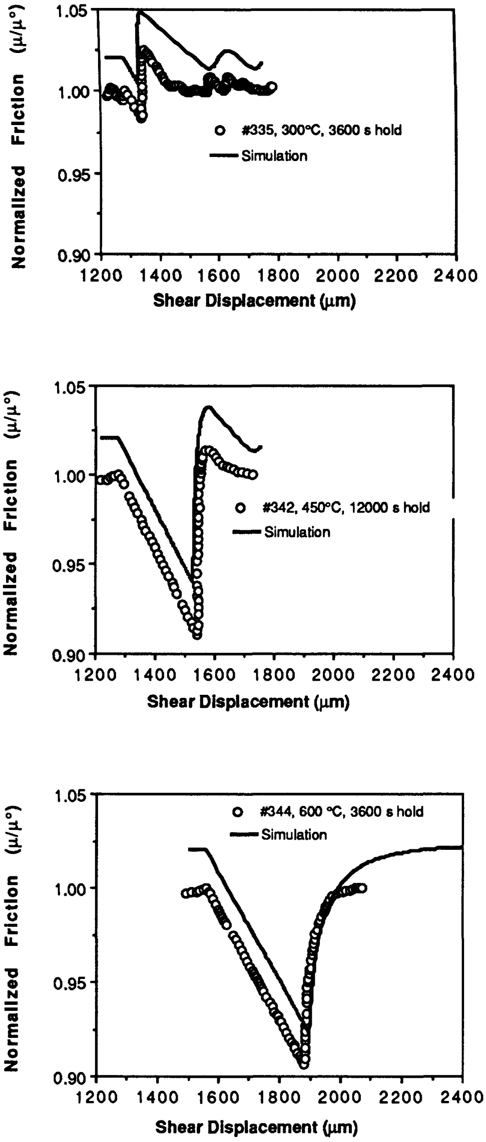

Fig 2. Representative variation in frictional strength as a function of displacement for Higgs' slide-hold-slide tests on wet quartz gouge at different temperatures. Simulations using the two-mechanism friction constitutive law are shown with solid lines, and are offset vertically for ease of comparison. This and previous figure show that the constitutive model can adequately describe the frictional behavior both during the relaxation (hold) and during subsequent sliding.

Mechanical Analysis of Large-Scale Folds Forming Above a Detachment

14-08-0001-G1700

Raymond C. Fletcher
Center for Tectonophysics
Texas A&M University
College Station, TX 77843
(409) 845-3251

Objective: For a class of earthquakes - e.g., the 1983 Coalinga Earthquake (M=6.7), the 1987 Whittier Narrows Earthquake (M=5.9)- the seismogenic faults occur within or are intimately related to large-scale folds which form above a shallowly-dipping basal detachment. The aim of the present study is to obtain a quantitative description of the mechanical environment of seismogenic faulting within large-scale folds, through theoretical modeling of fold initiation and growth, to apply the results to several natural structures, in order to test their value in interpreting the observed structure or the behavior in active fold growth, and to discuss the potential significance of the findings for the assessment of earthquake hazards.

Results: A study of the mechanics of sliding across a thrust ramp has been started to provide insight into the mechanics of "fault-bend folding", a process that is prominently employed in the interpretation and analysis of the form and kinematics of the fold and fault configurations implicated in fold-associated seismogenic faulting. Earlier studies (Berger and Johnson, 1980; Kilsdonk and Fletcher, 1989) obtained approximate solutions for stress and deformation in a deep isotropic viscous medium sliding across a thrust ramp. The method is accurate provided the thrust ramp has a dip of no greater than about 15°. The slip surface has been treated either as frictionless or as having finite sliding resistance at the thrust ramp (Berger and Johnson, 1980). In this study, we consider: (i) a frictionless detachment, (ii) a layer of finite thickness, H, (iii) an anisotropic viscous medium to account for the relative weakness of the rock mass in bed-parallel shear, (iv) the effect of gravity through the induced topography, (v) the decay of topography by surface processes, and (vi) quasi-static viscoelastic transients. Features (v) and (vi) have not yet been implemented.

A base level for the study of quasistatic transients is provided by first studying the steady-state. The parameters describing the behavior are (1) the ratio of layer thickness to ramp width, $T = H/2d$; (2) the ratio of lithostatic stress at the base of the layer to a stress associated with sliding, $S = \rho gH/[\eta_s(U/2d)]$, where U is the sliding velocity, and η_s is the viscosity in layer-parallel shear; (3), and the ratio of viscosity in layer-parallel shortening to η_s, $M = \eta_n/\eta_s$.

Steady-state surface profiles are shown in Figure 1. The upper profiles are for the case of an isotropic layer moving across a ramp whose width is equal to the layer thickness ($T = 1$); the variable parameter is $S = 0, 1, 2$, and 4. The ramp form and the horizontal mean position of the upper surface are shown at true scale. Surface profiles are shown at an exaggerated scale, and, for comparison, the ramp form itself is represented by a sharp corner. Thus, the form of the upper surface for the "zero gravity" case mimics the underlying ramp except that it is about twice as wide as the ramp itself, and is more rounded. For this case, the height in the upper-surface ramp form is indistinguishable from that of the ramp. The effect of gravity is to reduce the total topographic relief at the upper surface; this leads to a localization of topography above the ramp, where it is created. For $S = 1$ and 2, the spacing between the thrust ramp and the adjacent normal ramps is too small to prevent interaction, and the surface does not have a horizontal region between them. For $S = 4$ (e.g., $H = 10$ km, $U = 1$cm/a and $\eta = 10^{21}$ Pa-s) such regions are present, and an adequate approximation is achieved for an isolated ramp structure. The structure produced is a slightly asymmetric anticline whose maximum is nearly above the upper ramp corner. The layer is thinner downstream of the ramp by the ramp height, and so the mean horizontal elongation is $\varepsilon = 2\delta/H$. It is clear that in this case, the process more closely approximates thinning by extrusion through a frictionless die than "fault-bend folding". Fault-bend folding is a fair description of the process for the zero gravity case ($S = 0$) in the sense that the internal layering maintains uniform thickness. The zero-gravity case also corresponds to a limiting case in which the removal of topography by surface processes is so efficient as to keep the upper surface nearly planar. Although the surface would then be flat, the form of internal layer surfaces would closely approximate the ramp form. In the low-dip approximation used here, vertical axial planes cannot be distinguished from those that bisect the ramp-flat angles.

The fault-bend folding process assumes implicitly that the rock deforms chiefly in layer-parallel shear. Hence, it would be expected that a better approximation to it is attained if M is large. This is indeed the case, in that the zero-gravity surface profiles more closely approximate the ramp form. When gravity acts through the surface relief, the surface form is least changed in going from an isotropic layer to one that is anisotropic when the quantity $S^* = S/M$ is held constant (Figure 1, bottom). This implies that the important viscosity is that in layer-parallel shortening and extension, not that in layer-parallel shear.

The stress distributions within the layer, at the primary slip surface, and within the underlying substrate are pertinent to considerations of structural evolution and earthquake mechanics. For example, sites of high normal stress across the sliding surface are likely to be sites of asperities on frictional surfaces. The stress distribution within the layer may be though of as resulting from three contributions. (1) The stress distribution required by the presence of a thrust ramp is equivalent here to that for a frictionless indenter bounded on either side by frictionless rigid restraining surfaces. (2) The induced topography at the layer surface gives rise to a distribution of normal traction. (3) The background state of stress here may be considered lithostatic.

The normal stresses σ_{xx} and σ_{zz} are nearly equal along the detachment surface (Fig. 2); for a half-space ($T >> 1$) they would be equal. To the low-dip approximation used, the stresses σ_{xx} and σ_{zz} are parallel and normal to the detachment surface; the ramp and the surface topography is left off in a representation of the stress distribution (Figure 3). Both normal stresses are compressive along the ramp. The large compressive and tensile maxima just inside and outside the ramp corners are indicative of the stress singularities for an ideal sharp-cornered ramp. The positions of compressive maxima would be likely sites of asperities or of strong stress relaxation.

The stationary strain-rate field is illustrated (Figure 4) by plots of the components ε_{xx} and ε_{xz} for the case of an isotropic layer ($M = 1$, $T = 1$, $S = 0$). There is rounding of the ramp equal to that shown in Figure 3. Deformation is concentrated in the vicinity of the ramp corners. Rates of layer-parallel shearing are larger than those of layer-parallel shortening or extension. Except near the detachment surface, material extends parallel to layering as it moves above the ramp and shortens on either side. As M increases and the material becomes more anisotropic, the magnitude of ε_{xz} increase and that of ε_{xx} decreases.

<u>References:</u>

Berger, P., and A.M. Johnson, First order analysis of deformation of a thrust sheet moving over a ramp. Tectonophysics, 70, T9 - T24, 1980.

Kilsdonk, B., and R.C. Fletcher, An analytical model of hanging-wall and footwall deformation at ramps on normal and thrust faults, Tectonophysics, 163, 153 - 168, 1989.

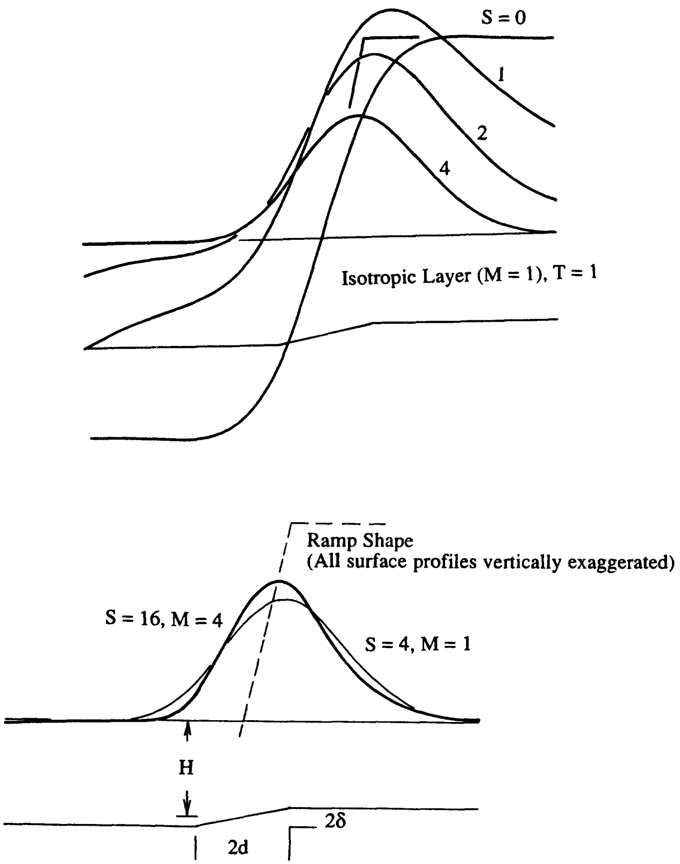

Figure 1. Steady-state surface profiles for the case of no erosion. The frictionless surface, across which the layer slides from left to right, has a planar thrust ramp. The portion of the slip surface shown is continued by reflection to the right and left, so that thrust ramps alternate with normal ramps. (Top) For $S = 1$ and 2, adjacent normal ramps and thrust ramps interact; for $S = 4$, the profile has planar segments upstream and downstream, and the structures at thrust ramps and normal ramps are isolated.

(Bottom) Comparison of structures for equal values of $S/M = \rho gh/\eta_n(U/2d)$, for $M = 1$ (thin line) and 4 (thick line). The anisotropic layer forms a narrower and somewhat higher anticline.

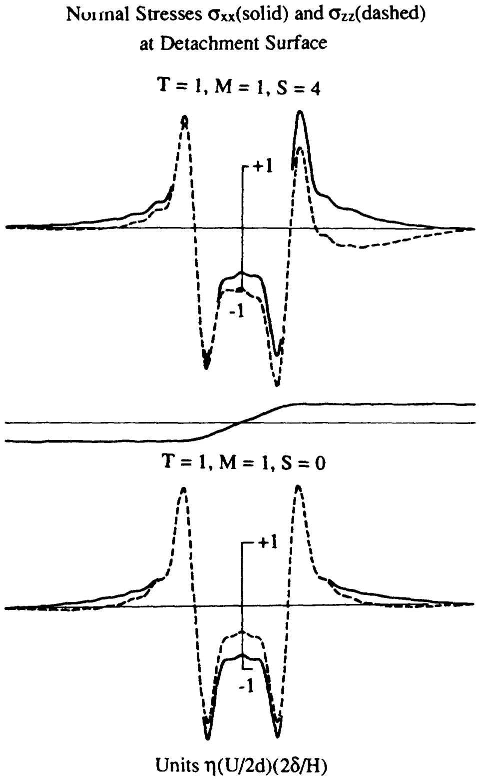

Figure 2. Normal stresses σ_{xx} and σ_{zz} at the detachment surface.

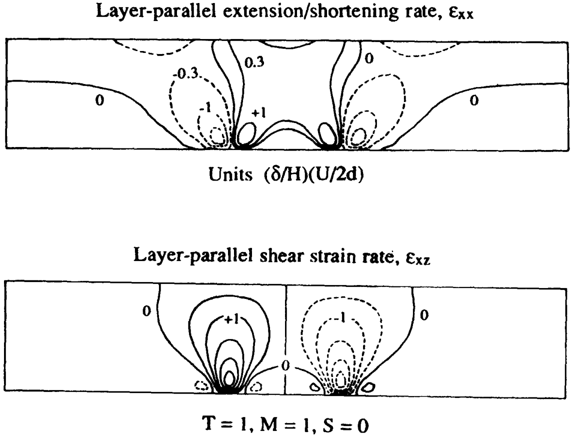

Figure 3. Deviatoric strain rates ε_{xx} and ε_{xz} throughout an isotropic layer (M = 1, T = 1, S = 0). Contours of ε_{xz} are at intervals of 0.5; contours of ε_{xx} are at 1, 0.3, 0, -0.3, -1, -1.8. Material moves through the stationary field of strain rate.

In Situ Stress Measurements

9960-01184

John Healy
Stephen Hickman
Branch of Tectonophysics
U.S. Geological Survey
345 Middlefield Road, MS 977
Menlo Park, CA 94025
415/329-4848

Investigations

Funding in this project has not been provided to conduct any new field measurements of in situ stress. During the last six month we worked on the reevaluation of data collected earlier on Yucca Mountain. Two oral reports on our Yucca Mountain stress measurements were presented at conferences in Death Valley, CA and Denver, CO. There are two technical reports in review and a third comprehensive data report is in preparation. Stephen Hickman is currently writing a review article on in situ stress for the 1990 IUGG U.S. National Report on Tectonophysics. We conducted borehole televiewer logging in a 3.2-km-deep oil exploration well that was recently drilled in the western Mojave Desert near the San Andreas fault. Although the high-density borehole fluids present did not permit a high-quality log to be obtained from this well, we are currently exploring options for taking over and cleaning out this well to allow additional testing. We have submitted a proposal for in situ stress and hydrologic measurements in a well drilled into the New Madrid Seismic Zone and are preparing an inventory of deep oil-exploration wells in this area that may be reopened for in situ stress measurements and borehole televiewer logging in the future.

Results

The results of this work reinforces our earlier conclusion that the stresses measured on Yucca Mountain are reflecting present day tectonic extension in this region and that the measured stresses are close to the values at which failure may occur.

Reports

(A) Baumgartner, J., Zoback, M.D., Healy, J., and O'Neill, B., 1989, A detailed interpretation of the Cajon Pass hydraulic fracturing stress measurements (abs.): EOS, Transactions of the American Geophysical Union, v. 70, no. 15, p. 480.

(A) Zoback, M.D. and Healy. J.H., 1989, Overview of in-situ stress measurements in the Cajon Pass scientific drillhole to a depth of 3.5 km (abs.): EOS, Transactions of the American Geophysical Union, v. 70, no. 15, p. 480.

(O) Healy, J.H., 1990, In situ stress measurements and the stability of Yucca Mountain, submitted.

Pressure Solution, Crack Healing and Crustal Stress

9960-04543

Stephen H. Hickman
Branch of Tectonophysics
U.S. Geological Survey
345 Middlefield Rd., MS 977
Menlo Park, CA 94025
(415) 329-4807

Investigations

1. To better understand the processes controlling the physical and temporal evolution of physical properties in the earth (e.g. permeability, seismic velocities, and density), the mechanisms and kinetics of solution-transport creep, and the micromechanics of friction and fault strengthening, I have begun a detailed experimental study of pressure solution and crack healing under load in simple quartz/water systems. This study will employ experiments with single crystals in well-controlled model geometries and experiments on polycrystalline aggregates (with Brian Evans at M.I.T.)

2. Although knowledge of the pathways and rates for fluid migration in the earth's crust is critical to a full understanding of such diverse phenomena as the mechanics of rock deformation and faulting, metamorphic reaction kinetics, and heat and mass transfer by circulating fluids, the permeabilities of rocks at depths of greater than a few kilometers are almost completely unknown. To obtain more accurate information on rock matrix permeability at depth, and to quantify the extent to which crack healing and sealing are occurring in the mid to upper continental crust, I have initiated a project to measure permeabilities and conduct quantitative microstuctural observations on cores recovered from the 12-km-deep Kola Deep Well in the U.S.S.R. (with David Lockner and James Byerlee at the U.S.G.S. in Menlo Park).

3. Although borehole breakouts have been widely used to study in-situ stresses, the extent to which variations in breakout geometry within a given well reflect variations in rock strength and the extent to which they reflect real fluctuations in the in-situ stress field is largely unknown. To improve our understanding of the mechanics of breakout formation, I have initiated a cooperative U.S./Soviet program to study the distribution, orientation, and morphology of breakouts from the Kola Deep Well using oriented four- and eight-arm caliper logs and strength measurements on cores obtained by Soviet scientists.

4. I am continuing to analyze and model the processes of crack healing and asperity adhesion in the solution-transport regime using data from experiments already conducted on halite single crystals.

Results

1. I have completed design and selection of the high pressure/temperature hydrothermal vessel and associated equipment for the single-crystal pressure solution and crack healing experiments and have submitted these items for competitive bidding and purchasing.

2. We have conducted constant flow-rate permeability measurements on three core samples recovered from the Kola well at depths of 11.4 to 12.0 km. Pore pressures used in these experiments (calculated assuming hydrostatic equilibrium with the ground surface) ranged from 112 - 117 MPa and effective confining pressures ($P_{eff} = P_{conf} - P_{pore}$) ranging from 10 - 400

MPa. The resulting permeabilities varied from approximately 25 μDa at a P_{eff} of 10 MPa to 0.1 nDa at a P_{eff} of 300 MPa. By comparison, Bayuk *et al.* [1986] reported minimum permeabilities of 8 to 100 μDa at effective confining pressures of up to 120 MPa, using cores recovered from depths of 3.7 - 9.9 km in the same well. Although the pore fluid pressure at depth in the Kola Well is not well constrained, by assuming that the *in-situ* pore pressure follows the hydrostat, and using a confining pressure equal to the calculated overburden stress (317 - 333 MPa), our measurements, if taken at face value, indicate *in situ* matrix permeabilities of 0.5 to 12 nDa at effective confining pressures appropriate to depths of 11.4 to 12.0 km. These values are 3 to 4 orders of magnitude lower than Bayuk *et al.*'s results, due primarily to the higher effective confining pressures used in our measurements. Furthermore, if our estimates of *in situ* fluid pressures are correct, then the irreversible stress-relief cracking that appears to have occurred during sample retrieval requires that our permeabilities be interpreted as upper bounds on the *in situ* matrix permeability. The strong pressure dependence of permeability observed in our samples illustrates the importance of measuring permeability under *in situ* pressures in order to obtain meaningful bounds on the matrix permeabilities at these great depths.

3. I have completed planning of a trip to the Kola Deep Well and three other deep wells in the Soviet Union to be conducted in July, 1990. During this trip, I will examine data collected from these wells, obtain copies of geophysical logs and laboratory data necessary for the analysis of breakouts from the Kola Well (and other wells, if appropriate), and obtain approximately 20 core samples from throughout the Kola Well to be used in permeability measurements and microstructural analyses at the U.S.G.S. in Menlo Park. At this time, I will also negotiate details of cooperative research projects in borehole geophysics and physical properties measurements and scientific personnel exchanges to be conducted in upcoming years.

References Cited

Bayuk, E. I., B. P. Belikov, L. I. Vernik, M. P. Volarovitch, Yu. I. Kuzxetsov, G. E. Kuzmenkova, and N. N. Pavlova, Rock density, porosity, and permeability, *in*: Ye. A. Kozlovsky (ed.), The Superdeep Well of the Kola Peninsula, pp. 332-338, Springer-Verlag, Berlin, 1987.

Reports

Brantley, S. L., B. Evans, S. Hickman, and D. Crerar, Healing of microcracks in quartz: Implications for fluid flow, *Geology*, *18*, 136-139, 1990.

Hickman, S., and B. Evans, Experimental pressure solution in halite, 1: The effect of grain/interphase boundary structure, *J. Geol. Soc. London*, in press, 1990.

Hickman, S., and B. Evans, An experimental study of intergranular pressure solution and sintering using halite single crystals, *in*: Proceedings of SEG Workshop on Permeability, Fluid Pressure and Pressure Seals in the Crust., submitted, 1990.

Lockner, D., S. Hickman, J. Byerlee, V. Kuksenko, A. Ponomarev, and A. Sidorin, Laboratory-Determined Permeability of Cores from the Kola Deep Well, USSR, *in*: Proceedings of SEG Workshop on Permeability, Fluid Pressure and Pressure Seals in the Crust., submitted, 1990.

EXPERIMENTAL ROCK MECHANICS

9960–01180

Stephen H. Kirby
Branch of Tectonophysics
U.S. Geological Survey
345 Middlefield Road, MS/977
Menlo Park, California 94025
(415) 329-4847

Investigations

We investigated polymorphic phase transformations under deviatoric stress in our laboratory and have sought to understand why their inelastic behavior varies so greatly from mineral to mineral.

We have successfully done sliding experiments on dunite under controlled hypothermal conditions.

A low–volume moist–argon pore–pressure system is under construction to investigate the fracture of dunite at high gas pressure and high temperature, the enviornment of intermediate–depth earthquakes under the island of Hawaii.

Results

A number of important solid–state phase transformations have now been investigated under deviatoric stress. Only three, the ice I → II, the tremolite → amorphous phase and the olivine → spinel transformation in Mg_2GeO_4 have displayed the anomalous faulting that is a promising candidate for the faulting mechanism of deep earthquakes. Recent work by Brad Hacker on the disproportioning reaction albite → jadeite + quartz and other transformations involving simple polymorphism (such as calcite → aragonite and quartz → coesite) that have been previously studied by others failed to show any evidence for anomalous faulting. Other than detailed differences in the crystal structures of these minerals, the only distinctive features of the transforming minerals that fault is that fault is that they have somewhat larger volume changes and, more importantly, have much larger latent heats of transformation. Both factors are important in the microphysics of growth of inclusions of the high–pressure, high–density phases. The albite breakdown reaction has a large volume change (−15.6%) and a large latent heat and yet does not show anomalous faulting. This finding suggests that only simple polymorphic phase changes with large volume reductions and evolved latent heats will produce transormation faults. If this phenomenology applies to the phase changes occurring in deeply subducting lithosphere, then the direct transformation of metastable olivine to spinel is the best candidate for transformation faulting in the deep earthquake environment. A **Science** article is in preparation describing our experiments and conclusions concerning the physical mechanism of deep earthquakes.

Preliminary experiments at 400 °C on the sliding resistance of dunite under a controlled pore pressure of 100 MPa and a confining pressure of 500 MPa were successful in reproducing the low sliding resistance in previous sealed tests where the pore pressure was not controlled. Also, evidence of active hydrothermal alteration on the sliding surface was found, again consistent with the earlier sealed tests. These recent results suggest an important role of retrograde metamorphic reactions in maintaining low shear stresses along crustal faults.

The gas pore–pressure system and new high–temperature furnace for fracture experiments on dunite at high pressures and temperatures are under construction and expected to be completed this summer. We will then be in a position to investigate the brittle faulting under conditions that simulate those found at intermediate depth beneath the island of Hawaii.

Reports

Kirby, S.H., Hemingway, B.S. and Lee, R., 1990, Anomalous fracture and thermal behavior of hydrous minerals, *AGU Geophysical Monograph* (in press).

Kronenberg, A.K., Kirby, S.H., and Pinkston, J., 1990, Basal slip and mechanical anisotropy of biotite, *Journal of Geophysiccal Research*, accepted.

Stern, L.A., Kirby, S.H., and Durham, W.B., 1989, Synthesis and deformation of CH_4-Clathrate for applications to the icy moons of the outer planets, *Trans. AGU*, v. 70, p. 1364.

Durham, W.B., Kirby, S.H., and Stern, L.A., 1989, Flow of NH_3–H_20 ice under planetary conditions, *Trans. AGU,* v. 70, p. 1364.

Dick, H.J.B., Meyer, R.S., Bloomer, S., Kirby, S.H., Stakes, D., and Mawer, C., 1989, Lithostratographic evolution of an *in situ* section of oceanic layer 3, Initial reports of the *Ocean Drilling Program*, v. 118, Part B, in review.

Rock Deformation

Eugene C. Robertson
Branch of Geologic Risk Assessment
U.S. Geological Survey
922 National Center
Reston, VA 22092
(703) 648-6792

Investigations

Correlation of the ratio of displacement to thickness of crushed zone on a fault to the compressive strength of the wall rock type may be useful in applying internal and sliding friction laws to earthquake prediction.

Results

In Figure 1, 76 displacement $\underline{d}$ points are plotted against thickness $\underline{t}$ of gouge and breccia measured on faults in mines predominantly (Robertson, 1983, 1987). The data could be grouped and regression lines fitted according to five rock types by

$$\underline{t} = a\underline{d}^{b} \qquad (1)$$

where a and b are constants. The variation in slopes from the linear diagonal (b = 1) is inherent in the variation of mechanical abrasion with petrography when selecting only by common rock names. Data from Otsuki (1978) on sandstone are also shown. Conceivably, $\underline{d}$, $\underline{t}$, and fault length and depth could be used to calculate work done to comminute fault walls, breccia and gouge, which could be compared with energy release by creep or an earthquake. The $\underline{t}$ values from the five regression lines at $\underline{d} = 1$ m are plotted in Figure 2 against the corresponding rack strengths $\underline{S}$ (Handin, 1966) at 50 MPa confining pressure. The forced line of negative linear slope fits the inverse equation

$$\underline{t} = c/\underline{S} \qquad (2)$$

where c = 7, with $\underline{t}$ in m, $\underline{S}$ in MPa.

From a review of sliding friction at low normal stress σ_n (< 100 MPa) by Byerlee (1978), the values of the coefficient of friction μ for four rocks are plotted in Figure 3 against $\underline{S}$ for those rocks (Handin, 1966) at 50 MPa confining pressure. The initial μ values are directly proportional to $\underline{S}$ values of these rocks

$$\mu = g\,\underline{S} \tag{3}$$

where $g = 10^{-3}$ MPa^{-1}. Coefficients of maximum friction are about 25 percent higher but are spread about the same for these rocks. At high normal stress (> 200 MPa) there are smaller differences in μ among the rock types. The constants c and g are only poorly constrained by the data in Figures 2 and 3.

These results may eventually be found applicable to the criteria for compressive and friction strength and help predict creep or earthquake failure of faults. Failure on a fault through intact rock is given by the Coulomb-Mohr criterion of strength in compression

$$\tau_c = \tau_0 + \sigma_n \tan\phi = 1/2\ \underline{S} \tag{4}$$

where τ_c is the shear stress at failure, τ_0 is the initial cohesive strength, σ_n is the effective normal stress across the fault plane, and ϕ is the internal friction angle. The law for friction strength by sliding is

$$\tau_f = \mu\ \sigma_n \tag{5}$$

where τ_f is the shear stress in sliding friction and σ_n is effective normal stress on the fault.

The relations of $\underline{d}$ and $\underline{t}$ with $\underline{S}$ and μ in Equations 1, 2, and 3 (Figs. 1, 2, and 3) are only approximate because of the uncertain petrography and physical properties and their shallow depth of observation. After thorough investigations, correlations of $\underline{d}$ and $\underline{t}$ with τ_c, τ_f, and μ eventually could be made from estimates of ambient shear τ and normal stress σ_n as they approach failure, using the strength laws of compressive and sliding friction. Approach of τ and σ_n to failure can be measured from related changes in wave velocities and attenuation (Robertson, 1975). Confining and pore pressure need to be accounted for, of course. Useful studies of stress level and strength limits could be made in an appropriate patch on a fault, a target where a seismic gap has been located for predicting seismic or aseismic energy release.

References cited:

Byerlee, J. D., Friction of rock, in Rock Friction and Earthquake Prediction, edited by J. D. Byerlee and Max Wyss, Birkhauser, Basel, pp. 583-991, 1978.

Handin, John, Strength and ductility, in Handbook of Physical Constants, edited by S. P. Clark, Jr., Geol. Soc. Amer. Memoir 97, pp. 223-289, 1966.

Otsuki, Kenshiro, On the relationship between the width of shear zone and the displacement along fault, J. Geol. Soc. Japan, 84, pp. 661-669, 1978.

Robertson, E. C., Multiple failure model of earthquakes, Amer. Geophs. Union EOS, 56, pp. 448, 1975.

Robertson, E. C., Relationship of fault displacement to gouge and breccia thickness, Mining Engineering, Am. Inst. Min. Met. Petrol. Engr., New York, 35, 1426-1432, 1983.

Robertson, E. C., fault breccia, displacement, and rock type, in Rock Mechanics: Proc. 28th Symp. Rock Mech., edited by I. W. Farmer et al., A. A. Balkema, Boston, pp. 65-72, 1987.

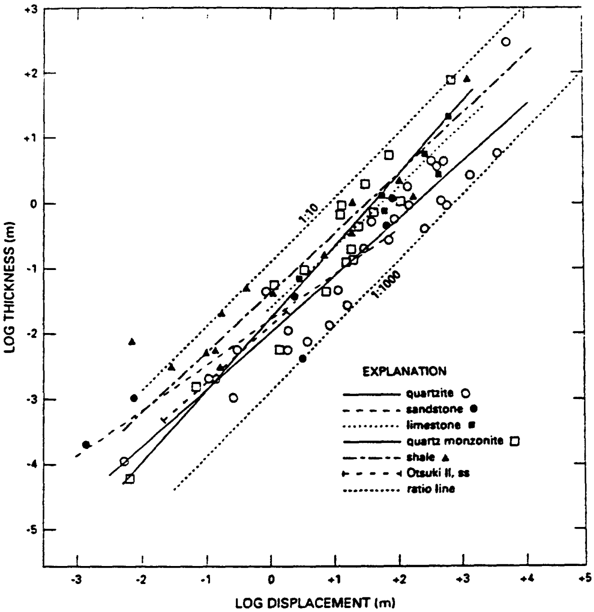

Figure 1. Dependence of thickness of gouge and breccia on displacement of faults in five rock types.

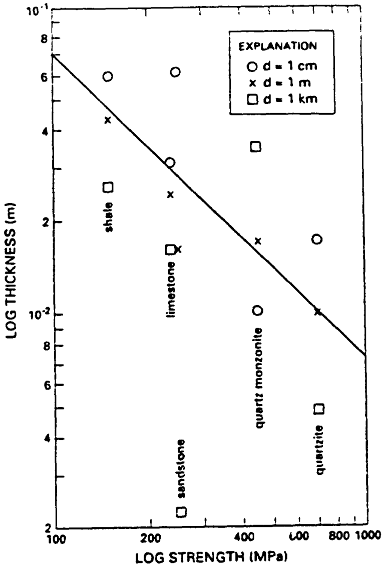

Figure 2. Thickness of crushed zone of faults in five wall rocks versus compressive strength.

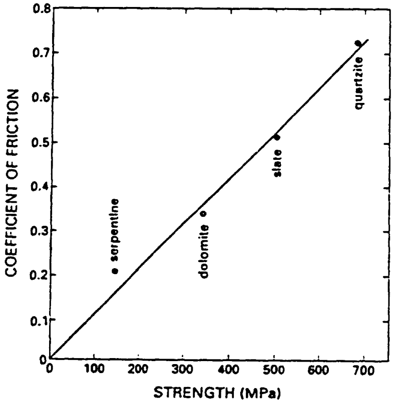

Figure 3. Initial friction coefficient versus compressive strength of four rocks.

Heat Flow and Tectonic Studies

9960-01177

John H. Sass
Branch of Tectonophysics
U.S. Geological Survey
2255 North Gemini Drive
Flagstaff, AZ 86001
(602) 527-7226
FTS: 765-7226

Arthur H. Lachenbruch
Colin F. Williams
Branch of Tectonophysics
U.S. Geological Survey
345 Middlefield Road
Menlo Park, CA 94025
(415) 329-4879/4881
FTS: 459-4879/4881

Investigations:

A geothermal study of the Santa Maria Basin and environs is continuing. Thirty-three idle oil wells have been logged, and samples have been collected for thermal conductivity determinations. Interpretations of the temperature profiles in terms of lithostratigraphy and active tectonics are under way.

Precision temperature monitoring in the USL-Pearson well near Parkfield is continuing. Monitored temperatures are stable to ±0.0002°C and show little variation in temperature over the past six months.

A final temperature log was obtained in the Cajon Pass well prior to an additional round of hydrologic testing. Two manuscripts for the JGR Cajon Pass special volume will be submitted to the journal early in the next report period.

Temperature data from DOE research well LVF 51-20 in Long Valley have been analyzed and thermal conductivity measurements on nine core samples have been completed.

Software for the new data-acquisition system is in the final phase of development.

Results:

Santa Maria Basin. The interdisciplinary USGS study of the Santa Maria Province, California, provides an opportunity for the coordination of traditional heat-flow investigations with concurrent stratigraphic and tectonic studies. To date, the Geothermal Studies Project has logged 19 idle oil wells in the onshore Santa Maria Basin, 5 wells in the offshore Santa Maria Basin, 3 wells in the onshore Ventura Basin, and 6 wells in the Cuyama Basin. These logs provide thermal data from the Guadalupe, Santa Maria Valley, Cat Canyon, Orcutt Hill, Lompoc, Zaca, Point Conception, Point Arguello, and South Cuyama oil fields.

Figure 1 presents a typical temperature and gradient plot from the Santa Maria Valley. The figure reveals a conductive thermal regime below a depth of 1700 feet, with gradients in the lower section of the well averaging approximately 50°C/km. The upper section displays a distinctive curvature characteristic of temperature logs from low-lying areas of the Santa Maria Basin. The curvature probably results from the combined effects of recent sedimentation and coastal uplift. Quantitative modeling of these effects is under way.

Parkfield. The Project's Long Term Temperature Monitor (LTTM) has been installed in the USL-Pearson 1B (PRSN) well, located approximately 1 mile west of the San Andreas fault and 15 miles northwest of Parkfield. Data collected over the past six months confirm the ±0.2 mK (±0.0002°C) resolution capability of the monitor. Except for some early problems with rain-related disturbances to the electronics, temperatures at a depth of 2600' have remained remarkably stable. It is expected that activity along the San Andreas fault near Parkfield will generate an identifiable thermal-hydrologic signal that could provide premonitory information and possibly data on strain-heating in the fault zone.

Cajon Pass. The temperature-depth-time record of 22 months post drilling to 3.5 km at Cajon Pass is one of the most complete and accurate records of the decay of drilling disturbances to these depths ever assembled (Figure 2). The temperature profiles emphasize the large amount of time required to re-establish pre-drilling temperatures after a long and complex drilling history. The curve labeled "Equil" (Figure 2) was calculated from extrapolation of the time-temperature relation for the previous four curves. The conspicuous structure in the gradient (Γ) curves centered on a depth of 2 km reflects the long-lived effects of lowering the water level in the well by 600+ m after setting casing to a depth of 1.8 km at the end of both the first and second phases of drilling.

Long Valley. Extrapolation of four post-drilling logs obtained between October 3 and November 14, 1989, results in an "equilibrium" temperature profile that is concave upward between the depths of 250 and 550 meters (Figure 3). This interval penetrated rocks of fairly uniform composition indicating that the temperatures are affected by recharge. The cored section between about 790 and 830 meters has an estimated thermal gradient of 53°C per kilometer and the harmonic mean of 20 determinations of thermal conductivity is 2.26 ± 0.13 (95% confidence limits). The resulting heat-flow estimate of 120 mW m^{-2} is typical of rapidly extending portions of the Basin and Range province but is a factor of 3 to 5 lower than estimates of the total energy flux from the caldera.

Data Acquisition and Reduction. Data-acquisition software for the PC-based logging system is nearly finished. Data reduction on the IBM PC system is established, and the Tektronix system in the lab/office has been retired. The Tektronix data-acquisition system in the logging truck is still active pending debugging of device interfaces and complete bench and field tests of the PC-based system.

Reports:

Lachenbruch, A. H., and McGarr, A., Stress and heat flow on the San Andreas fault: *U.S. Geological Survey Professional Paper,* in press, 1990.

Lachenbruch, A. H., and Morgan, P., Continental extension, magmatism, and elevation: Formal relations and rules of thumb: *Tectonophysics,* v. 174, p. 39-62, 1990.

Langseth, M. G., Lachenbruch, A. H., and Marshall, B. V., Geothermal observations in the Arctic region: *Decade of North American Geology,* in press, 1990.

Osterkamp, T. E., and Lachenbruch, A. H., Current thermal regime of permafrost in Alaska and the predicted global warming in *Proceedings, Workshop on "Climatic Change and Permafrost: Significance to Science and Engineering":* American Society of Civil Engineers, in press, 1990.

Osterkamp, T. E., and Lachenbruch, A. H., 1990, Thermal regime of permafrost in Alaska and predicted global warming: *Journal of Cold Regions Engineering,* v. 4, p. 38-42.

Sass, J. H., Lachenbruch, A. H., Moses, T. H., Jr., and Morgan, Paul, Heat flow from a scientific research well at Cajon Pass, California: [Approved by the Director on 3/14/90], to be published in *Journal of Geophysical Research,* 1990.

Williams, C. F., and Anderson, R. N., Thermophysical properties of the Earth's crust: *In situ* measurements from continent and ocean drilling: *Journal of Geophysical Research,* in press, 1990.

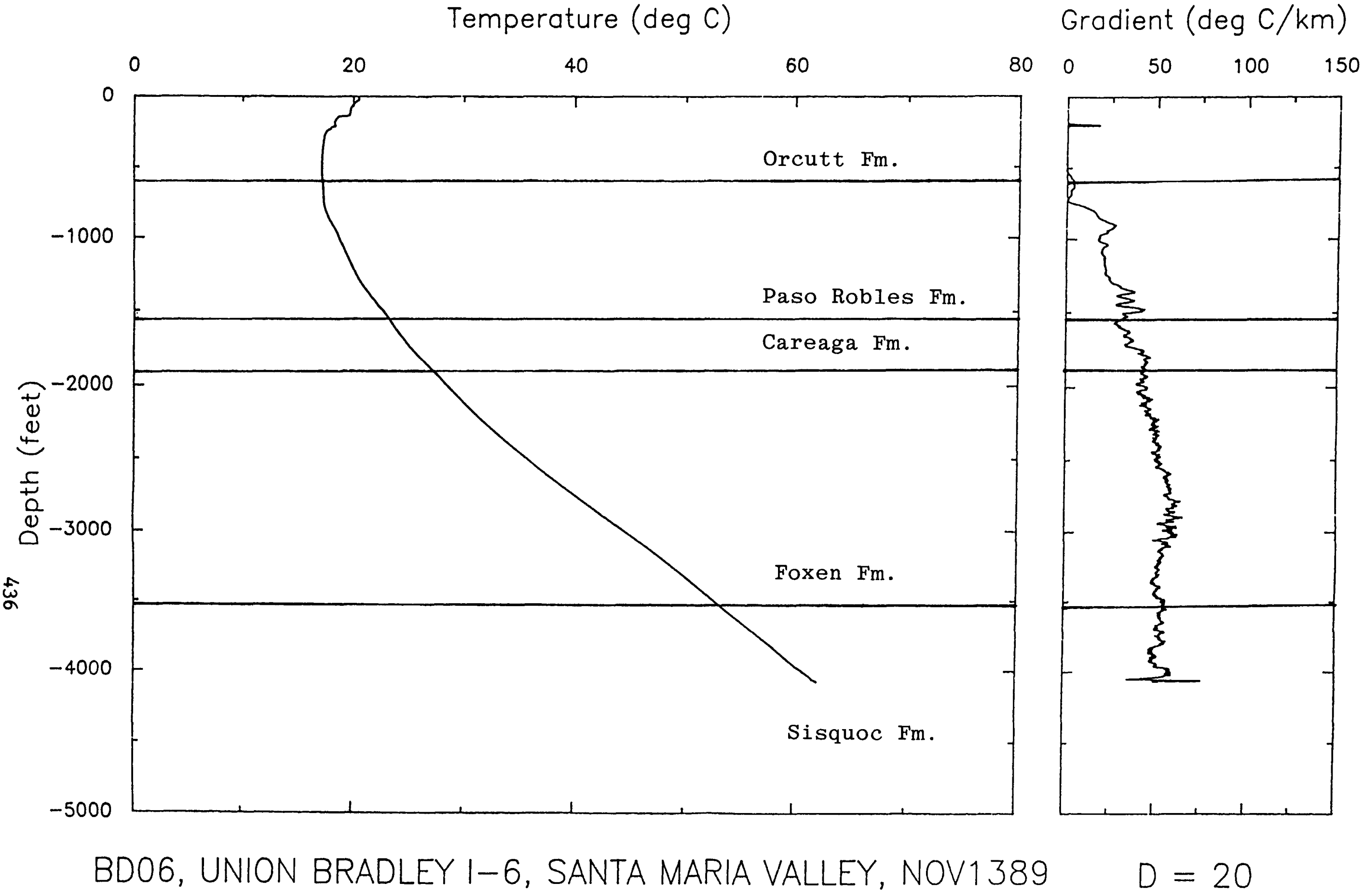
Temperature (deg C)
0
20
40
60
80
Gradient (deg C/km)
0
50
100
150
Depth (feet)
0
-1000
-2000
-3000
-4000
-5000
Orcutt Fm.
Paso Robles Fm.
Careaga Fm.
Foxen Fm.
Sisquoc Fm.
BD06, UNION BRADLEY I-6, SANTA MARIA VALLEY, NOV1389
D = 20

Figure 1

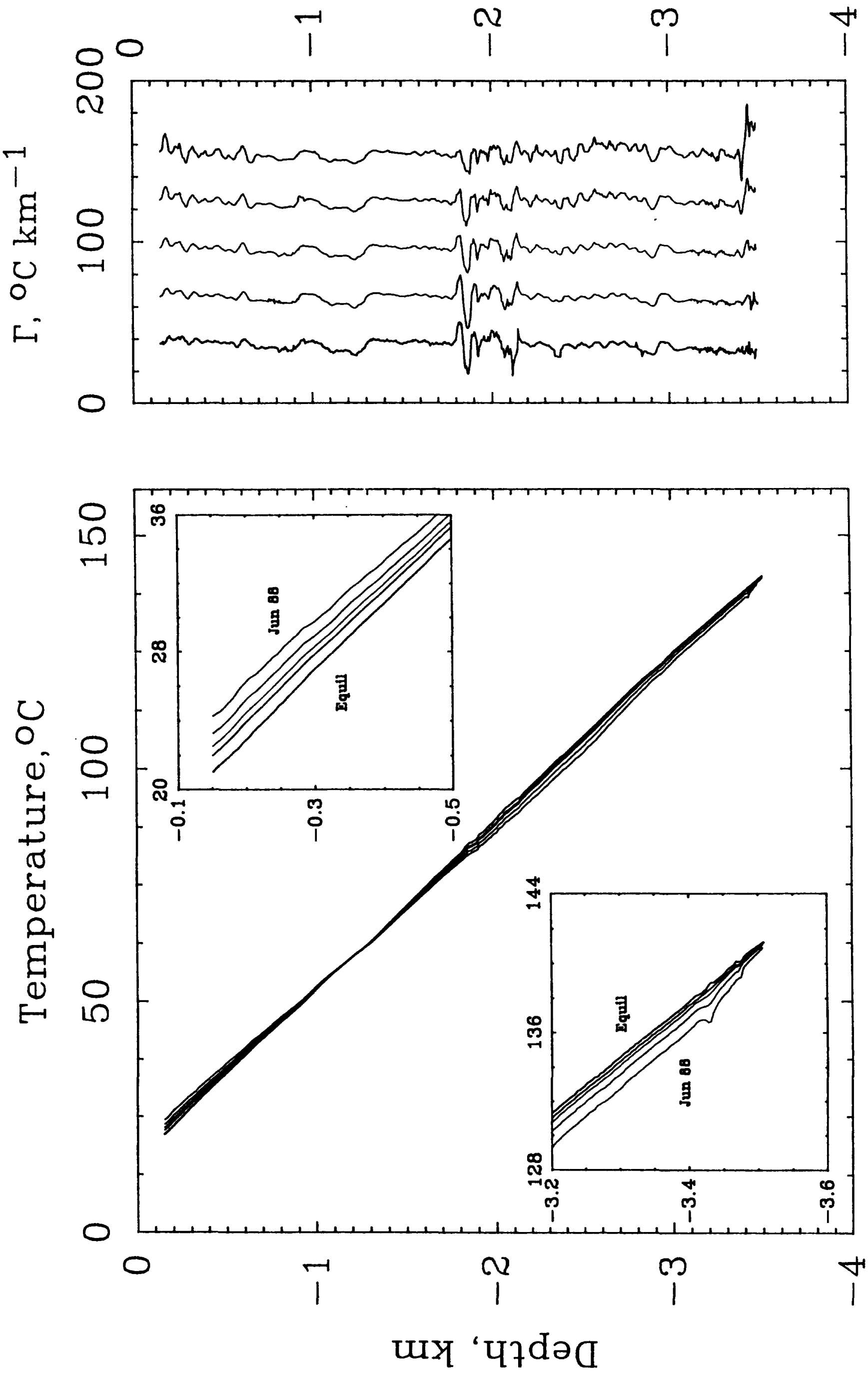
Temperature, °C
0
50
100
150
Depth, km
0
−1
−2
−3
−4
20
28
36
−0.1
−0.3
−0.5
Jun 88
Equil
128
136
144
−3.2
−3.4
−3.6
Equil
Jun 88
Γ, °C km−1
0
100
200
0
−1
−2
−3
−4

Figure 2

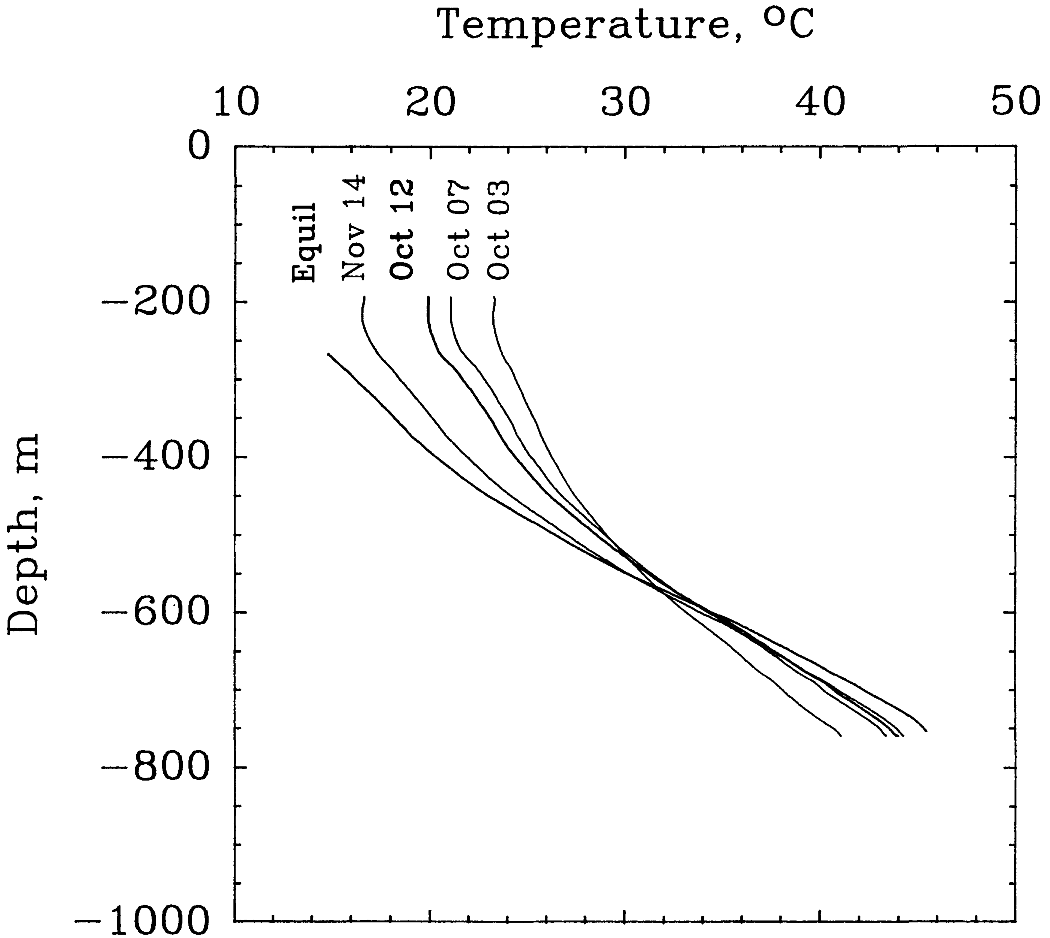
Temperature, °C
10
20
30
40
50
0
-200
-400
-600
-800
-1000
Depth, m
Equil
Nov 14
Oct 12
Oct 07
Oct 03

Figure 3

Micromechanics of Rock Friction

Grant No. 14-08-0001-G1668

Christopher H. Scholz
Ronald L. Biegel

Lamont-Doherty Geological Observatory
of Columbia University
Palisades, New York 10964
(914) 359-2900 Ext. 360

We are continuing to develop a theory to predict the frictional and wear properties of rock from topography data. From 1989 to present our project had three objectives: first, acquiring high-quality friction data for rock undergoing shear; second, modeling and testing frictional data on the initial slip stage; and lastly, determining an empirical law for wear of rock surfaces. Progress has been made in all three areas as discussed below.

1) A suite of experiments was performed in a rotary shear apparatus. Hand-lapped Westerly granite surfaces were prepared with #60 and #120 grit, roughnesses were measured with a profilometer. Experiments were run at normal stresses of 10, 15, and 20 MPa and slip velocities of 0.1 microns s^{-1} to total distances of several centimeters. Displacements were corrected for the deformation of the apparatus and sample. The first 200 microns of slip provided high-resolution displacement data to ±0.02 microns while slip distances of several centimeters were reached with somewhat lower displacement resolution.

The frictional properties of contacting rock surfaces were observed to evolve with displacement through three distinct phases. Stage one began the instant a shear load was applied and continued through the first few microns of displacement. The rock surfaces were observed to have a finite shear compliance from the start, and runs with smoother surfaces and/or higher normal stress had higher initial stiffness and strength at first yield. Shear stress normalized by normal stress increased with displacement from zero to 0.30 to 0.35. This first stage was successfully modeled using elastic contact theory as described below. A second stage began once a fully sliding surface was established and continued for 200 to 300 microns. The rougher surfaces exhibited positive slip hardening. We believe this is due to the onset of asperity interlock, ploughing and wear. The smoother surfaces showed less slip hardening than rough. Beyond 300 microns, relatively stable frictional properties characterized a third stage.

2) We developed a constitutive model which predicts during the early stages of frictional sliding the mechanical properties of two rough surfaces in contact under shear with constant normal load. The model uses the normal closure algorithm of Brown and Scholz (1985) to calculate the initial conditions imposed on individual asperities by the normal stress. The shear deformation is modeled by approximating the behavior of each contacting asperity with the elasticity solutions of Mindlin and Deresiewicz (1953). These solutions describe the development of slip at the contacts, a phenomenon which begins immediately upon application of the shear load.

The macroscopic mechanical properties of the surface are computed by imposing a shear displacement and summing the forces exerted by all the individual asperities. The micromechanical properties of each contact are a function of its geometry and elastic constants, the local normal load, and an asperity scale coefficient of friction. Initially, at the scale of an individual asperity, application of a finite shear displacement propagates an area of partial slip inward from the edge of the contact annulus until eventually the entire contact is fully sliding. We find that the presence of partial slip is the dominant phenomenon controlling the deformation of the contacting asperity and is highly dependent on the local normal load and size of the contact. As the shear load increases, more and more contacts begin to slip, with the contacts having lower local normal load sliding first.

The model was tested with experiments on lapped surfaces of Westerly Granite having a variety of surface roughnesses and normal loads (10, 15, and 20 MPa). Topography data from surface profiles constrained numerous geometric parameters in the model. The only free variable was an "asperity scale" coefficient of friction. We found that a coefficient of friction between 0.30 and 0.36, which is independent of normal load and surface roughness, gives good agreement between the model and the data. The model predicts the macroscopic shear compliance and friction for the first few microns of sample slip. It also predicts the effect of surface roughness and normal load on the initial friction curves. Additionally, it describes the first yield point of the friction curve which may correspond to a gradual transition from elastic deformation and partial slip of asperity contacts to a state of fully sliding contacts. Once a large population of contacts are fully sliding, the model under-estimates the frictional strength, indicating that displacement strengthening mechanisms have begun to operate.

3) Our experimental data shows that wear loss during frictional sliding is a function of normal stress on the sliding surface and the initial roughness of the surface. For a given normal stress and initial roughness, the wear loss-sliding displacement relationship indicates that the wear rate is initially higher, but then gradually decreases to a constant value. The wear process results in an evolution of the surface topography. Based on a model of two rough surfaces in elastic contact, a numerical model can describe wear in two different stages: a transient stage and a steady state stage. In the transient stage, the wear mechanism is interpreted as the shearing off of interlocking asperities. The total contribution by this mechanism is proportional to the overlapping volume of the asperities which is related to the initial roughness as well as the normal stress. In the steady state stage, wear is almost linear with displacement and the wear rate is proportional to the area of real contact between the two rough surfaces. The wear curves predicted by this model are in good agreement with the experimental results.

References

Brown, S. R. , and C. H. Scholz, Closure of random elastic surfaces in contact, J. Geophys. Res., 90, 5531-5545 (1985).

Mindlin, R. D., and H. Deresiewicz, Elastic spheres in contact under varying oblique forces, J. Appl. Mech., 20, 327-344 (1953).

Systems Analysis of Geologic Rate Processes:
SPACE-TIME MODELS FOR CALIFORNIA EARTHQUAKES

9980-02798

Herbert R. Shaw and Anne E. Gartner
Branch of Igneous and Geothermal Processes, U. S. Geological Survey
MS-910, 345 Middlefield Road, Menlo Park, CA 94025
(415) 329-5245, 5209

Objective: The objective of this report period was to compile the sequence information described in the last report, following Shaw (1987), and to plot areal recurrence patterns in the form of codified matrices (digram to 6-gram location 'word'-matrices are being compiled; e.g., a 'one-gram' is a histogram of location frequencies in a catalog). An ongoing objective is to relate these patterns to the dynamical and fractal properties of networks of coupled oscillators.

Results: We have completed digram matrices for M equal to or greater than about 5 for the historical record in California and environs (CDMG Catalogs to 10/25/82, and NEIS Catalogs to date), including events in an area enclosed by the approximate coordinates 114-126 W longitude and 30-43 N latitude. To date we are restricting the analysis to a set of 8 subregions, two of which were chosen to emphasize the precursory sequence patterns in the vicinities of San Francisco and Los Angeles, respectively.

References:

Shaw, H.R., A linguistic model of earthquake frequencies applied to the seismic history of California: U.S. Geological Survey, Open-File Report 87-296, 129 pp.

FAULT PATTERNS AND STRAIN BUDGETS

9960–02178

Robert W. Simpson
Branch of Tectonophysics
U.S. Geological Survey
345 Middlefield Road, MS/977
Menlo Park, California 94025
(415) 329–4865

Investigations

Three–dimensional dislocation models have been used to estimate the change in static stress on major Bay Area, California faults caused by the 1989 Loma Prieta earthquake. Delayed changes caused by aseismic afterslip on deeper parts of the vertical faults or on horizontal detachment surfaces extending under the Bay have also been explored. Other models were constructed to see if patterns of static stress change might explain pairing of large earthquakes that occurred on the two sides of the Bay in 1836–1838 and in 1865–1868.

Results

Changes in both shear stress and normal stress resulting from the Loma Prieta rupture have been calculated for Bay Area faults, as well as a signed combination equal to the increase in horizontal right–lateral shear plus a coefficient of friction times the increase in extensional normal stress. This combination is an approximate measure of the change in the Coulomb failure function (CFF) assuming that the faults are already loaded predominantly with horizontal right–lateral shear.

The largest changes in the CFF occur for the segments on the San Andreas fault to the north and south of the Loma Prieta rupture. In the models, these segments are now closer to failure by tens of bars as a result of the redistribution of stresses. On the Hayward fault, right–lateral shear stresses are slightly diminished. The CFF on the north and central parts of the Hayward fault indicates a slight relaxation (0 to -1 bars), whereas the CFF at the south end is higher (0 to $+1$ bars) because of the increase in extensional normal stress at the south end. Most of the Calaveras fault shows relaxation (negative changes in CFF), except for a part near Morgan Hill that shows slightly larger CFF values.

Although it is not clear that changes in CFF have anything to do with the timing of earthquakes, it does appear that the background seismicity rates on the Hayward fault decreased in the region of CFF relaxation after the Loma Prieta earthquake. This apparent correlation needs to be tested statistically.

Models were also constructed to test the effect of delayed post–seismic slip on deeper vertical parts (20–40 km) of Bay Area faults in response to static stress changes generated by Loma Prieta. As a result of slip at depth, amplitudes of stress in the upper seismogenic region change by less than 10–20 percent in general, and the overall pattern of stresses does not change very much.

For a horizontal detachment surface connecting the faults at depth under the Bay, the effects of delayed afterslip on the seismogenic layer can be as large or larger than the initial coseismic static stress changes. For a model with a detachment surface at 20 km depth, the regions of positive CFF at the south end of the Hayward fault and near Morgan Hill on the Calaveras fault were reduced in size and amplitude by afterslip on the horizontal plane. Thus detachment faults or horizontal decoupling zones may serve as a effective way to redistribute stresses over large horizontal distances.

Stress calculations to test if the 1836 earthquake on the northern Hayward fault could have triggered the 1838 earthquake on the Peninsula segment of the San Andreas fault suggest that increases in extensional normal stress (an unclamping effect) may be more important than increases in right–lateral shear. The same observation applies for the possible triggering of the 1868 Hayward earthquake by the 1865 San Andreas earthquake (which was possibly a Loma Prieta type event). Jim Brune (oral communication, 1989) has observed that moderate to large earthquakes alternating from one side of the Bay to the other in the 19th century tended to occur in a dilatational quadrant of the previous event. This observation also suggests that an increase in extensional forces may be important in triggering events across the Bay and that more work needs to be done to explore the significance of such patterns.

MECHANICS OF LITHOSPHERE PLATES

9960-03419

William D. Stuart
Branch of Tectonophysics
U.S. Geological Survey
Pasadena, California 91106
818 405-7816
FTS 961-7816

Investigations

Pacific–North America Plate Interaction

This work attempts to reconcile two related problems. The first problem is the cause of the variation along strike and depth of locking of the upper San Andreas fault. On the northern and southern sections the locking is firm, and thus conditions exist for the generation of great earthquakes. On the central section the locking is weak or absent, and slippage occurs as aseismic creep and small earthquakes. The second problem is to determine the tractions and body forces that cause tectonic plates in contact along western North America to move relative to one another. The assumption made for the analysis of both problems is that plate boundary faults obey a pressure dependent constitutive law, and this law links the two problems. That is, in principle fault properties are to be found simultaneously with plate motions.

Parkfield Prediction Methods

The goal of this work is to construct methods for trying to predict the next moderate Parkfield earthquake before it happens rather than after. There are two strategies. The first is to formulate an earthquake instability model for repeated earthquakes. The model simulates faulting and ground deformation for all parts of each cycle. In all models of this kind accelerating preseismic faulting and ground deformation occurs, and such anomalies, if large enough to detect, could be the basis of experimental predictions. This work is in collaboration with T. Tullis and R. Simpson. The second strategy is to construct a mechanical model that accounts for the seismic quiescence and rate changes of trilateration lines reported by Wyss, Aviles, Burford, Langbein, and colleagues.

Results

Pacific–North America Plate Interaction

A procedure has been developed to compute the stress and velocity fields for the Juan de Fuca plate as it interacts with the Gorda, Pacific, and North America plates. The procedure makes the plane stress approximation and uses edge dislocations to represent strike slip and opening mode boundaries. Subduction is represented by a new approximation that maps three dimensions into two.

Separately, a two-dimensional plane stress model for faulting of the San Andreas between the Mendocino triple junction and Ft. Tejon has been analyzed. The fault is postulated to have a constitutive law wherein the rate of healing after a great earthquake (e.g., 1906 San Francisco) increases with effective confining pressure, but shear strain counteracts the healing. The pressure-dependent healing hypothesis derives from an idea of J. Byerlee. This model explains the creeping section of the San Andreas as due to relatively low regional confining pressure that is not necessarily caused by high pore pressure.

Parkfield Prediction Methods

A second generation model now works and its computed fault slip history has been displayed as a movie on videotape by T. Tullis. S. Silverman is attempting to assemble a USGS facility to do the same. This model has several improvements over the model of *Stuart, Archuleta, and Lindh*, JGR, 1985. Early runs with the new model seem to produce pre-, co-, and post-seismic features that are known or plausible at Parkfield.

The rate changes of seismicity and trilateration lines appear to imply a decreased loading rate on the upper part of the San Andreas between Parkfield and Slack Canyon. It is easy to explain both kinds of observations by slippage on a sub-horizontal detachment fault at 10-15 km and adjacent to or intersecting the San Andreas. Such a fault would be expected to start slipping late in a seismic cycle, consistent with the observed rate changes starting about 1986.

Reports

Stuart, W.D., Why the northern San Andreas fault has great earthquakes (abs.), AGU Fall Annual Meeting, 1989.

Rice, J. R., and W. D. Stuart, Stressing in and near a strongly coupled subduction zone (abs.), AGU Fall Annual Meeting, 1989.

EXPERIMENTS ON ROCK FRICTION CONSTITUTIVE LAWS APPLIED TO EARTHQUAKE INSTABILITY ANALYSIS

USGS Contract 14-08-0001-G-1364

Terry E. Tullis
John D. Weeks
Department of Geological Sciences
Brown University
Providence, Rhode Island 02912
(401) 863-3829

INVESTIGATIONS:

1. Determination of the physical processes responsible for the evolution effect.

2. Development of a computer program to do formal inversion of friction data to obtain values of the constitutive parameters for a Ruina state-variable model.

3. Determination of the constitutive behavior of granite at large displacement.

4. Realistic modeling of the earth to study the implications of friction constitutive measurements for earthquake prediction.

5. Development of a bearing assembly to eliminate sample misalignment.

RESULTS:

1. We now have clear experimental evidence supporting our proposal that the evolution effect in rock friction is caused by the time-dependent diffusion of water away from the highly-stressed points of contact, resulting in an increase in true bonding across the sliding surfaces. We hypothesize that the evolution effect is caused by removal of contaminant water molecules from contacting points by diffusion under the driving potential of the normal force pressing the sliding surfaces together. The gradual removal of water would increase the adhesion of the surfaces and so cause time-dependent strengthening and the evolution effect (note that this is in contrast to theories that call on increases in the size of contacts with time). Thus, the evolution effect should be seen in hydrophilic materials in which water has a tendency to become attached to surfaces, but it should not exist for hydrophobic materials in which surfaces do not attract water. One specific prediction we made from our hypothesis was that talc should show no evolution effect because the basal planes of talc are hydrophobic; they are electrically neutral and do not attract the polar water molecule. In contrast, mica should show a moderate evolution effect because the basal planes of mica are electrically negative and attract positively charged ions in solution which are in turn hydrated, carrying with them a group of polar water molecules. This layer of hydrated ions results in a repulsive force and lowered adhesion between the mica surfaces. Thus, talc has no water to interfere with bonding at contact points, whereas mica, if electrolytes are present, will have layers of weakly bonded water that can diffuse away to improve bonding with time. Although the water present in our samples is adsorbed from the air and therefore contains no electrolytes, the strength of the evolution effect is likely to be non-zero for mica because thin films of water will probably contain some K^+ ions released from the mica surfaces. The evolution effect would be expected to be larger for framework silicates because the water is bound to the surfaces by hydrogen bonds even in the absence of an electrolytic solution.

We have done experiments on talc and flourophlogopite mica that support these predictions. We have tested for the presence of an evolution effect in these materials by looking for the presence or absence of a decay with sliding displacement following the direct response to a step change in velocity, and by looking for the presence or absence of an increase in the static coefficient of friction when sliding is resumed following a period of no sliding. Using both of these measures we have found that mica shows a small but definite evolution effect, whereas talc does not, just as predicted (Figure 1). Also as predicted, a stronger evolution effect is typically observed in granite and quartzite. Our results would appear to agree with those of Dieterich and Conrad (1984) although they interpreted their findings differently. They found that extremely dry quartzite both had higher frictional strength and lacked an evolution effect, as would be expected if the contaminate water layers had been removed by drying.

2. One of the goals of our work is to determine parameters for the Ruina state variable model that characterize rock friction behavior as observed in the laboratory. Because the models to describe rock friction constitutive behavior are highly non-linear and exhibit interaction with machine compliance, in the past this has meant trial and error forward modeling using a numerical solution of Ruina's differential equations. Determination of fit was done by eye. Needless to say, this was time-consuming and lacked accuracy and objectivity. In a major advance in our ability to interpret the measurements made in the laboratory, we have developed a computer program to numerically invert friction data for the values of the parameters of the constitutive law. The program uses an iterative least-squares method to solve the linearized problem $\mathbf{Gm} = \mathbf{d}$, where $\mathbf{G}$ is the matrix of partial derivatives of the model residuals with respect to the matrix of model parameters $\mathbf{m}$ and $\mathbf{d}$ is the matrix of differences between the predicted and observed values of the coefficient of friction. Nonlinearity of the model requires that the solution be iterated to achieve a good fit. A number of special problems had to be solved including the inability to form analytical solutions for the Ruina differential equations, numerical instability of the solution method, instability of the model itself, and the large amount of computation required.

The Ruina model, combined with equations giving the interaction of the constitutive law with the machine compliance, yields differential equations that cannot be solved except by numerical integration. Consequently, the matrix of partial derivatives must be calculated numerically by finite differences between a starting model and models having slightly perturbed parameters. This means that in order to fit a two state variable constitutive law to a data trace one iteration of the program requires seven numerical integrations of the differential equations - one for the predicted model and once each to calculate partials for each of six parameters ($\mathbf{a}$, $\mathbf{b}_1$, L_1, $\mathbf{b}_2$, L_2 and μ_0). The amount of computation required for running these forward models has been minimized by the use of a fifth-order Runge-Kutta method incorporating adaptive step-size control. Even so, each computation of the forward model may require a thousand or more iterations of this numerical integration routine. Thus, a large amount of computation is required; the speed of our new Hewlett Packard work station allows one iteration to be done in a matter of a few seconds. A few tens of iterations of the program are required for convergence to a high degree of precision.The nature of the model equations is such that instability can be a problem, both numerical instability of the iterated solution and actual instability of the model, representing unstable slip or earthquakes. Large differences in the magnitudes of the parameters led us to normalize the matrix of partial derivatives, $\mathbf{G}$. In addition, singular-value decomposition of the matrix is done in order to reduce computation and decrease the adverse effects of machine precision. The limitation of machine precision turns out to be significant and requires the use of double-precision computation. Finally, the likelihood that a given starting model would converge to a solution was improved by an unsophisticated damping method in which just half the corrections to the model parameters indicated for a given iteration are actually applied. This greatly decreases the chance of overshooting the desired solution in an unstable fashion. In Figure 2, a comparison is made between a previously published trial-and-error fit (dotted line) and a fit produced by application of the program (solid line). Both are fits to the same laboratory friction data (shown by x's) The starting model for the program is also shown (dot-dashed line). While the Tullis and Weeks fit appears quite good, it is clear that the inversion program has made a much better fit. The amount of difference between the Tullis and Weeks parameters and those resulting from the inversion program is sobering and illustrates the extreme sensitivity of the friction model to small changes. As this is a very recent development there are still problems to solve and enhancements to be made to the program. As mentioned above, numerical and model stability can be a problem. We plan to incorporate the methods of Tarantola and Valette (1982) which can take into account a priori information about model parameter values thereby enhancing the computational stability. We must also improve our ability to get information on the covariances, or interdependence of parameter values. This is very important and will be a top priority for further work.

3. We have developed new techniques to investigate the constitutive behavior of simulated granite gouge at large displacement. In the past, we observed that Teflon from sample jackets had contaminated the sliding surface and we feared that this was responsible for a switch from velocity weakening to velocity strengthening that occurred at a displacement of about 75 to 100 μm. We have developed a new sample geometry to allow experiments on granite gouge with no confining pressure and, consequently, no Teflon-containing jacket. This new assembly consists of a groove containing simulated gouge in one sample ring mated to a sample ring that fits into the groove to confine the gouge. The sample rings can be made of granite to assure that no foreign materials can contaminate the experiment, or they can be steel which is less likely to fail under the applied loads. This assembly is shown in Figure 3.

We have performed three experiments on simulated granite gouge using this assembly- two using granite rings which achieved 35 and 150 mm displacement, and one using the steel rings which achieved 319 mm displacement. The results of these experiments, conducted in rotary shear on gouge under a normal stress of 25 MPa but without any confining pressure, are not as simple as one might like. Still, they resolve some of the questions and promise that we may learn some very interesting things with more work. These results are shown in Figure 4, where we have superimposed the new results from the two types of grooved assemblies on the results previously reported for the assemblies having the sliding jacket assembly involving Teflon. The behavior of the gouge in the grooved steel holder was similar to that of the samples in which the Teflon may have been present, but at the highest displacement an additional change back to velocity weakening occurred. As the figure shows, all results show a similar decrease in **a-b** over the first 10 mm of sliding. This results in velocity weakening in the displacement interval 10-60 mm. One of the granite groove experiments failed while still in this velocity weakening regime. The steel groove experiment exhibits a shift to velocity strengthening identical to that shown by the jacketed samples, suggesting that the switch to velocity strengthening we observed in jacketed experiments are caused by the rock and not Teflon. However, the switch back to velocity weakening after 250 mm slip is a new observation having unknown origin. The second granite groove experiment is different from any previous experiments in having a period of unstable behavior from 9 to 95 mm with a return to stability after 120 mm. The overall shape of the evolution of **a-b** may be similar with an increase in **a-b** at about 100 mm, with the exception that in this experiment **a-b** simply was never positive. These results taken together suggest that characterizing the eventual behavior of the crushed granite simulated gouge as either velocity weakening or strengthening is not yet possible.

4. During the past year we have worked together with Bill Stuart to develop and test a three dimensional model of faulting applied to the geometry of the San Andreas fault at Parkfield, California. This is an extension to three dimensions of the type of modeling carried out by Tse and Rice (1986) for a two dimensional strike-slip fault model. The modeling uses constitutive parameters determined from laboratory studies including the depth variation in constitutive parameters that is expected from the San Andreas geotherm. A range of along-strike variation in constitutive parameters is used, keeping the range reasonable in terms of the variations found for different rock types in the laboratory. These three dimensional models will allow more reasonable estimates to be made of the magnitude of premonitory strain and geodetic signals to be expected prior to the next Parkfield earthquake. Preliminary models have been created and videos made from these models show interesting patterns of slip and seismicity in space and time.

5. We have made some significant progress in understanding the problem of Teflon contamination, and have devised a solution that has some additional advantages. Originally we thought that the Teflon was forced into the samples by the confining pressure applied to the sample. However, it now appears that the problem is caused by axial misalignment and the Teflon is wiped against the adjacent faces of the samples. We have made some measurements of the run-out of the samples and find that it varies between experiments and is more likely to occur at higher normal stress. We have designed a bearing assembly that will prevent this axial misalignment and at the same time will allow relative axial motion between the upper and lower samples. This assembly is shown in Figure 5. Although there will be a slight resistance to rotary and axial motion from friction in this bearing, we calculate this to be very low compared to the forces and torques arising from the sample. This assembly has the additional advantage that the associated redesign will allow us to measure both the rotary and axial displacements of the samples simultaneously using our internal resolver and internal LVDT. At present we are restricted to using either one or the other of these alone in any given experiment.

REPORTS:

Papers:

Blanpied, M. L., Weeks, J. D. and Tullis, T. E., 1990, The effects of sliding rate and shear heating on the friction constitutive behavior of granite, *J. Geophys. Res., in press.*

Blanpied, M. L., Tullis, T. E. and Weeks, J. D., Evolution of frictional behavior and fault zone textures in experimental granite faults with and without simulated gouge, *J. Geophys. Res., in press.*

Abstracts:

Blanpied, M. L., Weeks, J. D., and Tullis, T. E., Effects of sliding rate and shear heating on the velocity dependence of granite friction, *Eos, Trans. AGU, 70* 1303, 1989.

Reinen, L. A. and Weeks, J. D., Determination of rock friction constitutive parameters using a least squares inversion method, submitted to *Eos , Trans. AGU* for presentation at the spring meeting, 1990.

Tullis, T. E., Blanpied, M. L., and Weeks, J. D., The velocity dependence of granite friction with and without simulated gouge, *Eos, Trans. AGU, 70*, 1302, 1989.

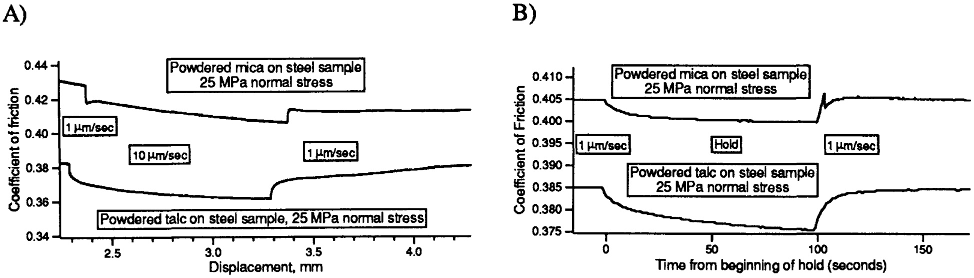

Figure 1. Comparison of response of talc and flourophlogopite mica to a velocity change (A) and stationary hold (B). Part (A) shows frictional strength for sliding first at 1, then at 10 and back to 1 $\mu m\ s^{-1}$. Talc shows no hint of transient peak following velocity changes, whereas the mica does, though not as strongly as for materials like granite or quartzite. Part (B) shows the response to a 100 second stationary hold. The figure shows the steady-state frictional strength achieved at 1 $\mu m\ s^{-1}$ followed by relaxation of stress during 100 second hold, and finally the response to re-loading at 1 $\mu m\ s^{-1}$. The evolution effect in the mica is expressed as a transient peak in strength upon re-loading (which, in this case, resulted in a small stick-slip event) and the relatively flat-bottomed decay.

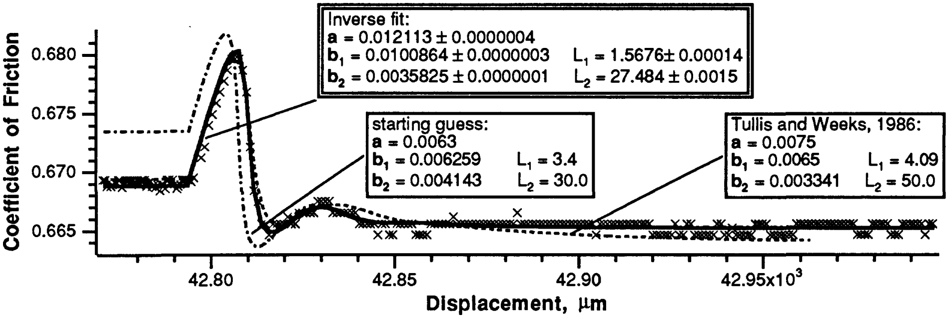

Figure 2. Example of friction model found by iterative least-squares inversion program. Model (solid line) is fit to data obtained in a laboratory sliding experiment (x's). The starting model for the inversion is shown by the dot-dashed line. For comparison, a trial-and-error fit from Tullis and Weeks (1986) is also shown (dotted line). The indicated precision of parameter values reflects only the variance of individual parameters with others held constant; it does not include covariances reflecting non-linear interactions of parameters.

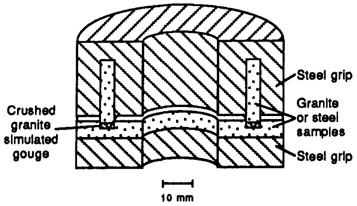

Figure 3. Schematic cross-section of grooved sample assembly. An upper ring-shaped sample rotates in a groove machined in the lower sample. The groove is about half filled by a 1 mm layer of simulated gouge. The samples may be either rock or steel. In the latter case, the samples and grips are made in a single piece. This assembly has been used with crushed granite simulated gouge on rock and steel, and with powdered talc and mica on steel.

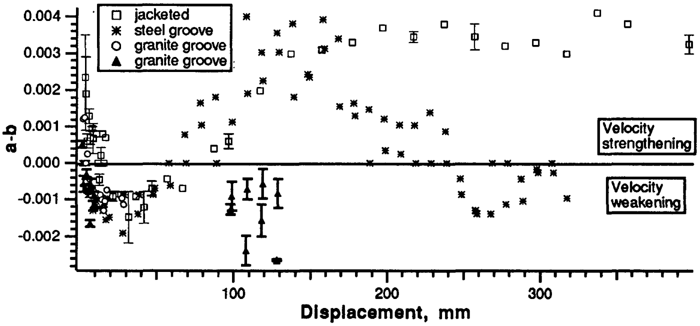

Figure 4. Comparison of steady-state velocity dependence of crushed granite simulated gouge as measured using a jacketed sample assembly with possible Teflon contamination (squares), our new grooved rock assembly (circles and triangles are from different experiments using this assembly), and the grooved steel assembly (stars). The experiments using the grooved rock assembly were terminated by failure of the lower sample (see Figure 3) after about 35 mm (circles) and 135 mm (triangles). The experiment represented by triangles slid unstably between 9 mm and 90 mm, preventing the measurement of steady-state velocity dependence in this interval; stability theory indicates that the velocity dependence here would have been even more velocity weakening than in the regions in which stable sliding prevailed.

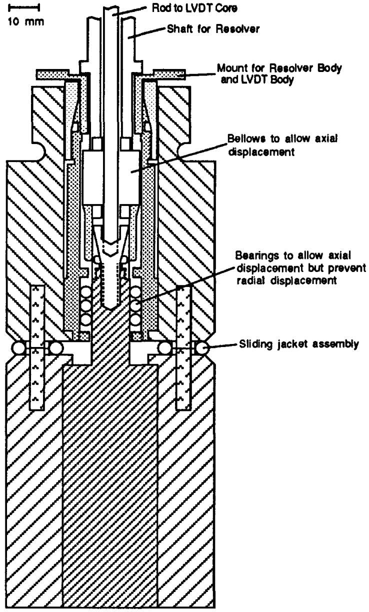

Figure 5. Diagram of bearing to prevent axial misalignment of sample rings,.while allowing rotary and axial motion. Unlike standard ball bearings, the surfaces on which the balls roll is cylindrical so that both axial and rotary motion are possible with the very low frictional forces associated with ball bearings. Much of the apparent complexity of the design is due to the mount for the resolver that measures rotary displacement, and a LVDT to measure axial displacement caused by compaction or dilation in response to sliding and application of normal stress.

Regional and National Seismic Hazard and Risk Assessment

9950-01207

S.T. Algermissen
Branch of Geologic Risk Assessment
U.S. Geological Survey
Denver Federal Center, MS 966
Denver, CO 80225
(303) 236-1611

Investigations

1. Following the October 17, 1989 Loma Prieta, California, earthquake a field team was dispatched to gather detailed information on damage to dwellings and Modified Mercalli Intensity in the stricken area.

2. Regional seismic source zones for a new generation of national probabilistic ground motion hazard maps are continuing to be revised, updated and documented.

3. Comparitive analyses of published ground-motion attenuation relations are continuing to determine which relations or combination of relations are best suited to modeling ground motion in a consistent manner nationwide.

4. Probabilistic ground-motion modeling that includes the probability of a great earthquake along the Cascadia subduction zone is being investigated for the Puget Sound and Portland areas.

5. Two loss investigations in California have been completed and manuscripts are in press. One study examines single family housing losses in the 1933 Long Beach, the 1971 San Fernando, the 1983 Coalinga, and 1987 Whittier Narrows earthquakes in the contexts of dwelling market value and insured values. The other investigation examines probable maximum loss to California mobile homes (manufactured housing).

6. A state-wide investigation of probabilistic losses to single-family dwellings for California has been completed.

7. Developmental work is continuing on the new seismic hazard and risk program, FRIENDLY. This program allows the analyst to perform probabilistic ground-motion hazard analysis interactively at a computer terminal. Conceptually, the ground-motion calculations are similar to those performed in the current program SEISRISK III. However, FRIENDLY is far more flexible with more sophisticated geometric treatments of fault sources.

Results

1. The epicentral Modified Mercalli intensity of the Loma Prieta earthquake was assessed as VIII based on structural damage to wood-framed dwellings and unreinforced masonry commercial buildings. Maximum intensities of IX, however, were assigned to sites of anomalous damage to freeway systems in San Francisco and Oakland, as well as to the Marina district of San Francisco. Ground-motion amplification by surficial sediments appears to have played a significant role in localizing pockets of extreme damage.

The largest peak horizontal acceleration of 0.64 g was measured in the epicentral region at Corralitos. The peak vertical acceleration at this location was 0.47 g. In the San Francisco-Oakland area, differences of 100 to 200 percent were observed in peak horzontal accelerations recorded on Bay Mud and Franciscan rock sites. These large differences are consistent with observed differences in MM intensitiy in this same region.

Damage in the Marina district was strongly influenced by the pounding of adjacent buildings and by 4-story apartment buildings having soft first stories. Certain blocks in which these buildings had been previously rehabilitated showed markedly less damage although exceptions were noted where there was extensitve ground distortion or settlement due to liquefaction.

The threshold of chimney damage usually corresponded to a density of less than 3 percent. At these lower levels, overall intensity evaluations corresponded to intensity VI. When density of chimney damage reached 30 percent, it was usually accompanied by other examples of damage indicating a local level of MM intensity VII. It appears that the density measure of intensity indicators can be used as a guide to isoseismal intensity and strong ground motion. The collected damage data will improve vulnerability relationships between shaking level and damage in loss estimation studies for dwellings.

2. Focal depths and nodal-plane dips of medium-sized earthquakes, hypocentral depth distributions from local networks, and geologic evidence are elements that help characterize the seismogenic crust in central and eastern North America. The seismogenic crust is thinner in the Appalachians than in the Precambrian craton. Most medium-sized earthquakes in the craton are 5-15 km deep, but an aseismic gap separates these from a few hypocenters 20-30 km deep. Network seismicity does not show the gap. The absence of surface ruptures is partly explained by the moderate nodal-plane dips of medium-sized earthquakes and a tendency for larger shocks in this range to have shallower dips. A manuscript is in review for eventual submittal to Seimological Research Letters.

The northwest two thirds of the Iapetan passive margin in eastern North America has a uniform style of seismicity distinct from styles in adjacent regions. The structure of the margin is dominated by north- to east-striking normal faults formed during late Proterozoic-early Paleozoic rifting. Slip on these Iapetan faults thinned the southeast third of the margin to about half its original thickness. The northwest two thirds contains Iapetan normal faults but lesser extension on them left this part of the margin comparatively intact. The boundary between intact and thinned parts of the margin and the southeast boundary of the entire margin are identified on deep seismic-reflection profiles. The northwest boundary of the margin is located by analogy to the width of the Mesozoic Atlantic margin. The location of the boundary is confirmed by comparison to sites of known and probable Iapetan faults. Northeast striking, steeply dipping Iapetan faults or fault zones at three and perhaps five or six locales of the intact part of the margin are undergoing seismic reactivation. The thinned part of the margin is aseismic beneath the overthrust metamorphic and igneous rocks of the Appalachian orogen. Seismicity at well-studied locales bordering the margin in the craton and the overthrust Appalachian core has different and more diverse characteristics than well-studied seismicity in the intact part of the margin. A manuscript is in internal review for eventual submittal to the Geological Society of America Bulletin.

3. Of particular interest in the comparison of strong-ground motion attenuation relations are three factors: (1) suitability of the attenuation relations to be adjusted for general crustal characteristics in the eastern and western U.S., (2) reasonableness of spectral shapes for a broad range of magnitudes and distances, and (3) provision for adjusting ground motion levels for differences in geological site condition. No single existing attenuation function performs well on all three factors.

A second Eastern U.S. ground-motion workshop sponsored by the National Center for Earthquake Engineering Research was attended in Troy, New York. The workshop was a followup of one attended in July, 1989 (Whitman, 1989) on desirable parameters for national hazard maps. The recent conference was convened for the purpose of recommending one or more standard site conditions to be used for a national map, with the intention of making feasible simple spectral adjustments for a small number of alternative site conditions. A general consensus was that a California attenuation, calibrated for "soft rock", would meet the standard condition requirement in the west and in the east when adjusted for the difference in anelastic attenuation. However, for the Appalachians and the northeastern U.S., where crystalline basement rock sites predominate, it was felt that this "hard rock" should be the standard site condition. There was no consensus on what existing attenuation function would be most appropriate. It was strongly doubted that an adjustment to a California "soft rock" attenuation relation to account for basement rock conditions would fit the observed eastern U.S. strong motion data.

4. Ground-motion acceleration, spectral velocity and Modified Mercalli intensity are being modeled probabilistically in the Puget Sound, Washington, and Portland, Oregon, areas. Attenuation relationships developed by Youngs and Coppersmith (1989) for both intraplate and interplate earthquakes are used for accelerations and spectral velocity. Intensity attenuation is based on new regressions of intraplate shocks in the subducted Juan de Fuca plate and shallower shocks in the North American plate in the Puget Sound area. Potential subduction zone interplate shocks are modeled along a dipping subduction zone interface as a Poisson process with an average interoccurrence time of 550 years. Acceleration and spectral response values are being determined for both rock and soil sites, and Modified Mercalli intensities are being determined for "average" site conditions.

Preliminary results indicate accelerations on rock at Seattle, Tacoma, Olympia, and Portland range from about .20 g to .12 g and on firm soil from .41 g to .25 g for a 50-year period of interest with a 10-percent chance of exceedance. Average Modified Mercalli intensities in the four cities range from VI to VII for the same period of interest and probability level. The results suggest that for a 50-year period of interest and a Poisson model of earthquake occurrence, a great interplate earthquake ($M_w = 8.5$) having an average recurrence of around 550 years contributes little to the expected ground motion.

5. Most of the methods for quantifying earthquake monetary losses to California wood frame dwellings have been based on summarized information on the 1933 Long Beach earthquake and on the partially analyzed 1971 San Fernando earthquake. Loss over deductible, for example, was not studied in the published reports which followed the 1971 San Fernando earthquake. The existing data from these two earthquakes, plus those from 1983 Coalinga and 1987 Whittier Narrows, and other events with less information, are re-examined in the contexts of dwelling market value and insured value.

Transferring data from specific earthquakes to generalized loss estimation methodology required commonality of data. Unusual construction characteristics were eliminated from the data as were unusual geologic effects. For examples discussed in the text, 1983 Coalinga information shows many dwellings unachored to their foundations. This circumstance was the result of houses moved to the city and placed on new foundations without anchors, contrary to generally accepted practice. In 1971 San Fernando, surface faulting and related ground movements at dwelling sites intensified damage. After standardizing the data, a transfer function was developed for earthquakes of other magnitudes.

Two key factors are examined: (a) Probable Maximum Loss and (b) loss over the deductible from the standpoints of market value and insured value. Analyses included one story, one and two story, split level, and two story structures. There are three age groups: pre-1940, 1940-49, and post-1949. Further subdivision is by type of first floor.

While measurable differences in expected monetary losses were found among most of these dwelling characteristics, those most important from a practical use standpoint are two age groupings: (1) pre-1940 construction, and (2) post-1939 construction. Available data allow the inclusion of any of the other dwelling characteristics which may be of user interest. The definition of the Probable Maximum Loss when applied to dwellings has practical difficulties due to uncertainties when evaluating the loss distribution curves. An alternative based on loss over deductible is proposed.

Proprietary and published earthquake loss data to mobile homes for five damaging earthquakes between 1971 and 1983 were examined. Mobile home losses were 2 to 4 times greater than losses to conventional wood frame dwellings in the 1971 San Fernando shock, which in part may be associated with the focal mechanism of the earthquake and the location of mobile homes with respect to the earthquake focus. The attenuation with distance, D, of percent loss to mobile homes derived for the San Fernando data is:

$$\text{Percent loss} = 7.81 - 0.34\ D$$

where D is distance in miles from the energy release.

For the earthquakes studied, the mobile home Probable Maximum Loss is estimated to be 40 percent for unbraced mobile homes, using the alternate "9 out of 10" PML definition. The average insured mobile home loss in the 12 mile wide PML zone for a magnitude 8.25 is estimated to be about 15 percent with a 1.5 uncertainty factor included.

6. All phases of the statewide California dwelling loss study have been completed to the point of providing losses to housing with 1 to 4 units per structure by county for periods of 10, 50 and 250 years. The general procedure for the analysis was as follows:

a. Determine three regional attenuation functions for intensity with distance in California using a method involving direct use of intensity observations and a relationship with M_s (Arnold, 1990).

b. Determine site responses in terms of intensity for about 2500 sites using about 7300 observations of intensity and distributing these over the 5000 centers of population for which housing statistics are known.

c. Update the number and replacement value of housing units since the 1980 Census. The values were found from an extensive survey of 180 California Boards of Realtors and numbers were derived from the Bureau of the Census estimates of net migration of population.

d. Using source zones already developed for California and the SEISRISK III program (Bender and Perkins, 1987), probabilistic intensities for each Census tract were obtained and losses were calculated using three different vulnerability functions.

7. The next generation seismic hazard and risk computer program, FRIENDLY, has been expanded to include nonhomogeneous source zones. A supplemental program has been coded to grid the geographic locations of historic earthquakes, and then to smooth the these locations. The output of this earthquake gridding program provides the input for the nonhomogeneous source zones in FRIENDLY. These programs are currently being tested.

Reports

Algermissen, S.T., Perkins, D.M., Thenhaus, P.C., Hanson, S.L., and Bender, B.L., 1990, Probabilistic earthquake acceleration and velocity maps for the United States and Puerto Rico: U.S. Geological Survey Miscellaneous Field Investigation Map, MF-2120, 2 shts., scale 1:5M.

Algermissen, S.T., 1990, Ground motion estimation in the Puget Sound and Portland areas, in, Hays, W.W., ed., Fourth Annual Workshop, National Earthquake Hazards Reduction Program, Puget Sound and Portland Area, [abs]., in press.

Arnold, E.P., 1990, $I_0 I$: Relationships between macroseismic epicenter, attenuation and magnitude: Earthquake Spectra, submitted.

Arnold, E.P., 1989, Program Seisrisk III adapted to personal computers: U.S. Geological Survey Open-File Report 89-557A-N.

Bender, B.K., 1990, Treatment of parameter uncertainty and variablility in seismic hazard maps: Submitted for Director's approval.

Hopper, M.G., Leyendecker, E.V., Thenhaus, P.C., Stover, C.W., Algermissen, S.T., Reagor, B.G., Perkins, D.M., Hanson, S.L., Brewer, L.R., and Baldwin, F.W., 1989, Damage and intenisty survey of the October, 17, 1989 Loma Prieta earthquake: American Geophysical Union Fall Meeting, December 4-8, 1989, San Francisco, California, Special session on the Loma Prieta Earthquake, [abs.].

Leyendecker, E.V., Thenhaus, P.C., Campbell, K.W., and Hopper, M.G., Hanson, S.L., Algermissen, S.T., and Perkins, D.M., 1990, Preliminary assessment of the distribution of intensity and strong ground motion for the Loma Prieta Earthquake: Earthquake Spectra, in press.

Leyendecker, E.V., Thenhaus, P.C., Campbell, K.W., and Hopper, M.G., Hanson, S.L., Algermissen, S.T., and Perkins, D.M., 1990, Preliminary assessment of the distribution of strong ground motion and intensity for the Loma Prieta Earthquake: Interagency Committee on Seismic safety and Construction Special Report on the October 17, 1989, Loma Prieta Earthquake, in press.

Steinbrugge, K.V., and Algermissen, S.T., 1990, Earthquake losses to single family housing: California experience: U.S. Geological Survey Bulletin, in press.

Steinbrugge, K.V., and Algermissen, S.T., 1990, California mobile homes (manufactured housing): Probable maximum loss (PML) and loss attentuation with distance: U.S. Geological Survey Bulletin, in press.

Thenhaus, P.C., 1989, Contributing author to: Plafker, G., and Galloway, J.P., eds., Lessons learned from the Loma Prieta, California, earthquake of October 17, 1989: U.S. Geological Survey Circular 1045.

Thenhaus, P.C., and Barnhard, T.P., 1989, Regional termination and segmentation of Quaternary fault belts in the Great Basin, Nevada and Utah: Seismological Society of America Bulletin, v. 79, p. 1426-1438.

References Cited

Arnold, E.P., 1990, $I_o l$: Relationships between macroseismic epicenter, attenuation and magnitude: Earthquake Spectra, submitted.

Bender, Bernice, and Perkins, D.M., 1987, SEISRISK III - A computer program for seismic risk hazard estimation: U.S. Geological Survey Bulletin 1772, 48p.

Whitman, R.V., 1989, Workshop on Ground Motion Parameters for Seismic Hazard Mapping, Buffalo, N.Y., July 17-18, 1989, National Center for Earthquake Engineering Technical Report NCEER-89-0038, 52p.

Youngs, R.R., and Coppersmith, K.J., 1989, Attenuation relationships for evaluation of seismic hazards from large subduction zone earthquakes, in, Hays, W.W., ed., Third Annual Workshop on "Earthquake Hazards in the Puget Sound, Portland Area": U.S. Geological Survey Open-File Report 89-465, p. 42-49.

REGIONAL AND LOCAL HAZARDS MAPPING IN THE EASTERN GREAT BASIN

9950-01738

R. Ernest Anderson
Branch of Geologic Risk Assessment
U.S. Geological Survey
Box 25046, MS 966, Denver Federal Center
Denver, CO 80225
(303) 236-1584

INVESTIGATIONS

Continued studies of Neogene shortening strains in the southern Great Basin by gathering additional data on fault-slip characteristics in the southern Mormon Mountains and East Mormon Mountains, Nevada.

RESULTS

Developed a model to explain how strike-slip deformation is absorbed or partially absorbed by folding during extensional deformation. The model is based on structures observed in the East Mormon Mountains. It is applied to other areas in the southeastern Great Basin where right steps are known or suspected in the left-oblique fault systems that characterize that area.

REPORTS

Anderson, R.E., 1989, Tectonic evolution of the intermontane system; Basin and Range, Colorado Plateau, and High Lava Plains, *in* Pakiser, L.C., and Mooney, W.D., eds., Geophysical framework of the continental United States: Geological Society of America, Memoir 172, p. 163-176.

Geologic studies for seismic zonation of the Puget Sound lowland

9540-04004

Brian F. Atwater
U.S. Geological Survey at Department of Geological Sciences
University of Washington AJ-20
Seattle, WA 98195
(206) 442-2927 FTS 399-2927

INVESTIGATIONS

Preparation and submission of 12 samples for precise radiocarbon dating of the most recent episode of sudden subsidence in coastal southern Washington. One of the samples comes from a western red cedar snag previously dated through tree-ring pattern matching by David K. Yamaguchi; the radiocarbon age will provide an independent check on Yamaguchi's dating. The other 11 samples come from stumps of Sitka spruce collected in September, 1989. The lab promises results in the fall of 1990.

RESULTS

The ring-width pattern and cell structure of the spruce samples collected for precise radiocarbon dating provide the first direct evidence that the most recent episode of sudden subsidence happened within a year.

The samples come from a suite of 12 stumps, each of which has well-preserved rings beneath the bark. The 12 stumps are rooted in the uppermost buried soil at northern Willapa Bay (7 stumps from two localities) and the Copalis River (5 stumps). The mud above all but two of these stumps (2 from the Copalis River) contains rhizomes of *Triglochin maritima*, whose preference for salt-water mud flats implies that the spruce trees should have been killed by the subsidence, as happened promptly to Sitka spruce in Alaska that subsided into the intertidal zone in 1964.

In 8 of the samples (2 from the Copalis River, 3 each from the Willapa Bay localities) the outermost 20-40 rings consistently show little or no outward decrease in thickness. In 4 of these 8 samples (1 from the Copalis River, 2 from each Willapa Bay locality) the outermost ring lacks thick-walled latewood cells (cells that form at the end of the spring-to-autumn growing season) or is composed entirely of cells with thin walls (D.K. Yamaguchi, written communication, 1989). In the other 4 samples either the outermost rings are obscured by pitch or, as is common in roots, the rings vary in thickness too greatly around the circumference to show any consistent pattern.

Lack of pronounced outward thinning of rings and absence of thick-walled cells in the outermost ring suggest rapid death. In particularly, the five trees lacking thick-walled cells in the outermost ring probably died during the growing season (D.K. Yamaguchi, written communication, 1989). Such rapid death is more consistent with coseismic subsidence than with a submergence of a more gradual sort, such as a regional rise in sea level caused by melting of glacial ice or an upward bulging of the geoid.

REPORTS (both submitted for internal USGS review)

Atwater, B.F., Nishenko, S.P., Phipps, J.B., and Hull, A.G., Buried Holocene lowlands and great-earthquake potential in coastal Washington: U.S. Geological Survey Bulletin.

Atwater, B.F., Coastal evidence for great earthquakes in western Washington, *in* Rogers, A.M., editor, Assessing and reducing earthquake hazards in the Pacific Northwest: U.S. Geological Survey Professional Paper.

April 13, 1990

Depth to Bedrock map in the greater Tacoma area, Washington

9950-04073

Jane M. Buchanan-Banks
Branch of Geologic Risk Assessment
U.S. Geological Survey
David A. Johnston Cascades Volcano Observatory
5400 MacArthur Boulevard
Vancouver, Washington 98661
(206) 696-7996

Investigations

Continuing research and compilation of data on depth to bedrock. Analysis of reconnaissance high resolution marine seismic surveys (Snaveley and others, 1977) to determine thickness of unconsolidated deposits beneath the seawater-sediment boundary within the southern Puget Basin.

Results

Analysis of most of the marine seismic survey lines provided only a minimum thickness of unconsolidated deposits; however, at one shot point in Budd Inlet north of Olympia, the sediment-bedrock contact was penetrated and a thickness of 120 m was determined.

Consultations planned with Sam Harding on interpretation of the new multichannel data in the Colvos Passage-Commencement Bay area (Harding and others, 1988) were delayed and eventually cancelled due to Sam's terminal illness.

All well locations plotted on the map were checked for accuracy of location and depth. The source diagram was revised and text and references updated. Bedrock outcrops on the map were divided into three groups using zipatone patterns to delineate volcanic and intrusive rocks, consolidated sedimentary rock, and unconsolidated-to-semiconsolidated sedimentary rocks of the Miocene Mashel Formation. Each group reflects differing geologic conditions which will likely result in different ground responses during an earthquake.

PUGET SOUND PALEOSEISMICITY

9950-04484

ROBERT C. BUCKNAM
U.S. Geological Survey
M.S. 966, Federal Center
Denver, Colorado 80225
(303) 236-1604

INVESTIGATIONS

1. Submittal of samples from sites in Puget Sound for ^{14}C analyses.

2. Reconnaissance study of late Holocene coastal deformation in Pakistan.

RESULTS

1. A ^{14}C age determination of subrounded fragments of charcoal provide a maximum estimate of the time of a 7-m uplift at Restoration Point, Bainbridge Island, Washington. The charcoal, from the upper 10 cm of a sandy mud containing brackish-water diatoms, gives a ^{14}C age of 1,580 ± 90 yr B.P. and a ^{13}C adjusted age of 1,560 ± 90 yr B.P. (Beta-36045). Using the CALIB program of Stuiver and Reimer (1986), the ^{13}C age corresponds to calendar-corrected dates of 1,420; 1,470; and 1,490 yr B.P. Using a laboratory error multiplier of 1, the one-sigma calibrated age range for the sample is 1,350 to 1,550 yr B.P.

2. Two recent papers (Byrne and others, 1989; Laane and Chen, 1989) have noted similarities between historic seismicity and tectonic processes along the Cascadia subduction zone and those along the Makran subduction zone off the coast of southwestern Pakistan. I spent 4 weeks in February and early March 1990 carrying out reconnaissance studies along the coast of Pakistan to evaluate the suitability of several areas for detailed studies of neotectonic deformation. The area offers an excellent opportunity to study the style of recent vertical coastal deformation adjacent to a shallow-dipping subduction zone with a thick accretionary wedge, features that the Makran shares with Cascadia. Such studies would also contribute to the development of a better understanding of the neotectonic setting and paleoseismic record in southern Pakistan in order to evaluate earthquake potential and seismic hazards.

Work in the area of Cape Monze, 35 km west of Karachi, led to the identification of 2 well defined, recently uplifted shorelines. The shorelines have small wave-cut platforms and encrustations of oysters and barnacles on the Tertiary limestone and sandstone bedrock. The lower shoreline is widely preserved in the area, and thick oyster and barnacle encrustations are present as much as 8 m above the estimated level of present mean high water. The higher shoreline is not as well preserved, with the upper limit of scarce oyster encrustations at 15 m above the estimated level of present mean high water. Samples of oysters were collected from both levels for ^{14}C analyses. Although widespread uplift in the Quaternary has been recognized in coastal Pakistan, age determinations from the oysters should provide some constraints on the timing and rates of Holocene deformation in the Karachi area.

References Cited

Byrne, D.E., Sykes, L.R., and Davis, D.M., 1989, The great Makran earthquake of 1945 and its implications for modes of plate boundary slip [abs.]: Eos, Transactions of the American Geophysical Union, v. 69, p. 1330.

Laane, J.L., and Chen, W.-P., 1989, The Makran earthquake of 1983 April 18: A possible analogue to the Puget Sound earthquake of 1965?: Geophysical Journal International, v. 98, p. 1-9.

Stuiver, M., and Reimer, P.J., 1986, A computer program of radiocarbon age calibration: Radiocarbon, v. 28, p. 1022-1030.

PUBLICATIONS

Bucknam, R.C., and Barnhard, T.P., 1989, Evidence of sudden late Holocene uplift in the central Puget lowland, Washington [abs.]: Eos, Transactions of the American Geophysical Union, v. 70, p. 1332.

Geology and Tectonic Evolution of the Western Transverse Ranges

9550-04063

Russell H. Campbell
Branch of Geologic Risk Assessment
U. S. Geological Survey
MS 922, National Center
Reston, Virginia 22092
(703)648-6784

Investigations

Recent project investigations include a review of evidence for Pliocene(?), Pleistocene and Holocene tectonic activity along the southern frontal fault system of the Transverse Ranges Province in the western Santa Monica Mountains. The review has been incorporated into the text that describes the structural geology of the Point Dume 7-1/2 minute quadrangle (GQ-map, in preparation), and is abstracted for this summary.

Results

The coastal zone along the southern flank of the western Santa Monica Mountains is dominated by the east-west structural grain common to the Transverse Ranges Province. In the adjacent offshore area, east-west trending structures dominate in the submarine shelf and slope at the north side of the Santa Monica Basin (Junger and Wagner, 1977). At the foot of the slope, a few miles south of the Malibu coastline, an east-west trending fault (the Anacapa Fault of Yerkes and Lee, 1979) marks the abrupt change from Transverse Ranges structure to the dominant northwesterly structural grain of the Peninsular Ranges Province.

Among the onshore coastal-zone geologic structures, the Malibu Coast fault (which also trends east-west, approximately parallel to the coastline) separates two markedly dissimilar geologic terrains that were first juxtaposed by major lateral displacement after late middle Miocene time (Campbell and Yerkes, 1976). Although the California fault map of Jennings and others (1975) indicates Quaternary activity for the Malibu Coast fault, and workers as early as Davis (1933) suggest that some geomorphic features may be offset left-laterally, it may be misleading to ascribe the known localities where fault displacements of late Pleistocene marine terrace deposits have been observed (Fig. 1.; see Yerkes and Wentworth, 1965; and Yerkes and Lee, 1987), to the "Malibu Coast fault."

From Point Dume on the west to Santa Monica in the east (approximately 20 miles), most of the known localities show displacement on short, discontinuous fault segments, each constrained to a relatively small, isolated area. At localities where strata older than Pliocene underlie the Pleistocene deposits, none of the young fault offsets is exactly coincident with the main trace of the throughgoing structure that separates the disparate pre-late middle Miocene stratigraphic sections.

From Late Cretaceous through early middle Miocene, the strata that now lie on the north side of the Malibu Coast fault form an accordant, nearly complete depositional sequence with indications of only minor, local folding and faulting. Major tectonic activity, accompanied by basaltic and andesitic volcanism, began in the middle of the middle Miocene (the basin-inception phase of the evolution of the Los Angeles basin, as described by Yerkes and others, 1965) and continued, probably episodically, into Pliocene time. Upper Pleistocene marine and nonmarine terrace deposits lie unconformably over the tilted, folded, and faulted upper Miocene and older strata. Although the terrace deposits have been broadly warped and locally faulted, their deformation is dramatically less intense than that in the underlying strata.

Structural and stratigraphic relations indicate that the middle Miocene deformation included significant crustal extension, detachment faulting, and tilting of major fault blocks, as well as a minimum of several tens of miles of lateral offset on the Malibu Coast fault (Campbell and others, 1966; Yerkes and Campbell, 1971; Campbell, 1973). If the deep marine depositional environments in which the late Miocene and early Pliocene strata of the Los Angeles and Ventura Basins were formed are considered to be manifestations of extensional deformation, the same style of deformation may have continued well into the Pliocene in the western Santa Monica Mountains. By late Pleistocene time, however, the sense of regional deformation along the Malibu Coast fault had been transformed from one of major lateral and/or extensional faulting to one dominated by north-over-south thrusting accompanied by uplift of the Santa Monica Mountains on the north relative to the Santa Monica basin offshore to the south. The deformation of the entire zone between the Anacapa and Malibu Coast faults shows late Pleistocene and Holocene(?) effects that can be attributed to a north-south compressional stress field, probably in association with some left-lateral oblique component.

Detailed mapping of a wave-cut surface overlain by 125,000-year old marine terrace deposits in the Pacific Palisades area by McGill (1987) shows evidence of relative uplift, local tilting and warping, and fault displacement. McGill (1987) interprets some evidence as indicating that nonmarine deposits as young as 25,000-30,000 years BP may have been offset by as much of 5 feet. Birkeland (1972) interprets the present configuration of elevated marine terraces to represent eustatic sea-level changes superimposed on a coastline that, near Point Dume, was being elevated at a rate of 1-1.2 feet (32-39 cm) per 1,000 years during the late Quaternary.

At a gravel pit locality about 2¼ miles (3.6 km) north of Point Dume, upper Pleistocene marine terrace deposits probably more than 250,000 years old (pre-Malibu terrace; see Birkeland, 1972, fig. 9) have been dropped at least 12 feet in a small north-northeast-trending graben bounded on both sides by basalts of the Zuma Volcanics (locality 1 of Yerkes and Wentworth, 1965, p. 151). Like most of the known offsets of the upper Pleistocene marine terrace deposits found in the general vicinity of the Malibu Coast fault, the bedrock units affected by the young offset are entirely on one side of the throughgoing bedrock fault, at this locality about 400 feet south of the trace of the Malibu Coast fault. Further east, several localities are entirely north of the trace of the Malibu Coast fault.

About 6 miles to the east, in Marie Canyon, the basal contact of 150,000-year-old marine terrace deposits (Corral terrace level of Birkeland, 1972) overlying dolomitic shales of the Monterey Shale is repeated by north-over-south thrusting approximately parallel to the bedding in the Monterey. As shown in Figure 2, the offset of the contact is at least 50 feet (16 m) on a northwest-trending fault that dips 22° to 35° northeast. The locality lies about 100 feet (32 m) south of the trace of the Malibu Coast fault. These exposures document that significant fault rupture of the surface has occurred on faults of the coastal zone within the past 150,000 years.

Contemporary vertical crustal movement in the area has been documented by Castle and others (1977) through analysis of precise leveling records. Comparison of 1971 and 1973 level surveys suggests that as much as 30 mm of uplift in that period may have accompanied the Point Mugu earthquake of February 21, 1973. Comparisons among four pre-earthquake level surveys (1960,1968, 1969, and 1971) indicate that aseismic vertical movements occurred prior to the earthquake. The aseismic movements appear to have been episodic and oscillatory (both up and down), but the 1960 through 1973 cumulative effect of aseismic and coseismic vertical deformation in the coastal part of the Point Dume quadrangle has been an uplift of between 15 and 30 mm (see Castle and others, 1977, fig. 2).

Yerkes and Lee (1979; 1986, p. 78-81), and Lee and others (1979) have summarized the regional seismicity of the western Transverse Ranges with an emphasis on the several hundred well-located events of M_L 2 to 6 that occurred between 1970 and 1976. The recorded earthquakes suggest that the seismic activity that is likely to have the greatest effect on the southern Santa Monica Mountains has occurred chiefly along the Anacapa fault, where focal mechanisms indicate reverse movement on north-dipping faults. The strongest earthquake of this group to occur in the western Santa Monica Mountains is the magnitude 6.0 Point Mugu earthquake of February 21, 1973.

Investigations of recent earthquakes in North Palm Springs, southern California (Morton and others, 1989), and in the Loma Prieta area, central California (Plafker and Galloway, 1989), have identified surface cracks and offsets that are attributed to distributed strain, rather than to a direct physical connection to the zone of seismogenic rupture at depth on the source fault. The distributions of localities of post-late Pleistocene faulting suggest that they, too, might have formed as a surficial response to seismogenic displacement at depth, possibly on the Anacapa fault, rather than being produced as intrinsic parts of seismogenic displacement on the Malibu Coast fault.

References Cited

Birkeland, P. W., 1972, Late Quaternary eustatic sea-level changes along the Malibu coast, Los Angeles County, California: Journal of Geology, v. 80, no.4, p. 432-448

Campbell, R. H., 1973, Generalized geologic map and sections, Santa Clara River to Santa Monica Bay, southern California; in Colburn, I. P., and Fritsche, A. E., eds., Cretaceous stratigraphy of the Santa Monica Mountains and Simi Hills, southern California: Geological Guidebook for the 1973 Fall Field Trip of the Pacific Section of the Society of Economic Paleontologists and Mineralogists, map in pocket, scale approximately 1:140,000

Campbell, R. H., Yerkes, R. F., and Wentworth, C. M., 1966, Detachment faults in the central Santa Monica Mountains, California; in Geological Survey research, 1966: U.S. Geological Survey Professional Paper 550-C, p. C1-C11

Campbell, R. H., and Yerkes, R. F., 1976, Cenozoic evolution of the Los Angeles basin area -- relation to plate tectonics; in Howell, D. G., ed., Aspects of the geologic history of the California continental borderland: Pacific Section, American Association of Petroleum Geologists, Miscellaneous Publication 24, p. 541-558

Castle, R. O., Church, J. P., Elliott, M. R., and Savage, J. C., 1977, Preseismic and coseismic elevation changes in the epicentral region of the Point Mugu earthquake of February 21, 1973: Bulletin of the Seismological Society of America, v. 67, no. 1., p. 219-231

Junger, Arne, and Wagner, H. C., 1977, Geology of the Santa Monica and San Pedro basins, California continental borderland: U.S. Geological Survey Map, MF-820, 1:250,000

Lee, W. H. K., Yerkes, R. F., and Simirenko, M., 1979, Recent earthquake activity and focal mechanisms in the western Transverse Ranges, California: U.S. Geological Survey Circular 799-A, 26 p.

McGill, J. T., 1989, Geologic maps of the Pacific Palisades area, Los Angeles, California: U.S. Geological Survey Map I-1828, 2 sheets, scale 1:4,800

Morton, D. M., Campbell, R. H., Jibson, R. W., Wesson, R. L., and Nicholson, C., 1989, Ground fractures and landslides produced by the North Palm Springs earthquake of July 8, 1986; in Sadler, P. M., and Morton, D. M., eds., Landslides in a semi_arid environment: Publications of the Inland Geological Society, v. 2, p. 183-196

Plafker, G., and Galloway, J. P., eds., 1989, Lessons learned from the Loma Prieta, California, earthquake of October 17, 1989: U.S. Geological Survey Circular 1045, 48 p.

Yerkes, R. F., McCulloh, T. H., Schoellhamer, J. E., and Vedder, J. G., 1965, Geology of the Los Angeles Basin, California -- an introduction: U.S. Geological Survey Professional Paper 420-A, 57p.

Yerkes, R. F., and Campbell, R. H., 1971, Cenozoic evolution of the Santa Monica Mountains-Los Angeles basin area II. Constraints on tectonic models; abs: Geological Society of America, Abstracts with Programs, v. 3, no. 2, p. 222-223

Yerkes, R. F., and Wentworth, C. M., 1964, Geologic report on the proposed Corral Canyon nuclear power plant site, Los Angeles County, California: U.S. Geological Survey administrative report prepared on behalf of the U.S. Atomic Energy Commission, December, 1964, 93 p.

Yerkes, R. F., and Wentworth, C. M., 1965, Structure, Quaternary history, and general geology of the Corral Canyon area, Los Angeles County, California: U.S. Geological Survey Open-File Report 864, 214 p.

Yerkes, R. F., and Lee, W. H. K., 1979, Late Quaternary deformation in the western Transverse Ranges, California: U.S. Geological Survey Circular 799-B, 37 p.

Yerkes, R. F., and Lee, W. H. K., 1987, Late Quaternary deformation in the western Transverse Ranges; in: Morton, D. M., and Yerkes, R. F., eds., Recent reverse faulting in the Transverse Ranges, California: U.S. Geological Survey Professional Paper 1339, p. 71-82

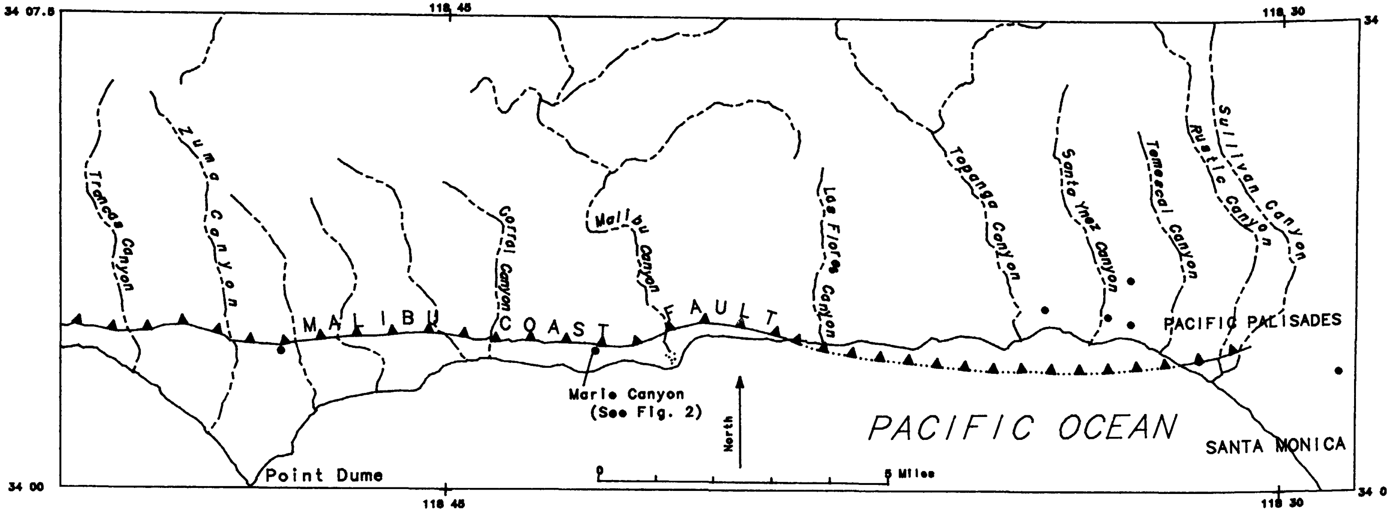

Figure 1. Outline map of part of south coastal Santa Monica Mountains, showing Malibu Coast Fault and localities of faulted upper Pleistocene or younger deposits. (Modified after Yerkes and Wentworth, 1965)

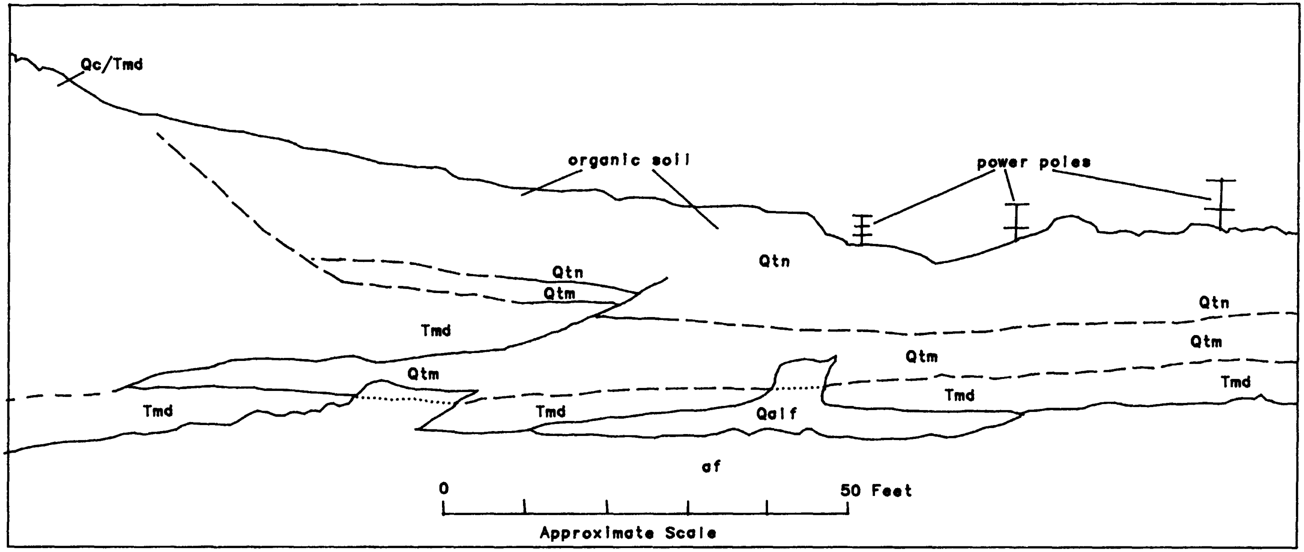

Figure 2. Sketch from a 1973 photograph of east bank of Marie Canyon, showing Monterey Formation (Tmd) bedrock thrust southward over Quaternary marine and nonmarine terrace deposits (Qtm and Qtn, respectively). Locality about 200 feet north of the Pacific Coast Highway and about 200 feet south of the trace of the Malibu Coast fault (as mapped by Yerkes and Campbell, 1980), which here constitutes the bedrock boundary between the Monterey Formation (middle and upper Miocene) on the south and the Sespe Formation (upper Eocene, Oligocene, and lower Miocene) to the north. (Qc/Tmd indicates thin colluvium overlying Monterey bedrock immediately above old erosional shoreline angle; af is construction fill in canyon bottom; Qalf is small fan deposited on fill) The cutbank was subsequently graded and planted with ground cover.

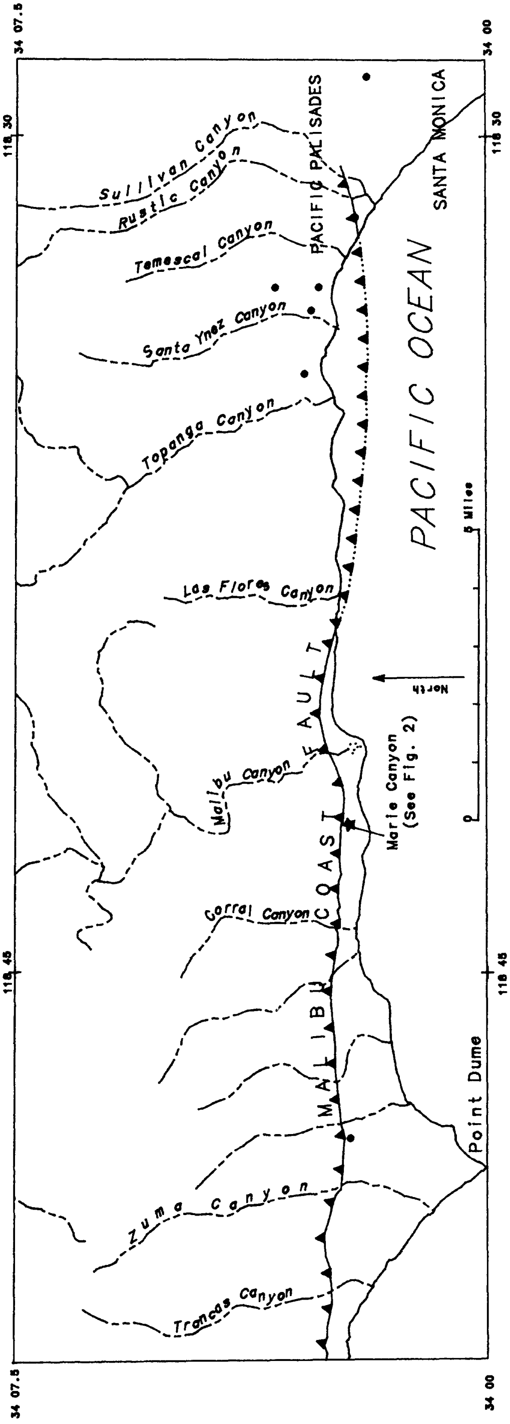
34 07.5
118 30
118 45
34 00
Sullivan Canyon
Rustic Canyon
Temescal Canyon
Santa Ynez Canyon
Topanga Canyon
Las Flores Canyon
Malibu Canyon
Corral Canyon
Zuma Canyon
Trancas Canyon
PACIFIC PALISADES
SANTA MONICA
PACIFIC OCEAN
MALIBU COAST FAULT
Marie Canyon
(See Fig. 2)
Point Dume
North
0
5 Miles

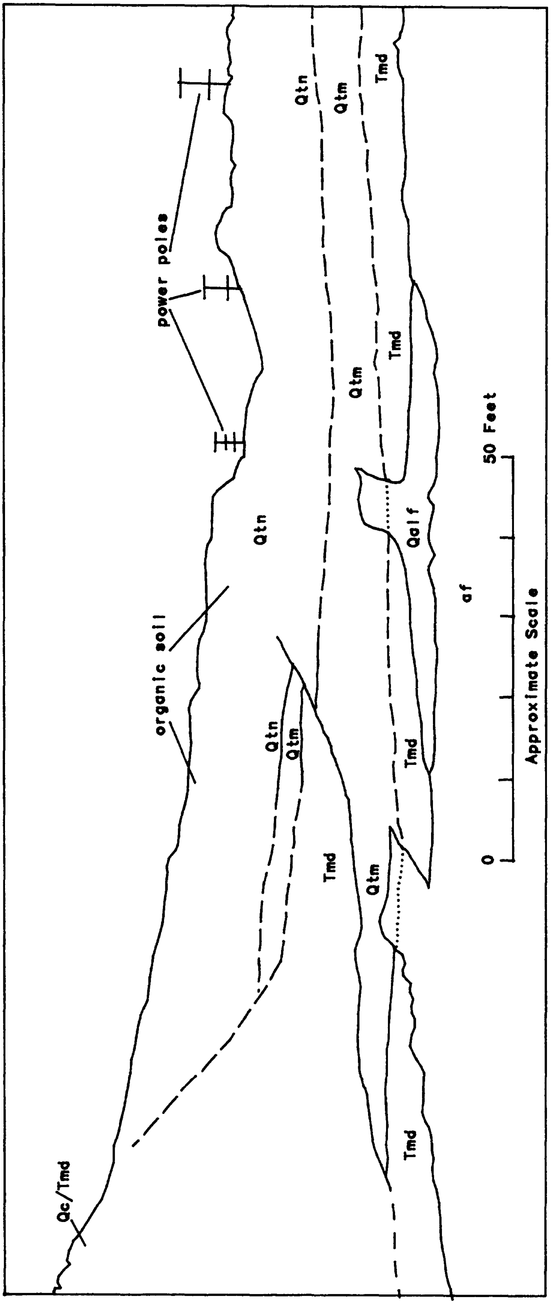
power poles
organic soil
Qtn
Qtm
Tmd
Qtn
Qtm
Tmd
Qtm
Tmd
Qtn
Qalf
af
Qtn
Qtm
Tmd
Tmd
Qtm
Tmd
Qc/Tmd
50 Feet
0
Approximate Scale

TECTONICS OF SEISMIC SOURCE ZONES, CENTRAL INTERIOR OF THE UNITED STATES

9950-04542

ANTHONY J. CRONE
Branch of Geologic Risk Assessment
U.S. Geological Survey
Box 25046, MS 966, Denver Federal Center
Denver, CO 80225
(303) 236-1595

INVESTIGATIONS

1. Cecil continued collection, analysis, and interpretation of potential-field data to clarify structural relations across the Wichita Frontal fault system in the area of the Meers fault (data collected in collaboration with L.-A. Bradley, BGRA, and S.L. Robbins and C. Williamson, Br. Sedimentary Processes).

2. Ellis initiated a study to evaluate and analyze the state of the contemporary stress field along the Wichita Frontal fault system, south-central and southwestern Oklahoma. With the exception of borehole-breakout data (Dart, 1987; Dart and Zoback, 1989), little information is currently available regarding the state of stress in parts of southern Oklahoma. Knowledge of the magnitude and orientation of the stress field may provide insight into the contemporary tectonics and seismic potential of individual faults in the Wichita Frontal fault system. Wellbore logs and drilling records from petroleum exploration and production in the region could contain information on the local and regional stress regimes.

3. Madole continued regional reconnaissance and detailed local studies of Quaternary alluvial stratigraphy in the vicinity of the Meers fault, southwestern Oklahoma.

4. Dart continued compiling and analyzing subsurface data from Oklahoma and the New Madrid seismic zone. He updated the existing catalog of borehole-breakout data for wells in Oklahoma and the Texas Panhandle. He completed the initial data-entry phase of subsurface stratigraphic information in the New Madrid region and completed a preliminary set of structure-contour and subcrop maps of various Paleozoic rock units in the region.

5. McKeown and Hamilton continued their analysis of geophysical, geologic, and seismic data related to understanding the structural and physical properties of the source zone that generates most of the earthquakes in the New Madrid seismic zone.

6. Hamilton, in collaboration with W.D. Mooney (USGS, Menlo Park, CA), analyzed selected seismic-refraction profiles in the New Madrid seismic zone to examine the attenuation of refracted seismic waves in the upper crust that pass through the Blytheville arch and major fault zones associated with Reelfoot rift.

7. Hamilton, McKeown, and Crone were key players in organizing and conducting the USGS-sponsored workshop to assess the need for an intensified program of scientific studies in the New Madrid seismic zone. They also assumed major responsibilities in preparing the two reports that resulted from the workshop.

8. Swolfs and Collins studied calcite-filled vein sets and measured bulk densities in an oriented core from selected depths between 7,973-8,002 ft and in unoriented cores from 10,200-10,229 ft and 11,400-11,426 ft in the Dow Chemical Co. #1 Garrigan well, Mississippi Co., Arkansas. The core is on loan to the USGS from the Arkansas Geological Commission through the efforts of E.E. Glick (USGS, Br. Central Regional Geology, Denver).

9. Diehl prepared a detailed stratigraphic log of the oriented core (7,973-8,002 ft) from the Dow Chemical Co. #1 Garrigan well, and continued petrographic and scanning-electron-microscope (SEM) studies of drill cuttings and junk-basket samples from the #1 Garrigan and the Dow Chemical Co. #1 Wilson wells, Mississippi Co., Arkansas.

10. Collins processed selected samples of well cuttings from Dow Chemical Co. #1 Garrigan well for analysis of insoluble residues.

RESULTS

1. (Cecil) Additional gravity and ground magnetic data, as well as exploratory VLF (Very Low Frequency) electromagnetic data were collected across the Meers fault at several locations. Samples of the exposed igneous rocks were collected for analyses of physical properties to aid in modeling of the gravity data. The data collection and compilation of aeromagnetic and gravity data for the 1:100,000 Lawton quadrangle is complete. The ¼-mile-spaced aeromagnetic data (USGS, 1975) is digitized and the density of gravity measurements has been filled in to ~3-mile-spacing. In addition, eight detailed ground magnetic profiles, five detailed gravity profiles, and four VLF profiles have been prepared across the Holocene Meers fault scarp and along the trace of the fault northwest and southeast of the scarp.

The VLF data show that the fault zone has a recognizable induced signal, though the signal-to-noise ratio is too low to perform additional quantitative analyses. The magnetic profiles show several notable features. The dike-like body, first recognized by Purucker (1986), is apparent on several of the profile lines as an anomaly of almost 1000 gammas. At the northwest end of the Meers fault scarp, splays of the fault that were previously interpreted on aeromagnetic data are visible. A profile line across the Meers fault less than one mile east of Ketch Creek shows a splay near the juncture of the Blue Creek Canyon and Meers faults. This splay is also shown on the surface rupture map of Ramelli and Slemmons (1986). Further analysis of the magnetic and gravity profiles will help determine the fault's attitude at depth and physical properties that characterize the part the fault that has Holocene movement.

2. (Ellis) An obscure study conducted in the early 1970's mapped the maximum and minimum stress gradients for a large part of central Oklahoma by utilizing data from hydraulic fracturing of oil wells. The stress gradients, displayed as contour plots, indicate areas of relatively high stress in the Washita Valley fault zone and the Arbuckle Mountains. Efforts are now underway to obtain the original data base used in this earlier study to evaluate its utility in mapping the magnitude and distributions of stress near the Wichita Frontal fault system. Hopefully, this data set will be supplemented by data from more recent wells. Analyses of these data will focus on examining the localized stress conditions near specific faults, integrating the stress magnitude estimates with existing stress-direction data, studying variations in the stress magnitude with depth, and confirming and (or) refining the stress distribution analysis derived from the previous study. The results of this analysis will be evaluated in the context of our current understanding of tectonic setting and seismicity in the central interior of the United States.

3. (Madole) A more complete understanding of the distribution and age of Quaternary alluvium in southwestern Oklahoma will help clarify the history of movement on the Meers fault. The southeastern end of the fault crosses East Cache Creek, a major drainage in the region. A reconnaissance study of Quaternary alluvium along East Cache Creek from near Lake Ellsworth southward to the Red River confirms that the basic stratigraphic units that were recognized and defined in previous studies (Madole, 1988) could be correlated on a regional basis. The Quaternary units that are exposed in East Cache Creek Valley do not appear to be vertically displaced across the projected trace of the Meers fault. The alluvial stratigraphy of East Cache Creek can be traced downvalley into the Red River Valley where Quaternary alluvium locally contains the 620-ka Lava Creek B volcanic ash. Hence, more detailed local studies in the East Cache Creek drainage and better regional correlations with alluvial units in the Red River Valley should refine the age control on early (?) and middle Pleistocene alluvium in the vicinity of the Meers fault, which will provide information on long-term slip-rates on the fault. Several ^{14}C samples were collected during the field work but have not yet been dated.

4. (Dart) The analysis of wellbore breakouts in Oklahoma and the Texas Panhandle has been completed and the results have been finalized for publication as a USGS Bulletin.

The catalog of digitized subsurface stratigraphic information in the New Madrid seismic zone is being updated with new information. The current data base consists of more than 400 entries from published and unpublished sources. Preliminary maps are being revised and refined. The quality of this data base is being expanded and improved by incorporating stratigraphic information derived from seismic-reflection profiles in the area. Plots of various stratigraphic units show a good correlation between the drill-hole data and the seismic-reflection profiles. Preliminary results of this subsurface mapping effort were presented at the 1989 Geological Society of America Annual Meetings in St. Louis, Missouri.

5. (McKeown and Hamilton) The spatial association of most earthquakes in the New Madrid seismic zone with the Blytheville arch (informally named "Charlie's ridge") and with the enigmatic Pascola arch has been known for several years (Crone and others, 1985; Hamilton and McKeown, 1988). However, the origin, extent, and physical properties of the arches, which are important to establishing the areal limits of the source zone, are controversial. Recently, the arches were interpreted to be the result of structural inversion of a very thick section of Cambrian rocks that were deposited in a deep trough along the axis of the Reelfoot rift (Hamilton and McKeown, 1988). The most recent analysis of seismic-reflection and drill-hole data suggests that the inversion is the result of diapirism. Combining stratigraphic information from the regional drill-hole data (compiled by R. Dart) with the areal extent of the Blytheville arch, as mapped from the seismic-reflection data, show that the Pascola arch is actually a dome-like structure that may be a continuation of the Blytheville arch. The epicenters of the three largest earthquakes of the 1811-12 sequence are imprecisely located, but they are within the limits of the Blytheville arch (whose exact boundaries are also imprecise) and its extension, the Pascola arch. The spatial correlation between the largest earthquakes in 1811-12 and the largest structural feature in Reelfoot rift raises the possibility that defining the limits of the arches will also delimit the source zones for major earthquakes in the New Madrid seismic zone.

6. (Hamilton) Detailed analysis of the seismic-refraction data from the New Madrid region show that refracted seismic waves that pass through the axial zone of seismicity and the fault zone along the southeastern margin of Reelfoot rift are highly attenuated. The high attenuation can be attributed to defocusing of seismic energy by a low velocity layer in the upper crust and (or) scattering and absorption of the waves. It is likely that the multiple episodes of deformation, which have affected Reelfoot rift since Cambrian time, have severely fractured and altered the rocks in major fault zones. Areas of greatly attenuated seismic waves may be a useful criterion for identifying major fault zones in intraplate settings. These results are being published in *Science*.

7. (Hamilton, McKeown, and Crone) The 1990 budget appropriations bill for the USGS requires that the USGS submit a report to Congress documenting the need, purpose, and importance of an intensified program to evaluate and mitigate the earthquake hazards in the New Madrid seismic zone. As a result of this Congressional mandate, a USGS-sponsored workshop was convened by R.M. Hamilton (USGS) and A.C. Johnston (Memphis St. Univ.) on November 15-16, 1989, at Memphis State University. The purpose of the workshop was to seek input from a wide spectrum of the scientific community on all aspects of the earthquake hazards in the New Madrid region. Approximately 60 individuals from various Federal and State agencies, Congressional committee members, academic institutions, and private organizations and corporations attended the workshop. During the two days of presentations and panel discussions, participants summarized the current state of knowledge on the New Madrid seismic zone, identified critical gaps in the existing data, defined topics that warranted further study, and prioritized recommendations for future research. Hamilton, McKeown, and Crone presented summary papers and led group discussions which defined research needs and priorities.

Two important products from the workshop are in preparation--the Report to Congress on research needs and priorities, and a USGS Circular which provides a general summary and supplemental supporting information for Congressional report. Hamilton has primary responsibility for compiling and editing the Circular and the Congressional report. McKeown and Crone contributed summary discussions to both publications.

8. (Swolfs and Collins) Two tectonically significant sets of extensional veins are present in the oriented core from the #1 Garrigan well and have been mapped in detail. The respective orientations of the near-vertical vein sets are N. 41° E. and N. 35° W. The N. 41° E. set is essentially parallel to the strike of Reelfoot rift. The fractures in this set are typically stratabound and are as much as 6 cm high and 3 mm wide. The N. 35° W. set is nearly perpendicular to the strike of the rift. This set is present throughout the length of the core, dips 80°SW., and contains individual veins that are as much as 1 mm wide. A steeply dipping set of veins, which are probably counterparts to the rift-normal set, are the only veins present in unoriented cores from depths of 10,200 ft and 11,400 ft in the same well. The presence of these rift-normal veins in the deeper parts of the well imply that this set of veins formed in response to a regional deformational event.

The stratification in the core from 7,973-8,002 ft has dips of 5° or less, assuming the drill hole is vertical. In contrast, the stratification in the core from 10,201-10,229 ft and 11,402-11,425 ft has dips of approximately 21°. These data indicate that either a major depositional or angular unconformity is present in the well between the depths of 8,002 and 10,20 ft. Bulk density values for the core are listed in Table 1.

TABLE 1.--Bulk-density measurements on core from selected intervals of the Dow Chemical Co. #1 Garrigan well, Mississippi County, Arkansas.

Density measurements are given in gm/cm^3

Depth (ft)	Low	High	Average
7,973-8,002	2.67	2.74	2.70
10,200-10,229	2.74	2.78	2.76
11,400-11,426	2.69	2.79	2.77

9. The detailed stratigraphic log of the oriented core from the #1 Garrigan well is interpreted to record of multiple cycles of subsidence in tidal flat and shallow-water marsh depositional setting. Repeated sequences of ripple-marked bedding and mud-flat sedimentation are interpreted as evidence of clastic deposition in a deltaic setting.

Petrographic analysis of the carbonate-filled fractures in unoriented cores from the #1 Garrigan well show several generations of cracking and resealing by authigenic minerals. The succession of minerals lining the vertical microfractures is similar to that observed in the fractures in samples from the Dow Chemical Co. #1 Wilson well, which is located about 27 km south of the Garrigan well. The earliest authigenic mineral is quartz followed by deposition of Fe-poor dolomite, Fe-rich dolomite, and finally Fe-rich calcite.

A section of core (11,420 ft) from the Garrigan well contains slickolites on a subhorizontal thrust fault. Authigenic minerals deposited on the slickolite consist of quartz followed by Fe-rich calcite. The dolomite phase is missing, which implies that either the dolomite has been replaced by calcite or no movement on this surface occurred during the episode of fracture-opening in which the dolomite was deposited.

The sequence of fracture-filling authigenic minerals in the basal clastic rocks in the #1 Wilson well record at least seven episodes of fracture opening, and therefore extension. Parallel sets of aligned fluid inclusions and quartz-filled microfractures are interpreted to record episodes of extension in Early Cambrian time. A later phase of concurrent clay-filled and carbonate-filled microfractures is inferred to record late Paleozoic tectonism. All of these vertical, mineral-filled fractures are commonly associated with and offset by horizontal stylolites. Tectonic and diagenetic stylolites are common. Authigenic monazite is present in the styolites, which may indicate a common origin with the authigenic monazite that is found in Hicks Dome in the fluorspar mineral district of southern Illinois.

10. The insoluble residues of 30 samples from the Dow Chemical Co. #1 Garrigan well show no distinctive changes in the mineralogy or the proportions of insoluble minerals that might serve as a tool for stratigraphic correlation. A special effort has been made to treat selected samples in a manner that would preserve highly soluble evaporitic minerals such as gypsum, anhydrite, and halite and fragile fossil fragments. No evaporitic mineral have been found. Foraminifera fragments were found in samples of Paleozoic rocks from depths of 3,810-80 and 8,560-8,620 ft.; they are probably of the genera *Nodosaris* or *Dentalina* (identified by M. Lagoe, Univ. Texas, Austin) which are mid-Mesozoic or younger. Therefore, these fossil fragments are contaminants that have collapsed from shallower parts of the well.

REFERENCES CITED

Crone, A.J., McKeown, F.A., Harding, S.T., Hamilton, R.M., Russ, D.P., and Zoback, M.D., 1985, Structure of the New Madrid seismic source zone in southeastern Missouri and northeastern Arkansas: Geology, v. 13, p. 547-550.

Dart, Richard, 1987, South-central United States well-bore breakout-data catalog: U.S. Geological Survey Open-File Report 87-405, 95 p.

Dart, R.L., and Zoback, M.L., 1989, Wellbore breakout stress analysis within the central and eastern continental United States: The Log Analyst, Jan-Feb. 1989, p. 12-25.

Hamilton, R.M., and McKeown, F.A., 1988, Structure of the Blytheville arch in the New Madrid seismic zone: Seismological Research Letters, v. 59, no. 4, p. 117-121.

Madole, R.F., 1988, Stratigraphic evidence of Holocene faulting in the mid-continent--The Meers fault, southwestern Oklahoma: Geological Society of America Bulletin, v. 100, no. 3, p. 392-401.

Purucker, Michael, 1986, Interpretation of an aeromagnetic survey along the Wichita Frontal fault zone, *in* Gilbert, M.C., ed., Petrology of the Cambrian Wichita Mountains igneous suite [Oklahoma]: Geological Survey Guidebook 23, p. 129-136.

Ramelli, A.R. and Slemmons, D.B., 1986, Neotectonic activity of the Meers fault, *in* Donovan, R.N., ed., The Slick Hills of Southwestern Oklahoma--Fragments of an aulocogen?: Oklahoma Geological Survey Guidebook 24, p. 45-54.

U.S. Geological Survey, 1975, Aeromagnetic map of the Wichita Mountains area, southwestern Oklahoma: U.S. Geological Survey Open-File Report 75-16, scale 1: 62,500, 1 oversized plate.

REPORTS

Crone, A.J., and Luza, K.V., 1990, Style and timing of Holocene surface faulting on the Meers fault, southwestern Oklahoma: Bulletin of the Geological Society of America, v. 102, no. 1, p. 1-17.

Dart, R.L., 1989, *In situ* stress analysis of wellbore breakouts from Oklahoma and the Texas Panhandle: U.S. Geological Survey Bulletin 1866-F, 82 p.

Hamilton, R.M. and Mooney, W.D., 1990, Seismic-wave attenuation with crustal faults in the New Madrid seismic zone: *Science*, in press.

Swolfs, H.S., McKeown, F.A., and Glick, E.E., 1990, Episodes of extension in Cambrian rocks in the Reelfoot rift, Mississippi embayment [abs.]: EOS, Transactions, American Geophysical Union, v. 71, in press.

SEISMOTECTONIC RESEARCH STUDIES

A.F. Espinosa
Branch of Geologic Risk Assessment
U.S. Geological Survey
Box 25046, MS 966, Denver Federal Center
Denver, CO 80225
(303) 236-1597

Investigations

1. Several tests are being performed in order to determine the accuracy of standard hypocenter estimation methods used in the analysis of regional seismic network data. Adaptation of a probabilistic approach to estimating hypocenters and examination of the underlying statistics in this estimation problem is underway.

2. Development of a detection threshold model for the Southern Great Basin Seismic Network (SGBSN) is in progress. Interpretation of the regional seismicity in the context of this threshold model and of a regional tectonic framework is being investigated.

3. Examination of the effects of source radiation on magnitude estimates is underway.

4. A simultaneous inversion of strong motion and teleseismic body-wave records is used to study the rupture history of the 1978 Tabas, Iran, earthquake. A nonlinear least-squares is used where the problem is parametrized in terms of both the slip amplitudes and the rupture times on a finite fault. This earthquake is one of the largest intraplate events, $M_S = 7.5$, for which there are several strong-motion recordings within one fault length, and has important implications for the estimation of strong ground motions in other intraplate environments; [i.e., New Madrid seismic zone].

5. Three-component strong-motion records from seventeen sites within one fault depth are modeled to study the rupture history of the 1987 Whittier, California, earthquake.

6. Teleseismic broadband body waves are inverted using both L2 and L1 norms to compare these two numerical approaches and to determine the rupture history of the 1989 Loma Prieta, California, earthquake.

7. Field investigation of the December 7, 1988, earthquake, $M_S = 6.9$, near Spitak, Armenia is being analyzed.

8. Field investigation of the June 10, 1987, earthquake, $m_b(Lg) = 5.2$, near Claremont, Illinois, is being analyzed.

9. Focal-mechanism solutions and their distribution in Alaska and the Aleutian Islands for 700 earthquakes, which took place from 1927 through 1987, are being cataloged. A focal-mechanism parameter catalog is being prepared for publication.

10. A focal-mechanism distribution map for Alaska and the Aleutian Islands is being prepared for publication.

11. Post-earthquake investigations were undertaken in the San Francisco Bay area after the October 17, 1989, Loma Prieta, earthquake. And follow-on field investigations have been conducted during the past six-months. The damage assessment was funded through the University of Colorado under a NSF Quick Response Research Grant. Direct field observations were made one day after the earthquake to a week later, when the transition to reconstruction occurred. This data is being edited and analyzed.

12. A continued analysis of the technical and societal aspects of the damage assessment process is underway. Several field visits and additional technical information has been compiled. A building-by-building analysis of damaged structures in the city and county of San Francisco was undertaken. Various structural characteristics, along with other building parameters, are been analyzed including a detailed vulnerability analysis of structures in the Marina District. Also, detailed information on actual losses (not estimated) is being collected and analyzed.

13. Preparation of the geologic map-report for the Anchorage B-8 SW quadrangle is in progress and awaits field checking, final geologic interpretation, and completion of the text which will include extensive surficial geologic information. Detailed interpretation of surficial geologic features of the eastern portions of the Anchorage A-8 NE and SE quadrangles and parts of adjacent quadrangles is in progress.

14. Results of previous field investigations of emergent tidal sediments and intercalated organic materials from which paleoseismicity of the region may be interpreted are being reevaluated using numerous radiocarbon dates from the region in cooperation with the Branch of Central Mineral Resources.

15. A surficial geologic map of the Eklutna River drainage basin, Municipality of Anchorage is in preparation from existing manuscripts and other relevant maps for inclusion in a Water Resources Division report.

16. Surficial geologic manifestations of the Chilean Tectonic Subduction Zone were investigated in middle and southern Chile during part of an austral summer as part of a special USGS grant. Samples of several types of organic materials have been analyzed and their relation to submerged and emerged sediments is under study in cooperation with the Branch of Central Mineral Resources.

17. Reinterpretation of some surficial geologic maps and detailed airphoto interpretation of sectors of the Gulkana A-1 and Nabesna B-6 quadrangles in Alaska is nearing completion in cooperation with the Branch of Alaskan Geology.

18. Studied relations among seismicity, tectonism, and hydrothermal regime in the west moat of the Long Valley caldera, California, is underway.

19. Studied relations among seismicity, tectonism, and hydrothermal regime in Chile, is in progress.

20. Calibration of temperature-sensing probes was undertaken. Corrected temperature logs obtained in wells in Long Valley caldera, California, during July 1989 for drift in thermistor probe is underway. Reduced and analyzed temperatures obtained in the air-filled part (upper 980 ft) of borehole PLV-1. Determined corrections for natural gamma-ray logs obtained in MLGRAP #1 and #2 due to variations in hole diameter, casing, cement, and fluid content.

21. Determined capillary corrections for acid-etch inclinometry in glass tubes of various diameters to temperatures of 80° C so that the inclinations of hot, small-diameter boreholes can be measured.

Results

1. Standard methods generally produce reliable epicenter estimates and associated uncertainties. Focal depth estimates can easily be biased by more than several kilometers due to large (several tenths of seconds) random data errors and (or) systematic velocity model errors (average velocity errors of several percent). The use of S-wave data can reduce this potential bias and estimates derived using the probabilistic approach are more robust with respect to random and systematic error. All methods invoke some model of the underlying statistics and all methods may produce poor results if the underlying statistics are incorrectly characterized.

2. There is a significant over-printing of a spatially variable detection threshold on the seismicity patterns observed in the SGBSN catalog data. This is accounted for when examining the distribution of epicenters. A strong correlation between concentrations of epicenters and zones of strike-slip faulting is apparent. There is also a high concentration of seismicity in the same area where nuclear testing is done. The seismicity is interpreted in terms of a semi-rigid block model such that the seismicity outlines the edges of a southern Great Basin block.

3. Theoretical calculations show that uncertainties in magnitude estimates of more than half a magnitude unit can easily be attributed to source effects and poor spatial sampling in magnitude calculations. These calculations also show that in some cases there can be an almost perfect trade-off between amplitude variations arising from source radiation effects and from attenuation.

4. The acceleration recordings for the Tabas earthquake were bandpass filtered, uniformly sampled, velocity records. Three, 3-component stations situated over or near the fault plane, and ten WWSSN long-period P-waves were selected for inversion. The fault plane is fixed, striking at 330°; with a dip of 25° NE, and is consistent with the long-period teleseismic solution. Our preferred slip model has three or four distinct subevents with maximum displacements between 1 and 2 m. Most of the faulting occurs above a depth of 15 km. The preferred model has a hypocenter depth between 5- and 10-km, a source duration time of 0.7 sec, and a rupture velocity of 2.5 km/sec. M_0 is 5.5 x 10**26 dyne-cm, which is consistent with M_0 values obtained using body waves, but is a factor of two less than M_0 obtained from long-period surface waves.

5. A constant-rupture and a variable-rupture velocity models are considered in this investigation. The results show a complex rupture process within a relatively small source volume, with at least four separate concentrations of slip. Two sources are associated with the hypocenter, the larger have a slip of 55 or 90 cm, depending on the rupture model. These sources have a radius of approximately 2 to 3 km and are ringed by a region of reduced slip. The aftershocks fall within this low-slip annulus. Other sources with slips from 40 to 70 cm, each ring the central source region and the aftershock pattern. The overall dimensions of the Whittier earthquake from the strong-motion inversions is 10 km long (along the strike), and 6 km wide (down the dip). The preferred dip is 30° and the preferred rupture velocity is 2.5 km/sec. M_0 estimates range from 7.4 to 10.0 x 10**24 dyne-cm, depending on the rupture model.

6. Broadband teleseismic P and SH waveforms from the GDSN and GEOSCOPE networks for the Loma Prieta earthquake have been collected. These data will be inverted to obtain the history of slip on a fault plane embedded in a layered half space.

7. A subset of 298 best-located aftershocks in Armenia define a pattern of seismicity about 60 km in length, and it has a broad bend near its mid-point (at the town of Spitak), changing from a near E-W alignment west of the bend to a S. 45-50° E. trend. The distribution of aftershocks west of Spitak is generally consistent with the predominant E-W to E-NE strike of the region's major topographic features. SE of Spitak, the aftershock alignment is subparallel with a NE trend of the mapped co-seismic surface ruptures. Sixteen composite focal-mechanism solutions were determined for events in the aftershock zone. For aftershocks west

of the "Spitak bend", three out of five solutions are in agreement with an easterly striking reverse fault with a small component of right-lateral strike-slip movement. The other two mechanisms indicate almost pure strike-slip displacement along an easterly striking nodal planes. Six composite solutions from the aftershocks in the "Spitak bend" show a mixture of easterly to southeasterly reverse as well as right-lateral strike-slip faulting. Five composite solutions for aftershocks within the southeast segment show a predominant right-lateral strike-slip solution with a southeasterly striking plane. Group composite solutions emphasize that the aftershock zone is in a very complex tectonic setting.

8. The Illinois earthquake occurred in the Wabash Valley seismic zone of southeastern Illinois and southeastern Indiana, and about 200 km of St. Louis, MO. It was felt over an area og about 433,000 km^2 with an I_0 = VI. The USGS and Memphis State University, in a joint effort, deployed 15 aftershock-monitoring-station network (later expanded to 21) and recorded more than 100 aftershocks in a four-day period. Results from 56 located events indicate a compact, tabular-shaped aftershock volume about 1.7 km long, 0.8 km wide, with some 3 1/2 km of vertical extent between about 6 1/2 and 12 km in depth. Six composite focal-mechanism solutions show the predominant mode of faulting as being reverse, including some strike-slip solutions similar to the mechanism of the main shock. The maximum principal stress direction (P-axes) is oriented easterly to east-southeasterly and is subhorizontal in plunge.

9. Results from the post-impact damage-assessment study included the identification of critically important technical and societal factors that affected the damage assessment process. Significant environmental factors included aftershocks and asbestos in earthquake-damaged buildings. Significant social, economic, and legal concerns also influenced the building evaluation process (for example, liability, housing disputes, etc.).

10. Results from the building-by-building assessment of damaged structures show that while building type and design factors were important, that mitigation and maintenance-related issues were significant.

11. The collection of actual-loss data (not post-earthquake estimates) is still in process. Since few final decisions and little repair has been completed on severely damaged structures, the actual-loss figures are still being collected and analyzed.

12. For the Anchorage B-8 SW quadrangle, Alaska, map units have been initially described, interpreted, and designated on overlays and base-map materials and the regional geologic framework part of the text completed.

13. Stratigraphic interpretation of emerged and submerged tidal deposits southeast of downtown Anchorage has resulted in the near completion of the pre-review level of a USGS Bulletin presently entitled, "The Girdwood Member of the Twenty Mile River Formation—late Holocene silt and peat stratigraphy, Turnagain Arm and vicinity, south central Alaska".

14. Scientific products resulting from geologic work in the Eklutna River drainage area, Alaska, were submitted to Water Resources Division, Alaska District.

15. Initial preparation of a paper describing partial results of research concerning emerged and submerged tidal sediments in southern Chile has been accomplished and a paper has been accepted for presentation at the 13th International Sedimentological Congress, Nottingham, U.K., entitled, "Stratigraphy of late Holocene intertidal deposits, Islagrande, De Chiloe region, southern Chile—evidence of relative sea-level changes".

16. The initial surficial geologic maps of the Gulkana A-1 quadrangle, Alaska and of the Nabesna B-6 quadrangle, Alaska were completed and submitted to colleagues in the Branch of Alaska Geology for their input.

17. The wells, MLGRAP #1 and #2, in the Town of Mammoth Lakes have been partly analyzed. The core was logged by Douglas Goodwin for The Town of Mammoth Lakes (California Division of Oil and Gas, Well Summary Report-Geothermal, 1988, A.P.I. Nos. 051-90120 and 051-90121). Temperatures were measured with a thermistor probe (time constant of 2 s in water) lowered at a rate of 3 m/min and recorded and plotted at 0.3-m intervals. Temperatures recorded in the air column are meaningless without further corrections, because the time constant of the probe is much longer in air than in water. Laboratory calibrations were made one month before logging and were repeated on October 21, 1989. Drift corrections have been applied to all of the temperatures obtained in Long Valley during July 1989.

18. The temperatures obtained in the air-filled part of borehole PLV-1 have been reduced and preliminary analysis indicates that the temperatures came into thermal equilibrium quite rapidly (< 1 hour). The temperature increase with depth is exponential. Since the tubing was not cemented in place, the possibility of flow along the hole can not be precluded.

19. The natural gama-ray logs obtained in MLGRAP #1 and #2 require corrections for hole diameter, casing, cement, and fluid content. These corrections were time-consuming, especially in MLGRAP #1, because of the complicated drilling history. A satisfactory correction scheme has been derived and applied to the logs so that they more accurately reflect the lithology.

20. The temperatures and thermal conductivity data for several drill holes in central Chile have been assembled and analyzed. The geologic background material has been obtained. Most of the information necessary to complete a report on the thermal regime of the area is in hand. However, detailed topographic maps necessary for terrain corrections have not been obtained yet.

Reports

Espinosa, A.F., and Rukstales, K.S., 1990, Focal mechanism solutions and maximum horizontal stress distributions for earthquakes in Alaska: Workshop on Focal Mechanism and Tectonics, Sponsored by the Universities of Madrid and of Paris; El Escorial, Spain.

Gomberg, J., 1990, Seismic network configuration, earthquake hypocenter estimation—A re-evaluation and a new approach to an old problem: U.S. Geological Survey Bulletin. (In press).

Gomberg, J., 1990, Seismicity, detection threshold, and a regional tectonic model of the southern Great Basin. (In preparation).

Gomberg, J., Shedlock, K., and Roecker, S., 1990, There is nothing better than good S—The effect of S wave arrival times on hypocenter estimation: Seismological Society of America Bulletin. (Submitted).

Hartzell, S., and Iida, M., 1990, Source complexity of the 1987 Whittier Narrows, California, earthquake from the inversion of strong motion records: Journal of Geophysical Research. (In press).

Hartzell, S., and Mendoza, C., 1990, Simultaneous inversion of strong motion records and teleseismic P-waveforms for fault slip and rupture times of the 1978 Tabas, Iran, earthquake: Seismological Research Letters. (In press).

Oaks, S.D., 1990, The damage assessment process in San Francisco, California after the October 17, 1989, Loma Prieta earthquake—A case study: EOS (American Geophysical Union Transactions), 71 (8), p. 289.

Oaks, S.D., 1990, The damage assessment process after the October 17, 1989, Loma Prieta earthquake—An analysis of the Application of ATC 20: Seismological Research Letters. (In press).

Oaks, S.D., 1990, The damage assessment process after the Loma Prieta earthquake—The application of ATC 20 and effects on relief and recovery, *in* The Loma Prieta earthquake—Short Term Impacts, Bolin, Robert, Ed., Natural Hazards Monograph #49: Boulder, Colorado, University of Colorado. (In press).

Oaks, S.D., 1990, The damage assessment process after the October 17, 1989, Loma Prieta earthquake—Effects on reconstruction and recovery, Hazard Reduction and Recovery Center Monograph: College Station, Texas, Texas A&M University.

Oaks, S.D., 1990, Vulnerability in the Marina District of San Francisco, California—An analysis of structural attributes and damage after the Loma Prieta earthquake: U.S. Geological Survey Professional Paper. (In press).

Richter, D.H., Ratte, J.C., Schmoll, H.R., and Yehle, L.A., 1989, Geologic map of the Gulkana B-1 quadrangle, Alaska: U.S. Geological Survey Geologic Quadrangle Map GQ 1655, scale 1:63,360.

Urban, T.C., and Diment, W.H., 1989a, Capillary corrections for acid-etch inclinometry in boreholes for glass tubes ranging in diameter from 6-25 mm and over a temperature range of 4-80 °C, *in* Abstracts of Papers, Third International Symposium on Borehole Geophysics for Minerals, Geotechnical, and Ground-Water Applications: Mineral and Geotechnical Logging Society, A Chapter-at-Large of the Society of Professional Well-Log Analysts, October 2-5, 1989, Las Vegas, Nevada, p. 20.

Urban, T.C., and Diment, W.H., 1989b, Capillary corrections for acid-etch inclinometry in boreholes for glass tubes ranging in diameter from 6-25 mm and over a temperature range of 4-80 °C, *in* Proceedings Third International Symposium on Borehole Geophysics for Minerals, Geotechnical, and Ground-Water Applications: Minerals and Geotechnical Logging Society, A Chapter-at-Large of the Society of Professional Well-Log Analysts, October 2-5, Las Vegas, Nevada, p. 233-260.

Urban, T.C., and Diment, W.H., 1989c, Capillary correction for acid-etch ininometry in boreholes for glass tubes ranging in diameter from 6-25 mm and over a temperature range of 4-80 °C including statistical analysis of the data: U.S. Geological Survey Open-File Report 89-632, 109 p.

Urban, T.C., and Diment, W.H., 1990a, Thermistor calibrations, techniques, and computer programs, 1968-1989: U.S. Geological Survey Open-File Report 90-216, 48 p.

Yehle, L.A., Schmoll, H.R., and Dobrovolny, Ernest, 1990, Geologic map of the Anchorage B-8 SE and part of the B-8 NE quadrangles, Alaska: U.S. Geological Survey Open-File Report 90-238, about 50 p., scale 1:25,000.

Ground Motion Modeling in the Eastern U. S.
With Emphasis on Effects of New Madrid Earthquakes
on Memphis and St. Louis

14-08-0001-G1769

Robert B. Herrmann
Department of Earth and Atmospheric Sciences
Saint Louis University
3507 Laclede Avenue
St. Louis, MO 63103
(314) 658-3131

Investigations

This program is focused on the specification of representative time histories for future large New Madrid earthquakes at target sites of Memphis, Tennessee and St. Louis, Missouri. This will be accomplished by a combination of deterministic and probabilistic techniques for the generation of time histories. Because of the unique environment of sites within the Mississippi River flood plain, e.g., 1000 meter thicknesses of very low velocity materials, effort is first directed toward constraining the wave propagation properties of the surface material.

Results

1. A three-component continuously recording accelerometer was installed south of New Madrid, Missouri in January. The accelerometer connects into the analog telemetry of the USGS/NRC Central Mississippi Valley Seismic Network and is recorded digitally along with the data from the regional network. Initial sensitivity was set at 10000 V/g, which caused clipping of magnitude 2.8 events within 10 km. In early April the gain was reduced to roughly 1000 V/g, so that larger events could be recorded on scale. Data from the vertical component agree with an adjacent 1 Hz velocity sensor upon integration. One major problem has to do with verifying the orientation of the horizontal components. The usual test of looking at P-wave particle motion is difficult to apply since ray paths are near vertical at the surface due to the low velocities of the sediments. These data will be used together with the CERI/Memphis State Panda Data to constrain the shear velocity and Q profile in the sediments.

2. Enhancements have been made to the random process theory technique to more correctly take into account crustal shear velocity and Q structure in the estimation of peak ground motion. The modification uses simple ray theory and the constraints of full wavenumber integration in a simple computational technique. Two papers have been submitted for publication. The peak acceleration of the 1988 Saguenay earthquake was correctly predicted as a function of distance.

3. Modifications to the random process theory model will be made to incorporate more realistic ray tracing techniques which take into account the transmission and free surface reflection coefficients that are not in the current model.

Publications

Ou, G.-B. and R. B. Herrmann (1990). Estimation theory for strong ground motion, *Seism. Res. Letters* **61,** (in press).

Ou, G.-B. and R. B. Herrmann (1990). A statistical model for peak ground motion from local to regional distances, *Bull. Seism. Soc. Am.* **61,** (in review).

Urban Hazards Seismic Field Investigations

9950-01919* (01896)
9950-03816

K.W. King
Branch of Geological Risk Assessment
U.S. Geological Survey
Box 25046, Denver Federal Center, MS 966
Denver, CO 80225
(303) 236-1591; (303) 236-1605

INVESTIGATIONS

The objectives of this project are: (1) to maintain an operation-instrumentation readiness for opportunities to support research in the earth science and engineering fields, (2) to develop integrated techniques and methodologies for efficiently and effectively documenting and processing high quality digital seismic data, seismic reflection and refraction data, seismic and geological borehole data, and surface/structure response data,(3) to develop improved methods to investigate subsurface geologic structures and geologic/engineering parameters (4) To improve the understanding of how shallow underlying geology affects ground motion.

Specific goals for this reporting period were (a) to document seismic data from the Loma Prieta earthquake, (b) to consolidate the seismic data documented from the Loma Prieta earthquake into a form appropriate for distribution (sites, geology, ground motions, time-histories, etc.), (c) to confirm all field calibrations and site locations used during the Loma Prieta operations, (d) to make a preliminary analysis of the Santa Cruz seismic data, (e) to finalize the Puget Sound site response analysis, and (f) to complete the seismic field operations for the Phoenix, National Park Service/USGS project.

Field Laboratory Efforts

(a-d) The Loma Prieta seismic field operations was a fully cooperative effort with USGS Menlo, EPRI, UC Santa Cruz, and State, County and City personnel. The operations equipment/crew responded to the earthquake within 24 hours. Twelve seismic experiments utilizing a total of 107 sites were completed. A new PC field-data-consolidation system was developed and utilized on all experiments. An open file report was published on the Santa Cruz field effort.

The field calibrations, site locations, seismometer orientations and world time are being corrected on all data headers. The data set is approximately 2 gigi-bytes in size and will be distributed on a CD in the near future.

Preliminary analysis of the seismic data indicates that relative spectral ratios of ground response generally compare well with observed damage distribution resulting from the Loma Prieta earthquake and are correlatable with the subsurface geology. The topographic-high experiment indicates that the ridge areas may be tuned to a narrow frequency band.

(e) Thus far, microearthquakes near Seattle seem to provide the best spectral ratio data to date. Because of funding limitations and project re-direction, data were recovered from only five sites. The data from the five sites have been analyzed and will be the subject of a formal report in 1990.

A cooperative building-testing project/report was completed with NBS. An eight-story building in Portland, Ore., and a seven-story building in Long Beach, Calif. were tested for engineering parameters.

(f) The seismic field effort at the Pueblo Grande ruins for the USGS/NPS preservation team project was completed. The data are now being analyzed.

PUBLICATIONS

King,K.W.,, Tarr, A.C., Carver, D.L., and Williams, R.A., 1989, Seismic ground response studies in Olympia, Washington and vicinity. (Director's Approval). (Submitted to and approved by BSSA).

King, K.W., and Williams, R.A., 1989, Seismic reflection profiling of subsurface cavities and related structures (abs.): Association of Engineering Geologists, Annual Meeting, 1989.

Williams, R.A., and King, K.W., 1989, Correlations between seismic shallow reflection, downhole, and ground response in the Salt Lake City, Utah, urban area. (In review).

Cranswick, E., K. W. King, P. Spudich, D. L. Carver, D. M. Worley, and R. Banfill (1990). Site response across the downtown Santa Cruz alluvial basin, EOS Trans., Am. Geoph. Union, **71**, no. 8, p. 287.

Cranswick, E., R. Banfill, K. W. King, R. Borcherdt, L. Bond, T. McCormick, and A. Johnston (1990). Processing digital seismograms in a Santa Cruz motel using locally rented IBM-PC-compatible microcomputers, EOS Trans., Am. Geoph. Union, **71**, no. 8, p. 287.

Andrews M., R. Banfill, D. Carver, M. Celebi, E. Cranswick, K. King, P. Spudich, and D. Worley (1990) Digital aftershock recordings of the October 17, 1989 Loma Prieta, California, earthquake, EOS Trans., Am. Geoph. Union, **71**, no. 8, p. 287.

Boore, D. M., S. Hough, S. P. Jarpe, and K. W. King (1990). Ground shaking from the 17 October Loma Prieta Earthquake, EOS Trans., Am. Geoph. Union, **71**, no. 8, p 290.

King, K. W., R. A. Williams, D. C. Carver, E. Cranswick, and D. M. Worley (1990) Site response and building damage in Santa Cruz, California, Seismological Society of America 85th annual meeting, May 2-4, 1990.

King, K. W., D. L. Carver, R. A. Williams, E. Cranswick, D. M. Worley, P. Spudich, L. Wennerberg, and M Celebi (1990) Preliminary evaluation of aftershocks recorded in the epicentral region of the 1989 Loma Prieta, California, earthquake: Effects of topography and geology on ground motion, Geophysical Research Letters, Am. Geoph. Union, v

King, K. W., D. Carver, E. Cranswick, R. Williams, and D. Worley (1990). Santa Cruz Seismic investigations: Loma Prieta Earthquake, U. S. Geological Survey Open-File Report(in review)

*defunct

CASCADIA SUBDUCTION ZONE: NEOTECTONICS OF THE ACCRETIONARY WEDGE AND ADJACENT ABYSSAL PLAIN OFF OREGON AND WASHINGTON

Contract 14-08-0001-G1800

Principal Investigator: LaVerne D. Kulm*
Co-Principal Investigator: Robert S. Yeats**
Graduate Research Assistant: Chris Goldfinger**

*College of Oceanography
**Department of Geosciences
Oregon State University
Corvallis, OR 97331
(503) 737-2296

Investigations

The overall objective of this study is to characterize and determine the timing of deformational events in the subducting Juan de Fuca plate (abyssal plain) and deformation front (accretionary wedge) of the Cascadia convergence zone off Oregon and Washington. We will try to identify and date discrete events and relate them to the distribution of earthquakes on the subducting oceanic plate and in the subduction zone.

When we learned in June, 1989, that the first year's NEHRP would be funded, we immediately placed special emphasis on selected neotectonic features in a region that was to be surveyed later in the year. An extensive and comprehensive sidescan survey and multichannel seismic reflection survey were completed off central and northern Oregon during August, September and October,1989, by the principal investigator under a separate, funded grant from the National Science Foundation. We obtained approximately 2,700 sq km of continuous SeaMARC-IA sidescan sonar coverage and 2000 km of 144-channel seismic reflection lines with the M/V GEOTIDE, operated by Digicon Geophysical Corporation, to study the deformational features and events on the continental slope and adjacent abyssal plain off Oregon (44° 30' to 45° 20' N latitude). A photographic mosaic of the navigated sidescan images and individual high-resolution sidescan swaths have been completed for the survey area. Several seismic lines have been processed, which clearly image the faults of the abyssal plain and the accretionary prism.

Non-classified SeaBeam bathymetry in this region was acquired earlier in 1987 and 1988 with the ATLANTIS-II by Oregon State University in a study sponsored by the National Science Foundation. All NOAA SeaBeam bathymetry is now declassified off Oregon, but it still remains classified off Washington, with the exception of pre-1984 data collected along the initial deformation front and the adjacent abyssal plain which remains unclassified.

Copies of all available seismic reflection records, both single channel and multichannel, covering the Oregon and Washington continental shelf, slope and abyssal plain have been obtained from various archives for the 1990 study of the neotectonics of this portion of the Cascadia subduction zone. All local and regional biostratigraphic and sedimentologic data have been compiled for the fault dating studies.

Results

1. Active Fault Zones Mapped on the Abyssal Plain

Faulting and associated fluid venting are presently occurring west of the main deformation front on the subducting Juan de Fuca plate (Kulm et al., 1989; Appelgate et al., 1989; Goldfinger et al., 1989). The SeaMARC-IA sidescan sonar survey conducted over the lower continental slope and abyssal plain between 44°30'N and 45°12'N latitude mapped in detail the surficial structures related to the subduction of the Juan de Fuca plate. Preliminary results (44° 30' to 44° 50'N) indicate that subduction-related NW-SE trending faults extend onto the abyssal plain 13-15 km seaward of the main deformation front (marginal ridge). In the northern part of the area, N-S trending faults occur on the abyssal plain seaward of the deformation front. Some of the NW-trending faults either crosscut, or are overlain by, mud volcanoes. Several faults are downthrown to the southwest and west, respectively. A high-resolution 3.5 kHz seismic record across one of these surficial NW-trending faults, located 13 km seaward of the main deformation front (44°51'N, 125°31.5'W), displays about 5 m of vertical separation and is downthrown to the southwest. A core was taken in the vicinity of the fault in an attempt to date it. Alternatively, some of these faults may be left-lateral strike-slip faults, which would show an apparent down to the south vertical separation due to offsetting the west-sloping abyssal plain.

A prominent linear fault scarp, striking 295° extends 17 km across the abyssal plain from the deformation front at 45°10'N latitude (Fault A; Appelgate, et al., 1989; Goldfinger et al., 1989). The fault displays along-strike reversals in vertical separation and a very straight trace, characteristic of strike-slip faults. On the eastern end of the fault a submarine channel that crosses the fault, 6 km seaward of the base of the marginal ridge, is offset about 100 m in a left-lateral sense. On the western end of the fault a prominent escarpment is also offset left-laterally, but the amount has not been determined. At the base of the marginal ridge, which forms the initial deformation front, this fault splays into a series of separate faults which can be traced eastward onto the ridge. A N-S oriented multichannel seismic record (single trace ship's monitor record) made across the fault shows stratigraphic displacement throughout the sedimentary section and possibly into the basaltic basement. A semi-conical mud volcano 250 m high and 4 km in diameter overlies the main fault 10 km west of the marginal ridge. A previous ALVIN submersible survey in 1988 established that methane-rich fluids are venting from the mud volcano and that live chemosynthetic clams occur over much of the volcano's southern flank. The fault is actively venting fluids as documented by the abundant chemosynthetic animals. Fluids from the mud volcano contain a high ^{3}He content (23%) which tentatively suggests the fluids are derived from the basaltic slab of the subducting plate. These combined characteristics suggest that the fault is presently active. Gravity cores were collected in the vicinity of the fault in our first attempt to date it.

A second NW-SE trending fault (Fault B) was imaged in sidescan on the abyssal plain to the south at 44° 52' N latitude. This fault crosscuts the base of a smaller mud volcano (1 km diameter, 125 m high) and is characterized by an escarpment that extends at least 5 km seaward from the base of the initial deformation front. A multichannel seismic record (single trace ship's monitor record) across the fault suggests that it is a major fault zone with apparent basement offset. This feature could be another strike-slip fault similar to the one found to the north, but it may be less well developed or less visible to sidescan due to the lack of offset topographic features.

A third fault (Fault C) was clearly identified in a N-S multichannel seismic record at 44° 32'N latitude on the abyssal plain, 5 km seaward of the initial deformation front. Its orientation is not yet confirmed; however, a reentrant in the deformation front suggests that this fault also has a NW-SE orientation, and one seafloor fault on the sidescan images, just landward of the seismic record, has the same orientation. Displacement of the thick stratigraphic section appears to extend to the seafloor. The strata have the appearance of an evolving fold with probable seaward vergence. The fault appears to offset the basement, which is downthrown to the south or southwest.

Three additional NW-trending faults occur on the abyssal plain off Washington. The thrust faults in Nitinat Fan are oriented perpendicular to the convergence direction. At some point faults penetrate the cap on the overpressured sedimentary section below the fan and the subsequent pressure release causes the now fluidized sediments to flow to the surface in narrow conduits without substantially disturbing the surrounding sediment. These materials then dewater and form a chaotic sediment pile (mud volcano). A NW-trending fault has been mapped immediately to the northwest of the mud volcano and projected into the mound. A prominent mound with 75 m of relief and about 2 km in diameter occurs about 3 km seaward of the base of the continental slope at 47°13'N. Bottom photographs show abundant jagged rock outcrops and fracture patterns but no bedding planes or evidence of coherent strata. These mound-like features (mud volcanoes) occur just seaward of the deformation front of other convergent margins.

2. Relationship of Abyssal Plain Faults to 1973 Earthquake

One of two major faults in the abyssal plain (i.e., faults A or B described above), mapped with sidescan sonar and multichannel seismics, may be related to a 1973 earthquake (M_s=5.7) along the eastern edge of the subducting oceanic plate (Spence, 1989, his Figure 7, event number 10). We will compare the motion of the mapped faults with that determined from first motions and tie the fault movements into the local and regional tectonic framework to evaluate the earthquake hazard. The recent study of stress distribution in the Juan de Fuca plate (Spence, 1989) of the 1973 event indicates a right-lateral strike-slip separation with one nodal plain at 300°, which is the same strike as faults A and B. The epicenter of the earthquake is located about 15 km north of the seaward projection of fault B, the most likely candidate for the 1973 earthquake.

3. Active Fault Zones Mapped on the Accretionary Wedge

Faulting and associated fluid venting are documented along the deformation front in the SeaMARC-IA sidescan sonar survey completed August, 1989 across the outer margin (44° 32'N-44° 50'N latitude) (Kulm et al., 1989). An 800 m-high ramp anticline characterizes the N-S trending seaward verging deformation front (marginal ridge) with an intervening basin and second ridge to the east. The frontal thrust is clearly imaged in the new multichannel seismic records along the initial deformation front, and several blind thrust faults occur up to 5 km seaward of the front within the abyssal plain sediments. Several N-S oriented scarps occur just to the east of the crest of the anticline and represent seafloor offsets of one or more faults associated with a backthrust also imaged in the new seismic data. Fluid migration along the backthrust is a probable source of methane- and CO_2-charged fluids, which were sampled with ALVIN at several active vent sites (Kulm, et al., 1989). The pore fluids and gases are derived from the tectonic-induced dewatering of the accreted and subducted abyssal sediments caused by the compressive stresses.

Numerous small and one large scale submarine sediment slumps were identified and mapped along the initial deformation front of the accretionary wedge using the SeaMARC-IA side scan sonar images and SeaBeam bathymetry. One gravity core was collected at the toe of the largest slump in an attempt to date the slump.

Reports

Appelgate, T.B., Kulm, L.D., Embley, R.W., Fox, C.G., 1989, Surficial structure of the central Oregon convergent margin: results from a SeaMARC-1A sidescan sonar survey: EOS, v. 70, p. 1345.

Goldfinger, C., Appelgate, T.B., Kulm, L.D., and Yeats, R.S., 1989, Sidescan sonar imaging of probable active faults on the Juan de Fuca plate adjacent to the central Oregon continental margin: EOS, v. 70, p. 1329.

Kulm, L.D., Appelgate, T.B., and Fox, C., 1989, Sidescan survey of structures and fluid vent sites on the central Oregon margin and subducting Juan de Fuca plate: EOS, v. 70, p. 1345.

Use of Temporal Correlation to Test a Proposed Seismic Origin for Giant Landslides in Seattle, Washington

14-08-0001-G1776

Gordon C. Jacoby
Tree-Ring Laboratory
Lamont-Doherty Geol. Obs.
Palisades, New York 10964
(914) 359-2900

Patrick L. Williams
Earth Science Division
Lawrence Berkeley Laboratory
University of California
Berkeley, California 94720
(415) 486-7156

Introduction

This investigation primarily addresses large-scale landslides submerged in Lake Washington in Seattle. Slide blocks moved to 0 to ≥40 m depths by deep-seated translational gliding from adjacent steep slopes. Historical block translations of this type are not recorded in the Puget Sound lowland area in the roughly 200 years since European settlers came into the Pacific Northwest (Manson and Thorson,1983). There have been some slope failures associated with moderate earthquakes in the Pacific Northwest. Atwater and his co-workers (Atwater, 1987 a & b, Yamaguchi et al. 1989)have identified stratigraphic evidence that several abrupt coastal subsidence events occurred along the Washington and Oregon coast during the past 3000 years. Testing for the coincidence of submergence ages with paleolandsliding and paleoliquifaction ages will critically test the great subduction-earthquake hypothesis and improve characterization of seismic risk in Washington State's urbanized areas. Regardless of whether the Lake Washington landslides were triggered by earthquakes of local or regional extent, or were produced nontectonically, they represent a significant geohazard in the Puget Sound region.

Lake Washington fills a 29-km-long basin adjacent to Seattle. Its surface area is approximately 80 km^2 (Figure 1). Lake-depth exceeds 60 m in several places. The basin was glacially-cut and is walled primarily by deposits of glacial outwash, glacial till and glacio-lacustrine silts and clay. Ice-contact (lodgement) till caps many of the upland surfaces (Waldron et al., 1962; Yount, 1983). The lake's boundaries are dominated by the characteristic oversteepened walls of glacial troughs. Steep slopes bound the lake except where the valley is partly filled by deltaic deposits, intersected by other ancient glacial valleys, or intersected by modern drainages. The late Pleistocene glacio-lacustrine Lawton Clay is widely present in the Seattle area. It is up to a few 10's of meters thick, is a ground-water barrier, and is overlain by the (commonly wet) silts and sands of the Esperance Sand. The contact of these units is associated with slope instability (e.g. Yount, 1983). The contact appears to be present between 0 and 70 m above the surface of Lake Washington at the three sites of proven late Holocene block sliding (Waldron et al., 1962), strongly suggesting the existence of an underappreciated regional slope-failure hazard.

Paleolandslides and Wood Preservation

A study of lake Washington stratigraphy, bathymetry, and Holocene history was completed by Gould et al. (manuscript, 1957) but never published. Gould et al. (1957) reported that three subareas having landslide topography are the sites of submerged forests (Figure 1). Because the deeply submerged stems are smooth and show no subaerial weathering effects, Gould et al. (1957) concluded that the trees were living at the time of submergence and their age "corresponds to the time of the landslide that placed them in their present position." Outer wood from a tree collected at the Kirkland site by Gould et al. had a radiocarbon age of 1160±80 radiocarbon years before present (RYBP) (Broecker and Kulp, 1957). We have found excellent preservation of sub-fossil trees at three sites in

Figure 1: Lake Washington and three landslide sites with dates

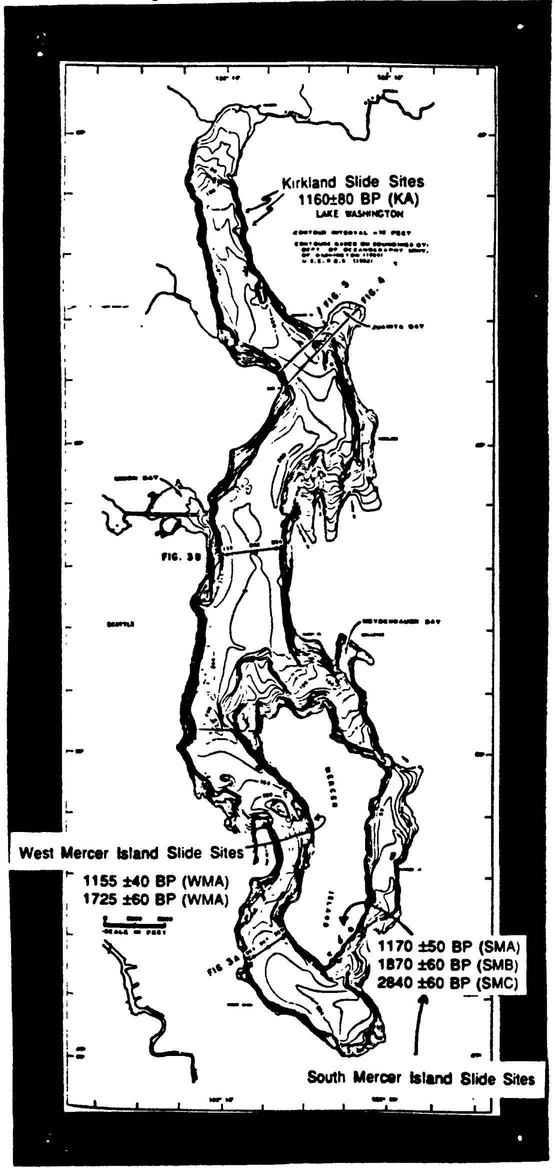

the lake. Prior to human modification in 1916 (lake level was lowered by about 3 m in that year), the depth extent of major wood decay on standing trees on slides was no more than 7 to 10 m below lake level. The depth limit of wood decay in Lake Washington is likely explained by lake stratification and reduced oxygen content of the deeper water.

Our Results to Date

We conducted reconnaissance surveys of the southeastern Mercer Island (SMI) and western Mercer Island (WMI) areas using single channel sonar (Williams and Jacoby, 1989). Geomorphic features interpreted to be landslide head-scarps and terraced and hummocky topography are present in the upland area adjacent to these areas. Sonar confirms the presence of tilted blocks and chaotic bathymetric features in the near-shore of both areas. In the first survey Williams collected wood from an uprooted tree on a prominent terrace of slide SMC (Figure 1) using SCUBA equipment. This wood was radiocarbon dated at 2840±60 RYBP (Williams and Jacoby, 1989). Youthfulness of this site is further indicated by the small accumulation (≤ 5 cm) of algal detritus on the submerged slide. At other near-shore sites in Lake Washington typically several decimeters of this material is present. Angular clasts of varved lacustrine clay were collected on the slide terrace. The presence of these clasts indicates block shattering and is thus suggestive of high energy conditions during sliding and a possible catastrophic failure mode.

All the carbon-14 dates are based on single analyses and the dates have not yet been dendrochronologically corrected. For the purposes of this discussion it is assumed that the dates are approximately correct. In the next phase of the project we must have duplicate or higher precision radiocarbon dates to confirm the ages. Radiocarbon dates from Kirkland, West Mercer Island and South Mercer Island indicate landslides at all three areas at around 1155 to 1170 RYBP (Figure 1). Even with the uncertainties of radiocarbon dating this is a relatively narrow time window and the hypothesis can be set forth that slides occurred simultaneously at all three locales. In the locale of South Mercer Island there are at least three slides. Figure 1 indicates the three slide sites which are named A, B, and C, from north to south. The specimen used for radiocarbon dating from site A is a wedge from a western redcedar with only 40 rings that show little variation for crossdating. This redcedar tree from site A was rooted in the slide as was the sample from the Kirkland site. The sample from the West Mercer Island site was not rooted. Radiocarbon dates also indicate slides at both West and South Mercer Island around 1725 to 1870 RYBP. These are close enough to be the same event but may also represent two separate events. Tree-ring dating of samples will resolve this issue.

We have already been able to cross-date several trees from different locations in Lake Washington. Two of the trees are the same ones sampled for radiocarbon analysis. The results of these analyses and the cross-dating is one chronology of over 170 years in length and another chronology of 285 years in length. The radiocarbon analysis places the last years of the first chronology at *ca.*1870 RYBP and the second chronology ends in *ca.* 1160 RYBP. Both chronologies can now be used to crossdate other samples from the lake. Cross-dating was achieved by ring-width comparisons and also confirmed by cross-dating of latewood density variations by microscopic examination. At the South Mercer Island site B the same tree used for radiocarbon dating also yielded a core sample with almost 150 rings. This sample cross-dates with the radiocarbon section from the same tree (as expected) and also cross-dates with a core from site A which has over 170 rings. The core sample from site A is from an unrooted tree. Therefore there are two interpretations. There were landslides at both sites around 1870 RYBP, meaning possibly two events at site A (1170 BP and 1870 BP). Or, the "1870 BP" sample from site A is from a tree dragged there from site B by US Corps of Engineers dredging activities to remove the trees as navigation hazards. Cores from SMB-6 and SMB-7 crossdate with samples from WMI-2 which is radiocarbon dated to 1155 RYBP. This result indicates a landslide at site SMB at 1155 RYBP in addition to the 1870 RYBP date from a rooted tree. Again unfortunately both SMB-6 and SMB-7 are not rooted so the same possibility for contamination by dragging exists. Site B is less than a half kilometer from site A. An uprooted sample from South Mercer Island site C was previously radiocarbon dated at 2840 RYBP. Our next sampling will concentrate on rooted trees to resolve the problem of multiple dates. If outer rings are found intact, age differences and timing of a single season are resolvable. If submergence occurred during the radial growth season, ring development would be similar and incomplete. If submergence occurred after the radial growth season, completed rings with latewood bands should be present. If outer rings indicate an event during the growing season, the drier time of year, it would lessen the chance that the event was due to ground saturation and collapse.

Summary

Our studies so far have produced approximate dates for at least three landslide events in Lake Washington over the past three thousand years. Two sets of dates are close enough to raise the possibility of simultaneous landslides at different places in the lake, a part of the original hypothesis of the research. The radiocarbon age ranges must be verified with more sample processing and many more cores are needed for dendrochronologic cross-dating. There has been loss of outer years from some of the trees and more effort will be needed to find and sample where the full trees are intact out to the bark. Such samples will closely establish the temporal correlation of different events at different sites. If ages of the Lake Washington slides closely match the ages of other candidate paleoseismic features in Washington and Oregon, the occurrence of large or great paleoearthquakes would be supported. However, if common ages of candidate paleoseismic features are found only locally, other mechanisms for landslide initiation must be be considered.

Regional tectonic events at about 300, 1100, 1700-1850, 2500, 2900 and 3100 years before present are suggested by a data review. Most prominent in these data is the candidate regional event at *ca.*1100 RYBP. Especially notable is the strong clustering of three radiocarbon tree ages from three remote Lake Washington sites (1155, 1160, and 1170 RYBP) and the crossdating of tree cores between the West Mercer and South Mercer sites. Despite the very mixed sources of dates, the preliminary correlations tend to support the occurrence of several regional earthquakes in late Holocene times.

REFERENCES CITED

Atwater, B.F., Evidence for great Holocene earthquakes along the outer coast of Washington state, Science, 236, 942-944, 1987a.

Atwater, B.F., Geologic studies for seismic zonation of the Puget lowland, in "National Earthquake Hazards Reduction Program, Summaries of Technical Reports", U.S. Geol. Surv. Open-File Rep. 88-16, 1987b.

Broecker, W.S. and J.L. Kulp, Lamont Natural Radiocarbon Measurements IV, Science, 124, 1324-1334, 1957.

Gould, H.R., T.F. Budinger and D.M. Ragan, Bathymetry and post-glacial sediments of Lake Washington, (manuscript), ca. 1957.

Manson, C.J., and G.W. Thorson, Landslides of Washington: an annotated bibliography through 1980, Wash. Div. of Geol. and Ear. Res. Open File Rept., 83-3, 78p., 1983.

Waldron, D. H., B. A. Liesch, D. R. Mullineaux and D. R. Crandell, Preliminary Map of Seattle and Vicinity, Washington, U. S. Geological Survey Miscellaneous Geologic Investigations Map, I-354, 1962.

Williams, P.L. and G.C. Jacoby, Evaluation of possible seismic triggering of giant landslides in Seattle, Washington (abstract), EOS Trans. AGU, 70, 1332, 1989

Yamaguchi, D.K., C.A. Woodhouse, and M.S. Reid, Tree-ring evidence for synchronous rapid submergence of the southwest Washington coast 300 years B.P. (abstract), EOS Trans. AGU, 70, 1332, 1989

Yount, J.C., Geologic units that likely control ground shaking in the greater Seattle area, in U.S. Geol. Surv. Open File Rept., 83-19, Earthquake Hazards of the Puget Sound Region, 268-279, 1983.

DATABASE MANAGEMENT

9910-03975

Charles S. Mueller
Branch of Engineering Seismology and Geology
U. S. Geological Survey
345 Middlefield Road, MS 977
Menlo Park, California 94025
(415) 329-5646

Investigations

1. Develop new techniques for playback, processing, management, and export of seismic waveform data, with emphasis on large aftershock datasets collected with portable digital event-recording seismographs (*e.g.*, GEOS).

2. Design and implement relational databases for strong-motion and aftershock data.

Results

1. New datsets played back, processed, and archived:
   Aftershocks of the 17 October 1989 Loma Prieta earthquake.

Reports

Mueller, C., 1990. Computer programs for analyzing digital seismic data, U. S. Geological Survey Open-File Report 90-35, 100 pages.

4/90

EARTHQUAKE RECURRENCE AND QUATERNARY DEFORMATION IN THE CASCADIA SUBDUCTION ZONE, COASTAL OREGON

9950-04180

ALAN R. NELSON, STEPHEN F. PERSONIUS, AND SUSAN RHEA

U.S. Geological Survey
Branch of Geologic Risk Assessment
MS 966, Box 25046
Denver, CO 80225
(303) 236-1596; FTS 776-1596

INVESTIGATIONS

There are three components to this project: (1) Nelson's study of coseismic changes in late Holocene sea level as revealed by salt marsh stratigraphy, (2) Personius' study of fluvial terrace remnants along major Coast Range rivers to determine style and rates of late Quaternary deformation, and (3) Rhea's study of river and drainage basin morphology in the Coast Range to determine relative rates of tectonic uplift.

RESULTS

Recurrence of coeismic changes in sea level in central Oregon

Nelson continued analysis of foraminifera and diatom data from modern transects in Oregon marshes and core WC-12 to estimate the magnitude of sudden sea level changes. Arrangements have been made for a geochemist specializing in experimental pretreatments of small radiocarbon samples to prepare high-quality samples to be collected by Nelson from one or two sites in August, 1990. Only the collegen fraction of the samples will be dated, eliminating the possibilty of younger carbon contaminating the samples. Special large-diameter coring techniques will be needed to recover suitable samples. If samples of sufficient quality can be found, statistical averaging of the ages on the samples will be valid and 90% confidence intervals on the time of marsh burial events may be reduced to 50-80 years. The results of our AMS radiocarbon samples submitted in April 1989 are still pending (U.S. AMS facility at Univ. of Arizona).

Nelson and Personius submitted a manuscript reviewing the status of paleoseismology studies along the Oregon coast for the USGS Profesional Paper on earthquake hazards in the Pacific Northwest in January (1990). Based on a comparison of the type of marsh stratigraphic records found along the coast, several models of rupture extent during Holocene great plate-interface earthquakes are suggested (Figs. 1-3). This type of synthesis suggests that the Cascadia zone is segmented and that most plate-interface events may have been closer to magnitude 8 than to 9.

Late Quaternary deformation rates indicated by fluvial terraces in central Oregon

Personius is continuing to examine fluvial terraces for evidence of late Quaternary deformation in the Oregon Coast Range. Radiocarbon analyses of Holocene terraces on the Umpqua, Smith, Siuslaw, and Siletz Rivers indicate relatively slow (0.2-0.6 mm/yr) rates of uplift (incision) of the central Oregon Coast Range. Incision rates appear to be higher in the upper parts of the drainages near the crest of the Coast Range. While not without some inconsistencies, thermoluminescence (TL) ages on fluvial sediment along the Umpqua River appear to yield similar rates for higher terraces. No evidence of active Holocene structures has been observed in the drainages examined in central Oregon, but an anticline in the underlying Eocene bedrock has warped older terraces (100-200 ka?) at one location along the Siuslaw River.

In south-central Oregon, radiocarbon ages on charcoal from the base of an abandoned channel of the Coquille River near Coquille, Oregon indicate no appreciable change in relative sea level in the past 2,500 yr in this area.

Differential uplift of the Oregon Coast Range

A manuscript summarizing Rhea's study of river valley and drainage basin morphology is almost ready for review. Rivers in the central Coast Range show patterns different from patterns for rivers in the southern Coast Range, the Klamath Mountains, or the Cascade Range. In the central region near the Yaquina River, river sinuosity values are higher than elsewhere, river gradients are variable, and river valleys seem to have developed differently than in the other areas. For example, on the central west slope of the Coast Range, the Yaquina River longitudinal profile is strongly convex, but the nearby Marys River, on the east slope of the Coast Range, has a more gradual profile. These types of patterns suggest the central Oregon Coast Range is experiencing more recent uplift or higher rates of uplift relative to areas to the north and south.

REPORTS

Grant, W.C., Atwater, B.F., Carver, G.A., Darienzo, M.E., Nelson, A.R., Peterson, C.D., and Vick, G.S., 1989, Radiocarbon dating of late Holocene coastal subsidence above the Cascadia subduction zone--Compilation for Washington, Oregon, and northern California: EOS, v. 70, no. 43, p. 1331.

Nelson, A.R., and Personius, S.F., (in press), Great earthquake potential in Oregon and Washington--An overview of recent coastal geologic studies and possible segmentation of the central Cascadia subduction zone, *in*, Weiss, A.J., compiler, Proceedings of 17th Water Reactor Safety Meeting, U.S. Nuclear Regulatory Commisssion, Office of Nuclear Regulatory Research, NUREG/CP-0105, 55 ms. p.

Nelson, A.R., and Personius, S.F., (in review), Great earthquake potential in Oregon and Washington--An overview of recent coastal geologic studies and their bearing on segmentation of Holocene ruptures in the central Cascadia subduction zone, *in*, Rogers, Kockelman, Priest, and Walsh, eds., Assessing and reducing earthquake hazards in the Pacific Northwest, U.S. Geological Survey Professional Paper, 69 ms. p.

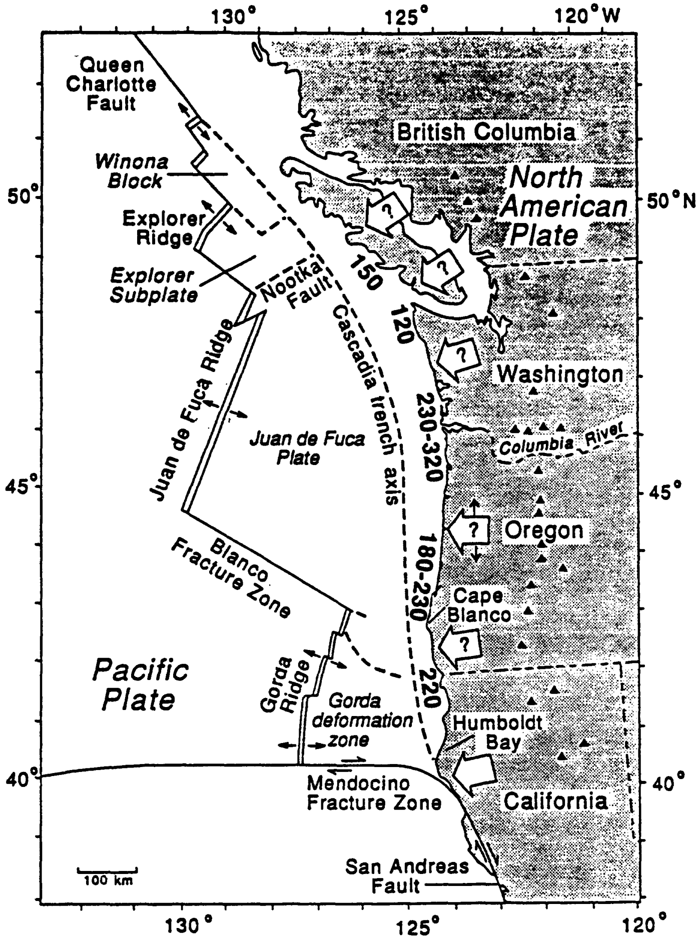

FIGURE 1.--Major features of the Cascadia subduction zone in the northwestern United States and southwestern Canada; modified from Rogers (1988), Spence (1989), and Wilson (1989). The large arrows mark generalized areas along the coast that coincide with boundaries between tectonic subplates, projections of boundaries between volcanic segments in the Cascade Range (Hughes and others, 1980), or other areas where seismicity and subducting plate parameters may change, and so could correspond with the boundaries between segments of the subducting-plate. No query is shown at the Mendocino fracture zone boundary because the location of this feature is accurately known. Distances between boundaries are shown only to suggest a range of possible segment lengths. The range of distances shown for segments north and south of 44.5° N reflects several locations for a possible boundary along this part of the coast. We do not know whether most Holocene ruptures along the CSZ have been influenced by these postulated boundaries. Small black triangles mark volcanoes in the Cascade Range.

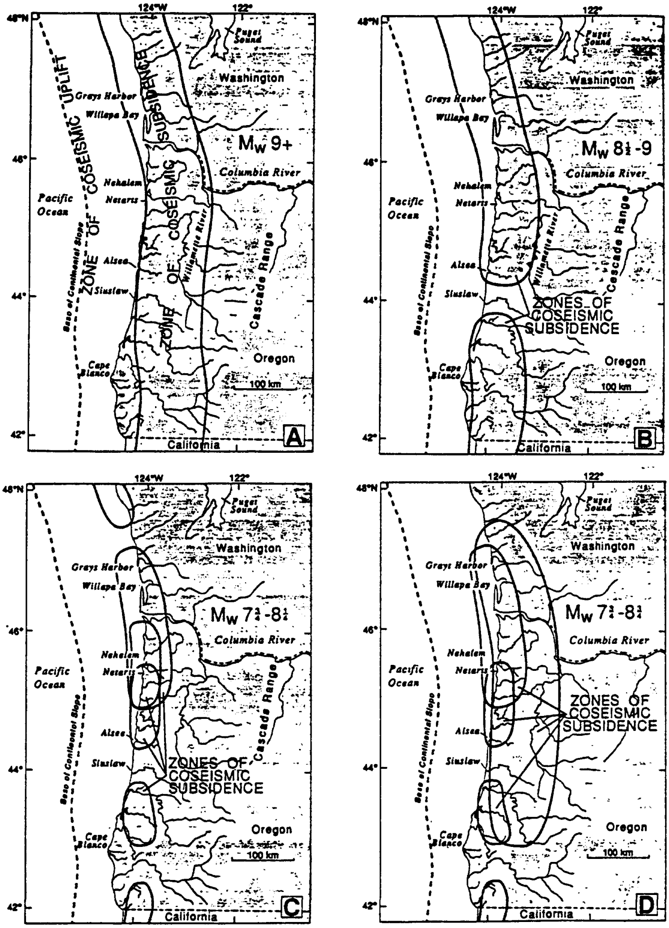

FIGURE 2.--Four possible models of the location of zones of coseismic subsidence during plate-interface ruptures in the central Cascadia subduction zone. A. A rupture of more than 700 km of the plate boundary from an earthquake of at least M_w 9 could produce a zone of coseismic uplift extending eastward (arcward) from the trench and a zone of coseismic subsidence east of the zone of uplift. Estuaries north of the Siuslaw River estuary contain stratigraphic sequences with evidence of coseisimic subsidence while the Siuslaw estuary contains evidence of a slow, uniform rise in relative sea level. Thus, if the edge of the zone of coseismic subsidence during M_w 9+ events trends between the Siuslaw and Alsea Bay estuaries, as shown, events of this magnitude may have occurred. The eastward extent of the zone of coseismic subsidence for such an event is unknown. B. Ruptures of 300-600 km of the plate boundary during M_w $8^{1/2}$-9 events would also produce extensive zones of coseismic subsidence. If these zones were located farther west than in (A) they could not include the Siuslaw estuary and the ruptures could not extend north or south of the Siuslaw River. C. If only single plate-boundary segments or portions of segments ruptured in events of less than M_w $8^{1/4}$, then zones of coseismic subsidence less than 250 km long could be produced. These smaller events might not produce any significant (>0.3 m) permanent subsidence and so could include the area of the Siuslaw estuary. Slip along some parts of the plate boundary could also be aseismic. D. A variation of models A and C is that events of M_w $7^{3/4}$-$8^{1/4}$ could be most common, with rare events of M_w $8^{3/4}$ that rupture two segments of the plate boundary. However, the zone of coseismic subsidence for the rare, largest events would have to be east of the Siuslaw estuary in this model.

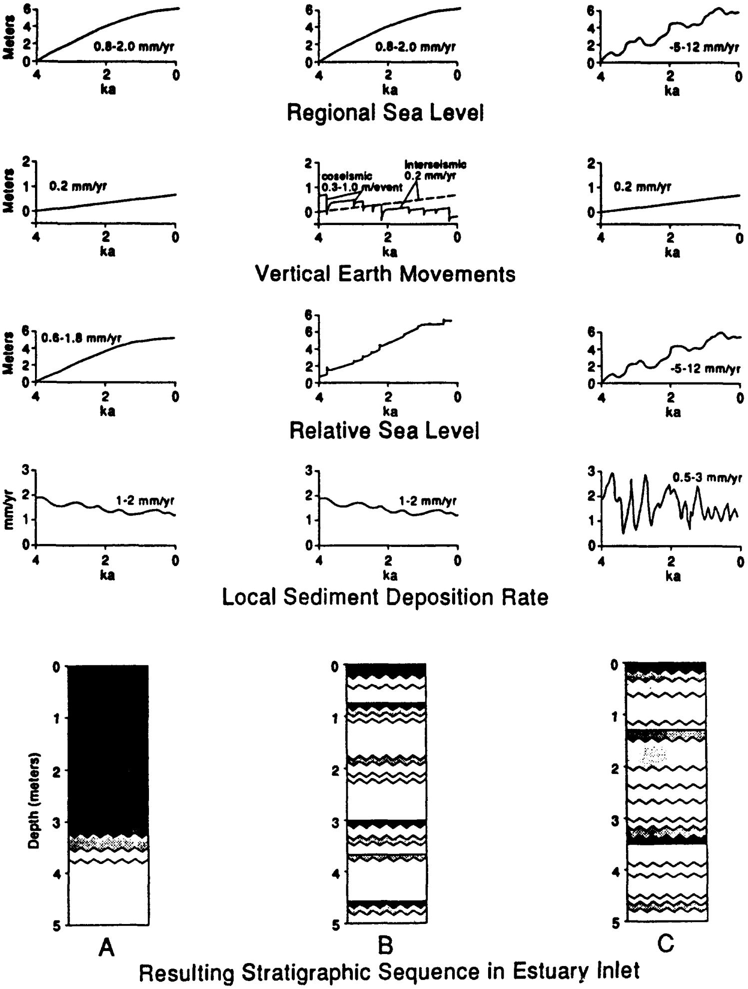

FIGURE 3.--Models of regional sea level rise, land level movements, the resulting relative sea level changes, and sediment depostion rates in tidal inlets during the late Holocene in the Pacific Northwest. The curves illustrate how different but plausible histories of sea level rise, coastal uplift, and sedimentation rates could produce different types of stratigraphic sequences in these inlets. The degree of darkness of lithologic units indicates amount of peat (dark) or mud (white) in unit. Serrated lines show gradational contacts; straight lines are abrupt contacts. Sequence A could only be produced in an inlet that had not experienced major (>0.3 m) sudden changes in relative sea level. The abrupt upper contacts on the peat units in sequence B suggest sudden (coseismic) subsidence. Gradational contacts characterize sequence C, which is produced by fluctuating regional sea level and rapidly changing sedimentation rates. Sequence B could easily be confused with sequence C, which was produced without any sudden changes in relative sea level.

Data Processing, Golden

9950-02088

Robert B. Park
Branch of Geologic Risk Assessment
U.S. Geological Survey
Box 25046, MS 966, Denver Federal Center
Denver, CO 80225
(303) 236-1638

Investigations

The purpose of this project is to provide the day-to-day management and systems maintenance and development for the Golden Data Processing Center. The Center supports Branch of Geologic Risk Assessment with a variety of computer services. The systems include a PDP 11/70, a VAX/750, a VAX/780, two MicroVAX's, two SUN servers, 5 SUN workstations, and a PDP 11/34. Total memory is 40 mbytes and disk space is approximately 7 G bytes. Peripherals include four plotters, ten mag-tape units, an analog tape unit, two line printers, 5 CRT terminals with graphics, and a Summagraphic digitizing table. Dial-up is available on all the major systems and hardwire lines are available for user terminals on the upper floors of the building. Users may access any of the systems through a Gandalf terminal switch. Operating systems used are RSX11 (11/34's), Unix (11/70), RT11 (LSI's) and VMS (VAX's).

Results

Computation performed is primarily related to the Hazards program; however, work is also done for the Induced Seismicity and Prediction programs as well as for DARPA, ACDA, and U.S. Bureau of Reclamation, among others.

The data center supports research in assessing seismic risk and the construction of national risk maps. It also provides capability for digitizing analog chart recordings and maps as well as analog tape. Also, most, if not all, of the research computing related to the hazards program are supported by the data center.

The data center also supports equipment for online digital monitoring of Nevada and Colorado Western Slope seismicity. Also, it provides capability for processing seismic data recorded on field analog and digital cassette tape in various formats.

Resonant Frequencies of Sedimentary Basins: Applications to Seismic Risk Evaluation

Contract USGS 14-08-0001-G1787

J.A. Rial

The University of North Carolina at Chapel Hill, Geology Department, Mitchell Hall,
CB#3315, Chapel Hill, NC 27599-3315; Tel: (919)9664553
E-mail: jar@antipode.geosci.unc.edu

INVESTIGATIONS:

Development of analytic and numerical methods to determine the natural frequencies of oscillation of three-dimensional models of sedimentary basins. The effort is focussed on both analytic and numerical methods. The analytic methods are derived from similar problems in classical dynamics and quantum chemistry. The numerical approach uses a modification of the Rayleigh-Ritz variational method to determine the resonant frequencies in basins of arbitrary geometry.

RESULTS:

Analytic solutions

Preliminary results of the mathematical approach originally proposed are reported in Rial (1989a, b). The analytic solutions obtained in Rial(1989a) are valid for separable geometries (those in which the scalar wave equation is separable). We have now incorporated in our study the semiclassical method for calculating eigenvalues of nonseparable oscillating systems, a technique introduced in molecular and quantum chemistry by Marcus (1973). The method is based upon the EBK (Einstein-Broullin-Keller) quantization rules for nonlinearly coupled oscillators, a particular case of which is the approach used in Rial(1989a). To compute the eigenvalues of a given resonant domain the resonance or "quantum" conditions along selected irreducible trajectories of normal ray congruences (a normal ray congruence is a family of rays orthogonal to any surface) are applied. These quantum conditions must be understood as constructive interference conditions to be satisfied by the wavelength of a particular eigenmode. For an N-dimensional nondegenerate system the conditions have the form (Keller,1985):

$$\kappa \int_{C_j} \text{grad}\,[S] \cdot \mathbf{ds} = 2\pi \left(n_j + \alpha_j/2 \right) \qquad (1)$$

$$j=1,2..N$$

where κ is the wavenumber, n_j and α_j are integers (α_j is named Maslov index). The Cj's are topologically independent closed paths (need not be along actual ray trajectories), and the generally multivalued phase function S= S(**x**) satisfies the eiconal equation $(\text{grad}[S])^2 = 1/v^2$, where v is the wavespeed. The left-hand-side of (1) is just the accumulated phase of the wave along the closed contour Cj. The vector **ds** is the vector element of arc-length along C_j. Condition (1) guarantees that the asymptotic solutions to the wave equation $(\Delta + \kappa^2)\Psi = 0$, given by $\Psi \sim A \exp\{i\kappa S\}$, are single-valued. Phase shifts due to reflections from boundaries are included when needed as additive factors to the RHS of (1). The Maslov index is typically equal to m/2, where m is the number of times the path crosses a given caustic. The domain of applicability of (1) may or may not be separable for the wave equation.

The importance of (1) has recently been demonstrated by a number of workers, such as Noid et. al. (1980), Knudsen et.al. (1986), Noid and Marcus (1986), and many others who have used it in the determination of eigenvalues and corresponding eigenfunctions of nonlinearly coupled oscillators. Such results are of great relevance to our problem because of the close analogy there is between the ray trajectories of multiply bouncing rays inside an arbitrarily shaped resonant sedimentary basin and the orbits described by the oscillators. The method of Marcus uses these orbits to compute the eigenfrequencies, we use the ray trajectories.

Our work also indicates that it is possible to find a system of differential equations that reproduces very accurately the ray trajectories in an arbitrary basin. Specifically, we have developed an approximate method that provides such a system of four nonlinear, coupled ordinary differential equations. Integration by a conventional Runge-Kutta method gives the trajectories of the bouncing points of the rays in an smooth basin of arbitrary shape. The constraints are that the inclines of the basin's bottom are small, and so the method is called SIBA (Small Incline Bottom Approximation). As a first approximation SIBA works remarkably well in reproducing both the ray trajectories and the corresponding Poincare sections for smooth basins, as shown below in Figure 1.

The SIBA equations are as follows:

Using cartesian coordinates we describe the sediment/rock interface of the basin as an arbitrary function $z = B(x,y) \le 0$, such that $z=0$ is the earth's surface. The plane given by the equation $a_1 x + a_2 y + a_3 z = a_0$, and such that

$$a_1 = -\partial B/\partial x\,; \quad a_2 = -\partial B/\partial y; \quad a_3 = 1\,; \quad \text{and} \quad a_0 = B(x,y)$$

is the plane tangent to the the basin's bottom at point (x,y). If we assume $|a_1| \ll 1$ and $|a_2| \ll 1$, it can be shown that the coordinates $x(t)$, $y(t)$ of the free-surface bouncing points of a multiply reflected ray inside a resonant basin whose lower boundary is given by a function B(x,y), satisfy the following system of ordinary, nonlinearly coupled differential equations:

$$\begin{aligned} dx/dt &= p_x \quad ; \quad dy/dt = p_y \\ dp_x/dt &= (1-u^2)\, a_1 / |B(x,y)| \\ dp_y/dt &= (1-u^2)\, a_2 / |B(x,y)| \end{aligned} \tag{2}$$

with $u^2 = p_x^2 + p_y^2$

It is easy to show that equations (2) can be derived using Newton's equations of motion

$$md^2X/dt^2 = - \text{grad}\,[\,V\,] \qquad (3)$$

with $V = V(x, y, p_x, p_y) = -(1 - u^2)\ln[-B(x,y)]$; $X = (x,y)$, and $m=1$

Figure 1 shows a comparison between ray trajectories obtained with ray tracing in a resonant basin of gaussian shape and those obtained by integration of the SIBA equations . A gaussian function is used for B(x,y) in (2). The figure also shows the Poincare sections of the phase space (position of bounce point vs. angle of the ray at reflection) along x and along y constructed following the method of Marcus (1973). The areas inside the closed curves generated by the Poincare sections in each coordinate direction are equal to the corresponding integrals in (1), and thus their numerical values can be used to determine the eigenvalues κ. The actual eigenvalues are those which make the corresponding values of the n_j of equation (1) become integers (Noid and Marcus, 1986).

The importance of SIBA bears on the fact that for any given basin of irregular geometry, integration of (2) is a much more stable process than ray tracing, in which round-off errors tend to accumulate at a very fast rate. Additionally, an analytic form such as SIBA allows us to study the entire phenomenon of multiple reflection, its dependence on basin geometry, the relative influences of separability and nonlinearities on the eigenvalues, and even the chaoticity (long term predictability) of the ray system.

When the ray trajectories are stable, as for instance, in the basin of Figure 1, the eigenfunctions are limited laterally by the modal caustics that are traced out by the ray paths, and the corresponding modes can be approximated by products of Hermite polynomials on x and y (these are solutions to Schroedinger-type equations), whose orders correspond to mode orders (Weinstein, 1969). An example of estimated eigenfunctions for the basin of Figure 1 is shown in Figure 2, where we show one of the non-degenerate modes. An example involving a basin of more complex geometry is shown in Figure 3. The modal shapes in this case are disjoint products of Airy functions which we are presently investigating.

Numerical solutions

The method of solution here is that of *a-priori/a-posteriori* inequalities as described by Kutler and Sigilito (1985). The eigenfunctions are approximated by sums of basis functions. Basis functions for a given basin geometry are guessed at by first determining the ray paths, as discussed above. Bounds on the error for an estimated eigenvalue are determined from previously derived inequalities using the basis function approximation to the associated eigenfunction. Currently, successful tests of a code for a two dimensional problem have been completed. The code for general three dimensional problems is under development.

As an example of the use of this method we show below (Table I) results for a two dimensional region or 'membrane' R, with square boundary and rigid boundaries. In our implementation we included IMSL subroutines to solve the generalized matrix eigenvalue problem. We used basis functions from the simple polynomials $x^n y^m$, n,m=0,1,... over a square situated with its diagonals along the x and y axes, for which the method's required iteration matrices may be easily derived analytically. To simplify the calculations we included only basis functions with appropriate symmetries. Table I gives results of our calculations of the first six such eigenvalues of the Helmholtz equation on a square with sides of length $\sqrt{2}$. It can be seen that results deteriorate rapidly for higher eigenvalues unless a correspondingly large number of basis functions is used. Few basis functions cannot approximate the eigenfunctions very well, so that the error bounds for the eigenvalues become large. Determining the optimal number of basis functions is however an uncomplicated matter, performed on a trial-and-error basis.

Table I

Calculated Bounding Interval	Exact Eigenvalue
(9.8686, 9.8706)	9.8696 $= \pi^2(1^2+1^2)/2$
(39.4745, 39.4863)	39.4784 $= \pi^2(2^2+2^2)/2$
(49.3401, 49.3559)	49.3480 $= \pi^2(3^2+1^2)/2$
(88.3932, 89.2637)	88.8264 $= \pi^2(3^2+3^2)/2$
(97.9736, 99.4284)	98.6960 $= \pi^2(4^2+2^2)/2$
(127.5261, 129.0924)	128.3049 $= \pi^2(5^2+1^2)/2$

ACKNOWLEDGEMENTS: Research Assistants Hui Ling and Nancy Saltzman contributed with computer code writing and numerical work.

REFERENCES

Keller, J.B. (1985) *SIAM Review*, **27**, pp458-504

Knudsen, S.K.,J.B.Delos & D.W. Noid (1986) *J.Chem.Phys.*,**84**(12),pp6886-94

Kutler, J.R. & Sigilito (1985) ***Estimating eigenvalues with a posteriori/a priori inequalities***, Pitman, Boston.

Marcus, R.A. (1973) *Faraday Diss.Chem. Soc.*, **55**, pp 34-44

Noid, D.W., M.L. Koszykowski &R.A. Marcus (1980) *J. Chem. Phys.*,**73** (1), pp 391-95

Noid, D.W. and R.A. Marcus(1986), *J.Chem.Phys.*, **85**(6), pp 3305-3311

Rial, J.A.(1989a) *Geophys. Jour. Int.*, **99**, pp81-90

Rial, J.A. (1989b), in ***Engineering Seismology and Site Response***, pp 263-77; A.S. Cakmak and I. Herrera (Editors). Computational Mech. Pubs., Southampton.

Weinstein, L.A. (1969) ***Open Resonators and Open Waveguides.*** The Golem Press, Boulder, Colorado.

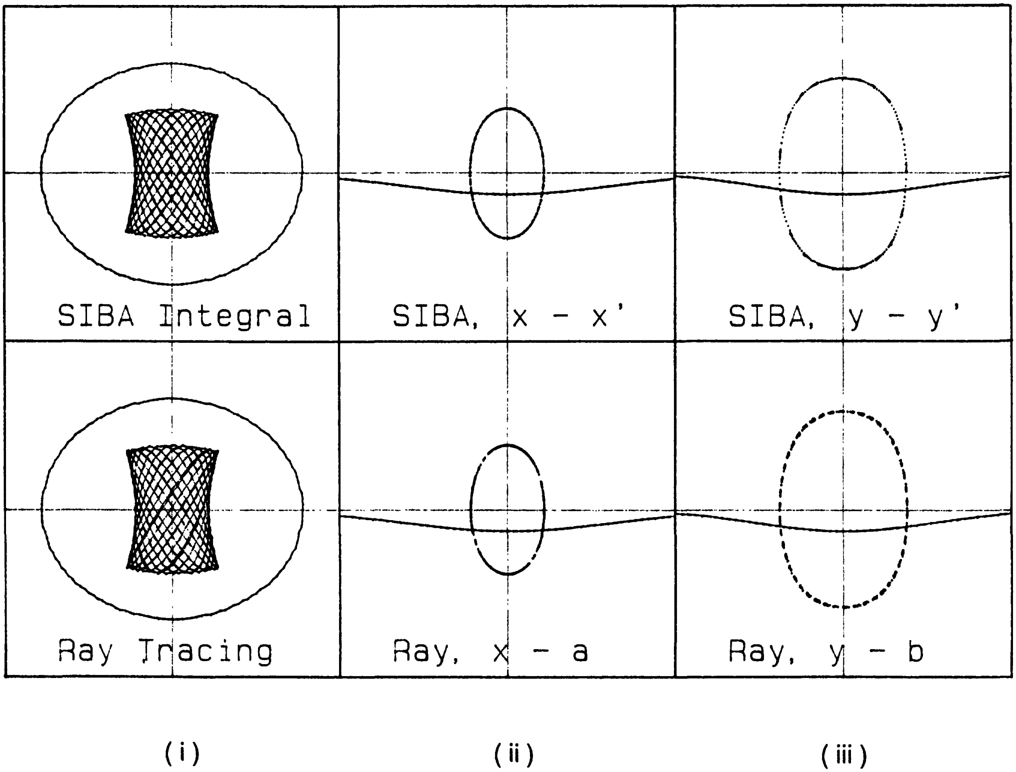

Figure 1. The orbits of bouncing points of seismic rays in a sedimentary basin of gaussian shape computed by SIBA and by conventional ray tracing. Panel (i) shows the trajectories of the rays on the x-y plane. The contour line at a depth 1/3 of the maximum basin depth is shown for reference. The maximum depth of the basin is 1/10 its longest horizontal dimension. Panels (ii) and (iii) are the two-dimensional Poincare sections of the six-dimensional phase space of the trajectories. Cross sections of the basin along the x and y directions are also shown (no vertical exageration). In panels (ii) and (iii) the vertical axes are $x' = dx/dt$, $y' = dy/dt$ for SIBA and **a** , **b** the direction cosines of the ray at the reflection point for the ray tracing plots. Since the wavespeed is taken as unity, the "velocities" x' and y' should be equivalent to **a** and **b** respectively. The eigenfrequencies of the basin are determined from the numerical values of the areas inside the closed curves of the Poincare sections that make the n_j in equation (1) become integers. The details of the eigenvalue estimation using the Poincare sections are described in Marcus (1973) and in Noid and Marcus (1986).

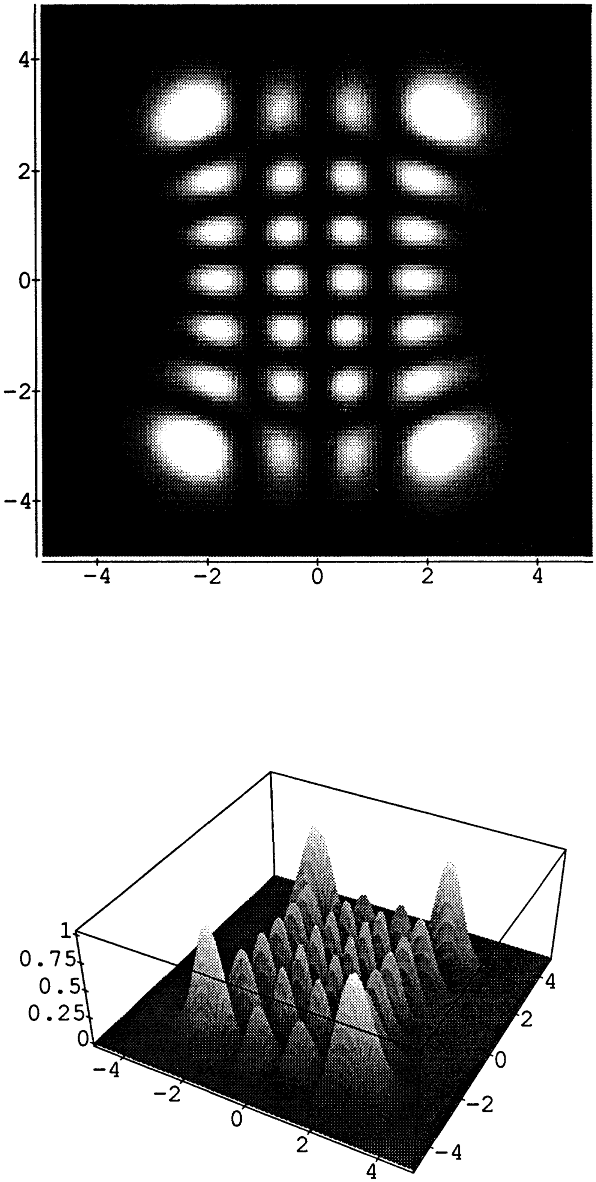

Figure 2. The m=3, n=6 eigenfunction for the basin in Fig. 1. The rays in Fig. 1 confine the mode, given here by products of Hermite polynomials in x and y. Scales are arbitrary.

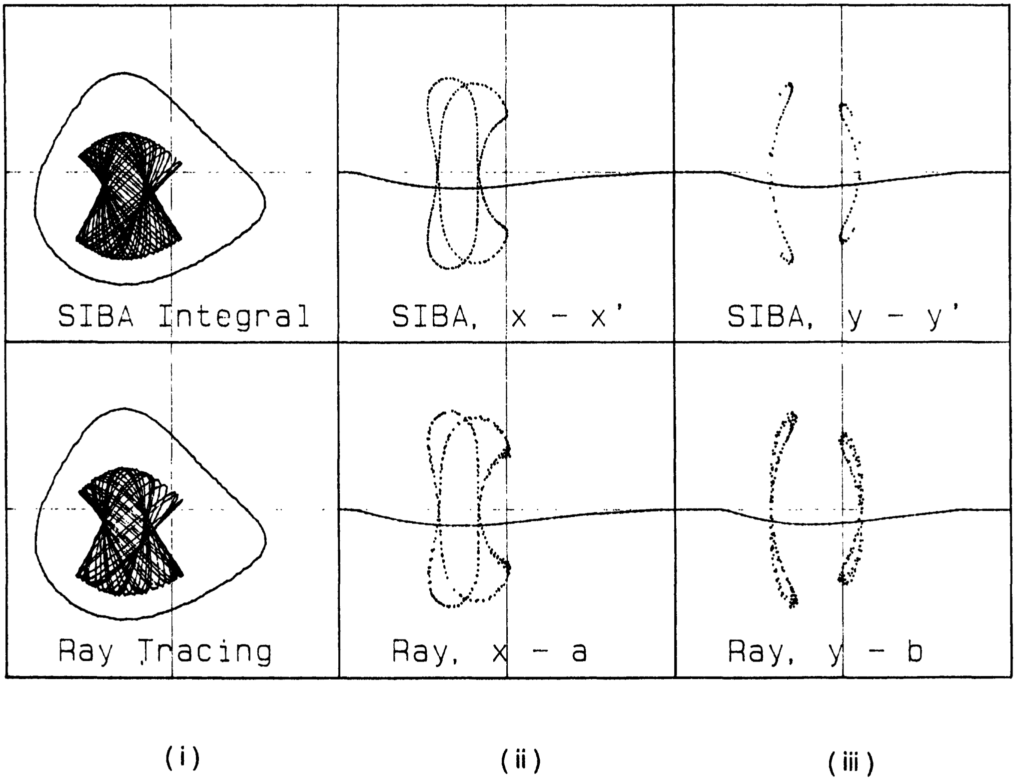

Figure 3. As in Figure 1 but for a more complex, nonsymmetrical resonant basin. The Poincare sections are again taken along the x=0 y=0 lines of (i), which here accounts for the complicated appearence of the closed curves in (ii) and (iii). Even in this case however, the accuracy of the SIBA approximation is very high. In contrast to the basin in Figure 1, it is not simple to find the analytic form of the eigenfunctions, which must consist of disjoint products of Airy functions or Hermite polynomials with coefficients that vary with the coordinates.

Investigations of Site Response

9950-03899

A. M. Rogers
Branch of Geologic Risk Assessment
U. S. Geological Survey
Box 25046, MS 966, DFC
Denver, Colorado 80225
303-236-6978

Investigations

Work during this period centered on several topics unrelated to this specific project.
1.) Considerable effort continues to be expended on the editorship of USGS Professional Paper 1560 "Evaluating Geologic Hazards in the Pacific Northwest". Over 40 papers are in preparation for this volume, submitted or to be submitted by both USGS and external scientists.
2.) Work on the NTS seismic network also continues. During this period two invited talks were given on the "Seismicity and Tectonics of the southern Great Basin" at a GSA/American Nuclear Society meeting in Las Vegas, and at the USGS sponsored CASEY meeting in Death Valley. Two papers on this topic have also been finalized during this period. In addition, work continues (in revision) on two site characterization plans as part of the QA requirements for this project.
3. I also led and finalized the writing for a consensus document for the Utah Geological and Mineralogical Survey entitled "Statement on the Ground Shaking Hazard in the Wasatch Basin" with S.T. Algermissen, K. Campbell, J. Pechmann, D. Perkins, M. Power, J.C. Tinsley, and L. Youd. This document will be included in a future publication regarding hazards in this region that is authored by W. Arabasz and D. Mabey.

Reports

Rogers, A.M., Harmsen, S.C., and Bufe, C.G., 1990, Selected characteristics of seismicity in the southern Great Basin of Nevada and California, in "U.S. Geological Survey Earth Science Studies for the Yucca Mountain Project--Selected Papers", U.S. Geological Survey Bulletin (in press).

Rogers, A.M., Harmsen, S.C., Corbett, E.J., Priestley, K., and DePolo, D., in press, The seismicity of Nevada and some adjacent parts of the Great Basin, in Neotectonics of North America, Decade of North American Geology, Slemmons, D.B., Engdahl, E.R., Blackwell, D., and Schwartz, D., eds.: Geological Society of America Special Paper, 36 ms. pages.

Rogers, A.M., 1989, The importance of geologic conditions on the level of strong shaking--Application to national probabilistic hazard mapping, in Proceedings of Conference XLVII, "A workshop on USGS's new generation of probabilistic ground motion maps and their applications to building codes", U.S. Geological Survey Open-File Report 89-364, p. 92-97.

Deep Structural Complexity and Site Response in Los Angeles Basin

14-08-0001-G1684

Mrinal K. Sen* and Chandan K. Saikia
Woodward-Clyde Consultants
566 El Dorado St.
Pasadena, CA 91101
(818)-449-7650

*Institute for Geophysics, University of Texas at Austin
8701 Mopac Blvd., Austin, TX 78759
(512)-471-0466

Investigations: The major objective of this project is to determine the effect of the lateral heterogeneity and local site conditions on strong ground motions in the Los Angeles basin. To achieve these goals we carried out waveform modeling of small to moderate sized earthquakes recorded in different parts of Los Angeles basin. The results of these studies were discussed in the previous summary (Sen, 1989) and will not be repeated. Here we will discuss the site characteristics of stations in the Los Angeles basin from regional events (NTS).

Results: From previous studies (Saikia and Burdick, 1990), we know which portions of seismograms from hard-rock site (Pasadena site, CIT) are due to regional phases, namely Pn, Pg, Lg, and shallow locally trapped surface waves. The appropriate ray parameter is a useful criterion in detecting which portion of the crustal structure is causing the variability in motions. That is, Pn is coming-up steeply and less affected by the edges of the basins and ridges relative to Lg, etc.

We analyzed the same data that were investigated by Rogers *et al.* (1979, 1980). The characteristic amplifications of the individual phases at sites of Los Angeles area relative to the corresponding phases recorded at Pasadena site (CIT) underlain by crystalline rock have been investigated. We have studied five explosions so far. Event Billet was one of the few events with recordings available at many sites. This event was recorded at Palos Verdes Estate (PVR) rock site (station underlain by a thin veneer of alluvium over sedimentary rock) and at a thick alluvium site at California State University (CSU) in Long Beach. It was also recorded at CIT, Tishman Airport Center (TAC), 800 W. Sixth Street (800WS) at Downtown Los Angeles. Figure 1 shows the locations of these sites marked by stars. Data are available for all components. Here we present the results obtained from the vertical component data analysis. Analysis of the other components will be discussed in a later report.

Each individual phase is windowed and tapered at both ends before transforming to the frequency domain. Possible noise contamination was removed by subtracting the spectrum of a noise window. This noise window was about 5 sec long and was taken from the seismograms before the onset of Pn signals. To obtain stable spectral ratio estimates, the spectral values are further smoothed by a triangular operator. The start time of the seismograms were not available, so we identified the earliest arriving signal as the Pn wave arrival and assumed it to have propagated to the sites with a phase velocity of 7.9 km/sec. A 5.0 sec window length was chosen for this phase. For the Pg and Lg waves, the windows were of 10 and 50 seconds durations with 6.5 and 3.6 km/sec phase velocities, respectively.

Figures 2-5 show the spectral ratios of individual phases relative to CIT. The seismograms of individual stations are shown on top of each spectral ratio panel. The signal within each rectangular window was used for the spectral analysis. The Pn signatures are distinct in each of these seismograms except for station 800WS. The spectral plots do suggest pronounced spectral amplification of Lg signals above 2.5 hz at the sedimentary site CSU at Long Beach. Signals above 5 hz are within the noise level and should not be trusted. Figure 3 shows the spectral ratios at four sites relative to CIT for the entire surface wave trend for a duration of 200 second starting at the onset of Lg waves (3.6 km/sec). The spectral ratios of the entire surface wave train appear to have more scalloping but behave similarly to the Lg waves. These results indicate that the surface waves are more affected by the shallow basin structures than are the body-wave phases. Quantitative modeling of these effects are currently being carried out.

References:

Rogers, A. M., P. A. Covington, R. B. Park, R. D. Borcherdt and D. M. Perkins, Nuclear Event Time Histories and Computed Site Transfer Functions for Locations in the Los Angeles Region, U. S. Geological Survey, *Open-File Report 80-1173*, Denver Federal Center, Denver, CO 80225, 1980.

Rogers, A. M., J. C. Tinsley, W. W. Hays, and K. W. King, Evaluation of the Relation Between Near-Surface Geological Units and Ground Response in the Vicinity of Long Beach, California, *Bull. Seis. Soc. Am., Vol 69*, 1603-1622, 1979.

Saikia, C. K. and L. J. Burdick, Fine structure of Pnl for Explosions, submitted to Journal of Geophysical Research for review, 1990.

Sen, M. K., Deep Structural Complexity and Site Response in Los Angeles Basin, *Nat. Earthq. Haz. Reduc. Prog. Summ. Tech. Rep.* V XXVIII, U.S. Geological Survey, *Open-File Report 89-453, 495-499.*

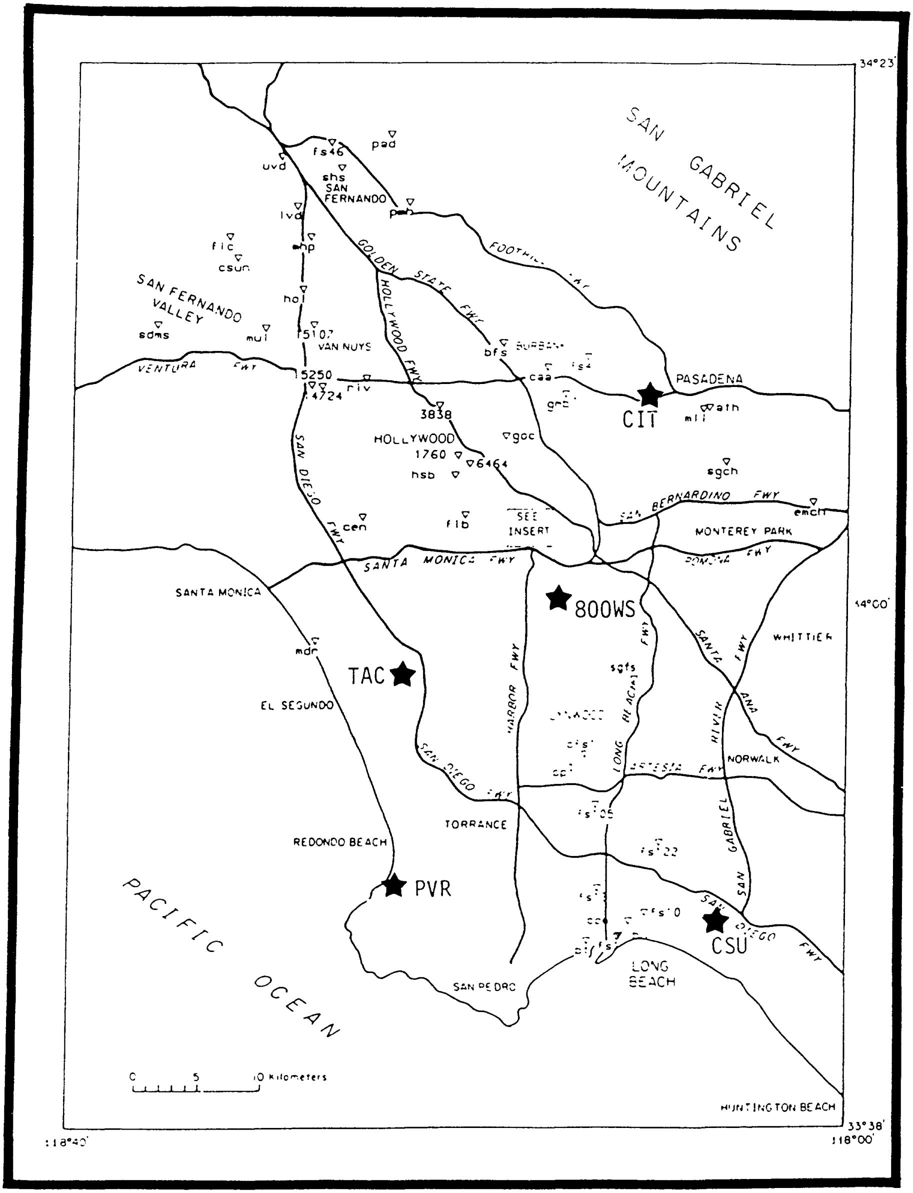

Figure 1. Locations of stations deployed by U.S.G.S. in the greater Los Angeles region. Star indicates the locations of the stations investigated in this study (Map taken from Rogers *et al.*, 1980).

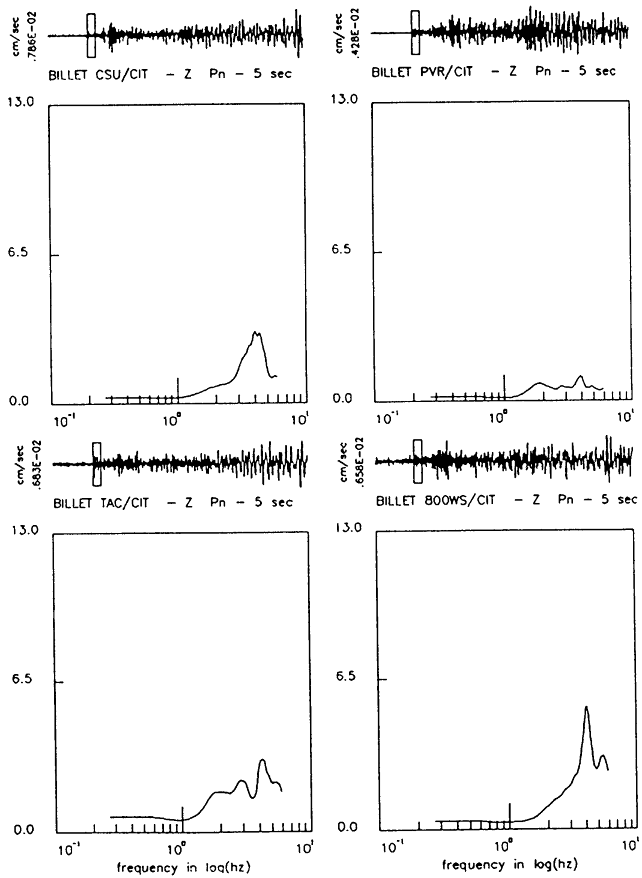

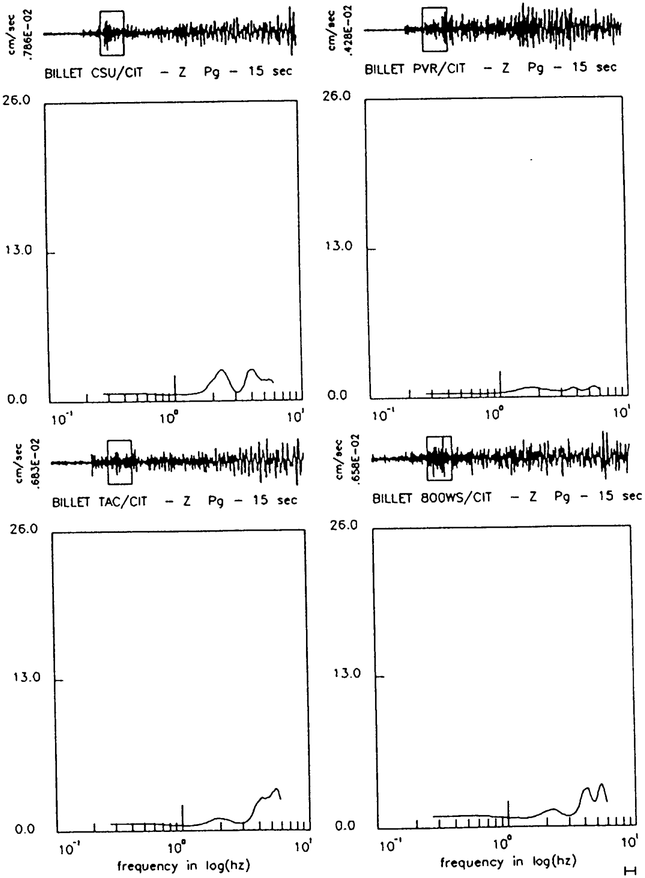

Figure 2. Spectral ratios of Pn (7.9 km/sec) waves recorded at CSU, PSR, TAC and 800WS from BILLET. A 5 sec time window was used. CIT was used as a reference station. Spectra were corrected for the noise contamination and smoothed by a traingular operator. (Vertical Component Data).

Figure 3. Spectral ratios of Pg (6.5 km/sec) waves recorded at CSU, PSR, TAC and 800WS from BILLET. A 15 sec time window was used. CIT was used as reference station. Spectra were corrected for the noise contamination and smoothed by a traingular operator. (Vertical Component Data).

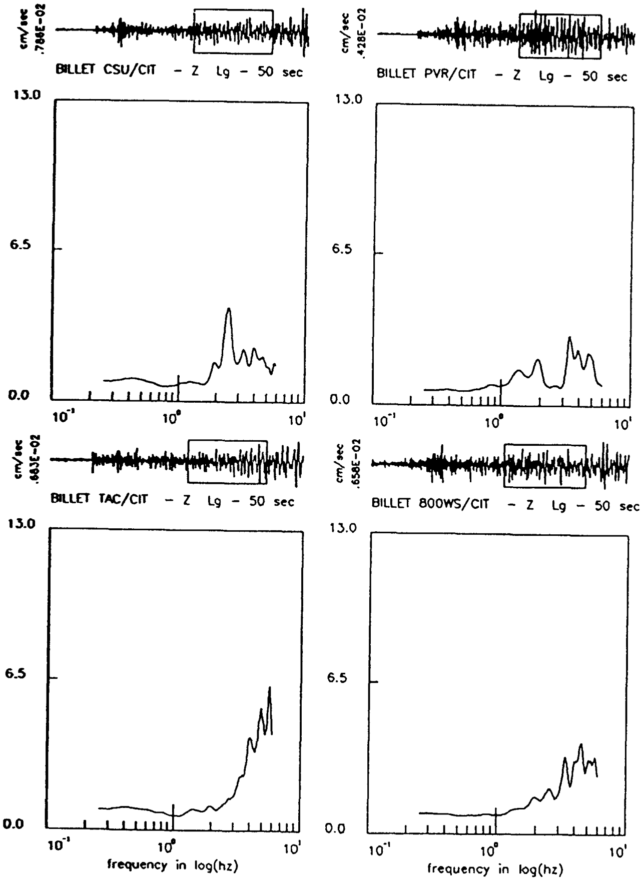

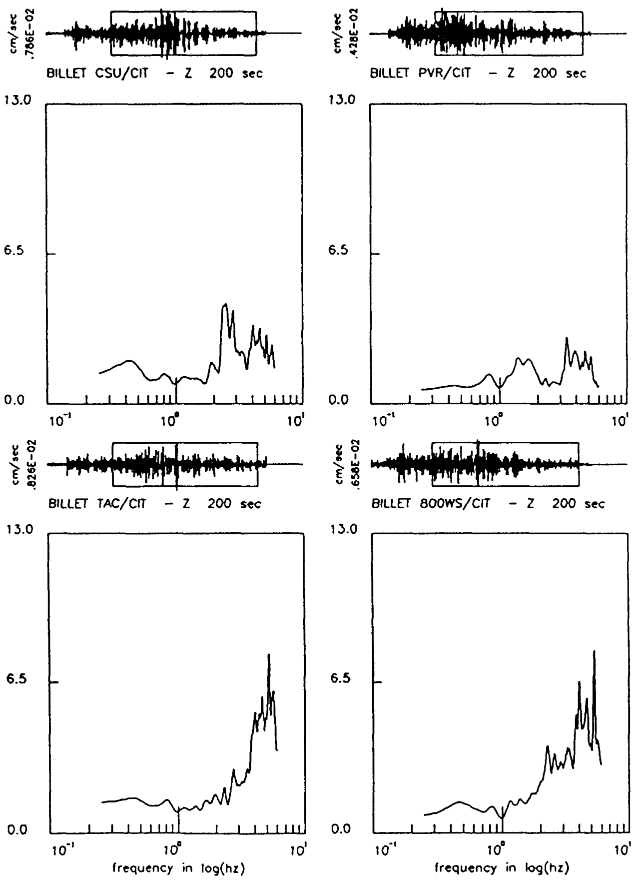

Figure 4. Spectral ratios of Lg (3.6 km/sec) waves recorded at CSU, PSR, TAC and 800WS from BILLET. A 5 sec time window was used. CIT was used as reference station. Spectra were corrected for the noise contamination and smoothed by a traingular operator. (Vertical Component Data).

Figure 5. Spectral ratios of surface waves starting at 3.6 km/sec recorded at CSU, PSR, TAC and 800WS from BILLET. A 50 sec time window was used. CIT was used as reference station. Spectra were corrected for the noise contamination and smoothed by a traingular operator. (Vertical Component Data).

Simulation and Empirical Studies of Ground Motion Attenuation in the Seattle-Portland Region

14-08-0001-G1516

Paul Somerville and Brian Cohee
Woodward-Clyde Consultants
566 El Dorado Street, Suite 100
Pasadena, CA 91101

PHASE I: SUBDUCTION EARTHQUAKES

OBJECTIVE

The objective of the first phase of this project is to estimate strong ground motions for hypothetical M_w=8.0 subduction zone thrust earthquakes in the Puget Sound - Portland region using a simulation method. The use of strong motion simulation procedures is motivated by the complete absence of subduction earthquakes on the Cascadia subduction zone during historical time (and the consequent absence of strong motion recordings of such events), and the paucity of applicable strong motion recordings from other subduction zones.

PUBLICATIONS

Somerville, P.G., M.K. Sen and B.P. Cohee (1990). Simulation of strong ground motions recorded during the 1985 Michoacan, Mexico and Valparaiso, Chile subduction earthquakes, *Bull. Seism. Soc. Am.*, submitted.

Cohee, B.P., P.G. Somerville and N.A. Abrahamson (1990). Ground motions from hypothesized M_w=8 earthquakes in the Pacific Northwest, *Bull. Seism. Soc. Am.*, submitted.

Somerville, P.G., B.P. Cohee and N.A. Abrahamson (1990) Ground motions from hypothesized M_w=8 Cascadia subduction earthquakes, submitted to the USGS Professional Paper *"Assessing and Reducing Earthquake Hazards in the Pacific Northwest."*

Cohee, B.P., P.G. Somerville and N.A. Abrahamson (1990). Simulated ground motions from subduction earthquakes in the Pacific Northwest, *Proc. 4th U.S. National Conference on Earthquake Engineering*, Palm Springs, May 1990.

Abrahamson, N.A., P.G. Somerville, and C. Allin Cornell (1990). Uncertainty in numerical strong motion predictions, *Proc. 4th U.S. National Conference on Earthquake Engineering*, Palm Springs, May 1990.

PHASE II: WADATI-BENIOFF ZONE EARTHQUAKES

OBJECTIVE

The objective of the second phase of this project is to estimate ground motions in the Puget Sound - Portland region resulting from earthquakes in the Wadati-Benioff zone that lies within the subducted oceanic plate downdip of the subduction zone plate interface (depths greater than 40 km). Both the 1949 Olympia and the 1965 Seattle earthquakes were events of this type.

METHOD

Accelerograms from the 1949 and 1965 earthquakes, together with recent, calibrated velocity recordings of smaller earthquakes provide an empirical data base that is used to define attenuation relations specific to this source zone. These are being compared with attenuation models derived from synthetic seismograms computed using crustal structure models appropriate for the Seattle-Portland region. The effects of laterally varying seismic velocity and Q structure on ground motion attenuation are being examined.

PROGRESS

Analysis of the five strong motion recordings from the 1949 and 1965 earthquakes using the complex polarization method of Vidale (1986, BSSA, pp.1393-1405), suggests wave propagation for the paths considered is fairly simple. Particle motion on the Olympia records is more regular and exhibits higher linear polarization compared to Seattle and Tacoma, suggesting the site is less influenced by local scattering. The large peak horizontal accelerations at Olympia appear to be caused by SH waves.

Attenuation structure appears to be highly variable under the three sites. During the 1965 earthquake, Olympia, at a hypocentral distance of 100 km, recorded significant energy above 12 Hz, while Seattle at a distance of 65 km, had very little energy above 6 Hz. Higher relative attenuation beneath Seattle is also seen in the record of the 1949 earthquake, even though this accelerogram was recorded at a different site some 5 km away from the location of the 1965 recording. In summary, the two records from Seattle show greater evidence of scattering and are more attenuated than the Olympia records, indicating strong variation in scattering Q structure in the study region.

Surface waves are not evident in the recordings, which is somewhat surprising considering the deep sedimentary basins and complex geologic structure of the area. The basin structures may cause focusing of energy, producing a different amplification pattern for each source location, but it is difficult to isolate these focusing effects given the scant regional distribution of the data. As a continuation of this work, we propose to explore the focusing potential of basins in the Puget Sound and Portland areas using the 3-D wave simulation method of Graves and Clayton (1990, Geophysics, pp.306-319).

SH finite difference wave simulation in a detailed 2-D velocity structure normal to the strike of the subduction zone indicates that amplitudes and waveforms at receiver locations in Puget Sound from deep (40-70 km) events in the slab are not strongly affected by the slab structure. For receiver locations further to the west, corresponding to updip propagation through the slab to the coastal areas of Washington, the direct S waveform develops some complexity from rays critically reflected within the slab, but the peak amplitudes are not strongly effected. Although the actual 3-D structure is certainly more complex than modeled, it appears that for receiver locations in Puget Sound, gross characteristics of wave propagation are fairly well approximated by a 1-D velocity model.

As mentioned above, the duration and peak amplitude of S waves appears to be strongly dependent on lateral variations in Q structure. In order to image the regional effect of Q structure on duration and amplitude, we have analyzed vertical short-period shear-wave velocity seismograms from 45 intraslab earthquakes (1.2<M<3.8) recorded on a calibrated 34 station subnet of the UW/USGS western Washington regional network. The station and earthquake locations are shown in Figure 1a. The data are bandpass filtered and scaled to a common gain. A 20 sec window is defined beginning 2 sec prior to the predicted S arrival. For each of the roughly 1000 seismograms, the peak velocity and acceleration, and the power in the 20 sec window is measured. A least-squares regression yields the relationship:

$$\ln(PGA) = -1.76\ln(r) + \sum_{i=1}^{nevents} d_i E_i$$

where *PGA* is the peak vertical acceleration of the S wave, r is hypocentral distance, and d_i is the coefficient for the E_i earthquake. We explicitly solve for d_i because the magnitudes of these events are poorly determined, but we may compare d_i with the original magnitudes to estimate the magnitude dependence. If the 34 stations are divided into three groups based on local site geology, the resulting regression formula is:

$$\ln(PGA) = -1.59\ln(r) + .62s_1 + 1.26s_2 + \sum_{i=1}^{nevents} d_i E_i$$

where s_1 is the soil-over-rock site dummy variable, and s_2 is the soil site dummy variable (1 for soil site, 0 otherwise). The default relationship (no site term) is appropriate for the rock sites.

Analysis of the residuals using the above regression formulas does not indicate the need for further terms in the regression. There is no trend in the residuals as a function of hypocentral distance, which confirms the observation that wave propagation for the ray paths producing the peak S amplitudes are fairly direct. There is, however, a pattern of positive residuals for azimuths (event to station) to the east and southeast.

To further explore this trend, we plot the mean residual for each station in Figure 1b-d. There is a clear grouping of the station residuals: positive residuals (larger than average amplitudes) in the east, and negative residuals in the west. The boundary between the positive and negative groups of station residuals is approximated by the 55 km depth contour of the subducted slab as identified by Crosson and Owens (1987, GRL, pp.824-827). If we treat the two groups independently, and make the hypothesis that the two groups have the same mean value, a maximum likelihood estimate indicates the probability of this hypothesis being true is less than 2 percent. On average, the stations to the east have peak vertical acceleration values 1.5 times larger than the stations to the west. We also regress on the *power* parameter measured for each seismogram, and plot the mean station residuals from the power regression formula in Figure 1d. This pattern is generally similar to the *PGA* station residuals shown in Figure 1c. The correlation between peak acceleration and power is consistent with the hypothesis that lateral variation in scattering Q is partly responsible for the observed variation in ground motion amplitudes from Wadati-Benioff earthquakes.

PUBLICATIONS

Cohee, B., N. Abrahamson and P. Somerville (1990). S-wave amplitudes from Wadati-Benioff earthquakes beneath western Washington, manuscript in preparation.

Cohee, B.P. and P.G. Somerville (1990). Simulated and empirical estimates of strong ground motion from Wadati-Benioff zone earthquakes beneath western Washington, *Seismological Research Letters*, 61, p. 24.

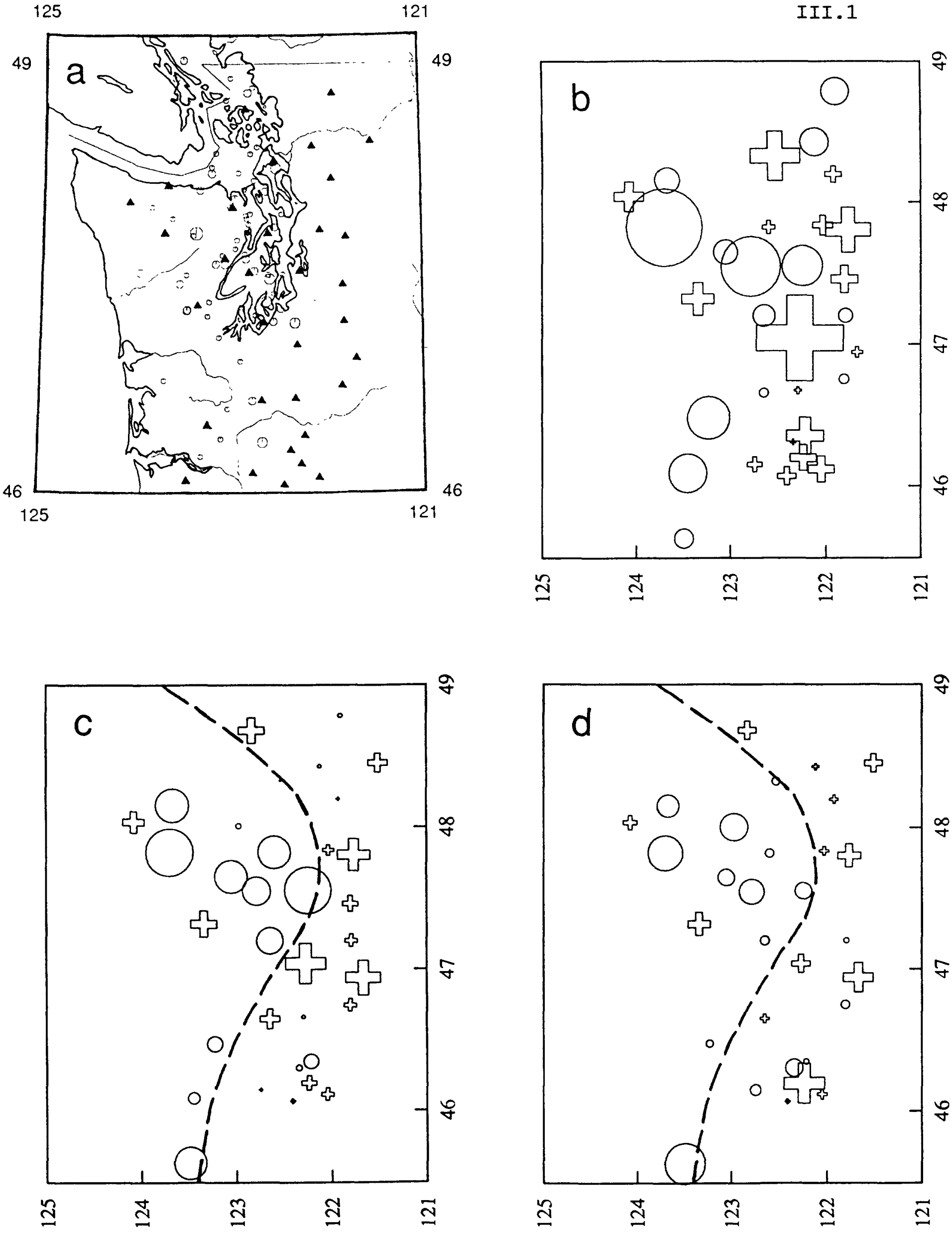

Figure 1a-d. a) map view of western Washington, calibrated stations are shown by triangles, epicenters are shown by open circles. b) mean station residuals for vertical S-wave peak acceleration (*PGA*) regression formula without site terms. c) mean station residuals for *PGA* regression formula using three site terms, dashed line is 55 km depth contour of the oceanic Moho, see text. d) mean station residuals for *power* regression formula using three site terms.

EXPERIMENTAL AND ANALYTICAL INVESTIGATIONS OF THREE GRAVELLY SITES WHICH LIQUEFIED DURING THE 1983 BORAH PEAK, IDAHO EARTHQUAKE

USGS 14-08-0001-G1779

Kenneth H. Stokoe, II, José M. Roesset and Ronald D. Andrus
The University of Texas at Austin
Department of Civil Engineering
ECJ 9.227
Austin, Texas 78712
(512) 471-4929

Investigation

Liquefaction of gravelly materials has been generated in several different earthquakes, including the 1891 Mino-Owari, Japan earthquake; 1929 Murchison, New Zealand earthquake; 1948 Fukui, Japan earthquake; 1964 Alaskan earthquake; 1974 Tangshan and 1975 Haicheng earthquakes, both in China; 1978 Miyayiken-Oki, Japan earthquakes; and the 1983 Borah Peak, Idaho earthquake. At present, there are no generally accepted guidelines for evaluating the susceptibility of soils which contain significant amounts of gravel. Recent studies by Andrus and Youd (1987), Stokoe et al (1988) and Harder (1988) at two sites (Pence Ranch and Whiskey Springs) which liquefied during the 1983 Borah Peak, Idaho earthquake, provide the most well-documented case histories of the field performance of loose gravelly sediments. The results from these studies are reasonably consistent with the susceptibility boundaries developed for sands and silts. However, the data are limited and incomplete.

This summer we plan to return to Pence Ranch and two additional gravelly sites which liquefied during the Borah Peak earthquake. The field work will involve test pit excavations, drilling, sampling and seismic testing. The test pits will be used to conduct large ring density tests as well as provide information concerning the sediment structure, grain size, depositional environment and age. SPT, CPT, and BPT tests will be performed at each site. Samples will be collected during test pit excavation and drilling. Data from sampling and penetration tests will be used to accurately define the relationship of q_c/N_{60} with D_{50} (Fig. 1) and the susceptibility boundaries of the empirical correlations for gravelly soils (Figs. 2-4). BPT data will be used to estimate equivalent SPT N-values in the gravelly soils. Seismic testing will include both SASW (Spectral-Analysis-of-Surface-Waves) and downhole techniques. Modified SASW procedures will permit deeper measurements of G_{max} which are required in the analytical studies. Dynamic tests will be performed in the laboratory on 6-in. (15-cm) reconstituted gravel specimens. A dynamic model will be developed from the results of the field and laboratory investigations combined with the limited amount of published data. Liquefaction susceptibility will be evaluated analytically at each site using both the cyclic stress and cyclic strain approaches.

Results

This project has just begun and our efforts thus far have gone into field and laboratory preparations as well as continued evaluation of the data collected in 1985.

Our efforts to apply existing empirical liquefaction assessment procedures to data collected at Pence Ranch will be briefly discussed in this summary.

Based on the penetration logs and sample borings, the generalized cross section of the lateral spread at Pence Ranch shown in Fig. 5 was constructed. The two units of most concern are C and D. SPT and CPT resistances in unit C ranged from 5 to 10 blows/ft and 4 to 202 tsf (4 to 197 kgf/cm^2), respectively. Unit D is characterized by N-values of 18 to 23 and tip resistances of 73 to 297 tsf (71 to 290 kgf/cm^2). Sediments within these units range from clean gravelly sand (SP-GP) to sandy gravel (GP). The most widely used simplified empirical approach for evaluating liquefaction potential of sands is a procedure by Seed and his colleagues based upon SPT and CPT test results. Without established guidelines to correct for gravel, the influence of gravel on the penetration resistance was ignored. Cyclic stress ratios are plotted versus average modified SPT and CPT penetration resistances in Figs. 2 and 3, respectively. Also shown in these figures are the liquefaction potential curves for materials with less than 5 percent fines. By applying the criteria of Seed and his colleagues directly to units C and D at Pence Ranch, unit C is predicted to liquefy and has significant shear deformation potential. This assessment is in agreement with field observations. Unit D is, however, also shown to be rather close to possible liquefaction in Fig. 2. It is difficult to clearly assess the liquefaction potential of units C and D using q_c and Fig. 3 because the average q_c/N_{60} value for these units is well beyond the limit of 5.3 presented in this plot. Seed and de Alba (1986) use the curve shown in Fig. 2 to generate the set of potential curves for q_c/N_{60} values of 4.4, 4.8 and 5.3. This would appear to suggest that additional curves could be drawn, using Fig. 2, for ratios of q_c/N_{60} greater than 5.3. However, by so doing would imply q_c to be sensitive to grain size and not $(N_1)_{60}$.

Another method of evaluating the liquefaction potential of sediments is based upon measured shear wave velocities and maximum ground acceleration (Bierschwale and Stokoe, 1984; and Stokoe et al, 1988b). The liquefaction potential is estimated by plotting the shear wave velocity versus the maximum ground acceleration estimated for a stiff site at the candidate-site location. (This method has evolved from the strain approach to liquefaction proposed by Dobry and his colleagues [1982].) Shear wave velocities determined using the SASW procedure ranged from 300 to 407 ft/sec (90 to 105 m/sec) in unit C and 369 to 750 ft/sec (115 to 215 m/sec) in unit D. The lowest value of shear wave velocity determined for units C and D at each test site are shown in Fig. 4. Unit C lies within the zone where liquefaction is predicted to occur which agrees with the field performance. Unit D has a lower potential than unit C. However, unit D is shown to lie in the region of likely liquefaction. It is difficult to properly assess the liquefaction potential of unit D because Fig. 4 was generated assuming no drainage and drainage may have occurred in unit D.

REFERENCES

Andrus, R.D. and Youd, T.L., (1987), "Subsurface Investigation of a Liquefaction-Induced Lateral Spread, Thousand Springs Valley, Idaho," U.S. Army Corps of Engineers, Geotechnical Laboratory Miscellaneous Paper GL-87-8, 131 p.

Bierschwale, J.G., and Stokoe, K.H., II, (1984), "Analytical Evaluation of Liquefaction Potential of Sands Subjected to the 1981 Westmorland Earthquake, Geotechnical Engineering Report GR84-15, Civil Engineering Department, The University of Texas at Austin, 231 p.

Dobry, R., Ladd, R.S., Yokel, F.Y., Chung, R.M., and Powell, D., (1982), "Prediction of Pore Water Pressure Buildup and Liquefaction of Sands During Earthquakes by the Cyclic Strain Method," *N.B.S. Bldg. Science Series* 138, U.S. Dept. of Commerce.

Harder, Jr., Leslie F., (1988), "Use of Penetration Tests to Determine the Liquefaction Potential of Soils During Earthquake Shaking," Ph.D. Dissertation, University of California, Berkeley, 565 p.

Seed, H. B., and de Alba, P., (1986), "Use of SPT and CPT Tests for Evaluating the Liquefaction Resistance of Sands," *Use of In Situ Tests in Geotechnical Engineering*, Samuel P. Clemence, editor, Geotechnical Special Publication No. 6, ASCE, pp. 281-302.

Seed, H. B., Tokimatsu, K., Harder, L. F., and Chung, R. M., (1985), "Influence of SPT Procedures in Soil Liquefaction Resistance Evaluations," *Journal of Geotechnical Engineering*, ASCE, Vol. 111, No. 12, pp. 1425-1445.

Stokoe, K.H., II, Andrus, R.D., Rix, G.J., Sanchez-Salinero, I., Sheu, J.C., and Mok, H.J., (1988a), "Field Investigation of Gravelly Soils Which Did and Did Not Liquefy During the 1983 Borah Peak, Idaho, Earthquake," Geotechnical Engineering Report GR87-1, Civil Engineering Dept., The University of Texas at Austin, 206 p.

Stokoe, K.H., II, Roesset, J.M., Bierschwale, J.G., and Aouad, M. (1988b), "Liquefaction Potential of Sands from Shear Wave Velocity," *Proceedings*, Ninth World Conference on Earthquake Engineering, Tokyo, Japan, April, pp. 213-218.

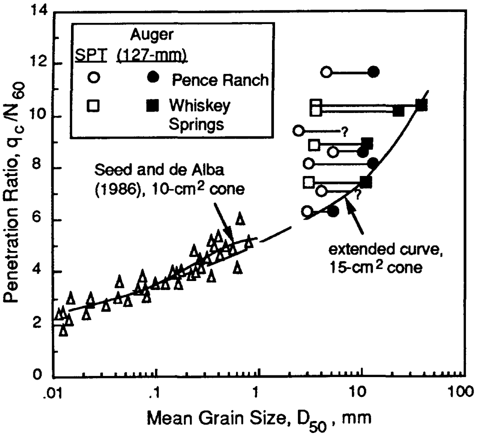

Fig. 1 Relationship between q_c/N_{60} and Mean Grain Size with Data from Pence Ranch and Whiskey Springs (from Stokoe et al, 1988a; after Andrus and Youd, 1987)

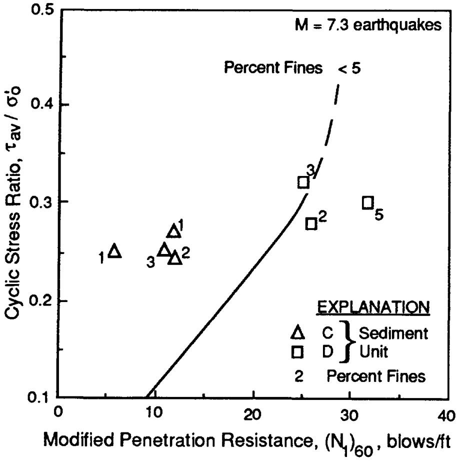

Fig. 2 Liquefaction Potential Chart Based on Modified N-Values with Results from Pence Ranch (Stokoe et al, 1988a)

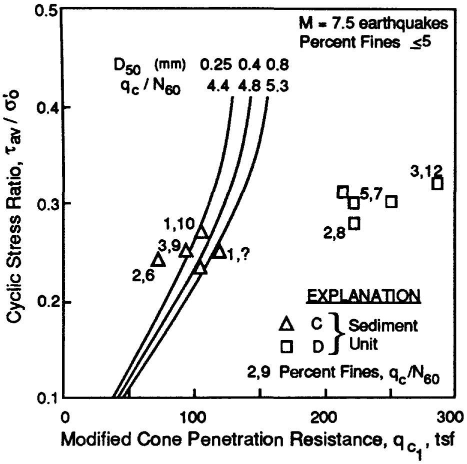

Fig. 3 Liquefaction Potential Chart Based on Modified Tip Resistance (Seed and de Alba, 1986) with Results from Pence Ranch (Stokoe et al, 1988a)

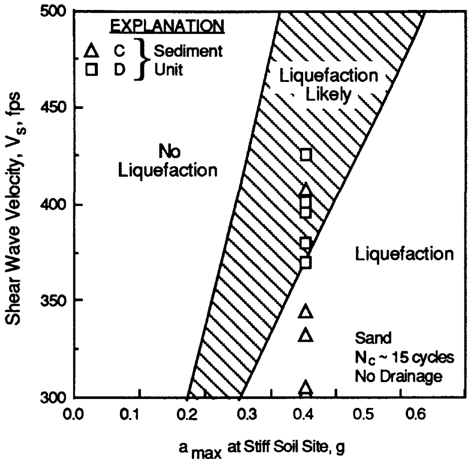

Fig. 4 Liquefaction Potential Chart Based on Shear Wave Velocity with Results from Pence Ranch (Stokoe et al, 1988a)

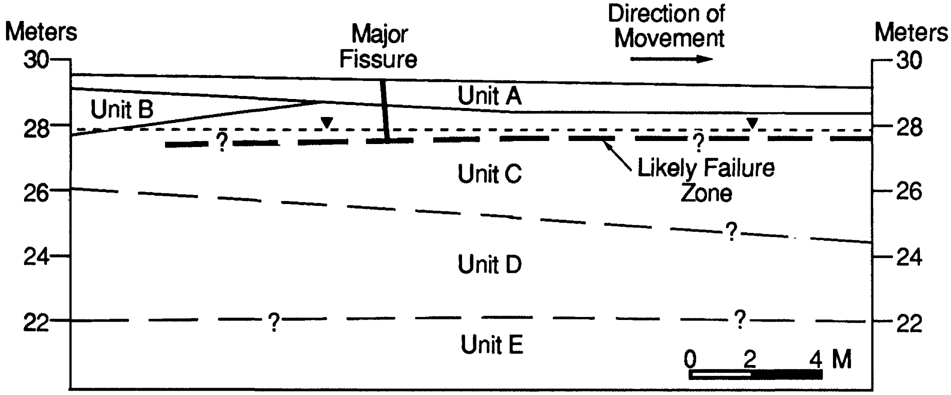

Fig. 5 Generalized Cross-Section of the Lateral Spread at Pence Ranch (after Stokoe et al, 1988a)

Quarternary Framework for Earthquake Studies
Los Angeles, California

9540-01611

John C. Tinsley
Branch of Western Regional Geology
U.S. Geological Survey
345 Middlefield Road M/S 975
Menlo Park, California 94025
(415) 329-4928

Investigations

1. Geology and relative ground motion, Wasatch region, Utah:

Analysis of geologic and geophysical data from 43 sites in the Salt Lake Valley continues, and writing of interpretative reports is in progress. The studies involve comparisons among parameters including thickness of key stratigraphic intervals, degree of cementation of materials, shear-wave velocity, and soil index parameters in relation to alluvium-to-rock spectral ratios in two period bands (0.2-0.7 sec and 0.7-1.0 sec). (J. Tinsley, K. King, R. Williams, and D. Trumm).

2. Regional Liquefaction Evaluation and Site Response studies, Los Angeles, CA; plans for FY 1990:

   A. USGS scientists and program managers are negotiating a Memorandum of Understanding with the Planning Department of the City of Los Angeles to encompass Open-File publication of USGS regional liquefaction hazard mapping (surficial geology, shallow groundwater database, and derivative hazard maps, scale 1:24,000). The mapping is expected to be a point of departure for revisions to the earthquake hazards element of the City's general plan. This will complete the release of USGS data and USGS-compiled data mustered in connection with the regional evaluation of liquefaction hazards by Tinsley and others (1985), published in USGS Professional Paper 1360. (J. Tinsley, D.M. Perkins, USGS, Golden, CO).

   B. A ground shaking hazards map (scale 1:24,000) of the Los Angeles 7.5' quadrangle is also part of the foregoing MOU. The maps and supporting data overlays will be drawn according to the methodology of Rogers and others (1985).

Results

1. An Open-File report presenting the basic data and summarizing the results of the study of the Salt Lake Valley is being prepared, re-scheduled for completion by the end of June, 1990.

2. A Memorandum of Understanding has been negotiated. Work progresses on all fronts.

References cited

Rogers, A.M., Tinsley, J.C., and Borcherdt, R.D., 1985, Predicting relative ground response: in Ziony, J.I., ed., Evaluating earthquake hazards in the Los Angeles region: U.S. Geological Survey Professional Paper 1360, p. 221-247.

Tinsley, J.C., Youd, T.L., Perkins, D.M., and Chen, A.T.F., 1985, Evaluating liquefaction potential in Ziony, J.I., ed., Evaluating earthquake hazards of the Los Angeles region, and earth science perspective: U.S. Geological Survey Professional Paper 1360, p. 263-316.

Seismic Reflection Investigations of Mesozoic Basins, Eastern U. S.

9950-03869

John D. Unger
Branch of Geologic Risk Assessment
U. S. Geological Survey
922 National Center
Reston, VA 22092
(703) 648-6790

Ongoing Investigations

1. To consolidate and synthesize the available seismic reflection data that pertain to the internal and external structure of Mesozoic basins, with special emphasis on the hypocentral areas of the present seismicity observed in South Carolina, New Jersey, New York, and Pennsylvania.
2. To use synthetic seismic reflection models of the basement structure along selected seismic reflection profiles as an aid to processing and interpreting these data and to develop better basement structural and velocity models for more accurate location of earthquake hypocenters.
3. To develop 2- and 3-dimensional Geographical Information System computer techniques to display, analyze, and interpret geological and geophysical data collected in and around Mesozoic basins and other seismogenic structures in the Eastern U. S., in order to better understand the tectonic history of the Appalachian orogen.

Results

This project continues data interpretation and analysis, which rely principally on the use of proprietary software from Dynamic Graphics Corp. (Interactive Surface Modeling and Interactive Volume Modeling) and ESRI (ARC/INFO). Research to date has resulted in promising possibilities for displaying interpreted seismic reflection data along with gravity, magnetic, and refraction information as three-dimensional models of the crust in and around Mesozoic basins. A key component of this process is the ability to integrate in-house software written on high resolution, color graphics workstations with the proprietary programs. This approach is expedited by being able to transfer data between the workstations and mini-computers, where these software packages reside, via high-speed networks.

Reports

Stewart, David B., Unger, John D., Wright, Bruce E., Phillips, Jeffrey D., and Liberty Lee M., 1989, Three-dimensional characterization of regional structures using an advanced geographic information system, in Schindler, K. S., ed., USGS Research on Mineral Resources--1989, Program and Abstracts, Fifth Annual V.E. McKelvey Forum on Mineral and Energy Resources: U.S. Geological Survey Circular 1035, p. 71-72.

Unger, John D. and Liberty, Lee M., 1989, Using workstations to develop digital models of the Earth's crust along a transect through the Northern Appalachians, in Proceedings of the 23rd Meeting of the Geoscience Information Society, ed., Joanne V. Lerud, vol. 19, p. 79-88.

Unger, J. D., Liberty, L. M., Phillips, J. D., and Wright, B. E., 1989, Creating a 3-dimensional transect of the earth's crust from carton to ocean basin across the Northern Appalachian orogen, in Raper, Jonathan, ed., Three Dimensional Applications in Geographic Information Systems: Taylor and Francis, London, p. 137-148.

A Search for Active Faults in the Willamette Valley, Oregon

14-08-0001-G1522

Robert S. Yeats
Department of Geosciences
Oregon State University
102 Wilkinson Hall
Corvallis, OR 97331-5506
503-737-1201

Investigations

The surface and subsurface geology as constrained by oil-exploratory wells, water wells, and industry multichannel seismic lines has been plotted on green-line mylars of 1:100,000 metric-series maps of the Willamette Valley. This map includes structure contours on the top of the Columbia River Basalt Group (CRB) in the northern Willamette Valley and Tualatin basin and the base of the upper Eocene-lower Oligocene Eugene Formation in the southern Willamette Valley, where the CRB is not present. The structure contour map of the CRB may be used to construct isopach maps of relatively unconsolidated sediment in the northern Willamette Valley and Tualatin basin.

Several cross sections are being constructed across the Willamette Valley, constrained by well data and seismic lines. In addition, structural cross sections constrained by detailed gravity surveys are being constructed for the Tualatin basin. A structure contour map is being constructed showing the base of relatively unconsolidated sediment in the southern Willamette Valley. This map may be used to construct isopachs of relatively unconsolidated sediment in the southern Willamette Valley.

Bob Yeats testified before the Emergency Board of the Oregon legislature in favor of emergency funding of S.B. 955, which assigned responsibilities to DOGAMI to evaluate earthquake hazards. In December, 1989, the emergency board granted $230,000 to DOGAMI for this purpose.

Results

Faults and broad folds in the Willamette Valley have been mapped and are shown on Figure 1. Mapping responsibilities are as follows: southern Willamette Valley, Erik Graven; Corvallis fault, Chris Goldfinger; northern Willamette Valley, Ken Werner; hills between northern Willamette Valley and Tualatin Valley, Marvin Beeson and Terry Tolan on contract to Department of Geology and Mineral Industries (DOGAMI); Tualatin Valley, Ian Madin and Tom Popowski.

The largest fault in the Valley is the Corvallis fault, previously believed to be a high-angle fault. Detailed gravity traverses across the fault by Chris Goldfinger and Kelly Basquez show that the Corvallis fault is a low-angle thrust dipping 10°-15° to the NW. However, there is no geological evidence of late Cenozoic activity. To the northeast, a fault with the same strike as the Corvallis fault cuts CRB in the Salem Hills; like the Corvallis fault, the southeast side is downthrown. However, there is no evidence that the fault in the Salem Hills connects across the Willamette Valley to the Corvallis fault.

Still further northeast, the northwest-facing range front of the Waldo Hills appears to be controlled by a fault with the northwest side downthrown. Investigations of this structure are still underway.

Ken Werner has shown that the Mt. Angel fault extends NW from Waldo Hills into the northern Willamette Valley, where the top of the CRB has a vertical separation of 250m (Figure 2). Nonmarine late Cenozoic sediments unconformably above the CRB appear to have a vertical separation of 70m, based on a multichannel seismic line (Figure 3). There is no evidence that the Mt. Angel fault is continuous with the Gales Creek fault southwest of the Tualatin basin, as previously believed.

Erik Graven has shown that the Owl Creek fault east of Corvallis brings the upper Eocene-lower Oligocene Eugene Formation close to the surface on the eastern upthrown side, apparently eroding away the late Cenozoic Calapooia Clay and the late Pleistocene Linn outwash gravels that overlie the Calapooia Clay unconformably (Figure 4). The Willamette Formation, part of the latest Pleistocene catastrophic flood deposits, shows no evidence of vertical separation across this fault.

To determine Quaternary slip rates on Willamette Valley structures, it will be necessary to (1) date the post-CRB sediments using magnetic stratigraphy, pollen sequences, and tephrochronology, and (2) run high-frequency, shallow-penetration seismic profiles across mapped faults to identify those faults cutting young sediments close enough to the surface to trench.

A second core hole through the Calapooia Clay was drilled and logged in March, funded by the Oregon Department of Transportation. This hole, located near Sublimity in the sub-basin east of the Salem Hills and south of the Waldo Hills contains predominantly fine-grained sediments, like those in the Corvallis corehole, but there is more evidence of contemporaneous Cascade volcanism. Assistance in logging the hole was provided by Erik Graven, Tom Popowski, Ken Werner, In-Chang Ryu and Alan Niem of OSU and Dave Weatherbee and Dave Morgan of USGS.

Report

Yeats, R.S., Goldfinger, C., Graven, E.P., Madin, I.P., Popowski, T.A., and Werner, K.S., 1990, Tectonics of the Willamette Valley, Oregon: To be submitted to U.S. Geological Survey professional paper on earthquake hazards in the Pacific Northwest.

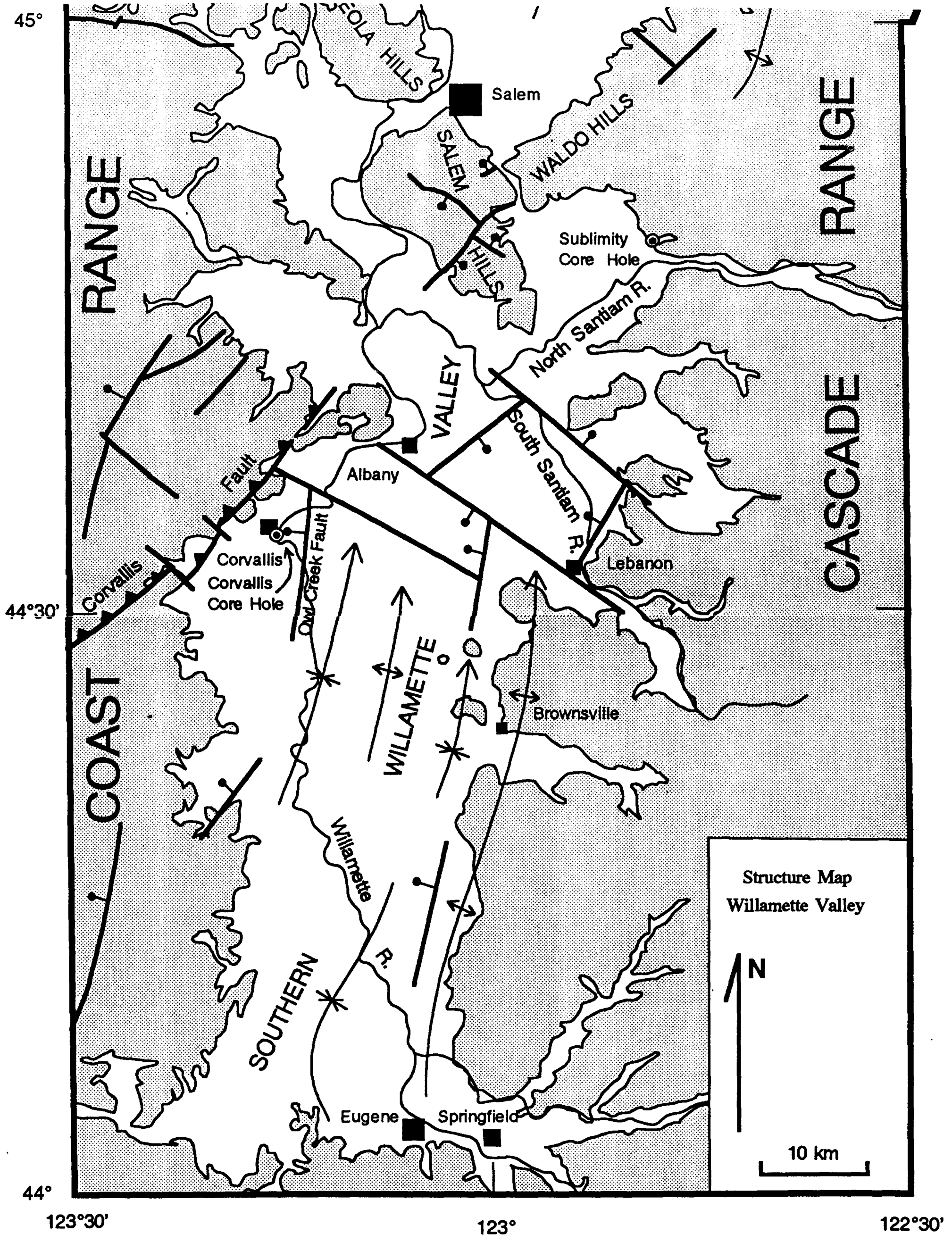

FIGURE 1 SOUTHERN PORTION OF STRUCTURE MAP

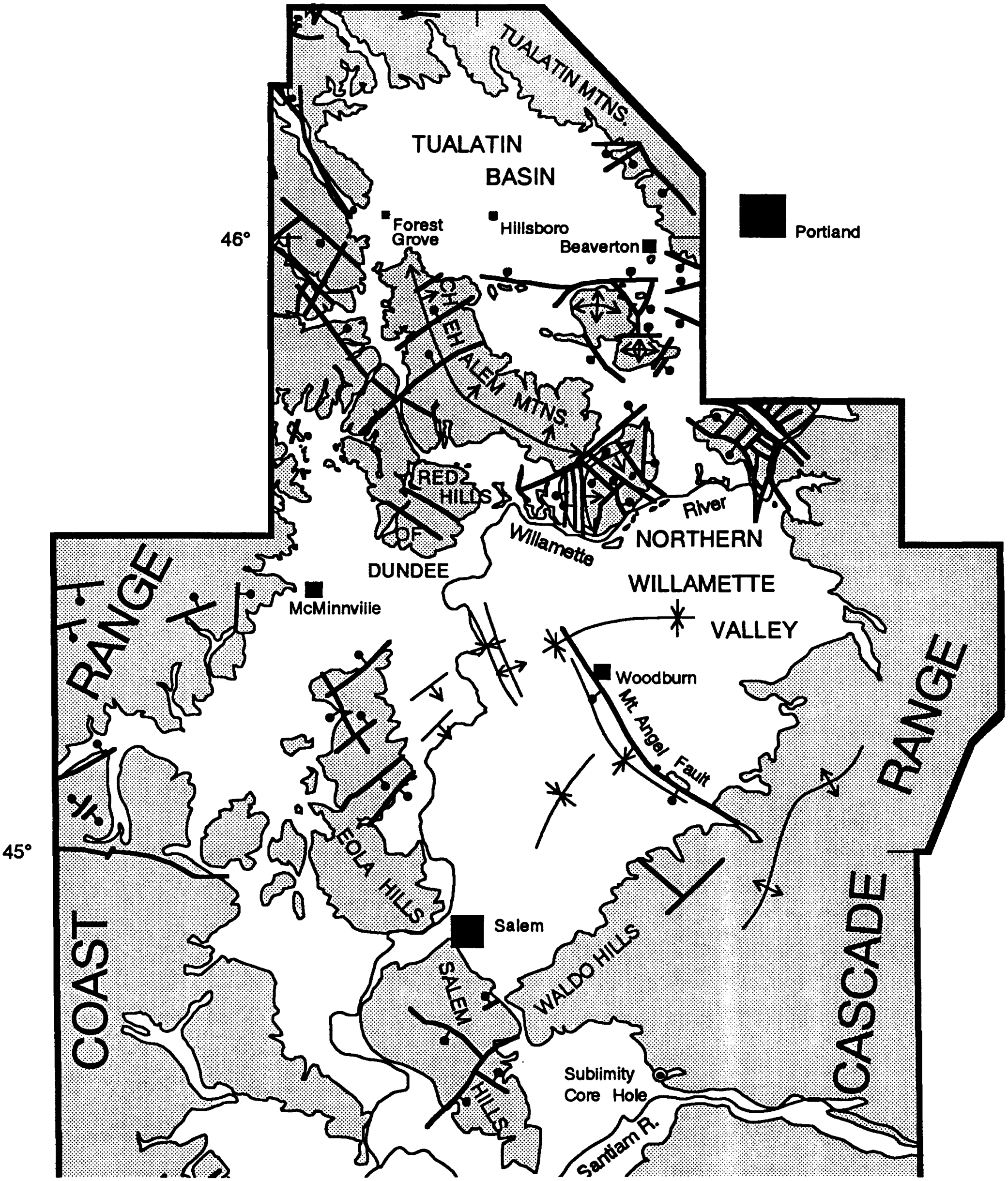

FIGURE 2 NORTHERN PORTION OF STRUCTURE MAP

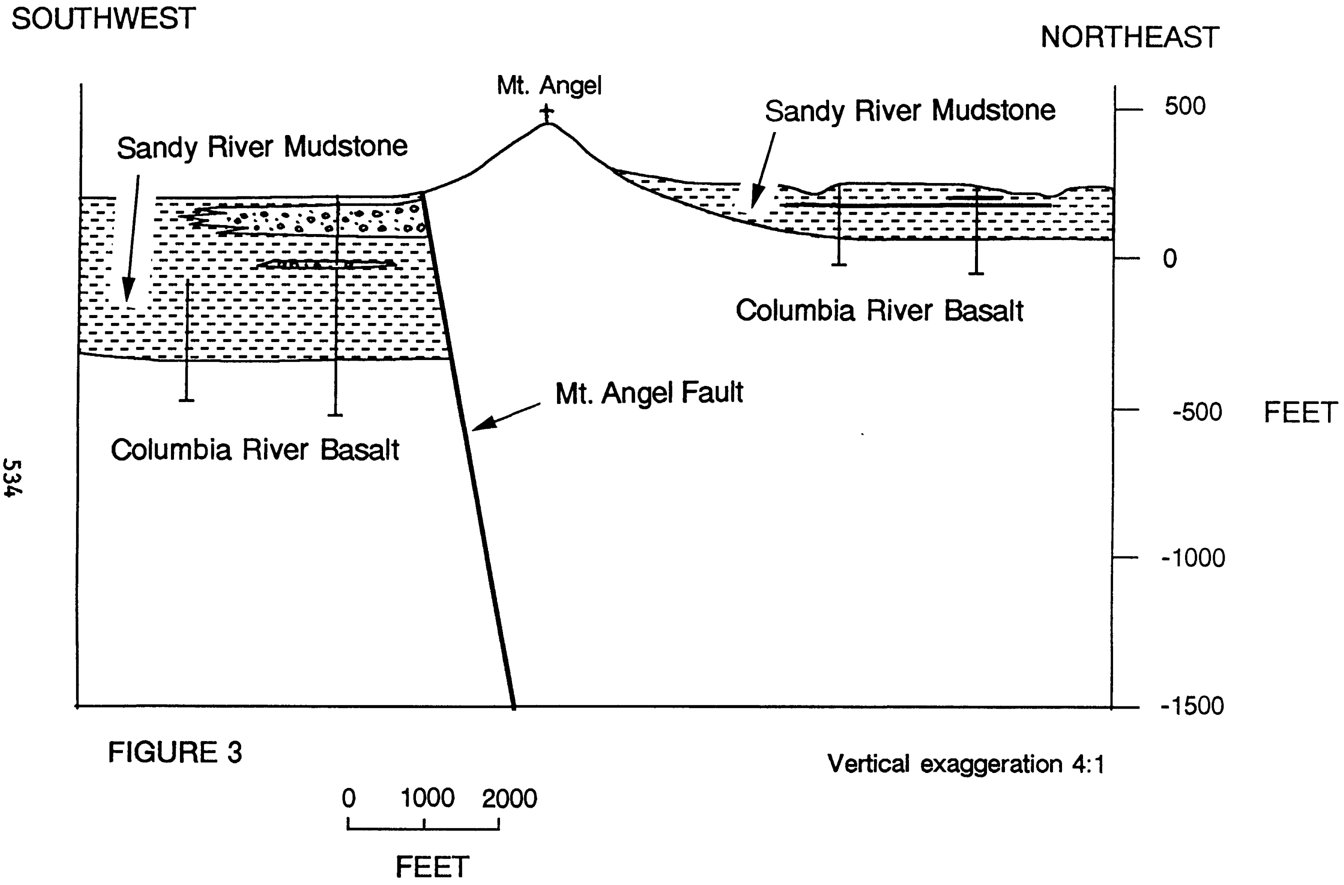
SOUTHWEST
NORTHEAST
Mt. Angel
Sandy River Mudstone
Sandy River Mudstone
Columbia River Basalt
Columbia River Basalt
Mt. Angel Fault
500
0
-500
-1000
-1500
FEET
Vertical exaggeration 4:1
0
1000
2000
FEET

FIGURE 3

FIGURE 4 PROPRIETARY SEISMIC LINE ACROSS MT. ANGEL FAULT

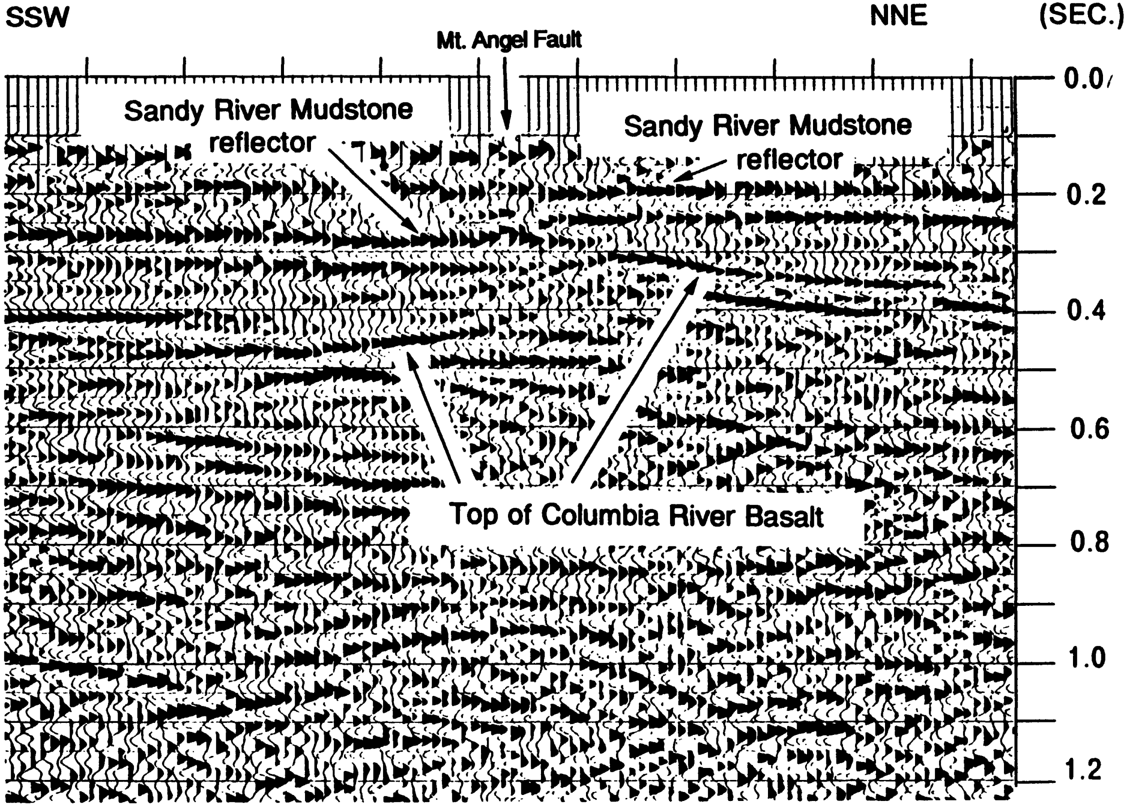

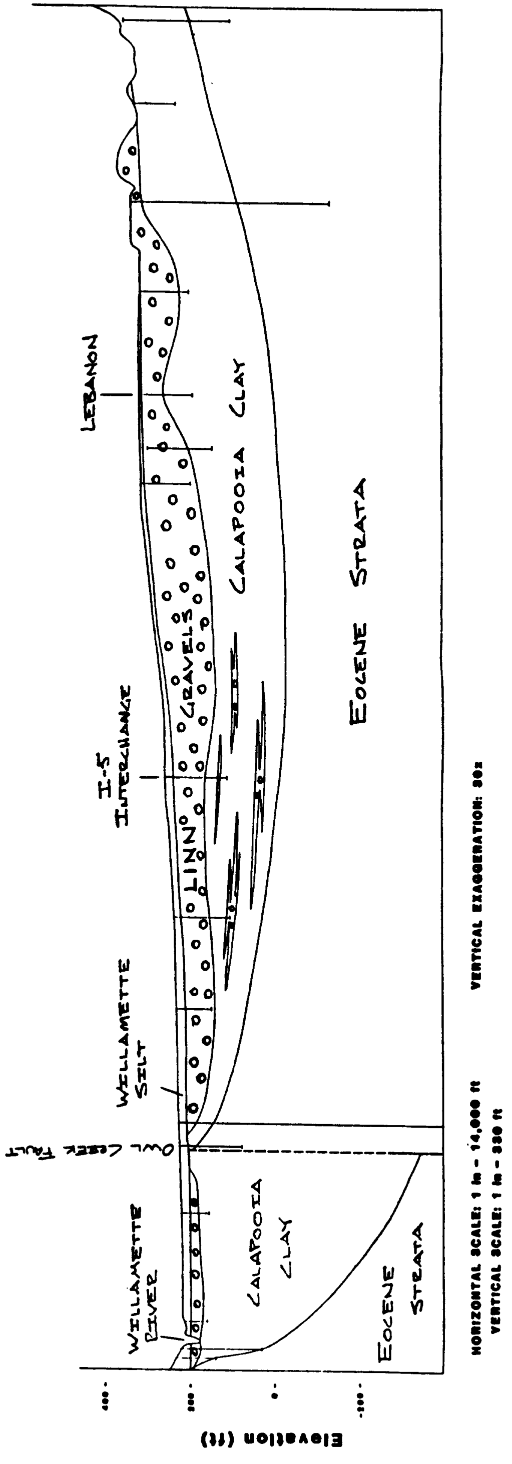
LEBANON
I-5 INTERCHANGE
WILLAMETTE SILT
OWL CREEK FAULT
WILLAMETTE RIVER
LINN GRAVELS
CALAPOOIA CLAY
EOCENE STRATA
CALAPOOIA CLAY
EOCENE STRATA
400
200
0
-200
Elevation (ft)
HORIZONTAL SCALE: 1 in - 14,000 ft
VERTICAL SCALE: 1 in - 330 ft
VERTICAL EXAGGERATION: 30x

Intraplate Stress and Deformation

9930-02669

Mary Lou Zoback
U. S. Geological Survey
Branch of Seismology
345 Middlefield Road, Mail Stop 977
Menlo Park, CA 94025
(415) 329-4760

Investigations

1. Continued compilation and interpretation of a quality-ranked global database of stress orientations and relative magnitudes. These data are stored in a dBase IV database management system in Menlo Park.

2. Continued analysis of dipmeter logs from the Puget Sound and surrounding region. In addition, several earthquake data sets were obtained from Steve Malone and from two of Bob Crosson's student's theses. The earthquake data and dipmeter data are currently being interpreted together.

3. Analysis of the subset of well-constrained intraplate events in North America using independently-derived stress data is nearly complete.

Results

1. Regional patterns of present-day tectonic stress can be used to evaluate the forces acting on the lithosphere and to investigate intraplate seismicity. Preliminary analysis of a global stress database indicates that most intraplate regions are characterized by a compressional stress regime; extension is limited almost entirely to thermally uplifted regions. In several plates the maximum horixontal stress is subparallel to the direction of absolute plate motion suggesting that the forces driving the plates also dominate the stress distribution in the plate interior.

The establishment of broad intraplate regions characterized by a relatively uniform stress field provides a critical framework for evaluating intraplate events which occur in these regions. Furthermore, once these first-order patterns have been established, we can begin to identify second-order patterns which have local origins (eg, weak faults, glacial rebound stresses, etc.).

2. Stress orientations inferred from analysis of wellbore breakouts, hydraulic fractures, and volcanic vent alignments are compared with earthquake focal mechanisms in the Pacific Northwest (Figure 1). Focal mechanisms considered are for crustal events of $M \geq 3.0$ and are generally well-constrained by first motions. Available dipmeter logs from petroleum wells drilled in Washington state after 1970 were analyzed for breakouts. These data are supplemented with breakout data from Oregon (Werner *et al.*,

1988, EOS) and hydrofrac data from Hanford (Paillet and Kim, 1987, JGR). Volcanic alignments for vents younger than 1 m.y. were also determined.

A general pattern of NE to NNE compression extends from the coast to about 160 km inland north of about latitude 46°N. Breakouts from wells in the Coast Ranges of Washington and NW Oregon indicate a N30°E SH_{max}, consistent with a N31°E SH_{max} inferred from focal mechanisms along the St. Helen's seismic zone and a N27°E SH_{max} inferred from focal mechanisms in south Vancouver Island. An iterative inversion of focal mechanisms for events beneath the central Puget Sound Basin yields a well-constrained SH_{max} of N20°E. This is consistent with a N15°E SH_{max} inferred from breakouts in one well in the basin. These data confirm the influence of NE directed Juan de Fuca–North American plate convergence along this section of the Cascadia subduction zone and suggest a strongly coupled plate boundary.

Although focal mechanisms just east of Puget Sound show highly variable P axes orientations, data from the region east of the central axis of the Cascades north of 46°N consistently indicate a N-S S_{Hmax}, probably related to Pacific–North American plate interaction. Sparse focal mechanism, breakout, and geologic data south of 46°N to just north of the Mendocino triple junction suggests this NS compression extends to the coastal region and indicates weak coupling with the subducted slab along this segment of the subduction zone.

3. To date, a set of well-constrained (±10°) focal mechanisms (32 events with $m_b > 4.0$) in the central and eastern United States and Canada have been analyzed in a preliminary fashion using using the independently determined stress orientation data Of these 32 earthquakes, 2 events are normal faulting events which are clearly anomalous with the regional compressional stress regime and another 3 events have slip vectors incompatible with the inferrred regional stress orientations. Both of these groups of events fall under hypothesis 3 above and require a local anomaly in the regional stress field to explain the seismicity. Five events require slip on extremely weak faults (apparent friction, "μ" < 0.4, compared to laboratory-determined frictional coefficients of $\mu =$ 0.6-0.85; Byerlee, 1979) or alternately, require pore pressures close to or exceeding the least principal stress (hypothesis 2 above). However, these 5 events may also represent local stress rotations not detected with current density of stress data sampling (hypothesis 3).

The remaining 22 events (70% of the dataset) are best categorized as being due to slip on "favorably" oriented pre-existing zones of weakness (hypothesis 1). For these events the angle between S_1 and the fault ranged between $30 - 45°$ and apparent frictional values were about 30% lower than assumed regional frictional strength value. Alternately, slip on these events could be explained by relatively modest increases in pore pressure (up to 70% of lithostatic compared to an assumed regional hydrostatic pore pressure which is about 37% of lithostatic).

The analysis also indicates that: 1) independent knowledge of S_{Hmax} orientation can be used to uniquely determine which of two nodal planes is the likely fault plane (for 27 of 28 events investigated, only one of the two nodal planes was consistent with a regional S_{Hmax} direction, even allowing for a ±15° uncertainty in the stress direction);

2) the central and eastern U. S. intraplate events are primarily strike-slip with nodal plane dips of $60 - 70°$, and 3) the southeastern Canadian events are dominantly thrust faulting events.

The results to date have highlighted a number of important topics to be investigated further and indicate that the analysis is doable and will yield interesting results. Identification of the actual fault plane for these events through this analysis is a powerful piece of information which permits further analysis of the actual in-situ conditions accompanying faulting as well as relationship of the fault planes to pre-existing structures. We will also compare focal depths of these events with the newest depth to basement map (currently in prep. by Muehlberger). Surprisingly, this simple piece of information has not been determined for the complete dataset.

The contrast in stress regime between southeastern Canada (primarily thrust events) and central and eastern U. S. (dominately strike-slip events) may result from the superposition of stresses related to to glacial rebound. Furthermore, the high level of seismicity in southeastern Canada and along the northeastern U.S.-Canadian border occurs in an area where glacial rebound is greatest and the dominant, circumferential rebound-related stresses (James, T.; EOS, 1988) are subparallel to the regional ENE S_{Hmax} orientation. Further to the west in the Great Lakes-southern Ontario region the circumferential rebound stresses are nearly perpendicular to the regional S_{Hmax} orientation and modern and historical seismicity is quite low. These observations of the contrasts in stress regime and in level of seismicity can be used a powerful constraints on absolute magnitudes and the depth dependent character of the regional stress field.

Reports and Publications

Zoback, M. L., *et al.*(23 coauthors), 1989, Global patterns of tectonic stress, Nature, v. 341, p. 291-298.

Magee, M. E., and Zoback, M. L., 1989, Present state of stress in the Pacific Northwest: EOS, Transactions of the American Geophysical Union, v. 70, p. 1332- 1333.

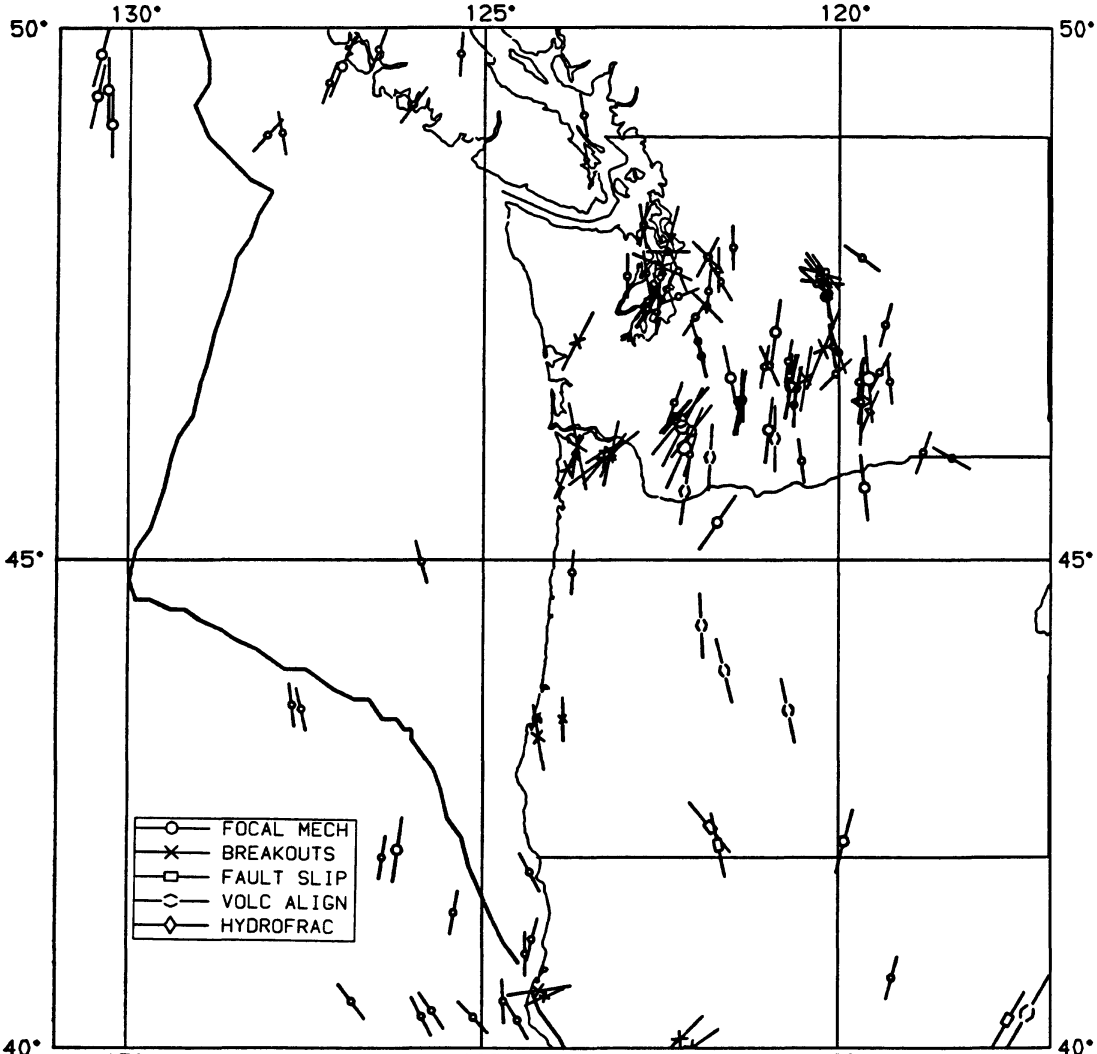

Figure 1: S_{Hmax} orientations inferred from earthquake focal mechanisms, well-bore breakouts, hydraulic fractures, and volcanic vent alignments. A general pattern of N 32° E to N 12° E compression extends from the coast to about 160 km inland north of about latitude 46° N. East of the central axis of the Cascades the data consistently indicate a N 5° E S_{Hmax} . Sparse data south of 46° N to just north of the Mendicino triple junction suggests this N-S compression extends to the coast in this region.

Figure 1

EARTHQUAKE LOSS ESTIMATION OF THE CITY OF EVERETT LIFELINE

14-08-0001-G1804

Donald B. Ballantyne
Kennedy/Jenks/Chilton
530 S. 336th St.
Federal Way, Washington 98003
(206) 874-0555

INTRODUCTION

The loss of function of individual lifeline systems in the City of Everett will be estimated in this project. The losses for each system will then be combined for all lifelines to assess the impact, particularly business interruption, on the City as a whole.

The cost of economic impact from business interruption is thought to be significantly greater than the cost to repair damage caused directly by the earthquake, particularly because of the major manufacturing plants being served by the City. While a catastrophic earthquake would have a devastating economic impact on a community, including significant business interruption losses, the probability of such an event is quite small. The impact of a moderate earthquake may be less severe in terms of repair costs. However, as a result of much shorter recurrence intervals, the average annual economic impact, taking into account business interruption, may be significantly greater for moderate earthquakes than for large earthquakes.

The City of Everett, located about 20 miles north of Seattle, has a population of almost 60,000. It is the largest city in Snohomish County. Even with its proximity to the Seattle metropolitan area, the City is quite self reliant in employment opportunities with the Boeing 747/767 manufacturing facility, Scott Paper Company, and the Navy developing a home port facility. Both Boeing and Scott Paper are participating in this study.

Individual lifeline systems have been modeled by each of the lifeline specialists on the project team. This project combines those results and establish the interrelationship of the impacts of all lifeline facilities.

System owner/operators and their respective lifeline systems participating in this project are as follows:

Water and Sewer	City of Everett
Power	Snohomish County PUD
Communications	GTE and US West
Transportation	Washington State DOT
Natural Gas	Washington Natural Gas

APPROACH

1) Vulnerability assessment methodologies from each lifeline will be reviewed and standardized. 2) Lifeline groups will be established coupling lifeline specialists and the respective system owner/operators and proceed with data acquisition.

3) An earthquake hazards assessment will be conducted considering ground motion, liquefaction, and landslides.

4) Each group will then assess the system vulnerability, and 5) develop mitigation recommendations.

6) A cross section of the community's economics will be established, and 7) based on scenarios for events similar to the 1949 and 1965 Puget Sound earthquake events, 8) losses to business estimated.

INTEGRATING EARTHQUAKE CASUALTIES INTO LOSS ESTIMATION

14-08-0001-G1785

Michael E. Durkin and Associates
22955 Leonora Drive
Woodland Hills, CA 91367
818) 704-1493

Investigations

During the last 10 years, considerable attention has been devoted to the general area of earthquake loss estimation; however, little attention has been devoted to more specific estimations of earthquake casualties. Yet casualties are of prime concern to those who commission loss estimations and make use of their results - public and private sector organizations whose responsibility is life safety.

In our current USGS grant entitled "INTEGRATING EARTHQUAKE CASUALTIES INTO LOSS ESTIMATION," we are drawing on findings from our eight year research program in earthquake injuries and health service response, including our USGS study of injuries in the Loma Prieta earthquake, to make injury estimations less speculative. We are examining the findings of other US and foreign researchers. We are also evaluating promising casualty estimation techniques, recently developed in Japan and Europe. This project aims to provide a sound basis for development of a comprehensive earthquake casualty loss estimation methodology that combines the most efficient and effective casualty estimation techniques and the most current theories and data.

This research entails two major phases: resource characterization, and suitability evaluation. During the resource characterization phase we are identifying all U.S. and foreign developments in earthquake casualty data and loss estimation techniques; we are characterizing these specific developments to permit possible application to existing broad-based loss estimation methodologies. In our suitability evaluation phase, we are systematically evaluating current loss estimation methods for their underlying assumptions, and mechanisms for calculating casualties; this evaluation is testing the ability of existing broad-based loss estimation methodologies to incorporate specific new casualty estimation techniques.

Results

In February and March we reviewed existing research for applicability to earthquake casualty estimation and began developing a comprehensive conceptual model for a U.S. earthquake casualty estimation process.

Our continuing analysis includes the following three major research classes: 1) studies aimed at producing actual casualty extimations or developing casualty estimation techniques, 2) empirical studies of earthquake casualties, and casualty studies for analogous disasters such as slope failure.

After creating a preliminary typology of casualty estimation approaches and procedures, we are now systematically characterizing this research body along relevent dimensions. To enable our later suitability assessment of candidate casualty estimation techniques, we are simultaneously constructing a comprehensive conceptual model with three major components: 1) an earthquake casualty demand framework for predicting casualty number and type as a function of geotechnical and structural variables, 2) a supply framework for estimating pre- and post-earthquake health service resource availability for meeting the casualty demand in a given target area, and 3) a mitigation framework for estimating the relative contribution of specific earthquake hazard reduction approaches to reducing the number and severity of earthquake casualties or increasing the post-earthquake health service resource supply. We are assessing available data and methods with framework needs to determine potential immediate applications, future applications with modification, and major gaps. Where possible, we are revising our U.S.G.S. Loma Prieta casualty study design to address modifications and gaps.

The October 17th Loma Prieta earthquake has prompted new seismic legislation - many with life safety and health provisions that our U.S.G.S. research can help shape. The earthquake and these subsequent bills have generated new state agency operational efforts which our results can assist. We are currently contributing research results to the following three policy activities:

1. AB 3827 Occupational Hazards: Earthquake Safety

This bill would require the Occupational Safety and Health Standards Board, within the Department of Industrial Relations, to adopt occupational safety standards and orders concerning nonstructural earthquake hazards. In the event of an earthquake, normal workplace safety standards are not sufficient to assure the protection of workers. Specifically, additional safety standards are needed to eliminate in workplaces the dangers posed by nonstructural components in the event of an earthquake.

We are reviewing our existing data base to see what workplace injuries are caused by nonstructural elements, their distribution, and their impact. We are also developing a process for estimating the relative injury potential of different nonstructural elements to help prioritize policy.

2. SB 2554: Joint Underwriting Association for Commercial Earthquake Insurance (Earthquake Insurance for Small Business)

Since January, we have analyzed, as part of our development of integrated earthquake casualty and loss estimation processes, detailed earthquake loss data for 831 small businesses in heavily damaged communities of Watsonville, Santa Cruz, and San Francisco's Marina District. Our summary report (2) shows the average dollar losses for commercial and rental broken down into non-real estate property, real estate, and business disruption. In our continuing research, we plan to focus on identifying damage and economic loss patterns for specific types of small businesses in specific construction.

3. Life Safety Criteria: Governor's Inquiry on the Loma Prieta Earthquake

Dr. Charles Thiel's role in producing the final committee report is enabling us to make our interim casualty research results available to the inquiry process. Study results are contributing to potential design criteria changes regulating all State structures so that important ones remain functional and the remainder protect life. Results are also supporting the position, of CalTrans structural engineers, that transportation system design should limit earthquake injuries and facilitate the provision of post-earthquake medical aid and other emergency services. Dr. Thiel is currently Project Director of the Applied Technology Council subcontract for our U.S.G.S. research.

The previous research contributions can assist similar policy and operational issues elsewhere in the U.S.

Reports

Durkin, Michael E., Anne H. Coulson, Martha Hijar, Jess Kraus, and Hitomi Ohashi Murakami, The Survival of People in Collapsed Buildings, EARTHQUAKE IN MEXICO: DISASTER CHRONICLES NO. 3 (Washington, D.C.: The Pan American Health Organization) pp. 55-70) July 1990.

Durkin, Michael, E., EARTHQUAKE IMPACT ON SMALL BUSINESS: SELECTED RESEARCH RESULTS, Report prepared for the California State Insurance Claims and Corporations Committee - Committee Hearing on Senate Bill 2554: Joint Underwriting Association for Commercial Earthquake Insurance, April 18, 1990. Copies available from author.

Frequency and Survivability Profiles of Highway Bridges Along the I-5 Corridor Between Everett, Washington and Salem, Oregon

14-08-0001-G1698

Dr. Ralph Alan Dusseau, Ph.D., P.E.
Wayne State University
5050 Cass, 1064 Mackenzie Hall
Detroit, Michigan 48202
(313) 577-3842

Objectives and Status

The objectives of this project were to inventory all bridges along I-5, I-205, and I-405 in western Washington State and northwestern Oregon and to incorporate the information gathered into a comprehensive I-5 Bridge Database. The total number of bridges that have been inventoried in Washington State are 554 along I-5, 98 along I-405 (in Seattle), and 30 along I-205 (in Vancouver). In Oregon, the total number inventoried is 278 along I-5, I-205, and I-405. The information for 455 Washington State bridges out of a total of 682 or 67% has been incorporated into the I-5 Bridge Database, while the data for 145 Oregon bridges out of a total of 278 or 52% has been recorded in the database.

Structure of the I-5 Bridge Database

The I-5 Bridge Database is being constructed using the dBASE IV software package. The names, sizes, and descriptions of the 98 fields that currently comprise the database are contained in Table 1. The data for each bridge is contained in two or more records. The total number of records used for a given bridge is based on the larger of the number of spans, supports, box-girder segments, joints, or soil borings, or the number of datapoints required to define the horizontal curves, vertical curves, deck tilts, or bent skews.

Each record in the database is assigned a 5-digit code which is stored in field #1 (CODE) with the format NNN.NN. The digits to the left of the decimal represent a unique number associated with each bridge (1 to 960) and the digits to the right of the decimal represent a unique number associated with the record number for that bridge (1 to 99). Thus 123.21 would represent the 21st record of bridge #123. The portion of field #1 (CODE) to the right of the decimal is generally the same as field #27 (NUMBER XX) which indexes the number of spans, supports, and joints.

The first record for each bridge contains general information such as the bridge number, compass bearing, total length, milepost, etc., which encompasses fields #2 to #12. Much of this general data is also included in the bridge lists of the Washington State Department of Transportation and the Oregon Department of Transportation. The first record also includes data on the deck and box-girder thicknesses in fields #13 to #18, the bridge materials in fields #30 to #33, and the main member sizes in fields #36 and #37. Each record (including the first) contains data on the following items where appropriate: one bridge span, one segment of box-girder, one bridge support and foundation, one bridge joint, one soil boring log, one horizontal curve, the deck tilt at one point, the bent skew at one point, and one vertical curve.

Assumptions and Notes

Data was recorded in the database utilizing the following assumptions:

1. The left abutment is the abutment with the lowest milepost number (which is generally the southernmost abutment).

2. The left and right segments or sides of the bridge deck are designations based on the assumption that the user is standing on the bridge centerline and facing in the direction of increasing milepost numbers (which is generally a northward direction for I-5, I-205, and I-405).

3. A positive radius for a horizontal curve is one in which the deck curves to the right when facing in the direction of increasing milepost numbers (which is generally a northward direction).

4. A positive deck tilt is one where the roadway deck tilts upward to the right and downward to the left assuming the user is standing on the bridge centerline and facing in the direction of increasing milepost numbers (which is generally a northward direction).

5. A positive bent skew is one that is counterclockwise when looking at a plan view of the bridge.

6. A positive roadway slope is one for which the roadway elevations increase in the direction of increasing milepost numbers (which is generally a northward direction).

The locations recorded in fields #25, #26, #34, #35, #80, #84, #89, #91, and #95 are all measured in feet with the left abutment as 0.00 and increasing in the direction of increasing milepost numbers which is generally a northward direction. If a longitudinal expansion joint divides the roadway deck into two sections, then the location recorded in field #25 (DATALOCA1) corresponds to the data for the left section of the deck which is stored in fields #19, #21, and #23, while the location recorded in field #26 (DATALOCA2) corresponds to the data for the right section of the deck which is stored in fields #20, #22, and #24. If the deck is monolithic, then fields #19, #21, #23, and #25 are used to describe the deck and fields #20, #22, #24, and #26 are blank.

Fields #34 and #35 (DATA FROM and DATA TO) are used to specify the beginning and ending locations of the box-girder segment whose data is recorded in fields #38 to #45. If field #35 is blank for a given segment of box-girder, then the data in fields #38 to #45 pertains only to the location designated in field #34 (DATA FROM). The data pertaining to horizontal curvature, deck tilt, bent skew, and vertical curvature, which are contained in fields #88 to #97, does not necessarily correspond to a particular span, support, or joint. Instead, the information in these fields is essentially raw data that could be used to generate the horizontal curvature, deck tilt, bent skew, vertical curvature, and deck elevations at any point along the length of the bridge.

Because most bridges along the I-5 corridor have some unique features that can not be incorporated directly into the records of the I-5 Bridge Database, a footnote file is being created for most bridges. The MS-DOS filenames for these footnote files are contained in field #98 (NOTES).

TABLE 1 FIELD STRUCTURE USED IN THE I-5 BRIDGE DATABASE

Field	Field Name	Width	Definition
1	CODE	6	- A unique number with format NNN.NN used to identify the database records associated with a given bridge. The digits to the left of the decimal represent a unique number associated with a given bridge (1 to 960) and the digits to the right of the decimal represent a unique number associated with a given record for that bridge (1 to 99).
2	BRIDGE NO	12	- A unique combination of digits assigned to each bridge by the state departments of transporation for Washington State or Oregon.
3	BR BEARING	12	- Compass bearing (in degrees & minutes) of the bridge centerline for bridges with straight segments; or, for continuously curved bridges, the compass bearing of the nearest straight segment of highway.
4	BRNG LOCA	7	- Location (in feet) at which the compass bearing is taken, measured along the centerline of the bridge from the left abutment.
5	TOTAL LENG	6	- Total overall length of the bridge (in feet) measured between the edges of the pavement at the left and right bridge abutments.
6	MILE POST	7	- The state route milepost of the bridge: as measured from 240.00 at the Linn-Marion County Line and increasing northward to 307.00 at the Washington State Line (Columbia River) for Oregon; and as measured from 0.00 at the Oregon State Line (Columbia River) and increasing northward to 217.66 at the Snohomish-Skagit County Line for Washington State.
7	CROSS NAME	30	- Descriptive name of the bridge using road, river, or other names, and using predefined abbreviations.
8	CONTR SECT	6	- A four-digit number for the Control Section in which the bridge is located.
9	LOCATION	20	- Distance (in miles) measured in the direction of increasing mileposts from a given feature such as a state line, county line, or state route junction.
10	IDENT NUMB	8	- State construction contract number or another unique combination of numbers.
11	YEAR	10	- Year the bridge was constructed for Oregon or year the bridge plans were approved for Washington State.
12	BRID APPR	6	- Type of roadway approach to the bridge abutments.
13	MAX DECKTH	6	- Maximum and minimum thicknesses (in inches) of the roadway deck or the top slab of concrete box-girder sections excluding any haunches, tapers, or other local changes in thickness.
14	MIN DECKTH	6	
15	MAX WALLTH	6	- Maximum and minimum thicknesses (in inches) of the interior and exterior vertical webs of box-girder sections excluding any local changes in thickness.
16	MIN WALLTH	6	
17	MAX BOT TH	6	- Maximum and minimum thicknesses (in inches) of the bottom slab for concrete box-girder sections or the bottom plate for steel box-girder sections excluding any local changes in thickness.
18	MIN BOT TH	6	

TABLE 1 (continued)

Field	Field Name	Width	Definition
19	DECK WID 1	7	- Width (in feet) of the roadway deck at DATALOCA 1 if the deck is monolithic; or width of the left section of the deck at DATALOCA 1 if the deck is divided into two sections by a longitudinal expansion joint.
20	DECK WID 2	7	- Width (in feet) of the righthand section of the roadway deck at DATALOCA 2 if the deck is divided into two sections by a longitudinal expansion joint.
21	NO MNMEM 1	4	- Number of main members (at DATALOCA 1) or box-girder cells (at DATA FROM or between DATA FROM & DATA TO) in the cross-section if the deck is monolithic; or number of main members in the left section of the cross-section at DATALOCA 1 if the deck is divided into two sections by a longitudinal expansion joint.
22	NO MNMEM 2	4	- Number of main members at DATALOCA 2 in the right section of the cross-section if the deck is divided into two segments by a longitudinal expansion joint.
23	MEM SPAC 1	7	- Spacing (in feet) of the main members at DATALOCA 1 if the cross-section of the roadway deck is monolithic; or spacing of the main members in the left section of the cross-section if the deck is divided into two sections by a longitudinal expansion joint.
24	MEM SPAC 2	7	- Spacing (in feet) of the main members at DATALOCA 2 in the right section of the cross-section if the deck is divided into two sections by a longitudinal expansion joint.
25	DATALOCA 1	9	- Location (in feet) at which the values DECK WID 1, NO MNMEM 1, and MEM SPAC 1 are valid, measured along the centerline of the bridge from the left abutment.
26	DATALOCA 2	9	- Location (in feet) at which the values DECK WID 2, NO MNMEM 2, and MEM SPAC 2 are valid, measured along the centerline of the bridge from the left abutment.
27	NUMBER XX	3	- Span number, support number, foundation number, and joint number associated with record CODE.
28	SPAN LENG	7	- Length (in feet) of span NUMBER XX.
29	SPAN TYPE	8	- Abbreviation indicating the type of bridge span for span NUMBER XX based on the bridge materials and the type of construction.
30	MAT DECK	4	- The 28-day compressive strength of the concrete roadway deck (in pounds per square inch).
31	MAT MNMEM	6	- Strength of the main members or the box-girder sections (in pounds per square inch for the 28-day compressive strength of concrete or in kips per square inch for the yield strength of steel).
32	MAT SUP	4	- Strength of the bridge supports (in pounds per square inch for the 28-day compressive strength of concrete supports or in kips per square inch for the yield strength of steel supports).
33	MAT FNDTN	4	- 28-day compressive strength of the concrete foundation (in pounds per square inch).

TABLE 1 (continued)

Field	Field Name	Width	Definition
34	DATA FROM	9	- Location (in feet) at which the box-girder cross-section data in fields #21, and #38 to #45 is valid, measured along the bridge centerline from the left abutment; or location which in conjunction with DATA TO represents the beginning and ending points, respectively, for a segment of box-girder over which the data in fields #21, and #38 to #45 is valid.
35	DATA TO	9	- Location (in feet) which in conjunction with DATA FROM represents the end and beginning points, respectively, for a box-girder segment over which the data in fields #21, and #38 to #45 is valid.
36	INT MN MEM	4	- Numbers denoting the interior and exterior main member sizes at DATALOCA 1 (consisting of the WSDOT designations for most prestressed concrete girders, the AISC designations for steel beams, or other designations for other types of bridge members).
37	EXT MN MEM	4	
38	MAX CEL HT	6	- Maximum and minimum cell heights (in feet) of the box-girder section(s) measured from the center of the top slab to the center of the bottom slab at DATA FROM or between DATA FROM and DATA TO.
39	MIN CEL HT	6	
40	MAX CEL WD	6	- Maximum and minimum cell widths (in feet) of the box-girder section(s) measured between the centers of adjacent webs at the midheight of the cells at DATA FROM or between DATA FROM and DATA TO.
41	MIN CEL WD	6	
42	MAX TOP WD	12	- Maximum and minimum top widths (in feet) of the box-girder section(s) measured between the centers of the exterior webs along the centerline of the top slab at DATA FROM or between DATA FROM and DATA TO.
43	MIN TOP WD	12	
44	MAX BOT WD	12	- Maximum and minimum bottom widths (in feet) of the box-girder section(s) measured between the exterior web centers along the centerline of the bottom slab at DATA FROM or between DATA FROM and DATA TO.
45	MIN BOT WD	12	
46	MAXTOPFLWD	6	- Maximum and minimum widths (in inches) for the top flange plates of the steel plate-girder section(s) for span NUMBER XX.
47	MINTOPFLWD	6	
48	MAXTOPFLTH	6	- Maximum and minimum total thicknesses (in inches) for the top flange plates of the steel plate-girder section(s) for span NUMBER XX.
49	MINTOPFLTH	6	
50	MAXBOTFLWD	6	- Maximum and minimum widths (in inches) for the bottom flange plates of the steel plate-girder section(s) for span NUMBER XX.
51	MINBOTFLWD	6	
52	MAXBOTFLTH	6	- Maximum and minimum total thicknesses (in inches) for the bottom flange plates of the steel plate-girder section(s) for span NUMBER XX.
53	MINBOTFLTH	6	
54	MAX WEB DP	6	- Maximum and minimum depths (in inches) for the web plates of the steel plate-girder section(s) for span NUMBER XX.
55	MIN WEB DP	6	
56	MAX WEB TH	6	- Maximum and minimum thicknesses (in inches) for the web plates of the steel plate-girder section(s) for span NUMBER XX.
57	MIN WEB TH	6	

TABLE 1 (continued)

Field	Field Name	Width	Definition
58	MAX TOPCHD	6	- Maximum and minimum cross-sectional areas (in square inches) for the top chord members of the side-trusses for span NUMBER XX.
59	MIN TOPCHD	6	
60	MAX BOTCHD	6	- Maximum and minimum cross-sectional areas (in square inches) for the bottom chord members of the side-trusses for span NUMBER XX.
61	MIN BOTCHD	6	
63	MAX PAN WD	6	- Maximum and minimum panel widths (in feet) of the side-trusses for span NUMBER XX.
63	MIN PAN WD	6	
64	MAX PAN HT	6	- Maximum and minimum panel heights (in feet) of the side-trusses for span NUMBER XX.
65	MIN PAN HT	6	
66	MAX DIAG	6	- Maximum and minimum cross-sectional areas (in square inches) for the diagonal members of the side-trusses for span NUMBER XX.
67	MIN DIAG	6	
68	FNDTN TYPE	8	- Abbreviation denoting the type of bridge foundation for foundation NUMBER XX.
69	FNDTN CAP	8	- Load capacity of foundation NUMBER XX (in kips per square foot for spread footings or kips per pile for pile foundations).
70	FNDTN LENG	12	- Typical length (in feet) measured perpendicular to the bent centerline for the footings or pile caps of foundation NUMBER XX.
71	FNDTN WID	9	- Typical width (in feet) measured parallel to the bent centerline for the footings or pile caps of foundation NUMBER XX.
72	FNDTN THCK	8	- Typical thickness (in feet) for the footings or pile caps of foundation NUMBER XX.
73	SUP TYPE	6	- Abbreviation denoting the type of bridge support for bent NUMBER XX.
74	SUP NUMBER	4	- Number of columns or wall segments in bent NUMBER XX.
75	SUP WIDTH	12	- Number denoting either the distance center-to-center (in feet) between the exterior columns measured along the centerline of bent NUMBER XX, or the wall width (in feet) measured along the centerline of bent NUMBER XX.
76	SUP SIZE	15	- Number(s) denoting the typical length and width (in feet) for rectangular columns, the typical diameter (in feet) for round columns, or the typical thickness of the wall (in feet) for bent NUMBER XX.
77	SUP HEIGHT	9	- Height of bent NUMBER XX (in feet) measured from the elevation of the deck centerline downward to either the elevation at the bottom of the center column footing or pile cap, the average elevation at the bottom of the two center-most column footings or pile caps, or the elevation directly below the centerline of the deck for wall footings.
78	JOINT TYPE	9	- Abbreviation denoting the type of bridge connection for joint NUMBER XX.
79	JOINT SEAT	9	- Width of the seat (in feet) upon which the members being connected rest for joint NUMBER XX.

TABLE 1 (continued)

Field	Field Name	Width	Definition
80	JOINT LOCA	9	- Location (in feet) of joint NUMBER XX measured along the centerline of the bridge from the left abutment.
81	JNT CLEAR	9	- Longitudinal clearance (in inches) of joint NUMBER XX, i.e. the amount of travel (in inches) that is permitted before the joint is fully closed.
82	JNT DETAIL	9	- Number denoting the corresponding detailed drawing for joint NUMBER XX as catalogued in a book of joint details for the I-5 bridges.
83	SLBG NUMB	6	- Number denoting the soil boring number as catalogued in a book of soil boring logs for the I-5 bridges.
84	SLBG LOCA	7	- Location (in feet) of SLBG NUMB as measured along the centerline of the bridge from the left abutment.
85	SLBG ELEV	7	- Elevation (in feet) above sea level of the original grade for SLBG NUMB.
86	LT ABUT EL	7	- Elevation (in feet) above sea level of the deck centerline at the left abutment.
87	RT ABUT EL	7	- Elevation (in feet) above sea level of the deck centerline at the right abutment.
88	RAD BTWN	10	- Radius (in feet) of the horizontal curve ending at location RAD LOCA. For the first bridge record, the curve begins at or before the left abutment. For subsequent bridge records, the curve begins at the location RAD LOCA of the previous bridge record.
89	RAD LOCA	9	- Location (in feet) at the end of the horizontal curve corresponding to radius RAD BTWN measured along the bridge centerline from the left abutment.
90	DECK TILT	9	- Lateral slope or tilt (in percent) of the roadway deck at location TILT LOCA.
91	TILT LOCA	9	- Location (in feet) at which the lateral slope DECK TILT is valid measured along the centerline of the bridge from the left abutment.
92	BENT SKEW	8	- Skew (in degrees) of the bent at location SKEW LOCA.
93	SKEW LOCA	9	- Location (in feet) at which the BENT SKEW is valid measured along the centerline of the bridge from the left abutment.
94	RDWYSLOPE1	7	- Vertical slope (in percent) of the roadway for the entire bridge deck; or vertical slope for a portion of the bridge deck to the left of the vertical curve corresponding to location PT VRT INT.
95	PT VRT INT	9	- Location (in feet) of the intersection point for the vertical curve with tangent slopes RDWYSLOPE1 on the left and RDWYSLOPE2 on the right as measured along the centerline of the bridge from the left abutment.
96	RDWYSLOPE2	7	- Vertical slope (in percent) of the roadway for a portion of the bridge deck to the right of the vertical curve corresponding to location PT VRT INT.
97	CURVE LENG	6	- Horizontal length (in feet) of the vertical curve with intersection point at location PT VRT INT.
98	NOTES	10	- MS-DOS filename for the bridge footnote.

Earthquake-Resistant Design and Structure Vulnerability
9950-04181

Edgar V. Leyendecker
Branch of Geologic Risk Assessment
U.S. Geological Survey
Denver Federal Center, M.S. 966
Denver, CO 80225
(303) 236-1601

Investigations

1. Work is continuing on improving measures of vulnerability of structures to damage, including the refinement of our understanding of earthquake damage and the applicability of the existing data base on earthquake damage.

2. Investigations continue for development/identification of cost-effective techniques for determining inventory at risk and on damage survey procedures. Revised procedures are planned for field testing.

3. Work was initiated to investigate structural damages occurring as a result of the Loma Prieta earthquake.

4. Studies continue on ground motion parameters used in structural design that might be most useful in national maps.

Results

1. Examination of current vulnerability relationships is continuing with a review of existing earthquake damage data bases and the new data obtained following the Loma Prieta earthquake.

2. Development of inventory at risk is costly and is a major impediment to accurate loss estimates. A study of the critical elements of inventory needed for loss assessment in urban areas, including field inventory techniques is in progress. Plans for preparation of inventory training procedures are continuing for trial use. Important strides have been made under the U.S.G.S. grant program and these results will be used where possible.

3. Field investigation of damages occurring as a result of the Loma Prieta earthquake were begun the day after the earthquake shook the Bay area. The data collected ranged from chimney damage to collapse of transportation networks. Both federal and private facilities were included. These data were used in the preparation of intensity maps. Data are continuing to be collected with the aim of improving correlations of damage with structural type, ground motion, and intensity.

4. Work is continuing on providing structural input to the ground motion parameters that should be included in national maps. USGS has participated in three recent workshops on the subject. One sponsored by USGS/SEAOC and two by the National Center for Earthquake Engineering Research. Proceedings of two of these workshops have been published and the third will be published in the near future. Studies are being conducted on attenuation relationships and the resulting spectral shapes with magnitude and distance. A number of cities have been selected for hazard analysis and the spectra that results from the analysis will be prepared for different exposure periods.

Reports

Hopper, M.G., Leyendecker, E.V., Thenhaus, P.C., Stover, C.W., Algermissen, S.T., Reagor, B.G., Perkins, D.M., Hanson, S.L., Brewer, L.R., and Baldwin, F.W., 1989, Damage and intensity survey of the October 17, 1989 Loma Prieta earthquake: American Geophysical Union Fall Meeting, December 4-8, 1989, San Francisco, California, Special session on the Loma Prieta earthquake.

Contributor to: Plafker, G., and Galloway, J.P., eds., 1989, Lessons learned from the Loma Prieta, California, earthquake of October 17, 1989: U.S. Geological Survey Circular 1045. Contribution was a discussion of Modified Mercalli Intensities and an MMI map of the earthquake (p. 17-20).

Leyendecker, E.V., Thenhaus, P.C., Campbell, K.W., Hopper, M.G., Hanson, S.L.,Algermissen, S.T., and Perkins, D.M., 1990, Preliminary assessment of the distribution of intensity and strong ground motion for the Loma Prieta Earthquake: Earthquake Spectra--The October 17, 1989, Loma Prieta Earthquake, Special Issue, in review.

Leyendecker, E.V., Thenhaus, P.C., Campbell, K.W., Hopper, M.G., Hanson, S.L., Algermissen, S.T., and Perkins, D.M., 1990, Preliminary assessment of the distribution of strong ground motion and intensity for the Loma Prieta Earthquake: Interagency Committee on Seismic Safety and Construction, Special Report on the October 17, 1989, Loma Prieta Earthquake, in review.

LATE QUATERNARY FAULTING, SOUTHERN SAN ANDREAS FAULT

9910-04098

Michael J. Rymer

Branch of Engineering Seismology and Geology
U.S. Geological Survey
345 Middlefield Road, MS/977
Menlo Park, CA 94025
(415) 329-5649

Investigations

1. Post-earthquake investigation of the 1989 Loma Prieta earthquake.

2. Trench investigations of the San Andreas fault in the Durmid Hill–Bombay Beach area.

3. Continued investigation of the Quaternary history of the San Andreas fault in the Coachella Valley, with special emphasis on structure and stratigraphy.

Results

1. Post-earthquake studies of the Loma Prieta earthquake were concentrated initially in the San Juan Bautista to Correlitos area to look for coseismic surface rupture. Starting the day after the earthquake, and for 4 months afterwards, measurements were made of line lengths in small-aperture nail quadrilaterals emplaced in paved roadways in the epicentral area and aftershock zone of the earthquake. The nail quadrilaterals show that only small amounts of postseismic slip occurred since the earthquake, thus not compensating for minor (<3 cm) surface faulting along the San Andreas fault in spite of the approximately 1.6 m of slip at depth. Two nail quadrilaterals were installed across the San Andreas fault and three across dominantly extensional cracks in the Summit Road area. The two sites on the San Andreas show about 3 to 5±2 mm of postseismic slip, whereas the three sites across extensional cracks show equivocal contractional motion, possibly due to the quick, crude measuring techniques used. Regardless, measurements at all sites show that large postseismic slip did not follow the earthquake.

2. Trenching, with R.V. Sharp, across faults in the Durmid Hill–Bombay Beach area showed that the "dog leg" section between Durmid Hill and Bombay Beach is a wide, extremely complex zone of right-lateral faulting. Also, the faults in this zone have trends parallel to that of the San Andreas. We, therefore, infer that this section of faults is in fact taking up most if not all the motion on the San Andreas fault and is part of the San Andreas fault. The age of deposits exposed in the trenches is not yet known. Samples for ^{14}C dating were collected, but have not yet been submitted. Likewise, samples for ^{14}C dating were collected from trenches studied by Scott Lindvall (Lindvall-Richter Associates) at Bombay Beach in June, 1989. Dating of deposits at both sites will help resolve the age of strata involved in the wide zones of faulting.

3. Mapping of Quaternary deposits in the Indio and Mecca Hills has revealed, among many other things, a more widespread presence of the Bishop ash (0.73 Ma) than previously known. New exposures of the Bishop ash were found in the central Indio Hills and the

western Mecca Hills, thus providing age control for the stratigraphic sequence and for development of tectonic features. Features in the western Mecca Hills are the most interesting, because they suggest that fault-normal compression with commensurate fault-parallel folds developed since deposition of the Bishop ash. Such fault-normal compression is in contrast to the more common right-lateral transpressive fold development exposed elsewhere in the Indio and Mecca Hills.

Reports

Rymer, M.J., 1989, Surface rupture in a fault stepover on the Superstition Hills fault, California, *in* Schwartz, D.P., and Sibson, R.H., eds., Fault segmentation and controls of rupture initiation and termination: U.S. Geological Survey Open-File Report 89–315, p. 309–323.

U.S. Geological Survey staff, 1989, Lessons learned from the Loma Prieta, California, earthquake of October 17, 1989: U.S. Geological Survey Circular 1045, 48 p.

U.S. Geological Survey staff, 1990, The Loma Prieta , California, earthquake: an anticipated event: Science, v. 247, p. 286–293.

Earthquake Hazards Studies, Metropolitan Los Angeles-Western Transverse Ranges Region

9540-02907

R.F. Yerkes
Branch of Western Regional Geology
345 Middlefield Road M/S 975
Menlo Park, California 94025
(415) 329-4946

Investigations and results

1. Historic earthquakes (W.H.K. Lee and Yerkes). Reinterpreting all available seismograms for 50 1984+ earthquakes in the Los Angeles basin-northern Peninsular Ranges region to assist in identifying the buried southern tectonic boundary of the Transverse Ranges and associated structural elements. This study was interrupted by equipment (VAX 750) demands of the Loma Prieta earthquake. A method for circumventing this bottleneck is being devised, but is not in place.

2. Geologic studies (Yerkes, C.M. Wentworth, and P.K. Showalter). As a necessary initial step in organizing a vast file of subsurface data we assembled, collated, and mapped, using GIS-Arc Info, data on 1385 exploratory wells of record in the Los Angeles 1:100,000 quadrangle. The digitized map shows bottom-hole geology for each well and oilfield boundaries with names; a separate register, keyed to the map, includes location, depth, and detailed geologic data on the wells.

Reports

Davis, T.L., Namson, J., and Yerkes, R.F., 1989, A cross section of the Los Angeles area: seismically active fold and thrust belt, the 1987 Whittier Narrows earthquake, and earthquake hazard: Jour. Geophys. Res., vol. 94, no. B7, p. 9644-9664, plate.

Yerkes, R.F., Oppenheimer, D.H., and Lee, W.H.K., 1989, Elsinore fault zone--seismicity vs. age of surface faults (abs.): EOS, vol. 70, no. 43, p. 1363.

Expert Synthesis and Translation of Earthquake Hazard Results —A Book for Non-Scientists in the Wasatch Front Region

14-08-0001-G1671

W.J. Arabasz and D.R. Mabey
Department of Geology and Geophysics
University of Utah
Salt Lake City, Utah 84112-1183
(801) 581-6274

Investigations:

This "implementation" project is part of the culmination of recent NEHRP focus on Utah's Wasatch Front region. The goals of the project are: (1) to coordinate with the scientific investigators who have worked in the Wasatch Front earthquake-hazards program—in order to develop a synthesis of important technical information, (2) to produce intermediate-level summaries from those discussions, and finally, (3) to "translate" the technical information into a book on the earthquake threat in Utah for non-earth scientists. The book is being designed to appeal to (i) the general public (who must encourage and support elected and appointed officials to make decisions on implementing earthquake-hazard-reduction measures), (ii) teachers and students, and (iii) decision-makers themselves. *(During the report period, a no-cost extension was requested—and granted—for this award. The project completion date is now September 30, 1990.)*

Results: October 1, 1989-March 31, 1990

Negotiations are under way for co-publication of the book by the University of Utah Press and by the Utah Geological & Mineral Survey. Targeting of the book as a so-called "trade title" for general readership in Utah is influencing some reshaping of the book for public appeal. Booksellers, for example, emphasize the need for "something people can grab and use" (hence, a request for chapters on "How to Prepare" and "What to do When it Hits"). In a similar vein, booksellers also emphasize the need for having a book that represents "the only book that people need in order to be educated about [earthquakes] in Utah."

For the upcoming "Sixth Annual Wasatch Front Earthquake Conference" (June 11-12, 1990), efforts are being made to produce another intermediate-stage summary (task 2). Direct experience with various user-groups during the past year emphasizes that technically-worded summaries produced by scientists and engineers are simply too complicated for them to understand. The informal document being prepared is modular and contains sections on: (1) a general introduction to Utah's earthquake threat; (2) a "translation" of technical conclusions produced in 1989 by working groups of scientists and engineers; (3) a motivational section, "Is Utah Ready to Take Action to Reduce its Earthquake Risk?" by G. Atwood and W. Hays; and (4) an instructional section on "Basic Strategies for Loss Reduction," by M. Lowe, G.E. Christenson, C.V. Nelson, R.M. Robison, and J. Tingey. The precisely-worded technical conclusions prepared by the working groups will be appended. This particular document is still, in effect, a working document for "those in the know." There remains an evident need to produce one or more simplified, graphic brochures for different types of decision-makers; the document at hand is intended to provide a starting point for such brochures.

Near-Surface Lithologic and Seismic Properties

9910-01168

J.F. Gibbs and W.B. Joyner
Branch of Engineering Seismology and Geology
345 Middlefield Road, MS 977
Menlo Park, California 94025
(415) 329-5631 or (415) 329-5640

Investigations

Measurements of seismic velocity and attenuation to determine the effect of local geology on strong ground motion and to aid in the interpretation of seismic source parameters.

Results

1. J. F. Gibbs participated in the Loma Prieta aftershock program from Oct. 18, 1989 to mid Jan. 1990 deploying and servicing General Earthquake Observation Systems (GEOS) recorders in the Marina district of San Francisco, on the Peninsula, East Bay, and in northern Santa Clara Valley. Numerous aftershocks were recorded at the above locations.

2. Preliminary results from borehole observations at the Gilroy strong motion station No. 2 indicate an average shear-wave Q of 10.2 ± 3.2 for the upper 115 m of alluvium, which is characteristic of much of the valley-fill underlying the heavily populated areas of Santa Clara Valley.

Reports

Gibbs, J.F., 1989, Near-surface P- and S-wave velocities from borehole measurements near Lake Hemet, California: U.S. Geological Survey Open-File Report 89-630, 10 p.

Gibbs, J.F., Roth, E.F., Fumal, T.E., Jasek, N.A., and Emslie, M.A., 1990, Seismic velocities from borehole measurements at four locations along a fifty-kilometer section of the San Andreas Fault near Parkfield, California: U.S. Geological Survey Open-File Report 90-248, 35 p.

Experimental Investigation of Liquefaction Potential

9910-01629

Thomas L. Holzer, John C. Tinsley III, and Michael J. Bennett
Branch of Engineering Seismology and Geology
U.S. Geological Survey
345 Middlefield Road
Menlo Park, CA 94025
(415) 329-5613

Investigations

1. Establishment and maintenance of an instrumented site in Parkfield, California, to monitor pore-pressure build-up in a sand undergoing liquefaction and strong ground motion during the predicted Parkfield earthquake.

2. Documentation of liquefaction effects in the Monterey Bay region from the October 17,1989, Loma Prieta, California, earthquake.

3. Documentation of liquefaction and causes of damage in the Marina District of San Francisco from the October 17, 1989, Loma Prieta, California, earthquake.

Results

1. The Parkfield liquefaction array with 14 pore pressure transducers and 5 three-component force-balanced accelerometers was maintained. Recording systems consist of two CRA-1 film recorders and a GEOS digital recording system connected to five transducers to improve the dynamic range. Geotechnical laboratory testing of undisturbed soil samples taken in November 1987 was complete and the liquefaction potential from the laboratory tests is presently being compared to the field results. Analysis of seismic refraction tests conducted during initial site exploration revealed evidence for unsaturation beneath the water table. Since unsaturation reduces liquefaction potential, the refine of the technique offers the potential for improving liquefaction assessments.

2. A map showing the distribution and nature of liquefaction-related ground failures at a scale of 1:24,000 is being prepared for the Monterey Bay-Hollister region, California. A comprehensive program of regional field studies and site specific investigations is in progress at 11 sites; the field phase is scheduled for completion in June, 1990. These studies include stratigraphic and geomorphic analyses of the facies associations of the ground failures; an evaluation of published USGS liquefaction potential map (Dupré and Tinsley, 1980) for the Monterey Bay region (scale 1:62,500), in light

of the Loma Prieta earthquake effects; comparisons of 1989 liquefaction effects with published reports of permanent ground failures arising from the 1906 San Francisco earthquake; cone penetrometer, standard penetrometer, and piezocone penetrometer studies of selected lateral spread ground failures to determine in-situ properties of failed and adjacent non-failed materials in relation to ground motion generated by the Loma Prieta earthquake; and comparisons among geotechnical properties of sediments involved in the failures of the natural deposits in relation to published curves for evaluating liquefaction susceptibility as used in standard engineering practice in the United States. Several sites have been located which may afford good potential to evaluate 1906 and earlier earthquakes using paleoliquefaction studies.

The initial compilation of ground failure effects using aerial photographic analysis coupled with field mapping and sampling of ejected sand is complete; particle size analysis of ejected sand samples is in progress in the soil laboratory at Menlo Park. From a stratigraphic perspective, there is a strong association between fluvial channel, levee, and point bar deposits and liquefaction effects observed following the October 17, 1989, earthquake, especially among deposits which are less than a few hundred years old.

Liquefaction was widespread within late Holocene fluvial deposits of the Pajaro and Salinas rivers, especially in tidewater reaches where ground water is within 1 to 2 meters of the ground surface year-round and the effects of prolonged drought on ground-water levels is minimal. In contrast to 1906, when wet soil moisture conditions contributed to widespread hillslope flow failures, in 1989, few if any slope failures related to liquefaction were reported. Intensity of liquefaction effects decreases upstream, as the fluvial deposits become more coarse, despite increasing proximity to the Loma Prieta earthquake seismic source zone. The proximity of a free-face within 50 to 150 m was commonly observed in lateral spread ground failures.

Components of displacements associated with ground failures measured in the field following the Loma Prieta earthquake range from a few millimeters to about 1 meter horizontally; settlements range from a few millimeters to less than 2 meters vertically.

3. Following the Loma Prieta mainshock, sand boils and ground cracks in the Marina District were mapped and portable seismographs were deployed to monitor aftershocks. Compilations of the geology of the district and a geotechnical drilling program also were conducted. Two earthquake effects were recognized - liquefaction and site amplification. Liquefaction was associated with a hydraulic fill that was placed in 1912 for the 1915 Panama-Pacific International Exposition. Fill material consists of a loose, clean, well-sorted sand. Site

amplification occurred over a broad area in the district. The area is one underlain by over 250 feet of unconsolidated natural deposits. Aftershock recordings revealed maximum amplification of six- to ten-fold. Our preliminary investigation reveals that both liquefaction and shaking caused damage to structures in the district. Structures were damaged on both natural deposits and artificial fills. Further investigation is required to define the relative significance of each of these hazards. Damage from earthquake shaking was abetted by inadequate stiffness of bottom stories and, in some cases, by the deterioration of timber or lack of proper anchoring of timber frames to their concrete strip foundations. Underground pipelines appear to have been damaged most severely by permanent differential ground displacements caused by liquefaction and consolidation of loose fills.

Publications

Holzer, T.L., Bennett, M.J., and Youd, T.L., 1989, Lateral spreading field experiments by the U.S. Geological Survey, in, Proceedings from the second U.S.-Japan Workshop on liquefaction, large ground deformation and their effects on lifelines (edited by T.D. O'Rourke and M. Hamada): National Center for Earthquake Engineering Research, Technical Report NCEER-89-0032, p. 82-101.

Plafker, G., and Galloway, J.P., 1989, Lessons learned from the Loma Prieta, California, earthquake of October 17, 1989: U.S. Geological Survey Circular 1045, 48p.

U.S. Geological Survey Staff, 1990, The Loma Prieta, California, earthquake: an anticipated event: Science, v. 247, p. 286-293.

U.S. Geological Survey Staff, 1990, Effects of the Loma Prieta earthquake on the Marina District, San Francisco, California: U.S. Geological Survey Open-File Report 90-253, 138p.

The Implementation of an Earthquake Hazard Mitigation Program in Salt Lake County: Phase II

Contract Number: 14-08-0001-G1797

Investigators: Gary Madsen, Loren Anderson,
and Gerold Barnes

Utah State University, Logan, Utah 84322-0730

(801) 750-1233, (801) 750-2775, (801) 468-2061

Investigators:

This is the second phase of a project to further develop an earthquake hazard preparedness program for Salt Lake County involving public officials, community groups, and the general public. The program is being designed to create heightened awareness of earthquake problems, generate public acceptance of earthquake hazard reduction programs, and establish an earthquake hazard mitigation plan for the county. We have already accomplished three primary tasks: 1) assessing earthquake hazard reduction priorities of public officials in the county, 2) assessing public awareness and understanding of earthquake hazards, and 3) developing an educational program for Salt Lake community groups. The second phase of the project began January 1, 1990. The final tasks are: 4) implementing the education program with materials designed for three distinct audiences (volunteer organizations, the business community, and local government officials), and 5) evaluating the program's effectiveness.

Results:

The initial three months of Phase II have been directed toward implementing the education program in Salt Lake County. Originally the educational program was developed into a slide-tape format. Through several pre-tests it was decided that this medium would be too cumbersome and complex to use with the large number of audiences for which the program was targeted. In addition, we wanted to include some recently obtained materials about the Loma Prieta earthquake. Therefore, we decided to add new information and to change the format to a videotape. This new version of the educational package is twenty-three minutes long and emphasizes three things: what are the major types of earthquake hazards effecting the Salt Lake Valley, what are mitigation strategies which can be directed toward new construction as well as existing buildings, and what can be done by individual households to reduce the risks associated with their residences as well as develop seventy-two hour emergency survival supplies.

The videotape has been reviewed extensively by numerous state and local government personnel and private citizens. It is now being presented to Salt Lake Valley public officials, community groups and the general public.

EARTHQUAKE RISK REDUCTION PROSPECTS:
PUGET SOUND - PORTLAND ASSESSMENT

Grant 14-08-0001-G1535
6/16/88-12/15/89

Peter J. May
Associate Professor
Political Science DO-30
University of Washington
Seattle, WA 98195
(206) 543-9842

Objective: This research has the broad objective of providing an understanding of the opportunities and problems associated with local earthquake risk reduction within the Puget Sound and Portland areas. The specific focus is upon local land use and building practices among the larger jurisdictions within the region.

Summary of Research Accomplishments: Information was collected for the major jurisdictions in the region comprising 6 Oregon counties, 16 Oregon cities, 13 Washington counties, 27 Washington cities, and 6 port districts. The data about risk perceptions and existing practices led to the identification of several different categories of risk reduction opportunities. This variation in situations also led to the development and consideration of four different state or regional-level implementation strategies that might be undertaken as new information about earthquake risks is developed. These findings are detailed in the final project report, *Anticipating Earthquakes: Risk Reduction Policies and Practices in the Puget Sound and Portland Areas*.

Reports Produced from this research:

Anticipating Earthquakes: Risk Reduction Policies and Practices in the Puget Sound and Portland Areas, November 1989, Seattle, WA: Institute for Public Policy and Management, University of Washington. (Final Project Report)

Earthquake Risk Reduction Profiles: Local Policies and Practices in the Puget Sound and Portland Areas, November 1989, Seattle, WA: Institute for Public Policy and Management, University of Washington. (Background Profiles to the Final Project Report)

Presentations based on this research:

"Anticipating Earthquakes: Local Policies and Practices in the Puget Sound and Portland Areas," presentation made to the annual meeting of the Western States Seismic Policy Council, Boise, Idaho, November 6-9, 1989.

"Washington Earthquake Policy Review," Presentation made to the House Committee on Energy and Utilities, Washington State Legislature, October 24, 1989.

"Federal Earthquake Risk Reduction Strategies," Invited seminar speaker at the National Center for Earthquake Engineering, State University of New York at Buffalo, June 22, 1989.

"Earthquake Risk Reduction Policies and Practices within the Puget Sound and Portland Areas," Presentation at the USGS-FEMA Workshop, Portland, Oregon, March 28-30, 1989.

"Earthquake Risk Reduction Prospects," Presentation at the USGS-FEMA Workshop, Olympia, WA, April 12-15, 1988.

Forthcoming papers:

"Earthquake Risk Reduction: Implementation Prospects for the Puget Sound and Portland Areas," Fourth US National Conference on Earthquake Engineering, May 20-24, 1990, Palm Springs, CA.

"Earthquake Risk Reduction Prospects for the Puget Sound and Portland Areas," submitted for the USGS Professional Paper.

Other project activities:

Assistance for dissertation work by Sarah Michaels, University of Colorado PhD candidate, on "Earthquake Issue Networks in Washington State and British Columbia".

Support for two graduate student assistants at the University of Washington.

EARTHQUAKE RISK REDUCTION PROSPECTS: PUGET SOUND - PORTLAND ASSESSMENT

Grant 14-08-0001-G1778
12/16/89-12/15/90

Peter J. May
Associate Professor
Political Science DO-30
University of Washington
Seattle, WA 98195
(206) 543-9842

Objective: This research has the broad objective of providing an understanding of the opportunities and problems associated with local earthquake risk reduction within the Puget Sound and Portland areas. The current research addresses professional practices and their relationship to local policies. It is aimed at providing a better understanding of the role of the professional standards of architects, geotechnical and structural engineers, and other design professionals in influencing local earthquake risk reduction. This is particularly unique and important in that it turns attention to the prospective role of the design professions in enhancing local earthquake risk reduction, rather than assuming risk reduction is necessarily accomplished through governmental actions.

Summary of Research To Date: Information is being collected about: (a) the role of different professional associations for design professionals in influencing risk reduction practices, (b) state licensing and registration requirements as they relate to professional practices, and (c) design professionals' perceptions of changes in practice over time.

Papers/Presentations based on this research:

"Loss Estimates as Unknown Numbers," Presentation at the USGS-FEMA NEHRP Workshop, Seattle, Washington, April 17-19, 1990.

Global Digital Network Operations

9920-02398

Howell M. Butler
Branch of Global Seismology and Geomagnetism
U.S. Geological Survey
Albuquerque Seismological Laboratory
Building 10002, Kirtland AFB-East
Albuquerque, New Mexico 87115-5000
(505) 844-4637

Investigations

The Global Digital Network Operations presently consists of 14 SRO/ASRO, 13 DWWSSN stations, and 80 WWSSN-type recording stations located in 58 countries and islands throughout the world. The primary objective of the project is to provide high-quality digital and analog seismic data for fundamental earthquake investigations and research, enhancing the United States capabilities to detect, locate, and identify earthquakes and underground nuclear explosions in support of test ban issues. Technical and operational support is provided as funds permit to keep the GSN operating at the highest percentage of recording time possible. This support includes operational supplies, replacement parts, repair service, modifications of existing equipment, installation os systems and on-site maintenance, training, and calibration. A service contract provides technicians to perform the support requirements as well as special projects such as on-site noise surveys, site preparations, and evaluation and testing of seismological and related instrumentation.

On-site Station Maintenance

1. Maintenance was performed at La Paz (ZOBO), Bolivia, during November.

2. Due to reduced project funding considerations, maintenance visits have been curtailed during this period. The systems at Bogota (BOCO), Colombia, and Lembang (LEM), Indonesia, have had catastrophic failures and will remain inoperative until funding is available for maintenance or replacement of the current system at those locations.

Results

The Global Digital Network continues with a combined total of 107 WWSSN/SRO/ASRO/DWWSSN/IRIS stations. The main effort of this project, as funding permits, is to furnish the types of support at a level needed to keep the GSN at the highest percentage of operational time in order to provide the improved geographical coverage with analog and digital data from highly sensitive short-period and broadband seismic sensor seismograph systems. Seventy-four WWSSN stations have been converted from photographic recording to thermal recording. Thirty-eight stations operate with six components. Six stations (BKS, DUG, FVM, GSC, HON, and LUB) continue with photographic recording.

U.S. Seismic Network

9920-01899

Marvin A. Carlson
Branch of Global Seismology and Geomagnetism
U.S. Geological Survey
Denver Federal Center
Box 25046, Mail Stop 967
Denver, Colorado 80225
(303) 236-1500

Investigations

U.S. Seismicity. Data from the U.S. Seismic Network (USSN) are used to obtain preliminary locations and magnitudes of significant earthquakes throughout the United States and the world.

Results

As an operational program, the USSN operated normally throughout the report period. Data were recorded continuously in real time at the National Earthquake Information Center's (NEIC) main office in Golden, Colorado. At the present time, 80 channels of SPZ data are being recorded at Golden on develocorder film. This includes data telemetered to Golden via satellite from both the Alaska Tsunami Warning Center, Palmer, Alaska, and the Pacific Tsunami Warning Center, Ewa Beach, Hawaii. A representative number of SPZ channels are also recorded on Helicorders to give NEIC real-time monitoring capability of the more active seismic areas of the United States. In addition, 18 channels of LPZ data are recorded in real time on multiple pen Helicorders.

Data from the USSN are interpreted by record analysts and the seismic readings are entered into the NEIS data base. The data are also used by NEIS standby personnel to monitor seismic activity in the United States and world wide on a real time basis. Additionally, the data are used to support the Alaska Tsunami Warning Center and the Pacific Tsunami Warning Service. At the present time, all earthquakes large enough to be recorded on several stations are worked up using the "Quick Quake" program to obtain a provisional solution as rapidly as possible. Finally, the data are used in such NEIS publications as the "Preliminary Determination of Epicenters" and the "Earthquake Data Report."

Development is continuing on an Event Detect and Earthquake Location System to process data generated by the USSN. We expect the new system to be ready for routine operational use during 1990. At that time, the use of develocorders for data storage will be discontinued. Ray Buland and David Ketchum have been doing the developmental programming for the new system. A VAX 3800 will be used as the primary computer of the Event Detect and Earthquake Location System.

Six stations of a pilot VSAT Network have been installed. Four of the stations are the former RSTN sites at McMinnville, Tennessee, St. Regis Falls, New York, Black Hills, South Dakota, and Red Lake, Ontario, which are now operated by the Branch of Global Seismology and Geomagnetism. The fifth site is the former AFTAC Array near Boulder, Wyoming, and the sixth site is at what was formerly the Newport Observatory, Newport, Washington, which is no longer a manned site. The data is transmitted via satellite to a shared Master Earth Station and on to the NEIC at Golden, Colorado, via AT&T long lines.

Earth Structure and its Effects upon Seismic Wave Propagation

9920-01736

George L. Choy
Branch of Global Seismology and Geomagnetism
U.S. Geological Survey
Denver Federal Center
Box 25046, Mail Stop 967
Denver, Colorado 80225
(303) 236-1506

Investigations

1. Effects of Earth structure on source parameters. The NEIS now uses broadband data to routinely compute parameters such as depth from differential arrival times, radiated energy and arrival times of late-arriving phases. To assure the accuracy of source parameters derived from waveforms we are developing corrections for the effects of wave propagation in the Earth.

2. Use of differential travel-time anomalies to infer lateral heterogeneity. We are investigating lateral heterogeneity in the Earth by analyzing differential travel times of phases that differ in ray path only in very narrow regions of the Earth. Because such phases often are associated with complications near a cusp or caustic, their arrival times can not be accurately read without special consideration of the effects of propagation in the Earth as well as additional processing to enhance arrivals.

3. Use of body wave pulse shapes to infer attenuation in the Earth. In previous work we developed techniques to determine the depth- and frequency-dependence of attenuation in the Earth. Resolution of this frequency dependence requires analysis of a continuous frequency band from several Hz to tens of seconds as well as consideration of the contributions of scattering and slab diffraction to apparent broadening of a pulse. We are now in the process of documenting Q for surface events and for events at different depths.

Results

1. Effects of Earth structure on source parameters. Body waves that touch internal caustics in the Earth are distorted in a way that can be mathematically corrected by Hilbert transformation. The correction for this pulse distortion has generally not been recognized in the practice of record interpretation. We are evaluating the effect on phases that are commonly read by analysts and the possible effect on tomographic inversions which take reported arrival times of body waves on face value.

2. Use of differential travel-time anomalies to infer lateral hetero geneity. We have developed a source-deconvolution technique that resolves

differential travel times of body waves near cusps and caustics. Application of this algorithm to PKP waves sampling the inner core suggests that regional velocity variations exist within the upper 200 km of the inner core. The regional variations are consistent with those obtained from global inversions of absolute PKP times. We are reading high quality arrival times of PcP and branches of PKP, corrected for propagation effects. This accumulation of data can be used to determine if propagation phenomena have biased the catalog data which have been used to derive models of lateral heterogeneity.

3. Use of body wave pulse shapes to infer attenuation in the Earth. The frequency-dependent Q model of Choy and Cormier (1987) has been crucial to the practical implementation of some algorithms that are used to compute source parameters. It was incorporated into a semi-automated version of the algorithm of Boatwright and Choy (1986) for use by the NEIC in computing radiated energies of earthquakes with $m_b > 5.8$. This Q model also provided the crucial attenuation correction in the technique described by Choy and Boatwright (1988) and Boatwright and Choy (1989) which derives acceleration spectrum from far-field broadband data. We are now attempting to separate intrinsic attenuation from scattering in waveforms. We synthesize waveforms using a method that simultaneously models causal attenuation and source finiteness. Under the assumption that intrinsic attenuation can be described by minimum phase operators, we can attribute discrepancies in the waveforms to scattering.

Reports

Boatwright, J. and Choy, G. L., 1989, Acceleration spectra for subduction zone earthquakes: Journal of Geophysical Research, v. 94, p. 15541-15553.

Choy, G. L. and Presgrave, B. W., 1989, Broadband seismogram analysis: A. Deep earthquake of Honshu, Japan of 7 September 1988, and B. Nepal-India border region earthquake of 20 August 1988, *in* Semi-Annual Technical Report: U.S. Geological Survey Open-file Report 89-207, p. 11-15.

Choy, G. L., 1990, Global digital data--Interpretation of the earthquake mechanism from broadband data: Proceedings of the PACRIM 90 Congress (submitted).

Choy, G. L. and J. Boatwright, 1990, Source characteristics of the Loma Prieta, California, earthquake of October 18, 1990 from global digital seismic data: Geophysical Research Letters (submitted).

Choy, G. L., Boatwright, J. and LaVonne, C. K., 1990, Teleseismic estimates of radiated energy from global seismicity of 1986-1988 [abs.]: EOS (American Geophysical Union, Transactions), v. 71, p. 258.

Choy, G. L. and Bowman, J. R., 1990, The rupture process of a multiple main shock sequence: Teleseismic, local and near-field analysis of the Tennant Creek earthquakes of 22 January 1988: Journal of Geophysical Research (in press).

Choy, G. L. and Kind, R., 1990, A preliminary broadband body-wave analysis of the Armenia S.S.R. earthquake of 7 December 1988: Geologisches Jahrbuch (submitted).

Choy, G. L., Presgrave, B. W., and LaVonne, C. K., Broadband seismogram analysis---The Ethiopian double earthquake of 20 August 1989, *in* Semi-Annual Technical Report: U.S. Geological Survey Open-file Report (submitted).

Reanalysis of Instrumentally Recorded United States Earthquakes

9920-01901

J. W. Dewey
Branch of Global Seismology and Geomagnetism
U.S. Geological Survey
Denver Federal Center
Box 25046, Mail Stop 967
Denver, Colorado 80225
(303) 236-1506

Investigations

1. Relocate instrumentally recorded U.S. earthquakes using the method of joint hypocenter determination (JHD) or the master event method, using subsidiary phases (Pg, S, Lg) in addition to first arriving P-waves, using regional travel-time tables, and expressing the uncertainty of the computed hypocenters in terms of confidence ellipsoids on the hypocentral coordinates.

2. Evaluate the implications of the revised hypocenters on regional tectonics and seismic risk.

Results

Jim Dewey has been studying the seismicity of a small region of northern Algeria near Ech Cheliff (named Orleansville in 1954 and El Asnam in 1980) which has produced two of the three largest earthquakes of this century in the 1800 km-long continental North African segment of the African/European plate boundary extending from Morocco through Tunisia. The MS=6.5 earthquake of September 9, 1954 killed over 1200 people, and the MS=7.3 earthquake of October 10, 1980 killed several thousand.

The Algerian earthquakes are important in analysis of U.S. seismic risk because they were caused by a type of faulting, predominantly reverse slip on faults in continental crust, that produces damaging earthquakes in some parts of the United States, such as the western Transverse Ranges and the flanks of the Coast Ranges of California and at various locations of the central and eastern U.S. An additional importance, which motivated Dewey's reanalysis of the earthquakes, concerns the characteristic-displacement model of earthquake occurrence. This model, widely used in earthquake hazards assessments, postulates that a given fault segment produces similar coseismic displacements through many cycles of strain accumulation and release, with each displacement releasing the strain that has accumulated across the fault since the previous earthquake. Based on earlier studies, it had appeared that many features of the 1980 (El Asnam) earthquake and its causative fault fit the characteristic-displacement model, but that the occurrence of the 1954 (Orleansville) earthquake was inconsistent with the model. The 1954 earthquake seemed to have occurred very near, perhaps on, a segment of the 1980 fault system that experienced high displacements in 1980, but the time period following the 1954 earthquake was too short to have allowed such large displacements to have accumulated across the 1980 fault plane. Dewey's research was begun on the hunch that the previously accepted position of the 1954 earthquake was incorrect, that the 1954 source was not close enough to the 1980 source to pose a challenge to the characteristic earthquake model, and that this could be revealed by a relocation of the 1954 earthquake sequence with respect to the 1980 earthquake sequence using the method of joint epicenter determination.

The hunch turned out to be wrong. Relocated epicenters of the 1954 mainshock and aftershocks occurring within 24 hours are situated in the midst of the region in which aftershocks were to occur in the 24 hours following the 1980 mainshock, on the boundaries of the segment of the 1980 fault system that was to experience maximum displacement in 1980.

The closeness of the 1954 mainshock and earliest aftershocks to a principal segment of the 1980 fault system implies that the 1954 earthquake involved either (1) rupture of the 1980 segment, or (2) rupture of a fault in the hanging-wall or footwall block of the 1980 segment. The first interpretation cannot be accommodated in the characteristic-displacement model of fault behavior but instead requires a model, such as the time-predictable model, that would permit slip in 1954 to have released only a small fraction of the elastic strain that was stored on the 1980 fault segment and that would later be released in 1980. However, the second interpretation, specifically with rupture in the hanging-wall block of the nearby 1980 fault segment, accounts more directly than the first interpretation for differences in the focal mechanisms and ground deformations associated with the two mainshocks. The second interpretation is therefore preferred. The second interpretation is consistent with a characteristic-displacement model of the 1980 fault system.

The 1954 and 1980 earthquakes provide grounds for both pessimism and optimism on the ultimate practicality of the characteristic-displacement model. Following the 1980 earthquake, paleoseismic studies were done by trenching the central segment of the 1980 fault system, the same segment on the boundaries of which the 1954 mainshock and earliest aftershocks occur. These studies showed that displacements similar to those of 1980 had occurred several times previously on the same fault segment in the late Holocene, but the trenches didn't show evidence for surface fault slip in 1954. Under the characteristic-displacement model, the paleoseismically determined offsets and the 1980 offset would be viewed as the characteristic displacements of their fault segment. A pessimistic assessment of the characteristic-displacement model arises from the fact that the 1954 earthquake was a very destructive earthquake, occurring very close to a prominent Holocene fault, that is not accounted for by the model as applied to the fault. Moreover, had the paleoseismic data and the characteristic-displacement model been available prior to the 1980 earthquake, it is easy to imagine that the 1954 earthquake, because of its relatively high magnitude, could have been viewed as possibly the culminating event of a seismic cycle on the fault zone, leading to an inappropriate downweighting of the intermediate-term seismic hazard thought to be associated with the fault. A positive assessment of the characteristic-displacement model would emphasize that, had model and paleoseismic data been available prior to

1980, a strict application of the model could have led to a warning that the 1954 earthquake might not be the culminating event of its seismic cycle, because it did not produce surface offsets such as those implied by the paleoseismic data.

Reports

Dewey, J. W., 1989, Hypocenter mapping and the extensibility of seismotectonic paradigms, in Litehiser, J. J., ed., Observatory Seismology: University of California Press, Berkeley, p. 225-239.

Dewey, J. W., Hill, D. P., Ellsworth, W. L., and Engdahl, E. R., 1989, Earthquakes, faults, and the seismotectonic framework of the contiguous United States, in Pakiser, L. C., and Mooney, W. D., eds., Geophysical Framework of the Continental United States: Memoir 172 of the Geological Society of America, p. 541-575.

Global Seismology

9920-03684

E. R. Engdahl
and
J. W. Dewey
Branch of Global Seismology and Geomagnetism
U.S. Geological Survey
Denver Federal Center
Box 25046, Mail Stop 967
Denver, Colorado 80225
(303) 236-1506

Investigations

1. Travel-Time Tables. Develop new standard global travel-time tables to locate earthquakes.

2. Arrival-Time Data. Develop a plan to establish an International Seismological Observing Period (ISOP)--a time interval during which there would be enhanced reporting of arrival-time data.

3. Earthquake Location in Island Arcs. Develop practical methods to accurately locate earthquakes in island arcs.

4. Subduction Zone Structure. Develop techniques to invert seismic travel times simultaneously for earthquake locations and subduction zone structure.

5. Global Synthesis. Synthesize recent observational results on the seismicity of the earth and analyze this seismicity in light of current models of global tectonic processes.

Results

1. Travel-Time Tables. New global travel-time tables to locate earthquakes are being developed by a working group of the IASPEI Sub-Commission on Earthquake Algorithms. The travel-time tables will be represented by a radially stratified Earth model with isotropic properties and with as good a fit as possible to the teleseismic observations of P, S, and core phases from the International Seismological Centre (ISC) catalog.

It has been agreed that a limited number of test events, for which the origin times and hypocenters are well constrained, will be used to check the performance of the velocity model as a representation of the new global travel times. This set of test events will include a broad geographic distribution of explosions (both nuclear and chemical) and earthquakes for which there are very strong constraints from local networks.

Test event data collected to date are used to investigate global differences in upper mantle structure with respect to a working velocity model developed by the IASPEI group. From high-quality arrival-time data associated with the test events, significant global differences in both average upper mantle structure and in lateral heterogeneity are observed. These differences are systematic and regionally dependent.

2. Arrival-Time Data. A Science Plan for the ISOP project has been developed. A summary of the highlights of this plan follows:

Definition: The International Seismological Observing Period (ISOP) is a specific time interval designated for enhanced international cooperation in the collection and dissemination of observatory measurements from the global seismographic network. The proposed ISOP project is sponsored jointly by the International Association of Seismology and Physics of the Earth's Interior (IASPEI), the IUGG Inter-Association Commission of the Study of the Earth's Deep Interior (SEDI), and by the Inter-Union Commission on the Lithosphere (ICL).

Goals: Seismology, the study of earthquakes and Earth structure using seismic waves, is an international science which requires data from global networks of observing stations. Current seismological practice relies heavily on a complex, worldwide infrastructure for the collection, processing, and dissemination of seismic data, involving the efforts of thousands of people in over 100 countries. The primary goal of ISOP is to strengthen this international infrastructure and increase the cooperation among nations that operate seismological observatories.

Measurements reported by the existing global network of seismic observatories and compiled by agencies such as the ISC are providing new information about earthquakes and Earth structure of fundamental importance to the Earth sciences. A goal of ISOP is to collect improved sets of observatory data for determining earthquake source parameters and Earth structure; in particular, the ISOP will encourage the measurement and reporting of later-arriving phases.

Other goals are to engage and educate young scientists, especially those from less developed countries, in modern seismological practice, including the use of digital seismic data for regional and global studies of seismic hazards, source processes, and Earth structure; to upgrade observatory practice so that a consistent set of waveform parameters can be derived from digitally recorded seismograms by local seismic analysts and transmitted to agencies such as the ISC for incorporation into internationally available catalogs; and to encourage and facilitate individual initiatives towards improving seismic measurements and data coverage.

Activities: Most improvements to observatory practice can be accomplished at very little cost and with only minor modifications to the organizational infrastructure of international seismology.

An important ISOP activity will be the enhanced reporting of the times of first- and later-arriving, high-frequency seismic phases. Under the project, there would be a concerted effort to improve the general distribution and reporting level of stations worldwide.

One approach to the problem of improved later-phase reporting is to select specific earthquakes for detailed observation by cooperating stations during a fixed ISOP period. From simulations of ISOP experiments of varying durations, it appears that a three-year ISOP experiment will provide a reasonably complete sample of seismicity from the major seismic zones of the Earth and that a simply parameterized selection algorithm based on seismological priorities can lead to a stable, manageable workload of about one event per day on average during the life of such an experiment.

The deployment of advanced digitally recording instrumentation provides an unprecedented opportunity to enhance the methods of seismogram interpretation and seismic parameter extraction through implementation of digital processing methods at seismic observatories worldwide. It must be ensured that this new information of scientific potential will be available to the seismological community at large. It is believed that this purpose is best served with an ISOP that promotes the development toward increased on-site analysis at digital stations.

Improvements in seismology require truly international cooperation, and the educational aspects of seismological practice form one of the goals of the ISOP. Thus, workshops will be needed to explain the ISOP objectives to network representatives, to train analysts in ISOP procedures, and to introduce them to modern techniques and applications of the data. Participants will thus benefit from theoretical results and practical experience that are to direct relevance to their own work. ISOP participation from developing countries will receive special attention.

3. Earthquake Location in Island Arcs. We compare relocated, teleseismically recorded seismicity before and after the May 7, 1986, Andreanof Islands earthquake (M_w=8) to the spatial and temporal distribution of seismic moment release during the mainshock. Relocated seismicity from 1964 through April 1987 clusters strongly along the main thrust zone, in similar locations for the pre- and post-mainshock periods.

We performed simultaneous iterative inversions of broadband teleseismic GDSN and NARS P-waveforms using the method of Kikuchi and Fukao (1987). Fault plane parameters (e.g., strike dip, depth, and extent of fault plane) consistent with regional tectonics and aftershock locations were specified. The results of the inversions are spatial and temporal maps of moment release on the fault plane. Most of the moment found by the inversion is localized in several regions of the fault plane. Resolution of the location and timing of the major subevents is good. The rupture was bilateral, with a highly variable rupture velocity. A shallow, updip region of the fault plane ruptured toward the end of the mainshock process.

The mainshock moment release tended to occur in regions of the fault plane in which no or few aftershocks or preshocks are located. This tendency suggests that regions of high moment release in the 1986 Andreanof Islands earthquake resulted from rupture of mechanically strong regions (i.e., asperities) on the fault plane, which exhibited little seismicity before or after the mainshock that ruptured them. We infer that the asperity regions were locked and quiescent before the mainshock, while surrounding seismically active areas did not store as much strain and slipped mostly aseismically.

4. Subduction Zone Structure. The use of published PP and pP phase data in tomographic delay-time inversions was investigated. Incorporation of PP and pP phases in tomographic studies potentially can improve the quality of the images because: (1) these phases sample Earth structure not ordinarily sampled by direct P phases; (2) these phases add rays that are oblique to rays of direct phases, which is especially important where the latter sample mantle structure in selected directions; and (3) pP data better constrain the earthquake focal depths. We demonstrated, from the distribution of reflection points and the cell hitcount, that PP and pP waves contributed positively to ray geometry in the cell model employed in the tomographic investigation and thus to the sampling by seismic waves of mantle structure below the Caribbean region. We note, however, that because of the relatively shallow seismicity in the area, the difference between ray paths of pP waves and the direct P wave is small.

We investigated the possibility that large errors (as compared to P) in reported PP and pP travel-time residuals may decrease the quality of the tomographic images. We did not attempt to improve the quality of the data set by the addition of high-quality digital data. Rather, we summarized the different sources of errors in ISC phase data nd assessed the contributions of these errors to the PP and pP delay times. We did not discern systematic biases in the reported PP data, which may be due to the random character of the errors or due to the properties of the ISC identification program. No evidence is found for the predominance of pwP phases, misidentified as pP, in the pP data set for the Caribbean region. The ISC reported focal depths are determined from direct P arrival times. We conclude that the pP delay times reported by the ISC are inconsistent with these depths. In the inversion, the large negative mean value of the pP delay-time distribution was accommodated by shallower focii and high-velocity images in the top layer of the cell model. The larger errors in PP and pP data relative to P data are recognized in the weighting scheme used in the inversion.

We showed that, despite the many sources of (large) errors in PP and pP data and the difficulty to assess their individual contributions, simultaneous inversion of ISC PP and pP data provide tomographic images consistent with P images. From this observation, we conclude that the ISC delay times of later arriving phases such as PP and pP do contain valuable information about velocity structures in Earth's mantle.

In contrast, lack of correlation between the results of the tomographic inversion of P, PP, and pP data and the image resulting from differential travel-time or reflection point residuals is not significant. We argued that one of the major drawbacks of the conventional approach to differential travel-time studies (e.g., Stewart, 1976) is that the residual is assumed to be caused primarily by velocity structures in the vicinity of the reflection point. The depth extent of the velocity anomalies contributing to the travel-time residuals is, however, not known and may comprise the whole upper mantle in the case where only teleseismic data are considered.

We demonstrated the improved spatial resolution when PP and pP phases are included in this tomographic study. Below large areas, we still have to cope with lack of spatial resolution, either due to serious underexposure by the particular seismic waves incorporated in the study or the low quality and high noise level of the data. These provide arguments for a further expansion and improvement of global networks of digital recorders, both on land and sea (bottom). We realize that, for the mantle below the Caribbean region, improvements due to the inclusion of PP and pP data on image resolution and changes in velocity structure are small. This is not surprising because (1) the number of pP and particularly PP data is very low with respect to the number of P data; (2) we had to decrease the influence of PP and pP data even further because of the higher level of data errors; and (3) the difference in ray geometry between pP waves and the direct P waves is small due to lack of seismicity at greater depths.

With these arguments in mind, we conclude that the incorporation of PP and pP phases in the P delay time tomographic study of the velocity structures in the Caribbean mantle has been successful. the modification and extension of software, necessary to incorporate the surface reflected PP and depth phase pP (together with PP-P and pP-P differential times) in tomographic investigations, is straightforward. Much care should be taken in correcting for bathymetry and topography and in the proper choice of a reference model. We argue that with relatively small efforts tomographic images can be obtained with higher spatial resolution.

In some respects, this study can be considered preliminary. With regard to the data errors, much work remains to be done. In particular, the effect of waveform distortions due to phase shifts (Hilbert transforms) in each frequency component of the PP phase (Choy and Richards, 1975) and the contamination of the pP delay times with reflections at surfaces other than those assumed (Engdahl and Billington, 1986; Schenk et al., 1989) need further attention. The examination of high-quality digital data, preferably broadband (Engdahl and Kind, 1986) may be essential for this purpose. Finally, the inconsistency between ISC focal depths and the reported pP delay times needs to be examined by those responsible for the routine processing of data at the ISC (Van der Hilst et al., 1990).

By virtue of the improvements realized in the Caribbean region, application of the method to areas with a greater depth distribution of earthquake focii is promising. We are presently working on a simultaneous tomographic inversion of P, PP, and pP delay time data (together with the differential residual times) to further investigate northwestern Pacific subduction zones. Because of the deep seismicity in that area, differences between pP and P ray paths are large and, consequently, shallow mantle structures below backarc (Sea of Japan) and intraplate areas (Philippine Plate) within this region will be better illuminated by pP waves. Better constraints on the shallow structures and on the focal depths also improve resolution of the subducted Pacific Plate in the down-dip direction. This improvement is important to the investigation of the morphology of the subducted slab near the 670 km discontinuity.

5. Global Synthesis. Nothing new to report.

Reports

Ekström, G., and Engdahl, E. R., 1989, Earthquake source parameters and stress distribution in the Adak Island region of the central Aleutian Islands, Alaska: Journal of Geophysical Research, v. 94, p. 15,499-15,519.

Engdahl, E. R., Billington, S., and Kisslinger, C., 1989, Teleseismically recorded seismicity before and after the May 7, 1986, Andreanof Islands, Alaska, earthquake: Journal of Geophysical Research, v. 94, p. 15,481-15,498.

Houston, H., and Engdahl, E. R., 1989, A comparison of the spatio-temporal distribution of moment release for the 1986 Andreanof Islands earthquake with relocated seismicity: Geophysical Research Letters, v. 16, p. 1421-1424.

Schwartz, S. Y., Dewey, J. W., and Lay, T., 1989, Influence of fault plane heterogeneity on the seismic behavior in the southern Kurile Islands arc: Journal of Geophysical Research, V. 94, P. 5637-5649.

Van der Hilst, R. D., and Engdahl, E. R., 1990, On the use of PP and pP data in delay time tomography: Geophysical Journal International (submitted).

Systems Engineering

9920-01262

Gary Holcomb
Branch of Global Seismology and Geomagnetism
U.S. Geological Survey
Albuquerque Seismological Laboratory
Building 10002, Kirtland AFB-East
Albuquerque, New Mexico 87115-5000
(505) 844-4637

Investigations

Engineering development to improve the quality of seismic instrumentation.

Results

The program to evaluate candidate National Seismic Network seismic sensor systems continued with considerable effort being extended to determine the precise source of noise sources within the sensors. A report summarizing the results of this series of tests was prepared and submitted to the contracting officer.

As part of a contract with Sandia National Laboratories, a series of evaluation tests was conducted on the Guralp CMG-3S borehole sensor system. This study is aimed at identifying noise levels and the sources of noise within this instrument system. The data has been partially analyzed, and a report of the results will follow.

A study of potential error sources in analyzing data obtained from side-by-side seismometer evaluations is underway. These error sources include sensor misalignment, numerical precision in the data processing, and model applicability.

Probabilistic Earthquake Assessment

9920-01506

Stuart P. Nishenko
Branch of Global Seismology and Geomagnetism
U.S. Geological Survey
Denver Federal Center
Box 25046, Mail Stop 967
Denver, Colorado 80225
(303) 236-1500

Investigations

1. Improve current probabilistic estimates for earthquakes within the United States and the circum-Pacific region.

2. Development of an operational methodology to provide rapid and reliable estimates of damage caused by moderate and large United States earthquakes.

Results

1a. Probabilistic estimates for the occurrence of damaging (i.e., $m_b > 6.0$) earthquakes in the eastern and central United States have been submitted for publication (Nishenko and Bollinger, 1990). These estimates are based on regional return times inferred from local network data, catalogs of eastern and central U.S. seismicity since 1727, and paleoseismic data. The conditional probability for an event of m_b 6 or larger in this region is at the 0.4 to 0.6 level for the next 30 years (i.e. 1990-2020). Probabilities for the recurrence of an event of $m_b > 7$ during this same time interval are at the 0.1 level. Both California and the central and eastern United States have equivalent chances of producing earthquakes with comparable damage areas when the differences in seismic wave attenuation for both regions are accounted for.

1b. As a consequence of the magnitude 7.1 Loma Prieta earthquake of 17 October 1989, the Working Group on Probabilities of Earthquakes in the San Francisco Bay Area was organized under the auspices of NEPEC. Activities of this Working Group are to review, and as necessary revise, the findings of the 1988 Working Group report (WGCEP, 1988) for the San Francisco Bay Region. The final report for the Bay Area working group will be presented to NEPEC this spring.

1c. Studies of historic great earthquakes along the central Peru subduction zone indicates significant variations in the size of events from cycle to cycle. Comparison of Modified Mercalli intensity patterns and tsunami wave heights by Beck and Nishenko (1990) indicates that events in 1940, 1966, and 1974 were smaller than events in 1687 and 1746. The magnitudes of these earlier events (M_W 8.7-8.8) appear to be in agreement with regional predictions of maximum magnitude based on the rate of plate convergence and sea floor age. In contrast to the simple, single asperity nature of the 20th century events, it is suggested that the older, larger events may represent multiple asperity ruptures.

2. The program to develop rapid estimates of earthquake damage is currently in the data gathering and analysis stage. Digital data bases (geologic, physiographic, and demographic) are being evaluated for use with other earthquake hazard and risk information. Comparisons of estimated and observed damage from previous earthquakes will be undertaken. Also, communications networks are being investigated to distribute damage information to vulnerable communities, local, state, and federal agencies, and the private sector.

Reports

Beck, S., and Nishenko, S. P., 1990, Variations in the mode of great earthquake rupture along the central Peru subduction zone: Geophysical Research Letters (in press).

Nishenko, S. P., and Bollinger, G. A., 1990, Forecasting damaging earthquakes in the central and eastern United States: Science (submitted).

Working Group on California Earthquake Probabilities, 1988, Probabilities of large earthquakes occurring in California on the San Andreas fault: U.S. Geological Survey Open-file Report, 88-398, 62 p.

Global Seismograph Network Evaluation and Development

9920-02384

Jon Peterson
Branch of Global Seismology and Geomagnetism
U.S. Geological Survey
Albuquerque Seismological Laboratory
Building 10002, Kirtland AFB-East
Albuquerque, New Mexico 87115-5000
(505) 844-4637

Investigations

Continued activities in support of the U.S.-USSR data exchange program and initiated development of software for PC-based utilization of network data and assessment of data quality.

Results

Plans have been developed to support the installation of a Soviet borehole seismograph system at the Albuquerque Seismological Laboratory. Facilities required, which include a recording building and a large-diameter borehole, are expected to be ready by mid 1990. Several special sets of GDSN and CDSN network data have been made available to the Soviets on floppy disks and copies of network volumes are now sent to the Soviet Union on a regular basis.

Interactive graphics programs for displaying and processing GSN network data are being developed for use on a PC or a Data Collection Center work station. The programs are intended to provide GSN stations with VBB seismographs, an inexpensive processing capability, and for use at the DCC for review of network data.

Digital Data Analysis

9920-01788

Stuart A. Sipkin
Branch of Global Seismology and Geomagnetism
U.S. Geological Survey
Denver Federal Center
Box 25046, Mail Stop 967
Denver, Colorado 80225
(303) 236-1506

Investigations

1. Moment Tensor Inversion. Apply methods for inverting body phase waveforms for the best point-source description to research problems.

2. Other Source Parameter Studies. Apply methods for inverting body phase waveforms for distributed kinematic and dynamic source properties.

3. Aftershock Source Properties. Examine mainshock and aftershock source properties to study the mechanics of aftershock occurrence.

4. Broadband Body-Wave Studies. Use broadband body phases to study lateral heterogeneity, attenuation, and scattering in the crust and mantle.

5. Earthquake Recurrence Statistics. Use earthquake recurrence statistics and related parameters to better understand the earthquake cycle and study how they can be used for prediction and forecasting purposes.

6. Earthquake Location Studies. Study techniques for improving the robustness, honesty, and portability of earthquake location algorithms, and participate in the construction and implementation of new standard travel-times for routine earthquake location.

7. NEIC Monthly Listing. Contribute both fault-plane solutions (using first-motion polarity) and moment tensors (using long-period body-phase waveforms) for all events of magnitude 5.8 or greater when sufficient data exists. Contribute waveform/focal-sphere figures of selected events.

Results

1. Moment Tensor Inversion. A paper listing the moment-tensor solutions for 426 moderate-to-large size earthquakes occurring from 1984 through 1987 has been published. A study of the 7 December 1988 Armenian earthquake was presented at the Fall 1989 AGU Meeting. The results indicate that the rupture consisted of two, and possibly three, subevents occurring at a centroidal depth of 5 km. The orientation of the mechanism changed during the rupture process, beginning as a thrust, but ending with strike-slip motion.

2. Other Source Parameter Studies. Linear and nonlinear methods of waveform inversion are being implemented to determine the fault-rupture history of large earthquakes. Preliminary results from a recent nonlinear inversion of teleseismic P-waveforms and strong-motion data recorded for the 1978 Tabas, Iran, earthquake suggest that this event ruptured mostly within the upper 15 km of the crust and occurred as a series of up to three distinct subevents. In addition, a linear method that inverts for the total slip as a function of position on the fault is being applied to teleseismic body-wave data recorded for recent large subduction earthquakes along the Mexico coast and for the October 1989 Loma Prieta earthquake.

3. Aftershock Source Properties. Work is continuing on the comparison of aftershock locations with distribution of fault slip derived from observed waveform data, especially for interplate thrust events.

4. Broadband Body-Wave Studies. A data set of relatively broadband shear-wave data has been assembled for the purpose of studying deep discontinuities in the Earth. Another data set is being assembled for the purpose of identifying near-receiver scattering of seismic waves. Software for both studies is being developed. Preliminary results indicate that, when deconvolving an instrument response, unless one is explicitly takes into account the properties of the filters being used, either bias or increased uncertainty in the results can be introduced, especially when taking integral measures of the displacement pulse. A new optimal method for deconvolving the instrument response is being developed.

5. Earthquake Recurrence Statistics. A paper has been submitted for publication in which the "generic," characteristic earthquake, recurrence interval, probability density function model has been extended to provide a marginal distribution for recurrence intervals which is independent of the uncertainty in the median recurrence interval. This permits the estimation of a single preferred value for the conditional earthquake forecast probability.

6. Earthquake Location Studies. As a result of participation in an IASPEI working group, tau-p travel time programs were provided on a UNIX platform. Subsequently, the tau-p package was modified to support the generation of a reference Earth model and results were presented to the IASPEI Commission on Practice. An article reviewing state-of-the-art earthquake location technology has been published as a chapter in the Encyclopedia of Solid Earth Geophysics. A journal article on the statistics of teleseismic body-wave travel-time residuals has been submitted for publication.

7. NEIC Monthly Listing. Since January 1981, first-motion fault-plane solutions for all events of magnitude 5.8 or greater have been contributed to the Monthly Listings. Since July 1982, moment-tensor solutions and waveform/focal-sphere plots have also been contributed. In the last six months, solutions for approximately 85 events have been published. An atlas of European seismicity is in preparation. Special maps showing the seismicity of Bangladesh and Pakistan have been made for the Office of Earthquakes,

Volcanos, and Engineering. A seismicity map of the Mediterranean Sea was made for UNDRO. A complete compilation of Mediterranean Sea seismicity is being prepared.

Reports

Buland, R. P., 1989, Earthquakes: location techniques, in James, D. E., ed. Encyclopedia of Solid Earth Geophysics: Van Nostrand Reinhold, p. 268-272.

Buland, R. P., 1990, Residual statistics: Bulletin Seismological Society of America (submitted).

Buland, R. P., and Nishenko, S. P., 1990, Preferred earthquake forecasts and conditional earthquake prediction: Bulletin Seismological Society of America (submitted).

Hartzell, S. H., and Mendoza, C., 1990, Simultaneous inversion of strong-motion records and teleseismic P-waveforms for fault slip and rupture times of the 1978 Tabas, Iran, earthquake [abs.]: Earthquake Notes (in press).

Hartzell, S. H., and Mendoza, C., 1990, Application of an iterative least-squares waveform inversion of strong motion and teleseismic records to the 1978 Tabas, Iran, earthquake: (in preparation).

Massé, R. P., and Needham, R. E., 1989, National Earthquake Information Center--NEIC: Earthquakes and Volcanos, v. 21, no. 1, p. 4-44.

Needham, R. E., and Sipkin, S. A., 1989, Teleseismic source parameters of the 7 December 1988 Armenian earthquake [abs.]: EOS (American Geophysical Union, Transactions), v. 70, no. 43, p. 1200.

Sipkin, S. A., 1990, Use of seismic-source-parameter catalogs to determine the roughness of a seismogenic zone [abs.]: Abstracts, ESC Workshop on Earthquake Source Mechanism and Seismotectonics, Madrid, Spain (in press).

Sipkin, S. A., and Lerner-Lam, A. L., 1989, Some caveats regarding broadband deconvolution [abs.]: EOS (American Geophysical Union, Transactions), v. 70, no. 43, p. 1194.

Sipkin, S. A., and Lerner-Lam, A. L., 1990, Pulse-shape distortion introduced by broadband deconvolution: (in preparation).

Sipkin, S. A., and Needham, R. E., 1988, Moment tensor solutions estimated using optimal filter theory--Global Seismicity, 1984-1987: Physics of the Earth and Planetary Interiors, v. 57, no. 3-4, 233-259.

Spence, W., Sipkin, S. A., and Choy, G. L., 1989, Measuring the size of an earthquake: Earthquakes and Volcanoes, v. 21, no. 1, p. 58-63.

Seismicity and Tectonics

9920-01206

William Spence
Branch of Global Seismology and Geomagnetism
U.S. Geological Survey
Denver Federal Center
Box 25046, Mail Stop 967
Denver, Colorado 80225
(303) 236-1506

Investigations

Studies carried out under this project focus on detailed investigations of large earthquakes, aftershock series, tectonic problems, and Earth structure. Studies in progress have the following objectives:

1. Determine the maximum depth and degree of velocity anomaly beneath the Rio Grande Rift and Jemez Lineament by use of a three-dimensional, seismic ray-tracing methodology (W. Spence and R. S. Gross).

2. Explore the consequences of the slab pull force acting at the zone of plate bending that is downdip of the lower end of an interface thrust zone (W. Spence and W. Z. Savage).

3. Develop a tectonic model for the Carpathian arc, Romania (G. Purcaru and W. Spence).

Results

1. The Jemez lineament is the most active volcanic feature in the southwestern United States. It is the southeastern tectonic boundary of the Colorado Plateau, it extends about 800 km from the Raton-Clayton volcanic field in northeast New Mexico to the San Carlos volcanic field in Arizona, and it crosses the Rio Grande rift at the Jemez Mountains. The lateral variations in P-wave velocity in the upper mantle beneath the central Jemez lineament and the central Rio Grande rift were investigated using teleseismic P-wave delays measured at a 23-station seismic network. The inversion used a method of damped, least-squares and velocity interpolations within a three-dimensional grid of points, rather than using blocks of fixed P-wave velocity. To a depth of about 160 km, the upper mantle P-wave velocity beneath the Rio Grande rift and Jemez lineament is very similar to that of the low velocity zone of the Basin and Range, being 4-6 percent lower than the P-wave velocity beneath the High Plains Province. While lateral variations showing low P-wave velocity in the upper mantle beneath the Rio Grande rift were not resolvable, the inversion shows a primary trend of 1-2 percent lower P-wave velocity underlying the Jemez lineament, at the depth interval of about 50-160 km. This result extends at least from Mt. Taylor through the Jemez volcanic center and through the Rio Grande rift. Three independent calculations of resolution indicate that these results are well-resolved. The most likely interpretation is that there are additional

concentrations of partial melt in the upper mantle beneath the Jemez lineament but not beneath the Rio Grande rift. This interpretation is consistent with the much greater volume of volcanism during the last 4.5 m.y. originating with Jemez lineament than originating with the Rio Grande rift. This result implies that the present volcanic potential of the Jemez lineament greatly exceeds that of the Rio Grande rift. It is argued that the source zones for magmas of the Jemez lineament move with the North American plate. If lithospheric thickness is defined as the thickness of the unit that participates coherently in plate motions, then the lithosphere of the western United States contains the source of the Jemez volcanics (and the "low-velocity zone") and has a thickness >200 km.

2. Interface thrust zones typically have dips in the range 8-15°, whereas lithospheres that are subducted into the mantle typically have dips in the range 40-70°, giving an average dip increase in the mantle of about 45°. These dip increases often occur within 40-60 km of plate length. These zones of sharp dip increases (slab bends) have not been given much attention because generally they lack large earthquakes. This is in sharp contrast to the well-studied zones of bending beneath oceanic trenches where there are frequent normal-faulting earthquakes. It has been noted by Ruff and Kanamori (1983) that great, interface thrust earthquakes terminate their downdip ruptures at the updip part of mantle slab bends. Spence (1987) showed that the slab pull force is the primary force that causes shallow, subduction earthquakes. Spence also interpreted the mantle slab bends as a pivot for the summed slab pull force of the more deeply subducted plate. In this study, we model the stress distribution in the mantle slab bend, acting under a slab pull load. We find that the observed lack of earthquakes in the mantle slab bend is due to ductility there. However, the strength of the work-hardened ductile portion of the slab bend is more than sufficient to transmit the slab pull load into the shallow subduction zone.

3. In the Vrancea region of the southeastern Carpathian arc, earthquakes extend to depths of 200 km, and have magnitudes as great as 7.5. Although tectonic reconstructions for this concave-westward arc are not definitive, especially for pre-Miocene time, we know that westward subduction at the Carpathian trench has terminated from northwest to southeast. Oceanic lithosphere is completely subducted and continental lithosphere is at the arc. Seismicity is most pronounced at the southeastern corner of the arc. Based on a variety of evidence, we propose a new tectonic model with a continuous subducted lithosphere, in which: (1) above 40 km depth the subducted lithosphere has a shallow dip; (2) between 40 and 70 km depth the dip of subducted plate steepens to near vertical; (3) the bending of the subducted plate is mostly aseismic; (4) the m_B 7.5 earthquakes at depths of 100-160 km result from downdip plate extension; (5) this extension results from the sinking of plate at depths of 100-160 and deeper; (6) stresses due to the sinking of deeply-subducted plate are communicated updip past the zone of plate bending into the shallow-dipping part of the plate; and (7) stresses in the shallow-dipping plate are communicated to the overriding plate and lead to broad regional deformation there.

Reports

Spence, William, and Gross, R. S., 1990, A tomographic glimpse of the upper mantle source of magmas of the Jemez lineament, New Mexico: Journal of Geophysical Research, v. 95 (in press).

United States Earthquakes

9920-01222

Carl W. Stover
Branch of Global Seismology and Geomagnetism
U.S. Geological Survey
Denver Federal Center
Box 25046, Mail Stop 967
Denver, Colorado 80225
(303) 236-1500

Investigations

One hundred and seventy-five earthquakes in the United States and Puerto Rico, were canvassed by a mail questionnaire for felt and damage data during the period October 1, 1989 to March 31, 1990. Seventy-one of these earthquakes occurred in California, 56 in Alaska, and 43 in eighteen other states, and 5 in Puerto Rico.

A damage survey of the epicentral region and the San Francisco Bay Area was made by Carl Stover, Glen Reagor, Frank Baldwin, and Lindie Brewer for the October 18, 1989 UTC, Santa Cruz Mountains (Loma Prieta), California, earthquake. The data is used for evaluating intensities and mapping the felt area.

Write computer programs to create a CD-ROM to be used as an earthquake data base, retrieval software for the data base, and a user's manual for the earthquake data packages for any IBM-compatible microcomputer equipped with a ISO 9660 interface.

Maintain and update the Earthquake Data Base System.

Results

Nine earthquakes caused damage during this period--eight in California and one in Missouri. Five of the California earthquakes and the Missouri earthquakes had maximum intensities of VI; two other California earthquakes had maximum intensities of VII; and the Santa Cruz Mountains (Loma Prieta), California, earthquake had a maximum intensity of IX. The Santa Cruz Mountains (Loma Prieta), California, earthquake on October 18, 1989 UTC (magnitude 7.1 M_S) caused 62 deaths, 3,757 injuries, over $6 billion in property damage; and was felt over a land area of 170,000 km^2 of California and Nevada. The most extensive damage occurred in Oakland, San Francisco, Santa Cruz, Watsonville, Hollister, and the rural area of the Santa Cruz Mountains near the San Andreas fault zone.

A Global Hypocenter Data Base CD-ROM has been created along with the retrieval software on two floppy disks, and a User's Guide. The CD-ROM contains 7 global and 12 regional catalogs covering a time period from 2100 BC through 1988. One floppy disk contains the retrieval program, the other contains a digitized map data base for the mapping portion of the software. The User's Guide is a step-by-step explanation of how to retrieve and display the data from the CD-ROM. Contact Glen Reagor at (303) 236-1500 for data or operational details.

The Earthquake Data Base System (EDBS) has been updated through the current PDE and through October 1989 Monthly Listing. Data are available on paper, tape, or floppy disk. This data base has been accessed 265 times by external users between October 1, 1989 and March 31, 1990. The most common users have been engineering companies, insurance companies, universities, government agencies, lawyers, and individuals. Contact Glen Reagor at (303) 236-1500 for information on the EDBS.

United States Earthquakes, 1985 (Bulletin) has been completed and submitted for printing.

Reports

Stover, C. W., Reagor, B. G., Baldwin, F. W., and Brewer, L. R., 1990 Preliminary isoseismal map for the Santa Cruz (Loma Prieta), California, earthquake of October 18, 1989 UTC: U.S. Geological Survey Open-File Report 90-18, 24 p.

Reagor, B. G., 1990, Computer programs for creation of the Global Hypocenter Data Base CD-ROM and its retrieval software (including the User's Guide and the Global Hypocenter Data Base Information packet).

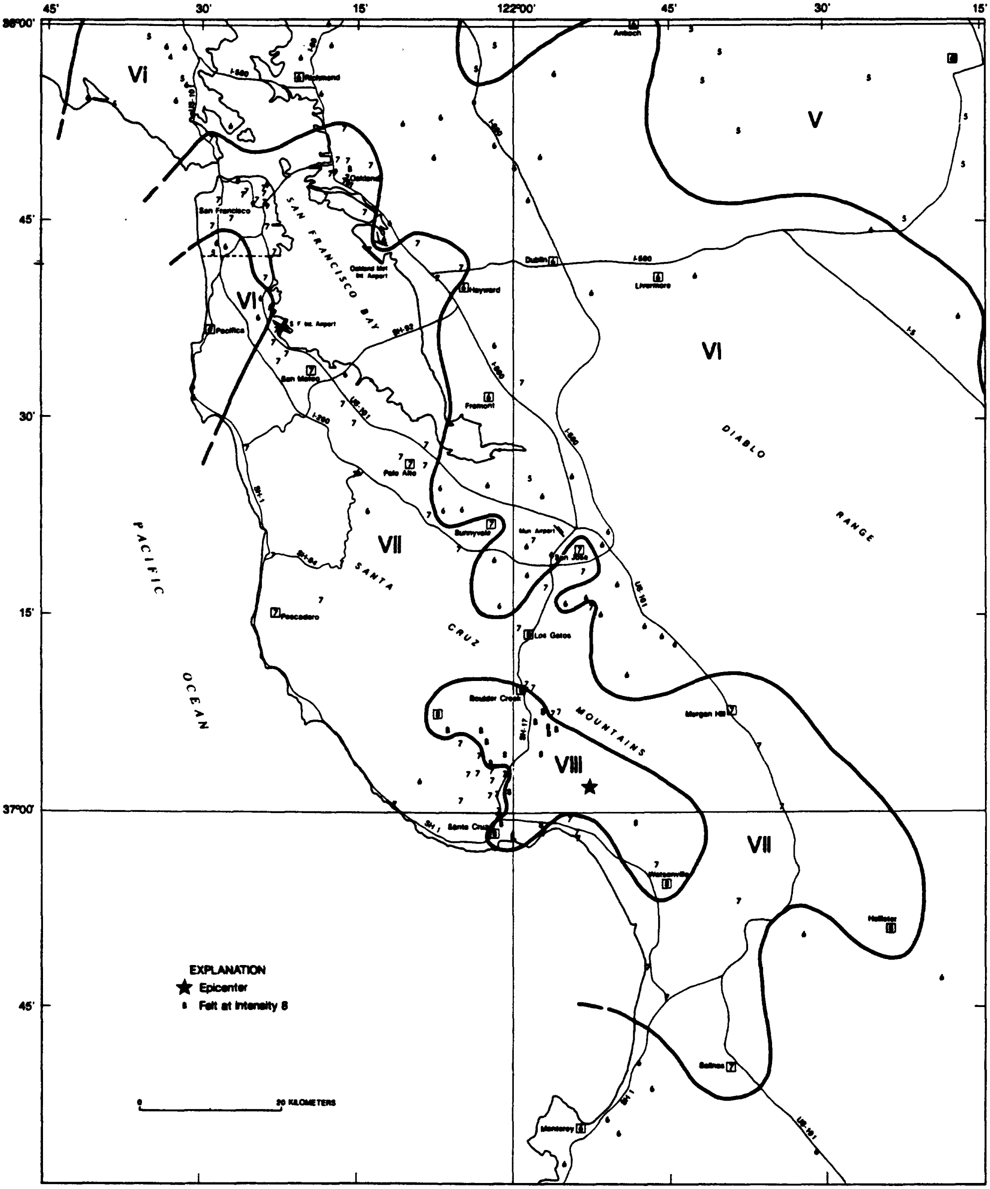

Figure 2. Isoseismal map for the San Francisco Bay region for the Santa Cruz (Loma Prieta), California, earthquake of October 18, 1989 UTC.

Global Seismicity Mapping

9920-04321

Susan K. Goter
Branch of Global Seismology and Geomagnetism
U.S. Geological Survey
Denver Federal Center
Box 25046, Mail Stop 969
Denver, Colorado 80225
(303) 236-1506

Investigations

1. State Seismicity Maps. Produce and distribute seismicity maps on shaded, elevation-tinted state map bases.

2. World Seismicity Poster. Produce and distribute a full-color poster showing earthquakes plotted on orthographic-projection base maps of the world.

Results

1. State Seismicity Maps. The aim of the state seismicity maps is to provide the most complete picture possible of where earthquakes have occurred historically in relation to geographic, geomorphic, and cultural features. This is accomplished by selecting or compiling an earthquake database that is then plotted and printed on a shaded, elevation-tinted base map.

Since this project began in 1988, state seismicity maps have been completed for California, Hawaii, and Alaska. Work is currently underway to produce a similar map for the state of Utah. This map will display earthquakes that occurred between 1884 and 1989. Although the magnitude threshold for earthquakes plotted on the map varies throughout the historical record, the lower magnitude cut-off for earthquakes that occurred after 1962 is 2.5. Epicenter symbol sizes plotted on the map are scaled into four magnitude categories. Earthquakes that occurred since 1975 are distinguished on this map from earlier events by the intensity of color of the epicentral symbol.

The resulting full-color maps are distributed to the research community worldwide, as well as to each high school in the state covered by the map.

2. World Seismicity Poster. Orthographic-projection views of three rotations of the Earth are shown on the poster in order to depict patterns of seismicity throughout the world. Each hemispherical view shows earthquakes plotted on a shaded, elevation-tinted base map. Because the orthographic projection simulates viewing a globe from space, the viewer is able to get a more accurate picture of seismicity patterns of our spherical Earth than can be achieved from the more commonly used Mercator projection.

The World Seismicity poster displays selected hypocenters for earthquakes that occurred from January 1979 to December 1988. Symbols are plotted at epicentral locations. Symbol colors represent three depth-of-focus classes. Symbol sizes are scaled into three magnitude ranges. Within each magnitude category, the earthquake database was thinned by plotting no more than one epicenter in any single cell of a 0.25 degree grid. Over 23,000 separate epicenter locations shown on the poster represent over 97,000 epicenters.

The resulting posters are distributed to the research community worldwide and are also available for purchase.

Reports

Goter, S. K., 1990, World Seismicity 1979-1988: U.S. Geological Survey NEIC Poster 1.
Goter, S. K., 1990, Seismicity of Utah, 1884-1989 (in preparation).

Data Processing Section

9920-02217

John Hoffman
Branch of Global Seismology and Geomagnetism
U.S. Geological Survey
Albuquerque Seismological Laboratory
Building 10002, Kirtland AFB-East
Albuquerque, New Mexico 87115-5000
(505) 844-4637

Investigations

1. IRIS/USGS Data Collection Center. The Incorporated Research Institutions for Seismology (IRIS) have designated the Albuquerque Seismological Laboratory (ASL) to be the data collection center (DCC) for a new global network of digitally recording seismograph stations. A new data processing system has been installed at the ASL, and a new data format has been developed which is becoming the international standard for seismic data recording and distribution.

2. Data Processing for the Global Digital Seismograph Network. All of the data received from the Global Digital Seismograph Network and other contributing stations is regularly reviewed, checked for quality, and archived at the ASL.

3. Network Volume Program. Data from the GDSN stations and other contributing networks are assembled into network volumes which are distributed to regional data centers and other government agencies.

Results

1. IRIS/USGS Data Collection Center. IRIS has developed the instrumentation for a network of 50 or more digital recording seismograph stations which will be primarily installed by USGS personnel over the next several years. All of the data from this network will be forwarded to the DCC located at the ASL. As part of this program, IRIS funded much of the new hardware required by the DCC to process this large amount of data. A new digital format known as the Standard for the Exchange of Earthquake Data (SEED) was developed by the USGS in cooperation with both IRIS and the Federation of Digital Broadband Seismograph Networks. The SEED format has been well received by the seismic community and is rapidly becoming a standard for both recording and distributing seismic data around the world. During the past year, most of the digital data archived at the ASL on magnetic tape has been transferred to an optical jukebox memory system which can automatically select any of 50 optical platters each of which can store up to 3.2 gigabytes of seismic data. In addition, the ASL has received 140 digital tapes containing seismic data recorded by the IRIS/IDA network of eight stations, four of which are located in the Soviet Union. These tapes contain approximately 14 gigabytes of seismic data which is presently being transferred to optical disk system. About 75 gigabytes of seismic data have

been recorded on the optical disk system, and an additional 35 gigabytes will be added during the next 6 months. At that time, all of the digital data ever received at the ASL will be online and available for instant recall. The optical platters on which this seismic data is archived have an estimated shelf life of 100 years.

2. Data Processing for the Global Digital Seismograph Network. During the past six months, 597 digital tapes (134 SRO/ASRO, 238 DWWSSN, 115 CDSN, 110 IRIS-1) from the Global Network and other contributing stations were edited, checked for quality, corrected when feasible, and archived at the ASL. The Global Network, supported by the USGS, is presently comprised of 12 SRO/ASRO stations, 14 DWWSSN stations, and one IRIS-1 station. In addition, there are 10 contributing stations which include the five stations from China Digital Seismograph Network and five IRIS-1 stations. Data from the eight IRIS/IDA stations, including the four in Russia, are also being received on a rather irregular basis. The data from the four Russian stations are frequently late due to delays in shipments between Russia and the United States.

3. Network Volume Program. The network volume program is a continuing program which assembles all of the data recorded by the Global Digital Seismograph Network plus the various contributing stations mentioned in the previous paragraph, for a specific calendar days or days onto one magnetic tape. This tape includes all the necessary station parameters, calibration data, transfer functions, and time-correction information for each station in the network. All of these tapes are recorded in the new SEED format, and copies are distributed to several university and government research groups for detailed analysis. These tapes are assembled approximately 60 days after real time in order to provide a sufficient time frame for recording the data at the stations, forwarding this data to the ASL, and processing the data at the DCC. The amount of data produced by the various networks each day is from 80 to 100 megabytes.

National Earthquake Information Service

9920-01194

Waverly J. Person
Branch of Global Seismology and Geomagnetism
U.S. Geological Survey
Denver Federal Center
Box 25046, Mail Stop 967
Denver, Colorado 80225
(303) 236-1500

Investigations and Results

The Quick Epicenter Determinations (QED) continues to be available to individuals and groups having access to a 300- or 1200-baud terminal with dial-up capabilities to a toll-free WATS number or a commercial telephone number in Golden, Colorado. It is also accessible via GEONET and public TYMNET. The time period of data available in the QED is approximately 3 weeks (from about 2 days behind real time to the current PDE in production). The QED program is available on a 24-hour basis, 7 days a week. From October 1, 1989, through March 31, 1990, there have been 8,179 logins to the QED program. A daily QED message, 7 days behind real time, is transmitted to 22 different agencies in the U.S. and throughout the world via electronic mail, including a scientific bulletin board operated by Dr. Francis Wu at the State University of New York at Binghamton. This bulletin board is accessible by anyone who is connected to BITNET. The daily QED message is also distributed to another 13 agencies via U.S. government communications (VADATS/DTS/AUTODIN), including worldwide distribution on the communications system of the World Meteorological Organization.

NEIS is making extensive use of electronic mail for data acquisition. Data are now being received via GEONET, TYMNET, internet, BITnet, DECNET/SPAN and uucp on a regular basis. Agencies sending data to NEIS via electronic mail include the following:

U.S. Bureau of Reclamation, Denver
Geological Survey of Canada, Ottawa
Geological Survey of Canada, Sidney, BC
Universidad Autonoma de Mexico, Mexico City
Universidade de Sao Paulo, Brazil
University of Bergen, Norway
Instituto Nazionale di Geofisica, Rome, Italy
Centro Cultura Scientifica Ettore Majorana, Erice, Sicily
Centre Seismologique Euro-Mediterraneen, Strasbourg, France
University of Thessaloniki, Greece
Kandilli Observatory, Istanbul, Turkey
Harvard University, Cambridge, MA (Centroid, Moment Tensor Solutions)

In addition, the following agencies contribute data to the PDE program by computer file transfer or remote login via the computer networks:

USGS Alaska Seismic Project, Menlo Park
USGS/California Institute of Technology, Pasadena
USGS Fredericksburg Observatory, Corbin, Virginia
USGS Guam Observatory, Mariana Islands
University of California, Berkeley
University of Southern California, Los Angeles
University of Washington, Seattle
John Carroll University, Cleveland, Ohio
North Illinois University, DeKalb
Oklahoma Geophysical Observatory, Leonard

Data acquisition by electronic mail is in the process of being established with Graefenberg Observatory in Germany and the Bureau Central Seismologique Francaise in France.

Telegraphic data are now being exchanged with the USSR on most larger earthquakes. The Soviet data are being received from the Central Seismological Observatory, Obninsk, under the auspices of the World Data Center system. Our designation as World Data Center A for Seismology played a key role in permitting this exchange to be established.

Data from the People's Republic of China via the American Embassy continue to be received in a very timely manner and in time for the PDE publication. We continue to receive four stations on a weekly basis from the State Seismological Bureau of the People's Republic of China. The Bulletins with additional data are now being received in time for the Monthly. We are currently establishing an exchange of bulletin data with them via floppy disk through the Embassy.

Special efforts are being made to receive more data from the Latin American countries on a more timely basis. The increased availability of telefax is permitting much more interaction with Latin American countries than in the past.

We have rapid data exchange (alarm quakes) with Centre Seismologique European-Mediterranean (CSEM), Strasbourg, France, and Instituto Nazionale de Geofisica, Rome, Italy, and Sicily, and data by telephone from Mundaring Geophysical Observatory, Mundaring, Western Australia and Pacific Tsunami Warning Center in Honolulu. The geophysical laboratory in Papeete, French Polynesia contributes a single-station estimate of seismic moment within about 24 hours of a large event in the Pacific region.

The Monthly Listing of Earthquakes is up to date. As of March 31, 1990, the Monthly Listing and Earthquake Data Report (EDR) have been completed through November 1989. The total number of events published for the period June through November 1989 was 7,355. By comparison, for 1970 only 4,353 events were published in the PDE for the entire year. Radiated energy, moment tensor, P-wave first-motion and broadband depth solutions continue to be determined by the USGS when possible and published in the Monthly Listing and EDR for any earthquake having an m_b magnitude $\geq$ 5.8. Centroid moment tensor solutions contributed by Harvard University continue to be published in the Monthly Listing and EDR. Waveform plots are being published for selected events having m_b magnitudes $\geq$ 5.8.

The Earthquake Early Alerting Service (EEAS) continues to provide information on recent earthquakes on a 24-hour basis to the Office of Earthquakes, Volcanoes and Engineering, scientists, news media, other government agencies, foreign countries, and the general public.

Forty-six releases were made from October 1, 1989, through March 31, 1989. In the United States, the most significant earthquakes were the magnitude 7.1 Loma Prieta earthquake of October 17, 1989, which kept the NEIS staff working continually for more than 48 hours. The second important U.S. earthquake was a magnitude 5.5 in southern California on February 28, 1990. The most significant foreign earthquakes were: a magnitude 5.4 in northeastern China on October 18, 1989; a magnitude 7.1 in the Solomon Islands on October 27; a magnitude 5.9 in Algeria on October 29; a magnitude 5.1 in Sichuan Province, China on November 20; a magnitude 5.6 in southern Iran on November 20; a magnitude 7.4 on Mindanao, Philippine Islands on December 15; a magnitude 5.5 earthquake in Newcastle, Australia, which killed nine people on December 27 (probably the first earthquake deaths in the country); a magnitude 7.0 in the Bismarck Sea on December 30; a magnitude 5.1 in eastern China on February 9, 1990; a magnitude 6.1 in Pakistan on March 4; a magnitude 7.1 in the Vanuatu Islands on March 4; and a magnitude 7.0 in Costa Rica on March 25.

Reports

Monthly Listing of Earthquakes and Earthquake Data Reports (EDR); six publications from June 1989 through November 1990. Compilers: W. Jacobs, L. Kerry, J. Minsch, R. Needham, W. Person, B. Presgrave, W. Schmieder.

Person, Waverly J., Seismological Notes: Bulletin of the Seismological Society of America, v. 79, no. 5, November-December 1988; v. 79, no. 6, January-February 1989; v. 80, no. 1, March-April 1989; v. 80, no. 2, May-June 1989.

Preliminary Determination of Epicenters (PDE); 35 weekly publications from October 5, 1989, numbers 37-89 through March 29, 1990, 10-90. Compilers: W. Jacobs, L. Kerry, J. Minsch, R. Needham, W. Person, B. Presgrave, W. Schmieder.

Quick Epicenter Determination (QED) (daily): Distributed only by electronic media.

Monthly Listing of Earthquakes, v. 60, no. 3, July-September 1989, v. 60, no. 4; October-December 1989 (Microfiche): Seismological Research Letters, Eastern Section, SSA. Compilers: W. Jacobs, L. Kerry, J. Minsch, R. Needham, W. Person, B. Presgrave, W. Schmieder.

Person, Waverly J., "Earthquakes and Volcanoes," v. 20, no. 6 "Earthquakes," July-August 1988; v. 21, no. 2 "Earthquakes," September-October 1988.

Seismic Review and Data Services

9920-01204

James N. Taggart
Branch of Global Seismology and Geomagnetism
U.S. Geological Survey
Denver Federal Center
Box 25046, Mail Stop 969
Denver, Colorado 80225
(303) 236-1506

Investigations

This project distributes copies at cost of filmed seismograms from the Worldwide Standardized Seismograph Network (WWSSN), the Canadian Standard Network (CSN), and various stations with historical (pre-1963) records. In addition, the project receives and processes the original WWSSN analogue seismograms for photography, and afterward returns them to the stations.

Results

A contract for the photography of original WWSSN seismograms and duplication of filmed seismograms, covering fiscal years 1990-1992, was finally signed in mid-December. Problems with moving and realigning the government-owned flatbed camera further delayed the start of photography until late February. As a result, only 60 station-months of WWSSN seismograms had been photographed by the end of this reporting period, and another 110 station-months were ready to be photographed. Nevertheless, the new contractor, American Micro Data of Denver, Colorado, is meeting quality specifications and should be on schedule (about 700 station-months completed) by the end of the fiscal year.

Nine standing orders for WWSSN and two standing orders for CSN fiscal year 1990 filmed seismograms have been received. The number of active stations in both networks continues to decrease slightly each year. As a result, the cost of the standing orders was reduced for the third successive year. CSN films through September 1989 have been received from Ottawa.

Fifteen special orders for filmed WWSSN seismograms have been filled under the new contract during this reporting period. About 20 additional requests have been received, mainly for filmed seismograms of the Loma Prieta, California, earthquake. Only a limited number of these seismograms have been received, and very few have been photographed.

This project is the principal source of filmed analogue seismograms for distribution through World Data Center A for Seismology, which was designated a part of the Branch structure in October 1986. The World Data Centers commonly exchange data for later distribution in their own regions of coverage.

Computer and Data Analysis Services

9920-04151

Madeleine Zirbes
Branch of Global Seismology and Geomagnetism
U.S. Geological Survey
Denver Federal Center
Box 25046, Mail Stop 967
Denver, Colorado 80225
(303) 236-1506

Investigations

1. NEIC Monthly Listing. Contribute waveform data for all events of magnitude 5.8 or greater when sufficient data exists.

2. Network Day Tape Support. Develop, distribute and support FORTRAN programs to access network-day tapes and station tapes.

3. SEED Support. Develop, distribute and support software for the Standard for the Exchange of Earthquake Data (SEED) format.

4. Event Tape Production and Distribution. Produce and distribute event tapes.

5. Event CD-ROM Production and Distribution. Produce and distribute event CD-ROM data.

Results

1. NEIC Monthly Listing. Since July 1982, digital waveform plots have been contributed to the Monthly Listings. USGS fault-plane and moment tensor solutions, and broadband data have also been incorporated into the focal sphere plots.

2. Network Day Tape Support. FORTRAN software to read and extract digital data from station tapes (1976-1979) and network day tapes (1980-1987) has been developed and distributed to the research community worldwide. Users are supported on a variety of computers.

3. SEED Support. A new Standard for the Exchange of Earthquake Data (SEED) has been created and tapes are now being produced (1988 to present) and distributed by the Albuquerque Seismic Laboratory. FORTRAN software has been developed to read and extract the digital data from the SEED tapes and this software is being made available to the research community.

4. Event Tape Production and Distribution. Event tapes have been produced from network day tapes for data from 1980 through 1986 for all events with magnitude 5.5 or greater. These tapes are distributed to 25 institutions worldwide, along with a waveform catalog that provides a visual display of the data available for each event.

5. Event CD-ROM Production and Distribution. Data from the event tapes are reformatted and sent to a CD-ROM mastering facility for replication. Five volumes have been produced, covering January 1980 through September 1985. The CD-ROMs are being distributed to over 200 Universities across the United States and geophysical research institutes worldwide. Retrieval software, SONIC (C) and CDRETRV (FORTRAN), has been developed for the IBM/PC/AT/386 compatibles and distributed. It allows easy access to the digital data.

Reports

CD-ROM Products

NEIC Earthquake Digital Data, Volume 5, January 1985 through September 1985.

General Earthquake Observation System (GEOS)
General Analysis and Playback Systems (GAPS)

9910-03009

Roger D. Borcherdt
Branch of Engineering Seismology and Geology
U.S. Geological Survey
345 Middlefield Road, MS 977
Menlo Park, California 94025
(415) 329-5619

Investigations

1. Complete construction and development of 100 portable, broad band, high-resolution digital data acquisition systems for use in a wide variety of active and passive seismic experiments.

2. Completed Program Plan for Large Array Seismic Observations **(LASO)**

3. Develop PC-based capabilities for retrieval, processing, and archival of large volumes of GEOS data.

4. Conduct Eurasian Seismic Studies Program.

5. Conduct Aftershock Investigations for Loma Prieta earthquake.

Results

1. The following design modifications for 55 new GEOS systems are in final testing stages:

   a.) Expanded data buffer (1 M/sample) design by M. Kennedy.
   b.) Extended gain with improved noise for amp/filter board by J. van Schaack and G. Jensen.
   c.) New tape controller for new 16 Mbyte tape cartridges by Phoenix Data, Inc.
   d.) Software drivers for mag tape controller by G. Maxwell.
   e.) Software for RS 232 for use in satellite, radio, and telephone telemetry and data transfer to field computer by G. Maxwell.
   f.) Software for incorporating design modifications, teleseismic trigger, and field playback are being pursued by G. Maxwell.
   g.) Completion of the 55 new GEOS units is expected by September 1990. Testing of first article is in progress but has been slowed by limited personnel resources.

2. An extensive scientific plan for management of a Large Array Seismic Observation program was developed and presented to office management by the **LASO** executive committee (R.D. Borchert, chair, M. Celebi, J. Filson, H.M. Iyer, M. Johnston, W. Mooney, A. Rogers.

3. GEOS maintenance laboratory under direction of J. Sena together with field support of G. Sembera and C. Dietel has facilitated the execution of several experiments within the last year, including experiments at Parkfield, Anza, Armenia, teleseismic receiver function experiments near Pace, Arizona, and ground response and near-source investigations of Loma Prieta earthquake.

4. Significant efforts have been devoted to planning for the Eurasian Seismic Studies Program in conjunction with J. Filson and D. Simpson. PC-based data playback and analysis capabilities (software and hardware) have been developed in conjunction with W. Lee, E. Cranswick, and C. Mueller. Selectable Omega/WWV timing capabilities for GEOS have been developed in conjunction with G. Jensen. Hardware and sensors required for deployment have been acquired for shipment on June 11, 1990.

Reports

Borcherdt, R.D. (editor), 1989, Results and data from seismologic and geologic studies of the earthquakes of December 7, 1988 near Spitak, Armenia, U.S.S.R.: U.S. Geological Survey Open-File Report 89-163, vols. I-V, 1958 p.

Borcherdt, R.D., Glassmoyer, G., Der Kiureghian, A., and Cranswick, E., 1989, Effect of site conditions on ground motions in Leninakan, Armenia, U.S.S.R. _in_ Borcherdt, R.D. (editor), 1989, Results and data from seismologic and geologic studies of the earthquakes of December 7, 1988 near Spitak, Armenia, U.S.S.R.: U.S. Geological Survey Open-File Report 89-163A, v.1, 188 p.

Borcherdt, R.D., Simpson, D., Langer, C., Sembera, G., Dietel, C., Cranswick, E., Mueller, C., Noce, T., Andrews, M., and Gasssmoyer, G., 1989, Seismological investigations (objectives and field experiments), _in_ Borcherdt, R.D. (editor), 1989, Results and data from seismologic and geologic studies of the earthquakes of December 7, 1988 near Spitak, Armenia, U.S.S.R.: U.S. Geological Survey Open-File Report 89-163A, v. 1, 188 p.

Borcherdt, R.D., Maxwell, G., Sena, J., Kennedy, M., Jensen, G., and van Schaak, J., 1989, Instrumentation used for seismological investigations -- Digital recording systems _in_ Borcherdt, R.D., (editor), 1989, Results and data from seismologic and geologic studies of the earthquakes of December 7, 1988 near Spitak, Armenia, U.S.S.R.: U.S. Geological Survey Open-File Report 89-163A, v.1, 188 p.

Agbabian, M.S., Borcherdt, R.D., Der Kiureghian, A., Filson, J.R., Krimgold, F., Lew, H.S., Mileti, D.S., Noji, E., O'Rourke, T., Schiff, A., Simpson, D., Sharp, R.V., Wyllie, Jr., L.A., Yanev, P.I., Armenian earthquake reconnaissance report: Jour. Earthq. Eng. Res. Inst., Spec. Suppl. Aug. 1989, 175 p.

Borcherdt, R.D., Celebi, M., Filson, J., Iyer, H.M., Johnston, M., Mooney, W., Rogers, A., 1989, A program for Large Array Seismic Observation (LASO): U.S. Geological Survey Administrative Report, 116 p.

Filson, J.R., Borcherdt, R.D., Langer, C., and Simpson, D., 1989, Seismology, in Wyllie, Jr., L.A., and Filson, J.R., eds., Armenian earthquake reconnaissance report: Earthquke Engineering Research Institute, Spectra, Special Supplement, August 1989, 175 p.

Borcherdt, R., Glassmoyer, G., Andrews, M., and Cranswick, E., 1989, Effects of site conditions on ground motion and damage, in Wyllie, Jr., L.A., and Filson, J.R., Armenian earthquake reconnaissance report: Earthquake Engineering Research Institute, Spectra, Special Supplement, August, 1989, 175 p.

Cara, M., Cisternas, A., Dorbath, L., Haessler, H., Romanowicz, B., Elyutin, A., Grazier, V., Givishiani, A., Mostinsky, A., Shehalin, N., Tumarkin, A., and Borcherdt, R., 1989, Plan for Spitak (Armenia 7.12.88) earthquake database: IASPEI-ICL Workshop on Regional Data Centers, Istanbul, Turkey, August 24, 19____, Proceedings, ______ p.

Borcherdt, R.D., Langer, C., Filson, J.R., Simpson, D.W., Glassmoyer, G., Andrews, M., and Cranswick, E., 1990, On the rupture zone and effects of local geologic conditions on damages and ground motions for the Armenian earthquakes of December 7, 1988: National Conference on Earthquake Engineering, 4th, Palm Springs, Calif., 1990, Proceedings, in press.

Borcherdt, R.D., Glassmoyer, G., Cranswick, E., and Andrews, M., 1989, Observed effects of site conditions on damages and ground motions in relation to one-dimensional model estimates of ground response for Leninakan, Armenia, U.S.S.R. [abs.]: EOS (American Geophysical Union Transactions), v. 70, p. 1199.

Frankel, A., Filson, J., Borcherdt, R., and Vidale, J., 1989, Numerical simulations of strong ground motions in the Leninakan basin produced by the 1988 Armenian earthquake and its aftershocks: EOS (American Geophysical Union Transactions), v. 70, p. 1200.

(See projects Borcherdt et al., 9910-02089, 9910-02689; Iyer; McGarr; Fletcher; Boatwright for additional reports based on GEOS data sets.)

National Strong-Motion Network: Data Processing

9910-02757

A.G. Brady
Branch of Engineering Seismology and Geology
345 Middlefield Road, MS 977
Menlo Park, California 94025
(415) 329-5664

Investigations

1. Processing data from the Loma Prieta earthquake, including the determination of long-period limits.

2. Software improvements for PC network in various staff offices within the Branch, and for the processing program.

3. Cataloging all strong-motion records from the cooperative network operated by USGS for 1987.

Results

1. Digitizing and processing of the records from Loma Prieta has commenced. Digitization is complete on records from 38 stations, and the first volume of processed data, with its accompanying tape, is available for distribution. Within the USGS, investigations have shown the contribution to damage of the Bay Bridge from ground resonances in the vicinity of the Oakland abutment.

2. Many subroutines in the accelerogram processing program have been streamlined and those parts dependent on current USGS hardware have been separated and treated for ability to transport. A limited PC version to be attached to a CDROM of strong motion uncorrected data is in preparation.

3. The annual report describing all strong-motion records recovered in a single year is called a "Catalogue of U.S. Geological Survey Strong-Motion Records, 19--" and its Table 1 lists all important parameters obtainable from the original record: earthquake epicenter and magnitude, station name and location, trigger and S-T times, and component directions, peak acceleration and duration.

Reports

Maley, R., A. Acosta, F. Ellis, E. Etheredge, L. Foote, D. Johnson, R. Porcella, M. Salsman, and J. Switzer, 1989, U.S. Geological Survey strong-motion records from the northern California (Loma Prieta) earthquake of October 17, 1989: U.S. Geological Survey Open-File Report No. 89-568, 85 p.

Brady, A.G., and P.N. Mork, 1990, Loma Prieta, California earthquake October 18 (GMT) 1989, processed strong-motion records, volume 1: U.S. Geological Survey Open-File Report 90-247, 274 p.

Porcella, R.L., and J.C. Switzer, 1989, Catalogue of U.S. Geological Survey strong-motion records, 1987: U.S. Geological Survey Circular 1044, 44 p.

National Strong-Motion Network: Engineering Data Analysis

9910-02760

A.G. Brady and G.N. Bycroft
Branch of Engineering Seismology and Geology
345 Middlefield Road, MS 977
Menlo Park, California 94025
(415) 329-5664 or (415) 329-5665

Investigations

Buildings and dams with extensive instrumentation triggered records from the M7.1 Loma Prieta earthquake of October 17, 1989. Anderson Dam is the closest USGS station to the epicenter, at 27 km, and is instrumented with 21 data channels of acceleration. Horizontal accelerations at the crest, downstream and left abutment from the recorders peaked at 0.39, 0.26, and 0.08 g, respectively. These records were studied for determination of the long-period content remaining relatively noise-free.

Results

A comparison of the Fourier amplitude spectra of the left abutment, 243° component, with that of a reference trace from the same film, processed in the same way, shows that these spectra have barely merged at periods as long as 40 sec, a time interval equal to the digitized record length. At a period of 10 sec, equal approximately to the estimated rupture duration, there is at least an order of magnitude between these spectral ordinates.

Ten-second waves crossing the array of instruments associated with this dam remain remarkably coherent. Having displacement amplitudes of 12 cm, the errors remain less than 1 cm, in accordance with estimates of displacement accuracy made from digitization tests.

Reports

Brady, A.G., and P.N. Mork, 1990, Loma Prieta, California, earthquake of October 18 (GMT), 1989, processed strong-motion records, volume 1: U.S. Geological Survey Open-File Report 90-247, 274 p.

Branch of Engineering Seismology and Geology Computer Project

9910-02085

Howard Bundock
Branch of Engineering Seismology and Geology
U. S. Geological Survey 345 Middlefield Road, MS 977
Menlo Park, California 94025
(415) 329-5621, FTS 459-5621

INVESTIGATIONS

The objectives of the Branch of Engineering Seismology and Geology Computer Project are to:

Maintain a strong capability for the processing, analysis and dissemination of all strong motion data collected on the National Strong Motion Network and data collected on portable arrays;

Support research projects in the Branch of Engineering Seismology and Geology by providing programming and computer support including digitizing, graphics, processing and plotting capabilities as an aid to earthquake investigations;

Manage and maintain computer hardware and software so that it is ready to process data rapidly in the event of an earthquake.

The Branch facilities include a VAX 8250 running VMS version 5.02 and a VAX 11/750 computer operating under VMS Version 4.6, a PDP 11/70 running RSX-11M+ and a PDP 11/73 computer. The Branch computers are part of a local area network with other Branch, OEVE, Geologic Division, and ISD computers, and we have access to computers Survey-wide over Geonet. Project personnel join other office branches in the support of the OEVE VAX 11/785.
Investigations during the first six months of FY90 included upgrade to version 5.2 of the VMS operating system software on Branch and Office computers. The project has also worked with other Branch representatives to install a new Local Area Network including personal computers for Branch scientists, mainly for word processing and spreadsheet capabilities. This network is ready to run, but holdups in hardware compatability have not allowed complete installation. The software has been tested on a separate circuit, however, and will be ready to run on same day the circuit comes on line. The project has been involved digitizing and preparing 3 dimensional graphics for use in the study of the recent Loma Prieta Earthquake. The project has also tested an 8mm cassette tape drive on the Office VAX for backup and archiving and has been active in testing a Digital Equipment Corporation Reduced Instruction Set high speed computer system. The project continues its support of the OEVE VAX 11/785 project. We have worked with computer specialists in other branches in planning a move of all computer hardware into space provided in an enclosed area in the same building. As an ongoing policy, we have kept our hardware up to current revision levels, and operating system, network, and other software at the most recent versions.

RESULTS

As a result of these and previous investigations, the project has:
Upgraded to VMS version 5.2 on its VAX 785 and upgraded various software packages as well;

With other Branch members, continued installation of a Local Area Network for IBM PC clones and Apple IIse microcomputers;

Tested a new tape drive for use of Branch and Office Scientists;

Tested and installed software for use on the Branch Personal Computer Network;

Managed and maintained the OEVE VAX 11/785;

Managed, maintained, updated Branch and Office computer system hardware and software.

REPORTS

None

INSTRUMENTATION OF STRUCTURES

9910-04099

Mehmet Celebi
Branch of Engineering Seismology and Geology
U.S. Geological Survey
345 Middlefield Road
Menlo Park, California 94025
415/329-5623

Investigations

1. The process of selection of structures to be recommended for strong-motion instrumentation has continued in Orange County, Hawaii, and Puget Sound (Seattle), Reno (Nevada), and Puerto Rico. This effort has also been extended to Salt Lake City.

2. The process to design instrumentation schemes for selected structures has continued. Applicable permits for a structure in Orange County, CA have been obtained. Current efforts are being made to obtain permits for structures in Hawaii and Seattle.

3. The process of implementation of instrumentation for those structures for which instrumentation schemes have been designed has been completed in Anchorage, Alaska. The strong-motion recording system in this building is now operational.

4. Non-destructive dynamic testing of Salt Lake City and County Building is to be carried out progressively to evaluate the dynamic characteristics of the building before and after being rehabilitated by base isolation.

5. The minimal instrumentation in a building in Alhambra, Southern California, has been upgraded to contain extensive instrumentation to acquire sufficient data to study complete response modes of the building. A set of records are obtained during the Uplands earthquake. This will be compared with the Whittier (October 1, 1987) earthquake data which was code-type.

6. Agreements have been made with UCLA to convert the wind-monitoring system in the Theme Buildings in Los Angeles (previously financed by NSF) into a strong-motion monitoring system. Plans are being made to implement the conversion.

7. Studies of records obtained from instrumented structures are carried out. In particular, the records obtained during the October 1, 1987 Whittier Narrows earthquake from 1100 Wilshire Finance Building (Los Angeles), the Bechtel Building (Norwalk), and the Santa Ana River Bridge (base-isolated) are being investigated. Papers and open-file reports are prepared.

8. Impressive set of records have been obtained during the October 17, 1989 Loma Prieta earthquake from Transamerica Building (San Francisco), Pacific Park Plaza (Emeryville), and others.

Results

1. The Hawaii committee on strong motion instrumentation of structures has completed its deliberations and a draft report is being prepared.

2. A final report of the puget Sound (Seattle) advisory committee for strong-motion instrumentation has been completed.

3. Papers resulting from study of records obtained from structures are prepared.

4. An invited talk is to be given on Seismic Monitoring of Structures at the NCEER, Buffalo, New York.

5. Invited talks on records from structures given in Taipei and Tokyo.

6. Invited talk on structural instrumentation and data to be given at U.C. Berkeley on April 30, 1990.

Reports

Celebi, M., 1989, Seismic monitoring of structures--objectives and analyses of records from structures: U.S.-Japan Panel, (Wind and Seismic Effects), May 1989.

Safak, E., and Celebi, M., 1990, A method to estimate center of rigidity using vibration recordings: ASCE, Journal of Structural Division, January 1990.

Celebi, M., Safak, E., and Youssef, N., 1989, Analyses of recorded responses of a unique building in Los Angeles to motions caused by Whittier Narrows earthquake of October 1, 1987: U.S. Geological Survey Open-File Report 89-542.

Celebi, M., and Safak, E., 1990, Study of earthquake records from select tall buildings, completed invited paper for Tall Buildings Conference, November, 1990.

Celebi, M., Safak, E., and Youssef, N., 1990, Coupled torsional response of a unique building: Proceedings, National Conference on Earthquake Engineering, 4th, Palm Springs, CA.

STRONG-MOTION INSTRUMENTATION NETWORK DESIGN, DEVELOPMENT, AND OPERATION

9910-02765

Edwin Etheredge, Ronald Porcella, Richard Maley
Branch of Engineering Seismology and Geology
U.S. Geological Survey
345 Middlefield Road
Menlo Park, CA 94025
415/329-5667

Investigations

The Strong-Motion laboratory, in cooperation with federal, state, and local agencies and advisory engineering committees, designs, develops, and operates an instrument program in 41 states and Puerto Rico. Program goals include: (1) recording of potentially damaging ground motion in regional networks, and in closely spaced sensor arrays; and (2) monitoring the structural response of buildings, bridges and dams using sensors placed in critical locations. The present coordinated network consists of approximately 1,000 recording units installed at 600 ground sites, 28 buildings, 5 bridges, 56 dams, and 2 pumping plants.

Results

A network of four accelerograph stations have been installed in the southern Los Angeles basin/Orange County area. Sites are located at:

STATION	INSTRUMENTATION
Irvine, Brinderson Tower Bldg. 13 story building	SMA-1 in basement
Newport Beach, 800 Marguerite one-story wood frame building	SMA-1 at ground level
Costa Mesa, John Wayne Airport Fire Station	SMA-1 at ground level
Costa Mesa, 2300 Placentia Fire Station	SMA-1 at ground level

RECENT EARTHQUAKE RECORDS

October 18, 1989 0004 Gmt Ml-7.0g
(Loma Prieta Earthquake)

Strong-motion accelerographs at 38 locations located in the general Bay area were triggered by the earthquake. These stations consist of 21 ground stations, 13 large buildings including 5 hospitals, 2 dams, and 2 bridge abutments.

Station Name	Peak Horizontal Ground Acceleration
Anderson Dam	0.26g
San Jose Interchange	0.18g
Cherry Flat Reservoir	0.09g
Sunnyvale	0.22g
Hollister Airport	0.29g
Palo Alto VA Hospital	0.38g
Hollister City Hall	0.25g
Calaveras Reservoir	0.13g
Hollister, SAGO	0.06g
Stanford, SLAC	0.29g
Menlo Park VA Hospital	0.27g
Fremont	0.20g
Crystal Springs Reservoir	0.12g
Sunol	0.10g
Redwood City	0.28g
Foster City	0.12g
Del Valle Dam	0.06g
Livermore VA Hospital	0.06g
Bear Valley No. 12	0.17g
Hayward City Hall	0.10g
Dublin	0.09g
Bear Valley No. 10	0.13g
Bear Valley No. 7	0.06g
S.F., 1295 Shafter	0.11g
S.F., State University	0.14g
S.F., 595 Market Street	0.13g
S.F., 600 Montgomery	0.18g
Emeryville	0.26g
Berkeley, Strawberry Canyon	0.08g
Berkeley, Haviland Hall	0.06g
Berkeley, 2168 Shattuck	0.11g
San Francisco, VA Hospital	0.16g
S.F., Golden Gate Bridge	0.24g
Richmond	0.11g
Martinez VA Hospital	0.07g
Larkspur	0.14g

September 21, 1989 1741 Gmt ML 4.8
Eel River Valley Array (Humboldt Co.)
Five strong-motion stations recorded this event. Maximum accelerations were recorded at Centerville Navy Facility (0.15g) and at Ferndale Fire Station (0.13g).

December 2, 1989 2316 Gmt ML 4.3
Anza Array
Seven strong-motion stations recorded this event. All ground accelerations were less than 0.05g.

December 24, 1989 0845 Gmt
Howard Hanson dam, Washington
The crest station recorded 0.08g. No other stations were triggered.

December 28m 1989 0941 Gmt
San Bernardino Array
Two strong-motion stations recorded this event. Maximum accelerations were less than 0.05g.

January 16, 1990 2008 Gmt ML 5.3
Eel River Valley Array (Humboldt Co.)
Ferndale and Fortuna stations were triggered by this event. Accelerations were less than 0.05g.

February 28, 1990 2343 Gmt ML 5.5
Upland Earthquake (Los Angeles)
Strong motion accelerograms were recorded from 47 stations located in Los Angeles/San Bernardino area. Accelerations on the order of 0.50g were recorded at San Antonio Dam and at Live Oak reservoir. A large water tank located at Metropolitan Water District's Weymouth Filter Plant recorded high-frequency tank vibrations at accelerations of about 0.85g. These three locations are within 10 km of the epicenter.

Reports

Maley, R., and others, 1989, Strong-Motion records from the Northern California (Loma Prieta Earthquake of October 17, 1989: U.S. Geological Survey Open-File Report 89-568.

4/90

Structural Analysis

9910-02759

Erdal Şafak and Mehmet Çelebi
Branch of Engineering, Seismology, and Geology
U.S. Geological Survey
345 Middlefield Road, MS 977
Menlo Park, California 94025
(415)-329-5648, FTS 459-5648

Investigations

1. Development of methodologies and computer software to analyze seismic recordings from instrumented structures.
2. Analyses of seismic recordings obtained from instrumented structures during the October 17, 1989 Loma Prieta earthquake.

Results

1. Two methods, one in the time domain and the other in the frequency domain, have been developed to determine the center of rigidity in buildings by using vibration recordings. The methods have been used to detect and identify torsional vibrations in several buildings, whose seismic records are available.
2. Full set of records from six extensively instrumented structures (five buildings and one dam) have been obtained during the October 17, 1989 Loma Prieta earthquake. The analysis of data from one of the buildings, the pyramid-shaped 60-story Transamerica Building has been completed. Another building, the tree-winged (Y shaped) 30-story Pacific Park Plaza, is currently being analyzed.

Reports

Şafak, E. and Çelebi, M., 1990, Method to estimate center of rigidity by using vibration recordings, ***Journal of Structural Engineering***, ASCE, Vol.116, No.1, Jan. 1990, pp.85-97.

Şafak, E., and Çelebi, M. 1990, New techniques in record analyses: Torsional vibrations, ***proceedings***, Fourth U.S Conference on Earthquake Engineering, May 20-24, 1990, Palm Springs, California.

Çelebi, M., and Şafak, E., 1990, Coupled torsional response of a tall building, ***proceedings***, Fourth U.S Conference on Earthquake Engineering, May 20-24, 1990, Palm Springs, California.

Çelebi, M., and Şafak, E., 1990, Recorded response of Transamerica Building: Part I-Data and preliminary analysis, ***Journal of Structural Engineering***, ASCE, submitted for publication.

Şafak , E., and Çelebi, M., 1990, Recorded response of Transamerica Building: Part II-System identification, ***Journal of Structural Engineering***, ASCE, submitted for publication.

Çelebi, M., Şafak, E., 1990, Study of earthquake records from selected tall buildings (invited paper), ***proceedings***, Tall Buildings Conference, Hong Kong, November 1990.

Physical Constraints on Source of Ground Motion

9910-01915

D. J. Andrews
Branch of Engineering Seismology and Geology
U.S. Geological Survey
345 Middlefield Road, MS 977
Menlo Park, California 94025
(415) 329-5606

INVESTIGATIONS

Looking for nonplanar features in earthquake sources. What can explain the complex focal mechanisms of aftershocks shallower than 10 km and the left-lateral surface breaks in the Loma Prieta earthquake?

RESULTS

Forward calculations have been done of simple 2-D models related to the Loma Prieta earthquake. Complex (including left-lateral) focal mechanisms of aftershocks shallower than 10 km strongly suggest that the upward propagation of the main rupture terminated at a weak subhorizontal decoupling layer. Such a layer of near-lithostatic fluid pressure has been suggested by Robert Fournier (manuscript in preparation). A calculation shows that a main rupture can terminate at such a decoupling layer, but that the layer needs to have heterogeneous strength to explain the complex response at shallower depths.

Ground Motion Prediction for Critical Structures

9910-01913

D. M. Boore
W. B. Joyner

Branch of Engineering Seismology and Geology
U. S. Geological Survey
345 Middlefield Road, MS 977
Menlo Park, California 94025

Investigations:

1. Study the ground motions produced by the October Loma Prieta earthquake.

Results:

Peak accelerations of the Loma Prieta main shock have been tabulated from instruments maintained by a number of organizations. We have analyzed a subset of 86 records from nominally free-field sites, which have been subdivided into rock, alluvium, and bay-mud categories according to data available in various reports. After correction for attenuation, the peak accelerations on rock, alluvium, and bay-mud sites are factors of 1.6, 1.8, and 4.5 larger, on the average, than Joyner and Boore's (1988) predicted values for a M=6.9 earthquake . The mean motions for the rock and alluvium sites are somewhat greater than one standard deviation away from the predicted value, but the mean acceleration from the bay-mud sites is well outside the range expected from analyses of data from previous earthquakes from rock and alluvium sites. Large amplitudes of motions on bay-mud sites relative to rock sites (a factor of 2.8 for the average of the recordings of the Loma Prieta main shock) has been found previously from recordings of distant earthquakes and explosions, but the Loma Prieta earthquake provided the first opportunity to study the relative amplitudes from strong-motion recordings.

Reports:

Boore, D. M., L. Seekins, and William B. Joyner (1990). Peak accelerations from the 17 October 1989 Loma Prieta earthquake, *Seismological Research Letters* **60**, 151–166.

Boore, D. M. (1989–1990). Contributions concerning the accelerations from the Loma Prieta earthquake published in *Science*, *U. S. Geological Survey Bulletin 1045*, and various publications of the *Earthquake Engineering Research Institute*.

9 April 1990

Anelastic Wave Propagation

9910-02689

Roger D. Borcherdt
Branch of Engineering Seismology and Geology
U.S. Geological Survey
345 Middlefield Road, MS 977
Menlo Park, California 94025
(415) 329-5619

Investigations:

Interpretation of colocated measurements of scalar volumetric strain and vectorial seismic displacement fields to infer additional characteristics of anelastic seismic wave fields. Analysis of strong motion and aftershock data collected during Loma Prieta earthquake of October 17, 1989.

Results:

Volumetric strain meters (Sacks-Evertson design) are installed at 15 sites along the San Andreas fault system, CA, to monitor long-term strain changes for earthquake prediction. Deployment of portable broad-band, high-resolution digital recorders (GEOS) at several sites extends the detection band for volumetric strain to periods shorter than 5 x 10^{-2} seconds and permits the simultaneous observation of seismic radiation fields using conventional short-period pendulum seismometers. Simultaneous observations establish that the strain detection bandwidth extends from periods greater than 10^{7} seconds to periods near 5 x 10^{-2} seconds with a dynamic range exceeding 140 db. Measurements of earth-strain noise for the period band, 10^{7} to 10^{-2} seconds, show that ground noise, not instrument noise, currently limits the measurement of strain over a bandwidth of more than eight orders of magnitude in period. Comparison of the short-period portion of earth-strain, noise spectra (20 to 5 x 10^{-2} secs) with average spectra determined from pendulum seismometers, suggest that observed noise is predominantly dilatational energy. Recordings of local and regional earthquakes indicate that dilatometers respond to *P* energy but not direct shear energy that straingrams can be used to resolve superimposed *P* and *S* waves for inference of wave characteristics not permitted by either sensor alone. Simultaneous measurements of incident *P*- and *S*-wave amplitudes provided single-station estimates of wave field inhomogeneity, free-surface reflection coefficients and local material velocity. Estimates of these parameters derived for the North Palm Springs earthquake (M_{ω}5.9) are respectively for the incident *P* wave 29°, -85°, 1.71, 2.9 km/s and for the incident *S* wave 17°, 79°, 0.85, 2.9 km/s. The empirical estimates of reflection coefficients are consistent with model estimates derived using an anelastic half-space model with incident inhomogeneous wave fields.

Preliminary analyses of ground motion data recorded during and after the Loma Prieta earthquake reiterate the importance of ground response earthquake hazard mitigation.

Reports

Borcherdt, R.D. and Glassmoyer, G., 1989, An exact anelastic model for the free-surface reflection of P and S-1 waves: *Bull. Seismol. Soc. Am.*, 79, 842-859.

Borcherdt, R.D., and Donovan, N.C., 1989, Geosciences, in Preliminary reconnaissance report, Loma Prieta earthquake October 17, 1989: *Eatrthquake Engineering Res. Inst. Special Publication 89-03*, p. 5-22.

Borcherdt, R.D., and Donovan, N.C., 1990, Geosciences overview, in Reconnaissance report, Loma Prieta earthquake October 17, 1989: *Earthquake Engineering Res. Inst.*, in press.

Glassmoyer, G., and Borcherdt, R.D., 1990, Source parameters and effects of bandwidth and local geology on high-frequency ground motions observed for aftershocks of northeastern Ohio earthquake of 31 January, 1986: *Seismol. Soc. of Am. Bull.*, accepted for publication.

Hough, S.E., Simpson, D., Lerner-Lan, A., Friberg, P.A., Busby, R., Shengold, L., Tuttle, M., Field, E.H., Jacob, K.H., Pacheco, J., Estabrook, C., Peterson, M., Johnson, D.H., Borcherdt, R.D., and Frankel, A., 1989, Observations of weak ground motion in the epicentral area and in west Oakland following the Loma Prieta earthquake of October 17, 1989, in Reconnaissance report for Loma Prieta earthquake of October 17, 1989: Earthquake Engineering Res. Inst., special suppl., *Spectra*, in press.

Hough, S.E., Friberg, P.A., Busby, R., Field, E.F., Jacob, K.H., and Borcherdt, R.D., Sediment induced amplification--A possible factor in the collapse of the Nimitz freeway during the October 17, 1989 Loma Prieta (CA) earthquake: accepted, *Nature*.

Excitation and Propagation of High-Frequency Seismic Waves
9910-04482

A. Frankel

Branch of Engineering Seismology and Geology
U.S. Geological Survey
345 Middlefield Rd., MS 977
Menlo Park, CA 94025
(703) 648-4119

Investigations

1. Develop methods to separate the shear-wave attenuation of the crust caused by anelasticity from that produced by scattering, using the energy-flux model of seismic coda. Investigate relationship between coda Q and the Q of direct shear waves.
2. Study the high-frequency seismic response of sedimentary basins using 2-D and 3-D finite-difference wave propagation codes.
3. Document and quantify the effects of near-surface attenuation on high-frequency seismic waves.
4. Use a self-similar model of complex rupture to quantify the relationship between the high-frequency spectral fall-off of an earthquake and the scaling of strength on a fault.

Results

1. I have compared the coda Q in New York State, South Africa, and southern California with the Q estimates of direct shear waves determined previously in Frankel et al. (1990). The frequency dependence of coda Q is found not to be equivalent to the frequency dependence of the direct shear wave Q. While coda Q values at 3 Hz for lapse times of 10-50 sec are similar to S-wave Q values determined with R^{-1} geometrical spreading, coda Q values at 15 and 30 Hz are substantially higher than S-wave Q values at these frequencies. The frequency dependence of coda Q changes with lapse time in New York State. The 3 Hz coda Q in South Africa for lapse times of 50-110 sec is about five times that of the Lg wave Q estimate. These findings support the idea that the coda decay is insensitive to the scattering attenuation, and are consistent with models of coda based on conservation of seismic energy during scattering.

2. I am continuing development of the 3-D finite difference code for elastic waves in a heterogeneous medium. A fourth-order accurate algorithm was incorporated into the program. A new way of inserting a seismic source with an arbitrary moment tensor was added to the code. I have been evaluating a method for including topography on the free surface. The 3-D code has been vectorized for use on a Cray supercomputer. This code will be used to model the local seismograms from the Loma Prieta earthquake and its aftershocks.

3. I have used a self-similar model of complex rupture involving nested sub-events to quantify the relations between the high-frequency fall-off of the displacement spectrum of an earthquake, the fractal dimension of its sub-event distribution, and the scaling of strength on a fault plane. This analysis indicates that the typically-observed spectral fall-off of ω^{-2} can be the result of scale-invariant strength along the fault zone. Such a scale-invariant strength also produces b-values of one for aftershock sequences.

Reports

Frankel, A., A. McGarr, J. Bicknell, J. Mori, L. Seeber, and E. Cranswick, Attenuation of high-frequency shear waves in the crust: measurements from New York State, South Africa, and southern California, paper submitted to *J. Geophys. Res.*, 1990.

Frankel, A., Effects of near-surface attenuation on the short-period waveforms and spectra of earthquakes and explosions, *EOS Trans. Amer. Geophys. Union,* **70,** 1188, 1989.

Frankel, A., J. Filson, R. Borcherdt, and J. Vidale, Numerical simulations of strong ground motions in the Leninakan basin produced by the 1988 Armenian earthquake and its aftershocks, *EOS Trans. Amer. Geophys. Union,* **70,** 1200, 1989.

Precise Velocity and Attenuation Measurements in Engineering Seismology

9910-02413

Hsi-Ping Liu
Branch of Engineering Seismology and Geology
U. S. Geological Survey
345 Middlefield Road, MS 977
Menlo Park, California 94025
(415) 329-5643

Investigations

Investigation of site geologic and seismic amplification conditions in the Marina district of San Francisco following the Loma Prieta earthquake of October 17, 1989. Although at a distance of ~ 100 km from the epicenter, the Marina district of San Francisco suffered severe damage during the Loma Prieta earthquake. After the earthquake, a soil boring to a total depth of 91 m was taken at the Winfield Scott School at Beach and Divisadero streets in order to investigate the effect of soil conditions on strong ground motion and liquefaction. The site was chosen because of the locally heavy damage sustained to structures, pavement, and public works near the school. Stratigraphic, soil engineering, and physical property data have been obtained from the soil samples. In addition, seismic velocities have been determined *in situ* using the downhole method. The hole itself will be used to install a downhole seismometer in order to investigate the effect of the soil column on seismic waves as they propagate to the earth's surface.

Results

1. The soil column consists of 4.3 m of filled sand overlying another 3.5 m of natural sand deposits. Below is an interbedded sequence of clayey sand and clay to a depth of 11.6 m interpreted to be the base of the Holocene Bay Mud. Below the Holocene Bay Mud is a layer of dense sand lying between 11.6 and 22.9 m depths and is characterized by a distinct yellow-brown color and high penetration resistance. The lower 57.9 m of the soil column consists of stiff olive-gray Pleistocene Bay Mud which overlies Franciscan bedrock at 79.5 m depth. The bedrock consists of hydrothermally altered serpentine embedded in clayey gouge material. Details of the stratigraphic description of the samples as well as results of laboratory testing such as water content, bulk density, grain size, Atterberg limits, and vane shear strength can be found in the report by Kayen *et al.* (1990).

2. The seismic velocities were deternmined *in situ* using the downhole method. An air-powered, impulsive, and horizontally polarized shear-wave (SH) source placed at the surface generated the shear waves, whereas the vertical impact of a sledge hammer on a steel plate generated the compressional (P) waves. The source offset was 1.88 m and 2.23 m from the center of the hole for the SH- and P-waves, respectively. The P-wave velocity has

a constant value through the Pleistocene Bay Mud at 1740 m/s and increases to 3000 m/s in the Franciscan bedrock. The shear-wave velocities of the artificially filled sand, natural sand deposits, and Holocene Bay Mud are 130 m/s, 175 m/s, and 145 m/s, respectively. The shear-wave velocity of the dense sand varies between 290 m/s and 455 m/s; the shear-wave velocity determined for the Pleistocene Bay Mud is 265 m/s. Shear wave arrivals travelling through soil deposits below 28 m depth were masked by the high-amplitude arrivals travelling down the borehole casing. We will conduct further experiments using the crosshole method in order to determine the shear-wave velocities below this depth.

Reports

Kayen, R. E., Liu, H.-P., Fumal, T. E., Westerlund, R. E., Warrick, R. E., Gibbs, J. F., and Lee, H. J., 1990, Engineering and seismic properties of the soil column at Winfield Scott School, San Francisco, *U. S. Geol. Surv. Prof. Pap.* , in press.

Liu, H.-P., 1990, Calculation of zero-offset vertical seismic profiles generated by a horizontal point force acting on the surface of an anelastic half-space, *Bull. Seismol. Soc. Am.* , in press.

Scaling of Seismic Sources

9910-04488

Art McGarr and John Bicknell
Branch of Engineering Seismology and Geology
345 Middlefield Road, MS 977
Menlo Park, California 94025
(415) 329-5645 or (415) 329-5625

Investigations

Seismic source parameters measured from surface records are compared to those from underground records in deep South Africa's gold mines to determine whether reported scaling transitions are a consequence of wave propagation or are due to corresponding scaling changes in the source processes.

Results

To estimate the seismic hazard to underground facilities or operations in the environs of a mining-induced tremor or a natural earthquake, it is very useful to be able to relate locally-recorded seismic wave forms to peak ground velocity and slip at the causative fault. With a minimum of assumptions, far-field S wave pulses are analyzed to define the faulting slip D and near-fault peak ground velocity $\dot{D}/2$ that give rise to the most significant ground motion. This most intense region of faulting, an assumed circular asperity, has radius r with a broader source zone of radius r_0 , which is traditionally calculated from the corner frequency of the S wave spectrum. In developing straightforward relationships between peak far-field velocity $\underline{v}$ and peak acceleration $\underline{a}$, and the source process of the asperity D and $\dot{D}$, as well as its radius r, the key model assumption is that $r = k\beta/\omega$, where $2\pi/\omega$ is the duration of the sinusoidal velocity pulse of maximum amplitude, β is the shear wave speed and k is a constant. Observations in deep-level gold mines of slip and slip velocity as well as laboratory observations of slip rate as a function of stress drop for stick-slip failure support a choice of $k = 2.34$, the value commonly used for estimating r_0. In particular, observations of fault slip up to 500 mm for mining-induced tremors in the moment magnitude range of 4 to 5 are consistent with $D = 8.1\ R\underline{v}/\beta$, where R is the hypocentral distance. Moreover, estimates based on underground damage of near-fault ground velocities ranging up to 3.5 m/s are in accord with $\dot{D}/2 = 1.28\ (\beta/\mu)\rho R\underline{a}$, where μ is the modulus of rigidity and p is the density. Alternatively, the average slip velocity $\bar{\dot{D}}$ can be expressed in terms of the stress drop $\Delta\sigma_i$ of the asperity $\bar{\dot{D}} = 0.51\ \beta\Delta\sigma_i/\mu$, and the agreement of this relationhip with measurements made during stick-slip failure in the laboratory is excellent. To the extent that seismic slip exterior to the asperity is a consequence of pre-event suppression of slip due to the asperity, the broader scale (r_0) slip can be related to that of the asperity. Just as the asperity radius $r =$ be estimated from $r = 2.34\ \beta\underline{v}/\underline{a}$, an alternative estimate for r_0 is given by $r_0 = \rho R\underline{a}\ M_0/\ [75.8\ (R\underline{v})^2]$, the results of which are generally in good agreement with estimates based on the spectral corner frequency method.

Reports

McGarr, A., Bicknell, J., Churcher, J., and Spottiswoode, S., 1990, Comparisons of ground motion from tremors and explosions in deep gold mines: submitted to *Journal of Geophysical Research.*

McGarr, A., 1990, Report on seismic hazard estimate for the Sudbury Neutrino Observatory: Branch of Engineering Seismology and Geology, U.S. Geological Survey, 15 p.

4/90

Emergency Earthquake Hazards

9540-04530

Thomas D. Gilmore
U.S. Geological Survey
Branch of Western Regional Geology
345 Middlefield Road M/S 975
Menlo Park, California 94025
(415) 329-4938

Investigations

This study focuses on describing, evaluating, and interpreting the patterns of historical vertical displacements disclosed by both direct and indirect comparisons among the results of reported geodetic levelings completed during the 20th-century within the Santa Cruz Mountains region. This geologically youthful and tectonically active region includes the epicentral areas of the 1989 Loma Prieta earthquake and other large-magnitude historical events, including the 1906 San Francisco earthquake. It has more recently become the focus of increasing geologic and geophysical investigations of future earthquake potential and has been identified by several USGS scientists as both the site of modern seismic gaps and imminent future earthquakes.

Results

Funding for this study only became available in March 1990, near the end of this reporting period. Consequently, no results have yet been obtained. Efforts focused on compiling and obtaining existing leveling data from the National Geodetic Survey and the U.S. Geological Survey and locating bench marks. Since the October earthquake, numerous inquiries from both within and outside the Geological Survey have been answered concerning the nature and locations of existing leveling in the Santa Cruz Mountains and plans for proposed relevelings. Results of relevelings completed following the 1989 earthquake are not yet available.

Reports

No reports were published or approved during the reporting period.

Emergency Earthquake Hazards

9540-04530

Ralph A. Haugerud
U.S. Geological Survey, MS 975
345 Middlefield Road
Menlo Park, California 94025
415-329-4955 (FTS 459-4955)

Investigations undertaken

In the weeks following the Loma Prieta earthquake, Steve Ellen and I, with help from several others, surveyed pavement damage in the region extending from southwest San Jose, through Los Gatos, and north towards Palo Alto. Since then we have been collecting reports of sidewalk damage from municipalities, and lists of underground gas and water pipe breaks from local utilities.

Immediately after the earthquake I also spent several days making pace, compass, and millimeter-scale traverses to survey the position, azimuth, and separation of cracks (most extensional) in asphalt roads in the epicentral region.

This work is relevant to Element I(Current Tectonic and Earthquake Potential Studies) and Element III (Regional Earthquake Hazards Assessment): It is leading to an increase understanding of the tectonics of this segment of the San Andreas fault system, as well as delineating a previously unappreciated hazard associated with some earthquakes on the San Andreas fault.

Results obtained

Along the NE margin of the Santa Cruz Mountains, damage was concentrated in linear zones along the rangefront (Figure 1). Deformation in downtown Los Gatos was associated with permanent NNE-SSW shortening of about 20-25 cm (measured from overlaps at breaks in concrete lining of Los Gatos Creek) and is probably tectonic, though not obviously associated with movement on a single fault strand. Pavement damage along the foot of Blossom Hill is of less certain origin: it may also be tectonic, but could be due to locally severe shaking. Overall, the pattern of pavement damage is suggestive of coseismic slip (triggered creep?) on reverse or thrust faults which separate the Santa Cruz Mountains from the Santa Clara Valley.

Data on asphalt pavement cracking in the epicentral region remain unexamined, largely because I am uncertain as to their significance.

Reports

Haugerud, R.A., and Ellen, S.D., 1990, Deformation along the northeast foot of the Santa Cruz Mountains during the Loma Prieta earthquake: EOS, v. 71, p. 288.

Ponti, D., Wells, R.E., Haugerud, R.A., Clark, M.M., and Hall, N.T., in press, Surface rupture aspects, in Earthquake Engineering Research Institute special volume on Loma Prieta earthquake. Received Director's approval 8 January 1990.

Haugerud, R.A., and Ellen, S.D., 1990, Stop 7. Coseismic ground deformation along the northeast margin of the Santa Cruz Mountains, in Schwartz, D.P., and Ponti, D.J., editors, Field guide to neotectonics of the San Andreas fault system, Santa Cruz Mountains, in light of the 1989 Loma Prieta earthquake: U.S. Geological Survey Open-file Report 90-274, p. 32-36.

also, contributions to

Staff of the U.S. Geological Survey, 1990, The Loma Prieta, California Earthquake: an anticipated event: Science, v. 247, p. 286-293.

Lessons learned from the Loma Prieta, California, earthquake of October 17, 1989: U.S. Geological Survey Circular 1045, 48 p.

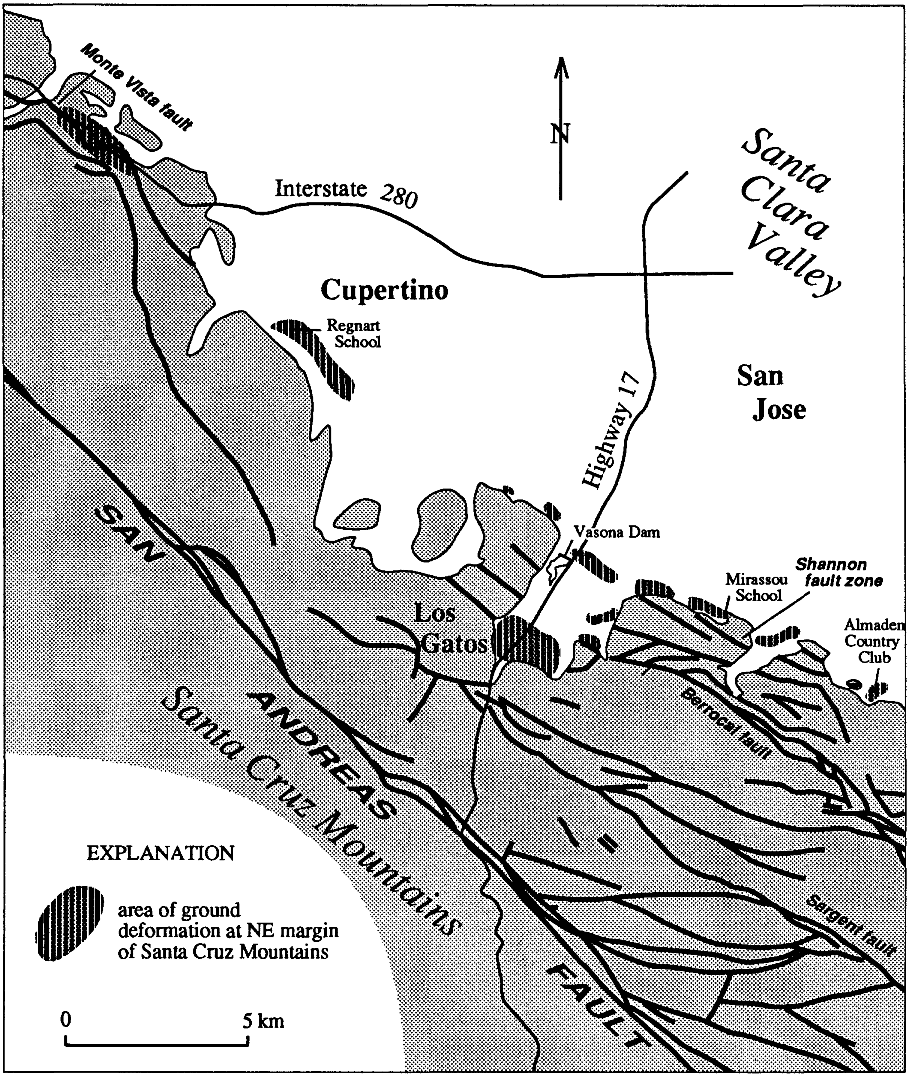

Figure 1. Map showing extent of observed ground deformation at northeast margin of Santa Cruz Mountains during Loma Prieta earthquake. Bedrock and older alluvium shaded; selected faults shown only where they cross bedrock or older alluvium. Modified from USGS OFR 90-274.

LOMA PRIETA AFTERSHOCKS: JOINT 3-D STRUCTURE AND HYPOCENTERS INVERSION FOR SOURCE DYNAMICS, USING UCB AND IRIS TEMPORARY NETWORK DATA AND CALNET LOCAL STATIONS

14-08-0001-G1840

T.V. McEvilly, W. Foxall and A. Michelini
Seismographic Station
University of California
Berkeley, CA 94720
415/642-3977

INTRODUCTION

Following the October 17, 1989, Loma Prieta earthquake (ML=7.0), the University of California, Seismographic Station at Berkeley (UCB) installed a five-station temporary network in the Santa Cruz Mountains to monitor the aftershock activity (Fig. 1.). Each station was equipped with three-component high- and low-gain seismometers and the data were digitally recorded on Sprengnether DR-100. The network operated for approximately seven weeks starting 36 hours from the main shock. The IRIS-PASSCAL network was also deployed in the aftershock zone for approximately the same period of time.

INVESTIGATION

The principal aim of the investigation is to study the tectonics of the region by analyzing the complex pattern of faulting that was activated in the area during the aftershock sequence. To this purpose we are pursuing two lines of research. In the first, we are determining the velocity structure of the area and calculating synthetic seismograms for the recorded larger aftershocks. The second consists of using the smaller aftershocks as empirical Green's functions to model the larger ones. We plan to use the data recorded by the UCB and IRIS temporary networks and those provided by the local USGS-CALNET stations.

RESULTS

We have finished the first part of the project that includes the calculation of a three-dimensional P-velocity model for the area by adopting a joint hypocenter/velocity inversion technique. We have used 89 earthquakes recorded by the USGS-CALNET stations and the temporary UCB network (Fig. 2.) that provided a total of approximately 2700 P arrival times (IRIS-PASSCAL data are not available yet). The model is parameterized in terms of cubic B-splines (Michelini and McEvilly, submitted for publication) which allows direct calculation of synthetic seismograms using dynamic ray-tracing (e.g. Cerveny, 1987). Plan views of the resolved velocity model at shallow depths (z=2,5 km) are shown in Figure 2 together with the isostatic gravity map for the same region. Cross-sections across the fault are shown in Figure 3 together with the corresponding sections of the resolving width function, which is calculated from the resolution matrix of the velocity parameters.

A good correlation is found between the isostatic gravity map and the shallow velocity structure at shallow depths and the local surface geology. A distinct low-velocity zone is imaged from the surface to about 4 km depth southwest of the San Andreas Fault (SAF) in the Santa Cruz Basin, which corresponds to Tertiary sediments outcropping at the surface. To the northeast a relatively high velocity body (Vp~5 Km/s) is imaged between the SAF and the Sargent Fault, approximately coinciding with gneissic rocks outcropping near Loma Prieta. Further to the northeast, lower velocities consistent with the Franciscan complex are found. At depths greater than 8 km, our model has velocities of approximately 6.8 km/s southwest of the SAF, which are too high for a granitic Salinian complex at these depths but could correspond to a mafic intrusion. At similar depths northeast of the SAF, velocities are again consistent with Franciscan rocks.

FURTHER WORK

We are currently finishing event association and at the end of the summer 1990 we will extend the joint inversion to the S-velocity model for selected areas with good source-receiver geometries. We will then move into the study of the rupture histories of the larger aftershocks by following the two lines of research mentioned above.

PRESENTATIONS

Michelini, A., Foxall, W. and T.V., McEvilly, 1990; Loma Prieta sequence: joint inversion for 3-D velocity structure and faulting geometry, *Seismol. Res. Lett.*, **61**, p. 48.

REFERENCES

Cerveny, V., 1987; Ray tracing algorithms in three-dimensional laterally varying layered structures, in *Seismic Tomography*, editor G. Nolet, *D. Reidel Publishing Company*, 99-133.

Michelini, A. and T.V. McEvilly, 1990; Seismological studies at Parkfield: I. Simultaneous inversion for velocity structure and hypocenters using cubic B-splines parameterization, submitted to *Bull. Sesim. Soc. Am.*.

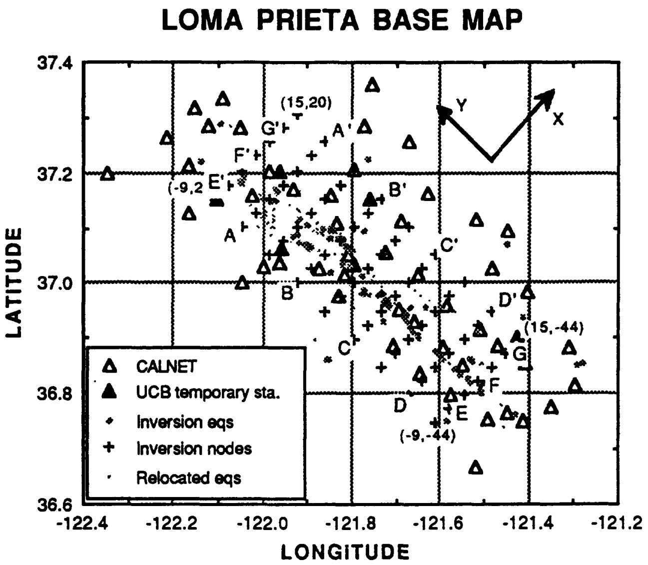

Figure 1. Base map of the Santa Cruz Mountains area. The vertical cross-sections A-A', B-B', C-C' and D-D' are shown in Figure 3.

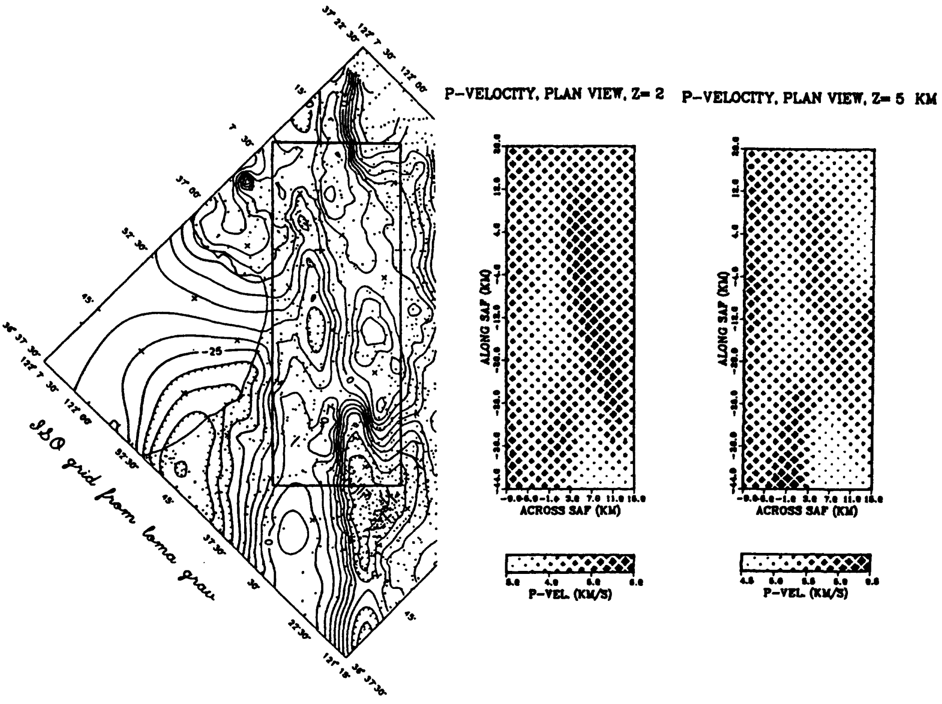

Figure 2. Isostatic gravity map and P-velocity plan view horizontal sections at depths of 2 and 5 km.

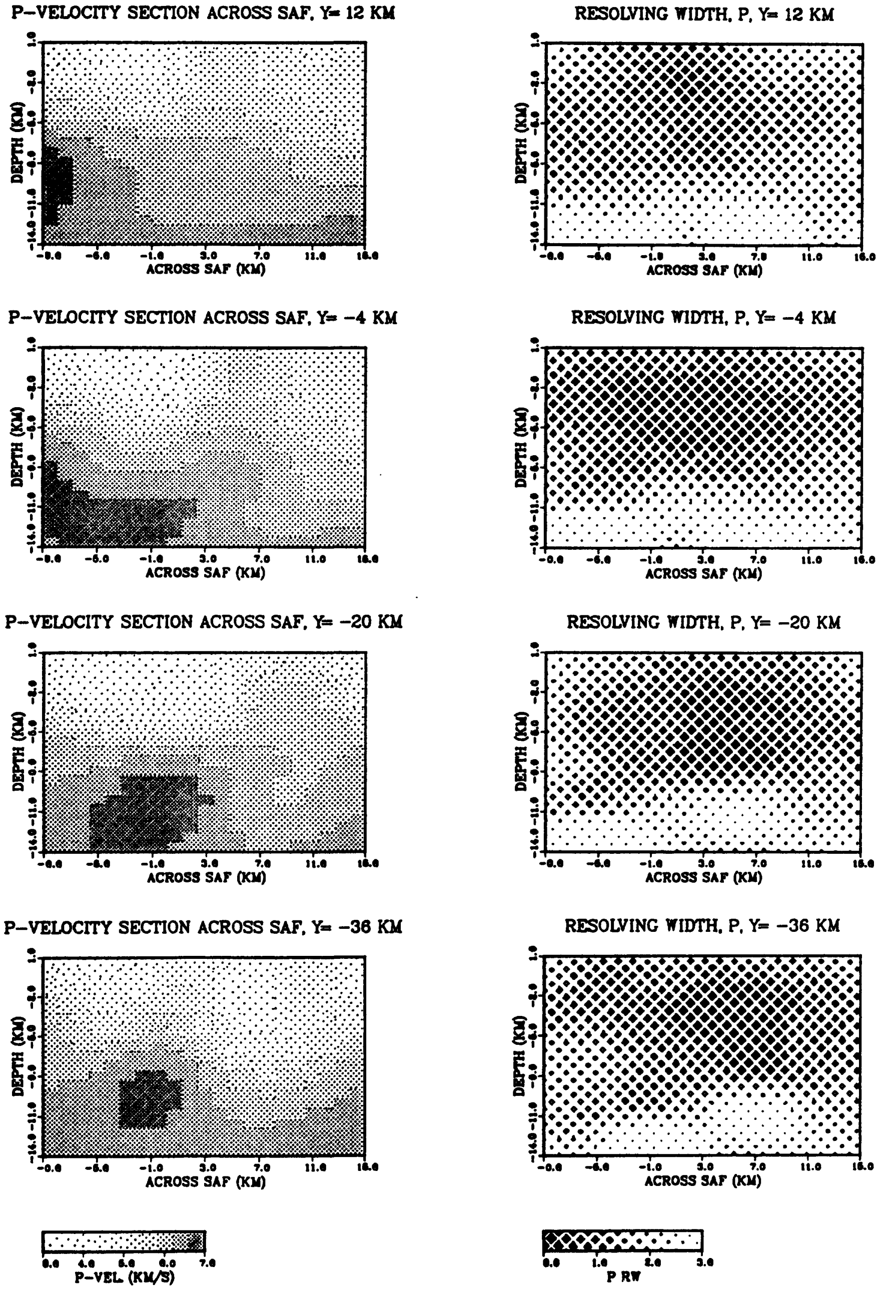

Figure 3. Vertical cross-sections of the P-velocity model (left) and corresponding sections for the resolving width function calculated from the resolution matrix of the velocity model parameters. Darker areas are better resolved (right).

ANALYSIS OF CONVERGENT DEFORMATION KINEMATICS AND RATES OF THE SANTA CRUZ MOUNTAINS AND RELATIONSHIP TO THE SAN ANDREAS FAULT AND THE LOMA PRIETA EARTHQUAKE

14-08-0001-G1830

Jay Namson and Thomas L. Davis

DAVIS AND NAMSON
CONSULTING GEOLOGISTS
1545 NORTH VERDUGO ROAD, SUITE 105
GLENDALE, CA 91208
(818) 507-6650

I. Objectives

A. Detection of seismically active blind thrusts in the Santa Cruz Mountains.

B. Determine the geometry, kinematics and slip rates of blind thrusts in the Santa Cruz Mountins.

C. Determine regional convergence rates and thrust fault slip rates in the Santa Cruz Mountians.

D. Determine the relationship between active convergence and strike-slip deformation of the Santa Cruz Mountains and the San Andreas Fault.

II. Approach: Compilation of surface and subsurface data, using detailed geologic maps and well data, into retro deformable cross sections.

III. Results: Most of the available geologic maps and well data have been identified and collected. Our level of funding will allow for the construction of only one regional cross section. The line of section chosen using the collected data was based on quality and the location of the Loma Prieta earthquake (Figure 1). Much of the geologic data have been compiled onto the cross section and analysis of the well data have begun.

FIGURE 1

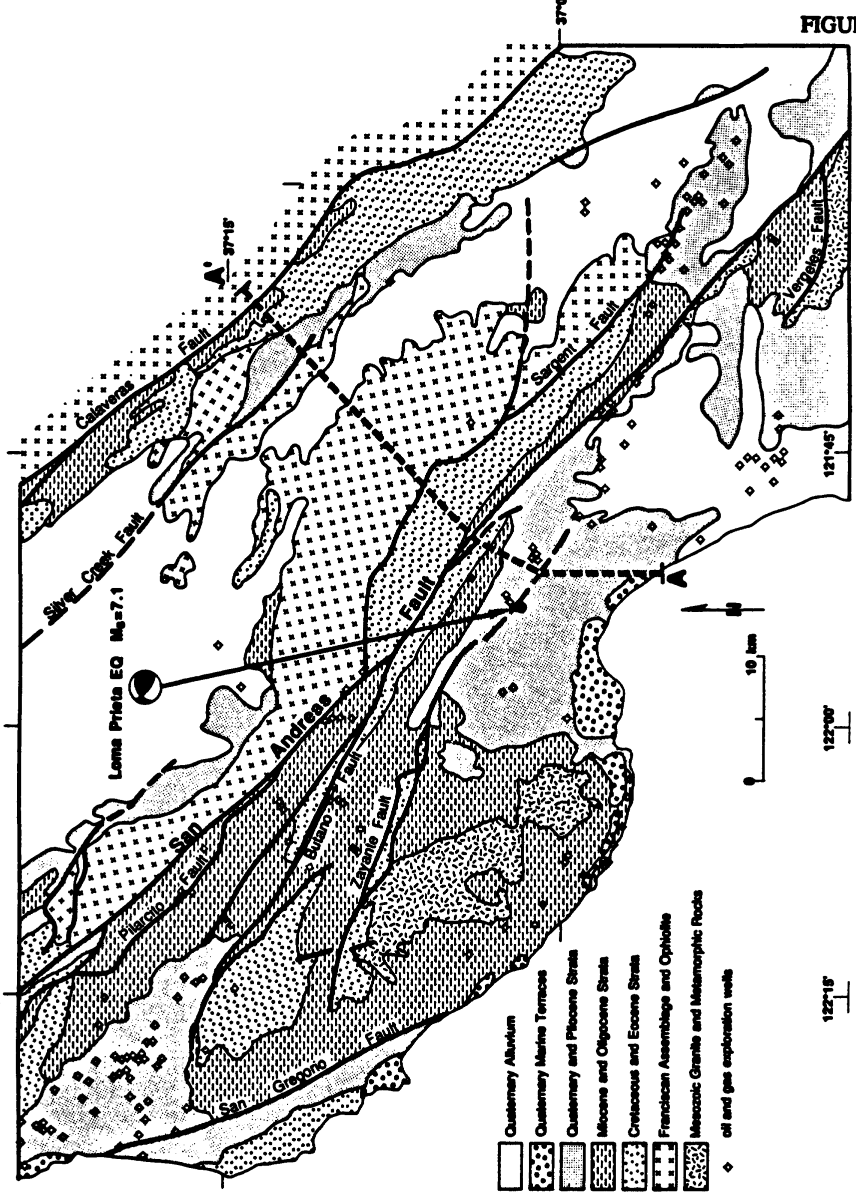
37°00'
37°15'
121°45'
122°00'
122°15'
A
A'
Calaveras Fault
Silver Creek Fault
San Andreas Fault
Sargent Fault
Vergeles Fault
Pilarcitos Fault
Butano Fault
Zayante Fault
San Gregorio Fault
Loma Prieta EQ M_S=7.1
N
0
10 km
Quaternary Alluvium
Quaternary Marine Terraces
Quaternary and Pliocene Strata
Miocene and Oligocene Strata
Cretaceous and Eocene Strata
Franciscan Assemblage and Ophiolite
Mesozoic Granite and Metamorphic Rocks
oil and gas exploration wells

GROUND MOTION PREDICTION IN REALISTIC EARTH STRUCTURES

9910-03010

Paul Spudich
Branch of Engineering Seismology and Geology
345 Middlefield Road, MS 977
Menlo Park, California 94025
415/329-5654

Investigations

1. Recording of aftershocks of the 1989 Loma Prieta earthquake for use as empirical Green's functions.

2. Recording of aftershocks of the 1989 Loma Prieta earthquake to study ground motion variations caused by topography and near-surface geology.

Results

1. Six-channel GEOS digital recorders equipped with 2-Hz triaxial geophones and triaxial force-balance accelerometers were co-sited with SMA-1 accelerometers that had recorded the main shock, in order to use the recorded aftershocks as empirical Green's functions for study of the main shock motions. USGS SMA-1's that were occupied were Fremont Porcella residence(*), Anderson Dam downstream(*), San Andreas Geophysical Laboratory(*), and Bear Valley Fire Station #1. We occupied the sites of California Strong Motion Instrumentation Program SMA-1's at halls Valley(*), Gilroy Gavilan College(*), Monterey City Hall(*), Capitola Fire Station (*), Coralitos(*), and Saratoga Aloha Street(*). Digital Sprengnether DR-200 recorders equipped with 2-Hz triaxial geophones only were installed at Lexington Dam abutment(*), UCSC Lick Observatory Electronics Shop(*), and Salinas. Most of the data were recovered from the sites marked by a(*) above. Participating in the GEOS deployment were Mary C. Andrews, John Boatwright, Chris Dietel, Gary Glassmoyer, Linda Haar, Charles Mueller, Thomas Noce, Joe Sena, and Leif Wennerberg. The Dr-200's were brought from the Golden office of the USGS by Ken King, David L. Carver, Robert A. Williams, Edward Cranswick,. Mark Marrimonte, and David M. Worley.

2. We installed a group of about 10 instruments on each of the two hills where topographic amplification of the main shock motions was suspected. The first was around Rebecca Lane near Boulder Creek, California, and the second was around Robinwood lane off Old San Jose Road in the epicentral region. Preliminary examination of the data suggests that on Rebecca Lane, the near surface site geology

was a much more important factor in the ground motions of the aftershocks than was topography. At Robinwood Lane there was no clear topographic amplification observed in the time domain, and frequency domain studies are in progress. To study the possible influence of surface geology on damage to buildings, we did several deployments in the cities of Santa Cruz and Los Gatos. About 15 sites distributed throughout Santa Cruz were occupied, and a 3-km long line of instruments were deployed across a the channel of the San Lorenzo River, near the area of heaviest damage. Preliminary examination of the data suggests that near-surface geology is correlated with the strength of shaking in aftershocks. A significant amplification of motions in the north-south direction at frequencies below 8 Hz was observed in the San Lorenzo River channel. In Los Gatos, about 15 sites were occupied in a general site study, and an L-shaped array having arms of about 0.5 km in length was deployed in the downtown area to determine whether ground strains induced by shaking could have caused the compressions observed in the downtown area. We also occupied about 8 sites where liquefaction had occurred, in collaboration with John Tinsley, but little data were recovered from this deployment owing to high ground noise caused by nearby agricultural activity.

Reports

Andrews, M., Banfill, R., Carver, D., Celebi, M., Cranswick, E., King, K., Spudich, P., and Worley, D., 1990, Digital aftershock recordings of the October 17, 1989 Loma Prieta, California, earthquake [abs.]: *EOS, Transactions of the American Geophysical Union*, v. __, p. 287.

Cranswick, E., King, K., Spudich, p., Carver, D., Worley, D., and Banfill, R., 1990, Site response across the downtown Santa Cruz alluvial basin [abs.]: *EOS, Transactions of the American Geophysical Union*, v. __, p. 287.

Cranswick, E., King, K., Spudich, P., Carver, D., Worley, D., Williams, R., and Banfill, R., 1990, Site response across the downtown Santa Cruz alluvial basin: *Geophysical Research Letters*, in press.

King, K., Carver, D., Williams, R.A., Cranswick, E., Worley, D., Spudich, P., Wennerberg, L., and Celebi, M., 1990, Preliminary evaluation of aftershocks recorded in the epicentral region of the 1989 Loma Prieta, California, earthquake--Effects of topography and geology on ground motion: *Geophysical Research Letters*, in press.

Liquefaction in the Monterey Bay Region
(Emergency Earthquake Hazards)

9910-01629

John C. Tinsley
Branch of Western Regional Geology
345 Middlefield Road M/S 975
Menlo Park, CA 94025
(415) 329-4928

Thomas L. Holzer
Branch of Engineering Geology and Seismology
345 Middlefield Road M/S 977
Menlo Park, CA 94025
(415) 329-5637

Investigations

A map showing the distribution and nature of liquefaction-related ground failures at a scale of 1:24,000 is being prepared for the Monterey Bay-Hollister region, California. A comprehensive program of regional field studies and site specific investigations is in progress at 11 sites; the field phase is scheduled for completion in June, 1990. These studies include stratigraphic and geomorphic analyses of the facies associations of the ground failures; an evaluation of published USGS liquefaction potential map (Dupre and Tinsley, 1980) for the Monterey Bay region (scale 1:62,500), in light of the Loma Prieta earthquake effects; comparisons of 1989 liquefaction effects with published reports of permanent ground failures arising from the 1907 San Francisco earthquake; cone penetrometer, standard penetrometer, and piezocone penetrometer studies of selected lateral spread ground failures to determine in-situ properties of failed and adjacent non-failed materials in relation to ground motion generated by the Loma Prieta earthquake; and comparisons among geotechnical properties of sediments involved in the failures of the natural deposits in relation to published curves for evaluating liquefaction susceptibility as used in standard engineering practice in the United States. Several sites have been located which may afford good potential to evaluate 1906 and earlier earthquakes using paleoliquefaction studies.

Results

The initial compilation of ground failure effects using aerial photographic analysis coupled with field mapping and sampling of ejected sand is complete; particle size analysis of ejected sand samples is in progress in the soil laboratory at Menlo Park. From a stratigraphic perspective, there is a strong association between fluvial channel, levee, and point bar deposits and liquefaction effects observed following the 10/17/89 earthquake, especially among deposits which are less than a few hundred years old.

Liquefaction was widespread within late Holocene fluvial deposits of the Pajaro and Salinas Rivers, especially in tidewater reaches where groundwater is within 1 to 2 meters of the ground surface year-round and the effects of prolonged drought on groundwater levels is minimal. In contrast to 1906, when wet soil moisture conditions contributed to widespread hillslope flow failures, in 1989, few if any slope failures related to liquefaction where reported. Intensity of liquefaction effects decreases upstream, as the fluvial deposits become more coarse, despite increasing proximity to the Loma Prieta earthquake seismic source zone. The proximity of a free-face within 50 to 150 m was commonly observed in lateral spread ground failures.

Components of displacements associated with ground failures measured in the field following the Loma Prieta earthquake range from a few millimeters to about 1 meter horizontally; settlements range from a few millimeters to less than 2 meters vertically.

References cited

Dupre, W.R. and Tinsley, J.C., 1980, Geology and liquefaction potential, northern Monterey and southern Santa Cruz Counties, California: U.S. Geological Survey Miscellaneous Field Studies Map MF-1199, 2 sheets, scale 1:62,500.

Geologic Investigations of Surface Fractures, Loma Prieta, California Earthquake

9540-04530

Ray E. Wells
U.S. Geological Survey
Branch of Western Regional Geology
345 Middlefield Road M/S 975
Menlo Park, California 94025
(415) 329-4933

INVESTIGATIONS

We have mapped anomalous but pervasive surface fractures that occurred above the northern end of the subsurface rupture zone during the Loma Prieta earthquake. We determined displacement vectors at over 200 stations and compared fracture trends and slip directions to underlying bedrock geologic structures and regional topographic slope.

RESULTS

Ground cracks as much as 100s of meters long with as much as 90 cm of displacement predominantly occur in an 8-km-long by 1 1/2-km-wide region at the northwest end of the subsurface rupture zone. They occur in areas underlain by steeply dipping Tertiary strata on the hanging wall (SW) block. Fracture trends roughly parallel the San Andreas fault, and displacement along most fractures is NNE-SSW extension, with components of left-lateral and vertical slip. Fracture trends and displacement directions are consistent along the zone, although the amount of displacement and continuity of the fractures generally decrease southeastward. Fracture trends roughly parallel the ridge crest along Summit Road but cut obliquely across Laurel Canyon and Skyland Ridge along strike to the southeast. The association of many fractures with linear scarps, troughs, and elongate depressions indicates repeated motion.

Most cracks in the Summit Road - Skyland Ridge area parallel the strike of bedding, even where bedding and fractures deviate from the overall trend. The displacement azimuths of some fractures coincide with the dip direction of beds. On Skyland Ridge cracks are most abundant in areas underlain by shale of the San Lorenzo Formation and mudstone of the Butano Formation, which are exposed in the core of the Laurel anticline. Areas underlain by massive sandstone of the Vaqueros and Butano Formations contain few cracks. The coincidence of ground cracks and shale beds is also evident in the Highway 17 roadcut near Summit Road. The surface breaks resulting from the Loma Prieta earthquake are similar to those reported in this area after the 1906 earthquake.

REPORTS

(P) Plafker, G., and Galloway, J.P., and 31 contributors, 1989, Lessons learned from the Loma Prieta, California earthquake of October 17, 1989, U.S. Geological Survey Circular 1045, 48 p.

(A) U.S. Geological Survey, 1990, Apparent lithologic and structural control of surface fracturing in the Summit Road area during the Loma Prieta earthquake of October 17, 1989: EOS, Transactions American Geophysical Union, in press, 1 p.

(O) U.S. Geological Survey, 1989, Preliminary map of fractures formed in the Summit Road-Skyland Ridge area during the Loma Prieta, California earthquake of October 17, 1989: 1 Sheet, scale 1:12,000: U.S.G.S. Open File Map 89-686.

(P) Ponti, D., Wells, R.E., and Haugerud, 1990, EERI Reconnaissance report on Loma Prieta earthquake surface ruptures, in press.

(P) U.S. Geological Survey, 1990, Loma Prieta California Earthquake: Anticipated event. Science, v. 247. p. 286-293.

Geologic Materials of the South San Francisco Bay Region (Emergency Earthquake Hazards)

9540-04530

Carl M. Wentworth
Branch of Western Regional Geology
U.S. Geological Survey
345 Middlefield Road
Menlo Park, CA 94025
(415) 329-4950

INVESTIGATIONS

A map showing the distribution of geologic materials in the south San Francisco Bay region is being prepared in digital form to support continuing efforts to understand the effects of the 1989 Loma Prieta earthquake and to help predict effects of future earthquakes in the region. Three existing sources are being compiled on a digital 1:125,000 topographic base (vector image of sheet 3 of the Bay region topographic map): Ellen and Wentworth, in press (hillside materials, same scale and base), Helley and Lajoie, 1979 (surficial materials, same scale and base), and Brabb, 1989 (geologic map of Santa Cruz County, 1:62,500). The map is being compiled using the commercial GIS system ARC/INFO under the control of a menu-driven shell called ALACARTE (separately developed by Fitzgibbon and Wentworth under support of the National Geologic Mapping Program, USGS). Geology is largely as of the mid-1970s; physical properties are based on summaries of field observations reported in the source reports and extrapolated by geologic unit.. When completed, the map will consist of a vector database with x,y coordinates in meters on the ground (Lambert Conformal Conic projection) that contains (1) lines identified by geologic type, (2) polygons identified by geologic and/or materials unit, and (3) summary unit descriptions in searchable form.

RESULTS

Linework for surficial materials has been scanned and vectorized and is being edited and for hillside materials and Santa Cruz County has been scanned, vectorized, edited, and tagged; polygons for Santa Cruz County have been tagged; the base has been scanned and vectorized in three layers - drainage, culture, and topographic contours. Geologic line symbols for plotting are available from ALACARTE. Color electrostatic plots of geologic linework on a three color base are of near publication quality. Loma Prieta aftershocks for the first two weeks have been successfully imported into ARC/INFO and plotted at 1:125,000 on the materials map and base as circles colored according to depth with radius proportional to magnitude.

INDEX 1

INDEX ALPHABETIZED BY PRINCIPAL INVESTIGATOR

INDEX 2

INDEX ALPHABETIZED BY INSTITUTION

☆U.S. GOVERNMENT PRINTING OFFICE: 1990-786-121/39228